ADA051932

THE PROPAGATION OF SATELLITE SIGNALS THROUGH TURBULENT MEDIA

January 1978

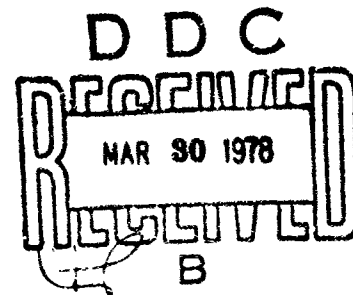Final Report

Approved for public release; distribution unlimited.

D D C

MAR 30 1978

B

Prepared for

Director

DEFENSE NUCLEAR AGENCY

Washington, DC 20305

AIR FORCE WEAPONS LABORATORY

Air Force Systems Command

Kirtland Air Force Base, NM 87117

This final report was prepared by the Air Force Weapons Laboratory, Kirtland Air Force Base, New Mexico under Job Order WDNB5401. Capt Leon A. Wittwer, DYC, was the Laboratory Project Officer.

When US Government drawings, specifications, or other data are used for any purpose other than a definitely related Government procurement operation, the Government thereby incurs no responsibility nor any obligation whatsoever, and the fact that the Government may have formulated, furnished, or in any way supplied the said drawings, specifications, or other data is not to be regarded by implication or otherwise as in any manner licensing the holder or any other person or corporation or conveying any rights or permission to manufacture, use, or sell any patented invention that may in any way be related thereto.

This report has been reviewed by the Office of Information (OI) and is releasable to the National Technical Information Service (NTIS). At NTIS, it will be available to the general public, including foreign nations.

This technical report has been reviewed and is approved for publication.

LEON A. WITTWER
Captain   USAF
Project Officer

FOR THE COMMANDER

JOHN D. HAWKINS
Major   USAF
Chief, Satellite and C³ Branch

PAUL J. DAILY
Colonel   USAF
Chief, Applied Physics Division

REPORT DOCUMENTATION PAGE	READ INSTRUCTIONS BEFORE COMPLETING FORM

1. REPORT NUMBER AFWL-TR-77-183	2. GOVT ACCESSION NO.	3. RECIPIENT'S CATALOG NUMBER

4. TITLE (and Subtitle)
THE PROPAGATION OF SATELLITE SIGNALS THROUGH TURBULENT MEDIA.

5. TYPE OF REPORT & PERIOD COVERED
Final Report.

6. PERFORMING ORG. REPORT NUMBER

7. AUTHOR(s)
Capt L. A. Wittwer

8. CONTRACT OR GRANT NUMBER(s)
WDNB5401

9. PERFORMING ORGANIZATION NAME AND ADDRESS
Air Force Weapons Laboratory (DYC)
Kirtland Air Force Base, New Mexico 87117

10. PROGRAM ELEMENT, PROJECT, TASK AREA & WORK UNIT NUMBERS
Subtask-S99QAXHB054; Work Unit-01; Title-Propagation Models for Satellite Comm.

11. CONTROLLING OFFICE NAME AND ADDRESS
Director
Defense Nuclear Agency
Washington, D.C. 20305

12. REPORT DATE
Jan 78

13. NUMBER OF PAGES
478

14. MONITORING AGENCY NAME & ADDRESS(if different from Controlling Office)
Air Force Weapons Laboratory (DYC)
Kirtland Air Force Base, New Mexico 87117

15. SECURITY CLASS. (of this report)
UNCLASSIFIED

15a. DECLASSIFICATION/DOWNGRADING SCHEDULE

16. DISTRIBUTION STATEMENT (of this Report)

Approved for public release; distribution unlimited.

17. DISTRIBUTION STATEMENT (of the abstract entered in Block 20, if different from Report)

19. KEY WORDS (Continue on reverse side if necessary and identify by block number)

Ionospheric Propagation   Scintillations
Radio Propagation
UHF Propagation
Striations

20. ABSTRACT (Continue on reverse side if necessary and identify by block number) (UNCLASSIFIED)
Calculations of the effects of striated ionospheres on satellite signals are presented and analyzed. The calculations include the effects of various striation power spectral densities and scale sizes. All types of propagation cases that are reasonably expected are included.

DD FORM 1473 EDITION OF 1 NOV 65 IS OBSOLETE

SECTION I

INTRODUCTION

The effects of turbulent media on propagation of various waveforms have been studied for many years. These studies have included starlight scintillation, underwater sound propagation, laser beam propagation and satellite link scintillations. Various theories and techniques have been developed to estimate turbulent effects under various conditions. The emphasis in this report is on satellite signal propagation. Calculational methods, particularly multiple phase screen algorithms have been developed that handle most cases of interest. However, no overall picture has been developed that encompasses the set of likely *in situ* environments, scale sizes, and other conditions of interest. The closest effort to date was by Singleton (ref. 1), but this work was quite limited in the cases studied. This lack has become particularly acute with the growing volume of signal data from the Defense Nuclear Agency (DNA) wideband satellite studies, Air Force Geophysics Laboratory (AFGL) aircraft studies, etc. This study is designed to remedy the situation by systematically calculating and presenting in typical data format signal propagation results that may be encountered. Features are identified in the data that allow interpretation of the *in situ* environments. Conceptually, the information presented should be viewed as "clean data"; i.e., experimental data without the problems of lack of stationarity, time-space ambiguities, sampling problems, data sample boundary problems and other experimental difficulties that becloud real data. One value of this point of view is to realize that features that are marginally detectable here are probably not useful in real data. Thus, this study defines the type and quality of information that can be obtained from signal propagation data.

Section II discusses the propagation algorithms particularly the Rytov method which is used for insight in interpreting and classifying results. Section III contains the data analysis. Section IV summarizes the conclusions.

---

1. Singleton, D. G., "Saturation and Focusing Effects in Radio-Star and Satellite Scintillations," J. Atoms. Terr. Phys., Vol 32, 1970.

SECTION II

PROPAGATION METHODS AND SPECTRAL MODELS

The calculations reported here were done with the multiple phase screen (MPS) method and the Rytov approximation (RA). These methods are described elsewhere (refs. 2 and 3) and only necessary extensions to these description are given here. The RA method calculates the correlation functions of the log amplitude and phase fluctuations through a turbulent medium. The basic two-dimensional equations are:

$$\overline{\chi(x)\,\chi(x+\rho)} = K^2 \int_{-\infty}^{\infty} \frac{d\,K_\rho}{2\pi} \int_{0}^{z_s} dz \, \sin^2\left[\frac{K_\rho^2}{2K}\left(z_s + z_g - z\right)\right] \Phi_2\left(z, K_\rho\right) e^{iK_\rho \rho} \quad (1)$$

$$\overline{\phi(x)\,\phi(x+\rho)} = K^2 \int_{-\infty}^{\infty} \frac{d\,K_\rho}{2\pi} \int_{0}^{z_s} dz \, \cos^2\left[\frac{K_\rho^2}{2K}\left(z_s + z_g - z\right)\right] \Phi_2\left(z, K_\rho\right) e^{iK_\rho \rho} \quad (2)$$

$$\overline{\phi(x)\,\chi(x+\rho)} = K^2 \int_{-\infty}^{\infty} \frac{d\,K_\rho}{2\pi} \int_{0}^{z_s} dz \, \sin\left[\frac{K_\rho^2}{2K}\left(z_s + z_g - z\right)\right]$$

$$(3)$$

$$\cos\left[\frac{K_\rho^2}{2K}\left(z_s + z_g \, z\right)\right] \Phi_2\left(z, K_\rho\right) e^{iK_\rho \rho}$$

2. Wittwer, L. A., UHF Propagation Effects in Scintillated Environments, AFWL-TR-76-304, Air Force Weapons Laboratory, Kirtland AFB, New Mexico, 1977.

3. Rino, C. L., Analysis of Scintillation Effects on Communication Systems, Stanford Research Institute (to be published).

where

z = coordinate along propagation line-of-sight (LOS)

X = coordinate perpendicular to LOS

z_s = turbulent layer thickness

z_g = distance from bottom of layer to receiver where the correlation functions are measured

K = rf wave number

Assume that there is no variation of the turbulent layer in the third coordinate and that the fluctuation statistics are isotropic. The medium is represented by

$$\Phi_2\left(z,K_\rho\right) = \int_{-\infty}^{\infty} \int_{-\infty}^{\infty} \overline{\Delta n_i\ (z,x)\ \Delta n_i\ (z,\epsilon,x+\rho)}e^{-iK_\rho\rho}d\rho d\epsilon \qquad (4)$$

where

$\Delta n_i = n_i - \overline{n_i}$

n_i = index of refraction

$\overline{n_i}$ = mean index of refraction

The prime value of the Rytov equations is that they provide a simple, quantitatively accurate estimate of the onset of phase and amplitude fluctuations and their power spectra. If $\Phi_2\left(z,K_\rho\right)$ has no z dependence then the integral over z can be done analytically, and we have for the log amplitude and phase power spectra

$$S_\phi\left(K_\rho\right) = \frac{K^2 z_s}{2}\left\{1 - \frac{K}{z_s K_\rho^2}\left[\sin\left(\frac{K_\rho^2\ z_g}{K}\right) - \sin\left(\frac{K_\rho^2}{K}\left(z_s + z_g\right)\right)\right]\right\}\Phi_2\left(K_\rho\right) \qquad (5)$$

$$S_\chi\left(K_\rho\right) = \frac{K^2 z_s}{2}\left\{1 + \frac{K}{z_s K_\rho^2}\left[\sin\left(\frac{K_\rho^2\ z_s}{K}\right) - \sin\left(\frac{K_\rho^2}{K}\left(z_s + z_g\right)\right)\right]\right\}\Phi_2\left(K_\rho\right) \qquad (6)$$

3

$$S_{\phi\chi}\left(K_\rho\right) = \frac{K^3}{2K_\rho^2}\left[\cos\left(\frac{K_\rho^3\,z_g}{K}\right) - \cos\left(\frac{K_\rho^2}{K}\left(z_s + z_g\right)\right)\right]\Phi_2\left(K_\rho\right) \tag{7}$$

The expressions in brackets in equations 5 through 7 can be looked at as filters which filter the $\Phi_2\left(K_\rho\right)$ spectrum to give the different spectra. Figure 1 shows the first two filter functions for $z_s = 10^7$ cm, $z_g = 3 \times 10^7$ and $K = 0.062$. The phase filter is roughly constant except for some oscillations. The log amplitude filter goes as K_ρ^4 until

$$K_\rho^2 = 5.5\,K\left[\frac{z_s}{\left(z_s + z_g{}^3 - z_g^3\right)}\right]^{1/2} \tag{8}$$

and is approximately constant afterward. This latter behavior can be used to evaluate measured signal amplitude spectra to determine $\Phi_2\left(K_\rho\right)$. Before actual data can be confidently analyzed, however, the practical limits of the preceeding equations must be known, as well as limitations on assuming

$$|E(x)| = 1 + \chi(x) \tag{9}$$

where $|E(x)|$ is the field amplitude. Equation 9 is not actually necessary, but most experimentalists measure amplitude and not log amplitude. The calculations discussed in section III amply demonstrate the range of validity of equations 5 through 7 and 9. Now look at $\Phi_2\left(K_\rho\right)$. Assume that the one dimensional index of refraction power spectral density is

$$S_i^{(1)}\left(K_\rho\right) = 2\,\overline{\Delta n_i^2}\,\frac{\Gamma\left(\nu + \frac{1}{2}\right)L^{-2\nu}}{\left(1/L^2 + K_\rho^2\right)^{\nu + 1/2}} \tag{10}$$

where L is the outer scale size and $2\nu + 1$ is the spectral index. If $\nu = 1/2$, we have the familiar K_ρ^{-2} spectra. If the fluctuations are two-dimensional and isotropic, then the two-dimensional power spectral density is
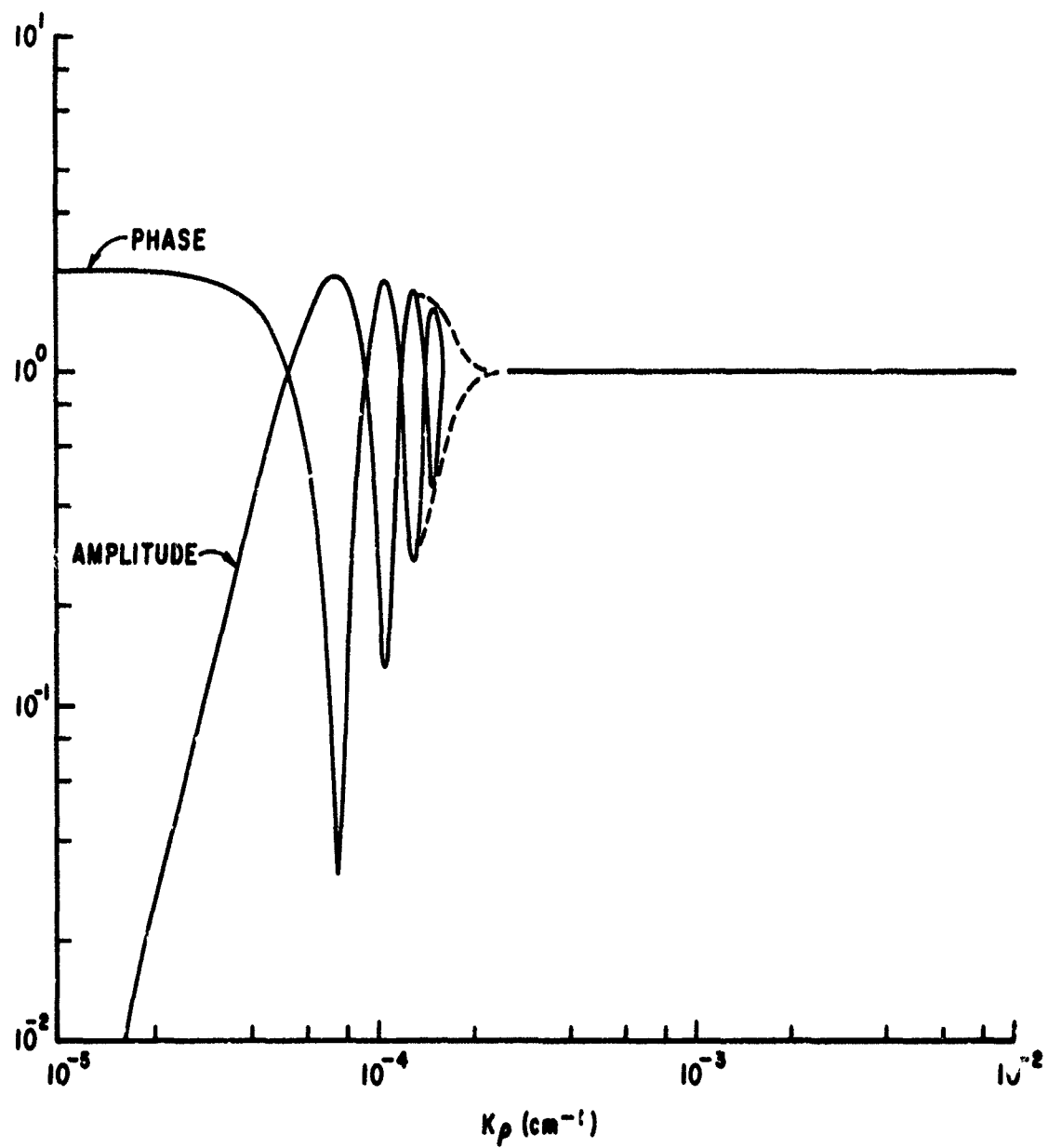
Figure 1. Amplitude and Phase Filter Functions

$$S_i^{(2)}\left(K_\rho, K_\epsilon\right) = 4\pi^{1/2} \cdot \frac{\overline{\Delta n_i^2}\ \Gamma(\nu + 1)\ L^{-2\nu}}{\left(1/L^2 + K_\rho^2 + K_\epsilon^2\right)^{\nu + 1}} \tag{11}$$

For three-dimensional isotropic fluctuations

$$S_i^{(3)}\left(K_\rho, K_\epsilon, K_z\right) = 8\pi \cdot \frac{\overline{\Delta n_i^2}\ \Gamma(\nu + 3/2)\ L^{-2\nu}}{\left(1/L^2 + K_\rho^2 + K_\epsilon^2 + K_z^2\right)^{\nu + 3/2}} \tag{12}$$

If the fluctuation statistics are not isotropic, equations 10 through 12 can be modified by generalizing the quadratic wave number terms. From equations (4) and 11 it is clear that

$$\Phi_2\left(K_\rho\right) = S_i^{(2)}\left(K_\rho, 0\right) \tag{13}$$

Thus $\Phi_2\left(K_\rho\right)$ is the two-dimensional index of refraction power spectral density with zero longitudinal wave number. The one dimension correlation function corresponding to equation 10 is

$$\overline{\Delta n_i\ (z,x)\ \Delta n_i\ (z,x + \rho)} = \frac{\overline{\Delta n_i^2}\ 2^{-\nu + 1}}{\pi^{1/2}}\ \left(\frac{\rho}{L}\right)^\nu K_\nu\left(\frac{\rho}{L}\right) \tag{14}$$

These formula are useable for $\nu > -1/2$ but some discussion is in order for $\nu \le 0$. For this case the one-dimensional power spectral density has infinite power, and the correlation function is unbounded at $\rho = 0$. The phase and log amplitude spectra, however, are still finite because only the spectrum near the outer scale contribute to the propagation. Thus, we can still use an infinite power spectrum in the sense that we are fitting the real *in situ* spectrum correctly near the sizes that determine the propagation. The use of $-1/2 < \nu \le 0$ does make the total mean square fluctuation power ambiguous because not all of it contributes to the propagation. Here, regard $\overline{\Delta n_i^2}$ as just an adjustable parameter

$$\overline{\Delta n_i^2} = \frac{\Phi_1\left(K_\rho = 0\right)}{2\Gamma\left(\nu + 1/2\right) L} \tag{15}$$

to determine by fitting to a measured power spectral density.

Other useful two-dimensional power spectral densities are

Chesnut (ref. 4):

$$S_i^{(2)}\left(K_\rho, K_\epsilon\right) = 4\pi \overline{\Delta n_i^2}\ e^{-\sqrt{2}}\ \left(K_\rho^2 + K_\epsilon^2\right)^{1/2} L \tag{16}$$

Gaussian:

$$S_i^{(2)}\left(K_\rho, K_\epsilon\right) = \pi \overline{\Delta n_i^2}\ L^2\ e^{-\left(K_\rho^2 + K_\epsilon^2\right)L^2/4} \tag{17}$$

Cylindrical Rod:

$$S_i^{(2)}\left(K_\rho, K_\epsilon\right) = 4\pi \overline{\Delta n_i^2}\ L^2 \left[\frac{J_1\left(\left(K_\rho^2 + K_\epsilon^2\right)^{1/2} L\right)}{\left(K_\rho^2 + K_\epsilon^2\right)^{1/2} L}\right]^2 \tag{18}$$

The one-dimensional spectra used in this study are shown in figure 2. Other useful functions for spectral modeling have been developed by Rino and Sachs (ref. 5).

Equations 5 and 6 can be used to develop expressions that determine the onset of amplitude and phase fluctuations. This was demonstrated in reference 2 for the power law expression and has since been generalized. The following is a summary for both guassian and power law spectra.
For

$$\frac{LK^2}{z_s + z_g} \leq 1$$

4. Chesnut, W. G., "Spatial-Frequency Analysis of Striated Nuclear Phenomena--
   Part 2: A Model of the Striated Checkmate Cloud," Stanford Rsch Institute
   (Unpublished)

5. Rino, C. L. and Sachs, D. L., "Striation Models for High Altitude Nuclear
   Propagation Effects," Stanford Research Institute (to be published).
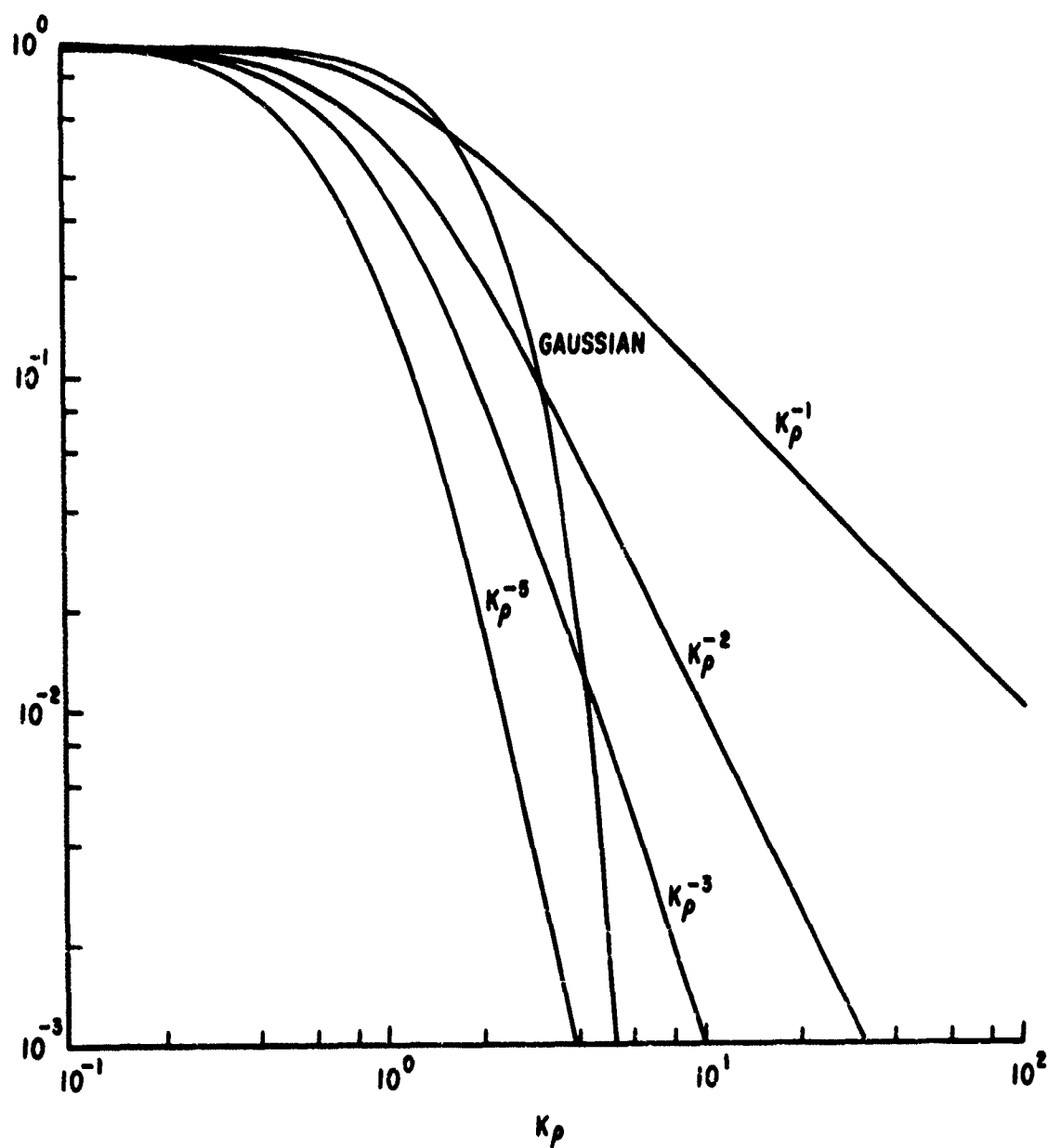
Figure 2. Selected One-Dimensional Power Spectra Normalized to 1 for $K_\rho = 0$

$$\overline{\phi^2} = \overline{\chi^2} = \left(\frac{2\pi e^2}{mc^2}\right)^2 \frac{\overline{\Delta n^2}}{K^2} \frac{L\ z_s}{K^2} \quad \text{(gaussian)} \tag{19}$$

$$\overline{\phi^2} = \overline{\chi^2} = \left(\frac{2\pi e^2}{mc^2}\right)^2 \frac{\overline{\Delta n^2}}{K^2} \frac{L\ z_s}{K^2}\ \Gamma\left(\nu + \frac{1}{2}\right) \quad \text{(power law)} \tag{20}$$

For

$$\frac{L^2 K}{z_s + z_g} \geq 1$$

$$\overline{\phi^2} = \left(\frac{2\pi e^2}{mc^2}\right)^2 \overline{\Delta n^2}\ \frac{2\ z_s\ L}{K^2} \quad \text{(gaussian)} \tag{21}$$

$$\overline{\chi^2} = \left(\frac{2\pi e^2}{mc^2}\right)^2 \overline{\Delta n^2}\ \pi^{1/2}\ \left[\frac{\left(z_s + z_g\right)^3 - z_g^3}{K^4\ L^3}\right] \quad \text{(gaussian)} \tag{22}$$

$$\overline{\phi^2} = \left(\frac{2\pi e^2}{mc^2}\right)^2 \overline{\Delta n^2}\ 2\ \frac{z_s\ L}{K^2}\ \Gamma\left(\nu + \frac{1}{2}\right) \quad \text{(power law)} \tag{23}$$

$$\overline{\chi^2} = C(\nu) \left(\frac{2\pi e^2}{mc^2}\right)^2 \overline{\Delta n^2}\ \frac{\left[\left(z_s + z_g\right)^3 - z_g^3\right]^{\nu/2 + 1/4}\ z_s^{-\nu/2 + 3/4}}{L^{2\nu}\ K^{\nu + 2.5}} \qquad \nu \leq 1.5 \tag{24a}$$

(power law)

9

$$\overline{\chi^2} = C(\nu)\left(\frac{2\pi e^2}{mc^2}\right)^2 \overline{\Delta n^2} \left[\frac{\left(z_s + z_g\right)^3 - z_g^3}{K^4 L^3}\right] \quad \nu > 1.5 \qquad (24b)$$

where

$$\Delta n = n - \overline{n}$$

n = electron density

$\overline{n}$ = mean electron density

$$C(\nu) = 0.9\ e^{-\nu/0.8} + 0.05$$

By setting $\overline{\phi^2} = \overline{\chi^2} = 0.1$, these expressions provide an accurate estimate of the conditions necessary for the development of phase and amplitude fluctuations for uniform layers.

Reference 2 demonstrates that if the scattering layer is sufficiently thick then the phase and amplitude distributions are a function of the *in situ* power spectral density. This work is expanded to include the phase, amplitude and signal power spectra. As in this reference, comparisons are made for a particular *in situ* spectrum between calculations made by assuming gaussian distributed fluctuations and by using explicit geometric figures.

The electron density using explicit geometric figures can be written as

$$n\left(x,z\right) = \sum_{i=0}^{N} f_i\ n_0\left(a_i\right) F\left(x,z,x_i,z_i,a_i\right) \qquad (25)$$

where

f_i = random variable with equally probable values of ± 1

$n_0\left(a_i\right)$ = peak on axis electron density

$F\left(x,z,x_i,z_i,a_i\right)$ = geometric function used to construct electron distribution

a_i = fluctuation size

N = number of striations

10

f_i is used to guarantee that $n(x,z)$ is zero mean. The fluctuation size, a_i, is distributed according to $P(a)$. The $\underline{P(a)}$ and $n_0(a)$ are chosen to give the correct *in situ* power spectral density and $\overline{\Delta n^2}$.

The MPS propagation requires the integrated phase of a plane wave going from z to $z + \Delta z$ on a mesh where $-T \leq x \leq T$. In two-dimensional calculations

$$\phi(x) = \frac{2\pi e^2}{mc^2} \; \frac{1}{K} \int\limits_{z}^{z+\Delta z} n\left(x, z'\right) d\, z' \tag{26}$$

For explicit representations, the striations are randomly located. If there is an average of $\overline{N}/A$ striations per unit area in the striated region, then each phase screen will have an average of $2\overline{N} \Delta z T/A$ striations contributing. The actual number N for any given screen is distributed according to the Poisson distribution

$$P_N(N) = \frac{\left(2\overline{N} \, \Delta z \, \frac{T}{A}\right)^N e^{-(2\overline{N} \, \Delta z T/A)}}{N!} \tag{27}$$

To calculate a screen, N is sampled along with N values of a_i and x_i. The phase screen is

$$\phi(x) = \frac{2\pi e^2}{mc^2} \frac{1}{K} \sum_{i=0}^{N} f_i \; n_0 \left(a_i\right) \int\limits_{-\infty}^{\infty} F\left(x, z, x_i, a_i\right) dz \tag{28}$$

The z limits are taken to infinity assuming that if a striation has its center within the $2T\Delta z$ area, then all of the phase effects of the striation are included in the phase screen being generated.

For gaussian distributed fluctuations, the phase screen is described in terms of a Fourier series.

$$\phi(x) = \frac{1}{2i} \sum_{m=-\infty}^{\infty} b_m \; e^{i \, \frac{m\pi x}{T}} \tag{29}$$

The b_m coefficients are independent, zero mean distributed variables with a variance of

$$\overline{b_m^2} = 2T \ K^2 \ \Delta z \ \phi_2 \left(\frac{m\pi}{T} \right) \tag{30}$$

where $\phi_2 \left(K_\rho \right)$ is the two-dimensional isotropic *in situ* power spectrum defined earlier.

Gaussian, K_ρ^{-2}, and cylindrical rod power spectral densities are used to illustrate the convergence of the second order propagation statistics. The first three spectra are constructed out of gaussian rods with

$$F \left(x,z,x_i,z_i,a_i \right) = e^{- \left[\left(x-x_i \right)^2 + \left(z-z_i \right)^2 \right] / a_i^2} \tag{31}$$

The distribution functions for a and $n_o(a)$ are

$$\left.\begin{array}{l} P(a) = \delta \left(L - 2^{1/2} \ a \right) \\[2em] n_0(a) = \left(\dfrac{2 \ \overline{\Delta n^2} \ A}{\overline{N} \ a^2 \ \pi} \right)^{1/2} \end{array}\right\} \quad \text{gaussian} \tag{32}$$

$$\left.\begin{array}{l} P(a) = \dfrac{\ell}{2^{1/2} \ a^2} \quad , \quad a \geq \dfrac{\ell}{2^{1/2}} \\[2em] n_0(a) = \left\{ \dfrac{4 \ \overline{\Delta n^2} \ A}{\overline{N}\ell L \pi^{3/2} \left(1 - \text{erf} \ (\ell/2L) \right)} \right\}^{1/2} e^{-a^2/4L^2} \end{array}\right\} K_\rho^{-2} \tag{33}$$

$$\left.\begin{array}{l} P(a) = \dfrac{\ell}{a^3} \quad , \quad a \geq \dfrac{\ell}{2^{1/2}} \\[2em] n_0(a) = \left\{ \dfrac{4 \ \overline{\Delta n^2} \ A}{\pi^{3/2} \ \overline{N} \ell^2 \left(1 - \text{erf} \left(\ell/2L \right) \right)} \right\}^{1/2} e^{-a^2/4L^2} \end{array}\right\} K_\rho^{-1} \tag{34}$$

where ℓ is the inner scale size, $\delta(a)$ is the Dirac delta function, and

$$\text{erf}(x) = \frac{2}{\pi^{1/2}} \int_0^X e^{-t^2} \, dt \tag{35}$$

The cylindrical rod function is

$$F\left(x, z, x_i, z_i, a_i\right) = 1 \quad , \quad \left[\left(x - x_i\right)^2 + \left(z - z_i\right)^2\right]^{1/2} \leq L \tag{36}$$

and

$$\left. \begin{array}{l} P(a) = \delta\left(L - 2^{1/2} a\right) \\[3em] n_0(a) = \left(\dfrac{\Delta n^2}{2\pi \, \overline{N} \, a^2}\right)^{1/2} \end{array} \right\} \quad \text{cylindrical rod} \tag{37}$$

The measure of thickness of a scattering layer is the mean free path defined as

$$\text{MFP} = \left[\frac{\overline{N}}{A} \int_{\ell/2^{1/2}}^\infty (2a) \left(2^{1/2} \frac{a}{L}\right) e^{-a^2/4L^2} \; P(a) \, da\right]^{-1} \tag{38}$$

for distributions where $P(a) \neq \delta\left(L - 2^{1/2} a\right)$ and

$$\text{MFP} = \left[\frac{2^{1/2} \, L \, \overline{N}}{A}\right]^{-1} \tag{39}$$

for the others.

For a given $\overline{\Delta n^2}$, spectral type, z_s, and L, $\overline{N}/A$ is varied to give the number of mean free paths desired. The calculations described in section III examine convergence for the second order signal statistics with scattering layers that are five mean free paths thick.

13

SECTION III

DATA ANALYSIS

Calculations were run for five *in situ* spectral types: K_ρ^{-1}, K_ρ^{-2}, K_ρ^{-3}, K_ρ^{-5}, and gaussian. Data taken by AFGL* and SRI** (the latter from the DNA Wideband Satellite) imply the existence of a K_ρ^{-1} spectrum in polar environments with a reasonable frequency of occurrence. Goldman (ref. 6) has derived conditions under which this spectrum might be expected. The K_ρ^{-2} spectrum has been observed in several ionospheric experiments (refs. 7 through 9)+. This spectrum is considered the result of the $\overline{E}X\overline{B}$ instability (refs. 6, 10 through 12). Recently it has been shown that K_ρ^{-2} can result from the decay of $\overline{E}X\overline{B}$ modes into drift modes (ref. 13). The K_ρ^{-3} spectrum also has been inferred from AFGL and SRI data. This spectrum has been calculated at NRL (ref. 14) in spread F simulation studies. The K_ρ^{-5} and gaussian spectra were used to examine the propagation effects of single size spectra, which have not appeared commonly in data.

In the following, the environments are described by specifying L, z_s, z_g, K, $\overline{\Delta n^2}$ and the type of fluctuation power spectral density. The propagation LOS is assumed to travel through the stationary fluctuations at $\overline{v} = 3 \times 10^4$ cm/sec. This velocity is used to transform spatial data to time data. In particular, to analyze the calculated spectral data, it is convenient to define three frequencies which correspond to the first Freznel zone size, the fluctuation scale size and the signal scale size, respectively.

$$f_F = \frac{\overline{v}}{2\pi}\left[5.5\ K\left(\frac{z_s}{\left(z_s + z_g\right)^3 - z_g^3}\right)^{1/2}\right]^{1/2} \tag{40}$$

---

* Whitney, H., Air Force Geophysics Laboratory, private communication.

** Rino, C. L., Stanford Research Institute, private communication.

+ Kelley, M. C., Cornell University, private communication.

NOTE: References 6 through 14 are listed at the back of this section.

$$f_s = \frac{\overline{v}}{(2\pi L)} \qquad \text{(power law)} \qquad (41a)$$

$$f_s = \frac{\overline{v}}{(\pi L)} \qquad \text{(gaussian)} \qquad (41b)$$

$$f_0 = \frac{1}{\left(2\pi \overline{\tau}_0\right)} = \frac{\overline{v}}{\left(2\pi \overline{\ell}_0\right)} \qquad (42)$$

The Fresnel frequency, f_F, corresponds approximately to the maximum in the amplitude filter function transformed to frequency space.

There are two classes of fluctuation power spectra as distinguished by the signal structures they give rise to. The first, called multisize spectra, includes all the power law spectra for $\nu < 1.5$. The name derives from the observation that the size of fluctuation that dominates the amplitude fluctuations for weak scatter and $f_s \leq f_F$ is determined by the Fresnel zone size and not the fluctuation scale size. Thus, any size fluctuation can dominate the amplitude effects given the proper circumstances. The second class, called single size spectra, includes power law with $\nu < 1.5$, gaussian, and exponential power spectral densities. For these cases the amplitude effects are dominated by a single size fluctuation, the scale size L.

For future purposes, it is useful to distinguish between weak and strong scatter cases. Weak scatter is defined as having $\chi^2 \leq 0.1$ and $S_4 \geq 0.5$ while strong scatter has $\chi^2 > 0.1$ or $S_4 \geq 0.5$. The definition for weak scatter has been chosen because as demonstrated by the calculations, the weak scatter region is where equations 5 through 7 and 9 are applicable.

The interplay of environmental parameters defines different types of signal properties for each spectrum. This is demonstrated by the propagation space plots in figures 4, 20, 39, 56 and 72 which were constructed using equations 19 through 24 to define $\overline{\chi^2} = 0.1$ and $\overline{\phi^2} = 0.1$ curves. In all but the gaussian plot, z_s, z_g, K and spectrum type are fixed, where $\overline{\Delta n^2}$ and L are the varied quantities. The gaussian case fixed $\overline{\Delta n^2}$ but varied z_s with all other variables the same as the other spectra calculations to examine the z_s dependence in equation 23. Each of the propagation space plots has three distinct regions shown schematically in figure 3.

15
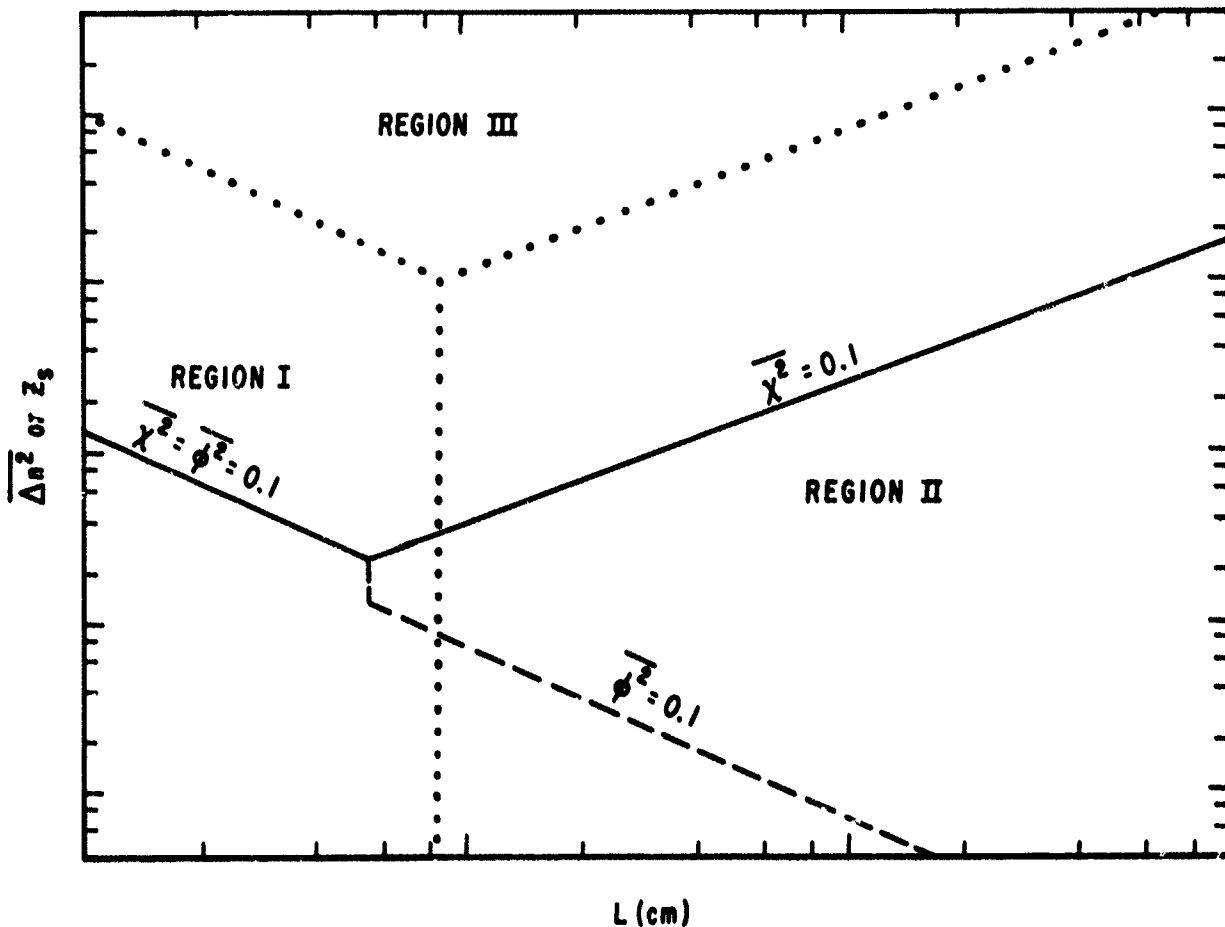
Figure 3. Propagation Space Plot for Generic Spectrum

a. Region I is characterized by gaussian quadrature evolving to Raleigh statistics as $\overline{\Delta n^2}$ or z_s increases and by $f_F \leq f_s$. The sets of figures 7 through 9, 42 through 44, 59 through 61 and 75 through 85 show the evolution of the signal statistics. It is evident from the complex signal plots, the amplitude distributions, and the phase distributions that the statistics are approximately gaussian quadrature. It is also clear that the distribution plots are not very sensitive to *in situ* spectral type. The different spectra do manifest themselves in the complex signal plots and the spectral densities. Figures 23a and 24a for the K_ρ^{-2} spectrum and figures 75a and 76a for the gaussian spectrum clearly show the relative lack of high frequency fluctuation in the gaussian case. The amplitude and phase spectra for the weak scatter cases are clearly explained by the Rytov approximation equations. Figures 23 and 75 are representative of $f_F < f_s$ where the peak in the amplitude filter function occurs before the break in Φ_2 at f_s.

16

The oscillatory behavior of the filter functions is apparent. The amplitude spectra begin with an approximate f^4 behavior to f_F and the Φ_2 behavior after f_F. For power law spectra with a characteristic well defined break at f_s, the region between f_s and f_F will be approximately flat. The phase spectrum for the most part mirrors Φ_2 with the phase filter function effects apparent. The Fresnel frequency is denoted by a deep notch. In some cases, the notch is easier to identify than the corresponding amplitude spectrum peak.

If f_F can be found by examining either the amplitude or phase spectrum and it is at the low frequency end of the flat portion of the amplitude spectrum, then f_F, f_s and the spectral type are unambiguously determined. The location of f_F must be identified because the same spectrum behavior can be generated with a power law spectrum with $\nu = 1$ where $f_F > f_s$, and f_F will be at the high frequency end of the flat portion of the amplitude spectrum.

Even if f_F is not obvious from the spectrum, often a good estimate can be obtained from knowledge of the propagation geometry and interpretation ambiguities can be reduced. Figures 7, 26, 42, 59 and 81 show several weak scatter spectra where $f_s \approx f_F$. The flat portion of the amplitude spectrum has disappeared and the spectrum now has a sharp peak. Let us define the difference between the approximate power law exponent of the amplitude spectrum for $f < f_s$ as α_d.

For the Φ_2 spectra considered here, $\alpha_d \gtrsim 5$ for these peaked spectra. This behavior unambiguously defines f_s, f_F and the spectral type. These sharp peaked data have been measured by AFGL.*

For all of the weak scatter cases with $f_F \leq f_s$, the signal power spectrum is approximately the sum of the amplitude and phase spectra. This is seen by examining equations 5 through 7 and noting that $\overline{\phi^2} \approx \overline{E_I^2}$ and $\overline{\chi^2} \approx \overline{E_I^2}$.

As $\overline{\Delta n^2}$ or z_s increases, the scattering becomes strong. The phase spectrum becomes ambiguous because of the rapid phase changes during deep fades. The amplitude spectrum now begins to distort in shape where, for weak scatter, it just increased in magnitude. The changes start at the lowest frequency and then work upward. The general trend is toward a flat spectrum with a break at f_0 and with the Φ_2 behavior beyond. Figure 27d shows a phenomenon that we will often see in

---

* Whitney, H., Air Force Geophysics Laboratory, private communication.

in strong scatter for all types of propagation. There is an apparent second
break in the amplitude spectrum that does not correspond to any characteristic
frequency. This break designates the failure point in frequency below which the
Rytov equations no longer hold. Thus, equations fail first at small f, and the
point of failure moves to higher frequency in a well-defined way eventually
coinciding reasonably well with f_0. Behavior such as in figure 27d has been
observed in data taken by AFGL.*

The complex signal spectrum does not change shape appreciably as $\overline{\Delta n^2}$
increases but the break at f_0 does move to higher frequency. The spectral shape
after f_0 tends to follow Φ_2. Figures 6, 22, 41, 58 and 74 show plots of S_4 versus
$\overline{\chi^2}$ for all of the spectra. The S_4 is approximately the same monotonic function
of $\overline{\chi^2}$ regardless of *in situ* spectrum when $f_s > f_r$.

b. Region II is characterized by doughnut statistics evolving to Rayleigh
as $\overline{\Delta n^2}$ increases and by $f_s > f_F$. Doughnut statistics are characterized by large
phase fluctuations and small amplitude fluctuations. These statistics are often
seen in the ambient ionosphere and are thought to be characteristic of other
disturbed ionospheres as well. The general behavior in region II is a function
of whether the *in situ* spectrum is multisize or single.

(1) Multisize Spectra. Figures 30, 31, 32 and 33 show a typical
sequence of multisize calculations from the K_ρ^{-2} data. The first two sets of
figures are weak scatter and demonstrate the preponderance of phase effects.
The dominance of phase effects increases with L as demonstrated by comparing
the above figures with figures 34, 35 and 36. The influence of the particular
type of multisize *in situ* spectrum is apparent in the complex signal plots seen
in figures 31 and 11 which correspond to environments that are significantly
different only in the *in situ* spectrum assumed.

Figures 35d and 35e show good weak scatter examples of phase and
amplitude for multisize spectra. The phase spectrum closely maps Φ_2 except for
the notch at f_F which represents the power lost to the amplitude fluctuations.
The amplitude spectrum demonstrates the behavior expected from examining the
Rytov equations. There are three distinct spectral regions. The first is for
$f < f_s$ and is driven by the f^4 behavior of the amplitude filter function because

---

* Whitney, H., Air Force Geophysics Laboratory, private communication.

Φ_2 is approximately flat. For $f_s < f < f_F$, $\Phi_2 \propto f^{-3}$ and the filter function still goes as f^4 resulting in an approximate f^1 behavior. For $f > f_F$, the filter function becomes flat and the amplitude spectrum goes as Φ_2, the difference, α_d, in the power law exponent for $f > f_s$ and $f < f_s$ is approximately 4 regardless of the spectral type. It is clear that the amplitude spectral shape near the peak is only a function of the spectral type and not L.

Since the total amplitude power is dominated by the spectrum near the peak, amplitude for multisize spectra can be characterized by the spectral type and $\overline{\chi^2}$. This is an important result. It says that if lines are drawn in region II parallel with the $\overline{\chi^2} = 0.1$ curve, the amplitude spectrum, power, and distribution are constant along any of the lines. This is very useful in that a calculation for a given $\overline{\chi^2}$ defines the amplitude effects for all L and $\overline{\Delta n^2}$ with the same $\overline{\chi^2}$ with $f_F < f_s$. This means that from amplitude data alone, only the distance away from the $\overline{\chi^2} = 0.1$ line is determinable and not the position along that line. Thus, only $\overline{\Delta n^2} L^{-2\nu}$ can be determined. If L or $\overline{\Delta n^2}$ can be deduced from the phase or other data, then the ambiguity can be resolved. The complex signal spectrum for $\overline{\phi^2} \leq 0.1$ is proportional to Φ_2. As the propagation effects increase, the break denoted by f_0 moves to higher frequency keeping the Φ_2 behavior for $f > f_0$. These calculations show that both f_s and f_F are usually apparent in the weak scatter amplitude and phase spectra as long as the frequency range is large enough. Past scintillation data have tended to emphasize resolution at ever higher frequencies. The low frequency data are also quite valuable particularly to find f_s even when the corresponding wavelengths may be as large as the characteristic dimension of the ionosphere. As $\overline{\Delta n^2}$ increases, $\overline{\chi^2}$ becomes larger than 0.1, S_4 becomes larger than 0.5, and the propagation signal scattering becomes strong. The phase spectrum for all *in situ* spectra becomes dominated by large rapid phase changes and no longer accurately maps Φ_2. The amplitude spectrum evolves qualitatively as in region I as the scattering becomes strong. The Rytov equations begin to fail starting at the lower frequencies. The tendency is for the low frequencies to flatten out to a break at approximately f_0 and Φ_2 behavior beyond f_0. See figures 30d, 31d, 32d, and 33d. The amplitude statistics continue to be constant along lines parallel to $\overline{\chi^2} = 0.1$ in the strong scatter region. The complex signal spectrum changes are characterized by the increases in f_0 with little change in spectrum. The S_4 and $\overline{\chi^2}$ increase essentially monotonically to limits of 1.0 and 0.46, respectively. The amplitude distributions

evolve to Rayleigh showing little spectral dependence. In addition, the amplitude distributions always have a smaller population of deep fades than a Rayleigh distribution (figures 37b, 32b and 53b). This is the source of the statement that Rayleigh statistics are a worst case for amplitude sensitive systems. The discussion of single size spectra shows that this is not always true.

For both weak and strong scatter S_4 is the same well defined, single valued function of $\overline{\chi^2}$ that was found in region I. From the discussion of the amplitude spectrum, it is apparent why this is true for any given spectral type, but it is not obvious why the same function works for all multisize spectra and for all spectra in region I. The most probable cause is that (in the cases quoted) the majority of amplitude power comes from a narrow spectral range.

(2) Single Size Spectra

The behavior of single size spectra in region II is significantly different and distinctive from that of the multisize spectra. The complex signal plots clearly lack the high frequency content of the multisize spectra (figures 64a, 65a, 84a and 85a). For weak scatter, the amplitude and phase spectra are precisely what would be expected from the Rytov equations. The basic difference from earlier cases is that now Φ_2 breaks faster than f^{-4} and the amplitude spectrum peak is now determined by the scale size and not the Fresnel zone size. Figures 86 through 90 show a typical sequence of calculations as $\overline{\Delta n^2}$ increases for the gaussian spectrum. Figures 68 through 71 show weak and strong scatter cases for the K_ρ^{-5} spectrum. These figures clearly demonstrate the folding of the filter functions with Φ_2. In figures 68d, the amplitude spectrum goes as f^4 for $f < f_s$, f^{-2} for $f_s < f < f_F$, and f^{-6} for $f > f_F$. The Rytov equations show that for any $\nu > 1.5$ there is some $f_s < f_F$ for which that portion of the amplitude spectrum containing most of the power goes as $K_\rho^{-4} \Phi_2 \left(K_\rho \right)$ independent of f_F. The size of the ratio f_F/f_s required to make the amplitude spectrum and, hence, the amplitude statistics independent of f_F depends upon how large ν is. In the K_ρ^{-5} and the gaussian calculations, we just barely reach the region of f_F independence as judged by the amplitude spectrum before the numerical limits of the propagation algorithm are reached. For very small f_s compared to f_F then, we see that the amplitude statistics and spectrum are constant on curves parallel to the $\overline{\chi^2} = 0.1$ curve. We also see that the S_4 versus $\overline{\chi^2}$ curve becomes invariant along $\overline{\chi^2} = $ constant and roughly independent of single size spectral type. This function is different from the corresponding function for multisize spectra and offers an easy way to partially classify spectra from S_4 and $\overline{\chi^2}$ data (figures

58 and 74). It must be remembered, however, that f_s must be sufficiently small compared to f_F for the two types of spectra to be distinguishable in this manner.

Figures 56 and 72 show the propagation space plots for the K_ρ^{-5} and gaussian spectra, respectively, with $S_4 = 0.5$ plotted in addition to the $\overline{\chi^2} = 0.1$ curve. The criterion for weak scatter is now driven by S_4 alone. The larger S_4 for a given $\overline{\chi^2}$ compared to a multisize case is evident from the complex signal plots. These plots are characterized by a lack of deep fades and large signal enhancements (figures 65a, 70a, 71a, 88a, 92a, 65b, 70b, 88b and 92b). It is these enhancements that drive S_4 preferentially to $\overline{\chi^2}$. The amplitude distributions also illustrate the presence of large enhancements and low deep fade populations.

As $\overline{\Delta n^2}$ or z_s increases and the scattering goes from weak to strong, the spectra no longer obey the Rytov equations. The phase spectrum becomes dominated by passes near the origin and becomes useless. The amplitude spectrum tend to distort and change at all frequencies, not just the low frequencies as in the multisize spectra. A new break appears which is correlated with f_0 (figures 66d, 71d, 84d, 87d, 89d and 92d). The slope for $f > f_0$ tends to a 5.0 to 5.5 power law for both the gaussian and the K_ρ^{-5} spectra.

The intermediate slope has a range of slopes. The most interesting feature of the strong scatter is that S_4 becomes significantly greater than one driven by the large signal enhancements. The peak in the amplitude distribution moves to deeper fades and soon this case poses a more severe fade threat than Rayleigh in having more deep fades. Eventually as $\overline{\Delta n^2}$ increases, S_4 peaks, then goes to 1; and the amplitude distribution goes to Rayleigh. The complex signal spectrum shows a unique behavior not seen in multiple size spectra. At large frequencies, the Φ_2 behavior maintains itself. At the lower frequencies, however, the spectrum is evolving to a gaussian. Figures 69f and 66f demonstrate this behavior. Eventually, the complex signal spectrum will be gaussian for all important frequencies.

Figure 33a shows a complex signal plot for a K_ρ^{-2} case that has Rayleigh statistics; figure 85a is a corresponding Rayleigh case for the gaussian spectrum. Even though both are Rayleigh, the difference in high frequency content is evident. This is traceable to a K_ρ^{-3} complex signal spectrum in one case and a gaussian in the other. It seems clear that eyeball analysis of signal plots is a useful technique for differentiating types of spectra.

c. Region III is the limiting statistics of the assumed spectra. The amplitude statistics are Rayleigh. The amplitude spectrum is flat at $f < f_0$ and drops off rapidly above f_0. The complex signal spectrum evolves to an approximate gaussian for all cases except for where the asymptotic strong scatter limit is approximately K_ρ^{-2}. The shapes of these spectra, except perhaps for the K_ρ^{-2}, do not contain much useable information about the environment. The only parameter remaining which characterizes both the complex signal and amplitude spectra is ℓ_0. Figures 5, 21, 40, 57 and 73 show plots of $\ell_0/L_\perp$ for all the studied spectra. The $L_\perp$ and $L_{\parallel}$ are the environment scale sizes perpendicular and parallel, respectively, to the propagation LOS. The plots are similar except for the K_ρ^{-1} case.

Figures 93 through 96 show the results comparing the signal statistics for gaussian distributed fluctuations with those from an explicit representation of the striations for four different *in situ* power spectral densities. The explicit representation results are represented by dashed histograms on the distribution plots and circles on the power spectrum plots. Table 6 shows various other statistical measures for comparison. All of the calculations with explicit geometric representations are five mean free paths thick.

Figures 93 and 94 represent the gaussian and cylindrical rod *in situ* power spectra, respectively. The agreement is evident between the gaussian distributed fluctuations and the explicit representations. Figures 95 and 96 are for the K_ρ^{-2} and K_ρ^{-1} cases, respectively. Again, the agreement is excellent up to about 3 hertz. The lack of agreement above 3 hertz results from the minimum size, ℓ, used in the explicit representations, because ℓ was set to 2×10^3 cm which corresponds roughly to 3 hertz. Table 6 shows that the agreement extends to other important statistical measures. These results demonstrate conclusively that for layers that are five or more mean free paths thick the *in situ* power spectral density is necessary and sufficient for calculating the required signal statistics. The assumption to gaussian fluctuations for the use of explicit representation is merely a matter of convenience.

SECTION IV

CONCLUSIONS

This report illuminates the basic character of propagation through turbulent environments characterized by different *in situ* power spectral densities. The Rytov method was used to develop analytic comprehendable expressions for the phase and amplitude power spectral densities, equations 5 and 6, for relatively uniform layers. Expressions (equations 19 through 24) were also developed for the mean square log amplitude and phase fluctuation power. Calculations using the MPS algorithm shows that these expressions hold quite well as long as $\overline{\chi^2} \leq 0.1$ and $S_4 < 0.5$, subsequently defined as weak scatter criteria, even with the additional assumption that $|E(x,z)| \approx 1 + \chi(x,z)$. Numerous examples show that features exist in weak scatter spectra that, via the Rytov expressions, allow determination of scale sizes, Fresnel zone sizes, spectral indices, and other valuable information.

For any given *in situ* power spectral density, three classes of propagation effects exist which correspond to the three regions of a propagation space plot. The distinctive character of each of these regions is readily apparent in the signal statistics. In region II, distinguished by $f_s < f_F$, the study shows that the general behavior of the propagation is a function of whether the *in situ* spectrum is single or multisized. The multisize effects are dominated by the first Fresnel zone size, while the single size cases are dominated by the scale size. In both cases for f_F sufficiently large compared to f_s, the amplitude statistics become constant along lines parallel to the $\overline{\chi^2} = 0.1$ curve in the propagation space plots for both weak and strong scatter. This result is very important in that a single set of calculations can characterize the amplitude effects for all $f_s < f_F$. The two types of spectra are further differentiated by their plots of S_4 versus $\overline{\chi^2}$. The differences in these curves are sufficient to constitute a very good test as to spectrum type. In addition, the curve for the multisize spectrum holds for all spectra for $f_s \geq f_F$.

All of these results imply that for the best environmental analysis, weak scatter cases are best at the highest propagation frequencies possible to maximize the fluctuation power being analyzed. A number of calculations examine how thick

a turbulent layer has to be so that the propagation effects only depend uniquely on the *in situ* power spectral density and the propagation geometry. Results show that five mean free paths are sufficient to minimize any dissimilarities between different electron density representations which have common power spectral densities.

REFERENCES

1. Singleton, D. G., "Saturation and Focusing Effects in Radio-Star and Satellite Scintillations," J. Atmos. Terr. Phys., Vol 32, 1970.

2. Wittwer, L. A., UHF Propagation Effects in Scintillated Environments, AFWL-TR-76-304, Air Force Weapons Laboratory, Kirtland AFB, NM, August 1977.

3. Rino, C. L., Analysis of Scintillation Effects on Communication Systems, Stanford Research Institute (to be published).

4. Chesnut, W. G., "Spatial-Frequency Analysis of Striated Nuclear Phenomena--Part 2: A Model of the Striated Checkmate Cloud," Stanford Research Institute (unpublished).

5. Rino, C. L. and Sachs, D. L., "Striation Models for High Altitude Nuclear Propagation Effects," Stanford Research Institute (to be published).

7. Phelps, A. D. R. and Sagalyn, R. C., "Plasma Density Irregularities in the High-Latitude Top Side Ionosphere," J. of Geophysical Rsch, Vol 81, No. 4, February 1976.

8. Dyson, P. L., McClure, J. P., and Hanson W. B., In Situ Measurements of the Spectral Characteristics of F Region Ionospheric Irregularities, Vol 79, April, 1974.

9. Morse, F. A., et al., EQUION, An Equatorial Ionospheric Irregularity Experiment, SSL-76 (6960-04)-2, Aerospace Corporation, El Segundo, Calif., April 1976.

10. Scannapieco, A. J., Ossakow, S. L., Goldman, S. R., and Pierre, J. M., "Plasma Cloud Late-Time Striation Spectra," J. Geophys. Rsch., Vol 81, 1976.

11. Ragnlien, T. O. and Weinstock, J., "Theory of the Nonlinear Spectrum of the Gradient Drift Instability in the Equatrial Electrojet," J. Geophys. Rsch., Vol 79, November 1974.

12. Sleeper, A. M. and Weinstock, J., "Nonlinear Theory of Density Fluctuation in Turbulent Plasmas," Phys. Fluids, Vol 15, 1972.

13. Chaturvedi, P. K. and Kaw, P. K., "An Interpretation for the Power Law Spectrum of Spread F Irregularities," J. Geophys. Rsch., Vol 81, 1976.

14. Scannapieco, A. J., Goldman, S. R., Ossakow, S. L., Bock, D. L. and McDonald, B. E., "Threoretical and Numerical Simulation Studies of Midlatitude F Region Irregularities," NRL Memorandum Report 3014, Naval Research Laboratory, Wash D. C., March 1975.

APPENDIX

CALCULATION DATA

This appendix contains the sets of data which different *in situ* power spectra, L, and propagation geometry. All of the striated layers are uniform in their statistical properties.

The signal incident on a striated layer beginning at z = 0 is a plane wave. Two signal representations are used.

$$E(x,z) = \widehat{E}_R(x,z) + i\, E_I(x,z) \tag{A1-a}$$

$$E(x,z) = e^{\chi(x,z)\, +\, i\,\phi(x,z)} \tag{A1-b}$$

where

$$E(x,0) = \overline{E}(0) = 1.0$$

The propagation LOS is assumed to sweep through the striated medium at a velocity, $\overline{v}$, of 3×10^4 cm/sec. The field representation above can be converted to time by setting $x = \overline{v}t$.

The field at the receiver plane where $z = z_s + z_g$ is described by a variety of measures: ℓ_0; $\overline{\phi^2}$, $\overline{\phi^2}\star$, $\overline{\chi^2}$, S_4, $\overline{E_R^2}$, $\overline{E_I^2}$, $S_A(f)$, $S_\phi(f)$, $S_s(f)$, α_ϕ, α_A, α_s, P(A) and P(ϕ).

The ℓ_0 is the e^{-1} point in the complex correlation function.

$$\overline{E^\star\left(x, z_s + z_g\right) E\left(x + \ell_0, z_s + z_g\right)} - \overline{E}\left(z_s + z_g\right)^2 = e^{-1}\left(1 - \overline{E}\left(z_s + z_g\right)^2\right) \tag{A2}$$

$\overline{\phi^2}$ is the variance of the signal phase. The $\overline{\phi^2}\star$ is defined as

$$\overline{\phi^2}\star = \frac{K^2 z_s}{2\pi} \int_{-\infty}^{\infty} \phi_2\left(K_\rho\right) d\,K_\rho \tag{A3}$$

27

$\overline{\phi^2}*$ is the quantity used to define mean square phase fluctuation. Only in certain situations is $\overline{\phi^2}*$ a real statistical quantity. When the mean square phase fluctuation is measurable and unambiguous, it will be described without the asterisk.

The $\overline{\chi^2}$ and S_4 are commonly used measures of the amplitude fluctuations. The S_4 is defined as

$$S_4 = \left[\frac{\left(\overline{E^4} - \overline{E^2}^2 \right)}{\overline{E^2}^2} \right]^{1/2} \qquad (A4)$$

Both $\overline{\chi^2}$ and S_4 are determined from the calculated signals. Because of the particular method used to calculate $\overline{\chi^2}$ and S_4, the quoted values are reliable only for $\overline{\chi^2} \geq 10^{-3}$.

The $\overline{E_R^2}$ and $\overline{E_I^2}$ are included to provide an additional measure of fluctuation power. These two measures are particularly useful for indicating gaussian quadrature statistics; they also define $\overline{E}$.

The $S_A(f)$, $S_\phi(f)$ and $S_S(f)$ are the amplitude, phase and signal power spectral densities, respectively. All of these spectra are two-sided where frequency integrals are over f where $-\infty < f < \infty$. The signal spectrum is

$$S_S(f) = \int_{-\infty}^{\infty} \left[\overline{E^*(t) E(t + \tau)} - \overline{E}^2 \right] e^{i2\pi f\tau} d\tau \qquad (A5)$$

Most of these spectra will have regions with a well-defined power law or gaussian behavior as they decrease at higher frequencies. The power law indices are designated as α_A, α_ϕ, and α_S. The G denotes a gaussian-like spectrum.

The P(A) and P(ϕ) are histogram probability distributions for the amplitude and phase. The Rayleigh amplitude distribution is plotted on each amplitude plot for comparison purposes; ϕ is limited by $\pm \pi$ in calculating the phase distribution.

Several of the cases with large amplitude fluctuations do not have phase power spectral densities included. This is because the signal as shown in a complex signal plot passes often very near the origin during a deep fade. When this happens, the phase measuring algorithm has to guess on which side of the origin the signal passed as it processes the digitally represented signal. If it guesses incorrectly, discontinuities are introduced and the spectrum rapidly

approaches an f^{-2} behavior regardless of the real spectrum. The spectrum contains no useful information. If the signal were analog, this numerical problem would not exist; but, as shown earlier the signal passes near the origin during deep fades will still come to dominate the real spectrum.

This appendix is arranged in subsections, each containing the data for a particular assumed *in situ* environment. The subsection contains a table that summarizes the relevant parameters for the calculations, a propagation space plot, an $\ell_0/L_\perp$ plot, an S_4 versus $\overline{\chi^2}$ plot and the plots unique to each specific calculation. These sets are ordered in increasing $\overline{\Delta n^2}$ for each L starting with the smallest values of L. The gaussian data are ordered by increasing z_s instead of $\overline{\Delta n^2}$. Each set of plots for a given L and $\overline{\Delta n^2}$ or z_s has the same figure number indexed by letters, this includes a plot of the complex signal, amplitude distribution, phase distribution, amplitude spectrum, phase spectrum and complex signal spectrum. The phase spectrum (letter designation "e") is ommitted when numerically ambiguous. The last subsection contains the data for the scattering layer thickness arguments.

Table 1

K_ρ^{-1} SPECTRUM

	$z_g = 2 \times 10^7$			$z_s = 5 \times 10^7$			$K = 1.46$		K_ρ^{-1} SPECTRUM		
FIG.	L	$\overline{\Delta n^2}$	$\overline{\phi^2}$	$\overline{\chi^2}$	S_4	ℓ_0	$\overline{E_R^2}$	$\overline{E_I^2}$	α_A	α_ϕ	α_S
7	3.5×10^3	4×10^{11}	0.29	0.18	0.63	3.1×10^3	0.12	0.18	1.9		2.0
8	3.5×10^3	2×10^{12}	1.8*	0.43	0.93	2.0×10^3	0.38	0.43	1.9		1.9
9	3.5×10^3	10^{13}	9.0*	0.46	0.99	4.1×10^2	0.50	0.50	1.9		1.9
10	2.0×10^4	3×10^{10}	0.13	0.02	0.25	3.2×10^4	0.02	0.11	1.9	2.1	2.1
11	2.0×10^4	1.5×10^{11}	0.67	0.10	0.51	1.7×10^4	0.15	0.36	2.0	1.9	1.9
12	2.0×10^4	4.6×10^{11}	2.7*	0.31	0.78	9.0×10^3	0.39	0.49	1.9		1.9
13	2.0×10^4	1.5×10^{12}	7.7*	0.44	0.95	2.8×10^3	0.51	0.49	0.6, 2.0		1.9
14	8×10^4	1.5×10^{10}	0.28	0.01	0.19	8.0×10^4	0.04	0.21	2.1	2.1	1.1
15	8×10^4	1.5×10^{11}	3.1	0.11	0.53	3.3×10^4	0.43	0.51	2.0	1.9	1.9
16	8×10^4	4.6×10^{11}	9.5*	0.32	0.79	9.4×10^4	0.50	0.50	1.9		2.1
17	3×10^5	2.5×10^9	0.18	0.001	0.07	3.2×10^5	0.02	0.15	2.0	1.9	2.0
18	3×10^5	2.0×10^{10}	1.4	0.01	0.19	1.81×10^5	0.29	0.47	2.0	2.0	2.0
19	3×10^5	1.5×10^{11}	12.*	0.10	0.53	2.8×10^4	0.49	0.51	2.0		1.9

Figure 4. Propagation Space Plot for K_ρ^{-1} Spectrum
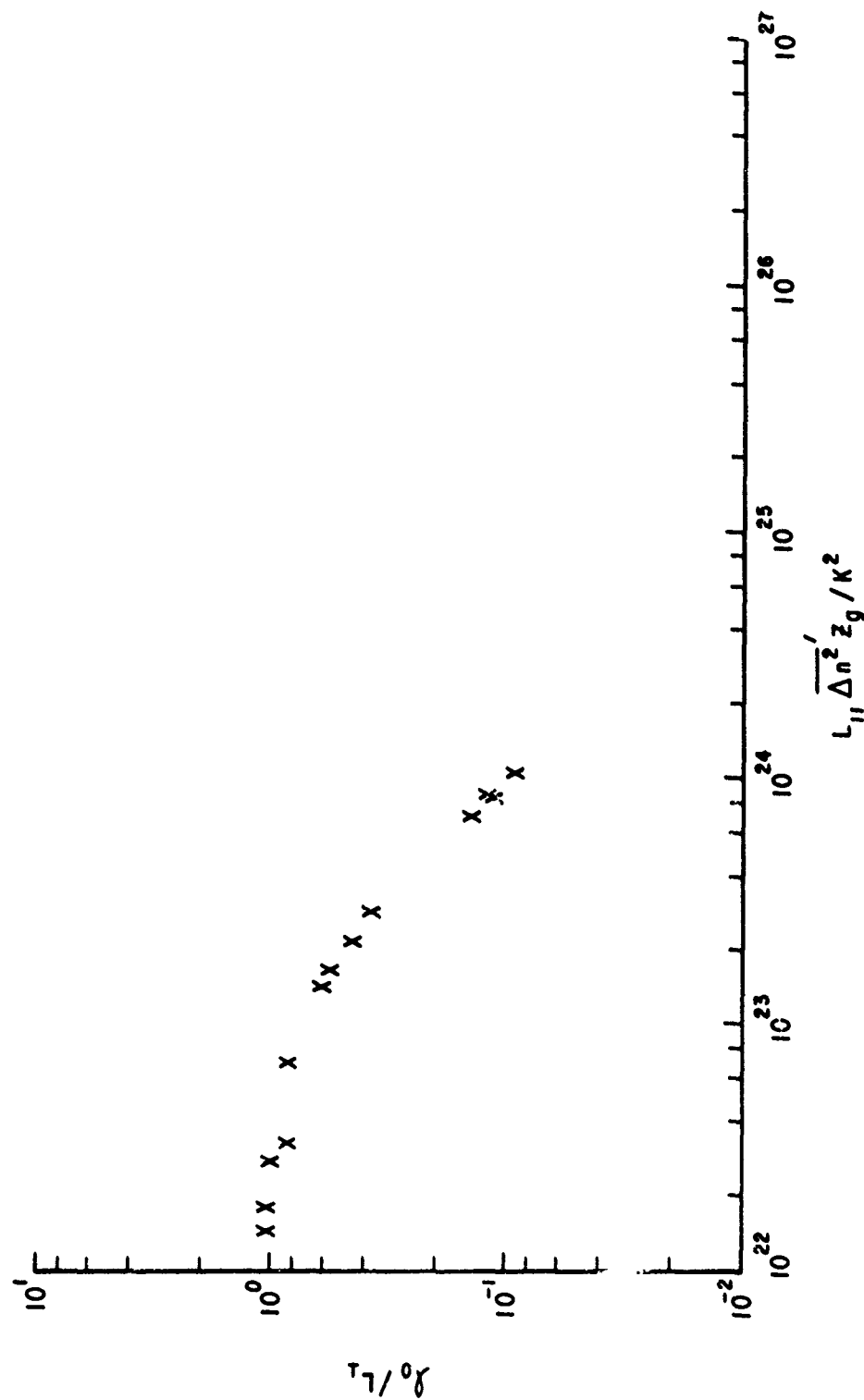
Figure 5. ℓ_0 for K_ρ^{-1} Spectrum
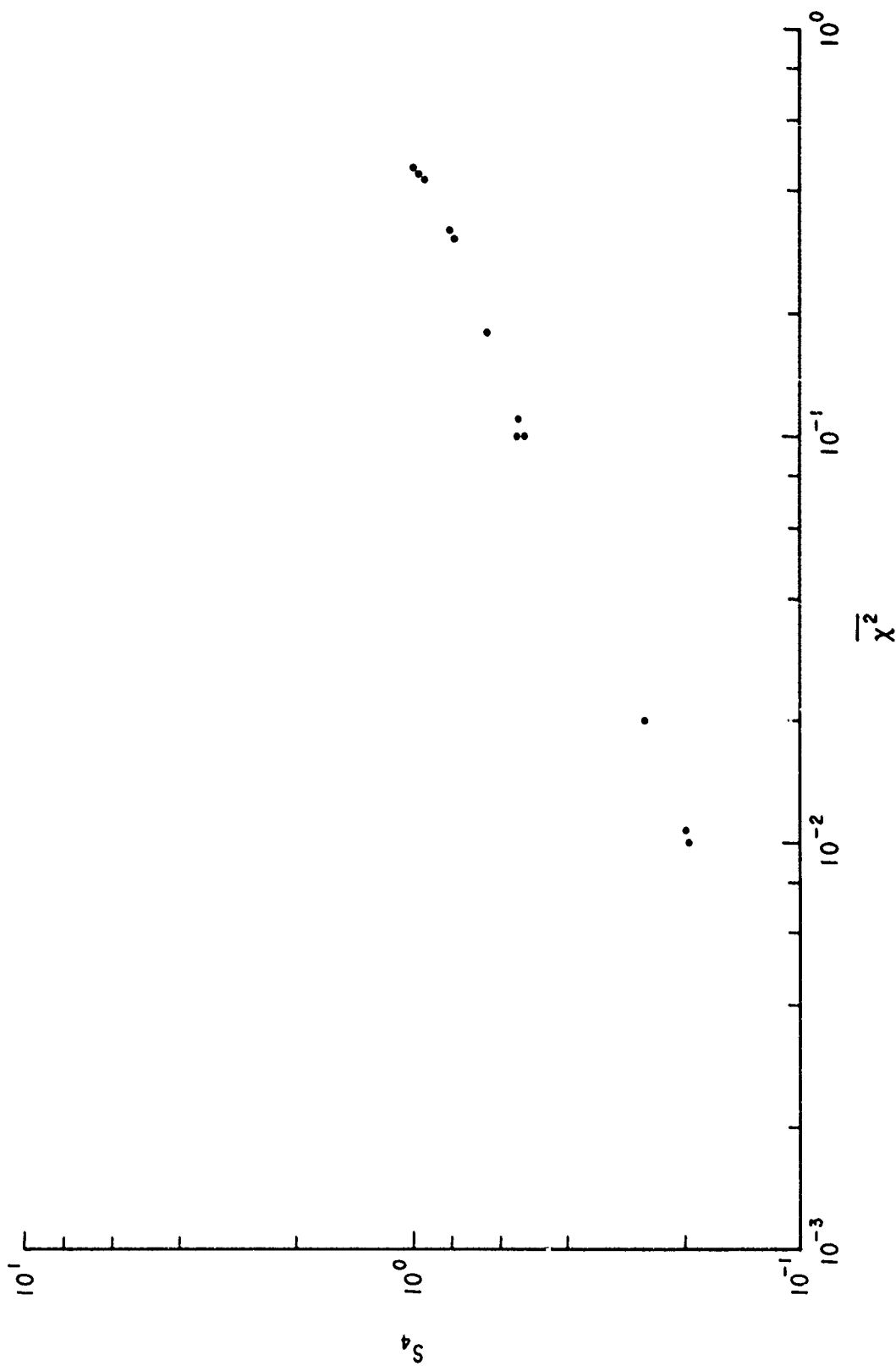
Figure 6. S_4 vs. $\overline{\chi^2}$ for K_ρ^{-1} Spectrum
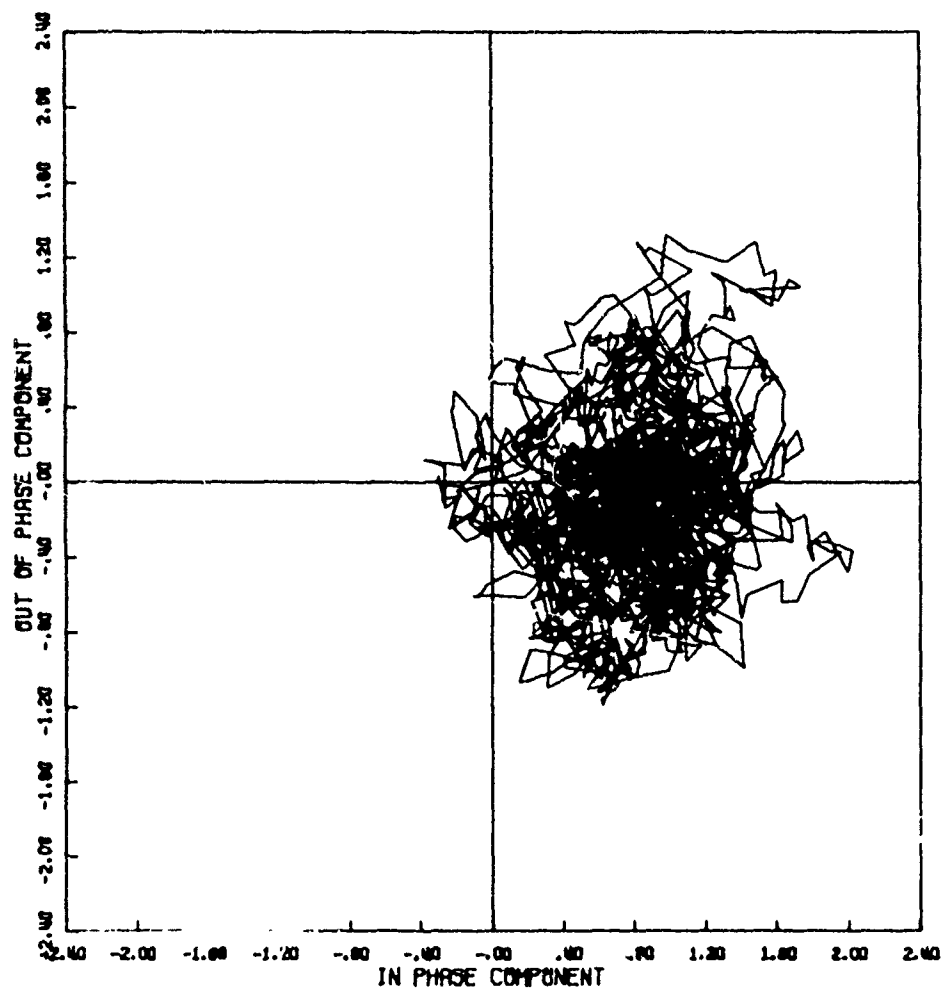
Figure 7a. Signal Phase Plot
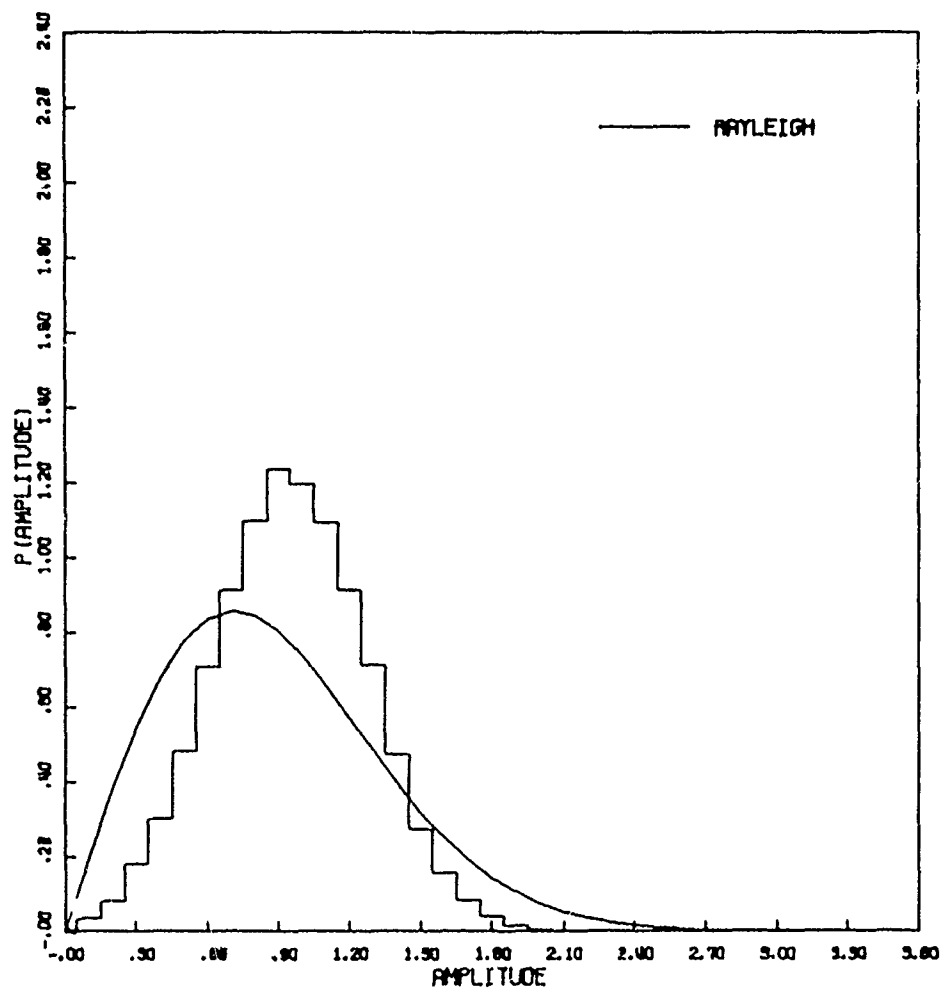
Figure 7b. Amplitude Distribution
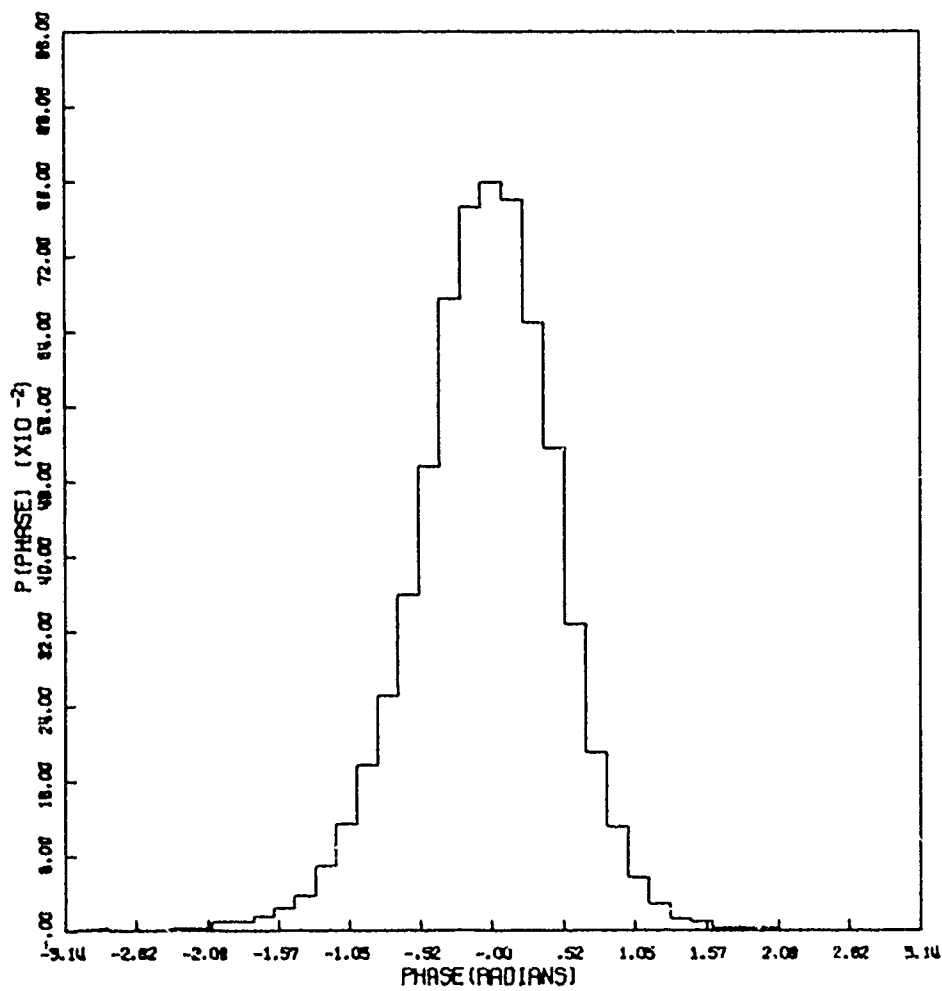
Figure 7c.   Phase Distribution
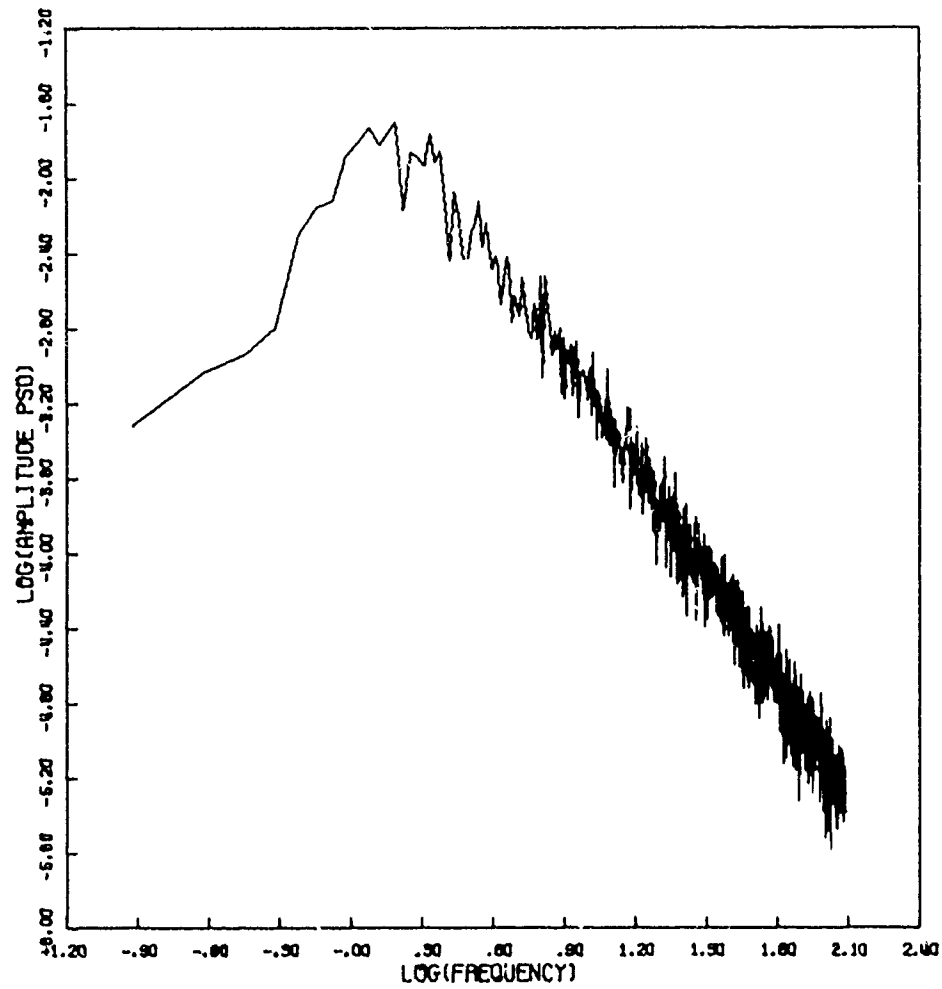
Figure 7d. Amplitude Power Spectral Density
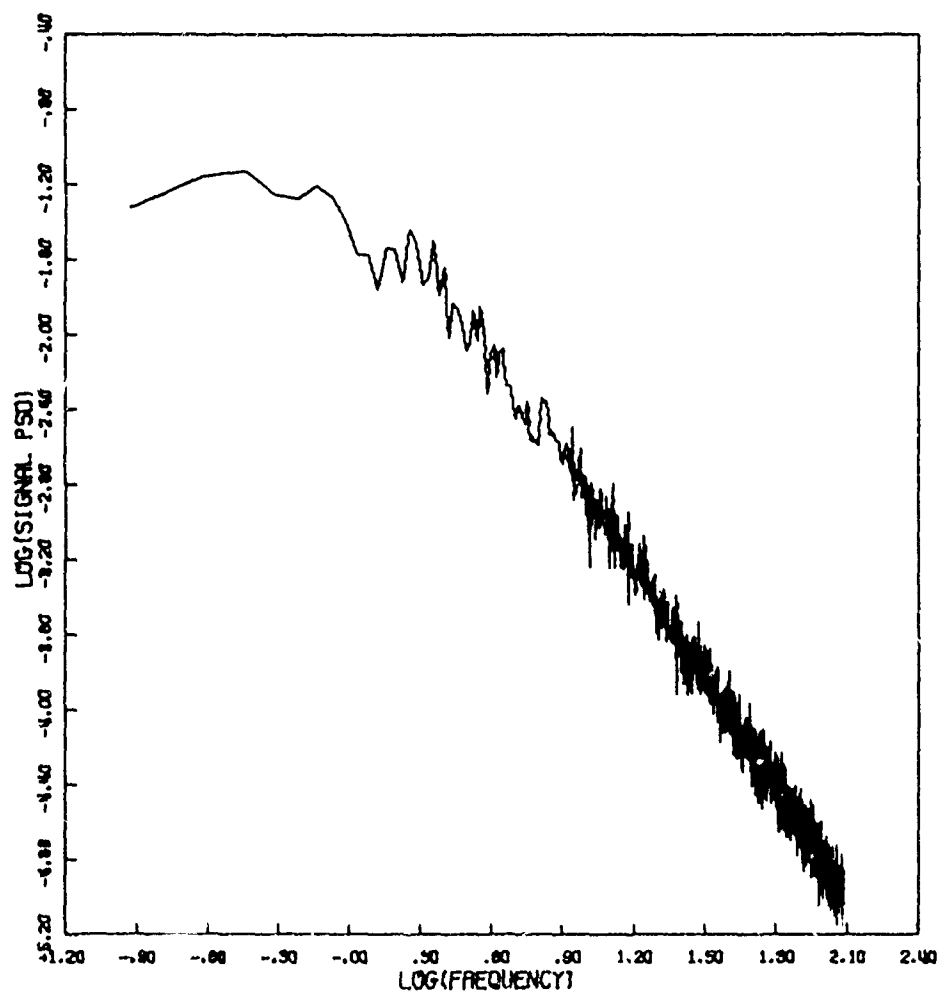
Figure 7f. Signal Power Spectral Density
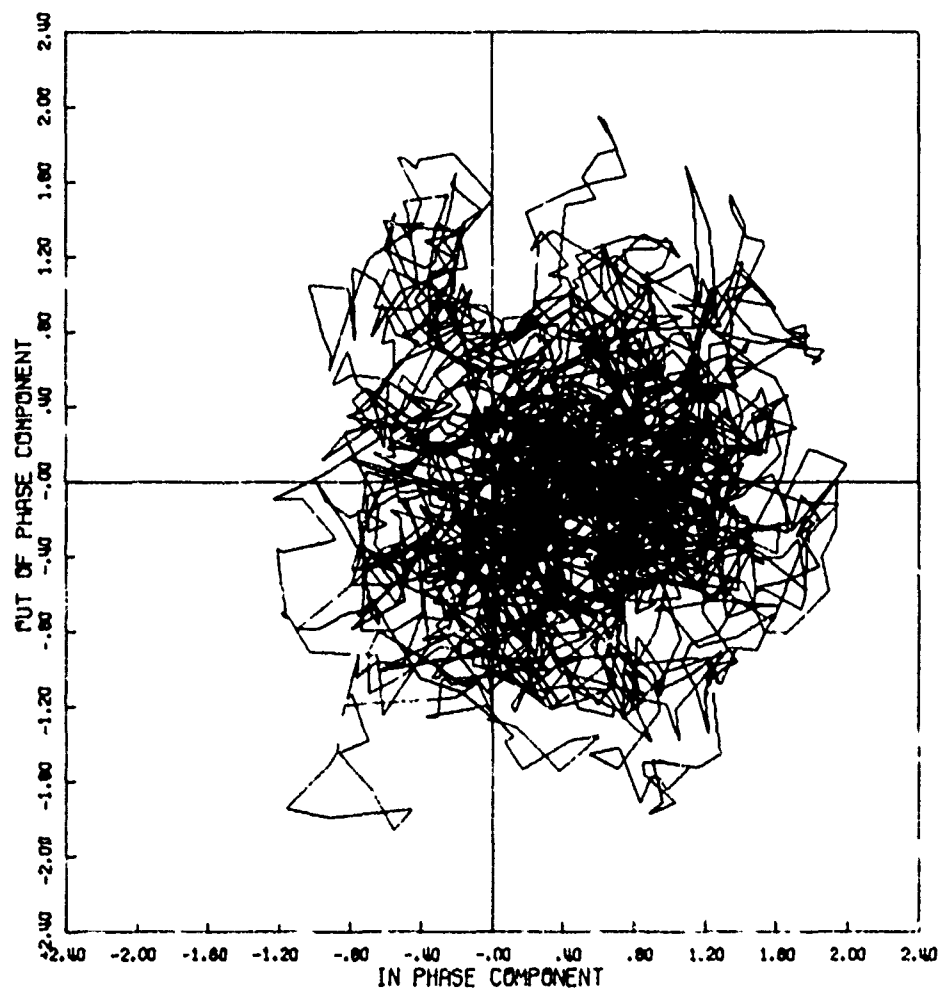
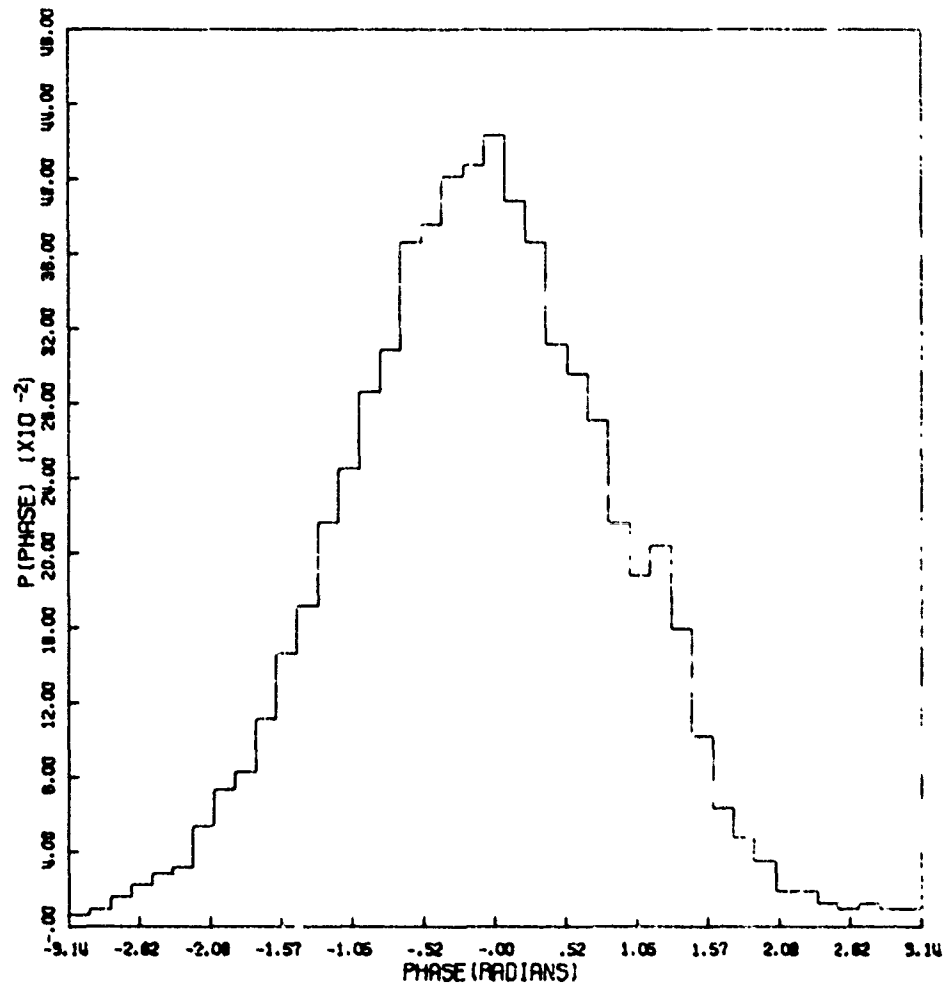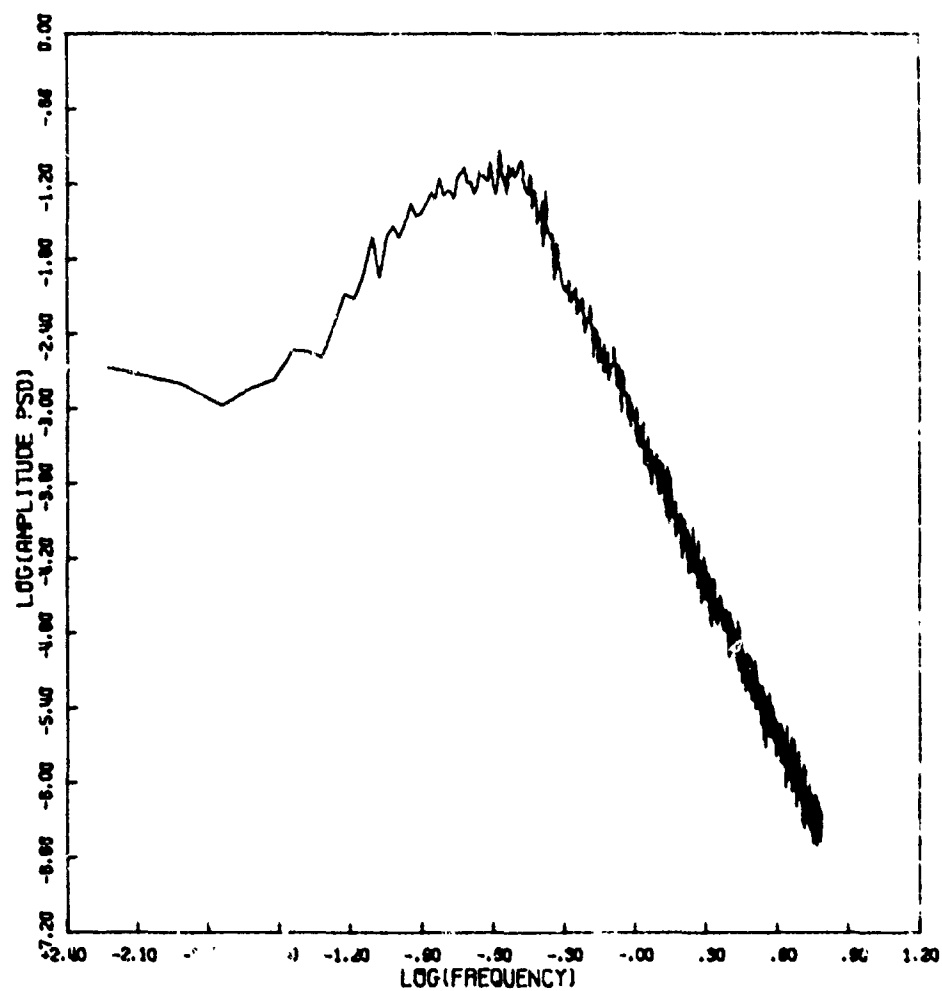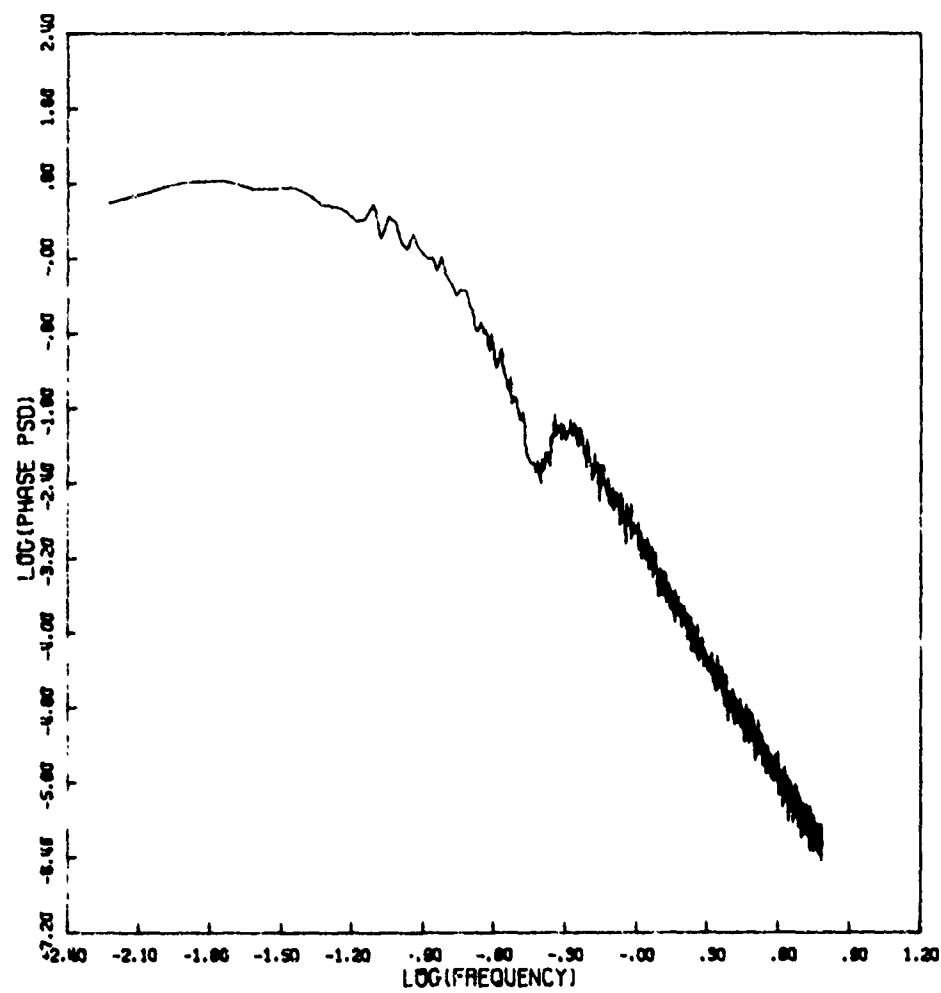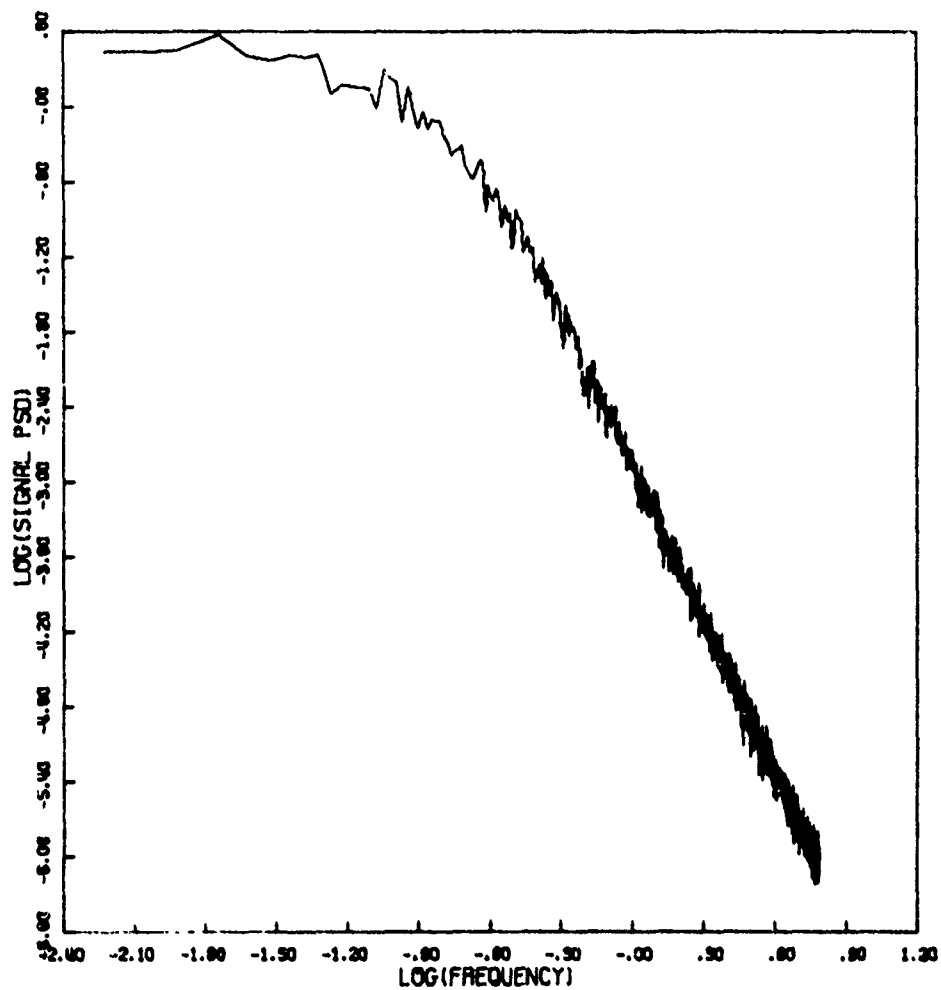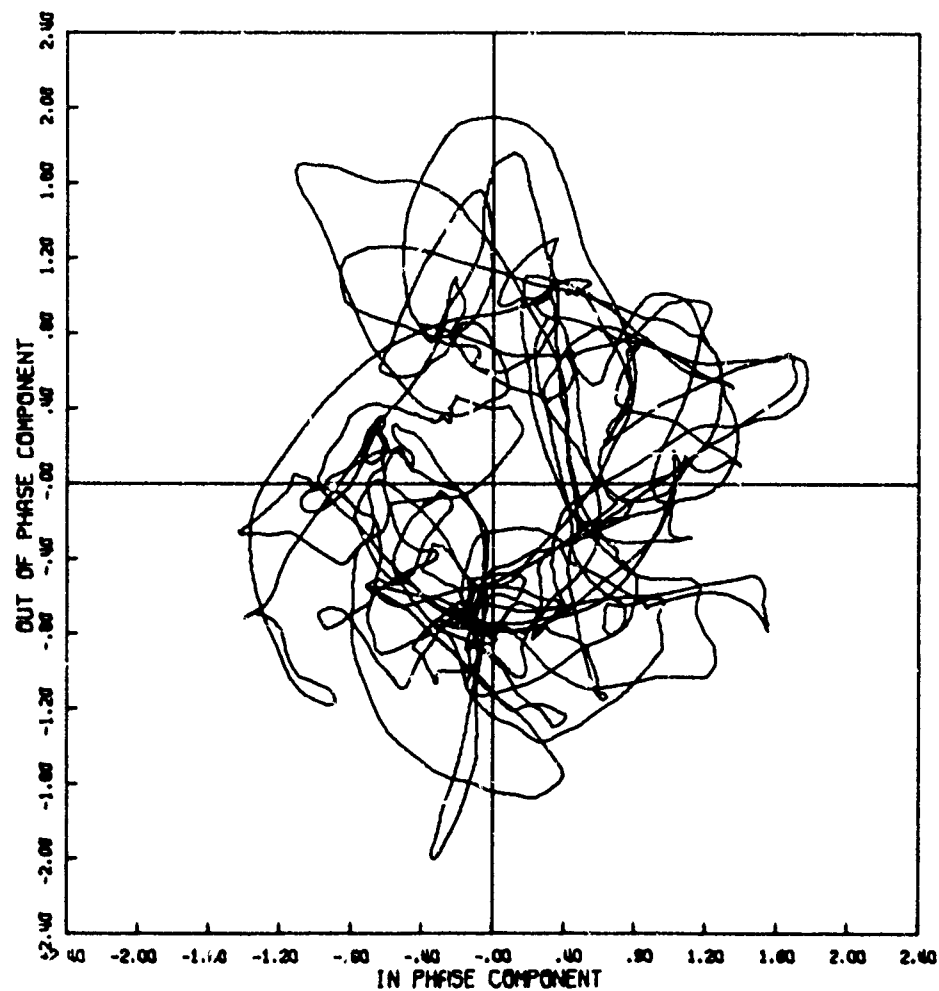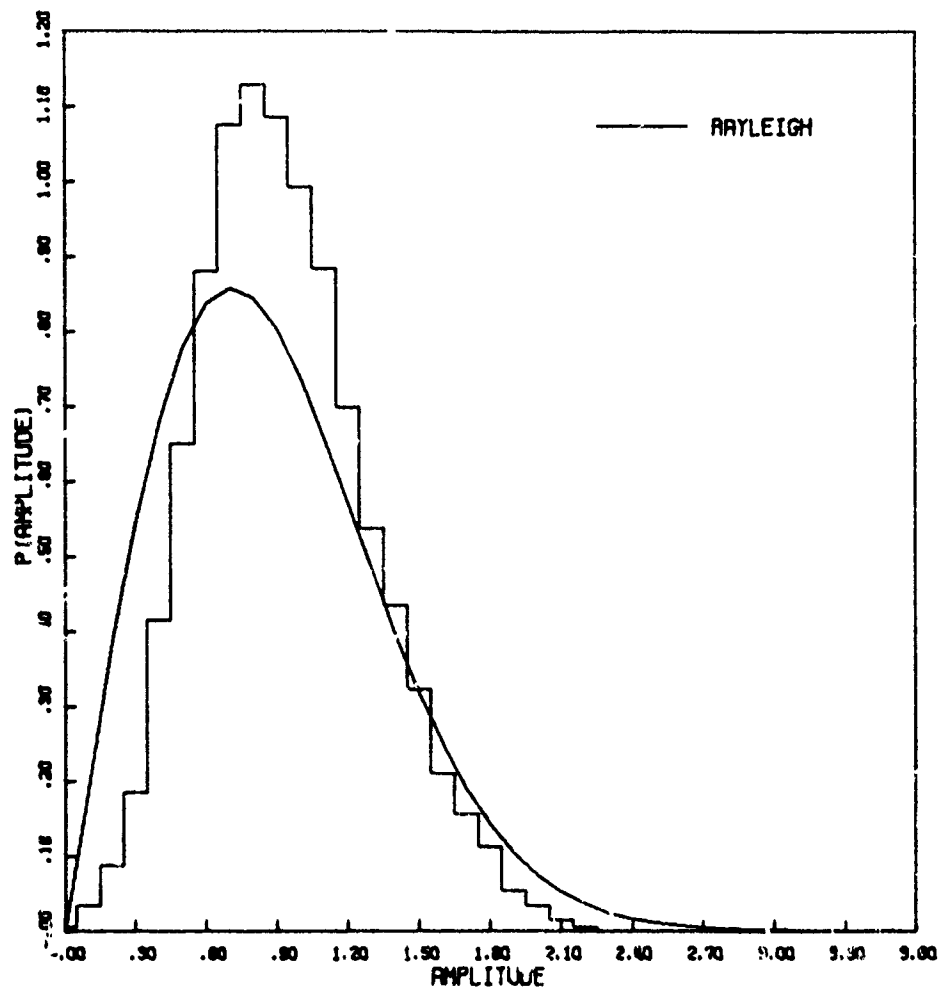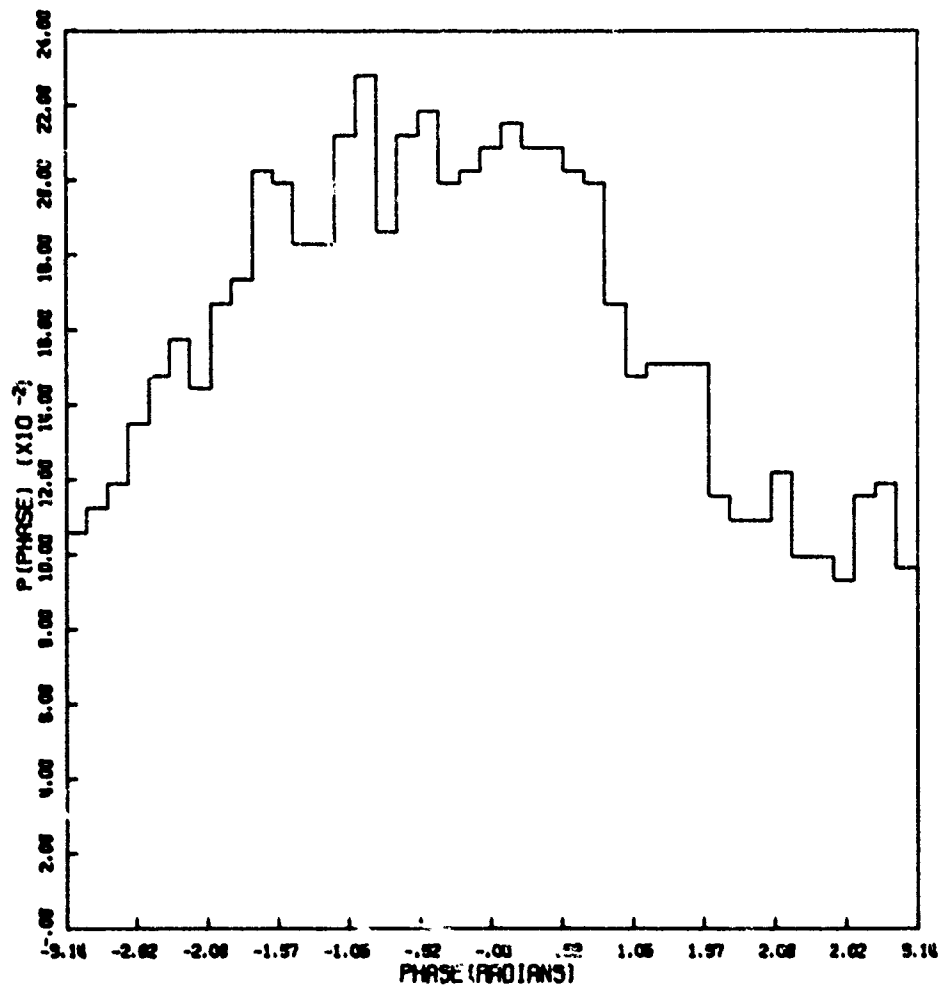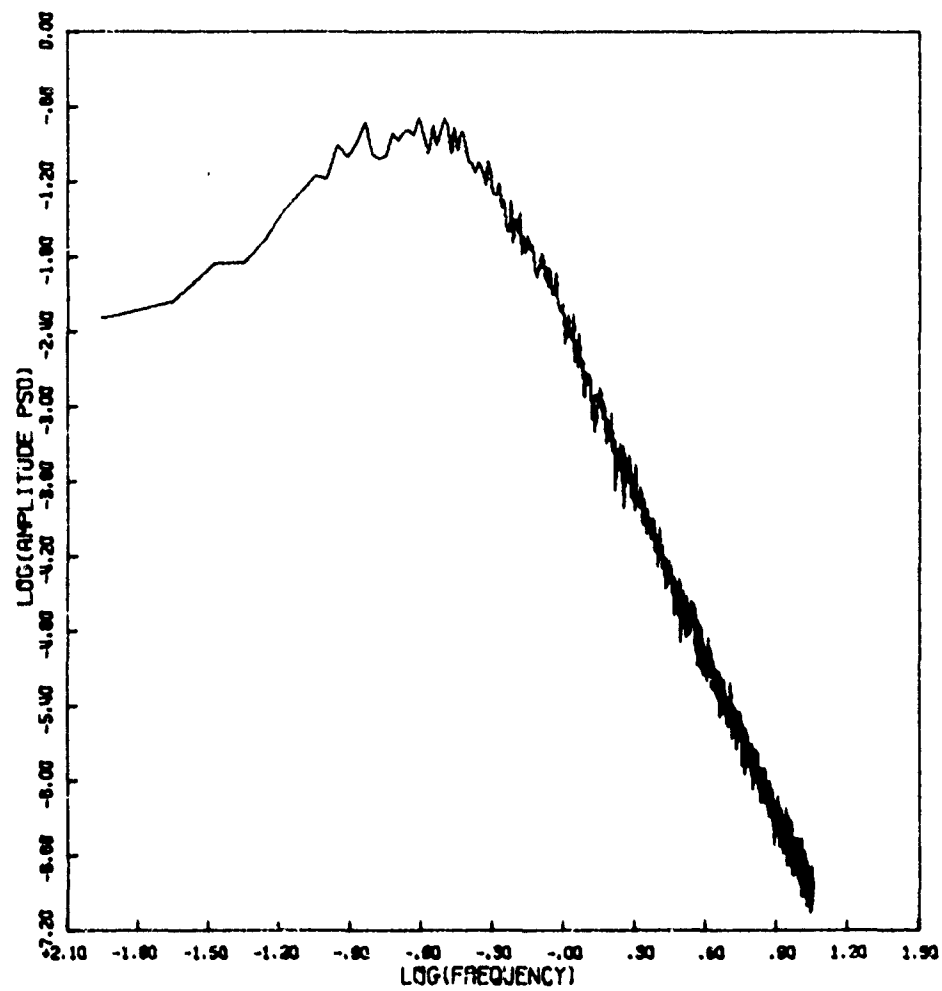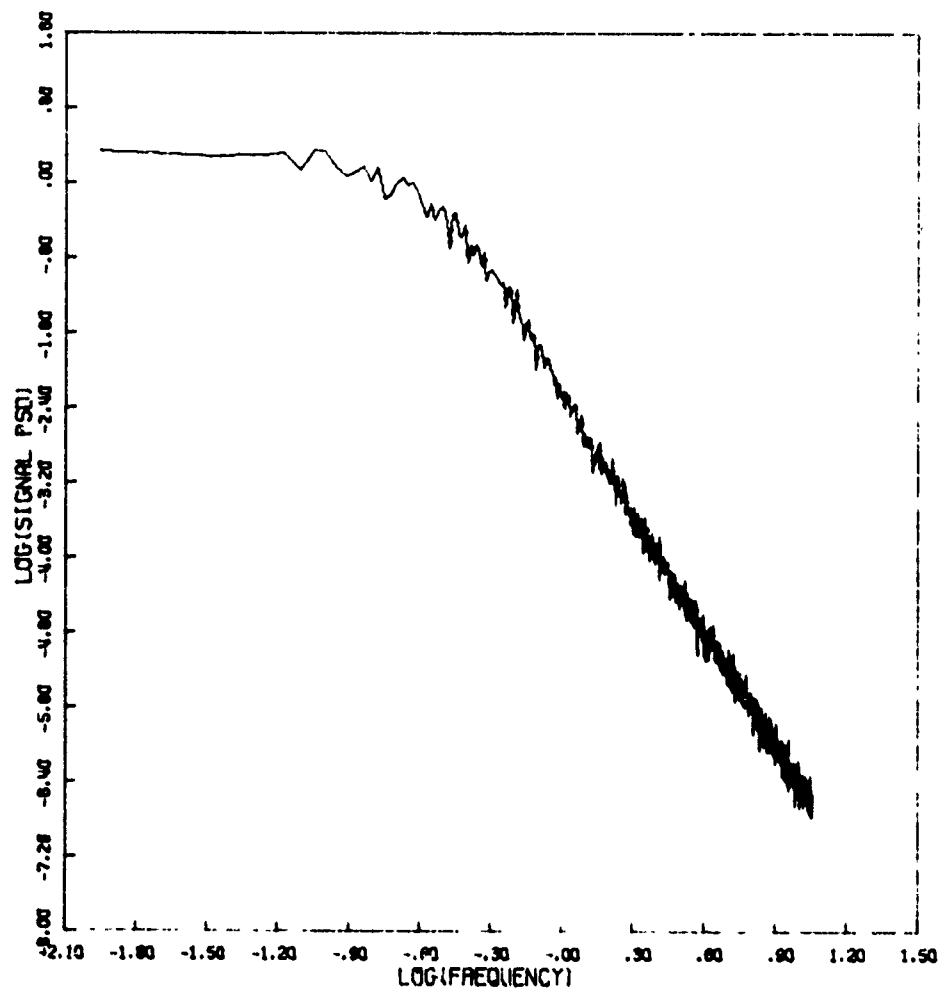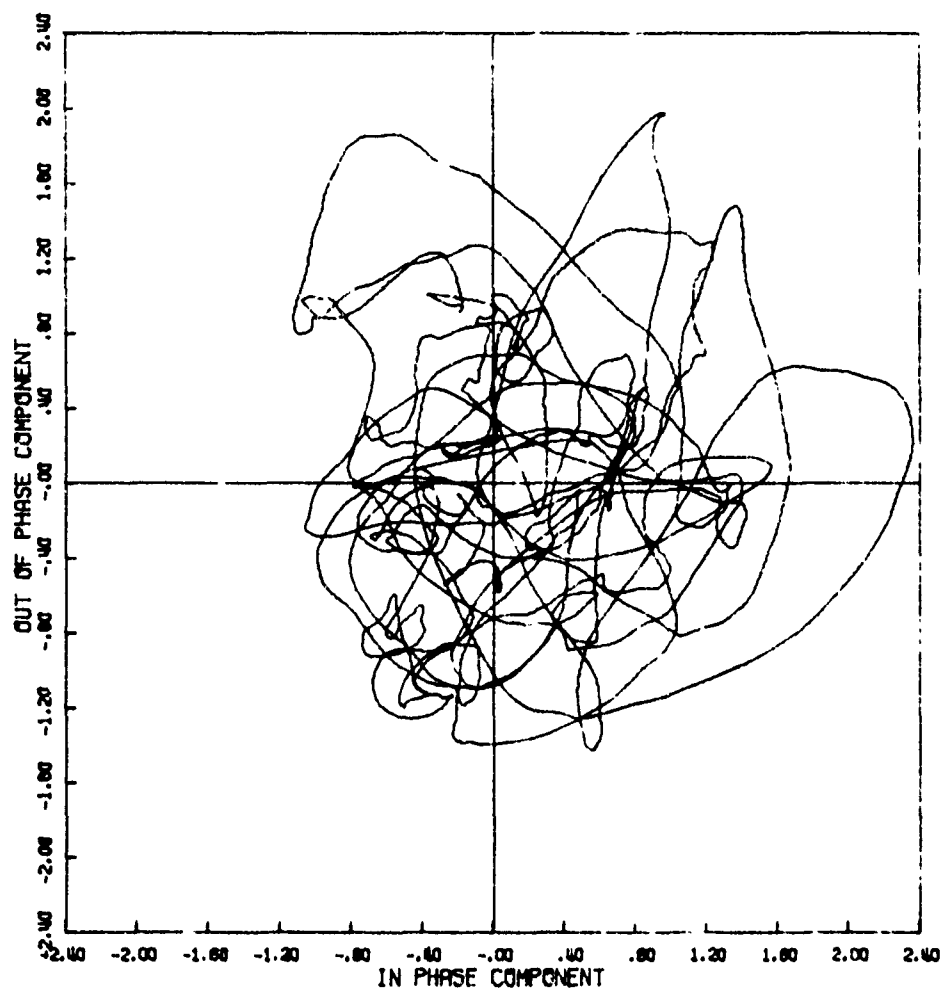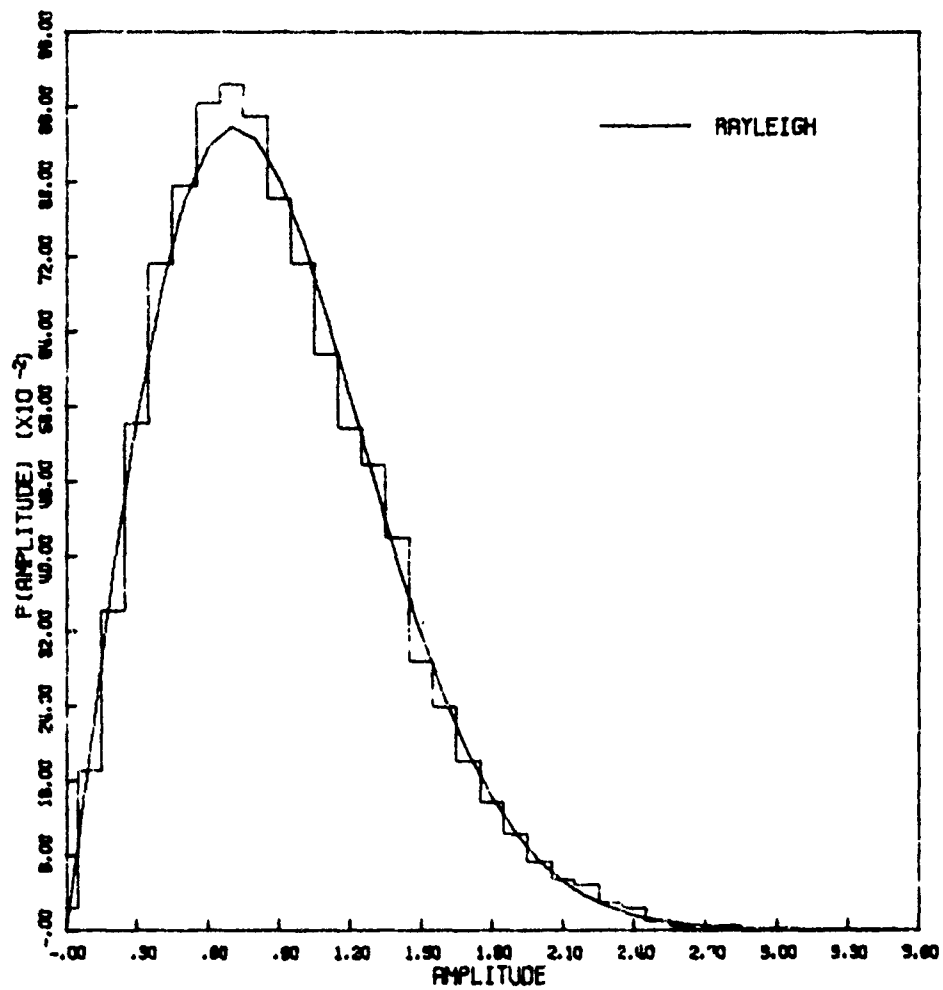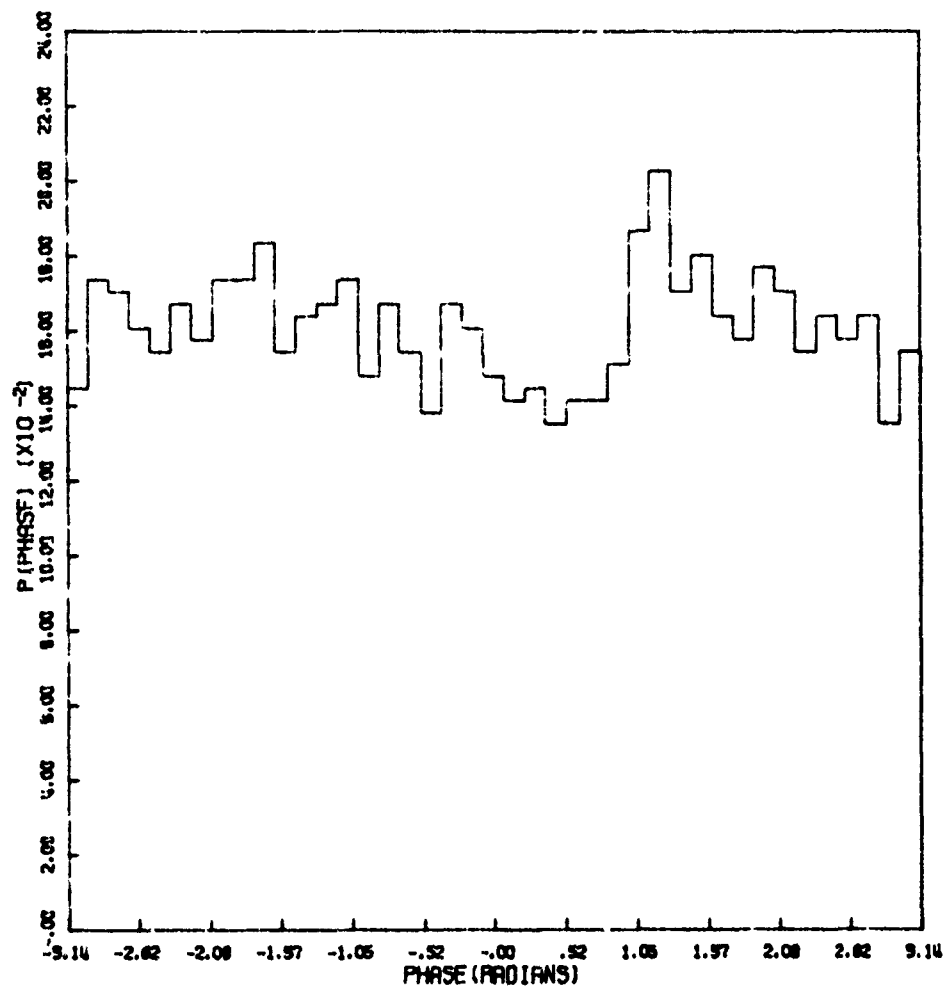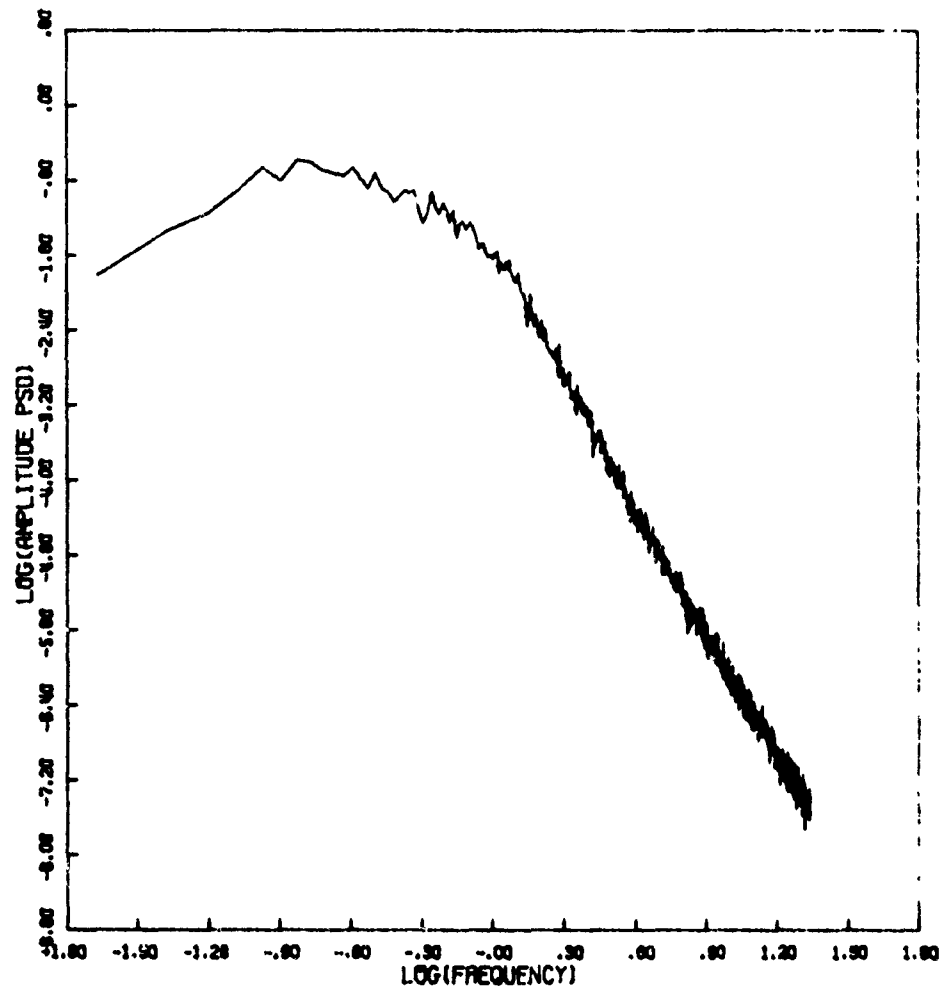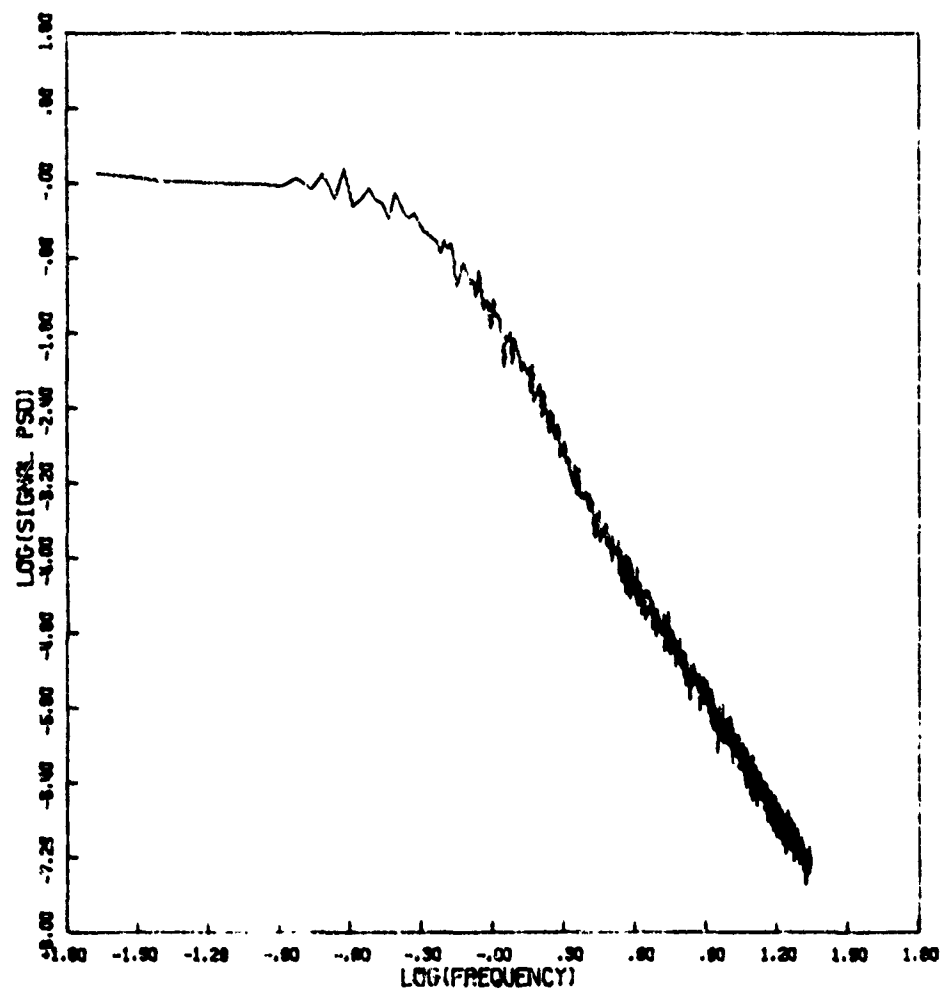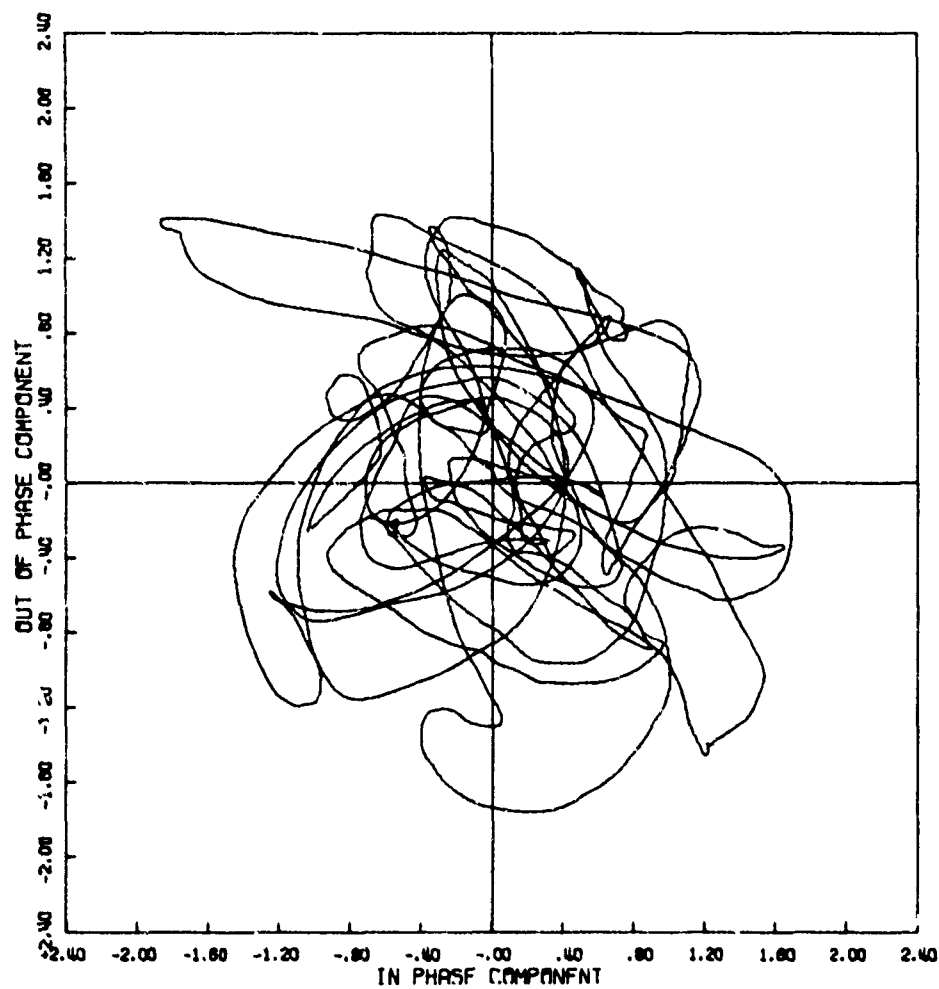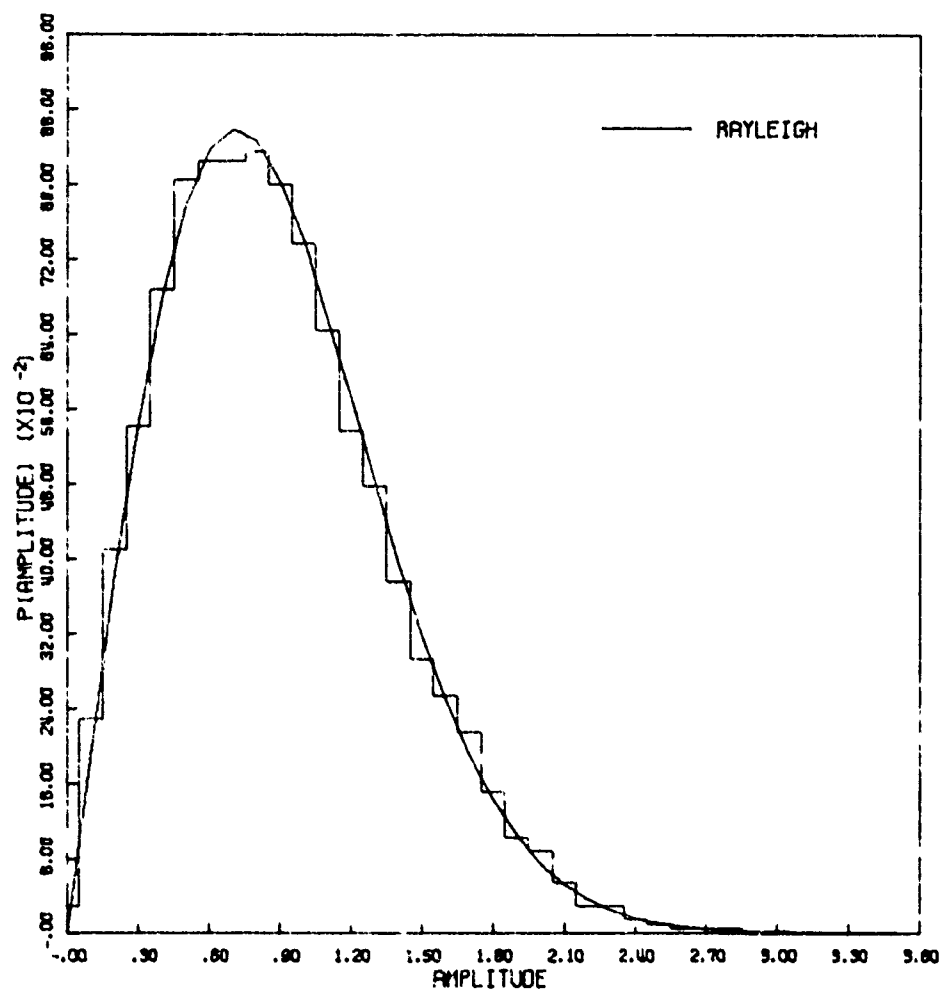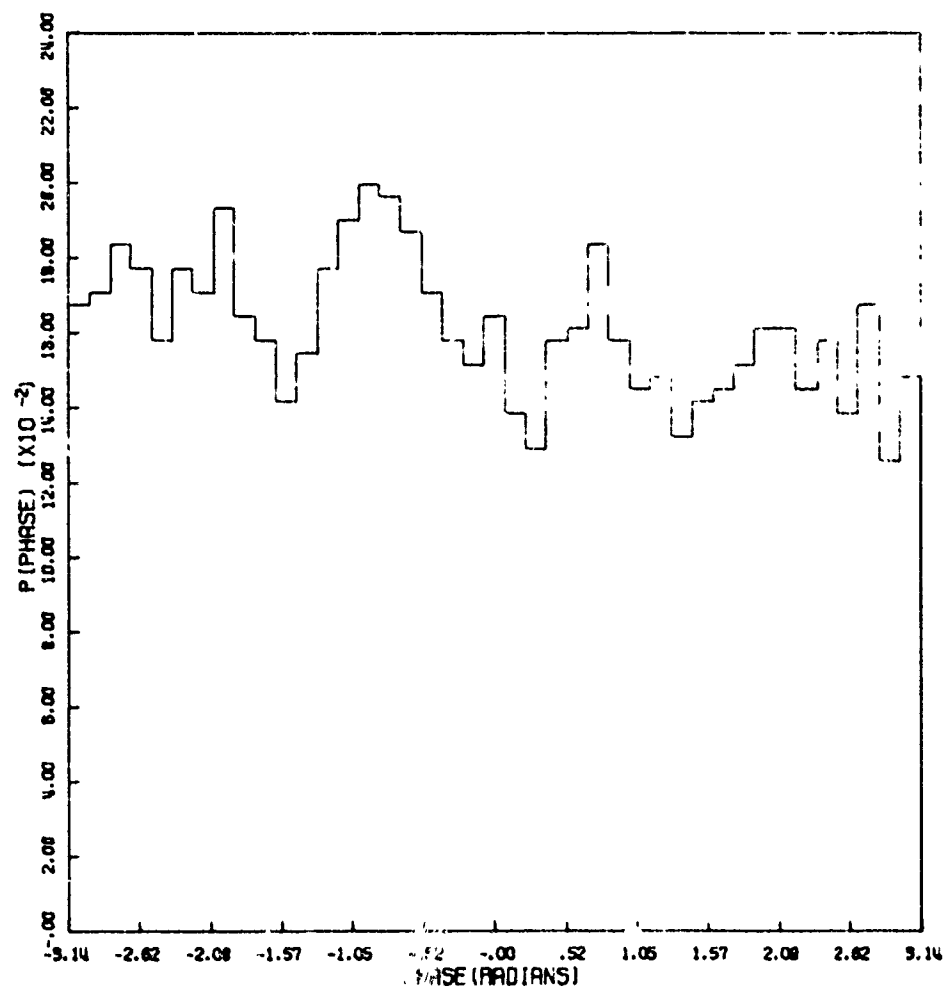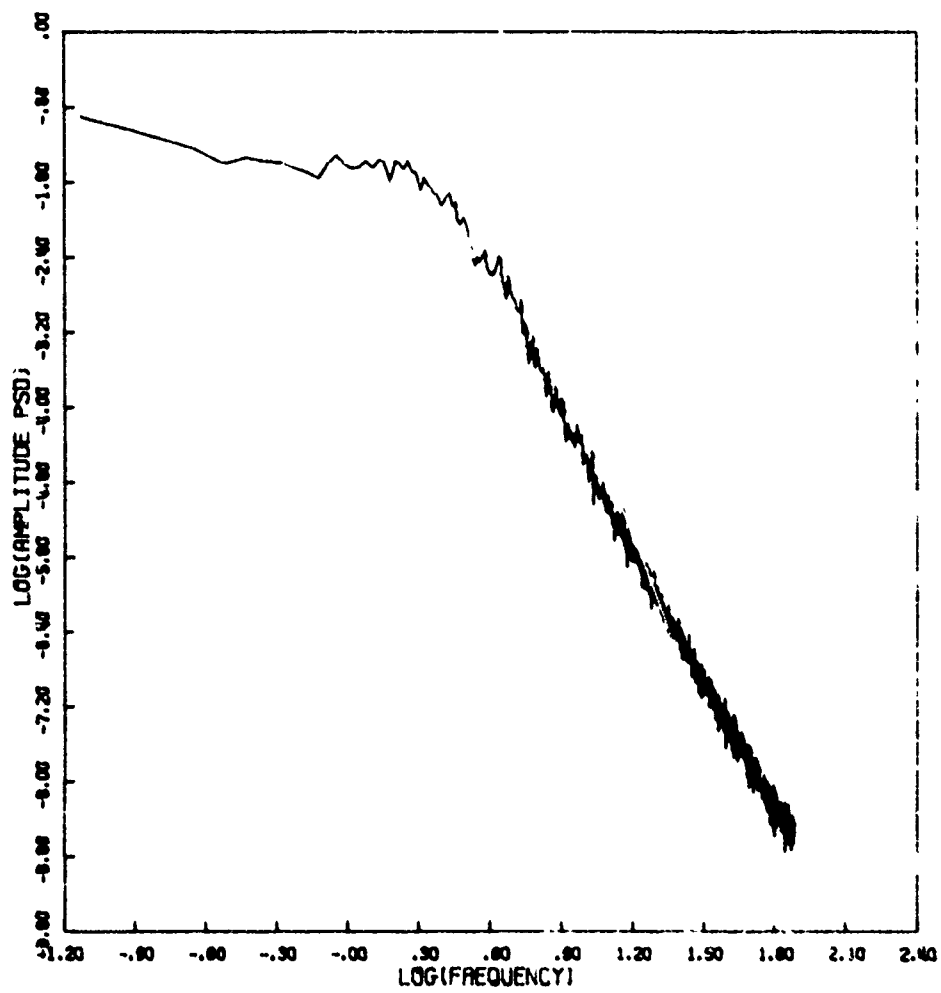Figure 8a.   Signal Phase Plot
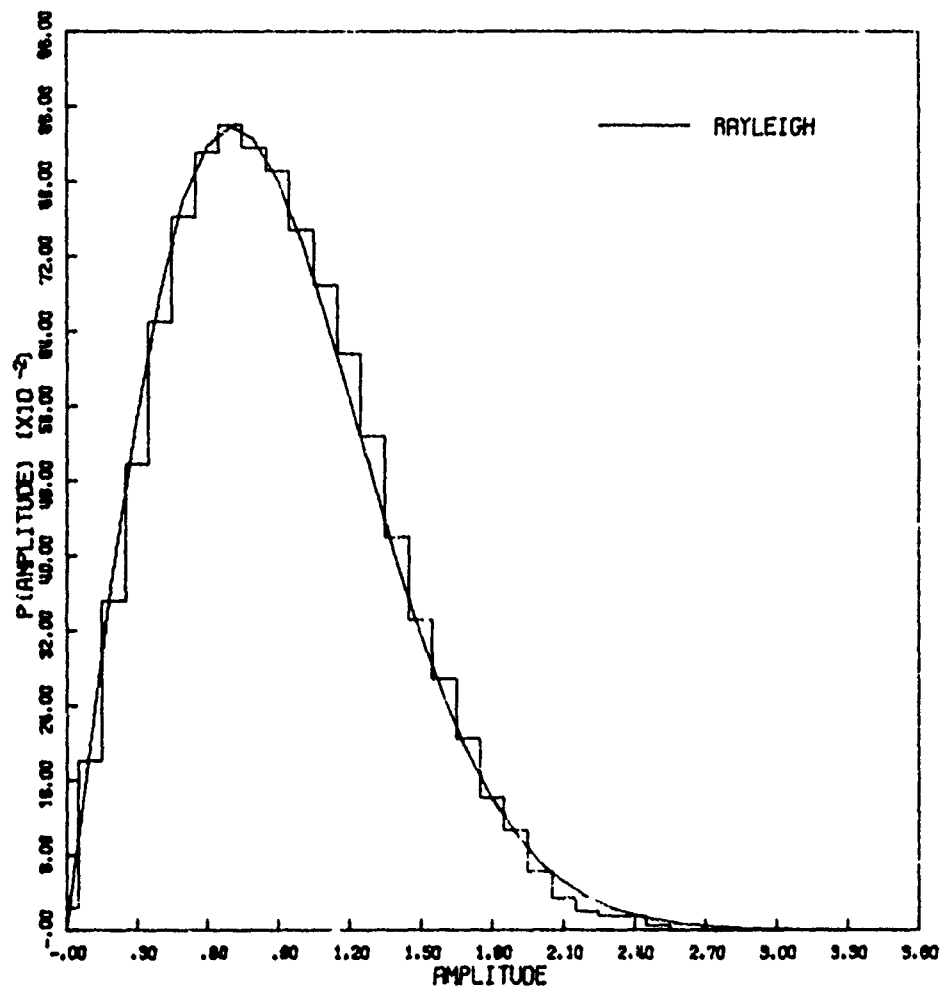
Figure 8b. Amplitude Distribution
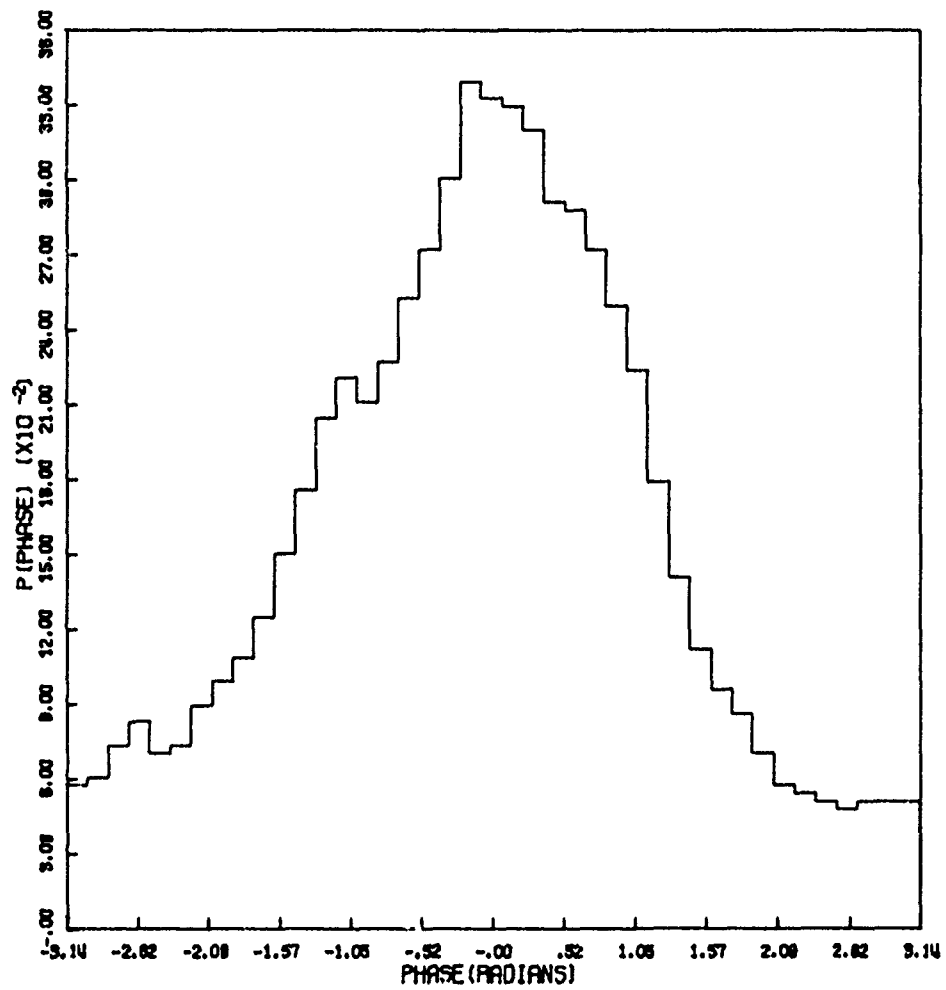
Figure 8c.   Phase Distribution
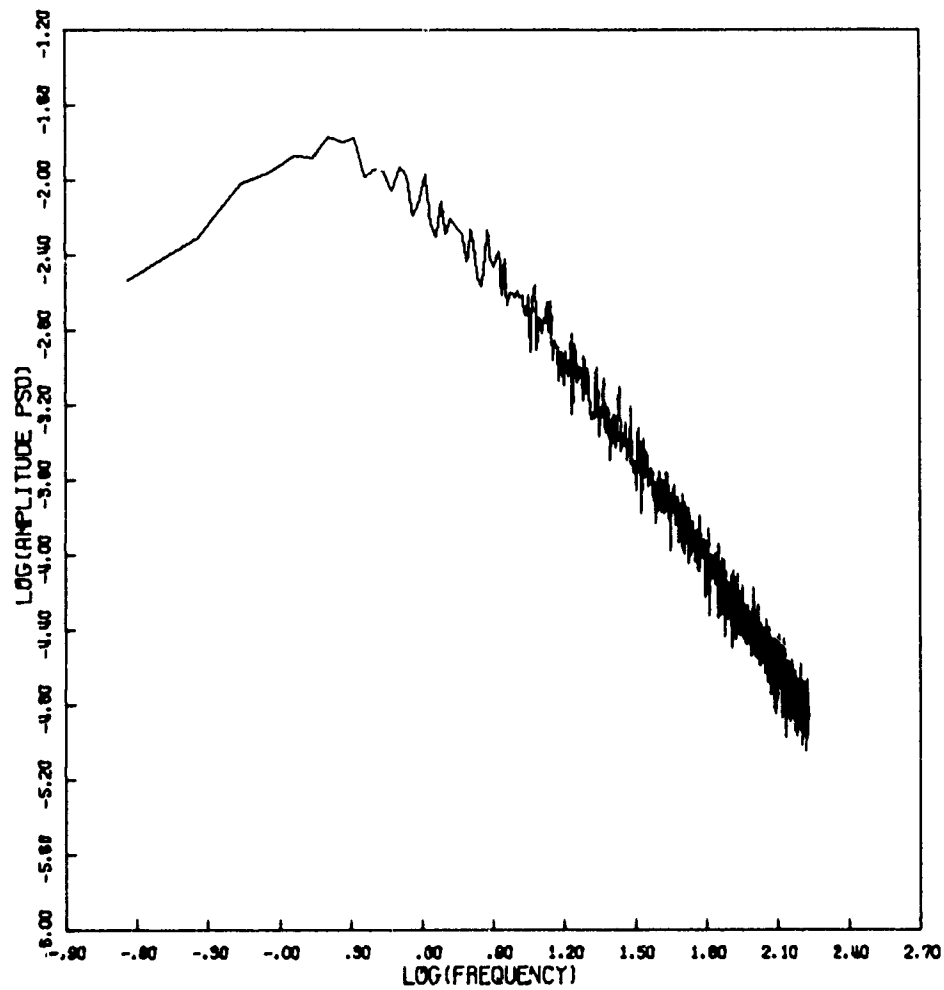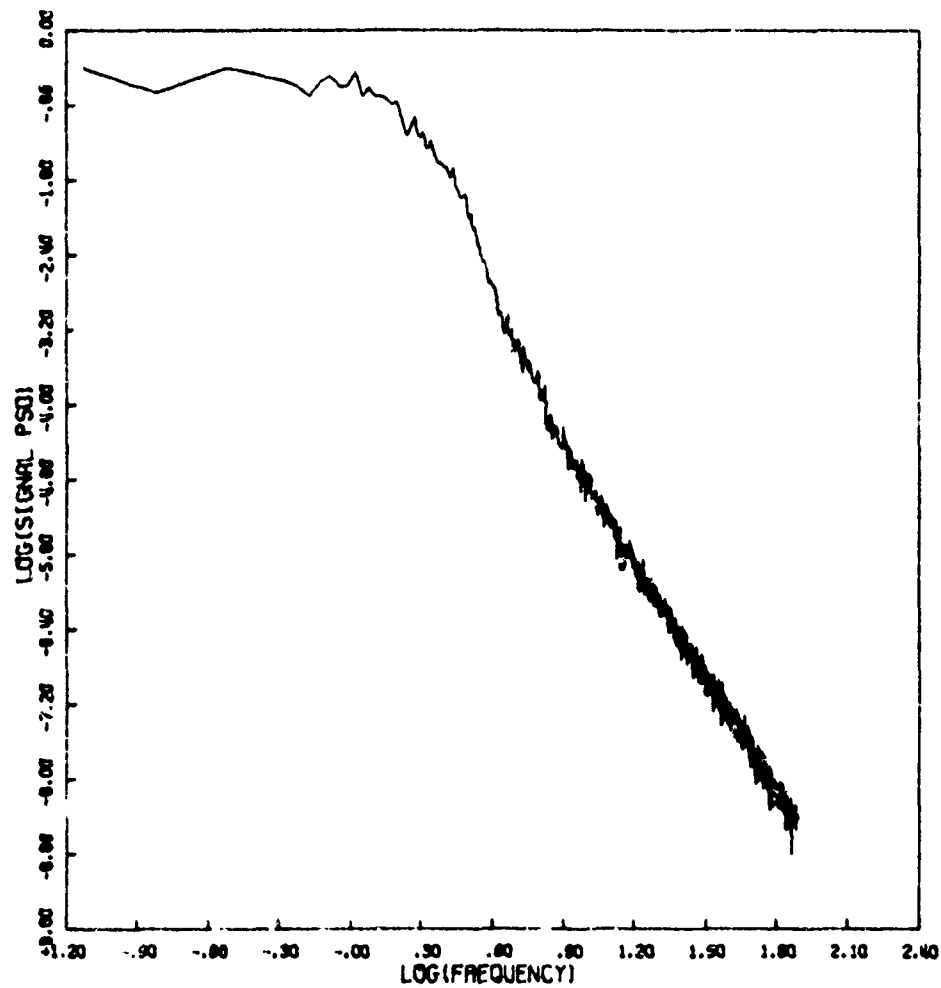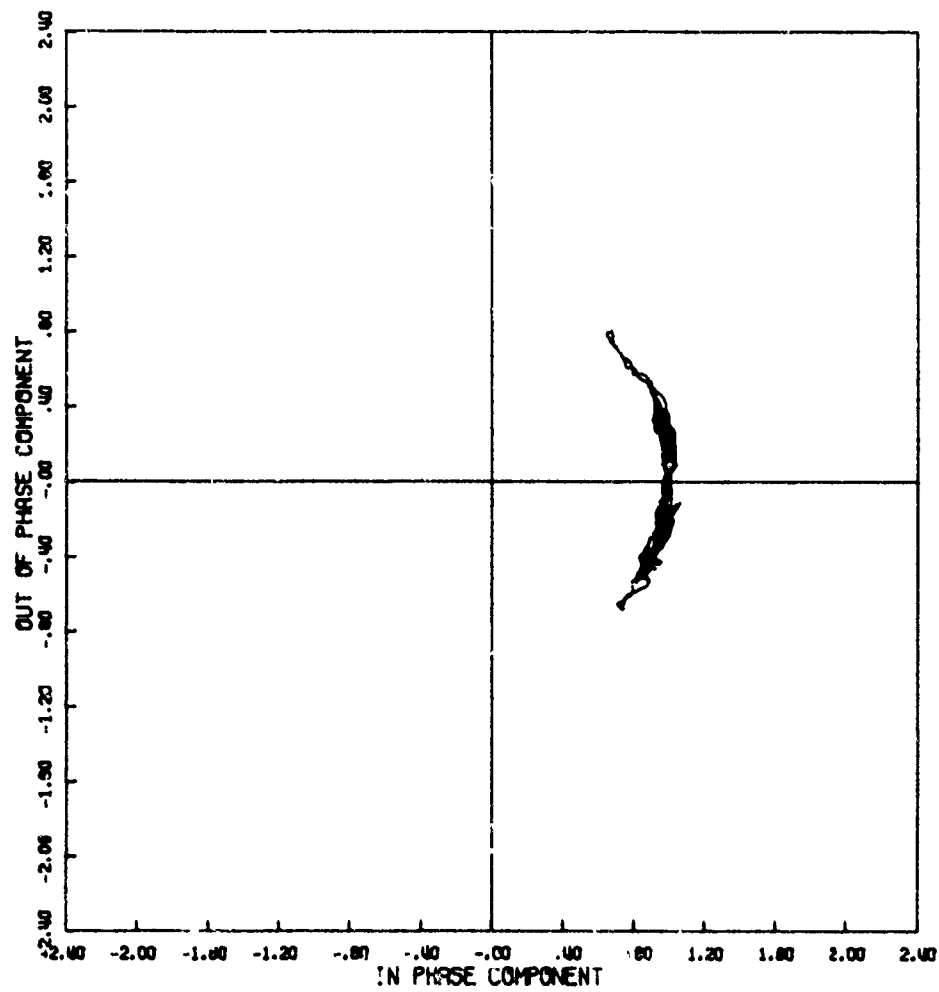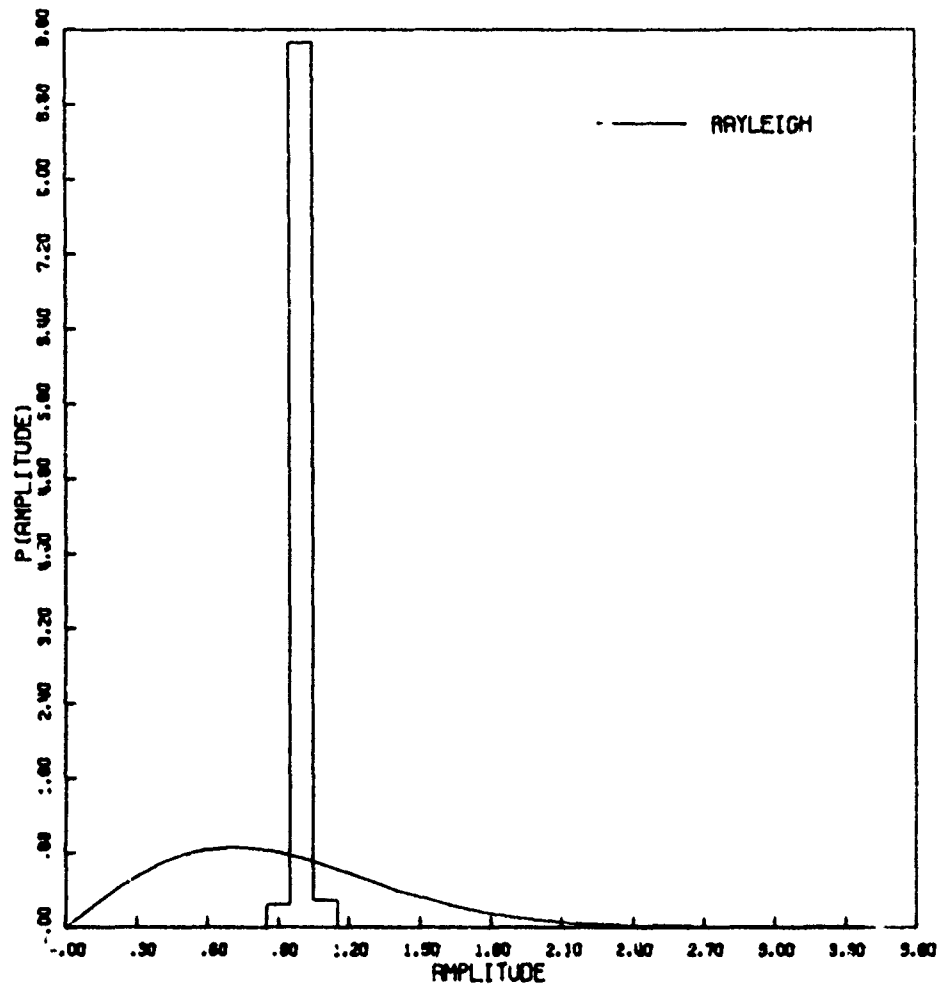
Figure 8d.   Amplitude Power Spectral Density
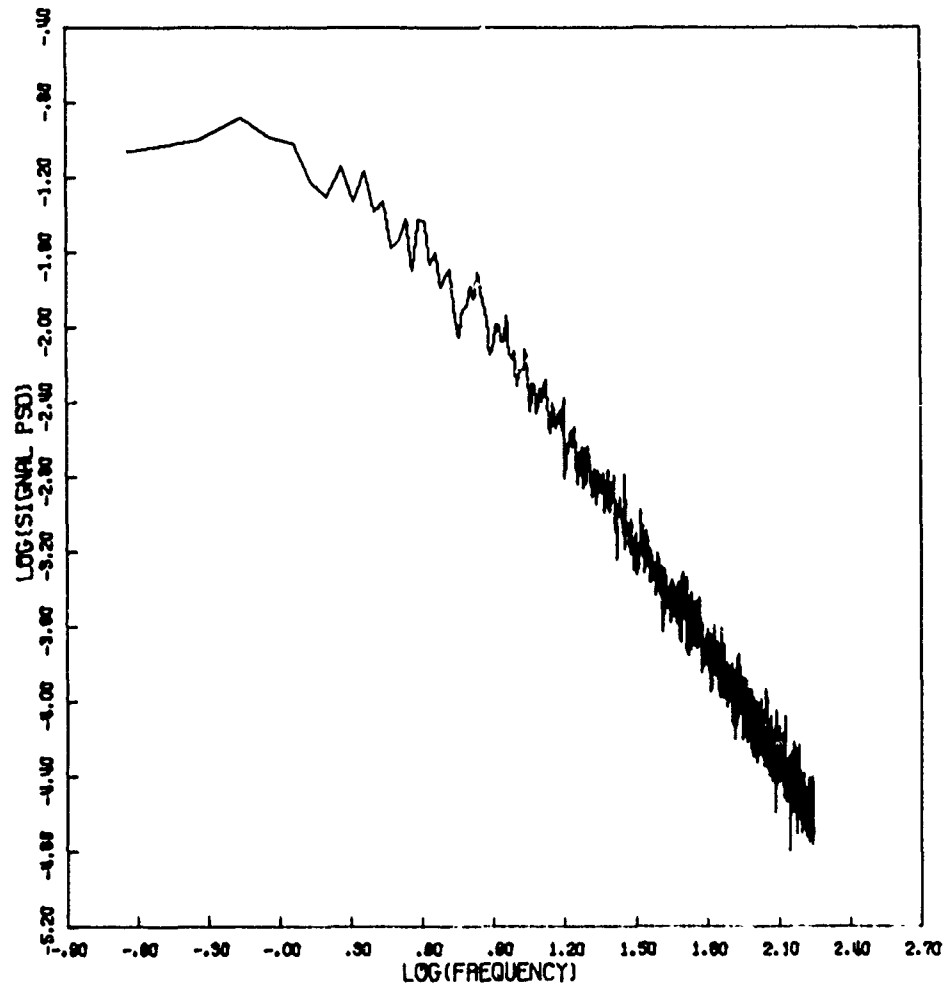
Figure 8e. Signal Power Spectral Density
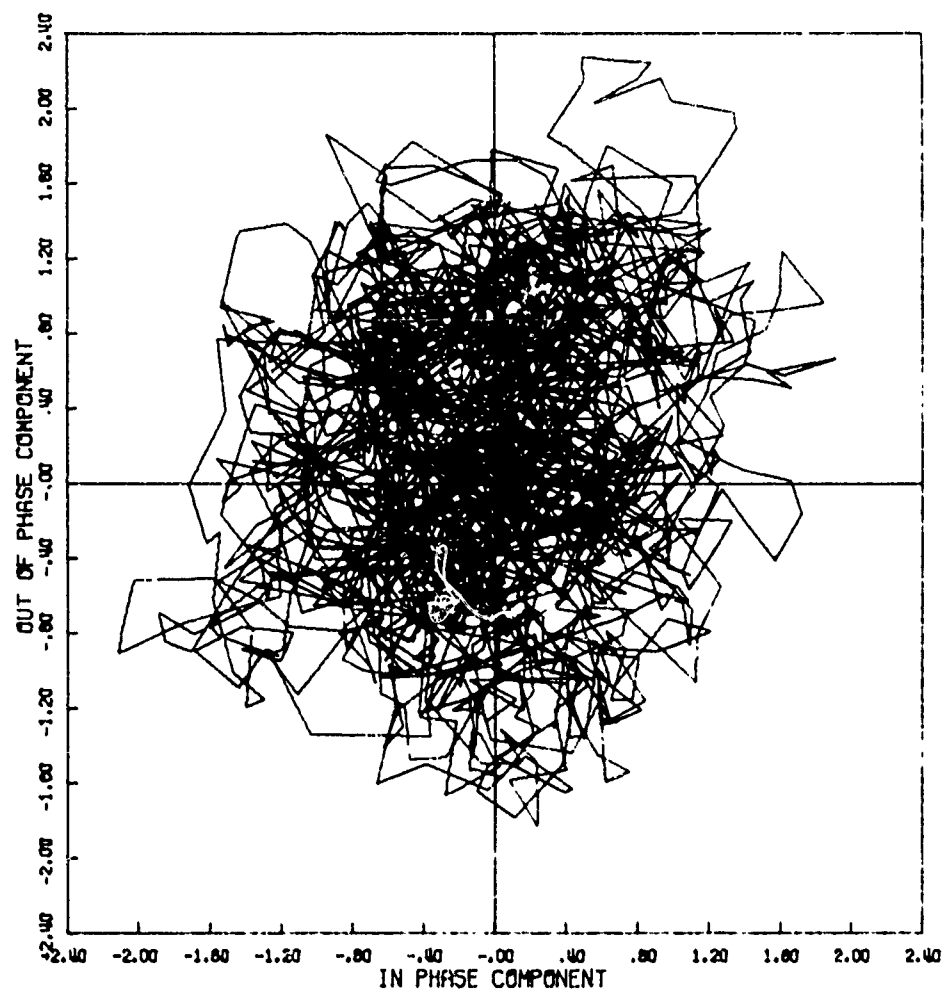
Figure 9a. Signal Phase Plot
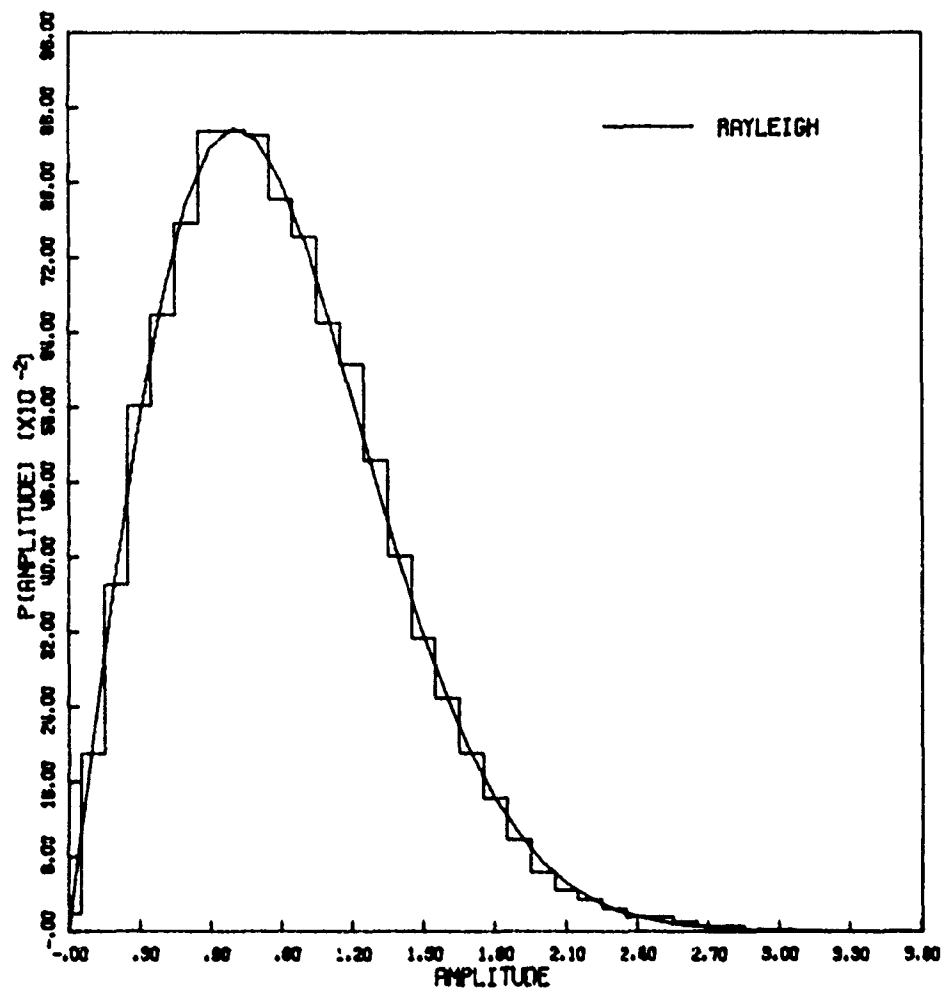
Figure 9b. Amplitude Distribution
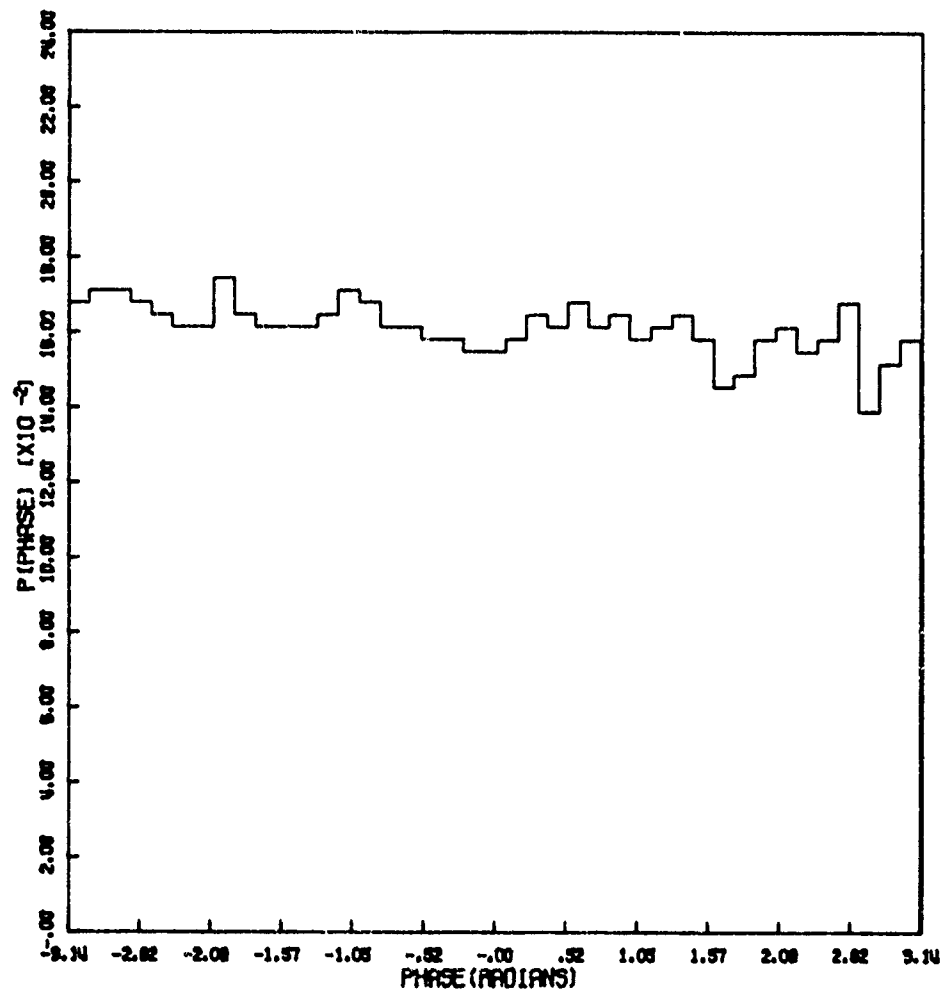
Figure 9c. Phase Distribution
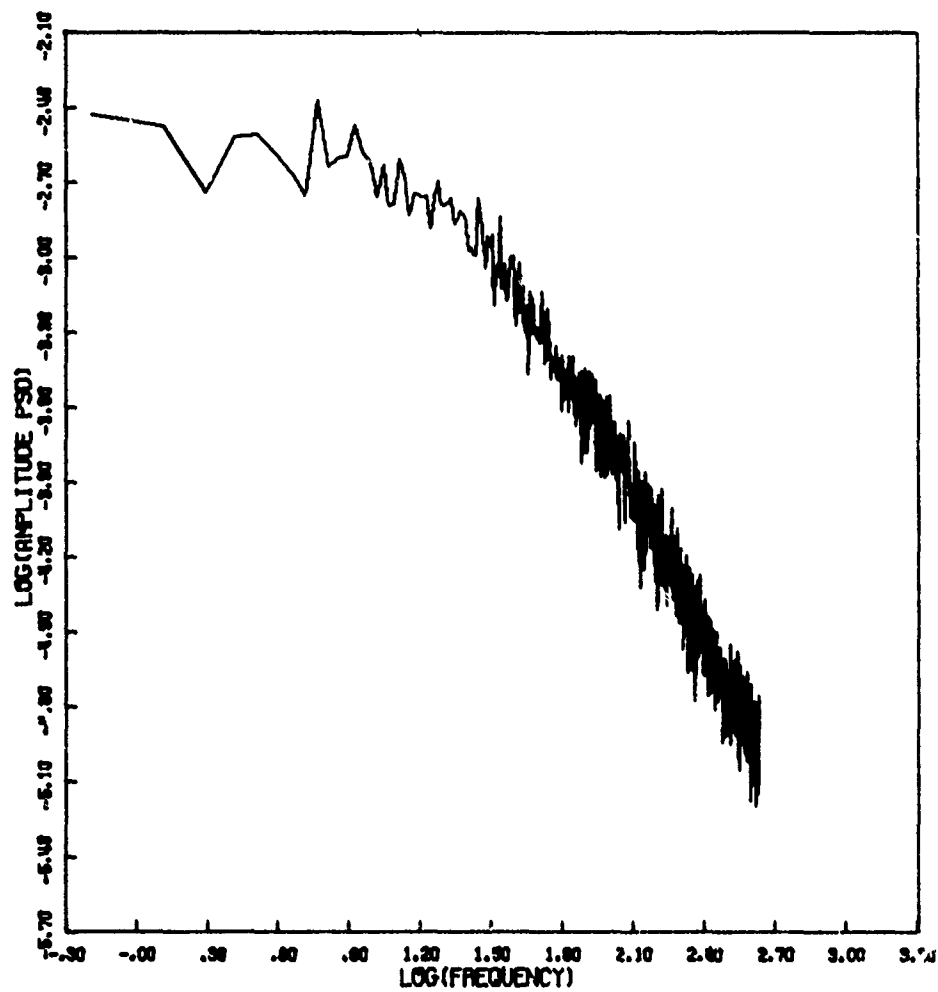
Figure 9d.   Amplitude Power Spectral Density
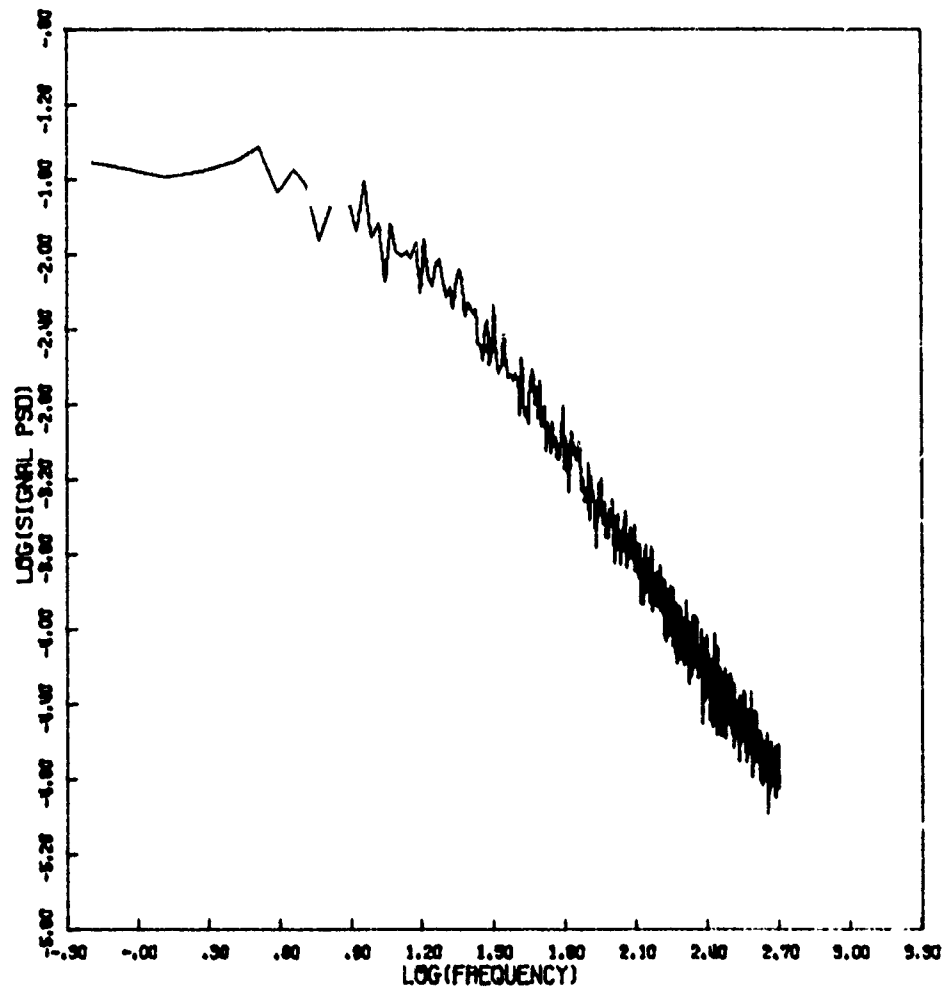
Figure 9e.   Signal Power Spectral Density
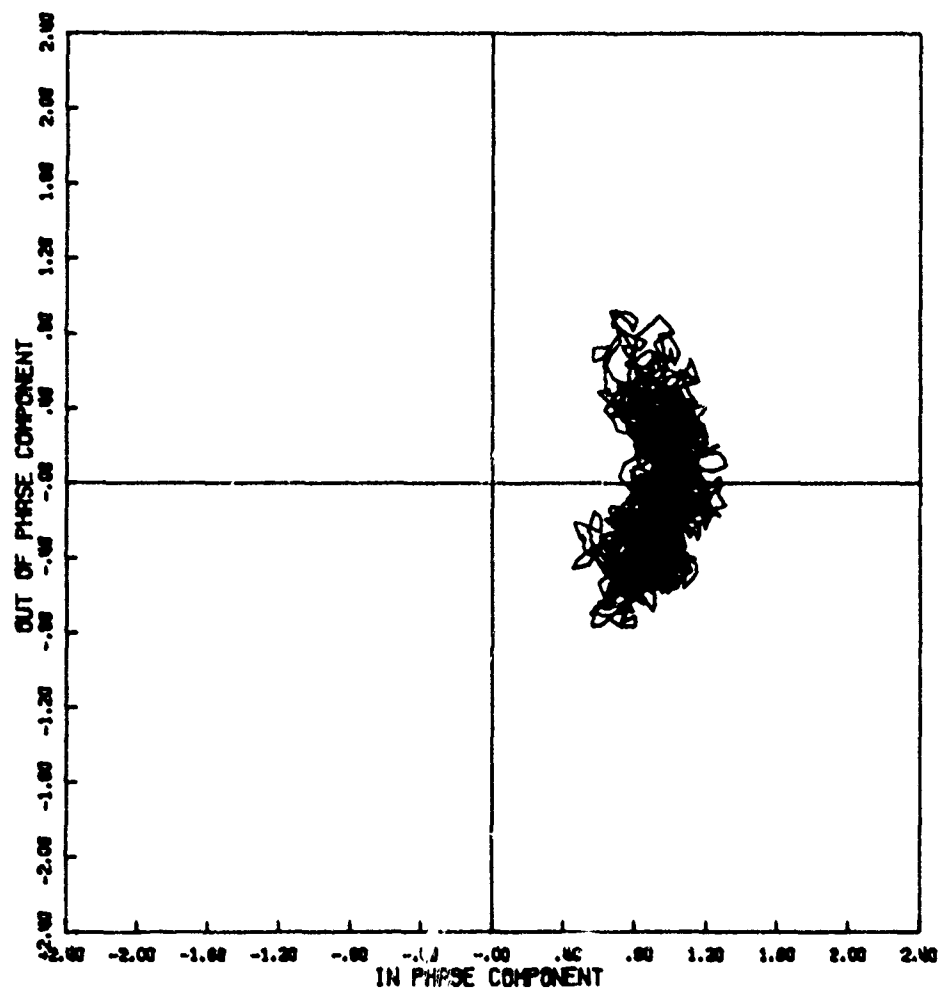
Figure 10a. Signal Phase Plot
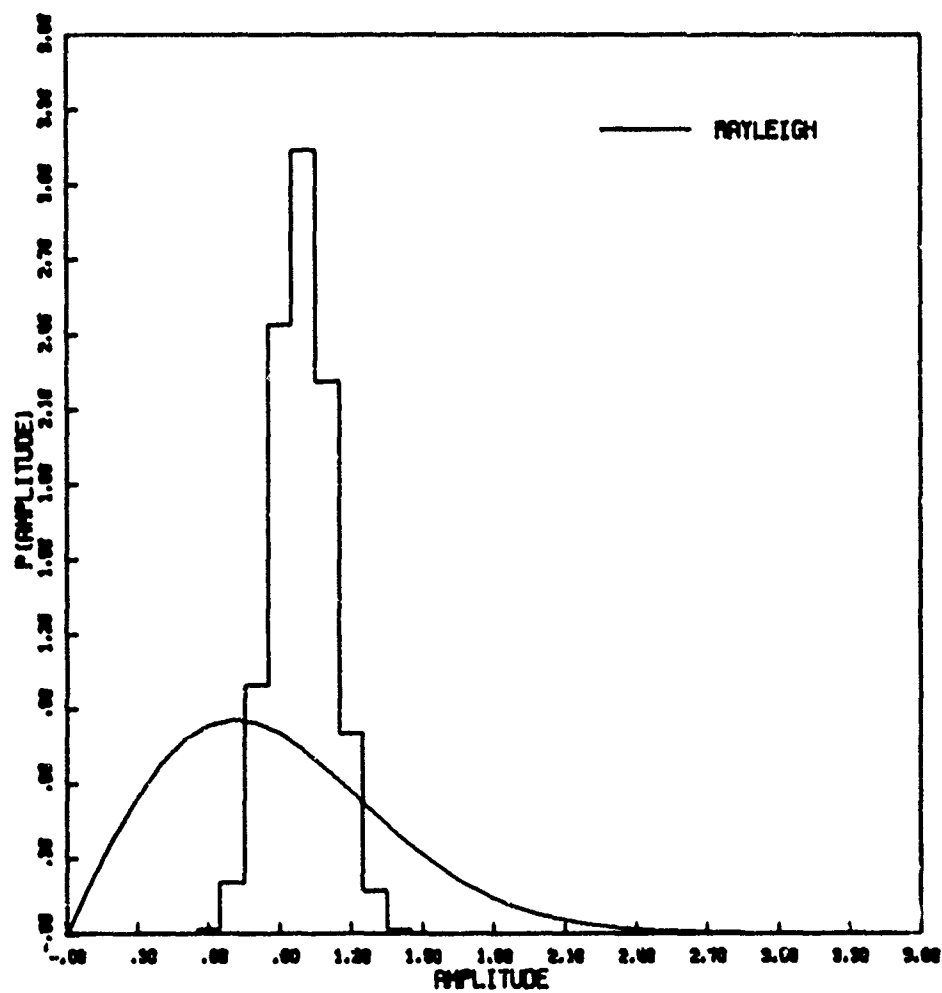
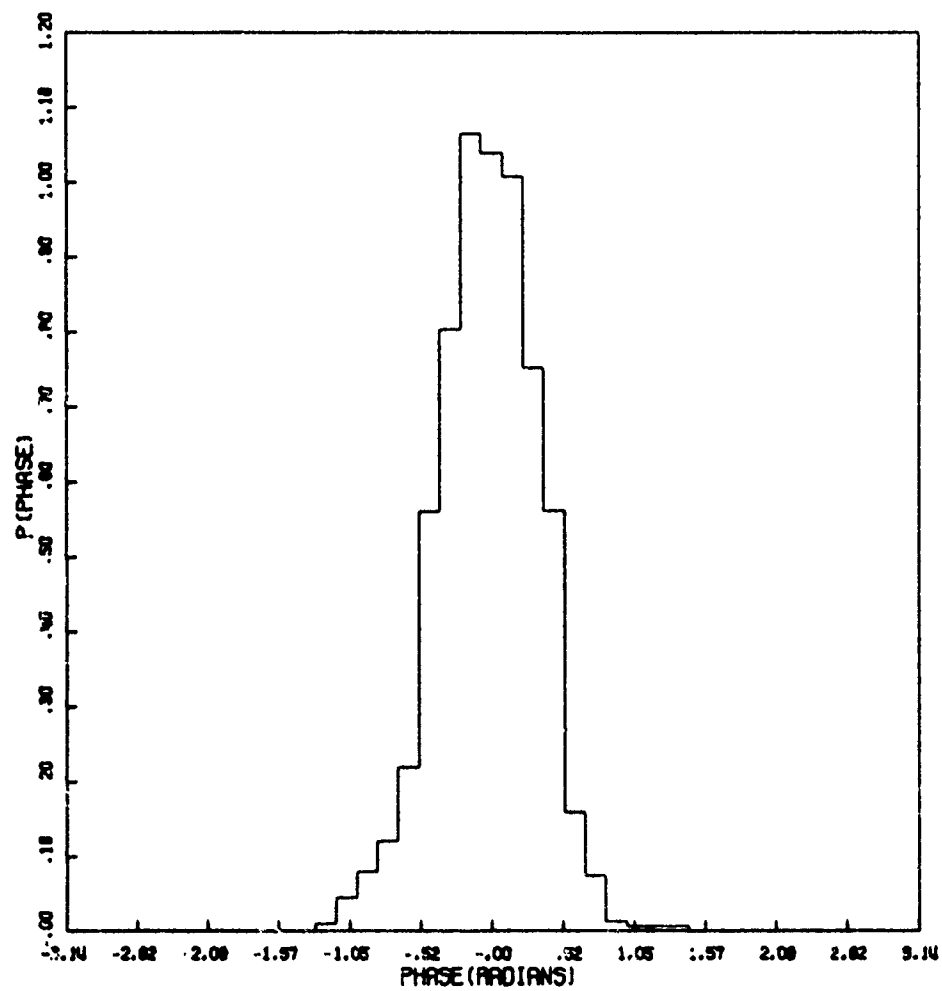Figure 10b. Amplitude Distribution
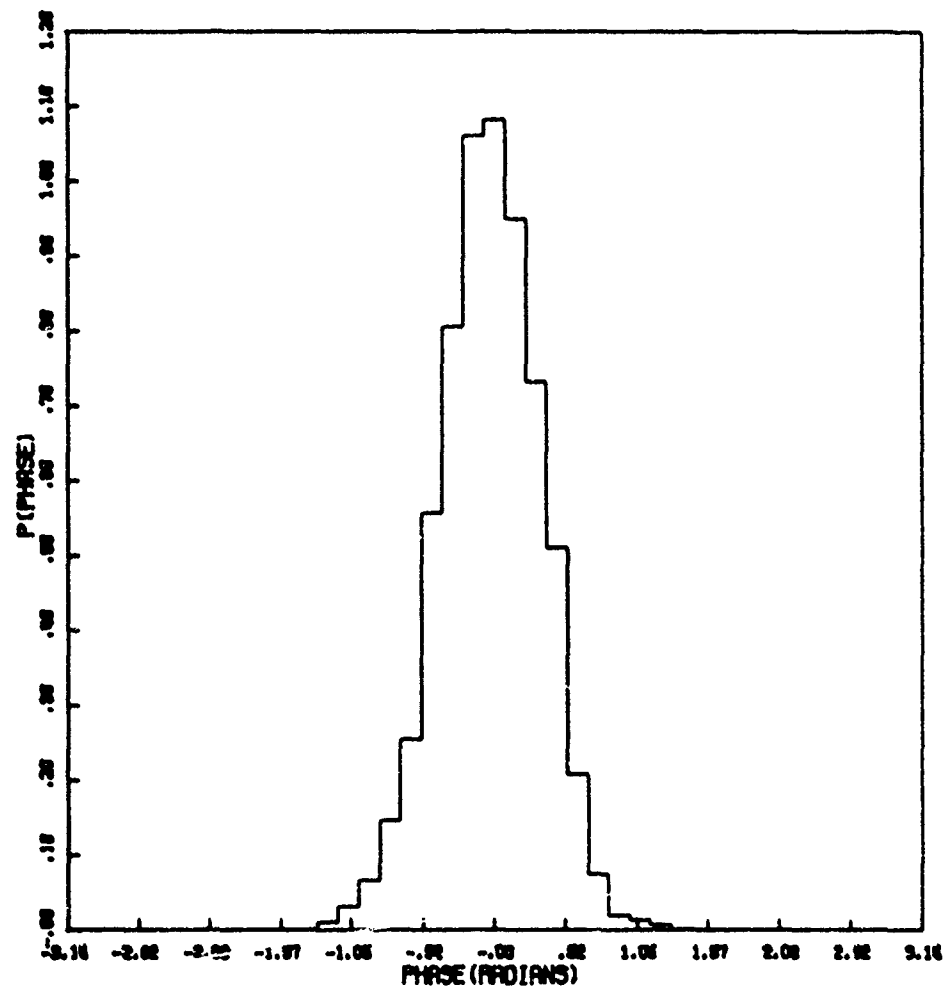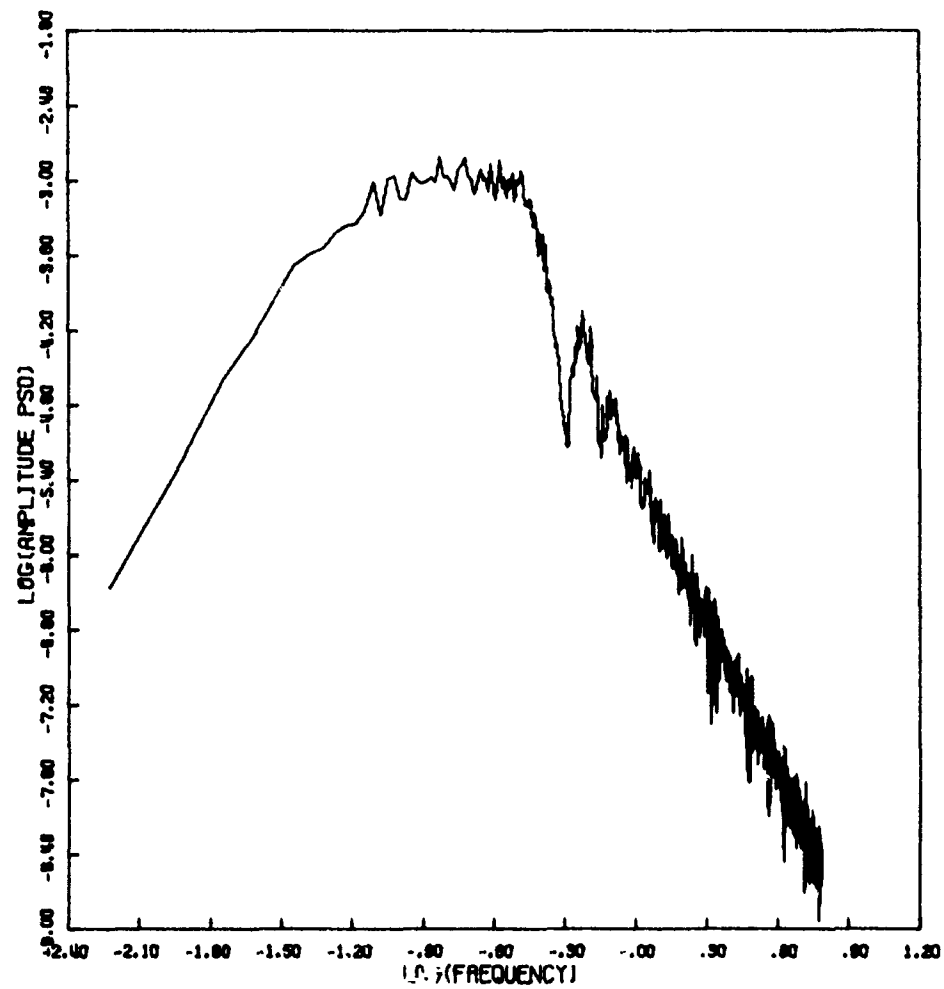
Figure 10c. Phase Distribution
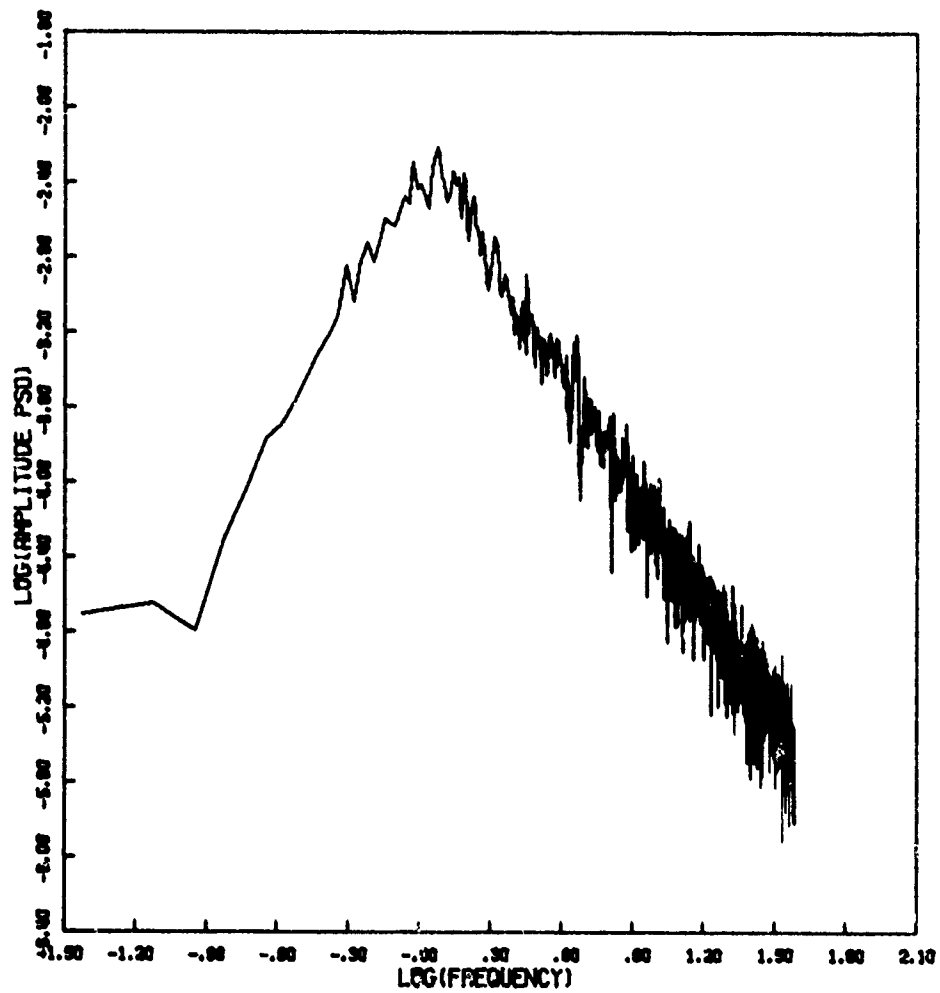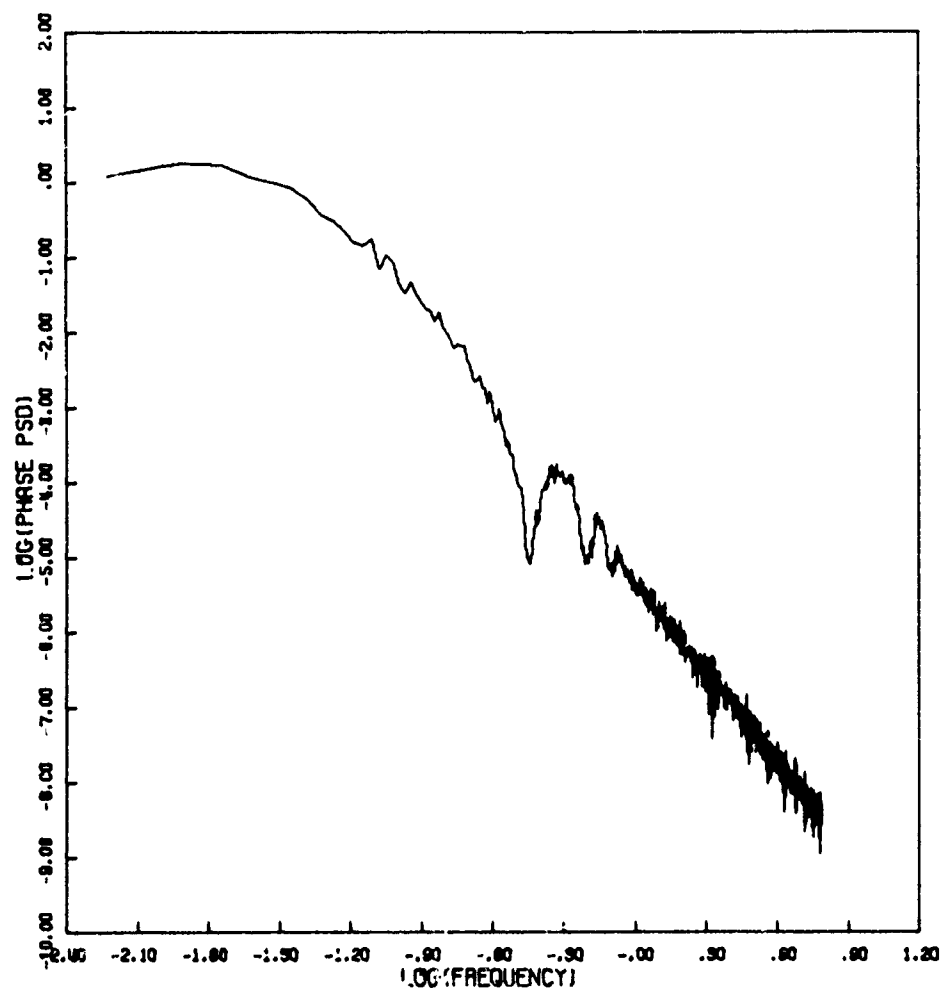
Figure 10d. Amplitude Power Spectral Density
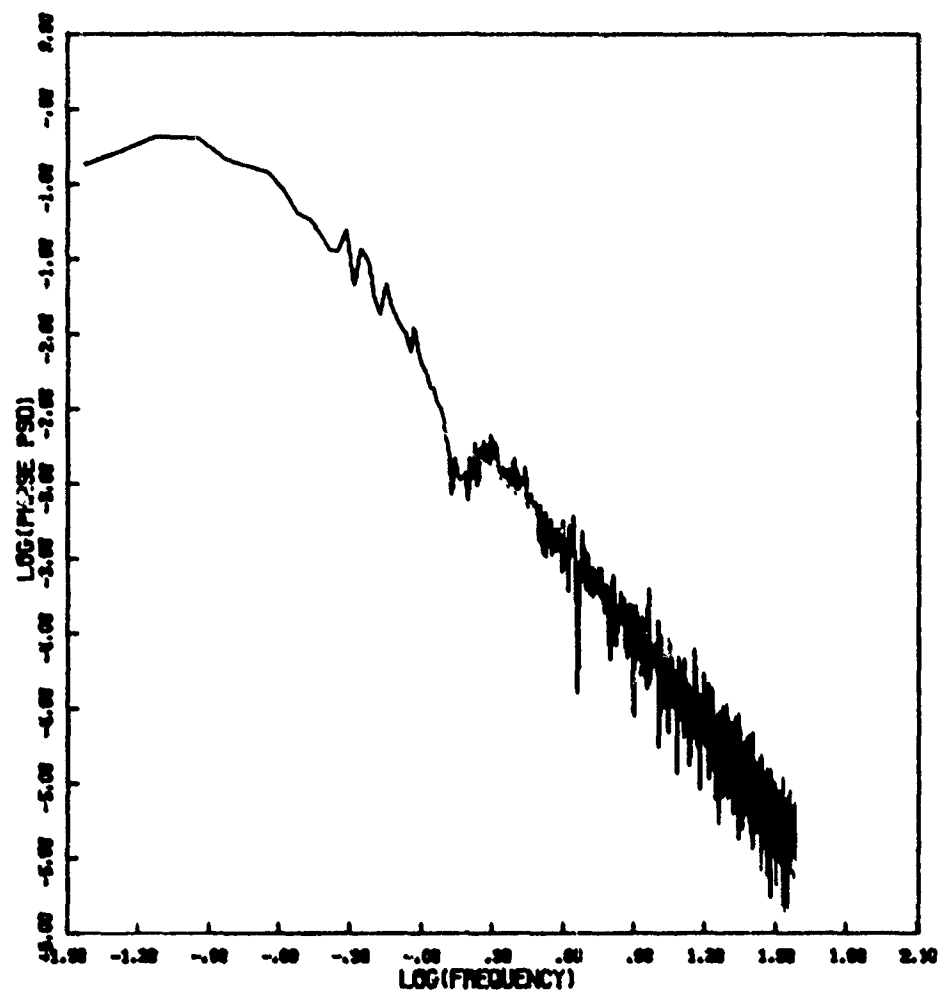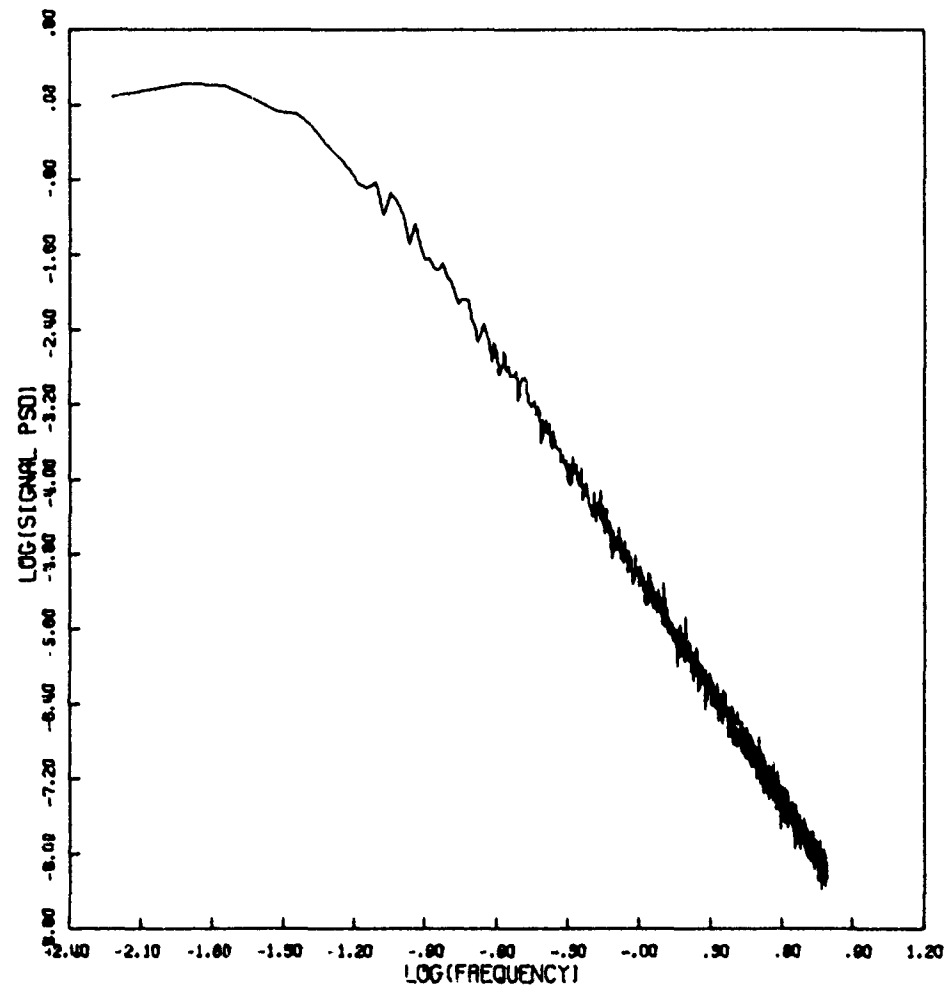
Figure 10e.   Phase Power Spectral Density
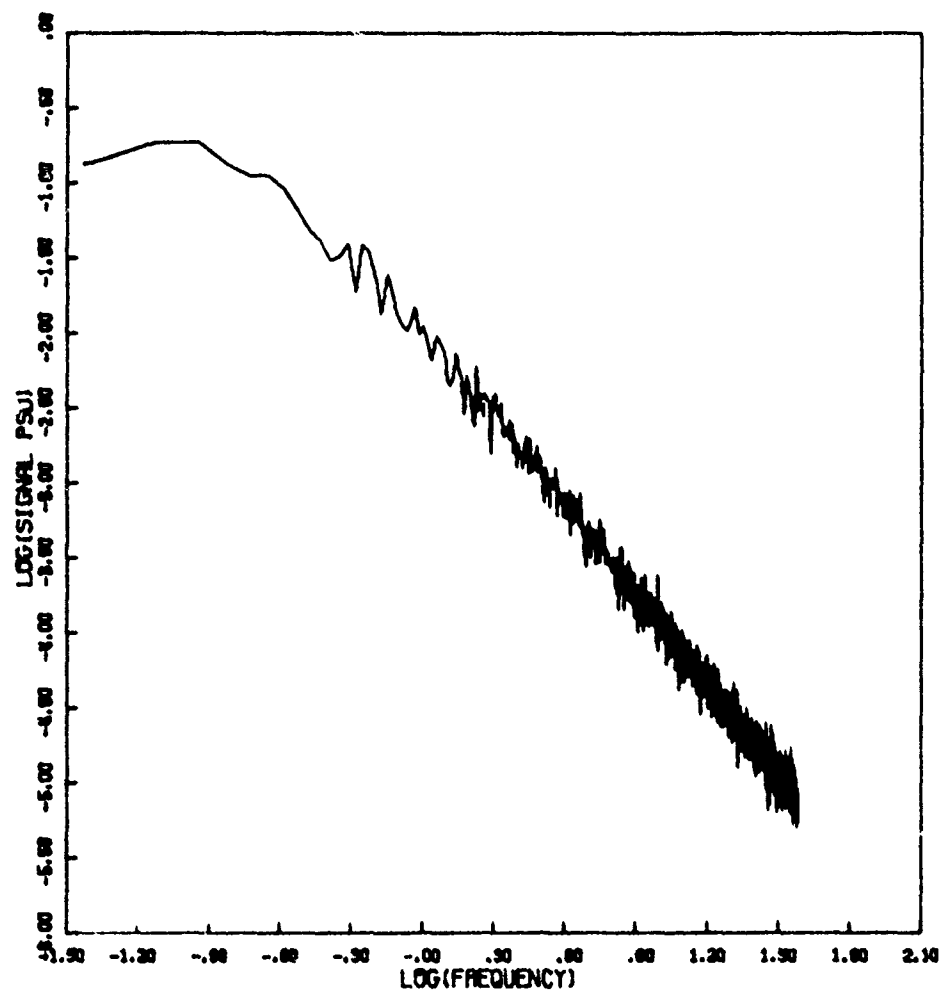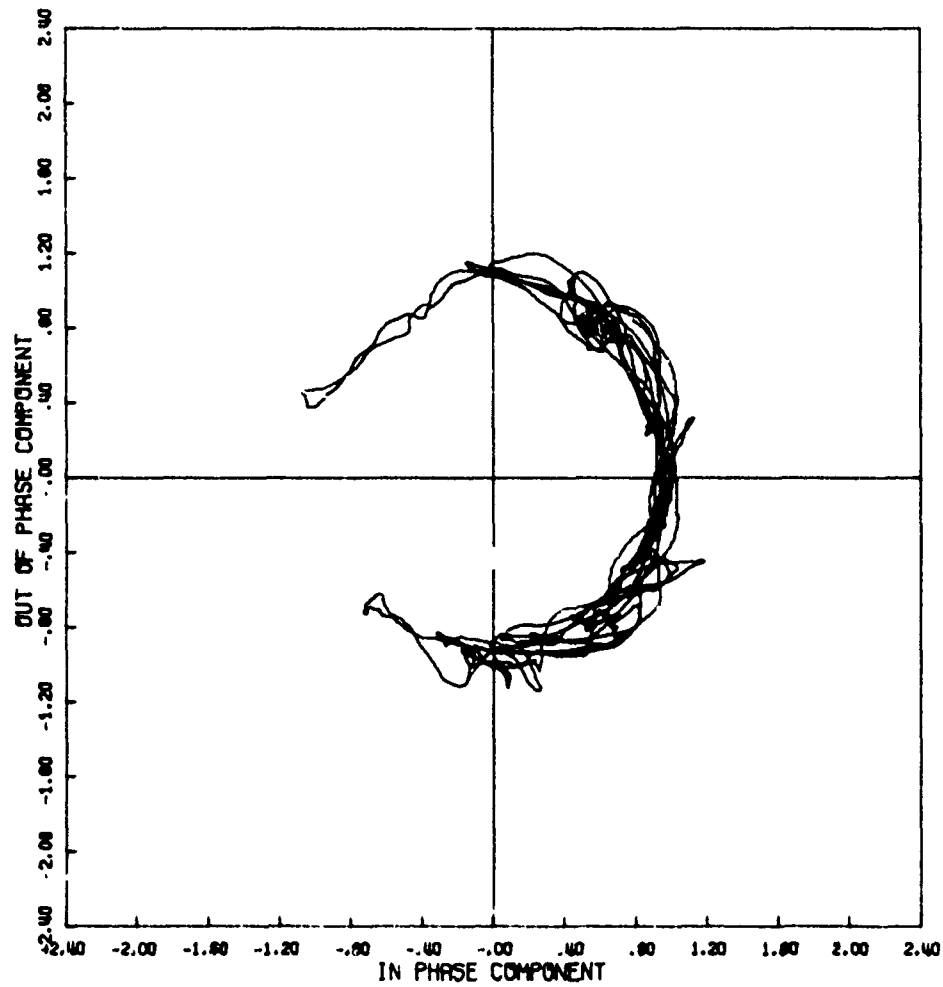
Figure 10f. Signal Power Spectral Density
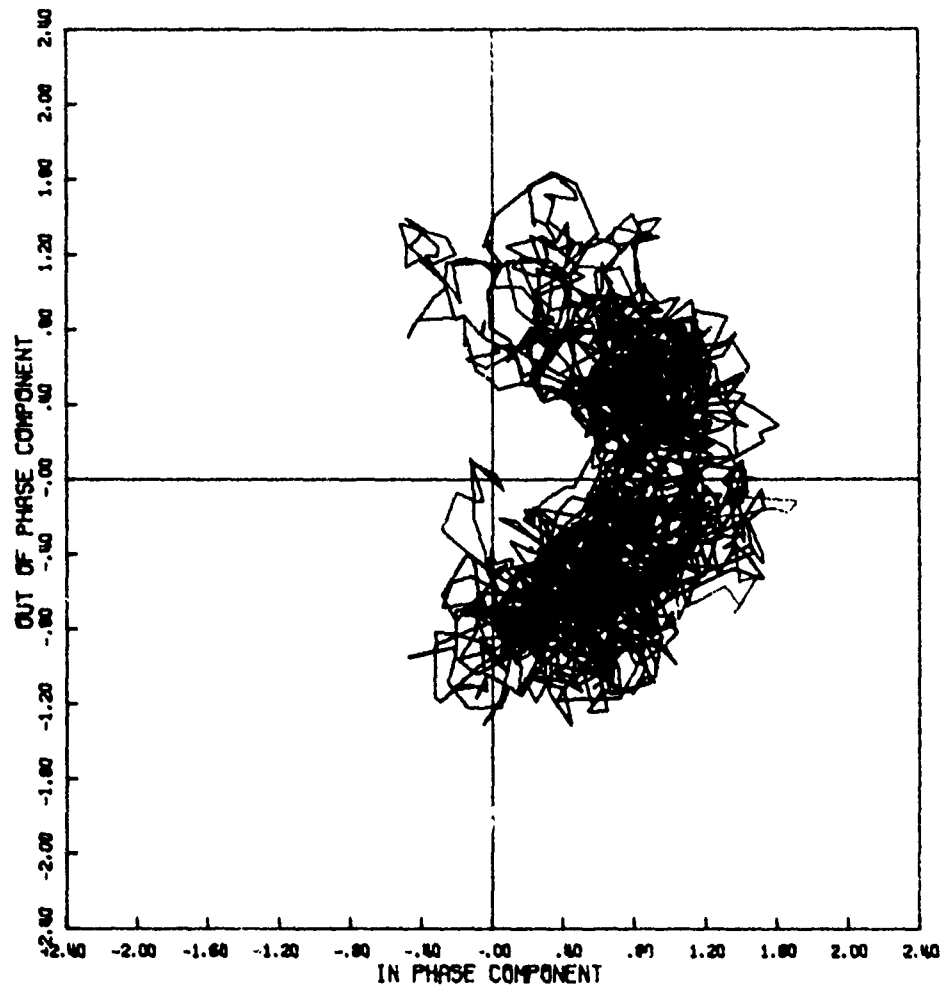
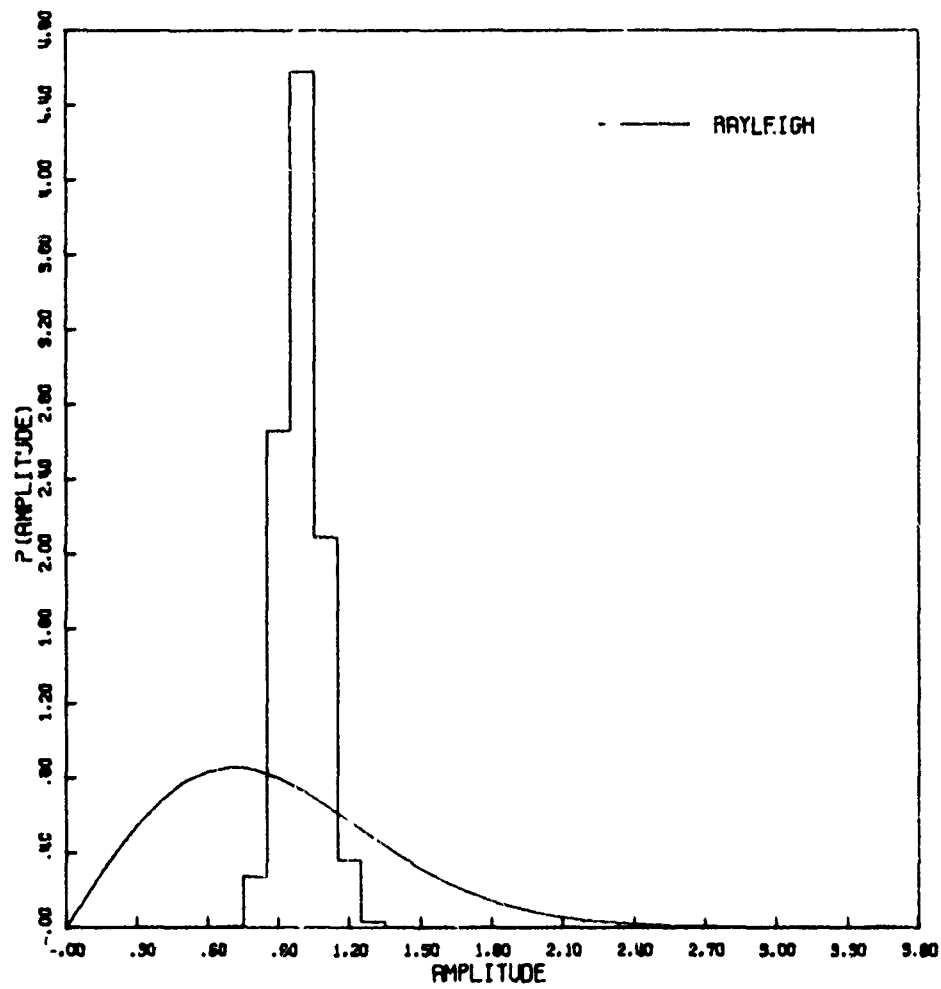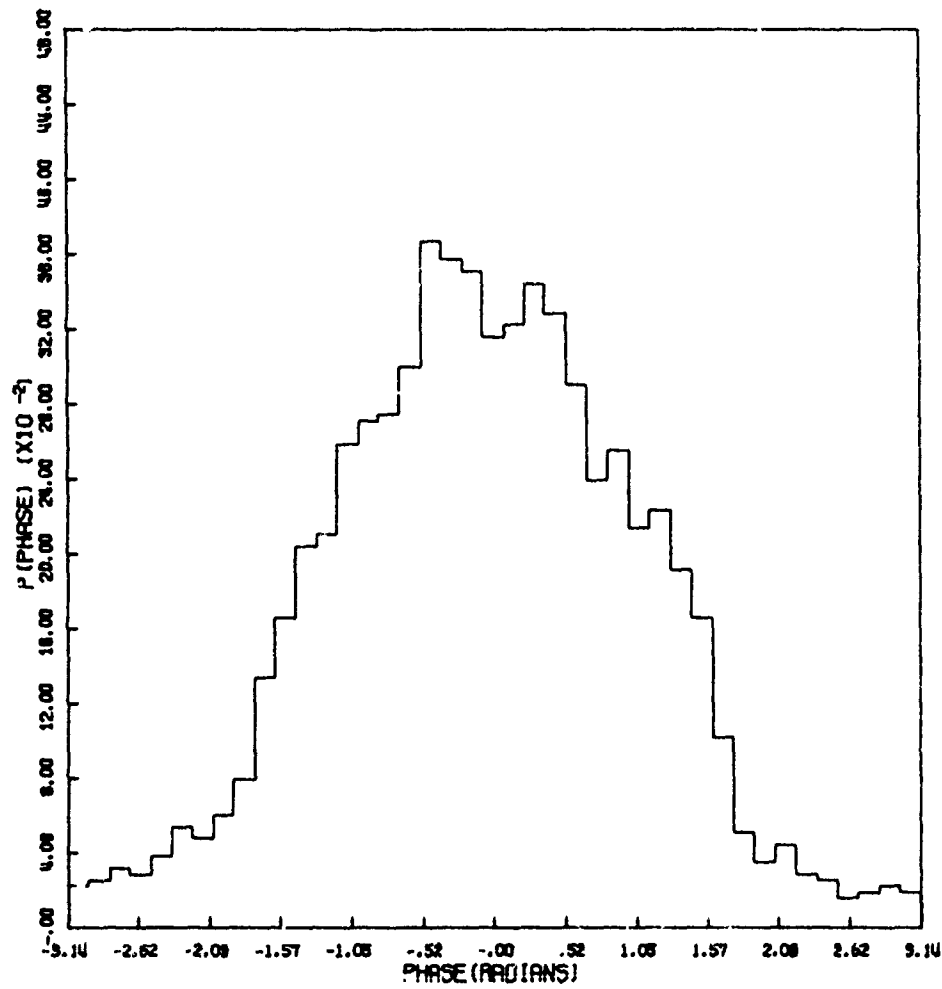Figure 11a. Signal Phase Plot
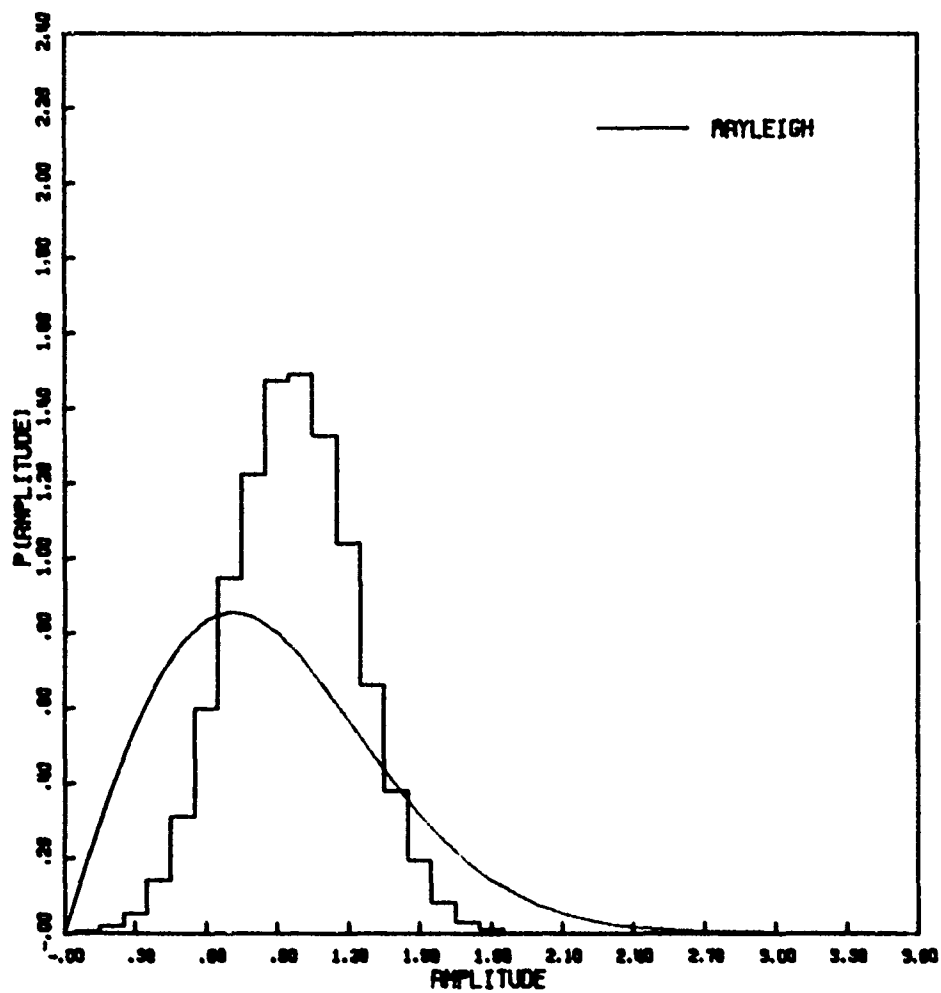
Figure 11b. Amplitude Distribution
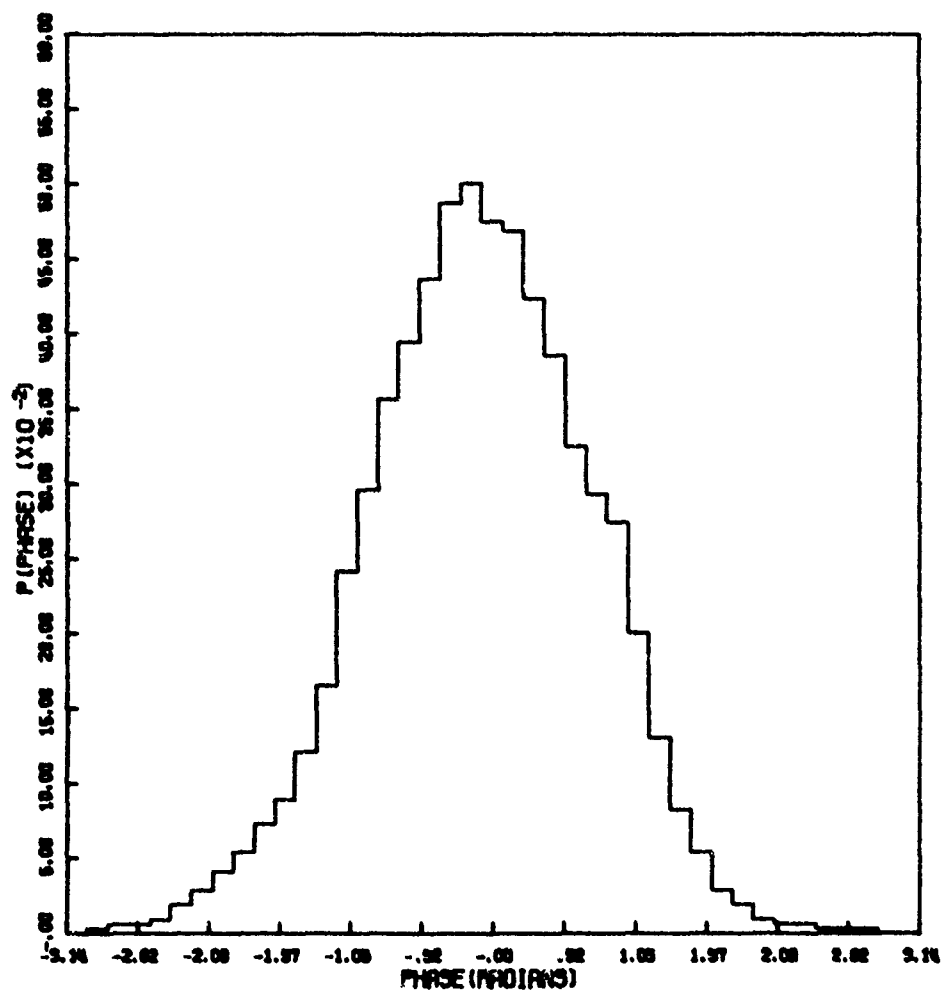
Figure 11c.   Phase Distribution
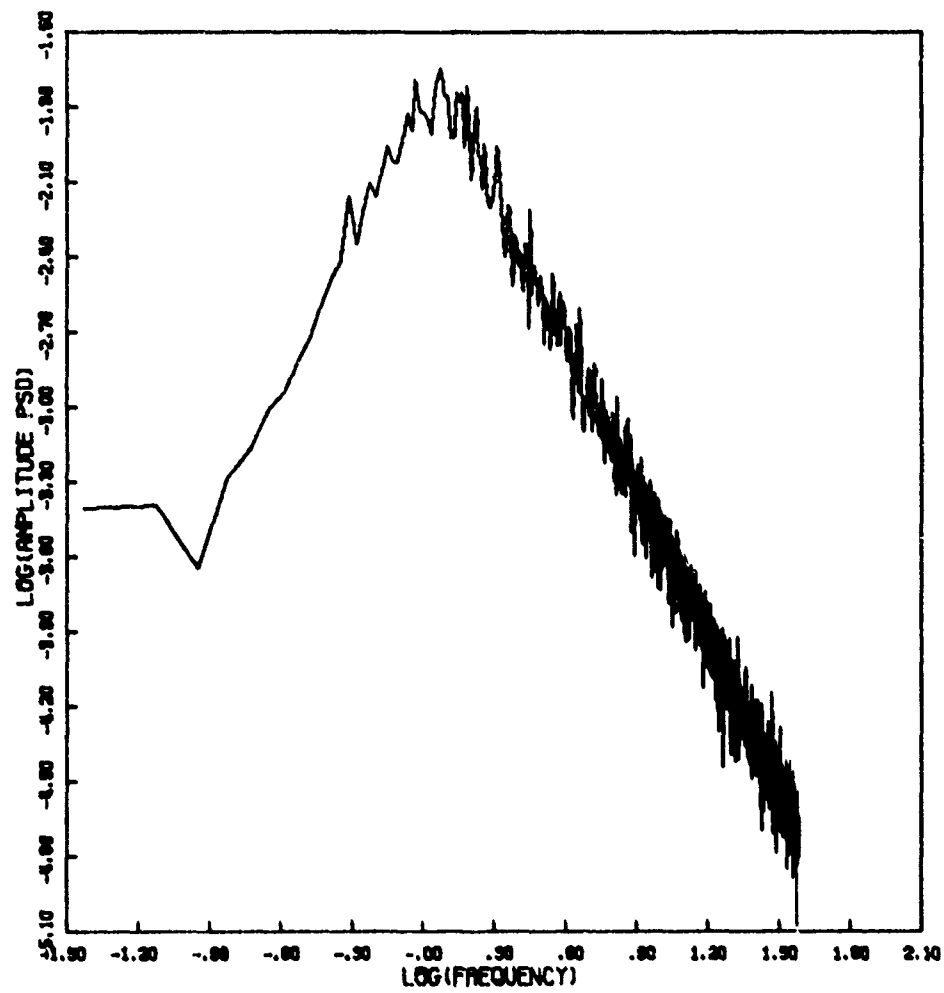
Figure 11d. Amplitude Power Spectral Density
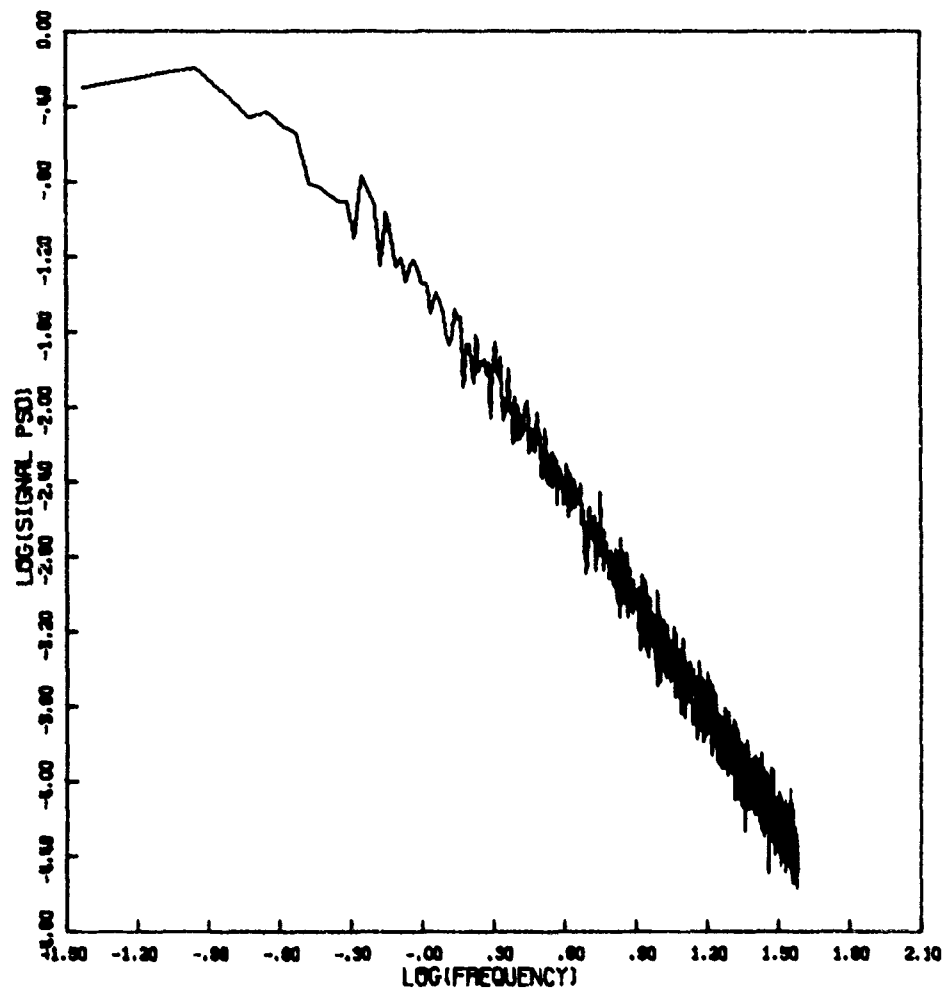
Figure 11e. Signal Power Spectral Density
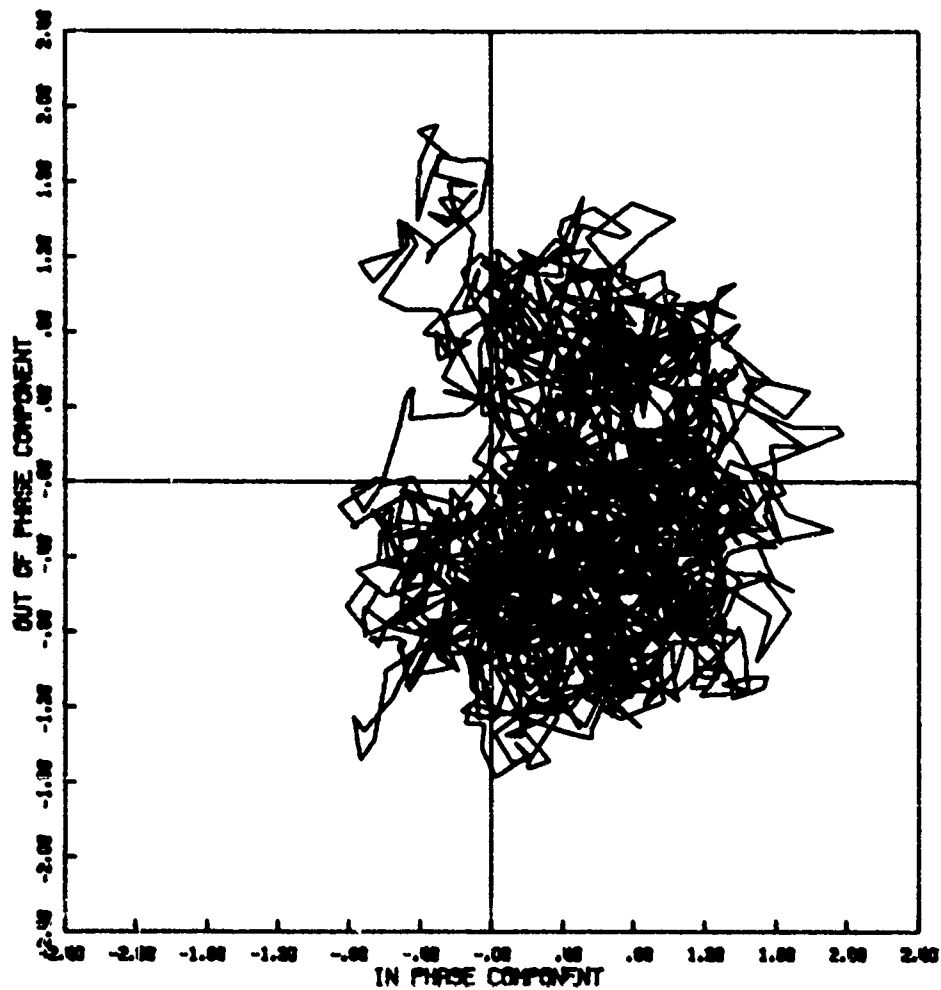
Figure 12a. Signal Phase Plot
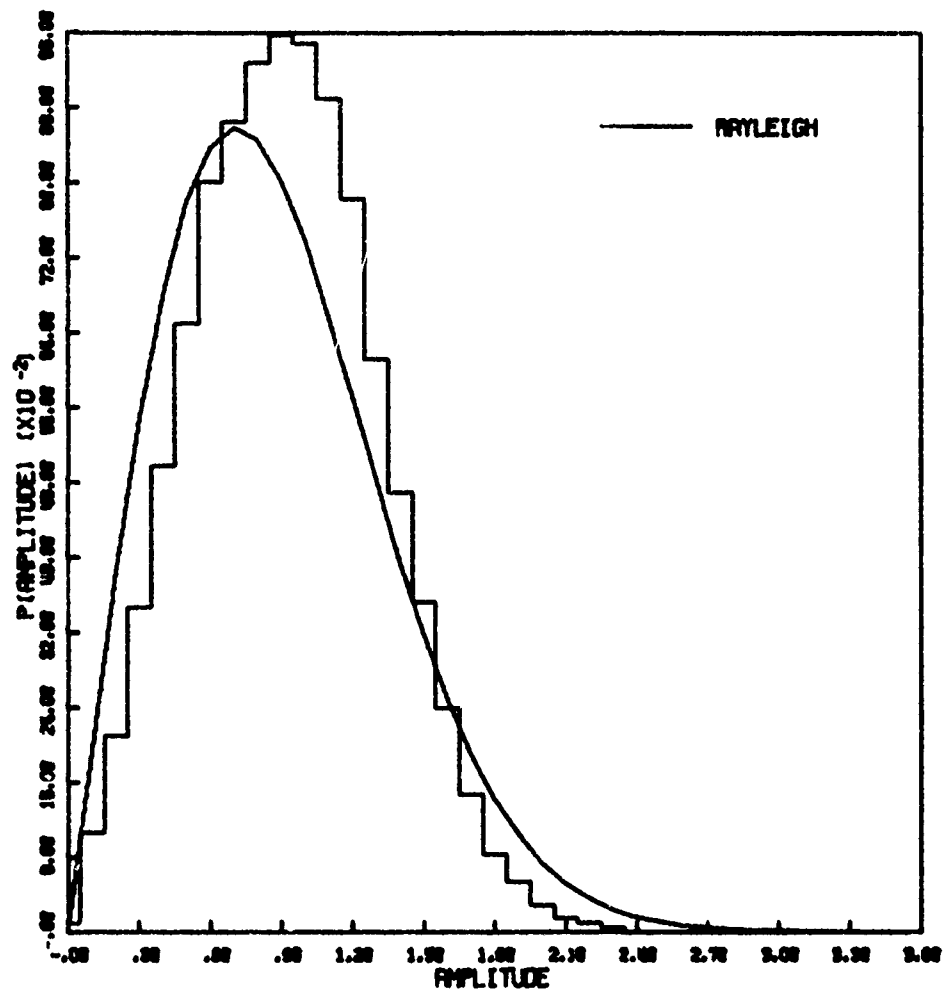
Figure 12b. Amplitude Distribution
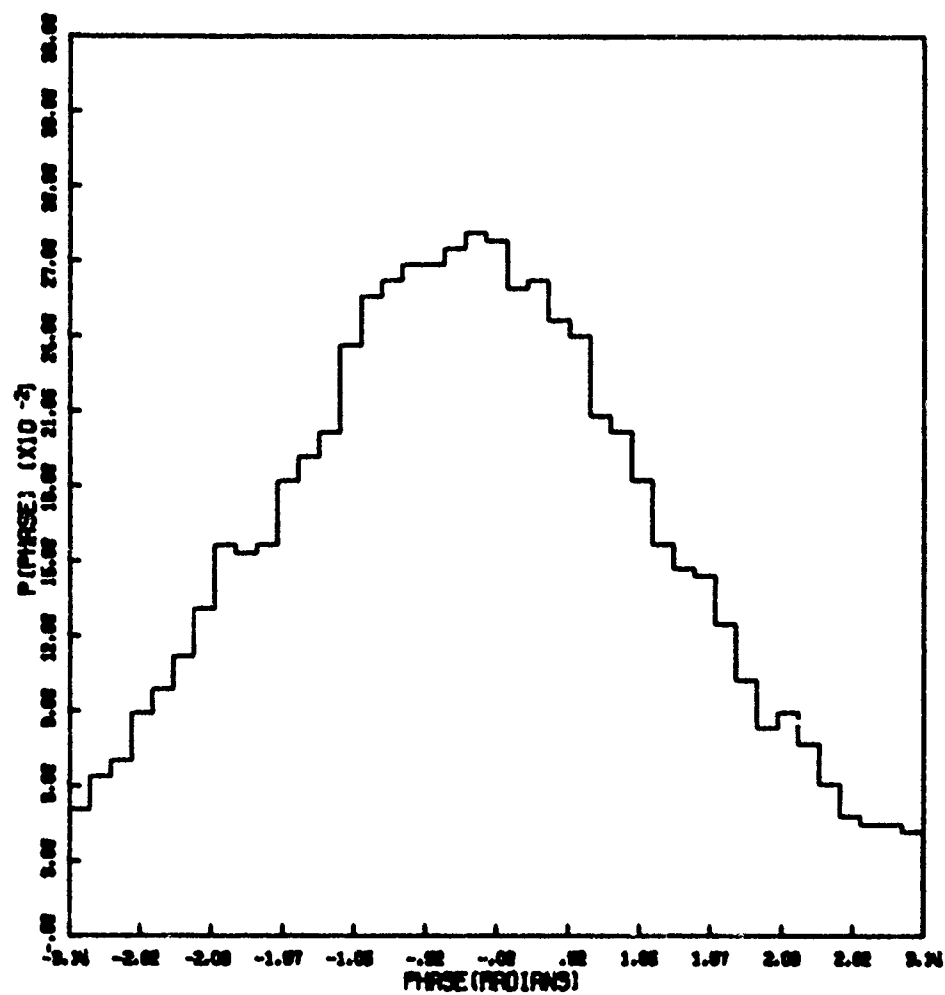
Figure 12c.   Phase Distribution
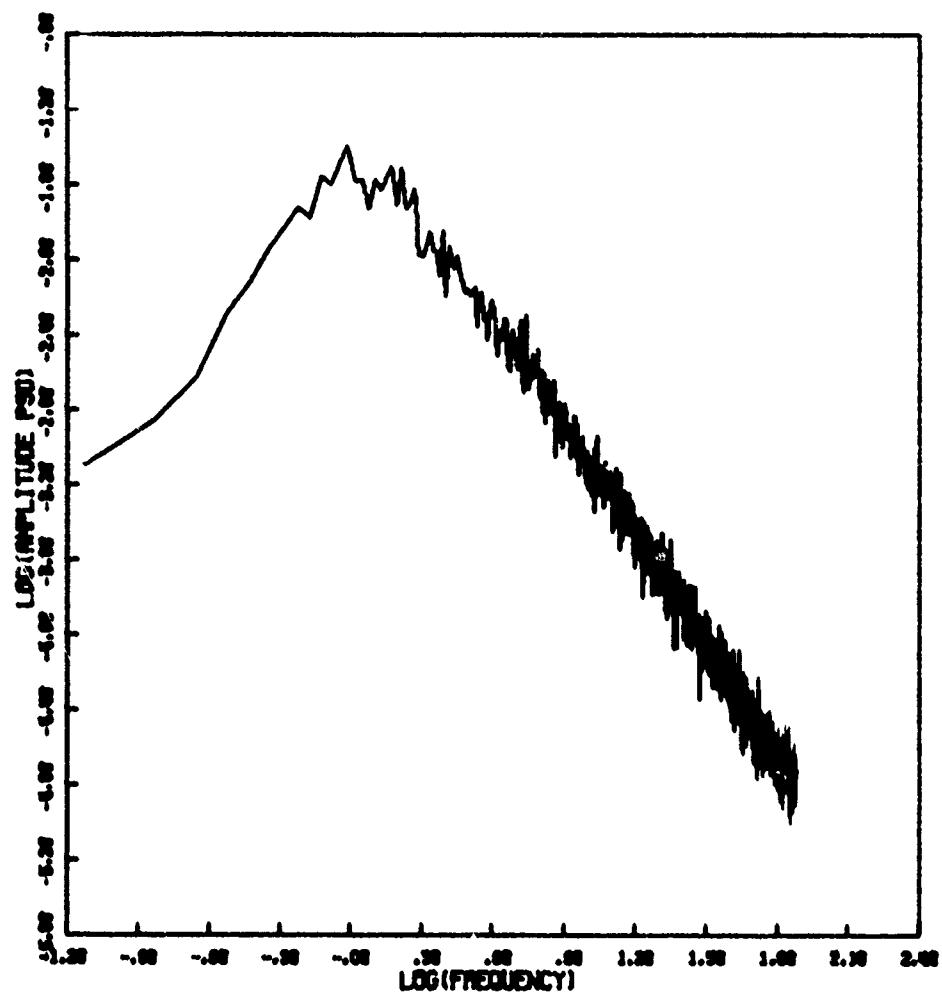
Figure 12d. Amplitude Power Spectral Density
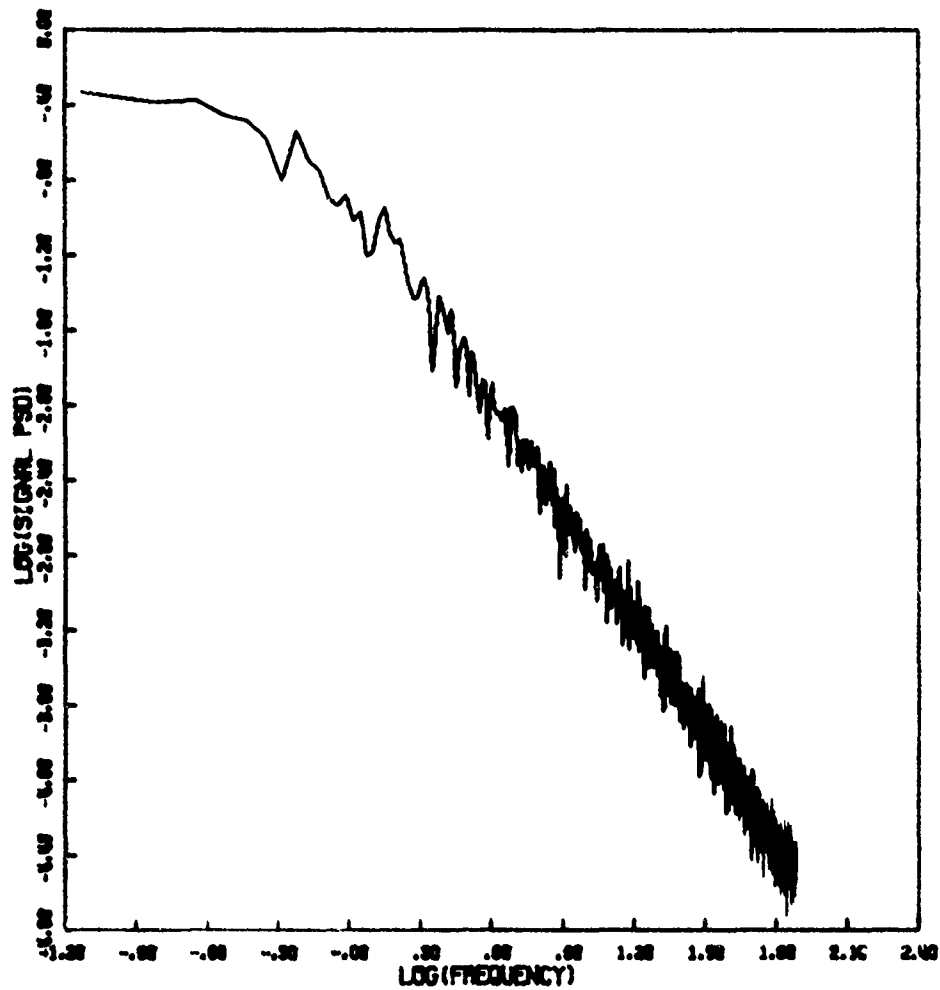
Figure 12e. Signal Power Spectral Density
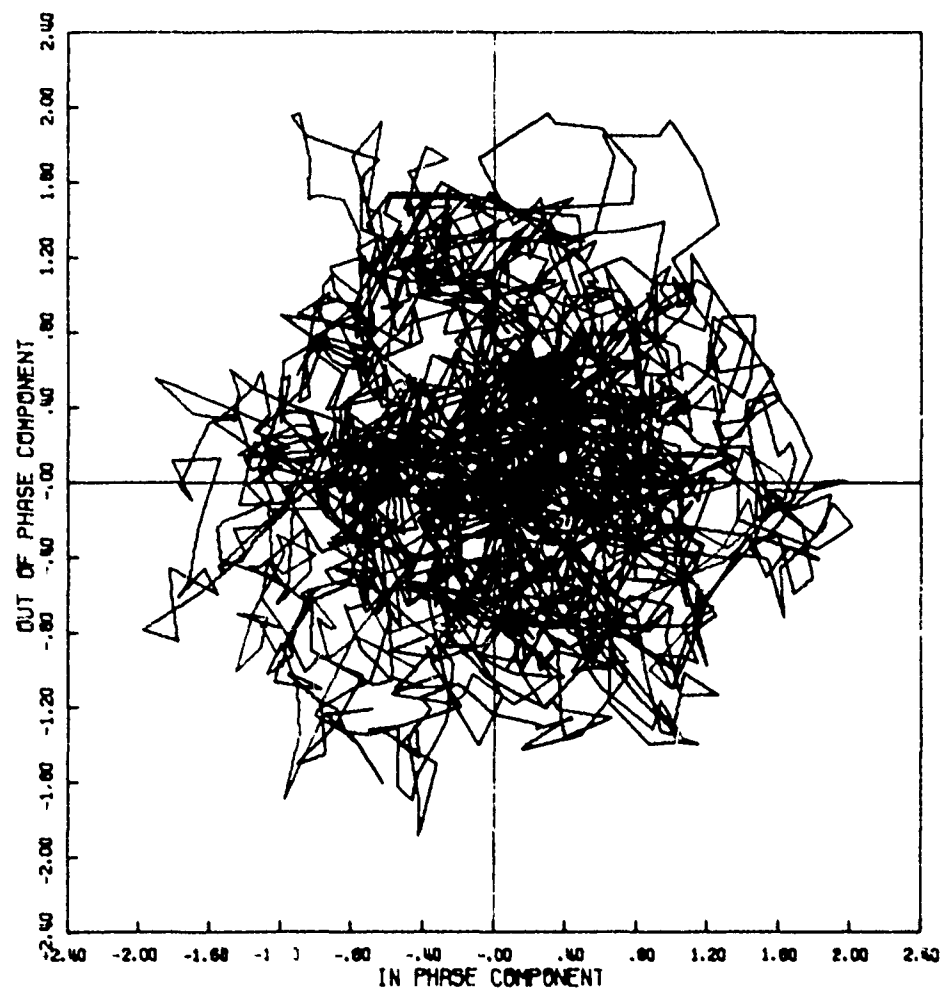
Figure 13a.   Signal Phase Plot
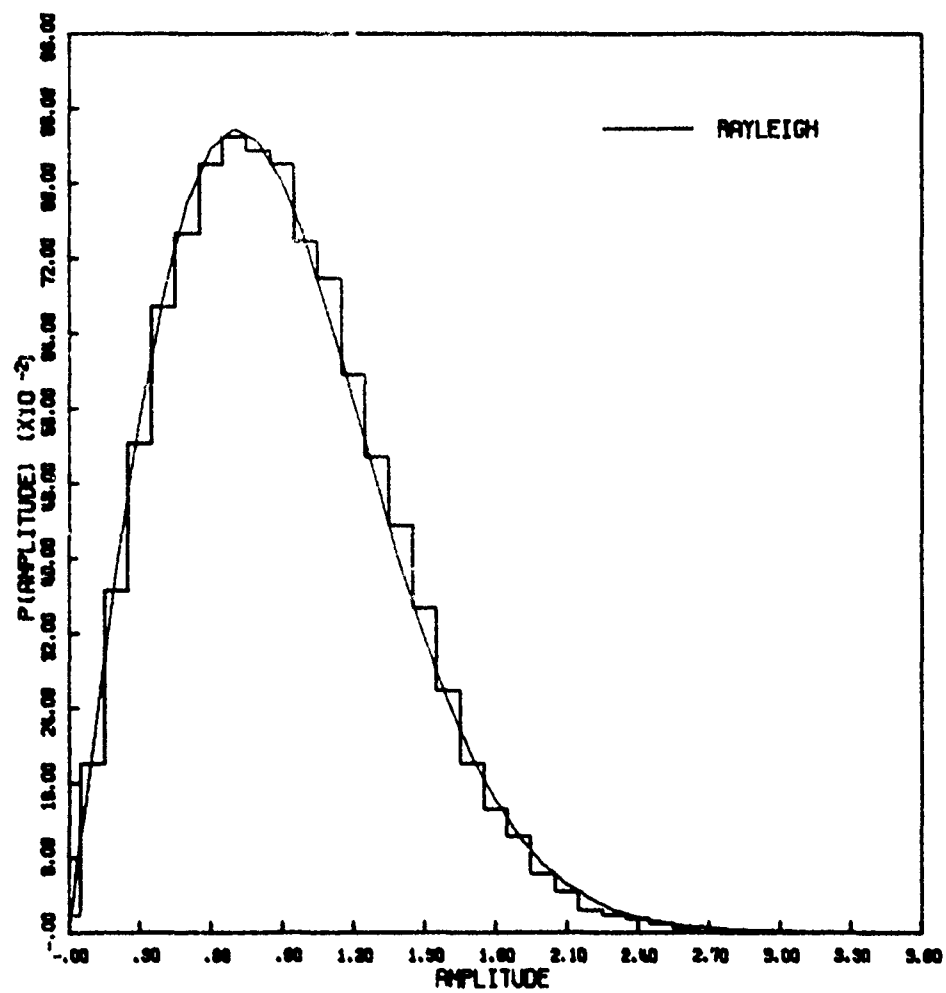
Figure 13b. Amplitude Distribution
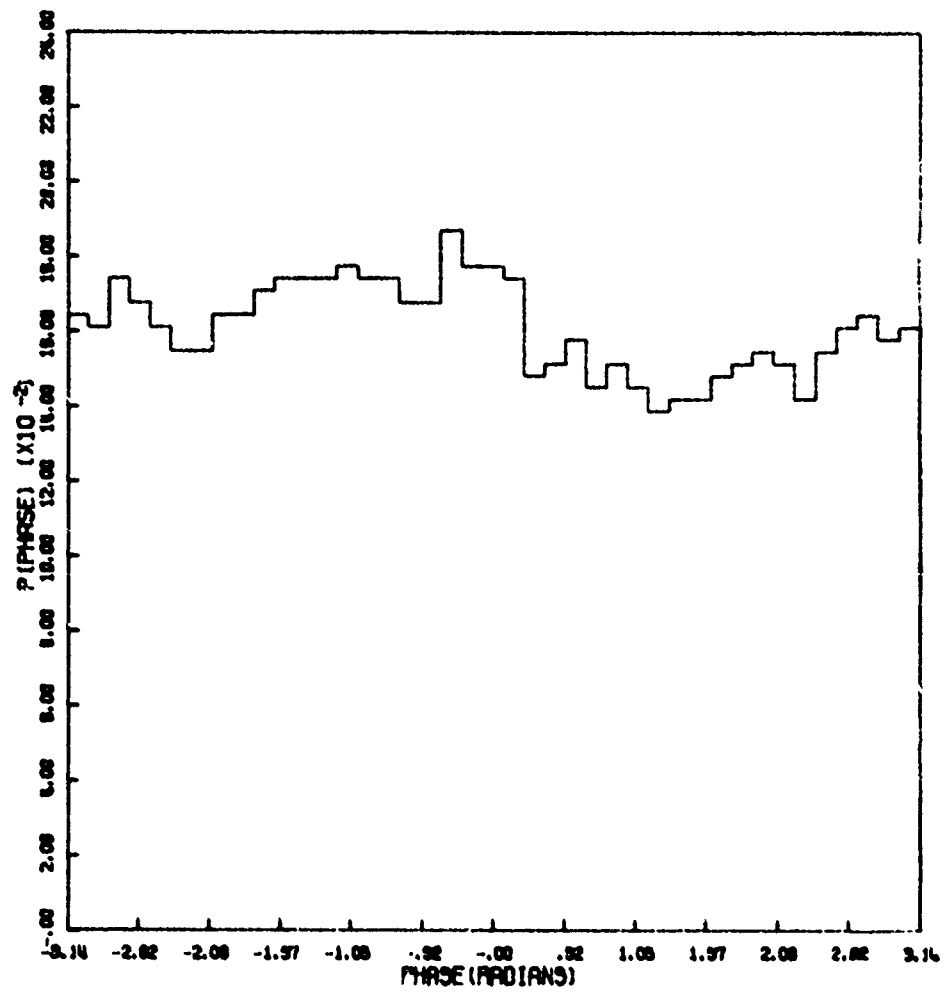
Figure 13c.   Phase Distribution
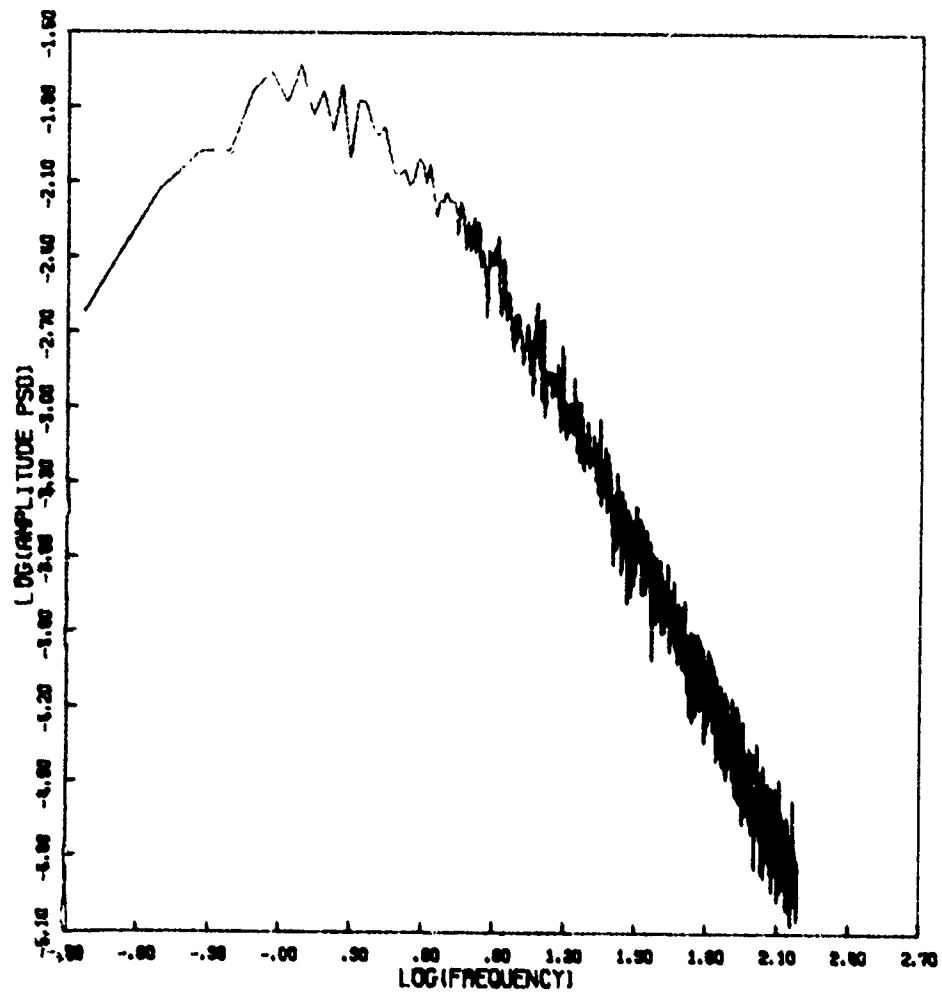
Figure 13d.   Amplitude Power Spectral Density
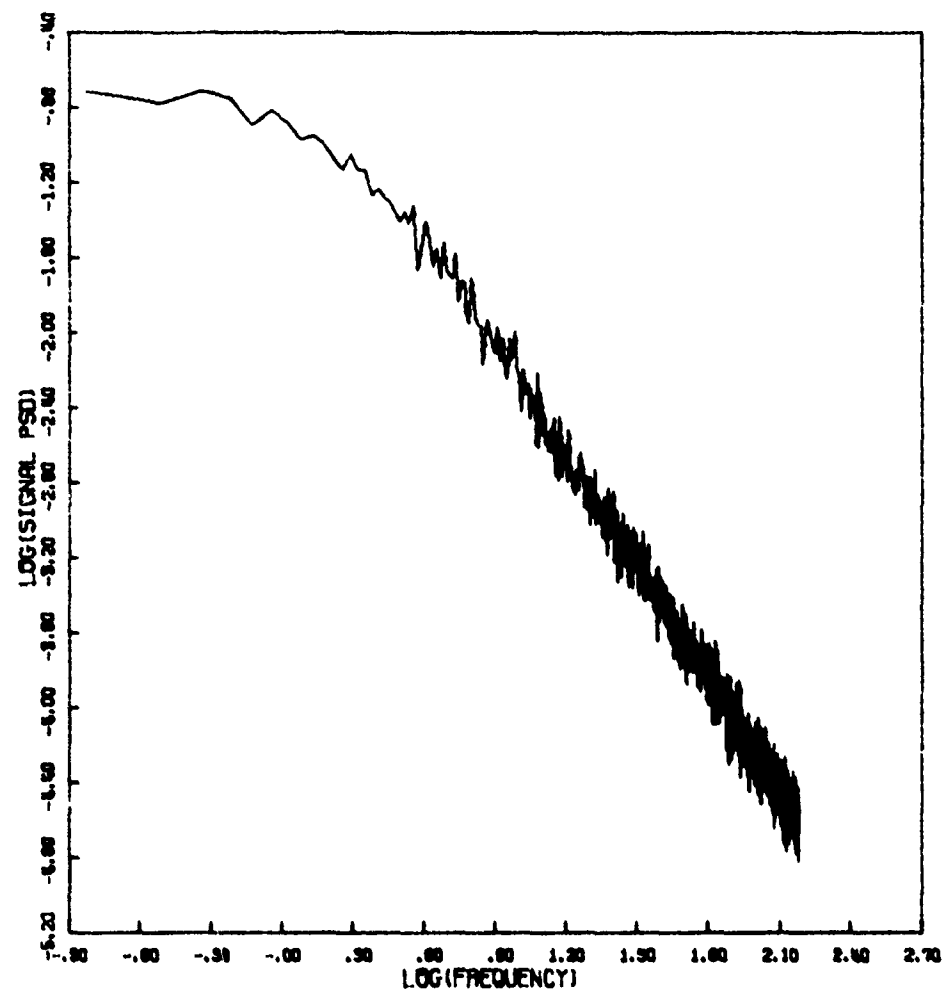
Figure 13e.   Signal Power Spectral Density
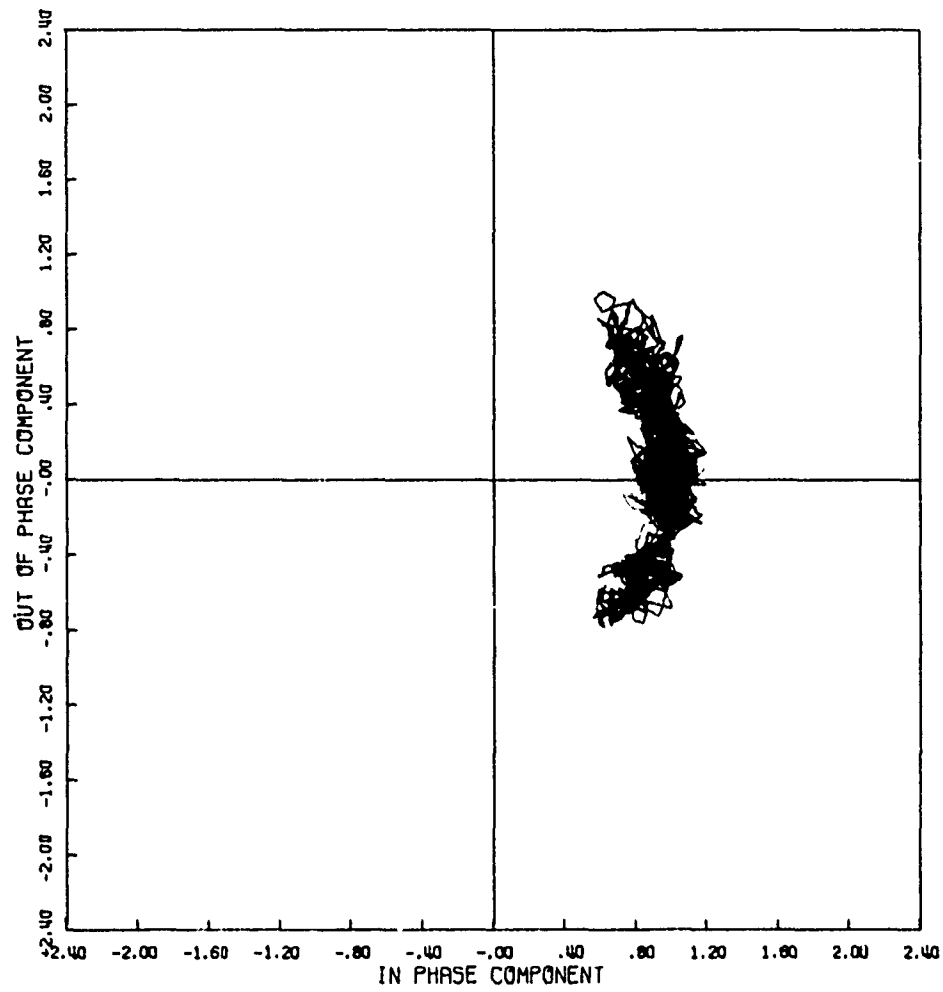
Figure 14a. Signal Phase Plot
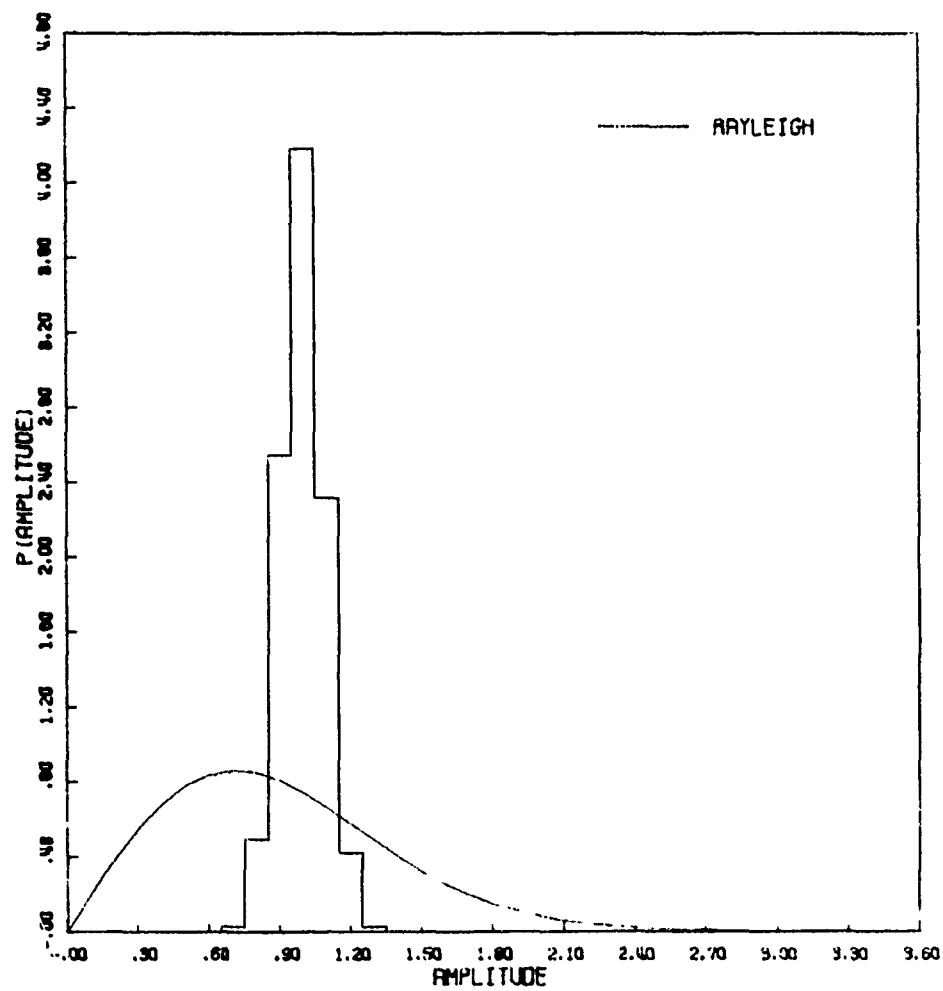
Figure 14b.   Amplitude Distribution
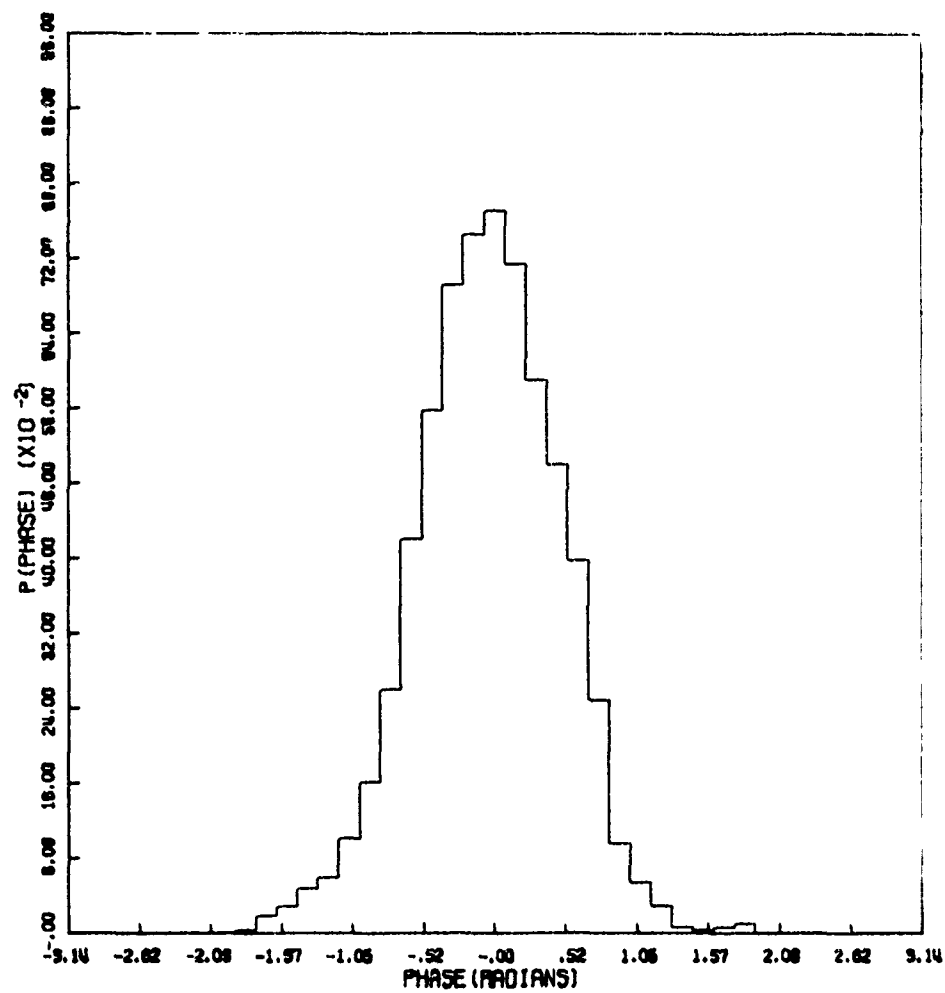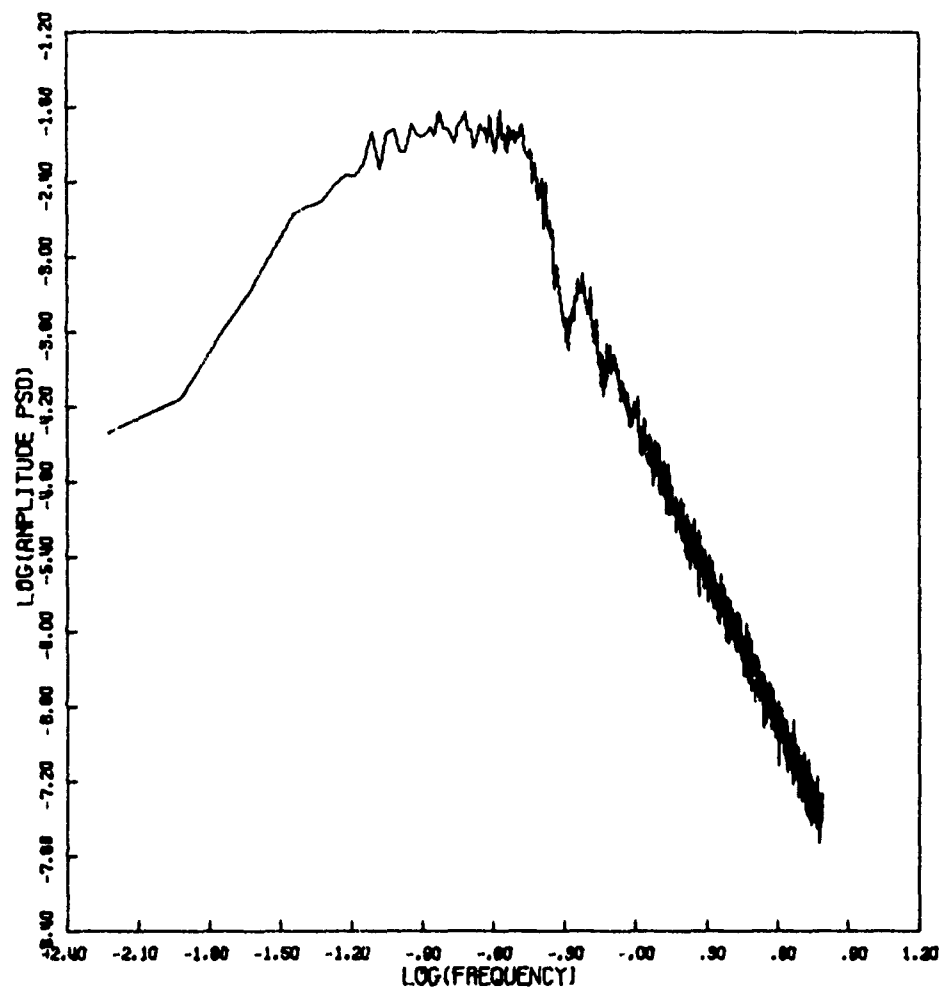
Figure 14c. Phase Distribution
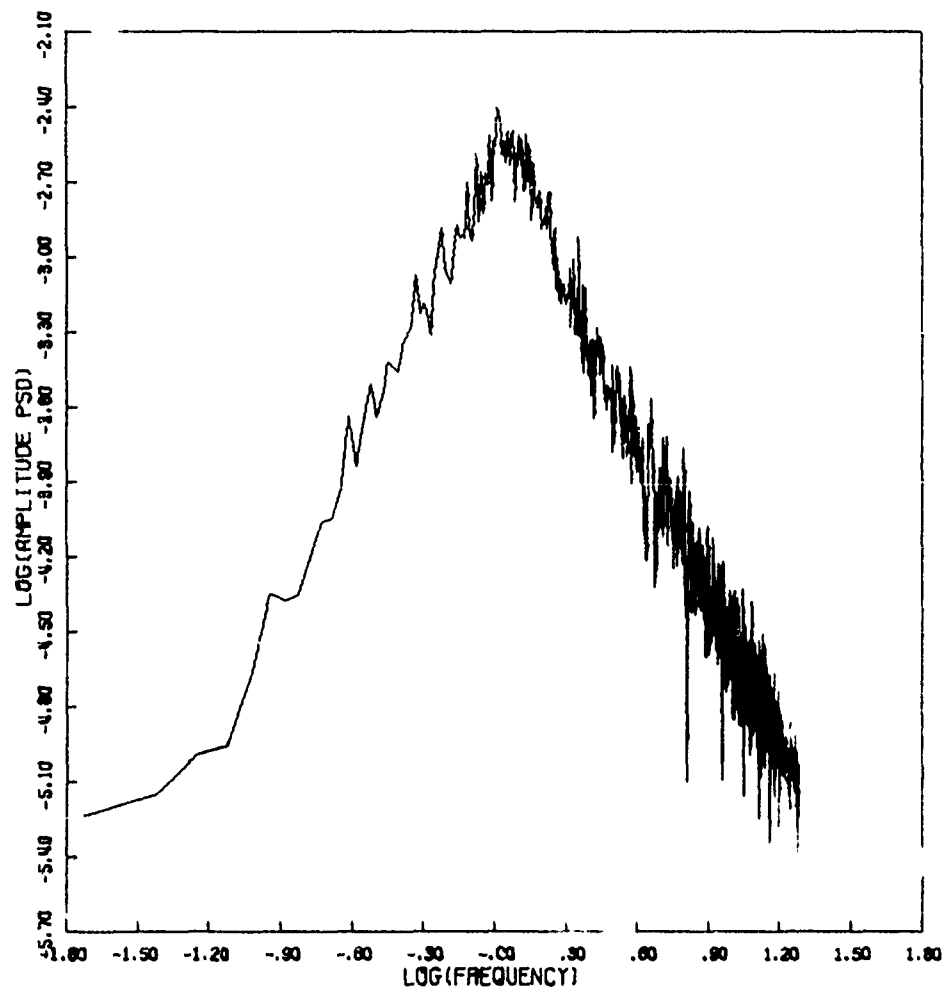
Figure 14d. Amplitude Power Spectral Density
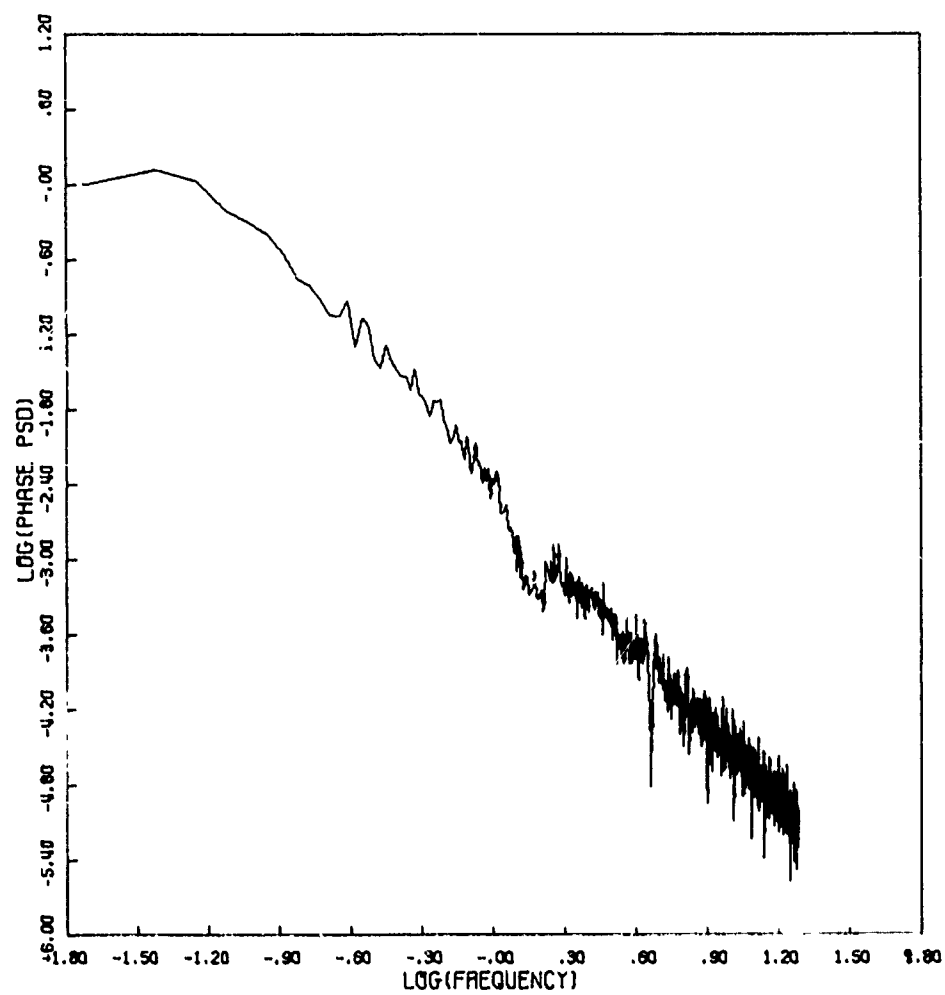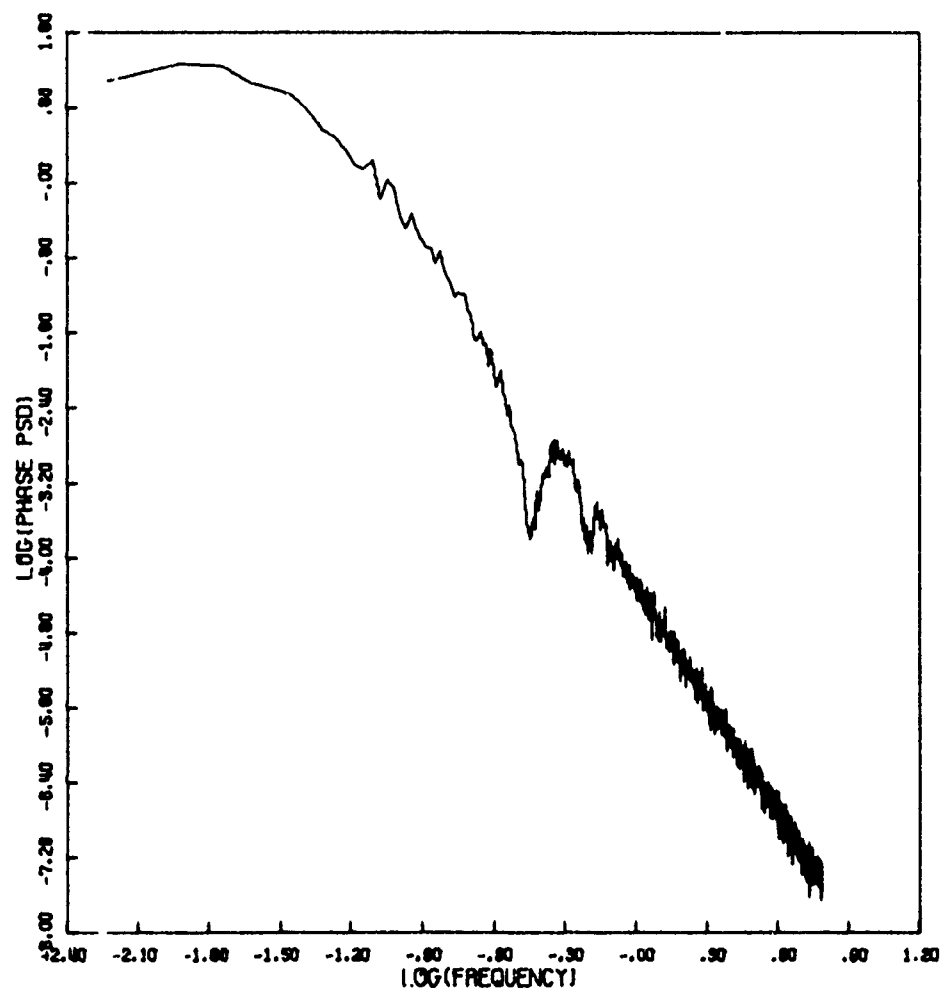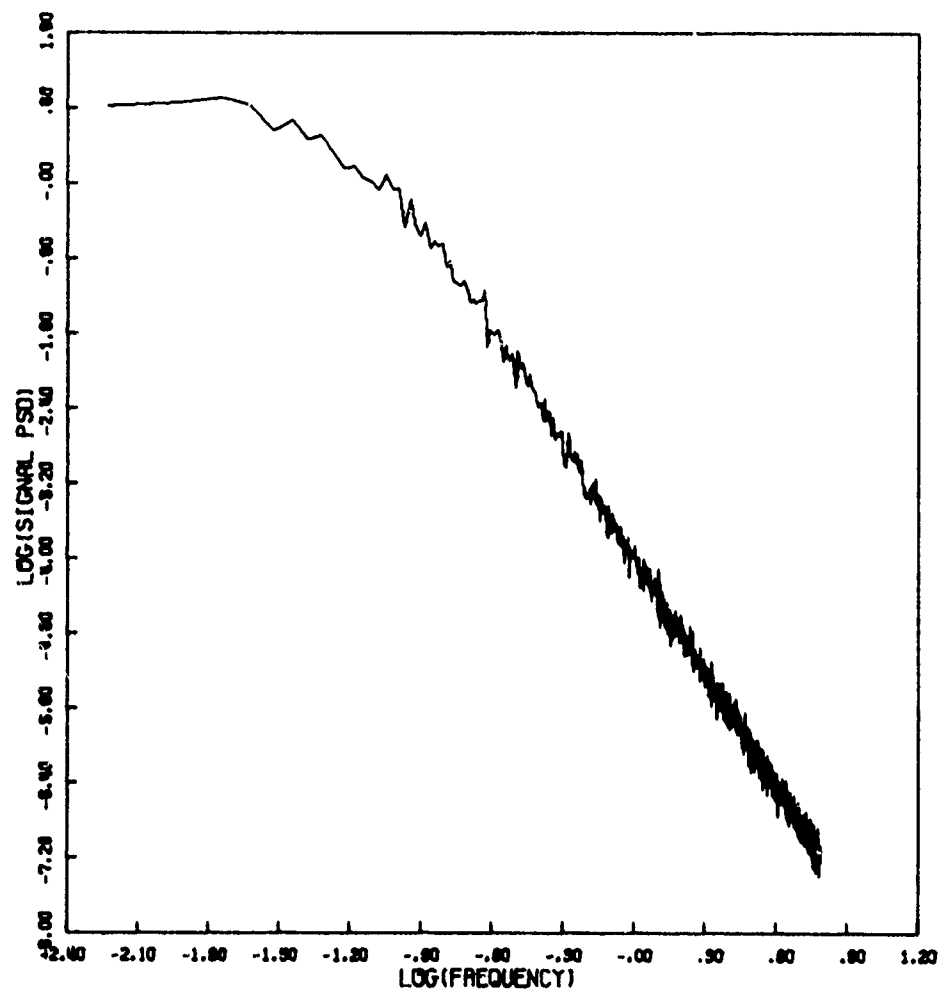
Figure 14e.   Phase Power Spectral Density
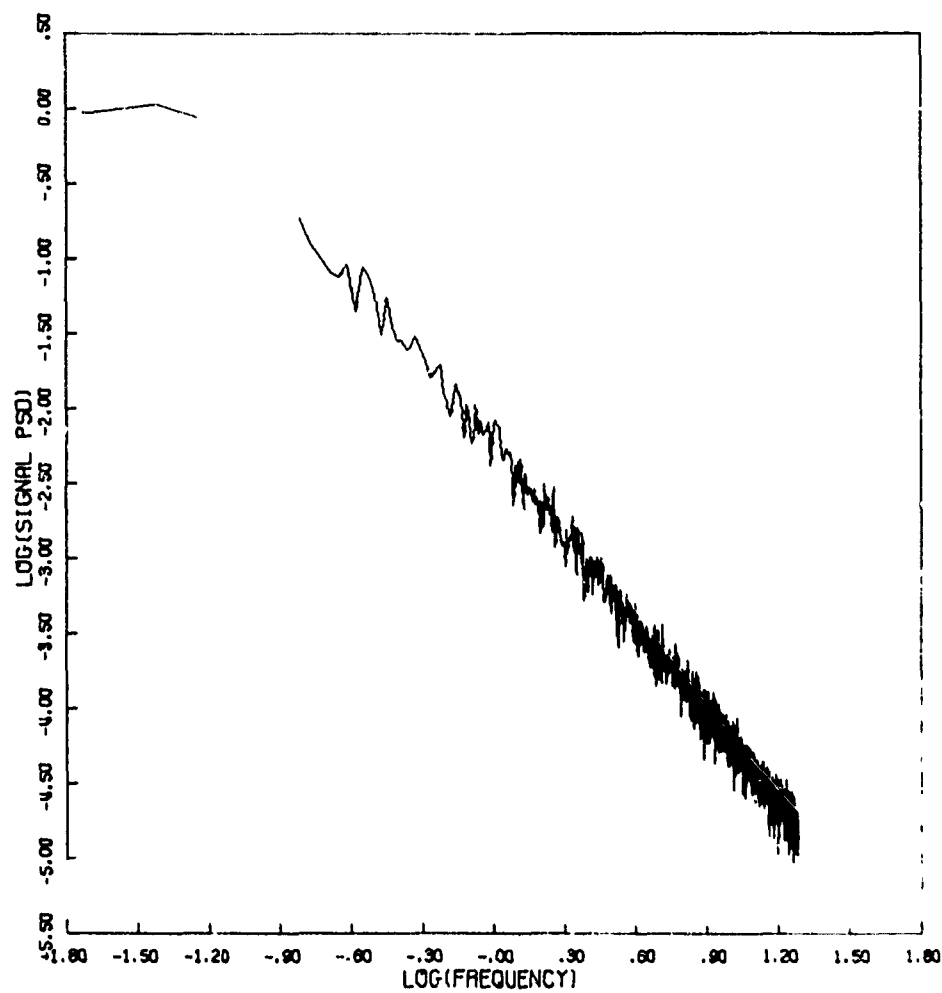
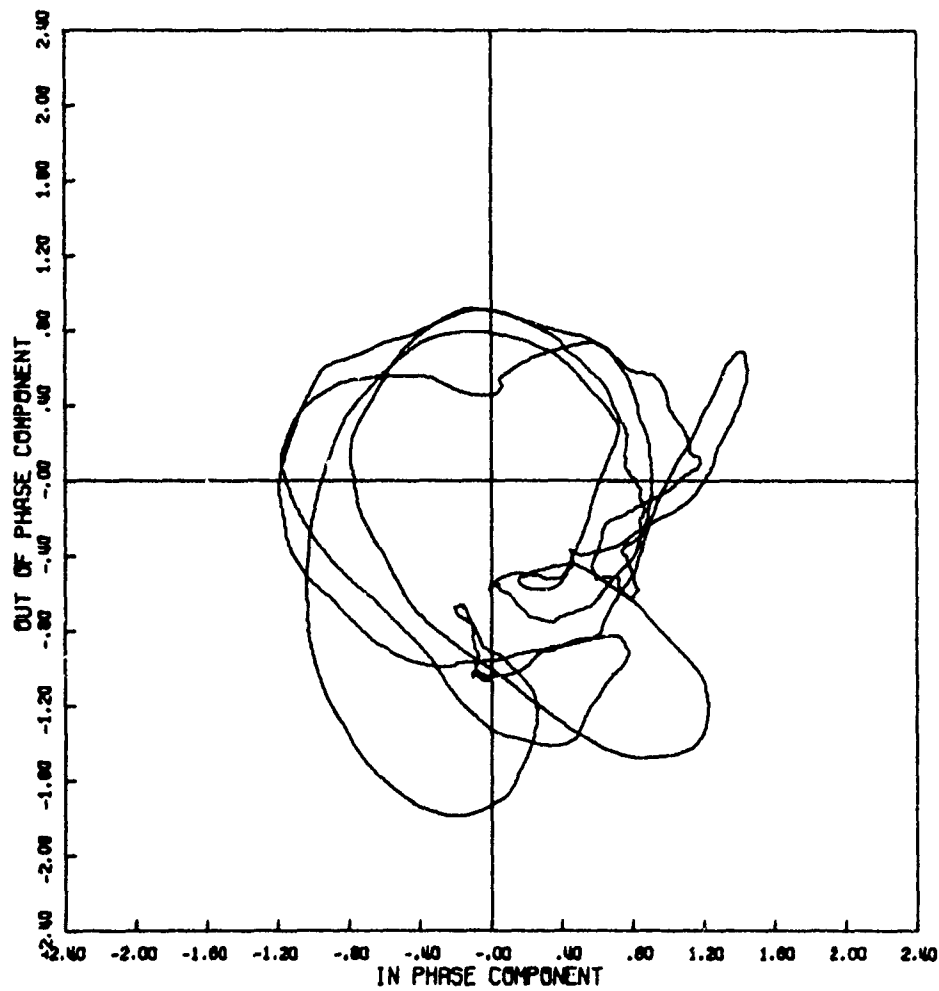Figure 14f.   Signal Power Spectral Density
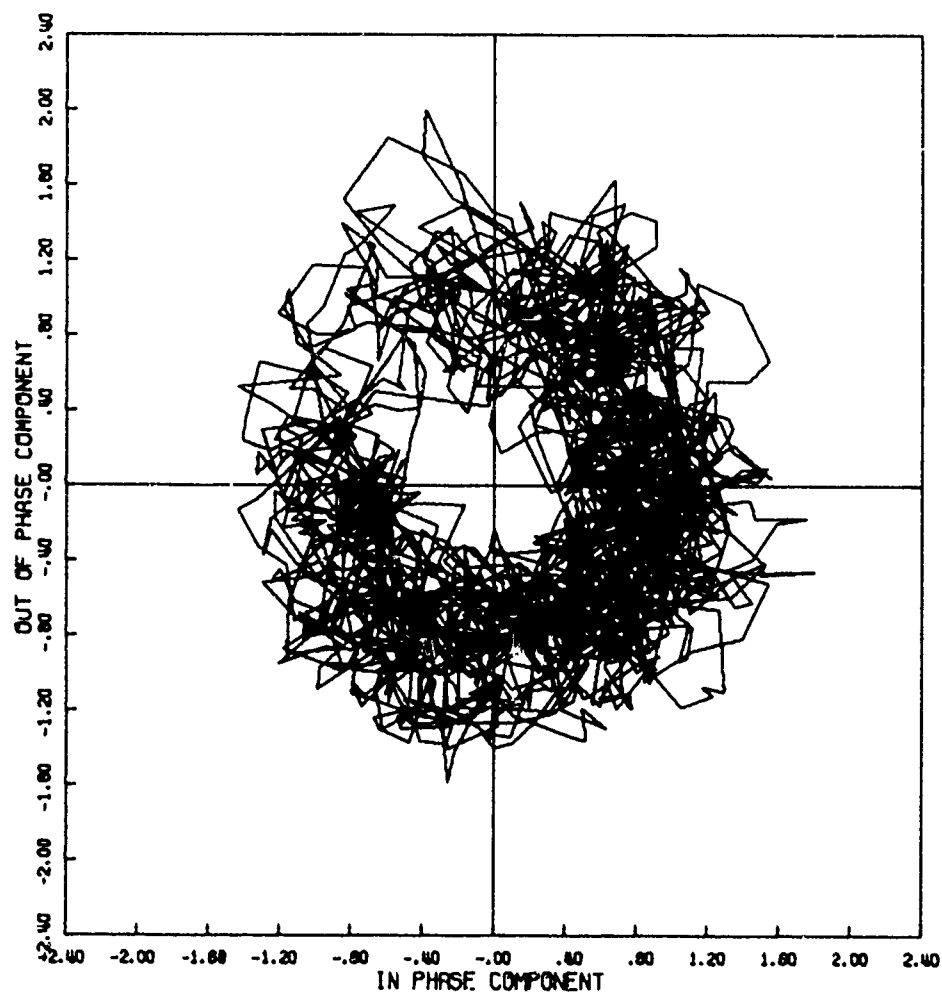
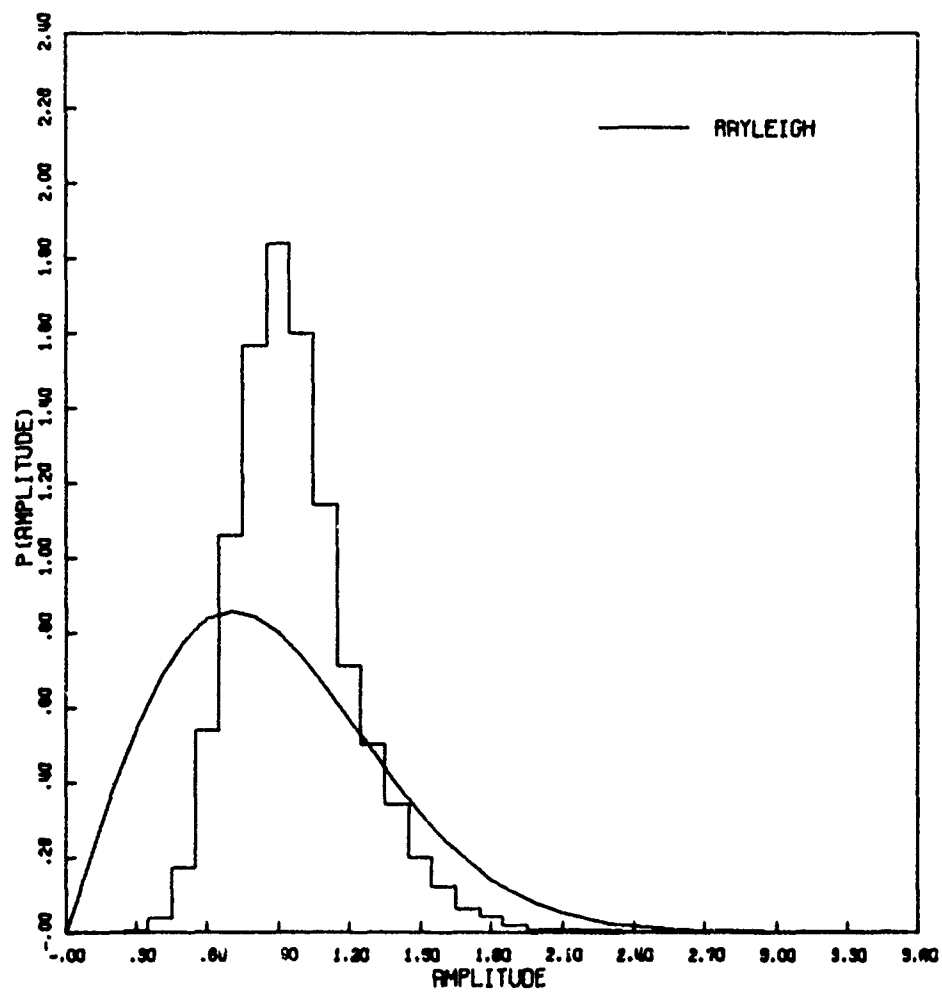Figure 15a.   Signal Phase Plot
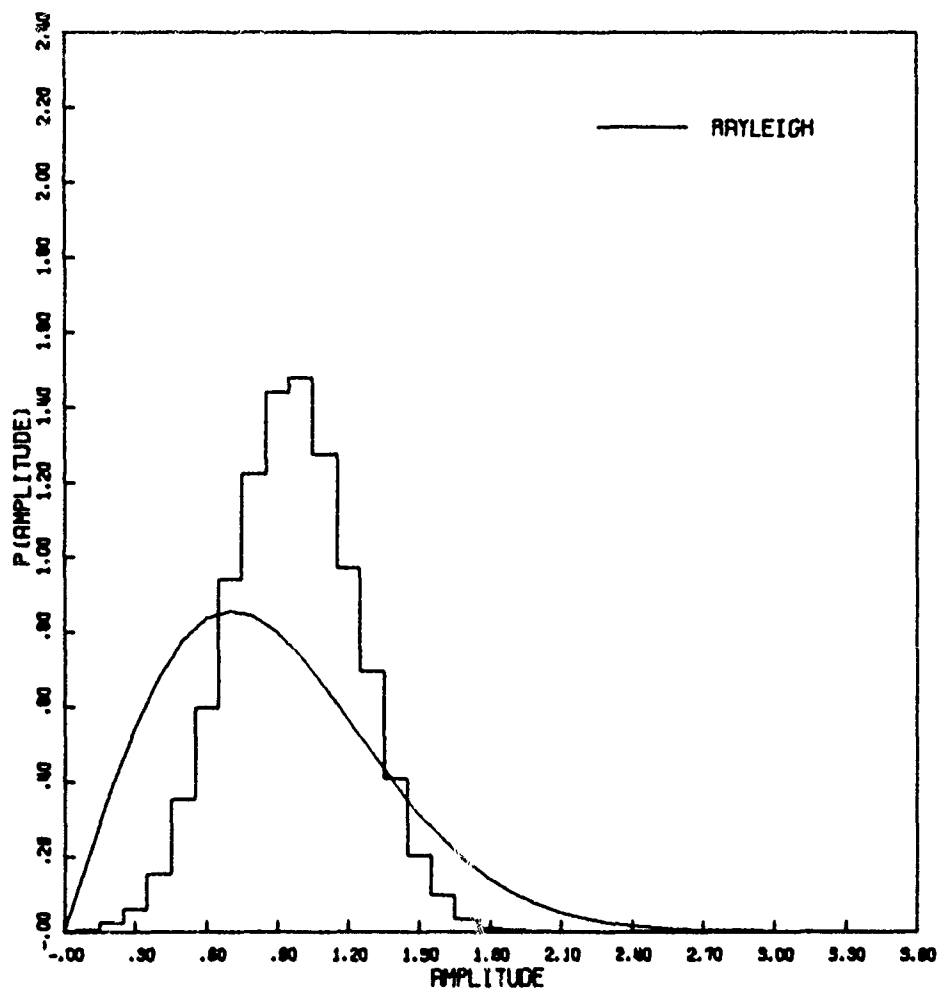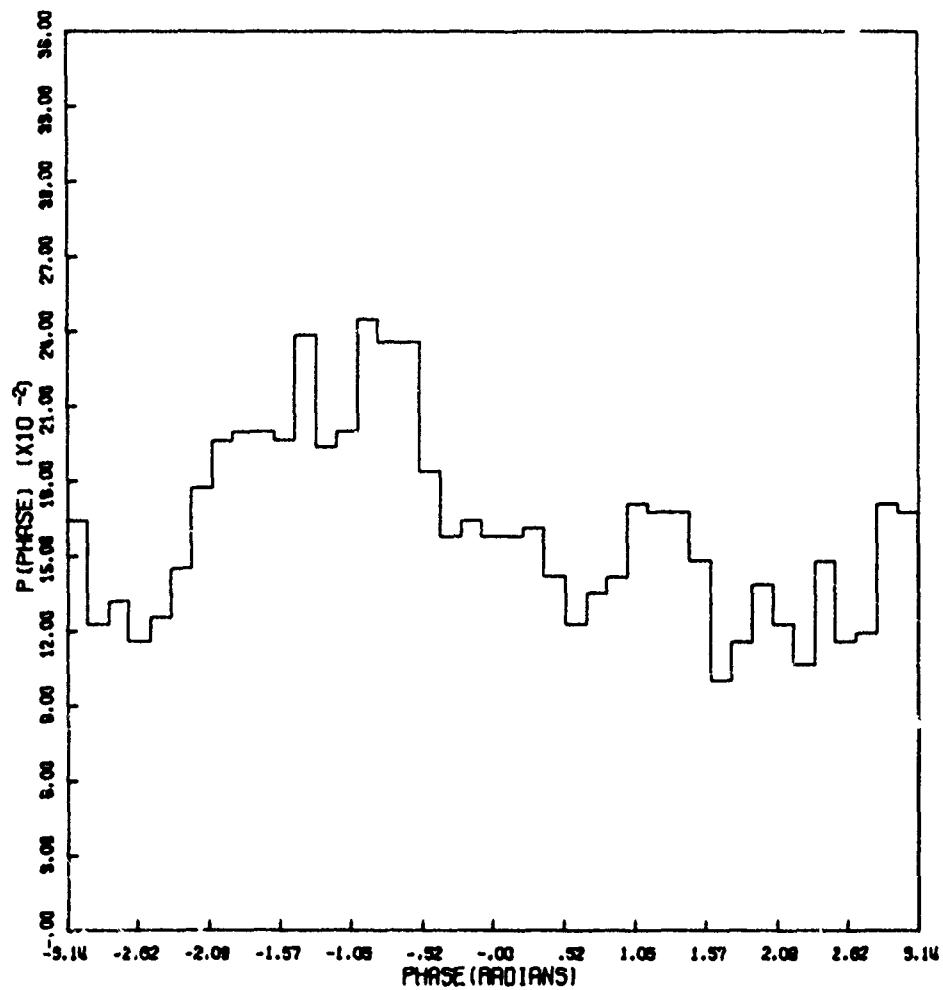
Figure 15b. Amplitude Distribution
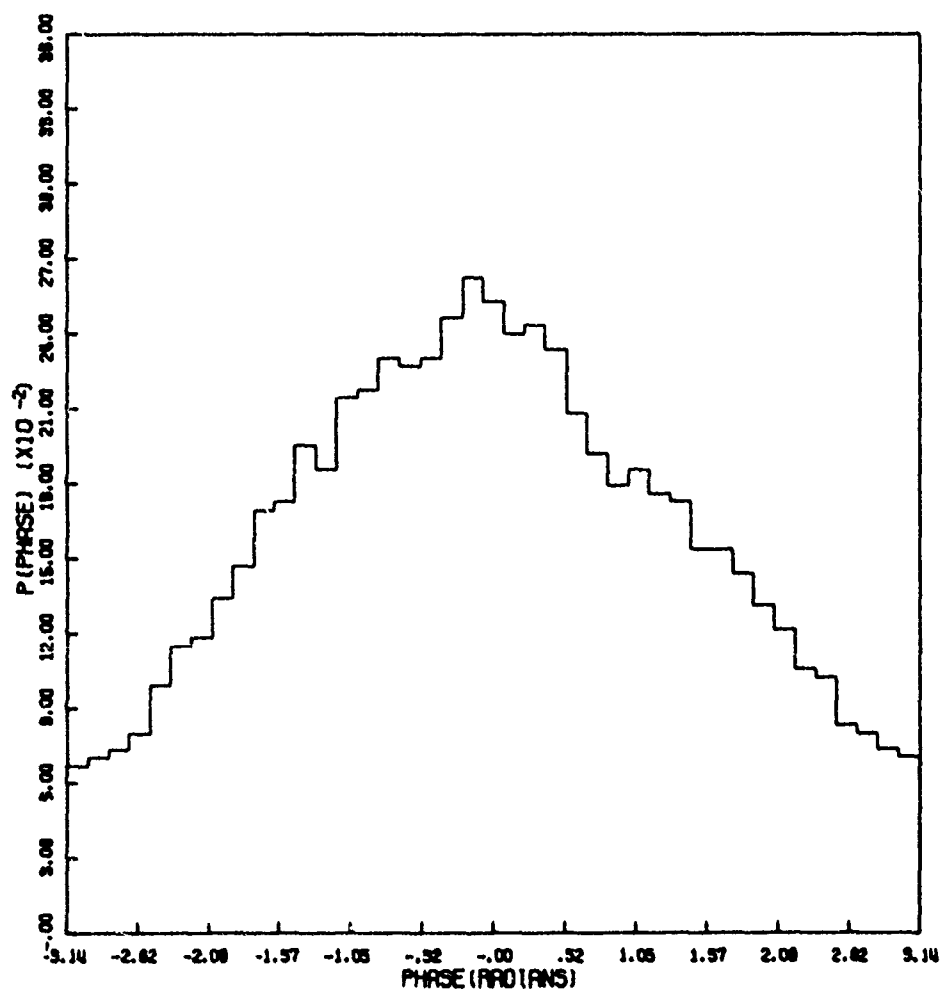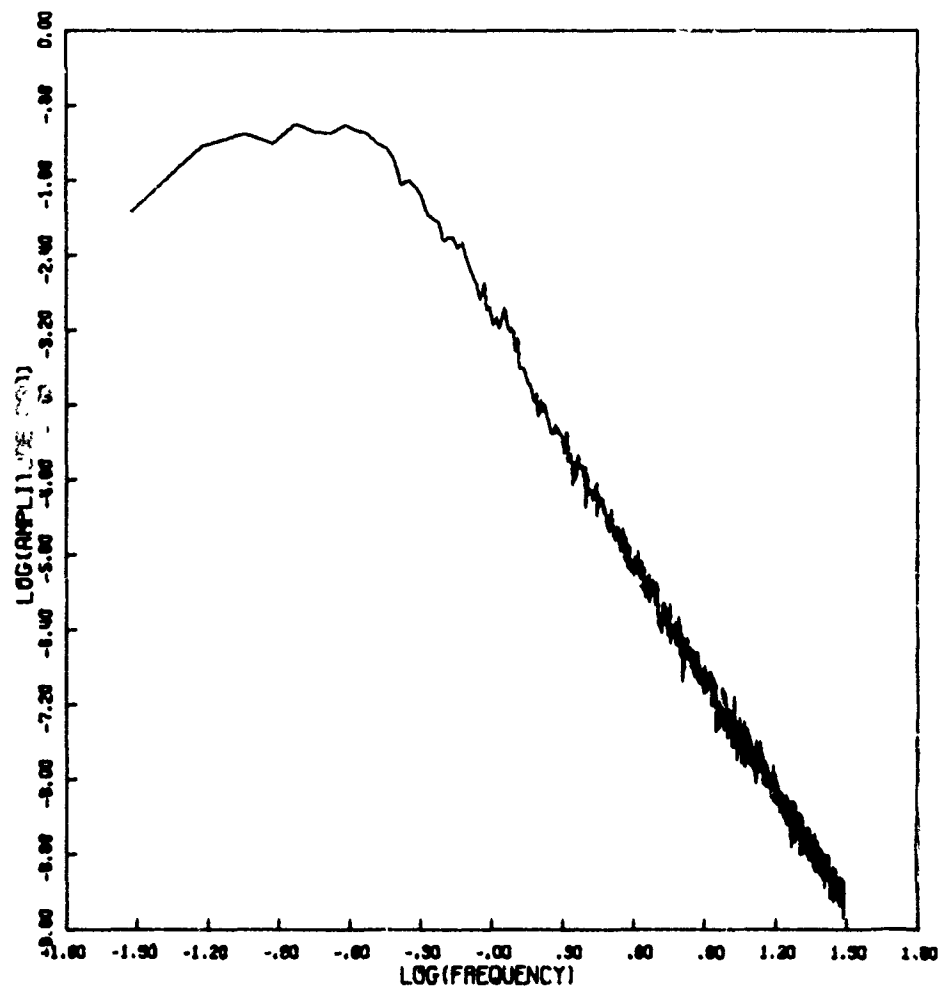
Figure 15c. Phase Distribution
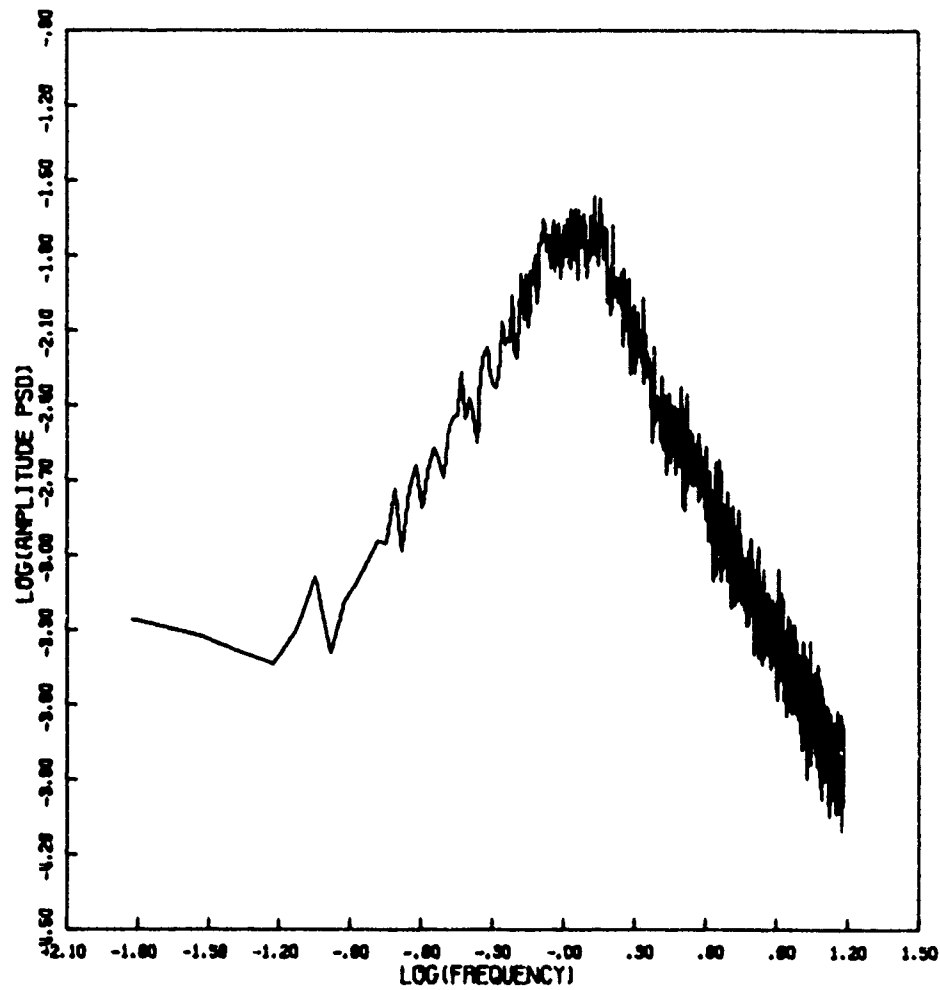
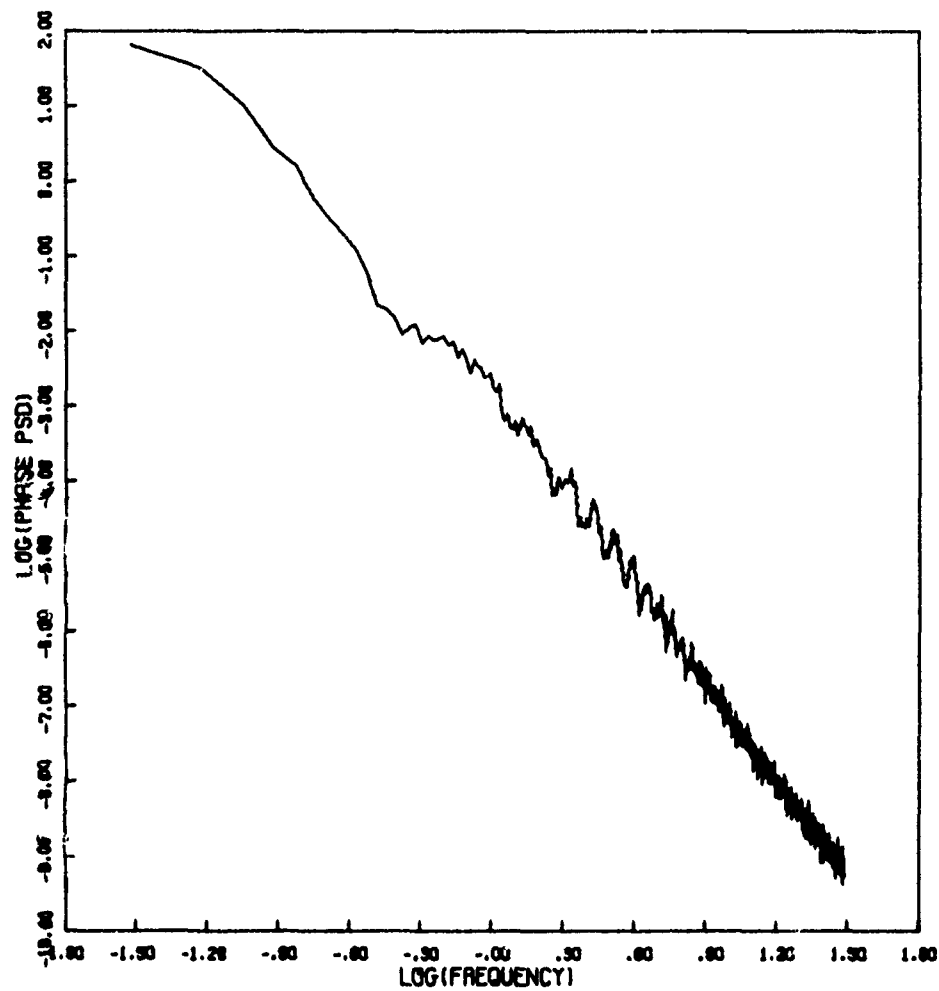Figure 15d.   Amplitude Power Spectral Density
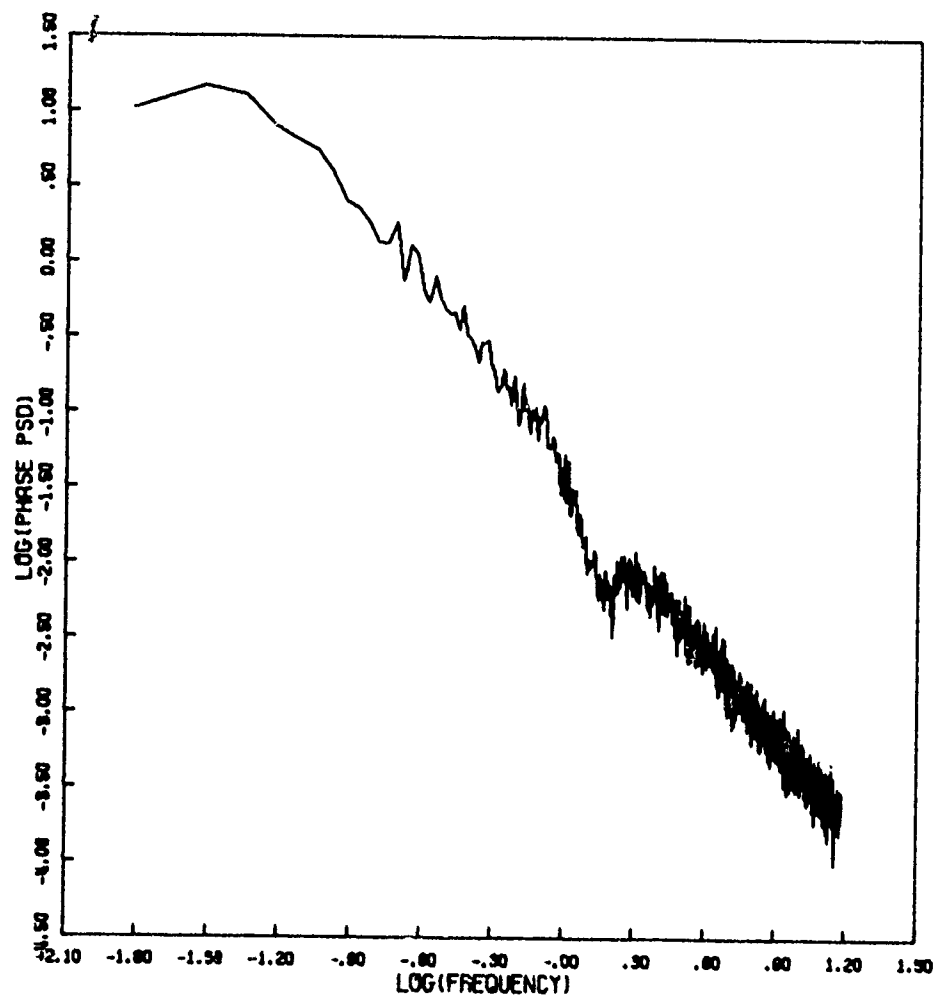
Figure 15e.   Phase Power Spectral Density
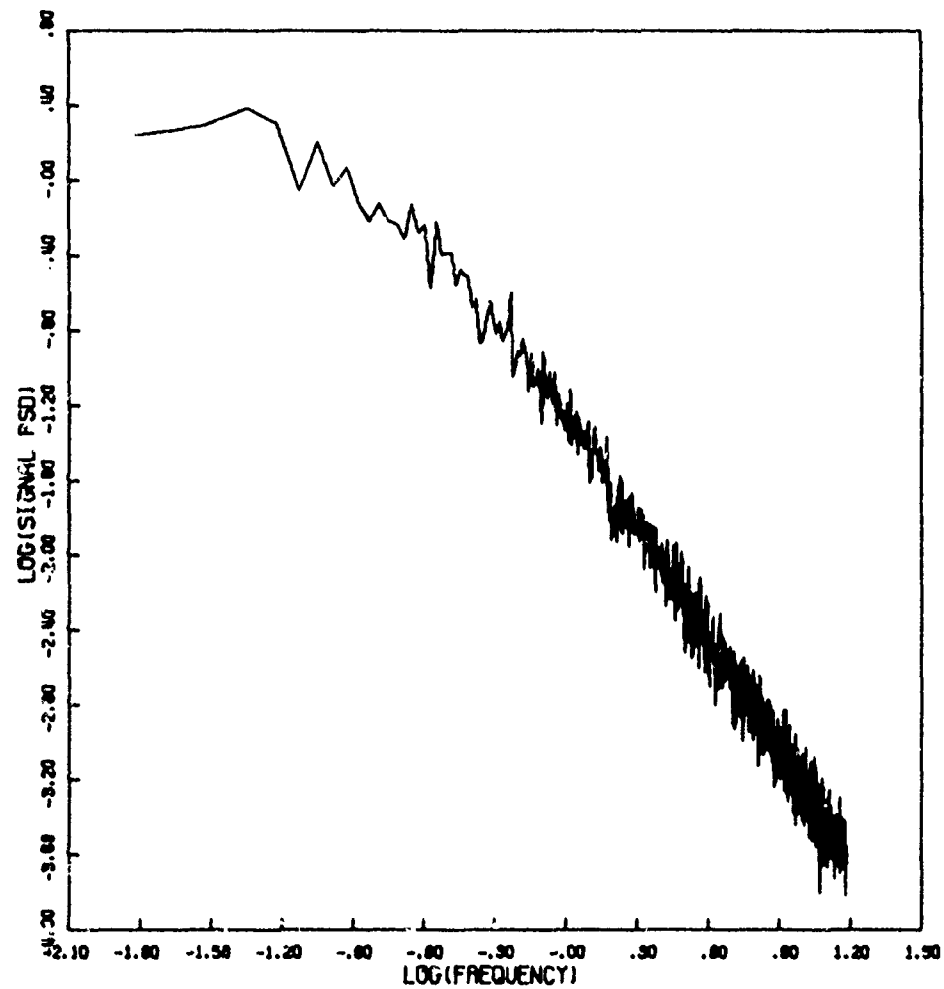
Figure 15f. Signal Power Spectral Density
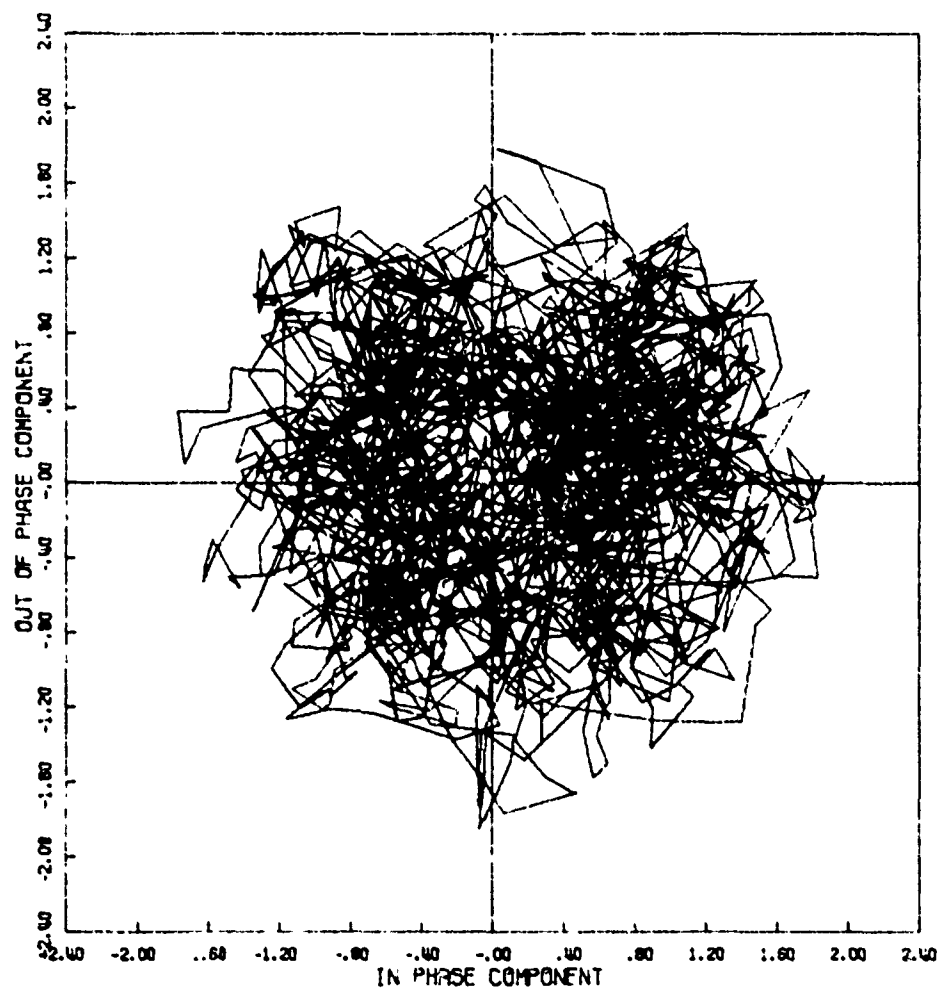
Figure 16a. Signal Phase Plot
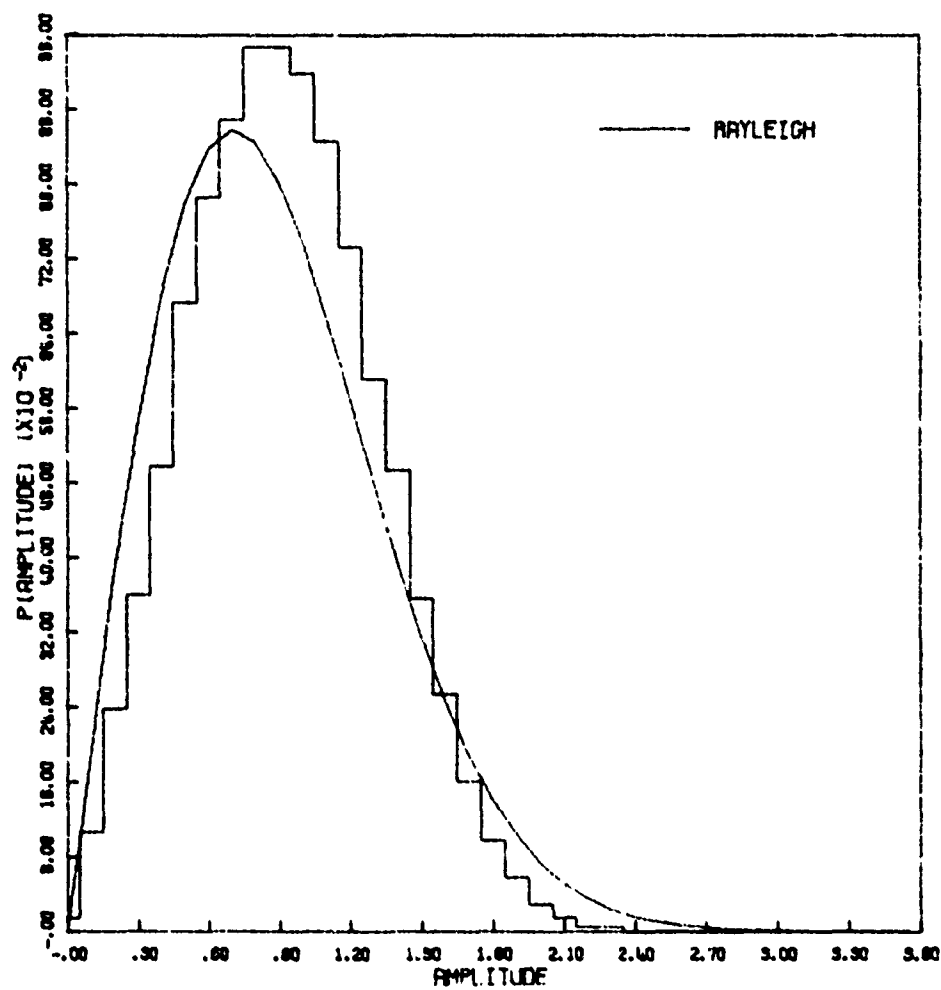
Figure 16b. Amplitude Distribution
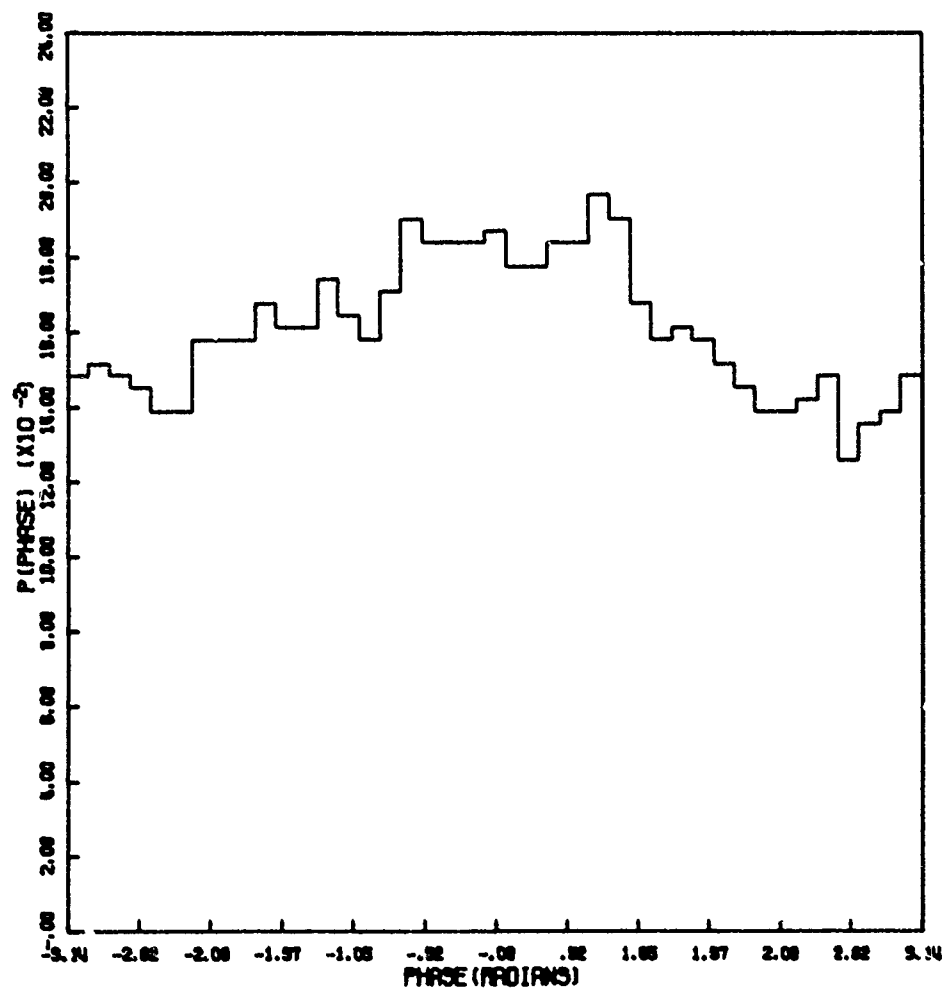
Figure 16c. Phase Distribution
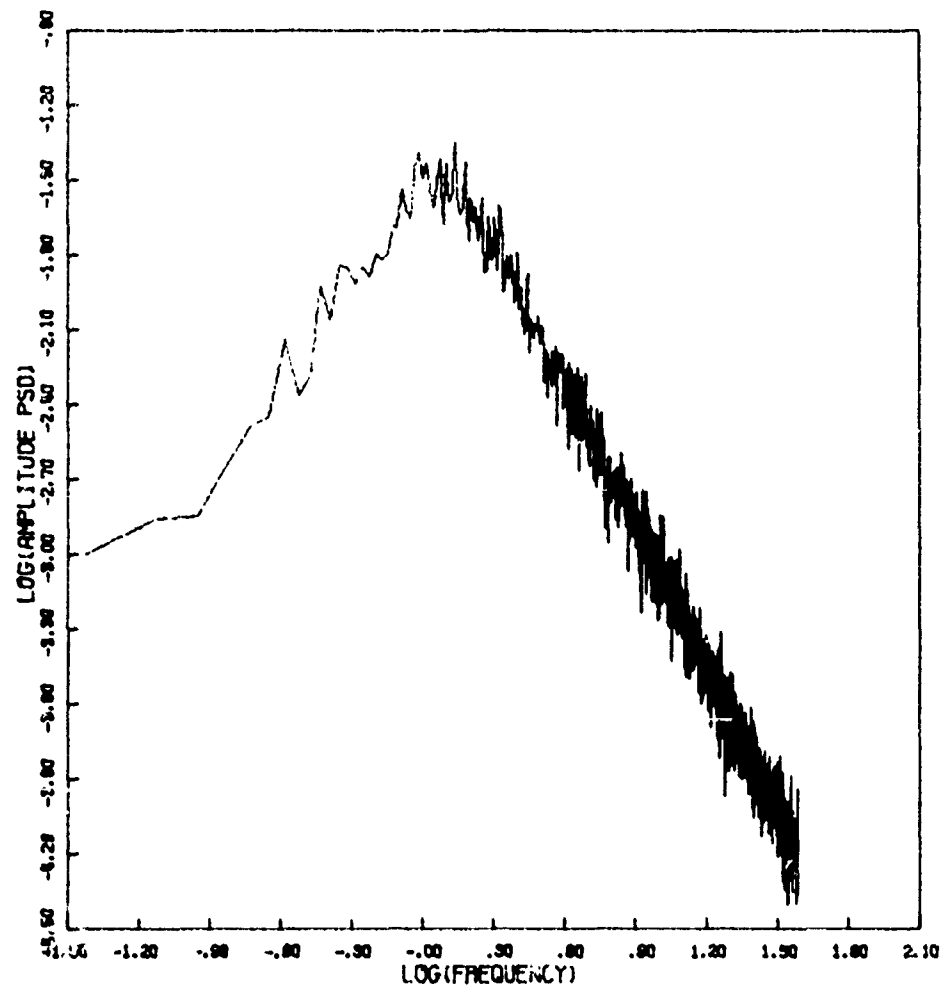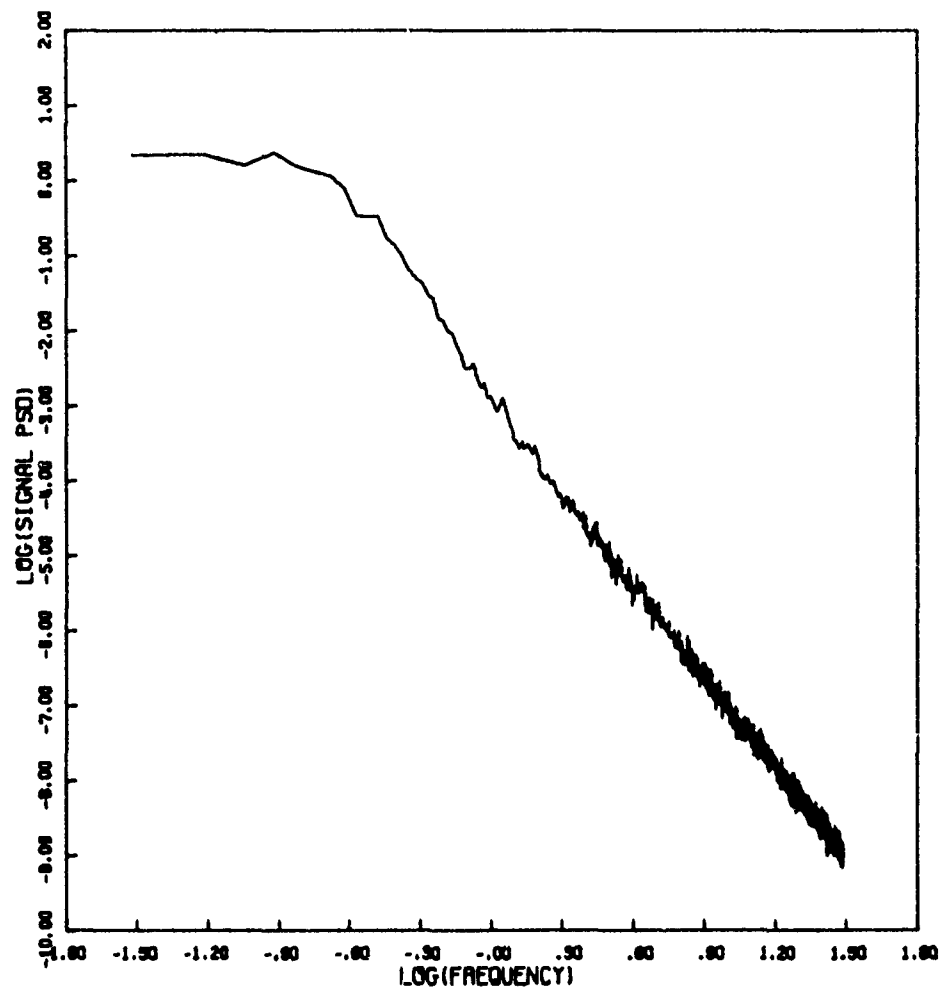
Figure 16d.   Amplitude Power Spectral Density
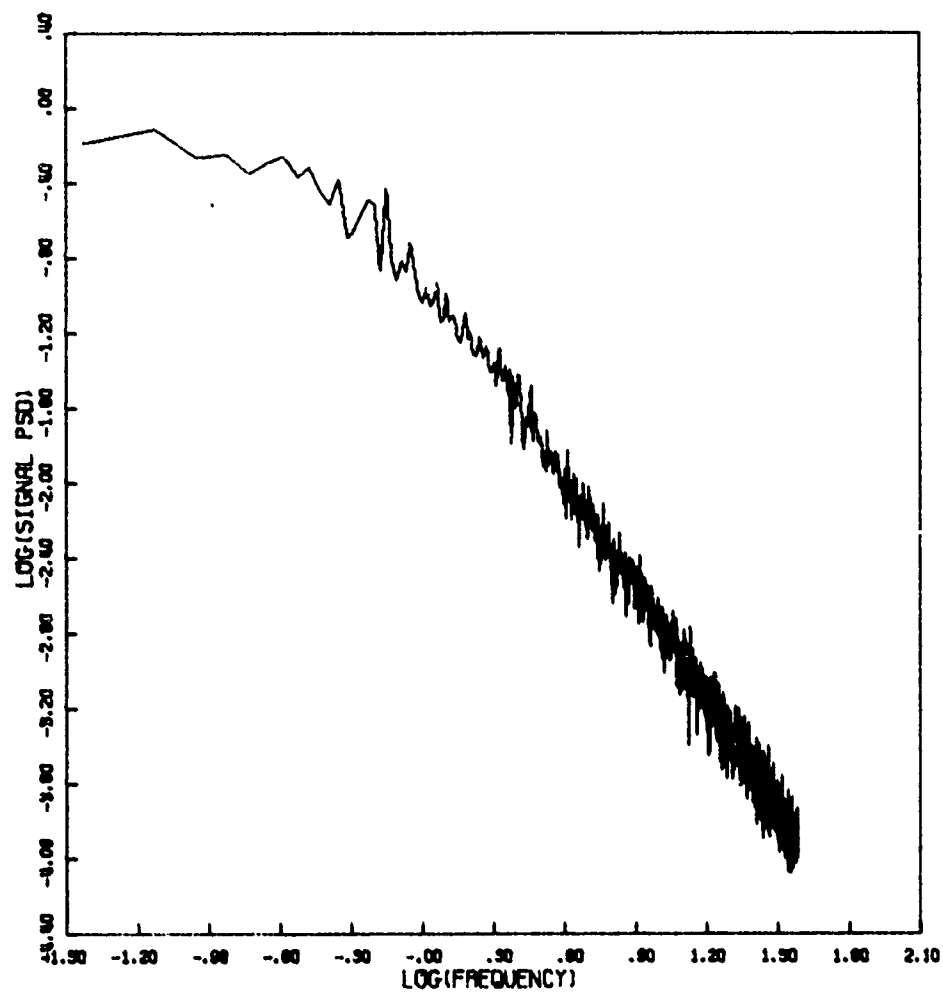
Figure 16f. Signal Power Spectral Density
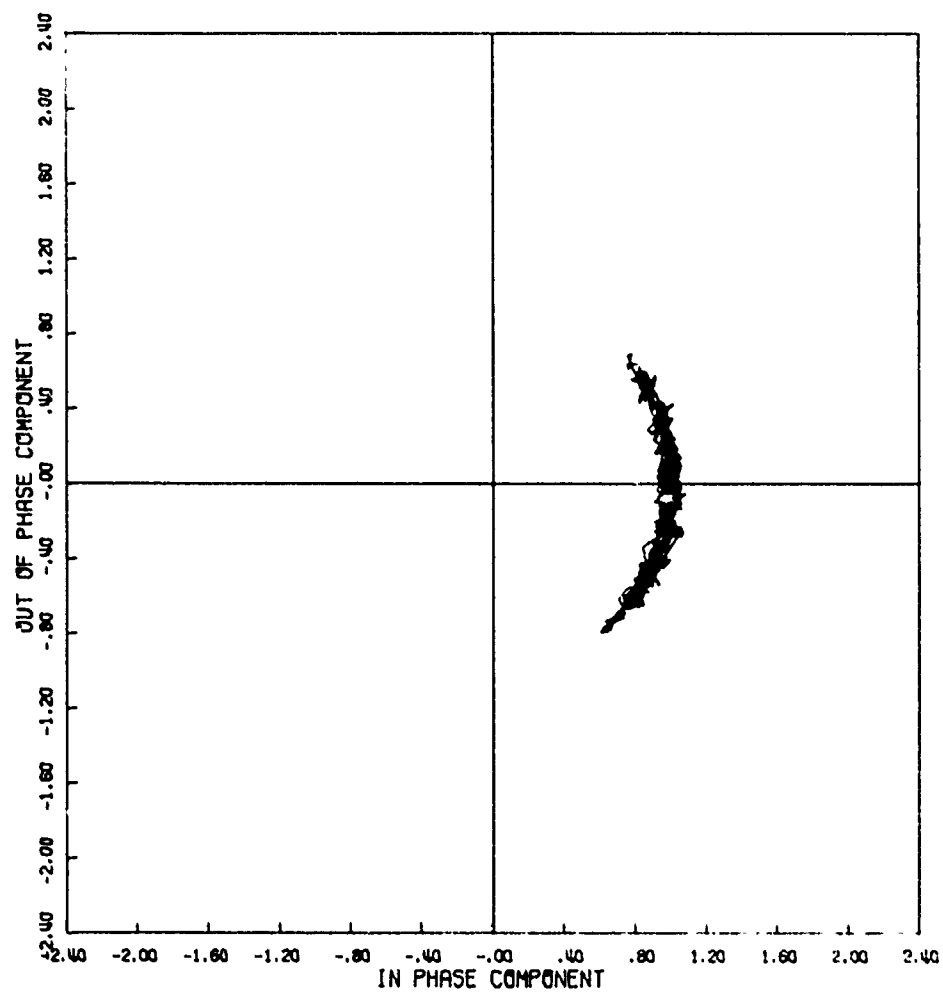
Figure 17a. Signal Phase Plot
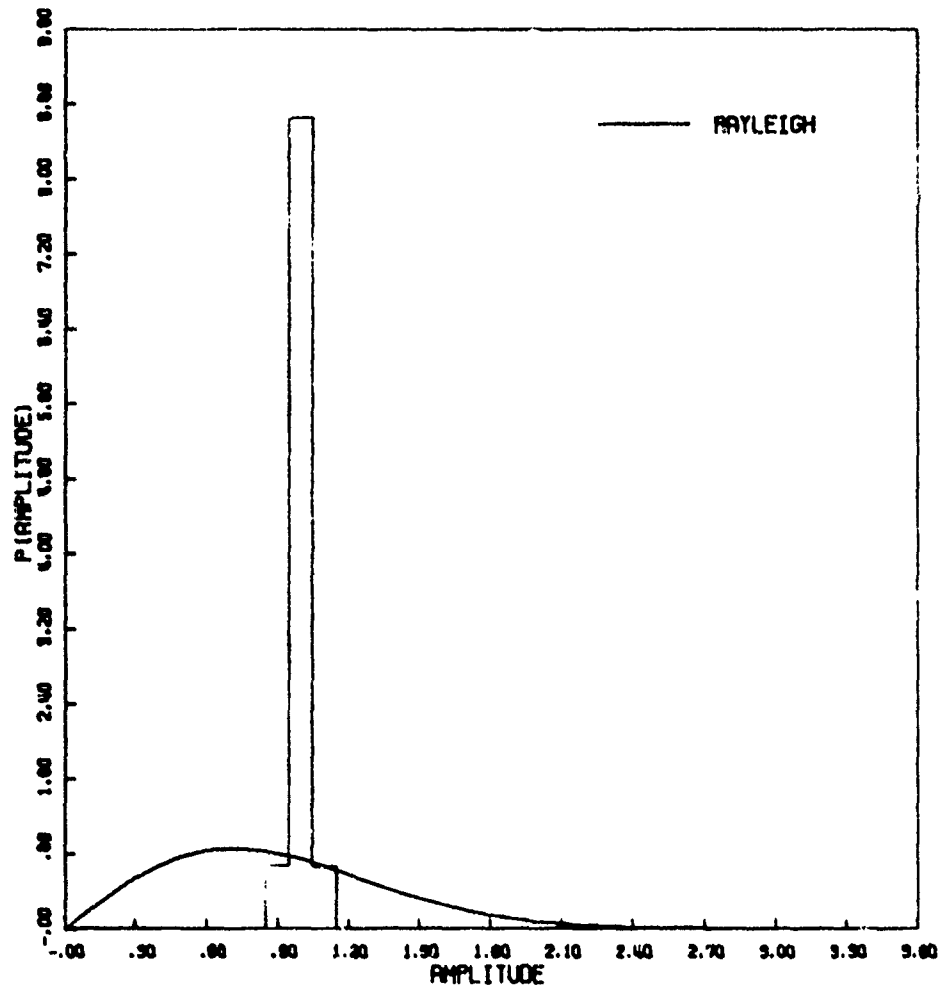
Figure 17b.   Amplitude Distribution
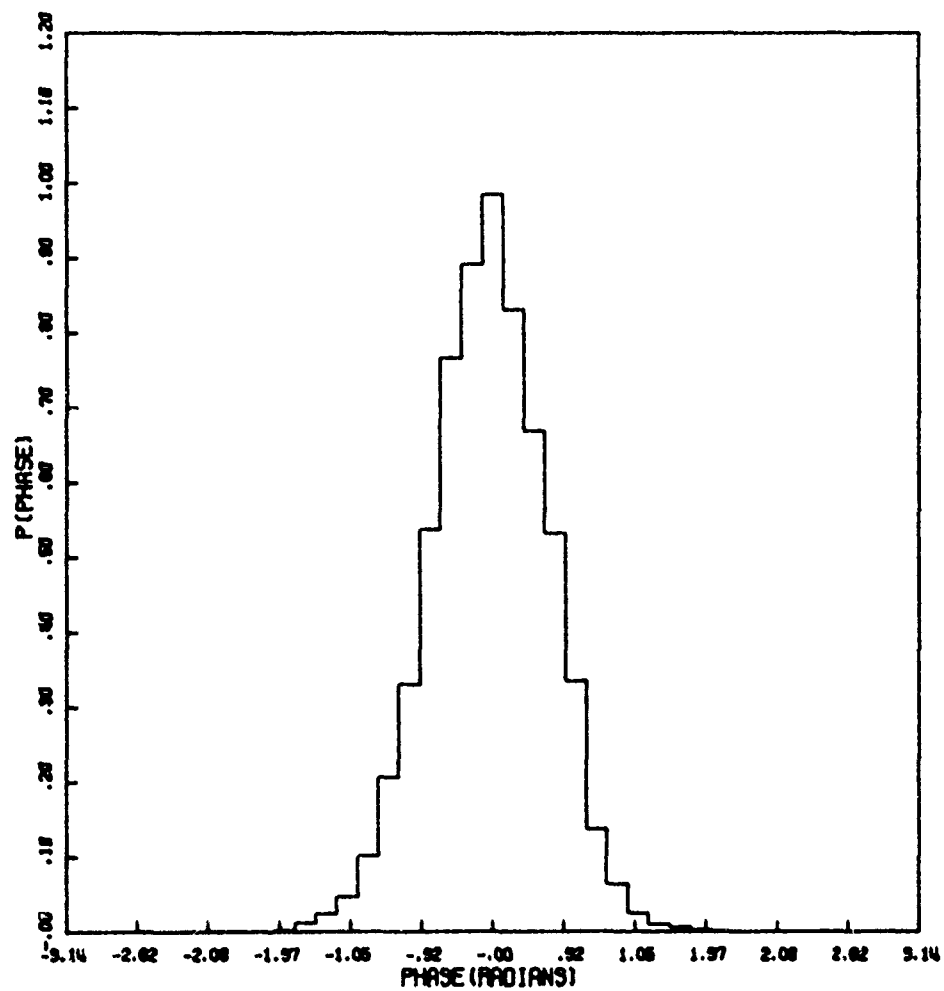
Figure 17c. Phase Distribution
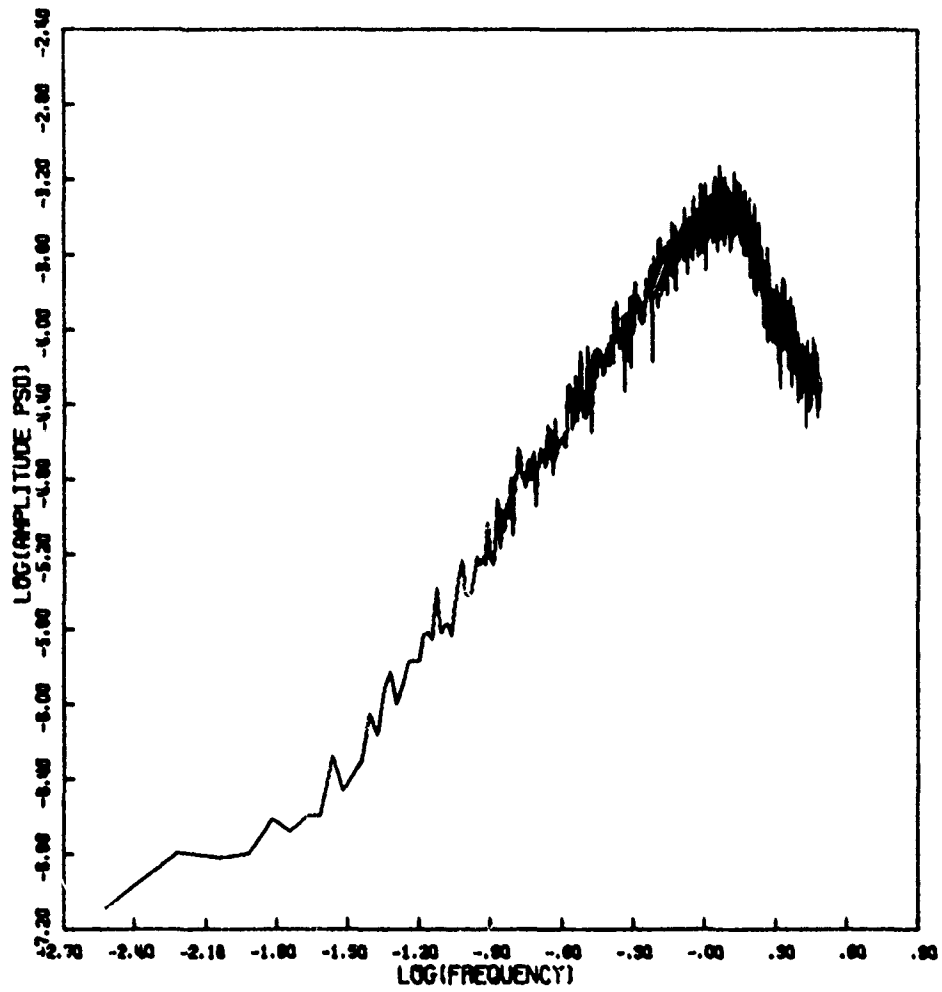
Figure 17d. Amplitude Power Spectral Density
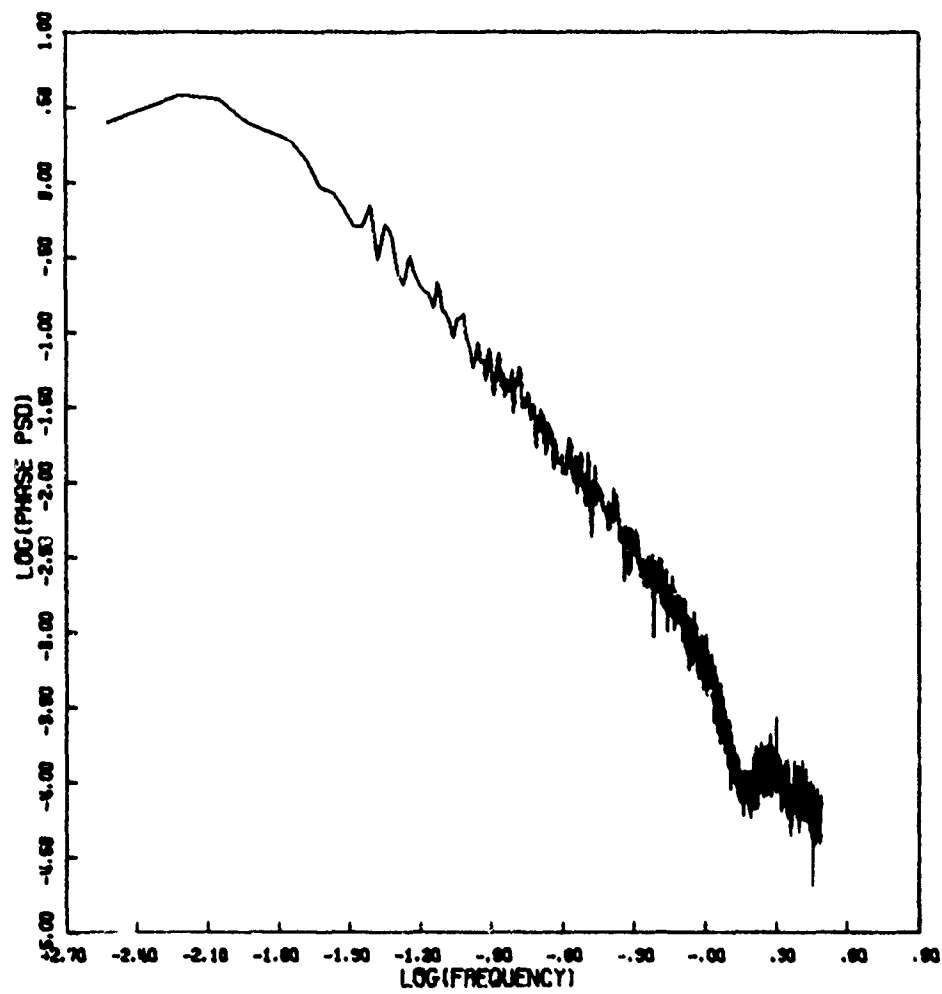
Figure 17e. Phase Power Spectral Density
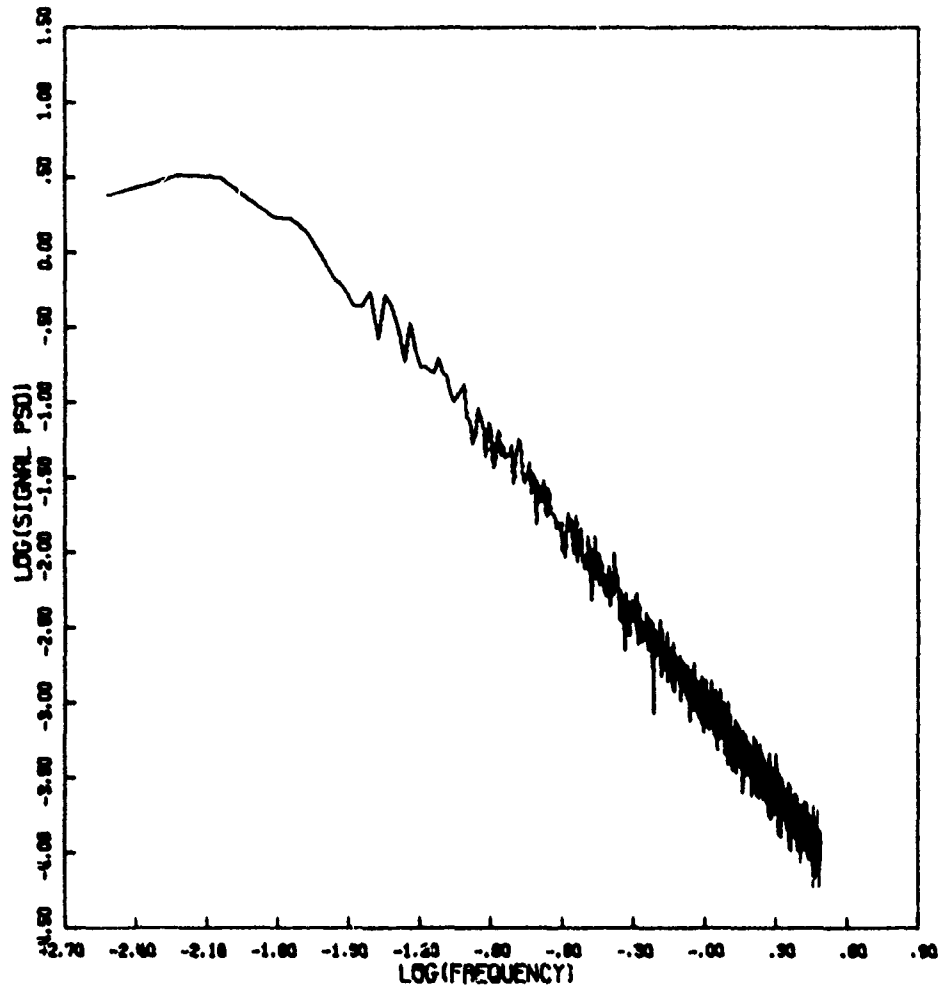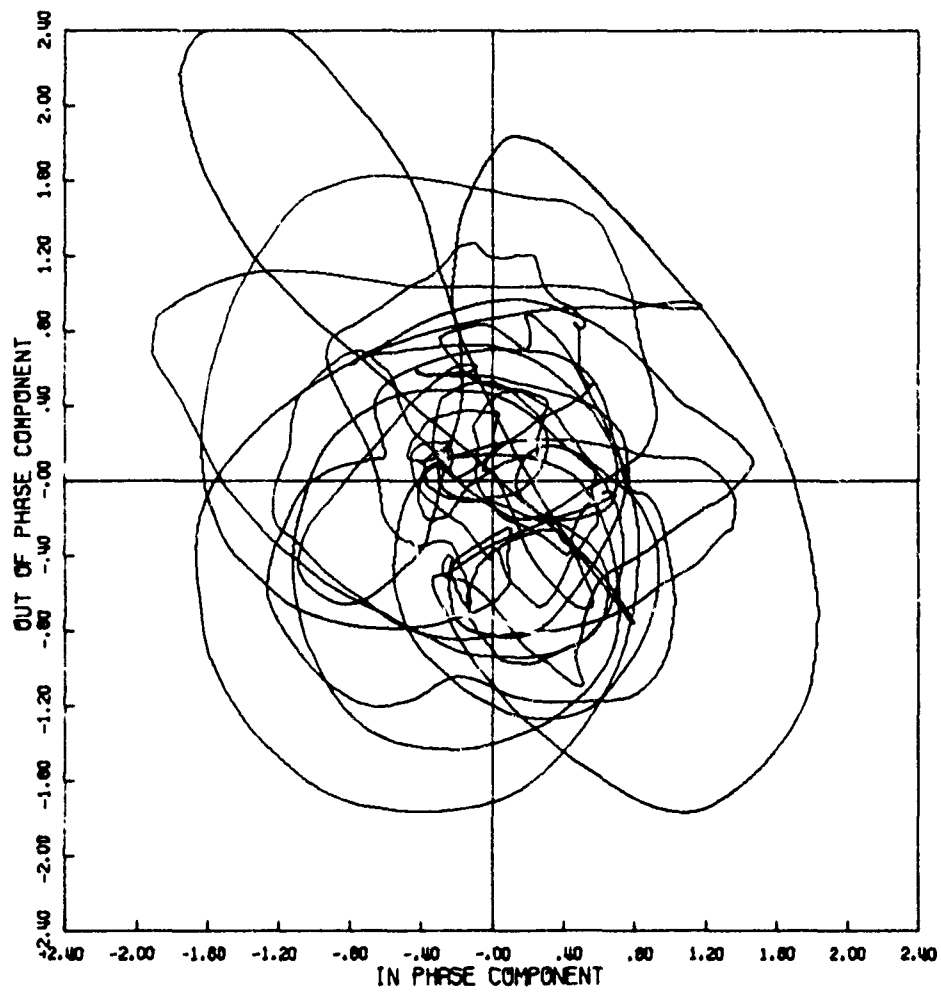
Figure 17f. Signal Power Spectral Density
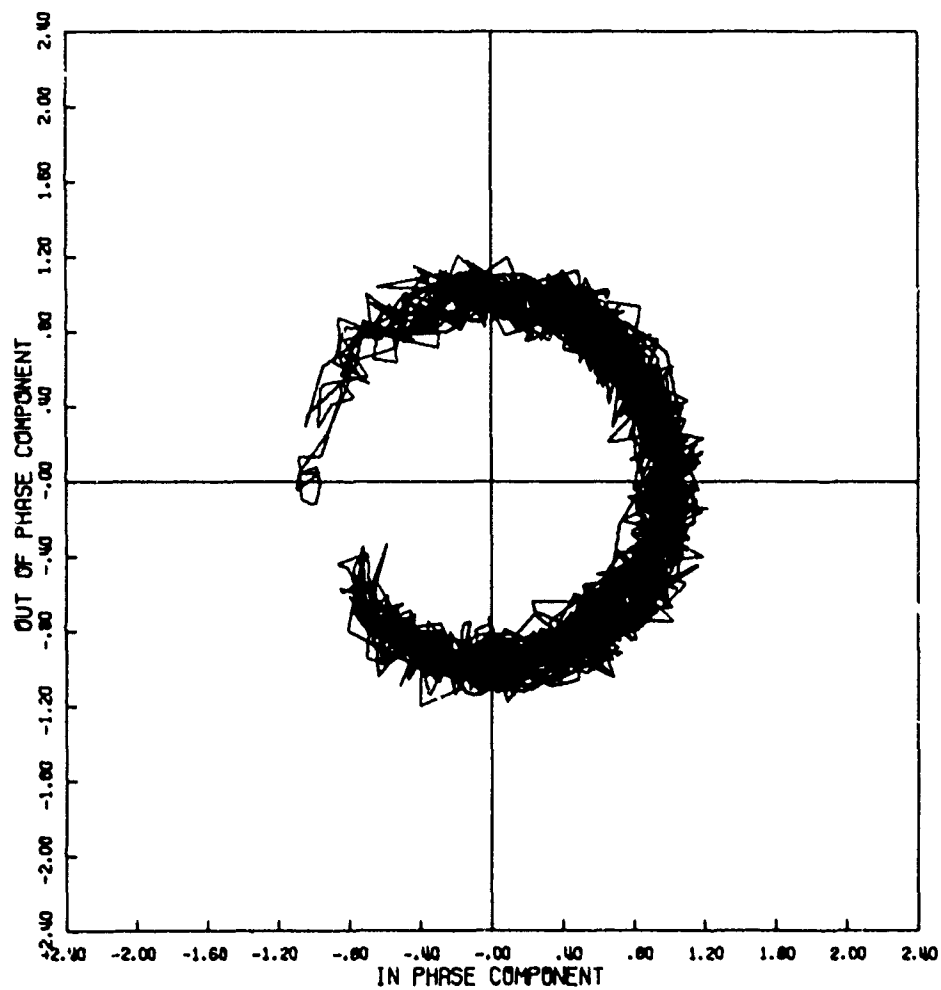
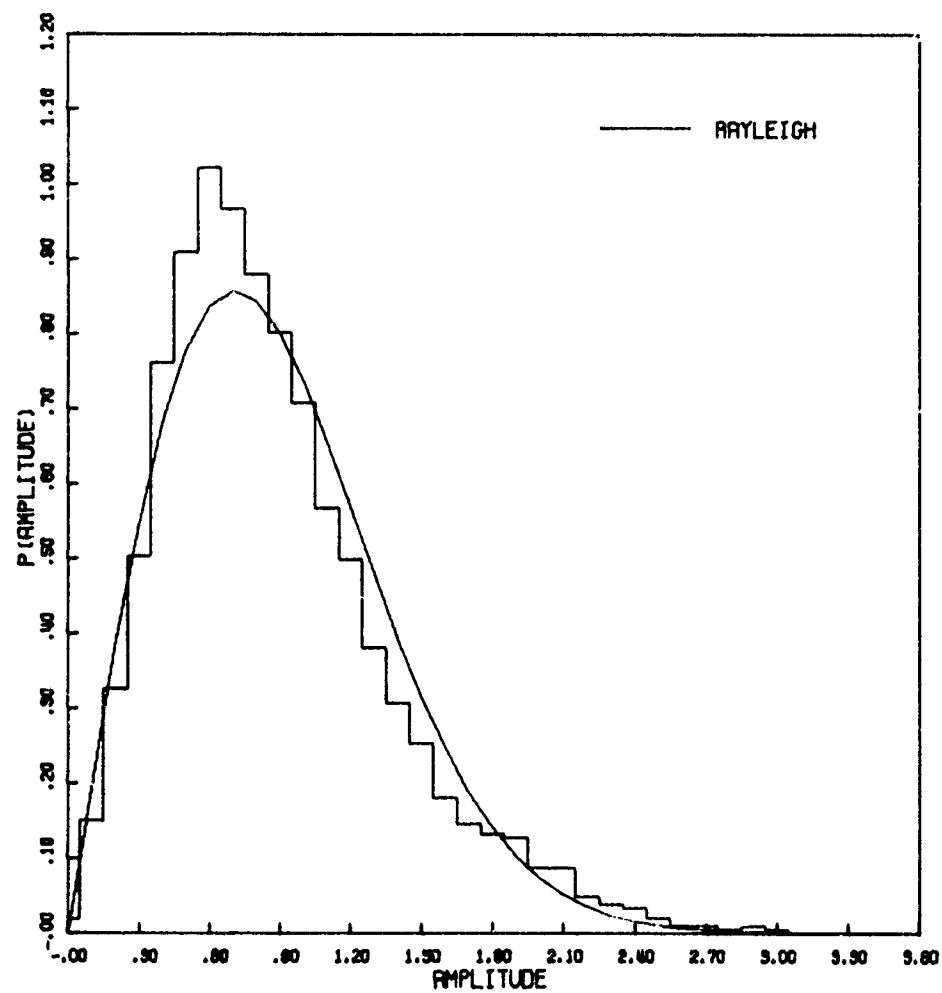Figure 18a. Signal Phase Plot
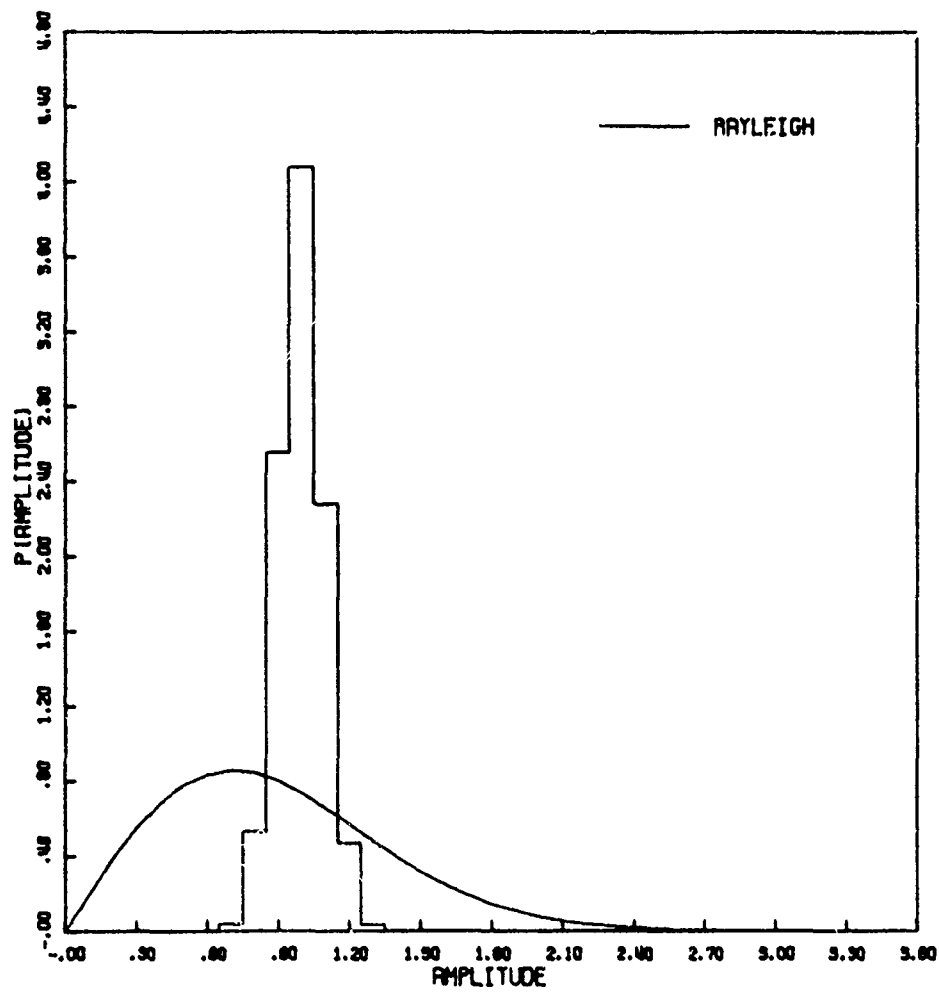
Figure 18b.   Amplitude Distribution
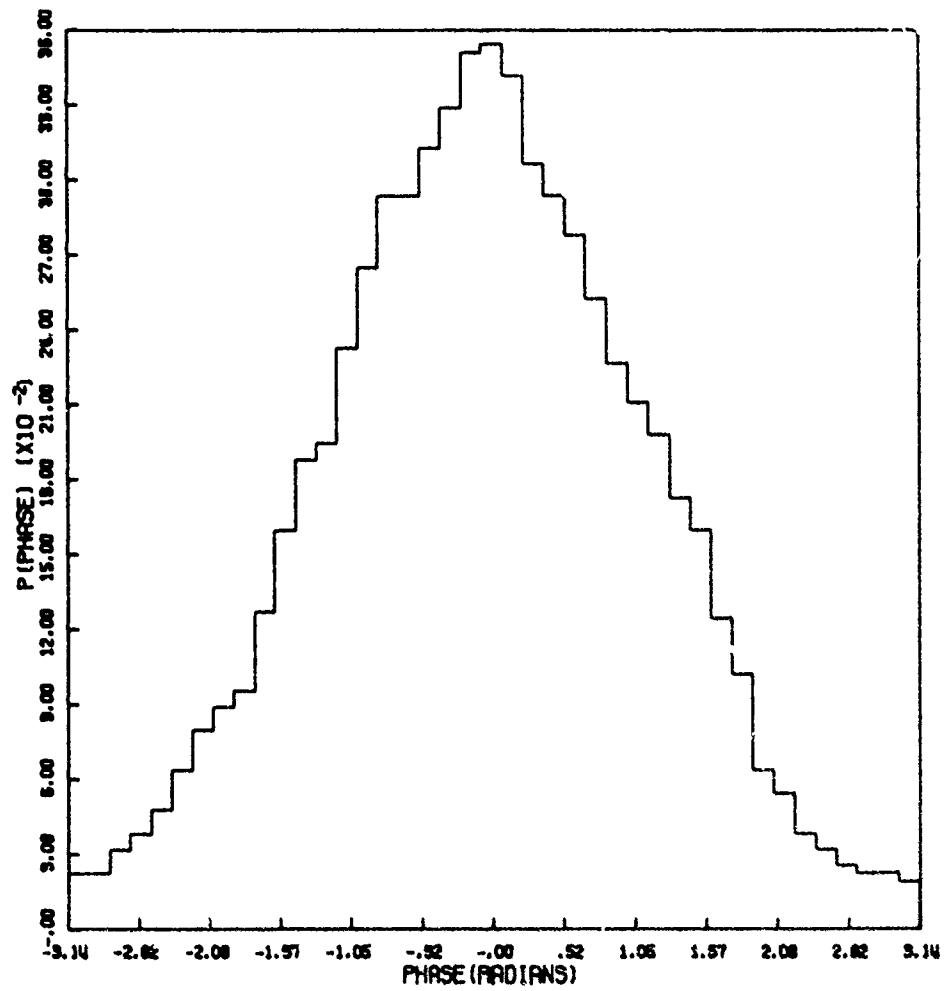
Figure 18c. Phase Distribution
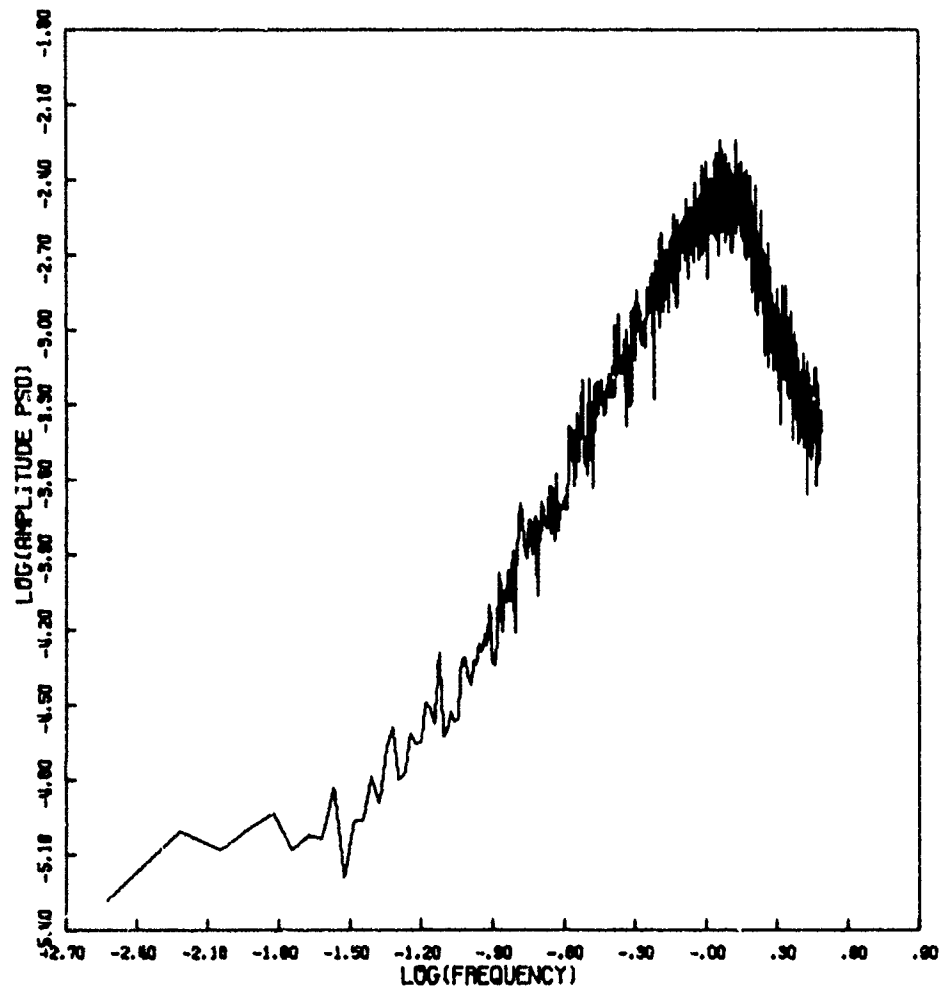
Figure 18d. Amplitude Power Spectral Density
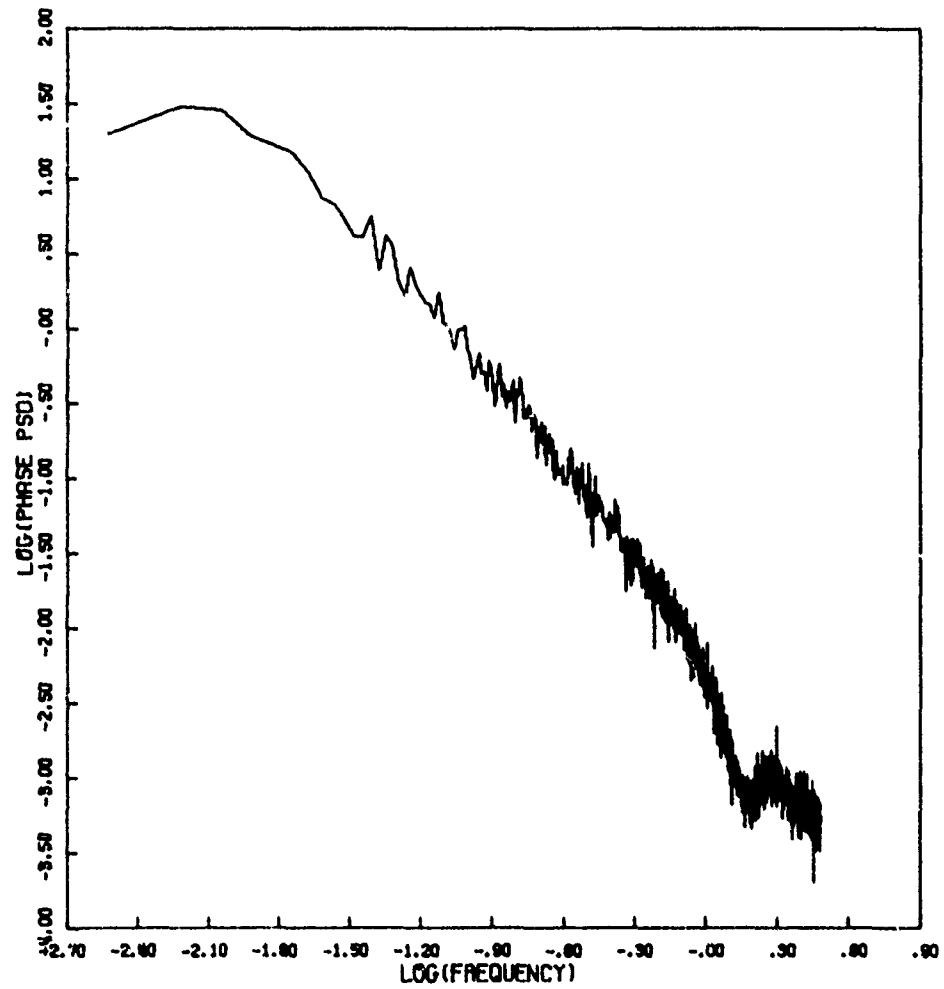
Figure 18e.   Phase Power Spectral Density
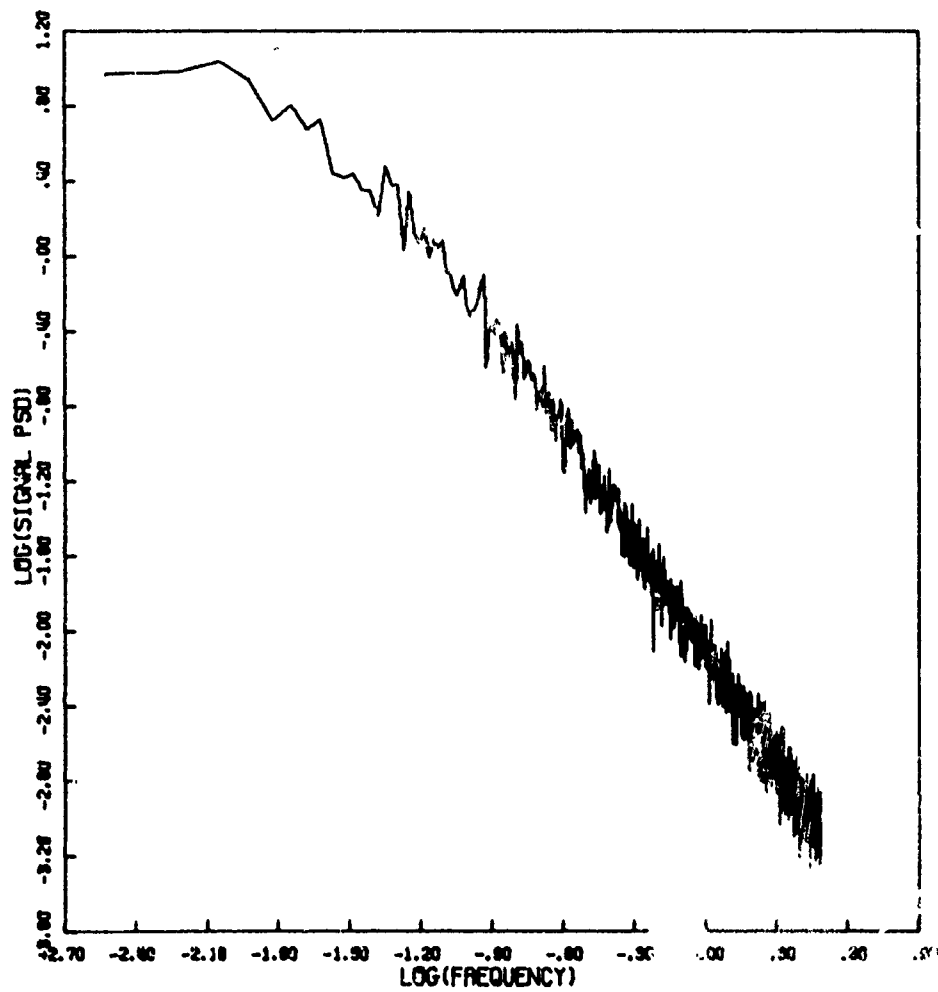
Figure 18f.   Signal Power Spectral Density
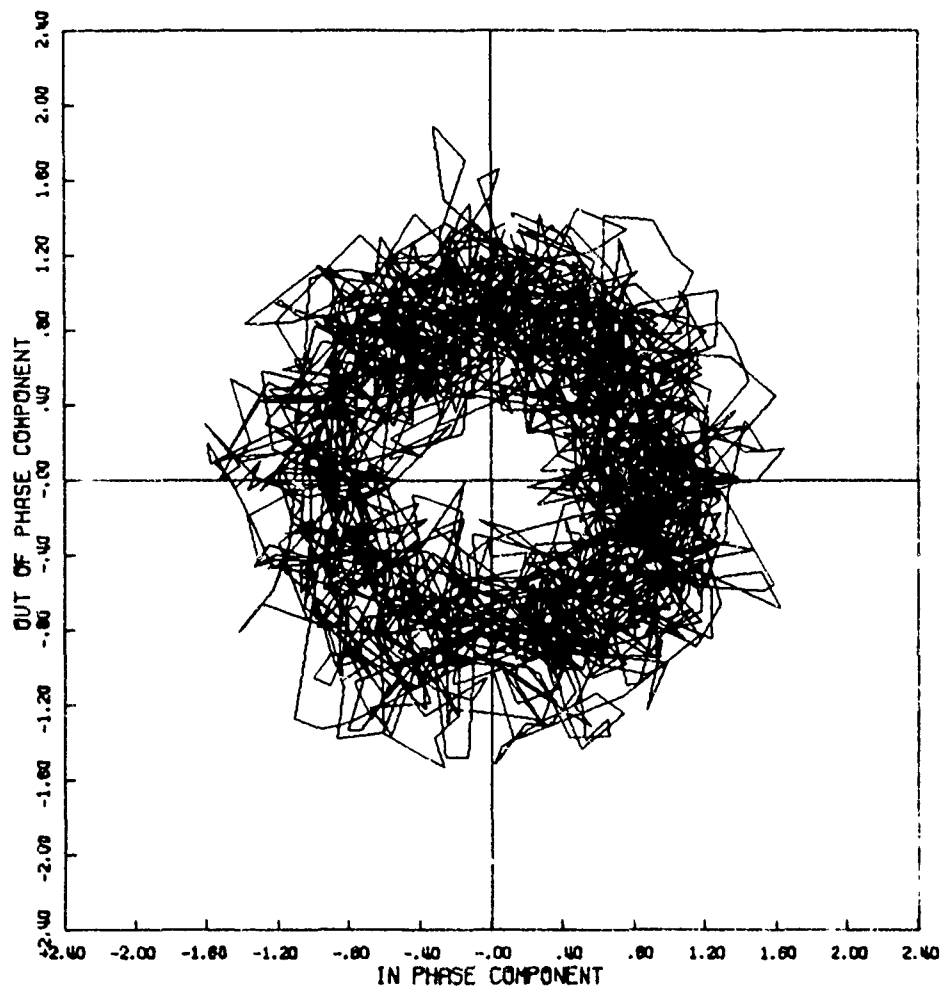
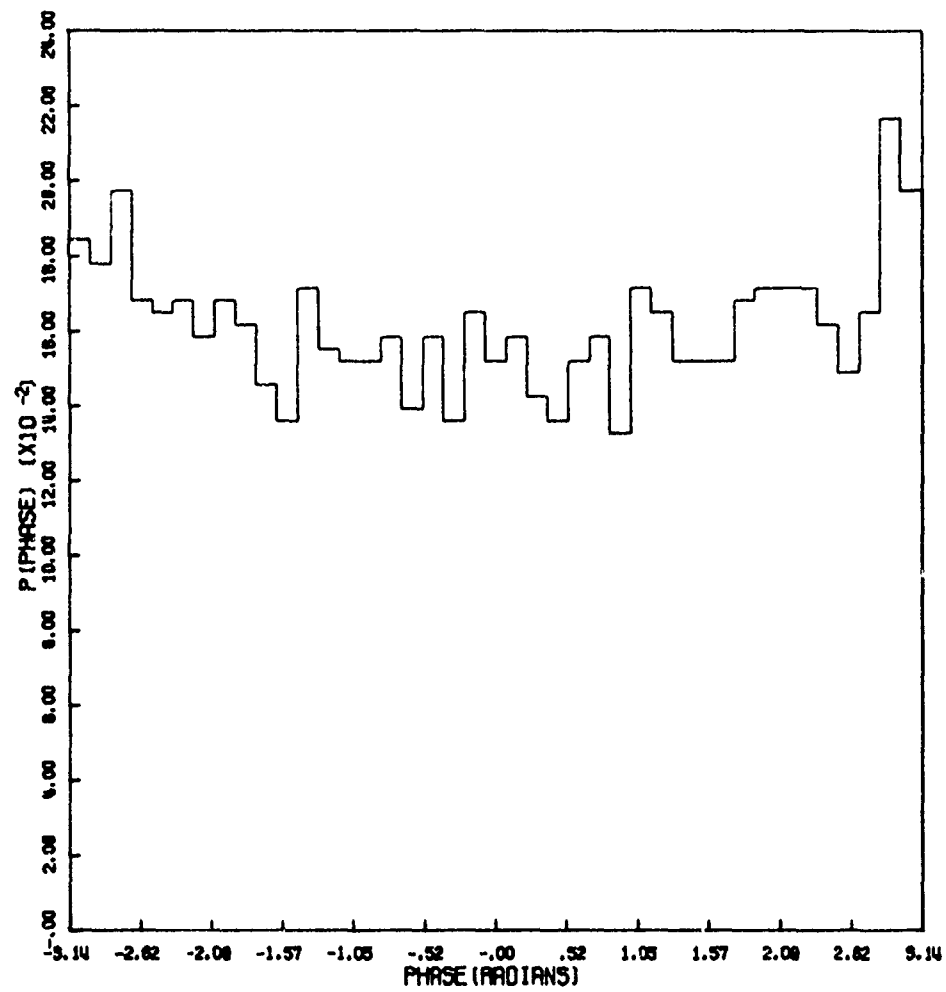Figure 19a. Signal Phase Plot
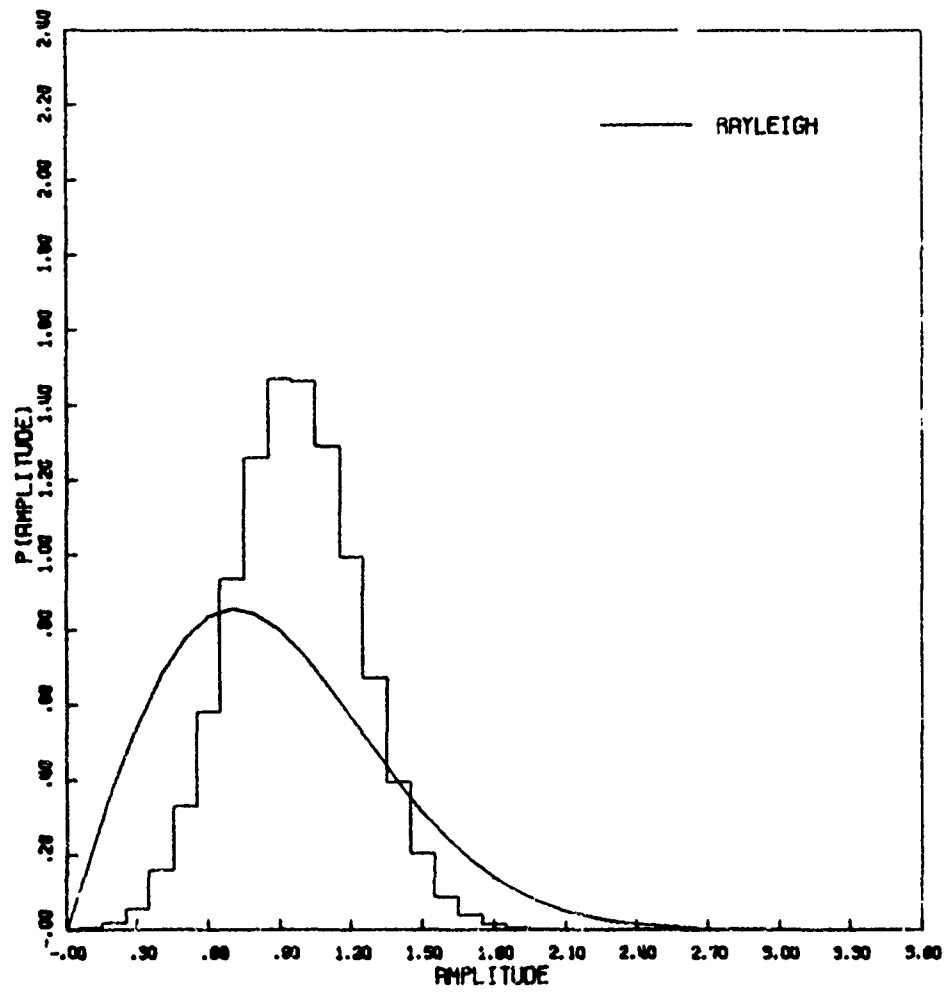
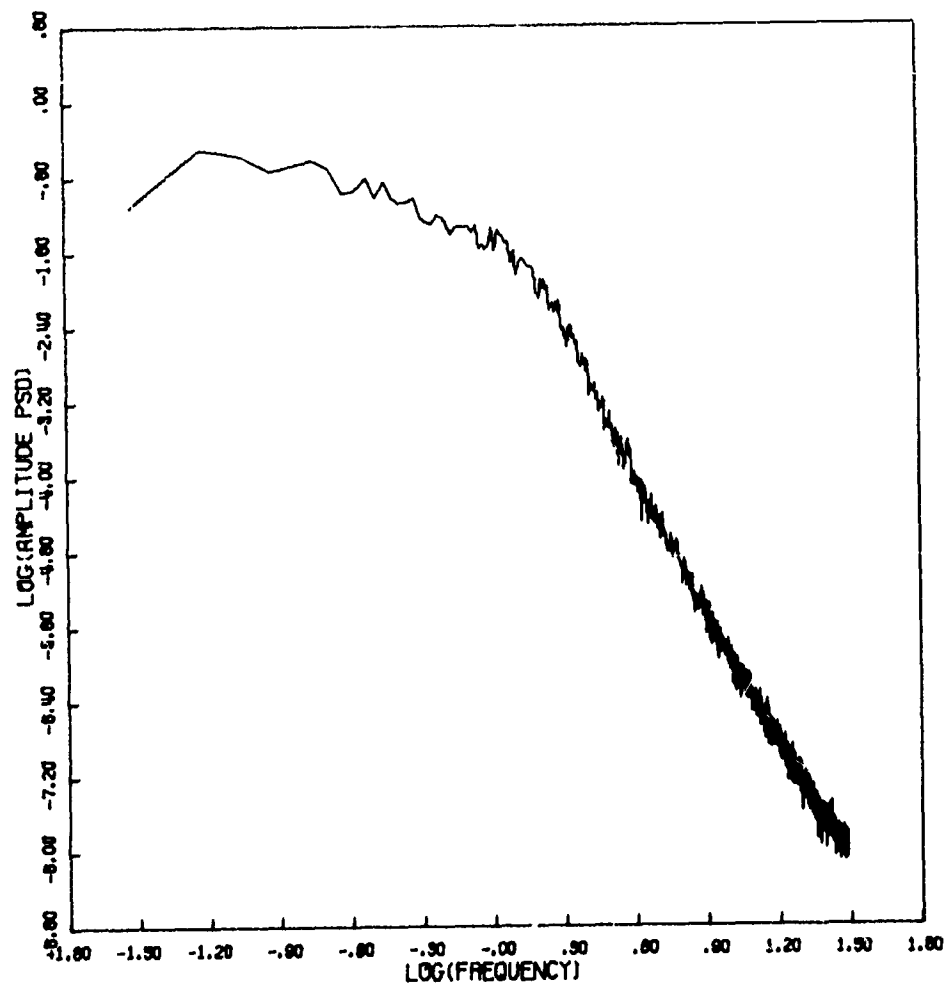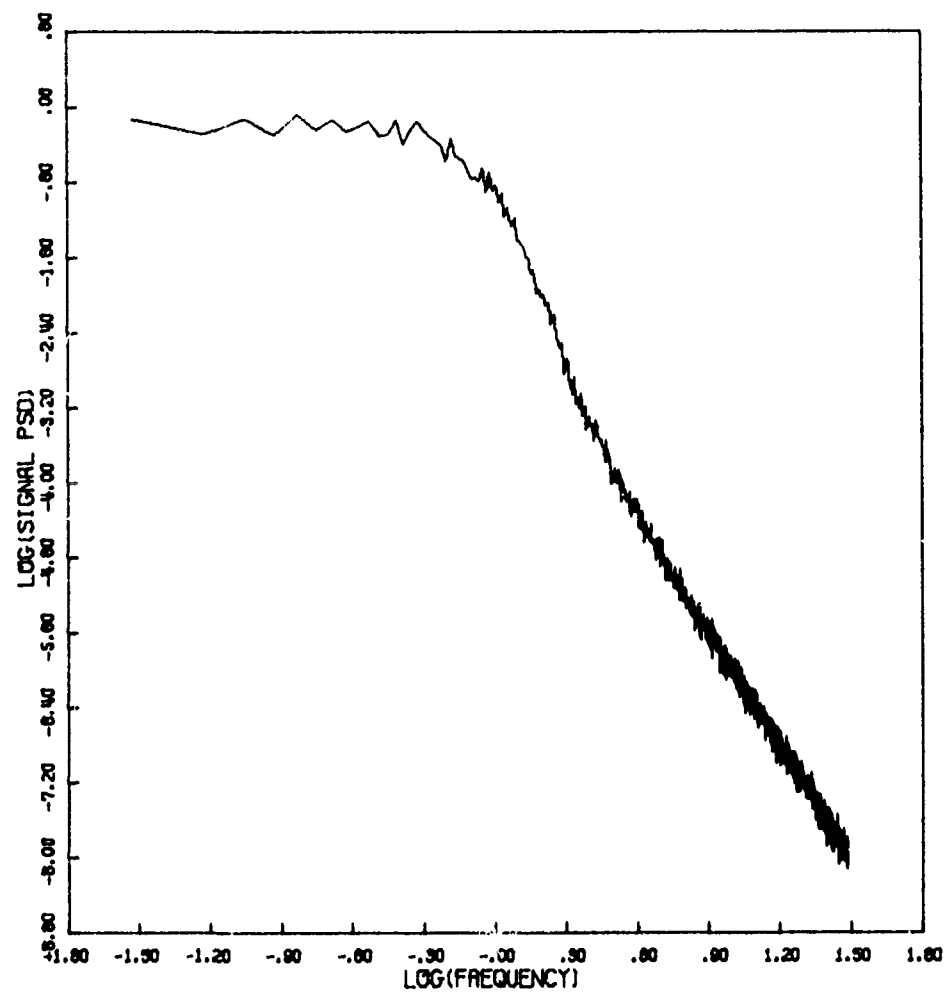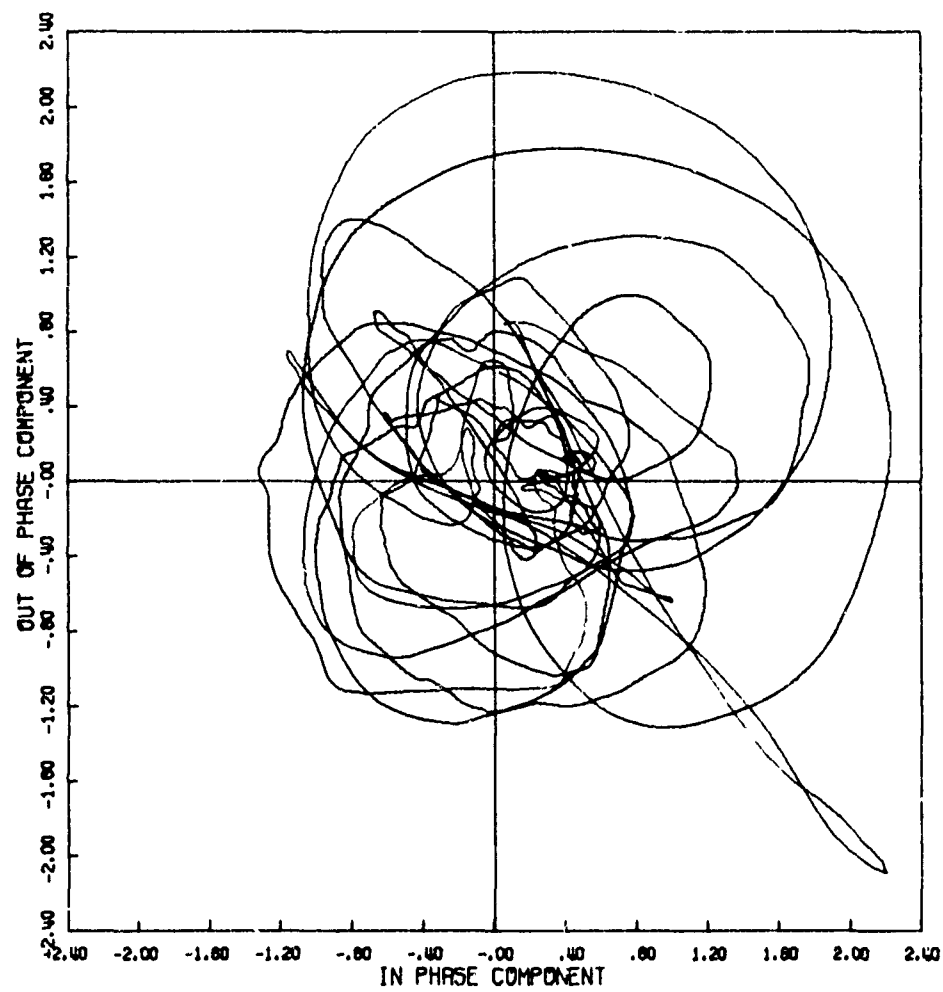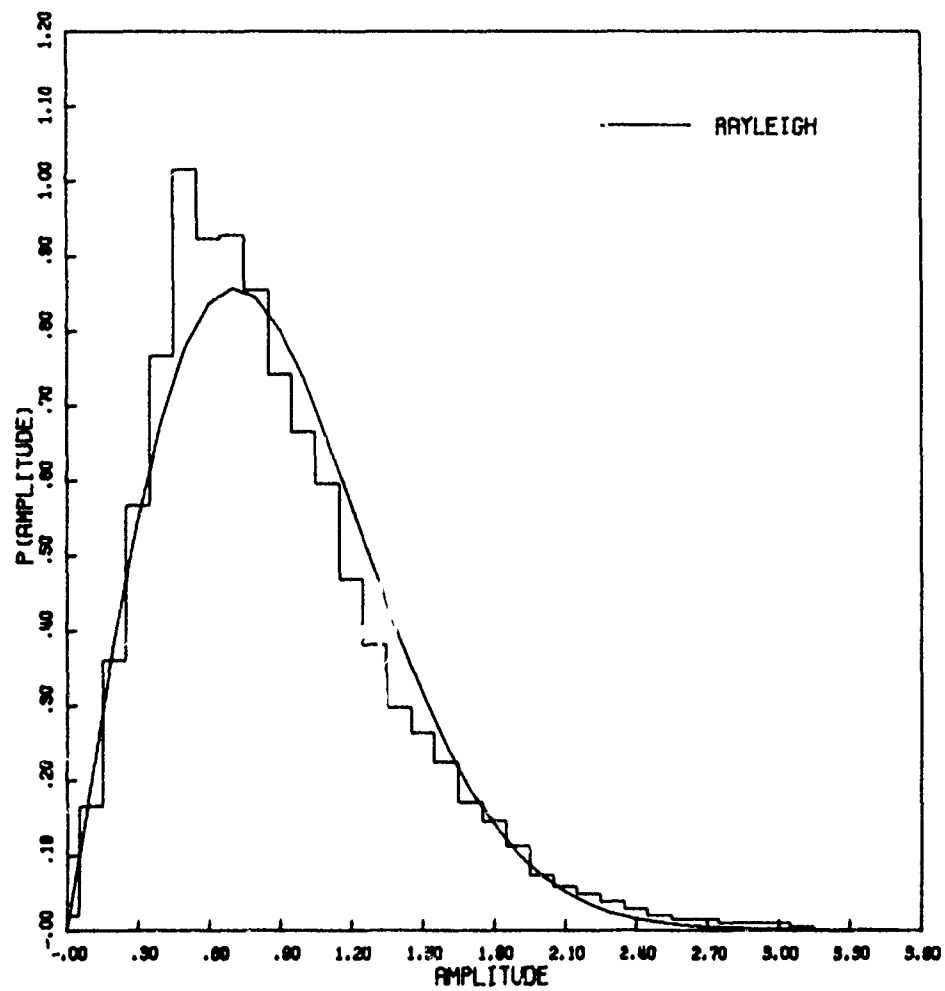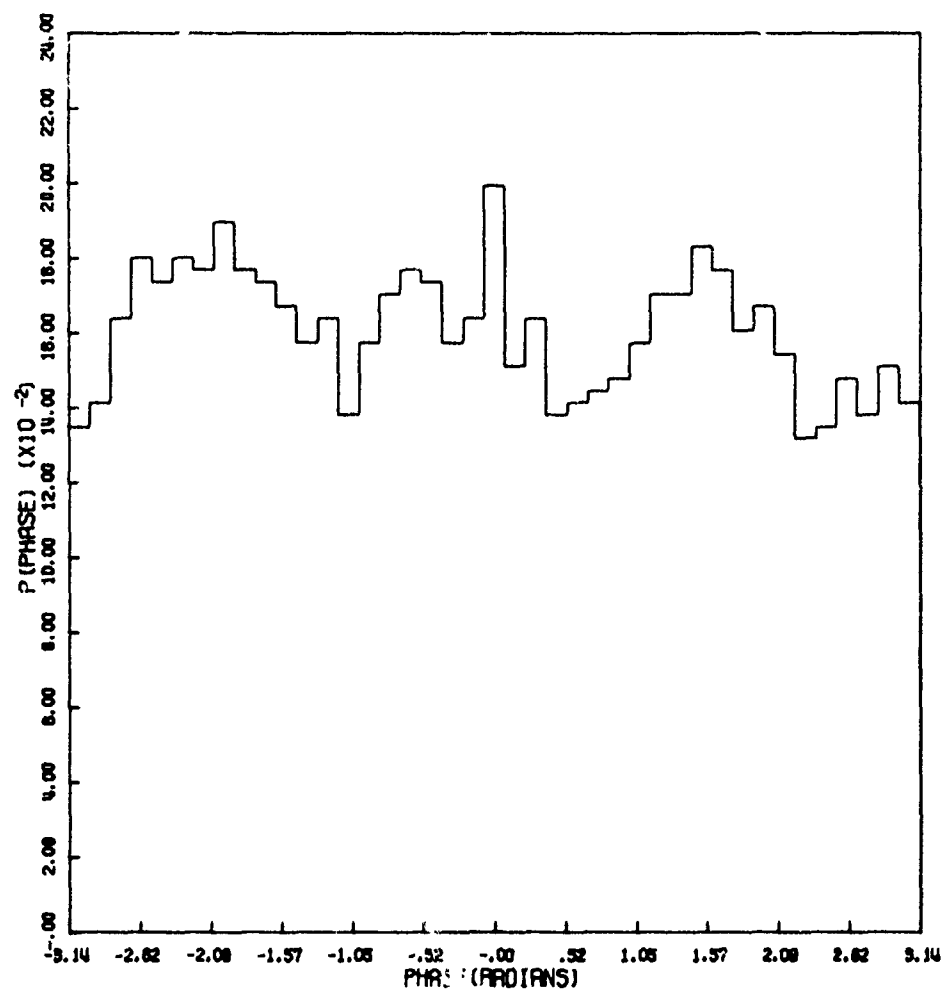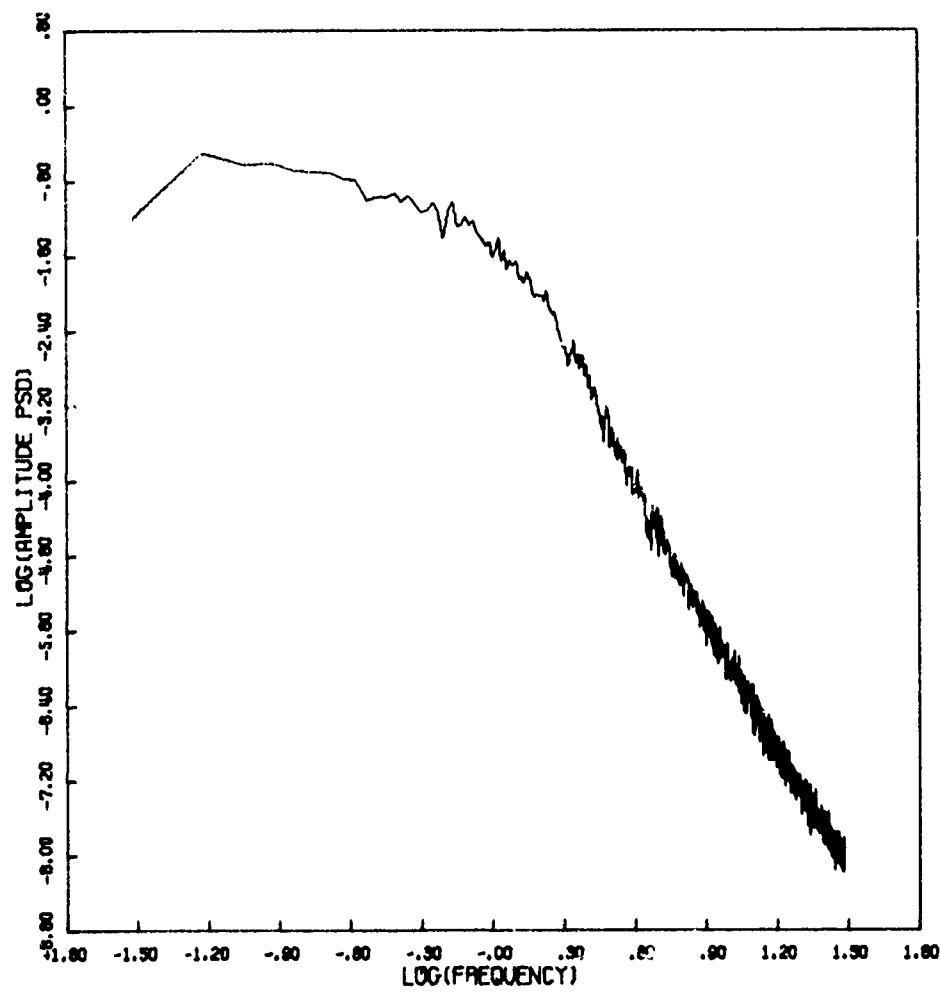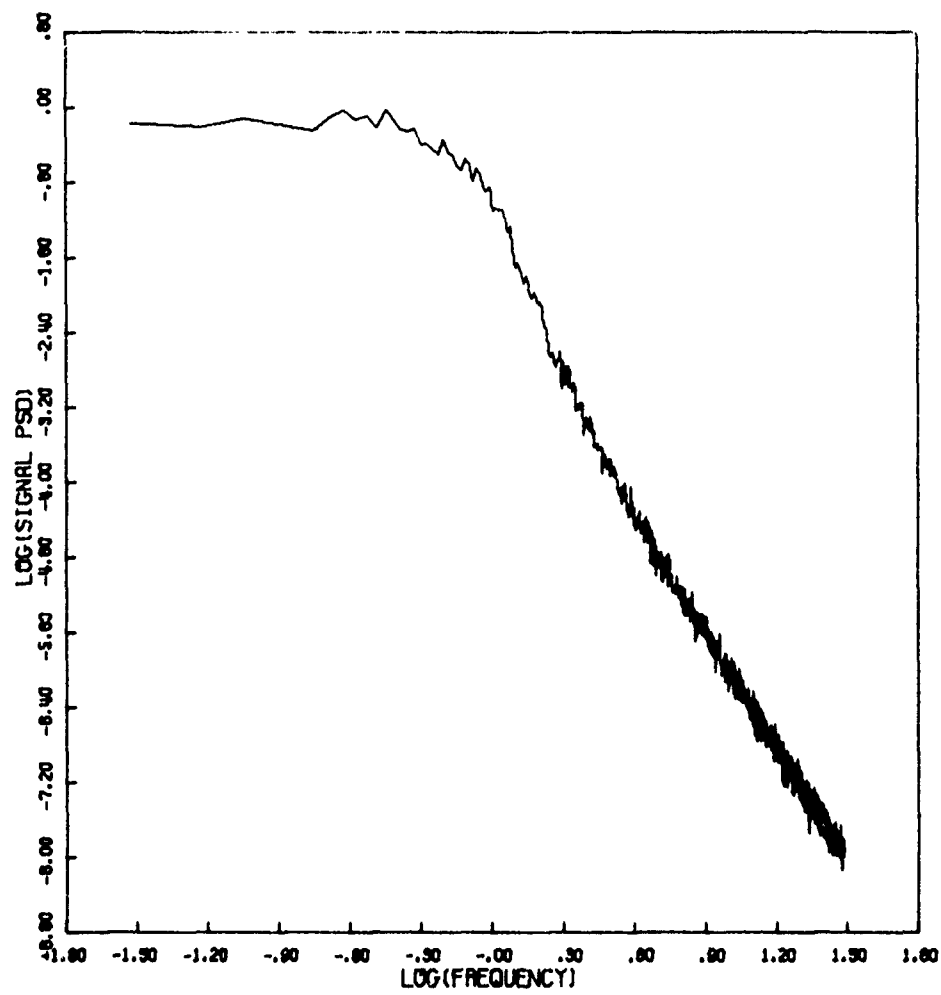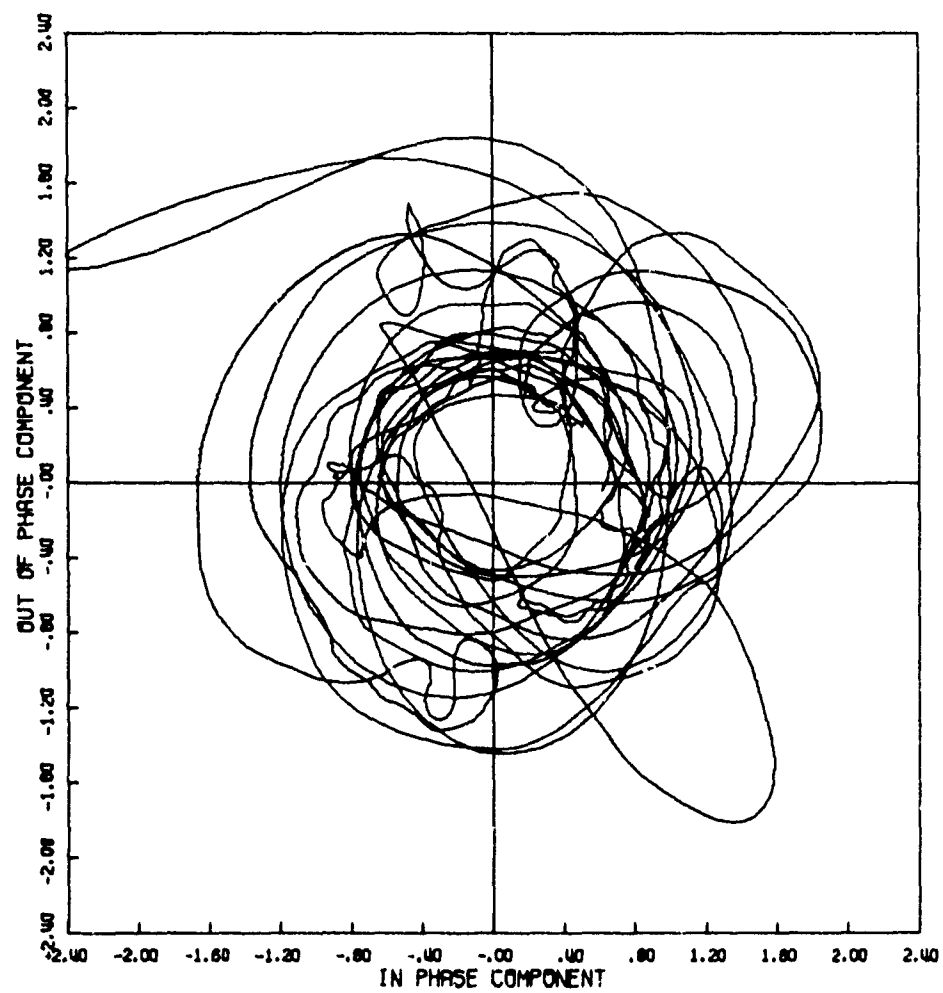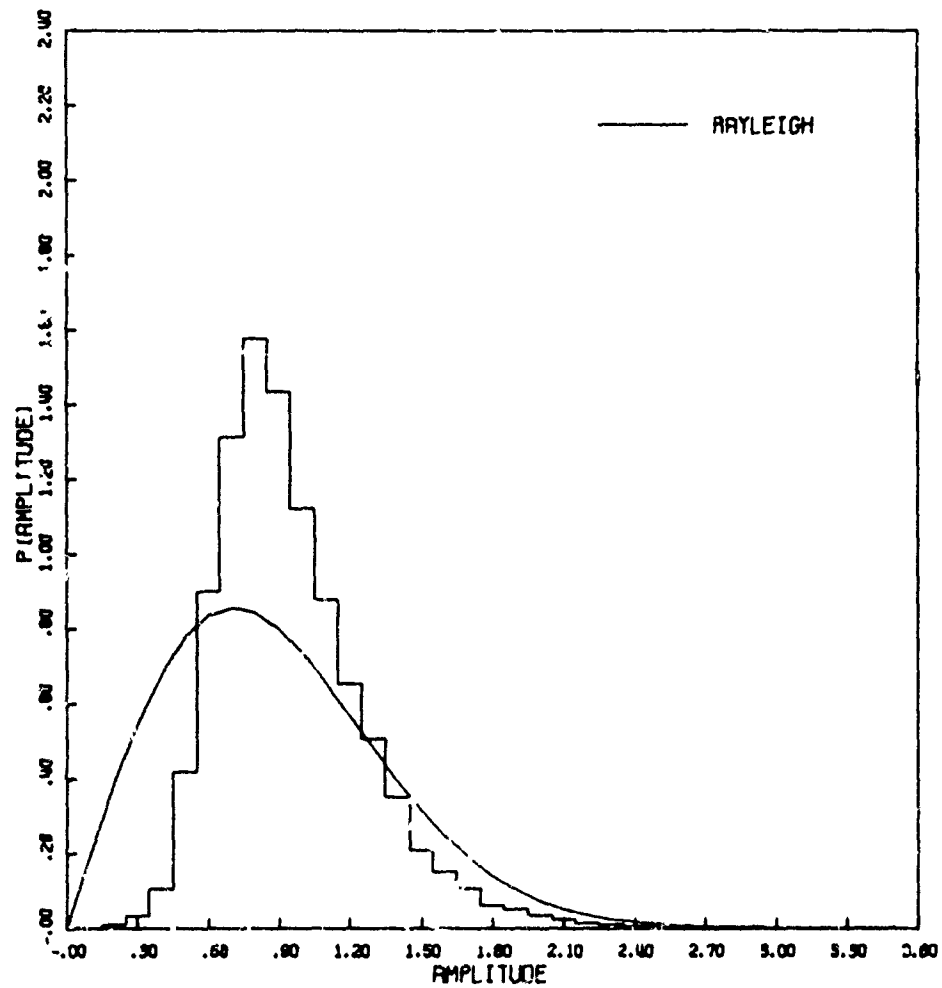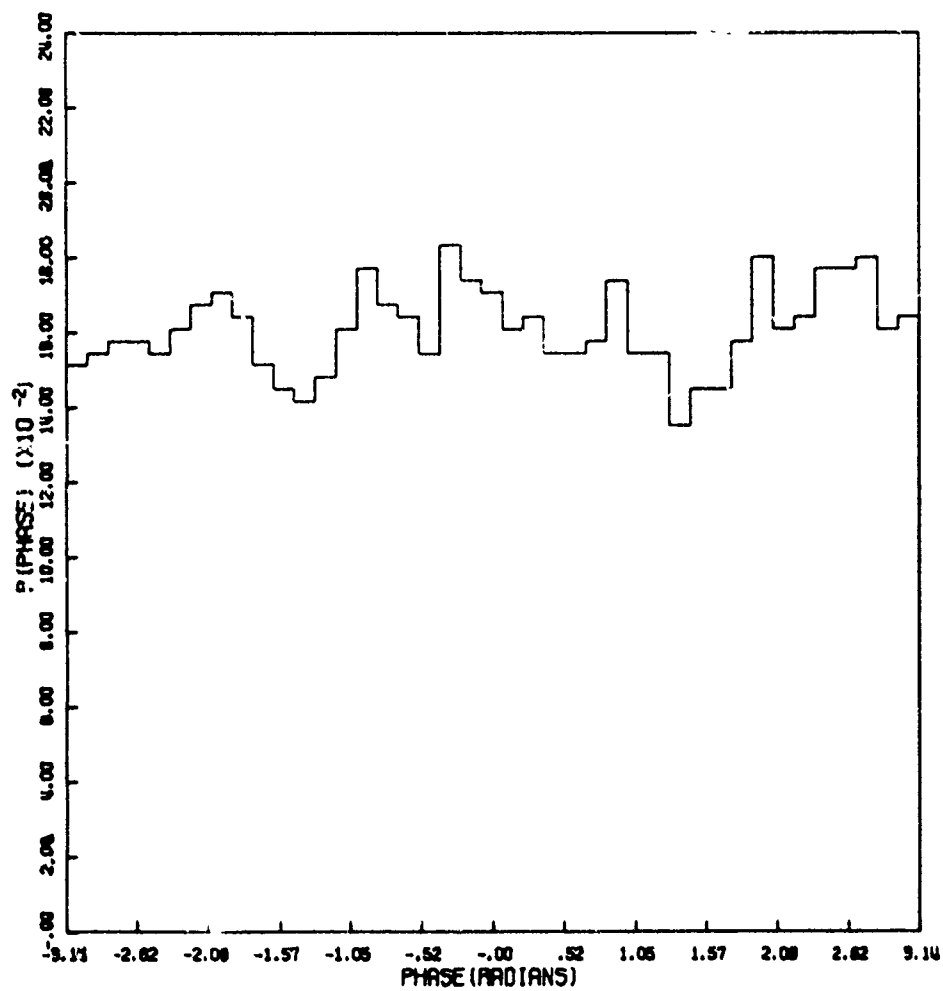Figure 19b. Amplitude Distribution
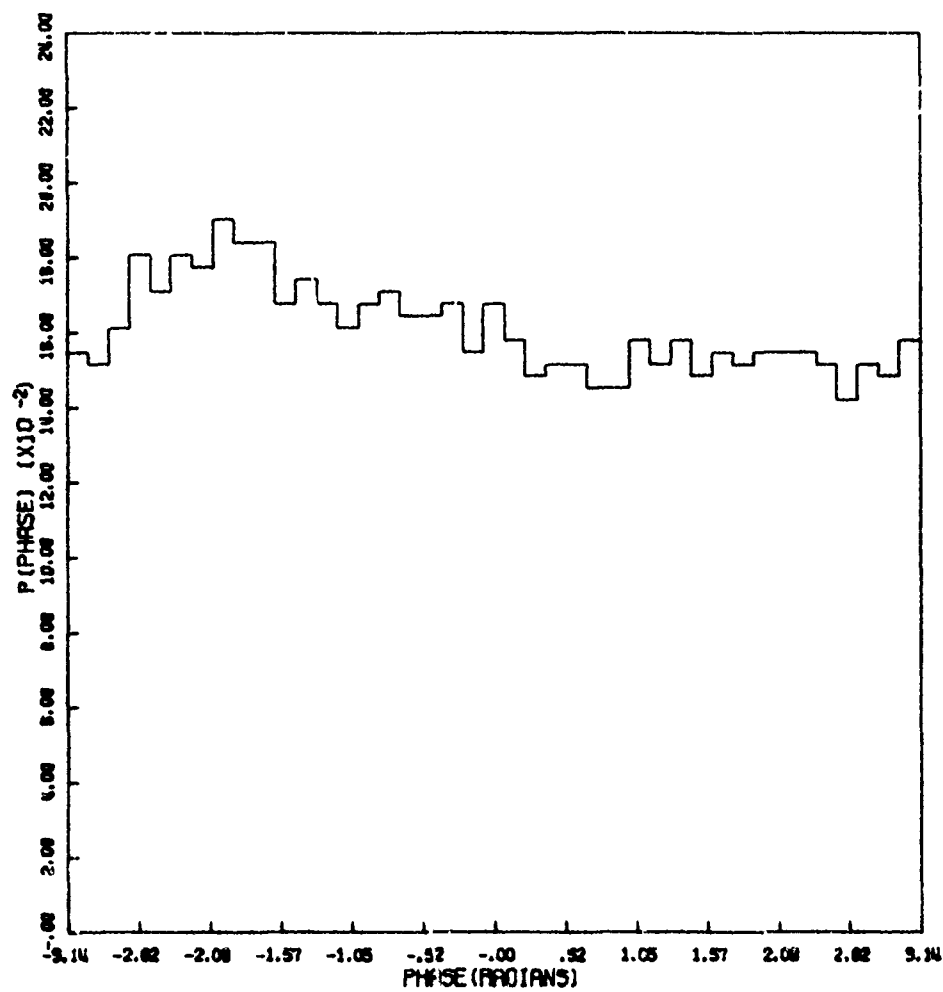
Figure 19c. Phase Distribution
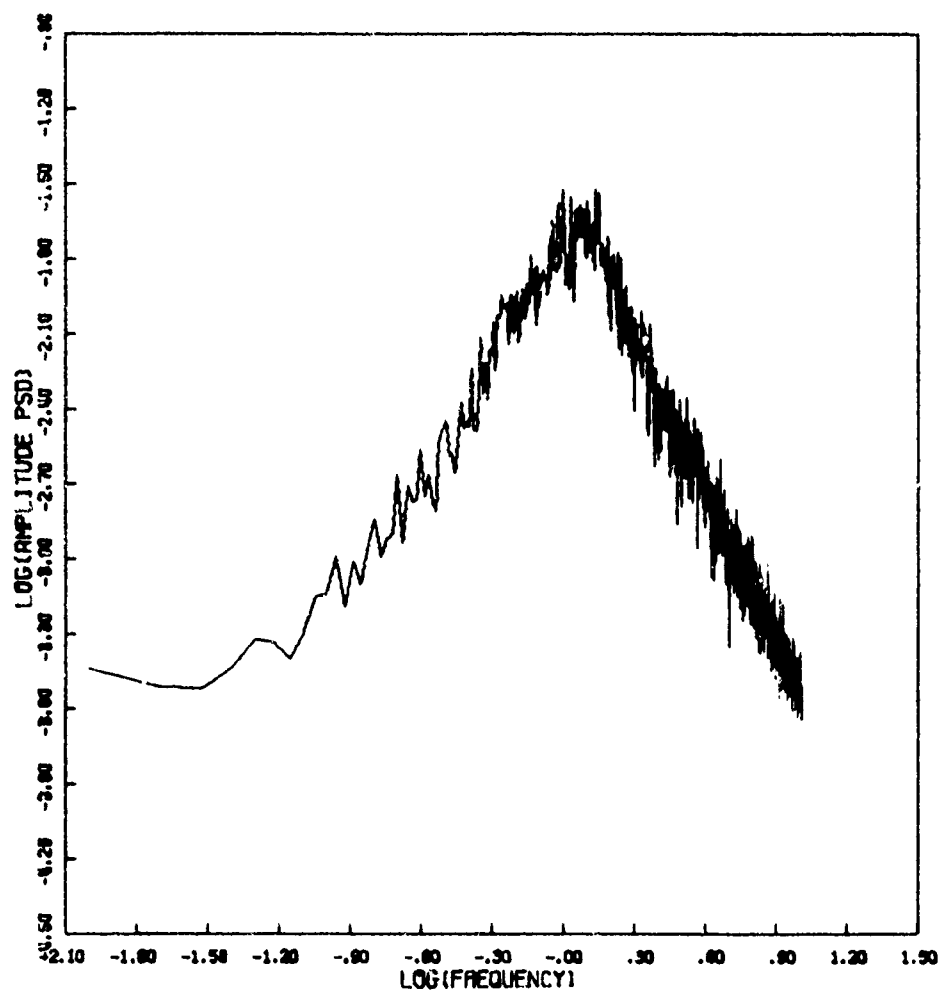
Figure 19d.   Amplitude Power Spectral Density
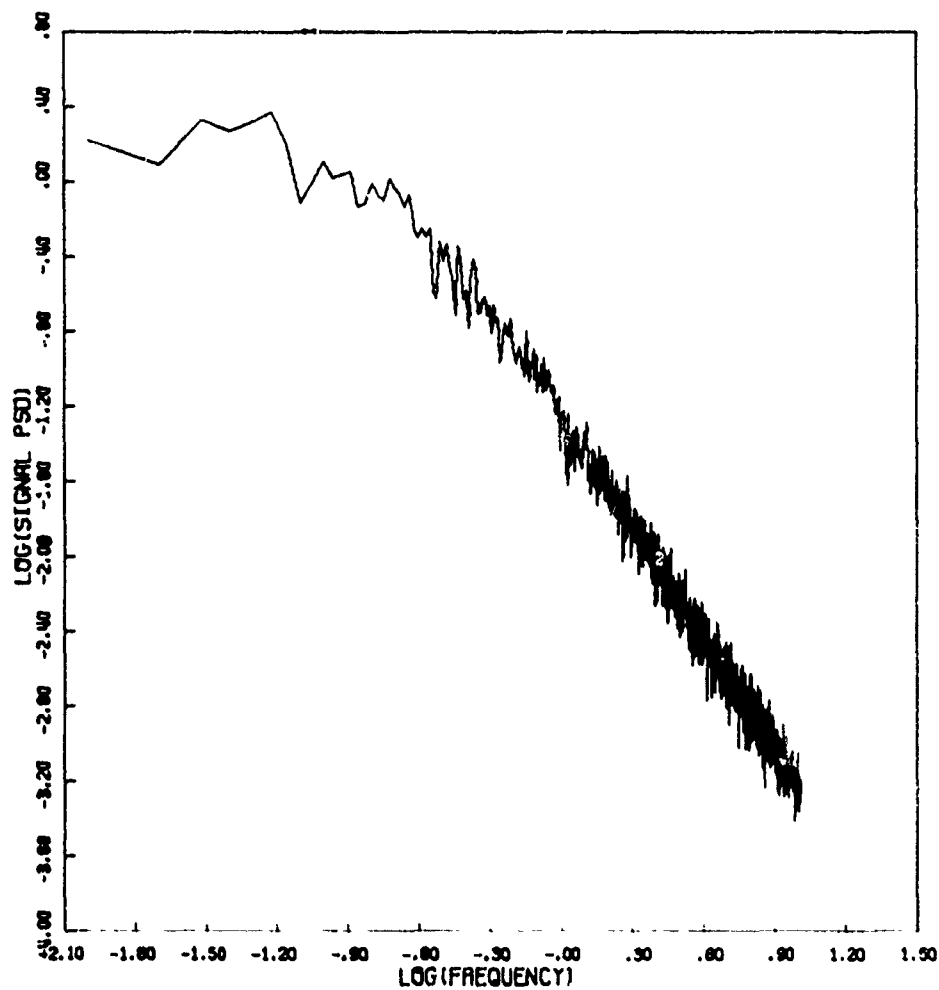
Figure 19f.   Signal Power Spectral Density

Table 2

K_ρ^{-2} SPECTRUM

	$z_g = 2\times10^7$		$z_s = 5\times10^7$			K = 1.47			K_ρ^{-2} SPECTRUM		
FIG.	L	$\overline{\Delta n^2}$	$\overline{\phi^2}$	$\overline{\chi^2}$	S_4	ℓ_o	$\overline{E_R^2}$	$\overline{E_I^2}$	α_A	α_ϕ	α_s
23	1.25×10^3	10^{12}	0.1	0.08	0.5	2×10^3	0.07	0.09	2.8	2.8	2.8
24	1.25×10^3	10^{13}	1.8*	0.43	0.95	1.3×10^3	0.39	0.44	2.7		2.8
25	1.25×10^3	10^{14}	18.2*	0.46	0.99	2.8×10^2	0.49	0.51	3.4		3.0
26	5×10^3	3×10^{11}	0.14	0.05	0.39	7.5×10^3	0.05	0.14	2.9	3.0	2.7
27	5×10^3	3×10^{12}	2.2*	0.41	0.87	4.8×10^3	0.42	0.47	1.3, 3.1		3.2
28	5×10^3	3×10^{13}	22.*	0.45	0.98	9.8×10^2	0.47	0.53	3.5		3.2
29	10^4	5×10^{11}	0.50	0.08	0.48	1.3×10^4	0.17	0.38	2.8	2.9	2.9
30	2×10^4	3×10^{10}	0.08	0.003	0.11	3.3×10^4	0.01	0.07	3.0	2.8	2.7
31	2×10^4	3×10^{11}	0.87	0.025	0.31	2.7×10^4	0.16	0.40	2.9	2.9	2.9
32	2×10^4	3×10^{12}	8.7*	0.31	0.84	7.4×10^3	0.51	0.49	3.3		3.0
33	2×10^4	3×10^{13}	67.*	0.46	1.01	1.7×10^3	0.50	0.50	3.7		3.5
34	8×10^4	10^{10}	0.12	~ 0	~ 0	1.4×10^5	0.004	0.095	2.9	3.0	3.0
35	8×10^4	10^{11}	1.2	0.003	0.11	9.9×10^4	0.20	0.46	2.8	2.8	2.8
36	8×10^4	1.2×10^{12}	14.	0.03	0.33	2.2×10^4	0.51	0.49	3.0	3.0	3.1
37	8×10^4	10^{13}	116.*	0.28	0.85	5.6×10^3	0.50	0.50	3.3		3.0
38	2.5×10^5	3.8×10^{12}	138.	0.03	0.33	1.7×10^4	0.51	0.49	3.1	3.1	3.4

Figure 20. Propagation Space Plot for K_ρ^{-2} Spectrum
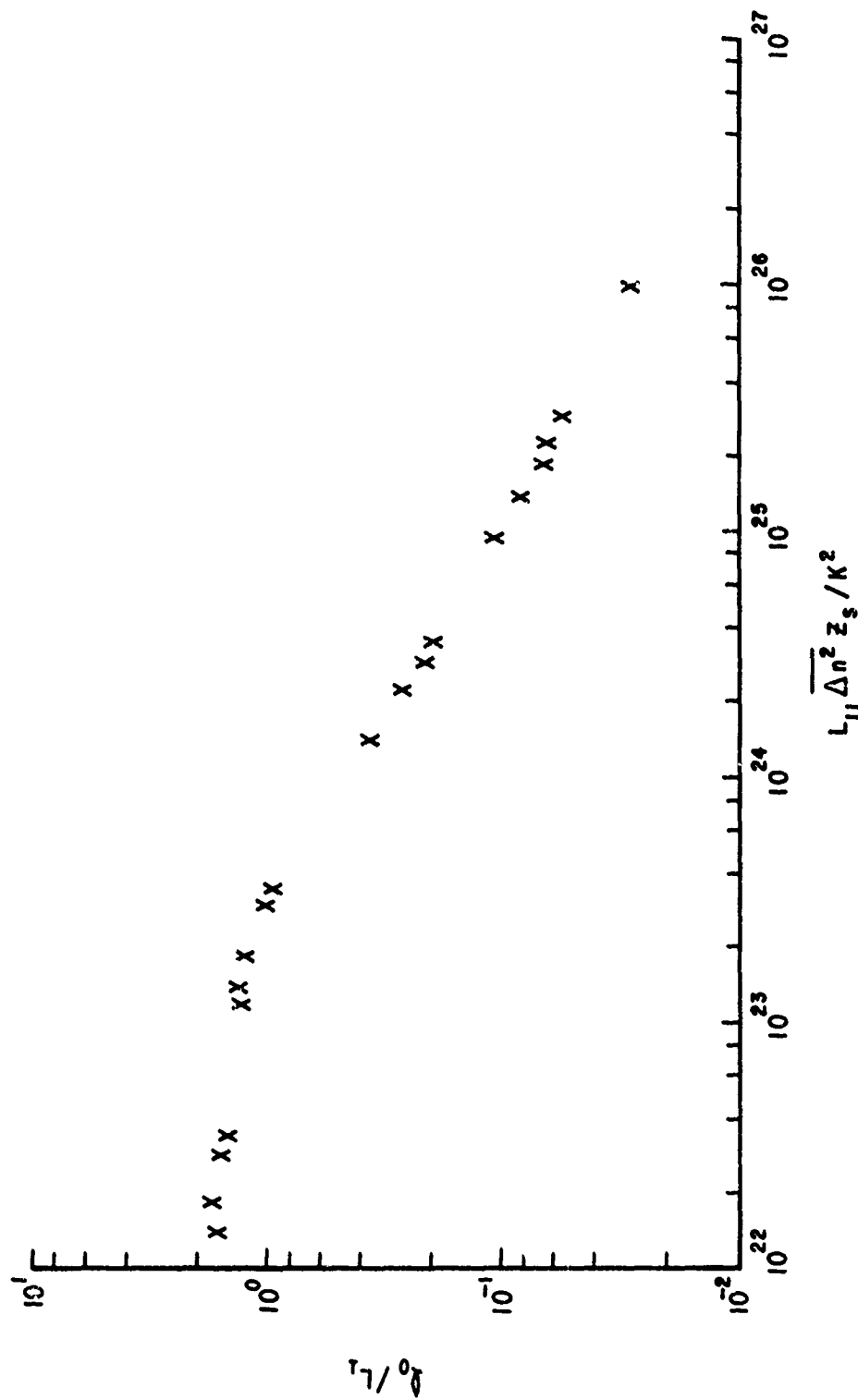
Figure 21. ℓ_0 for K_ρ^{-2} Spectrum
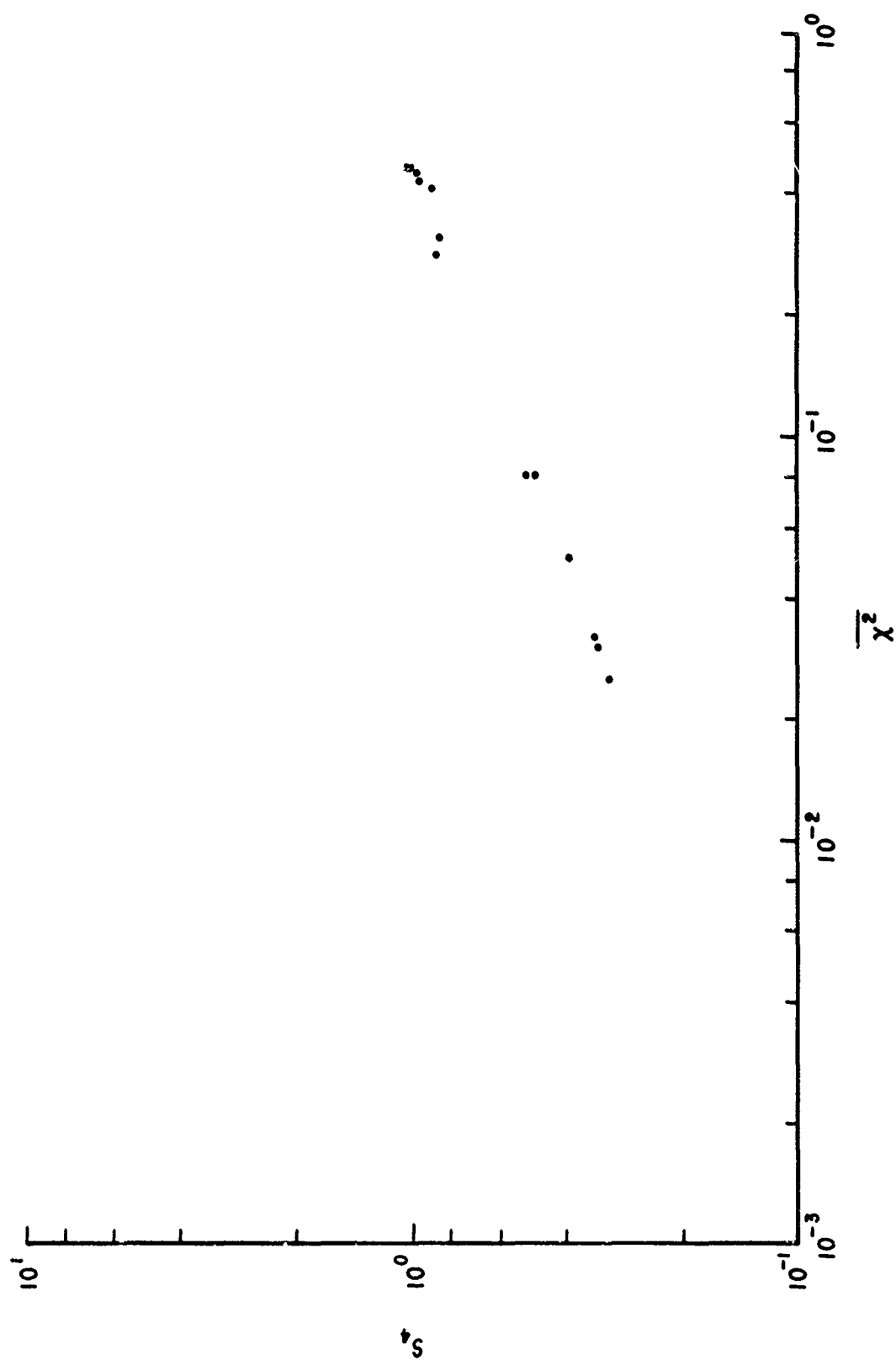
Figure 22. S_4 vs. $\overline{\chi^2}$ for K_ρ^{-2} Spectrum
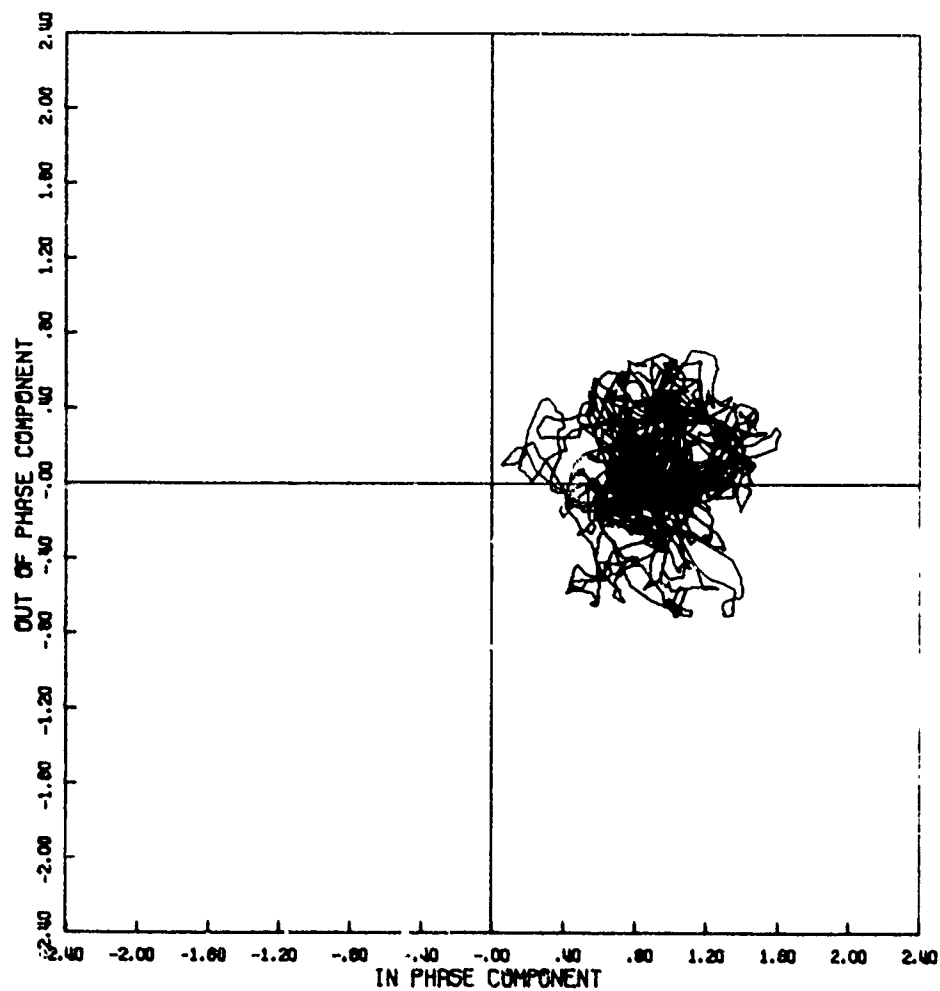
Figure 23a.   Signal Phase Plot
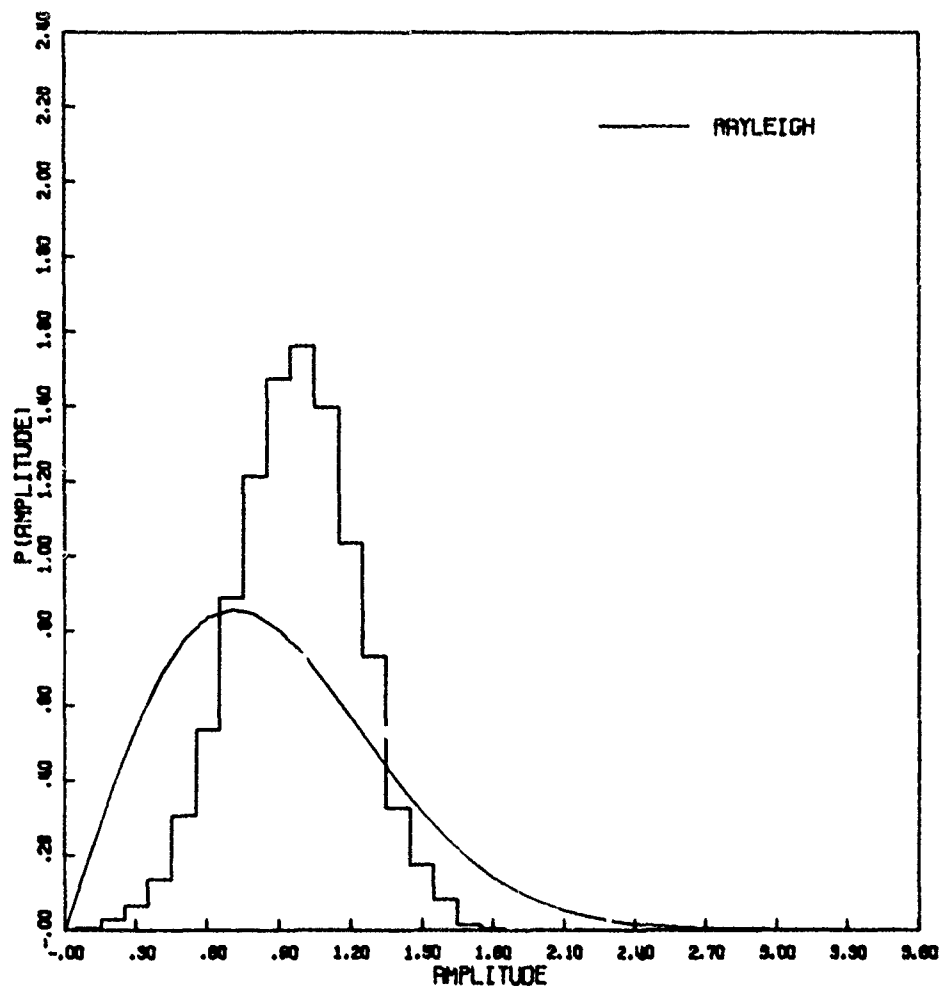
Figure 23b. Amplitude Distribution
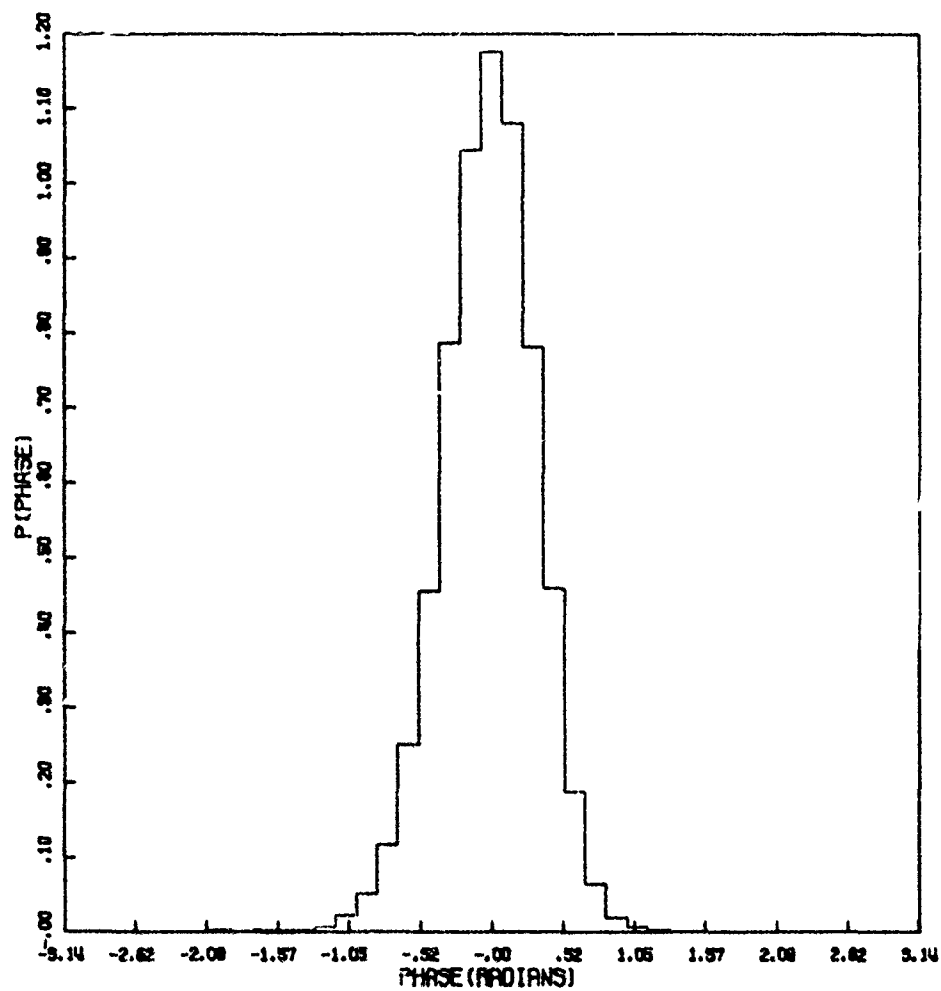
Figure 23c.   Phase Distribution
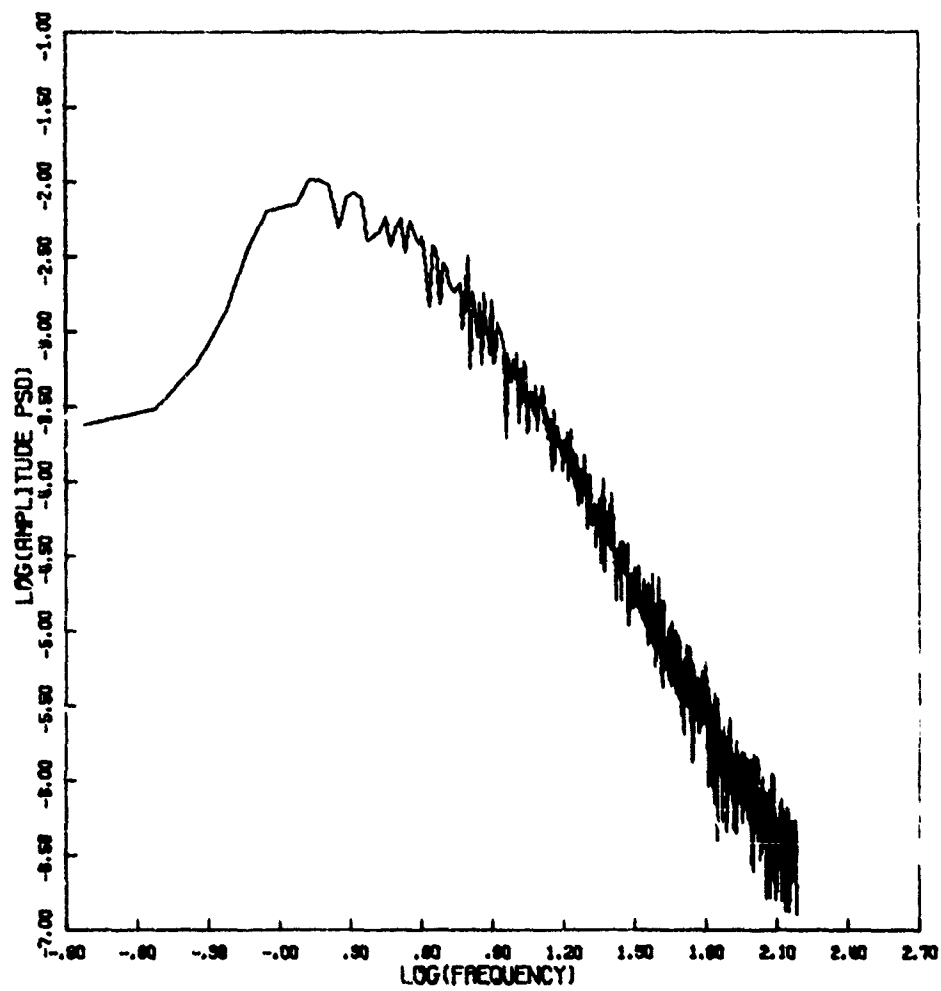
Figure 23d.   Amplitude Power Spectral Density
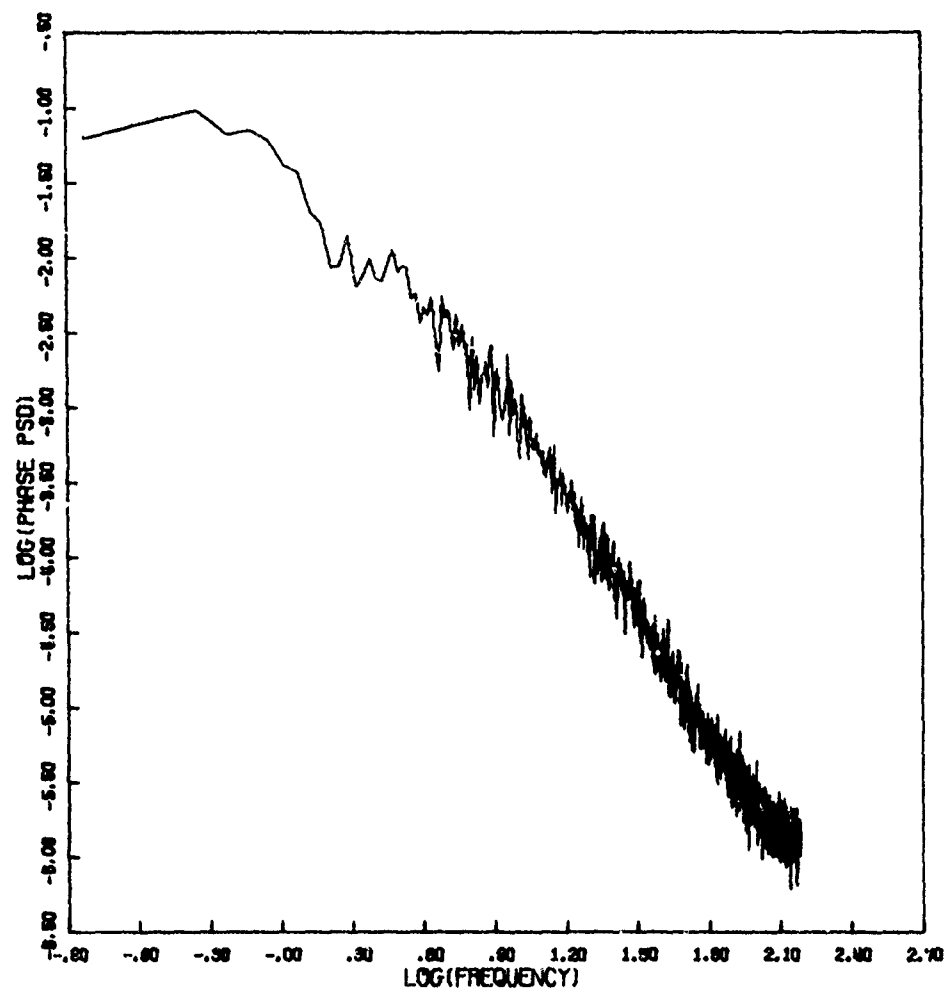
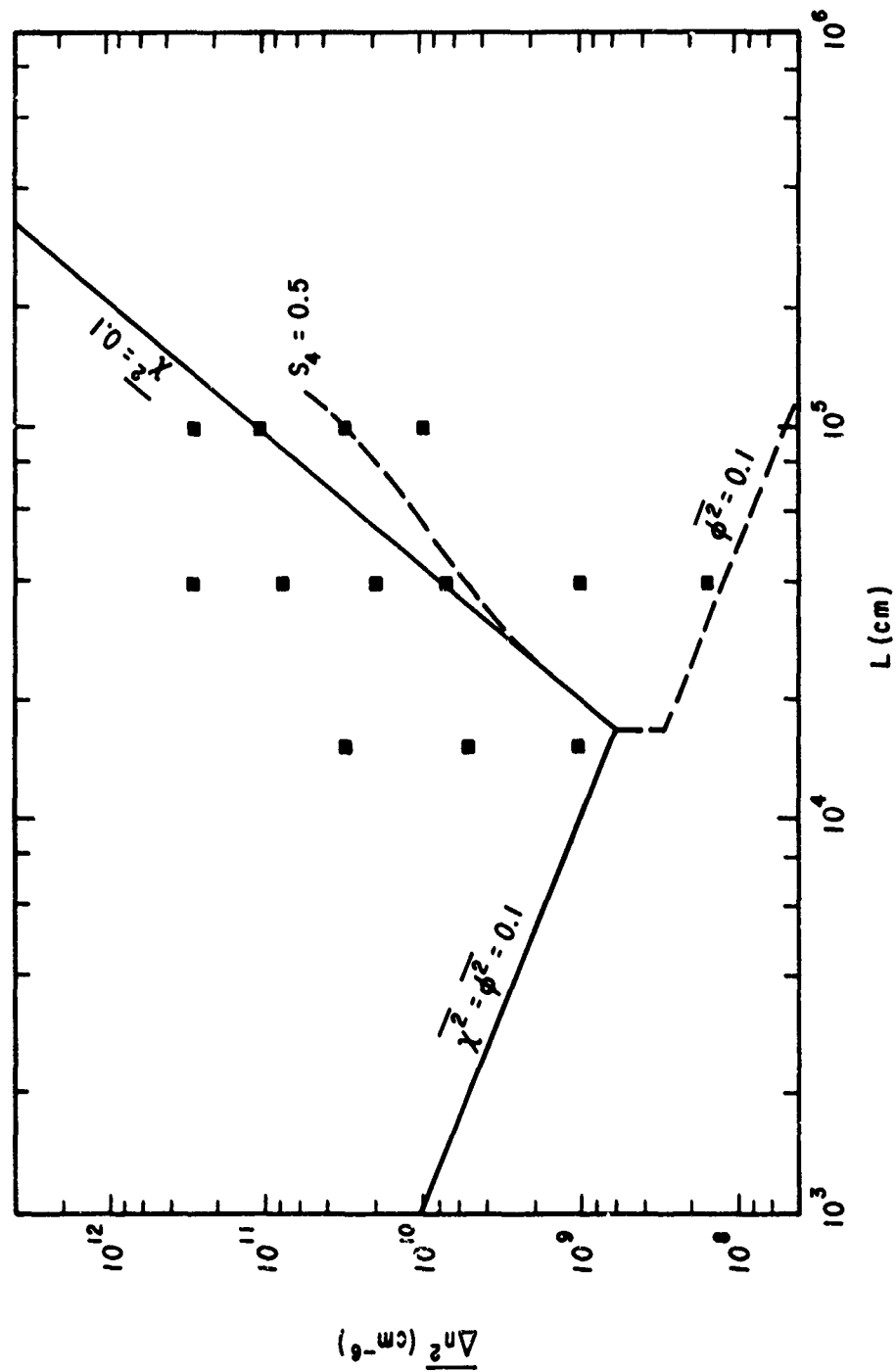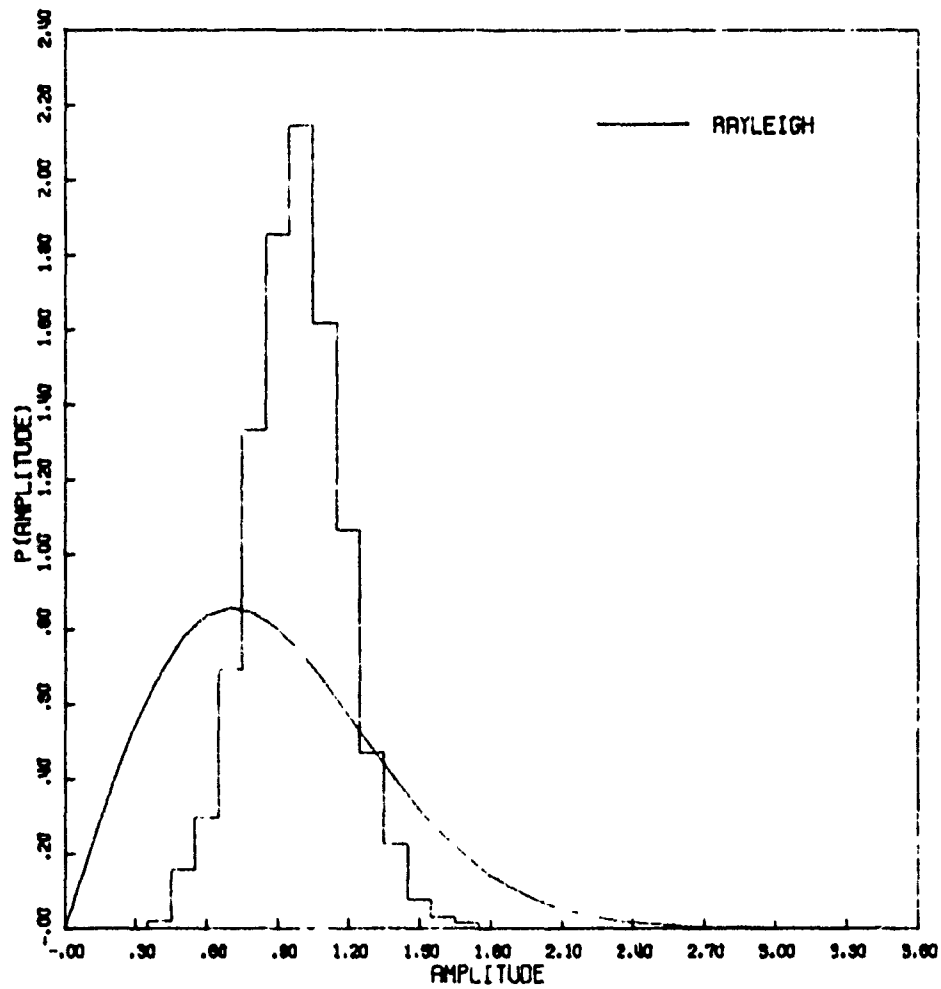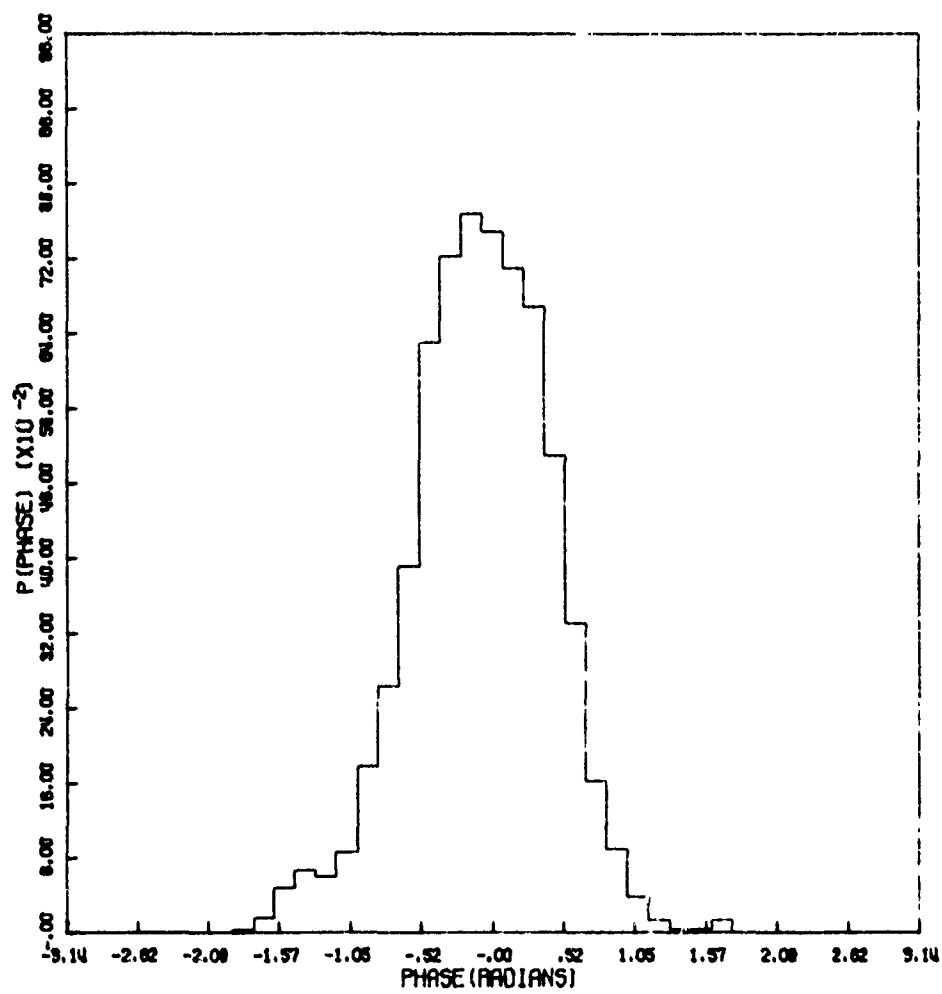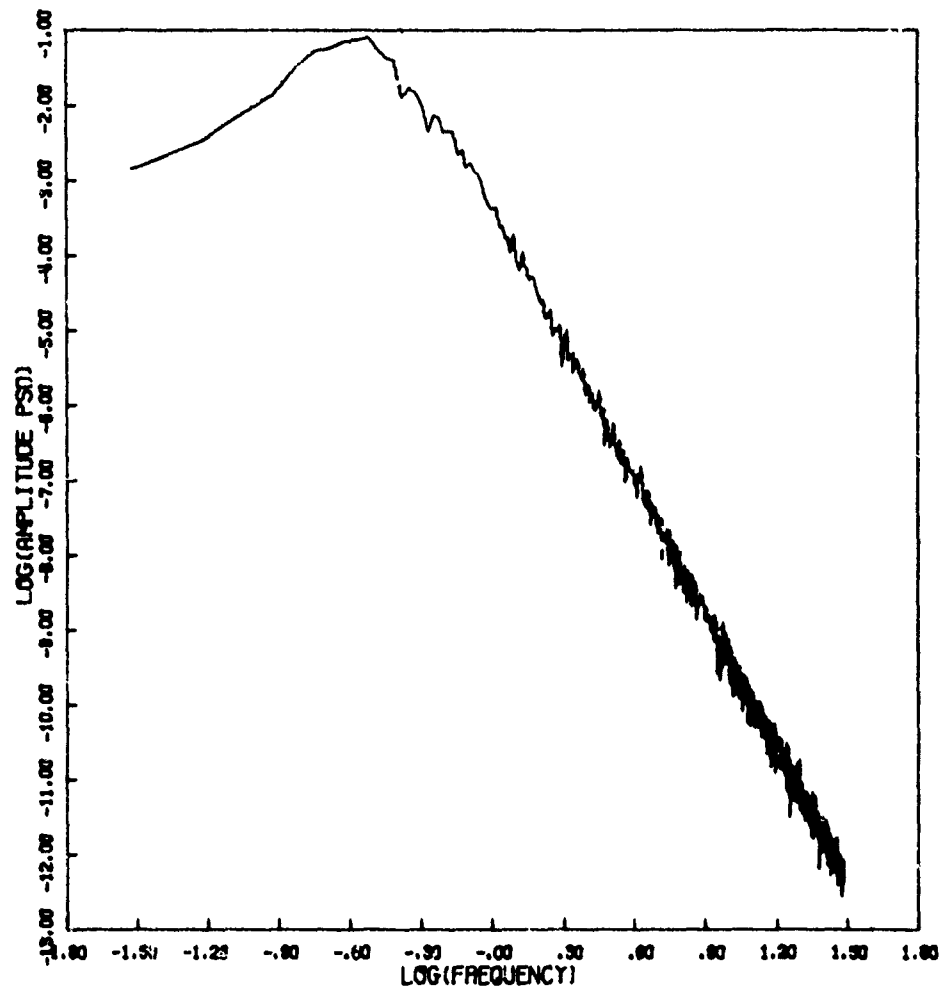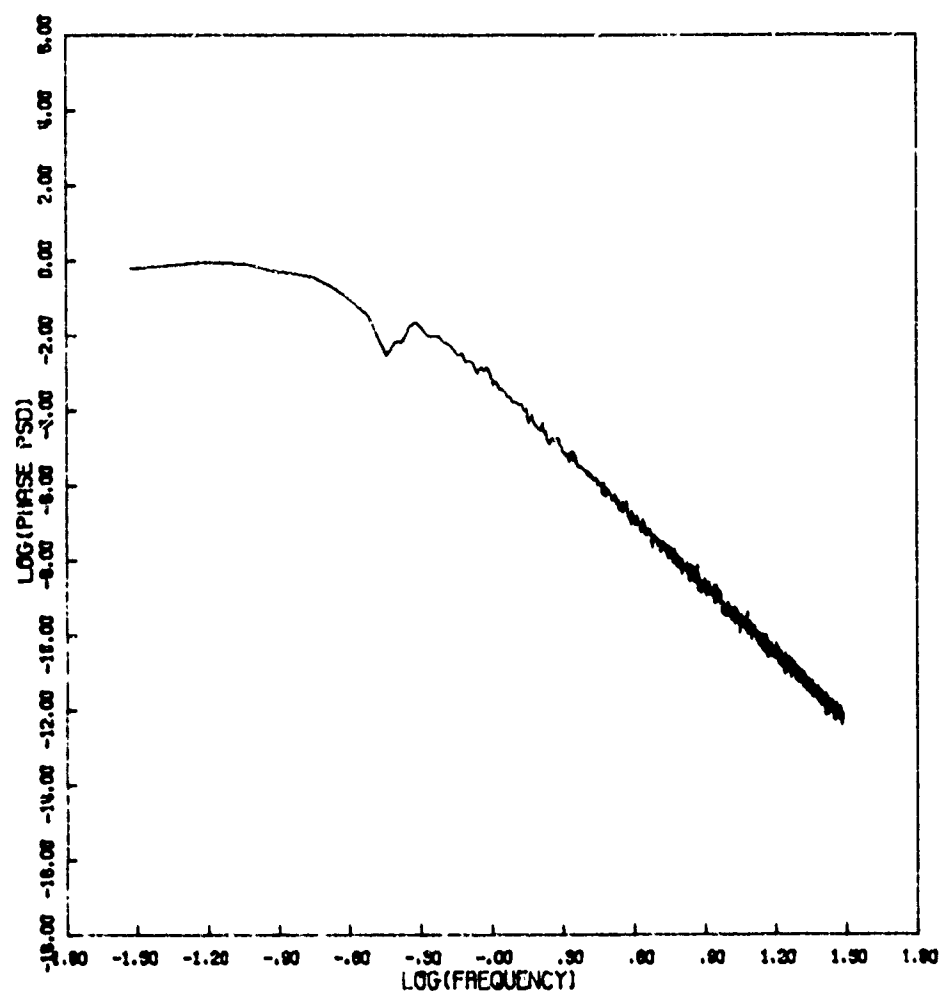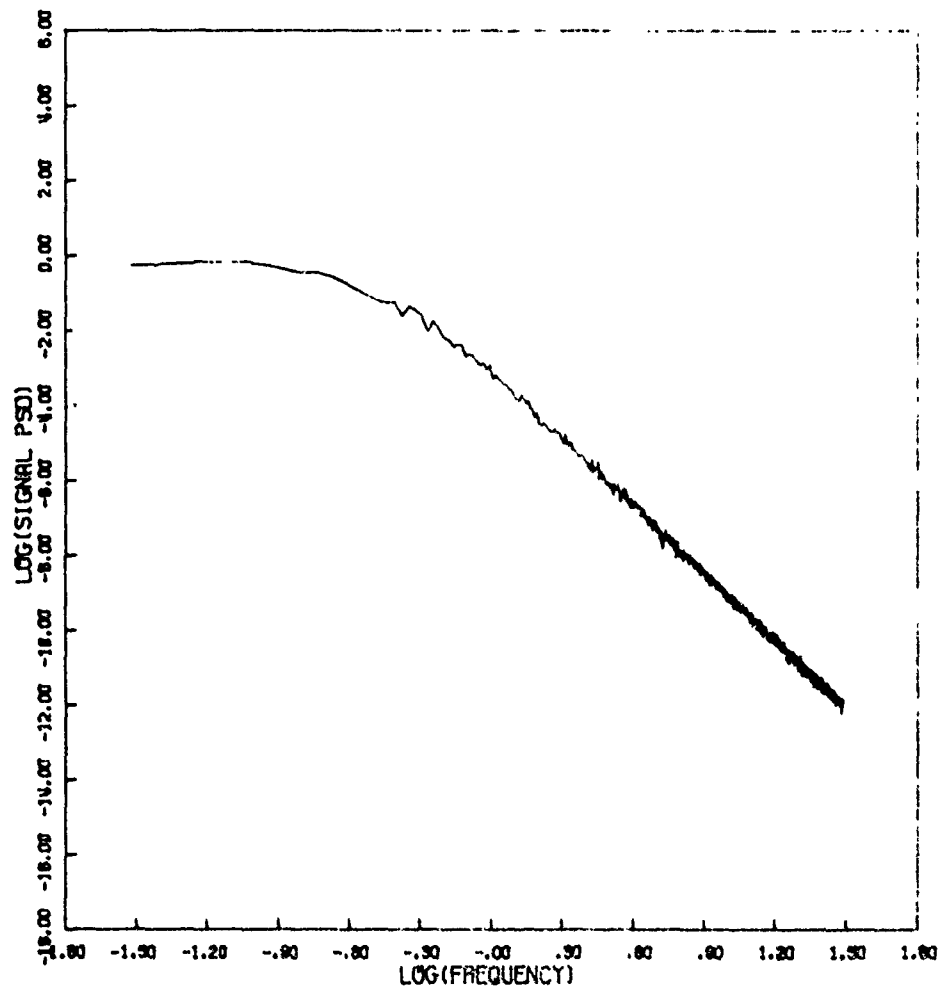Figure 23e.   Phase Power Spectral Density
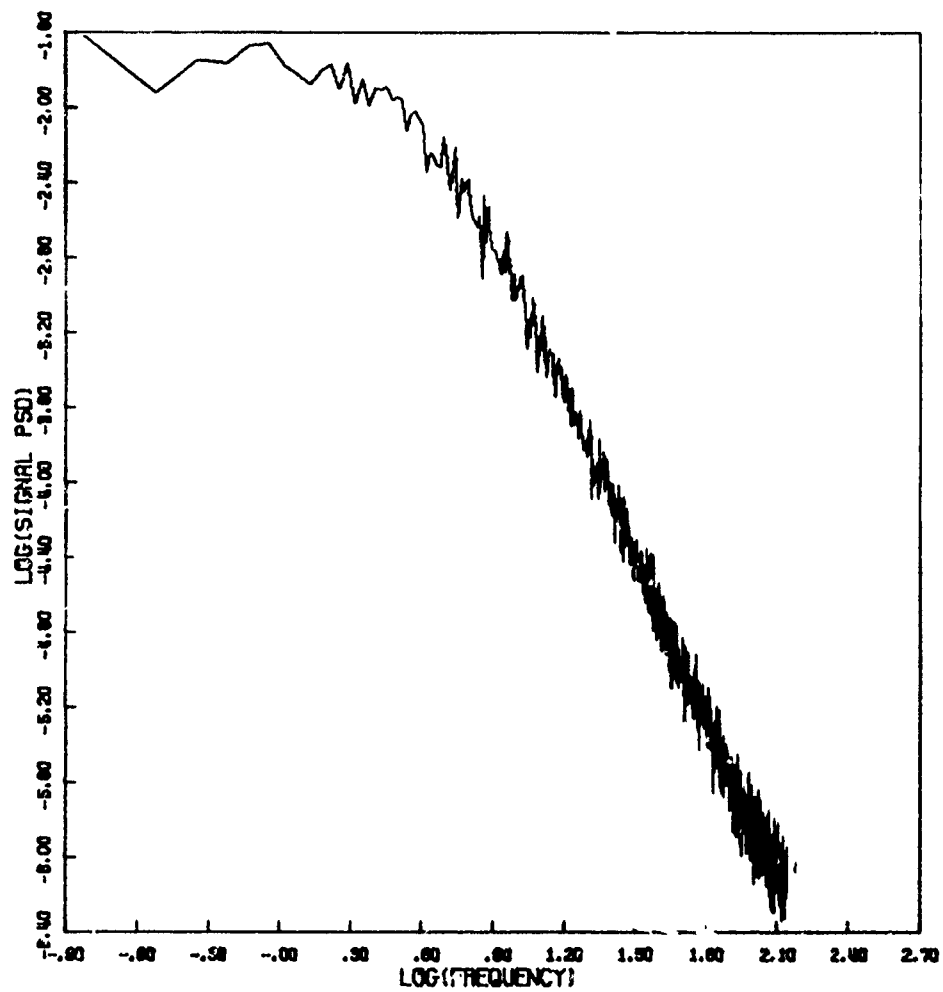
Figure 23f. Signal Power Spectral Density
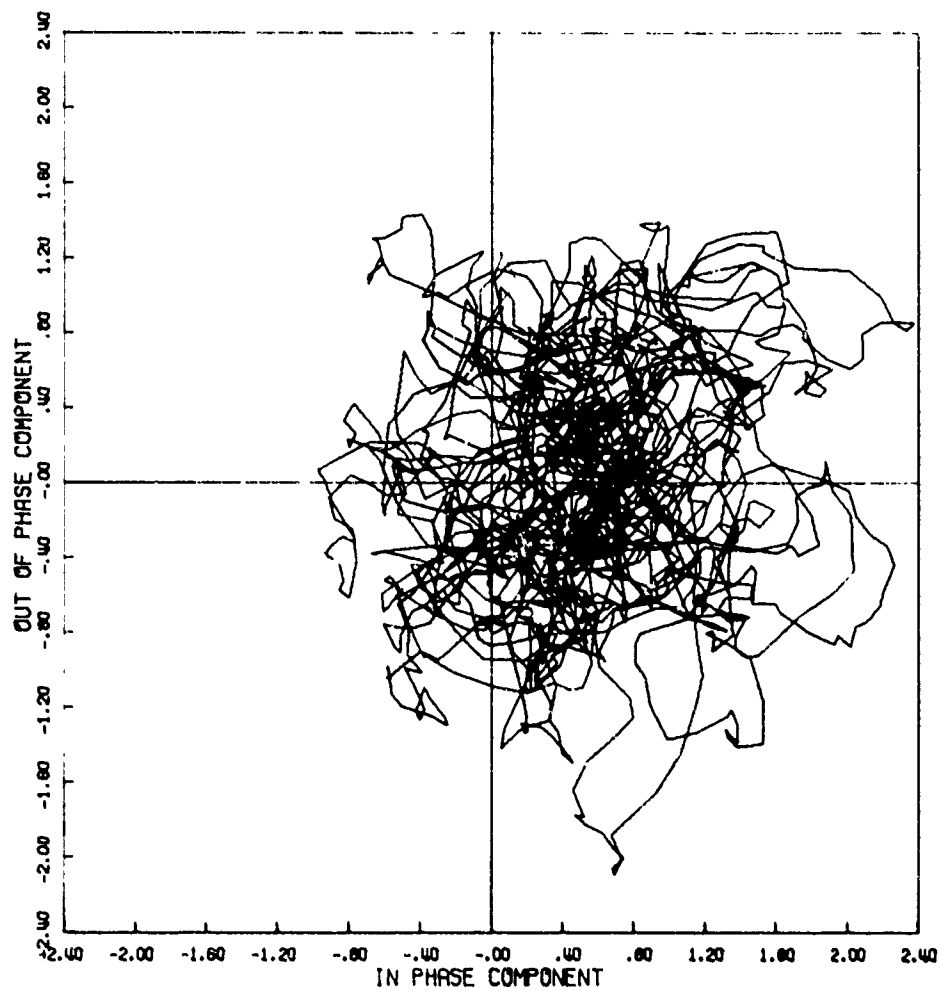
Figure 24a. Signal Phase Plot
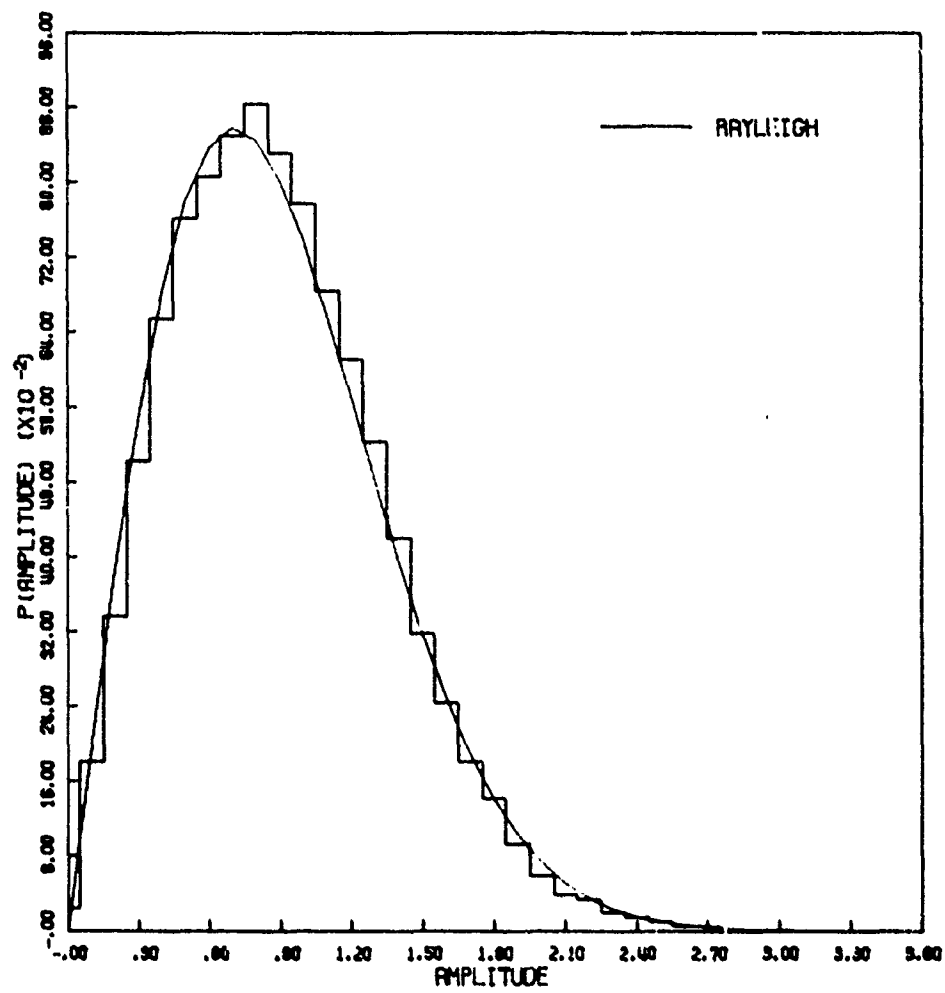
Figure 24b. Amplitude Distribution
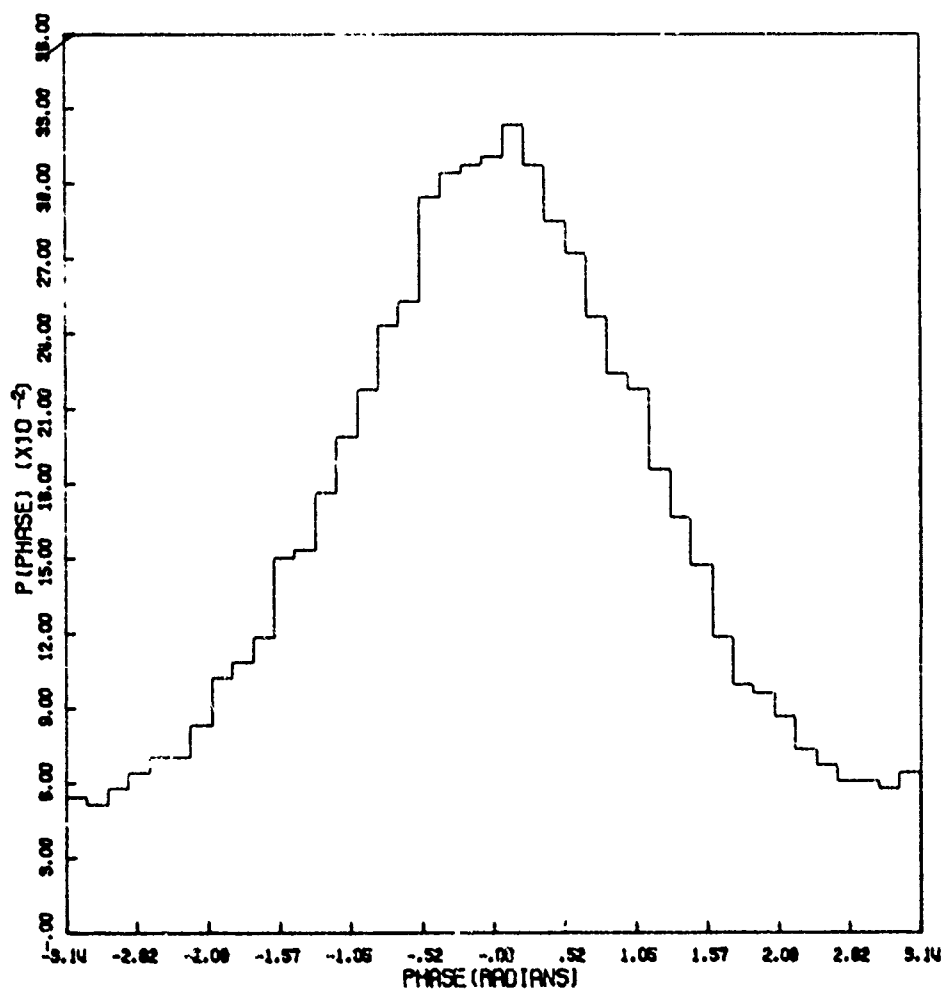
Figure 24c. Phase Distribution
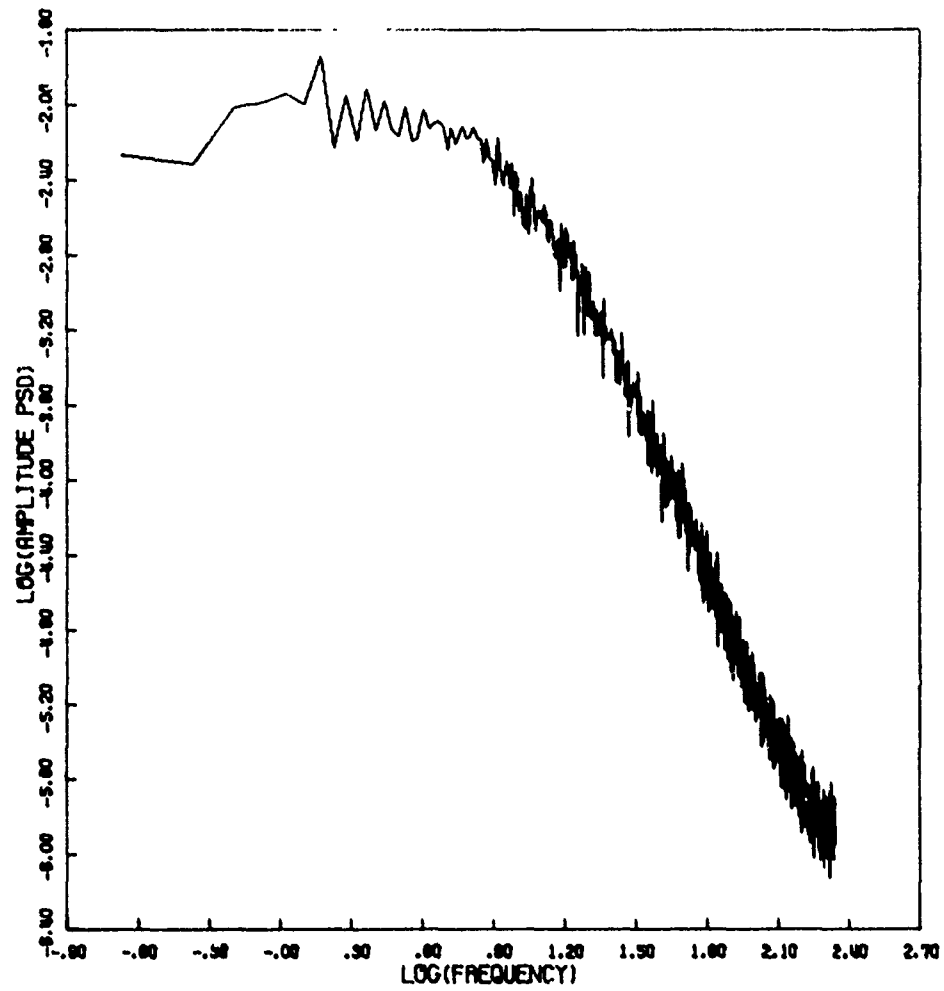
Figure 24d. Amplitude Power Spectral Density
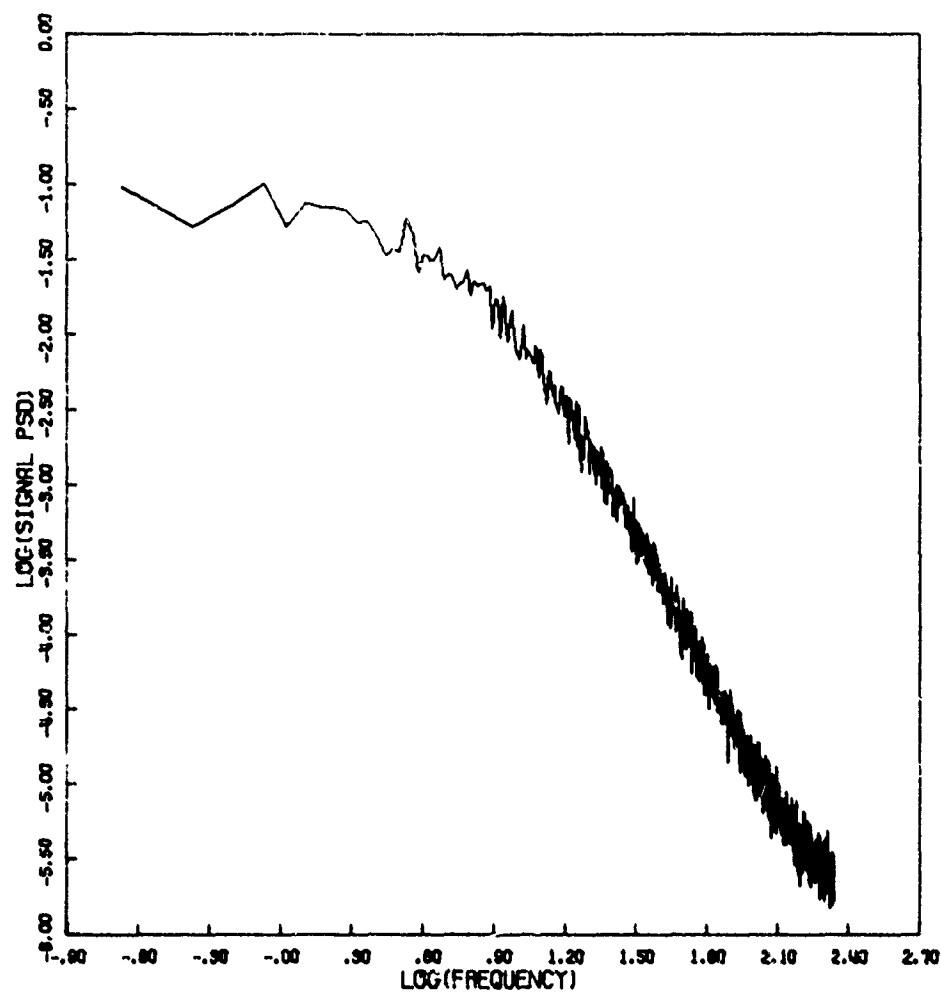
Figure 24f. Signal Power Spectral Density
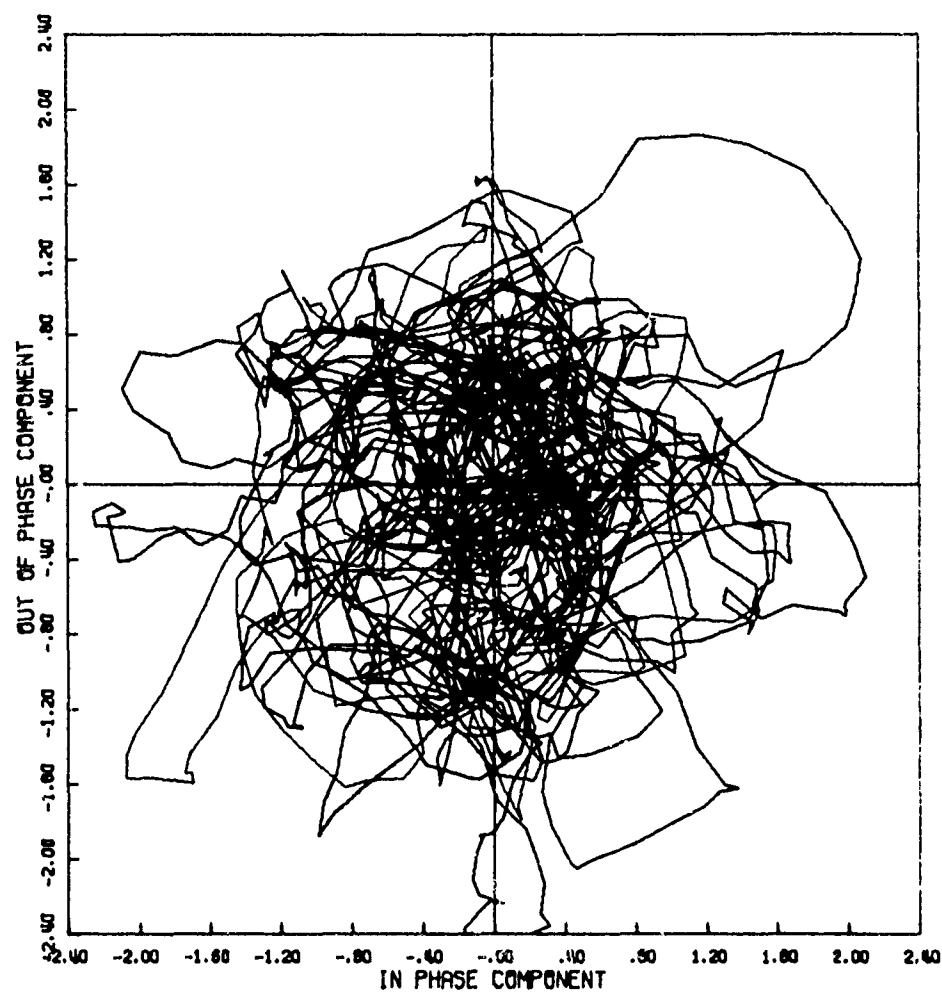
Figure 25a. Signal Phase Plot
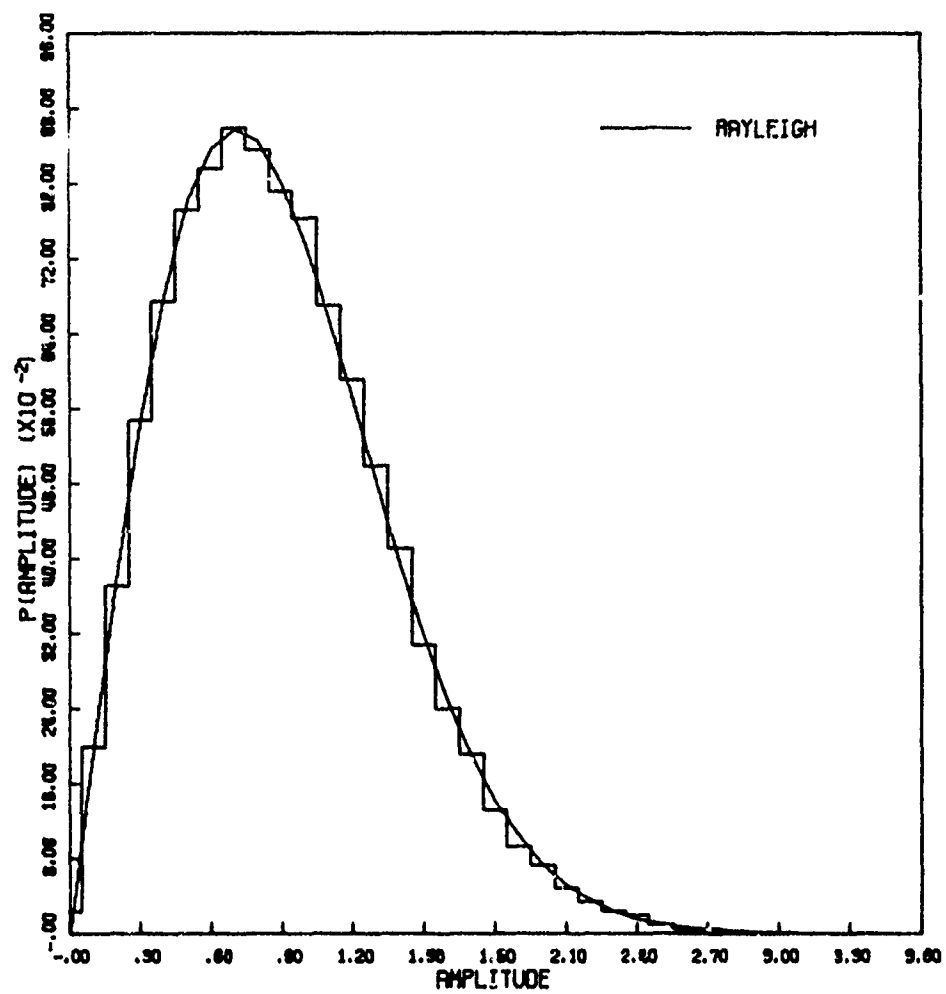
Figure 25b.   Amplitude Distribution
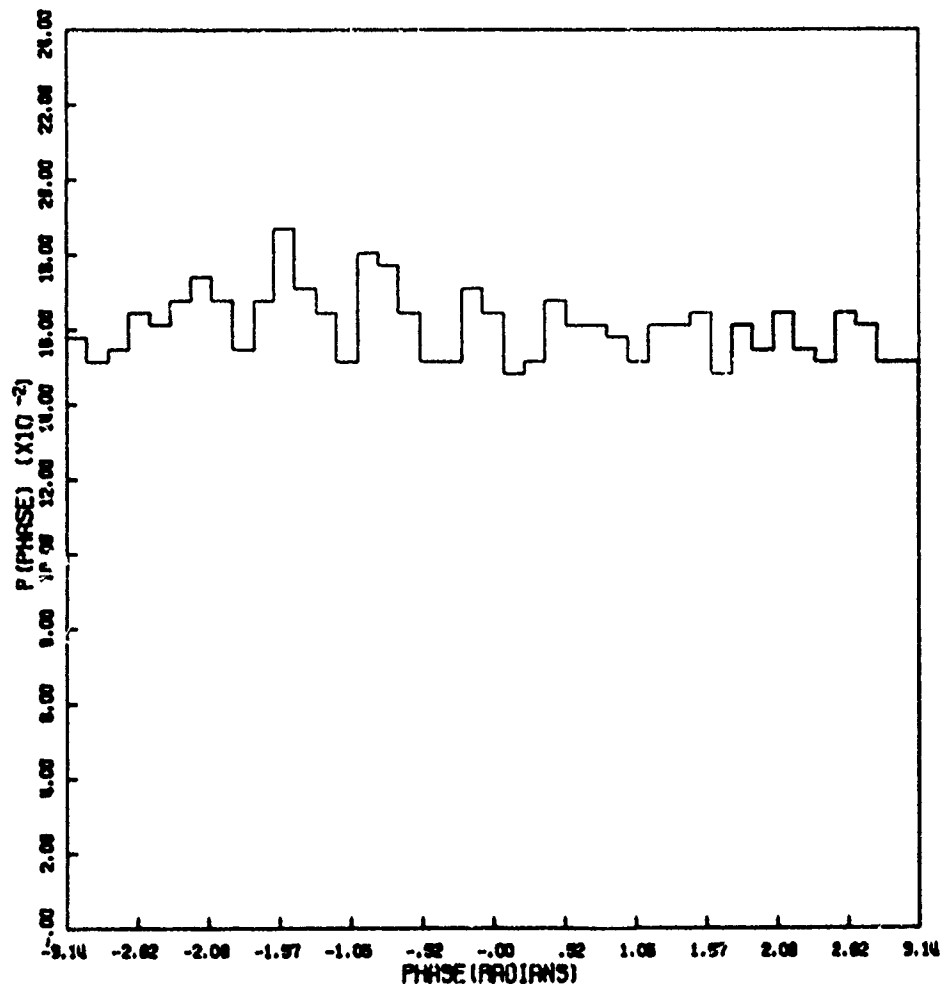
Figure 25c. Phase Distribution
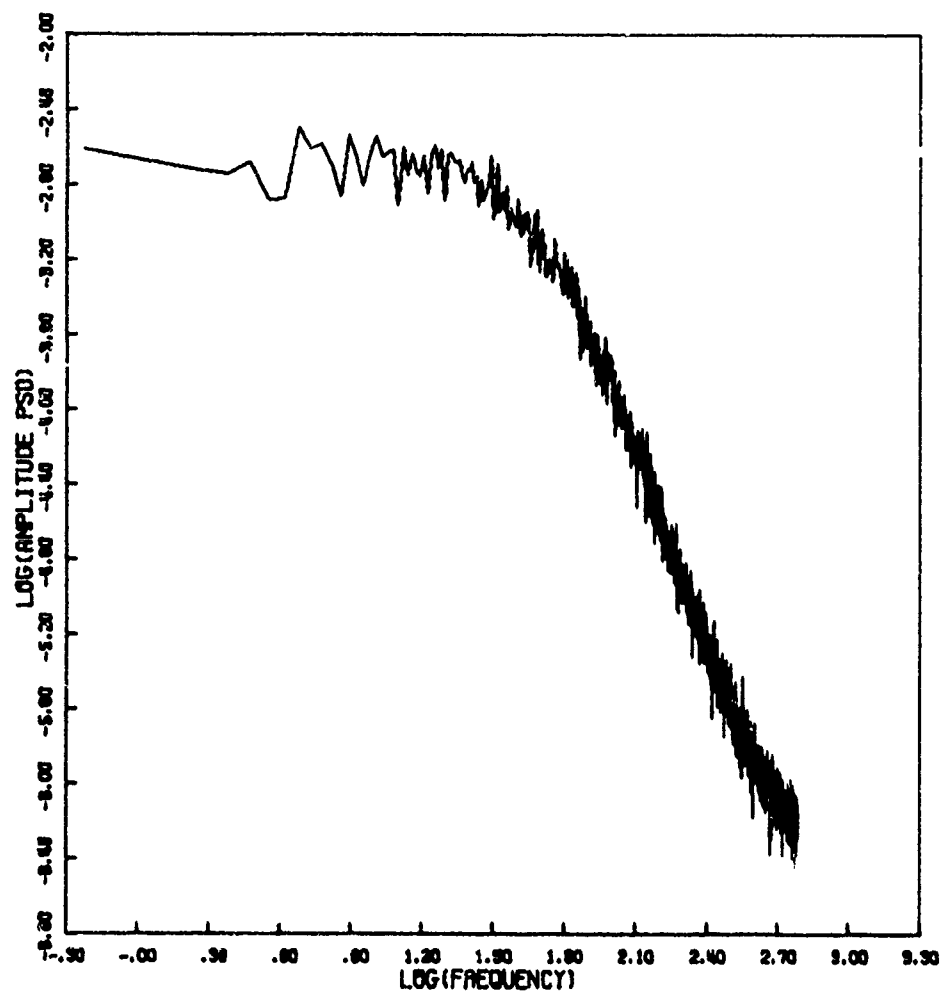
Figure 25d.   Amplitude Power Spectral Density
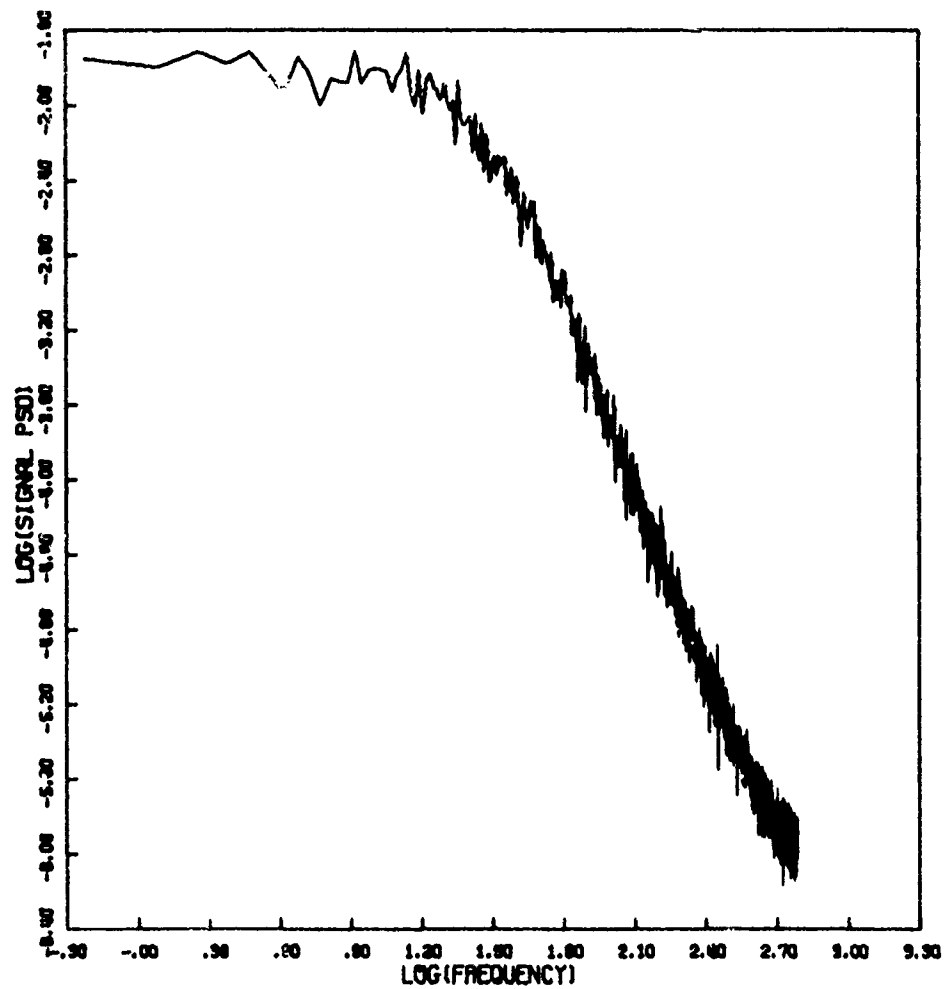
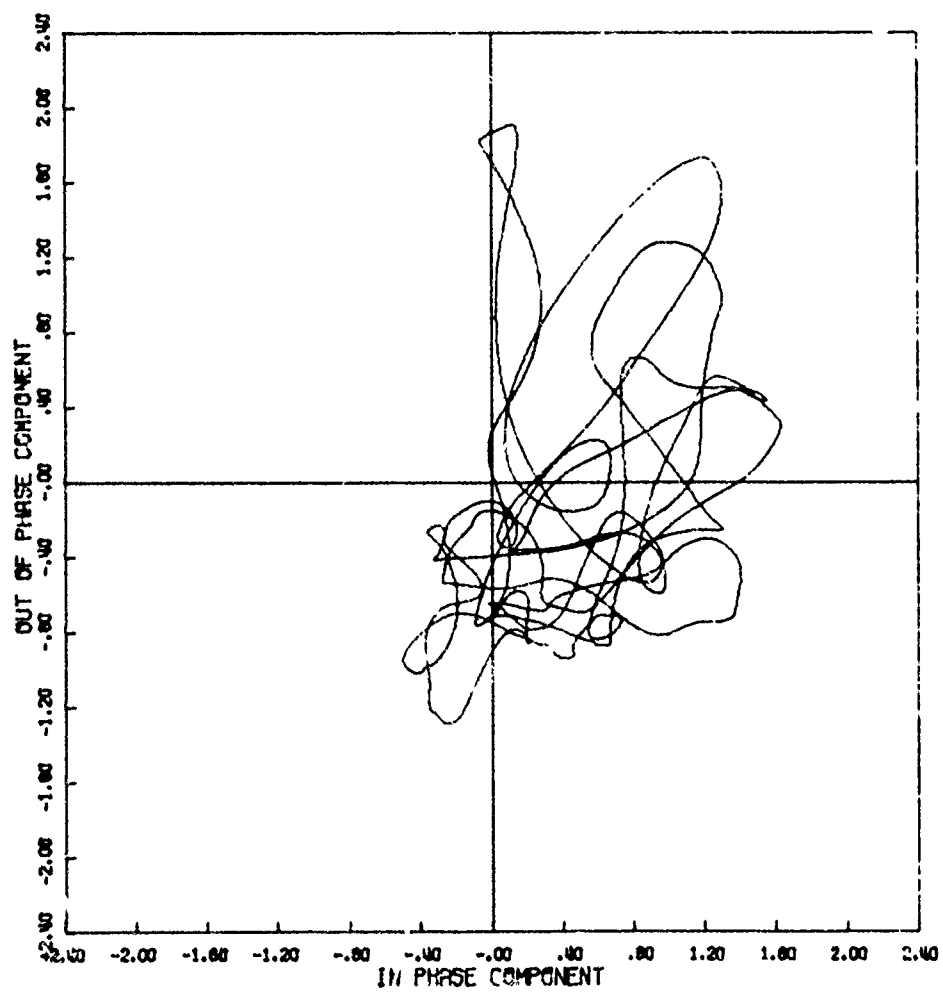Figure 25f.   Signal Power Spectral Density
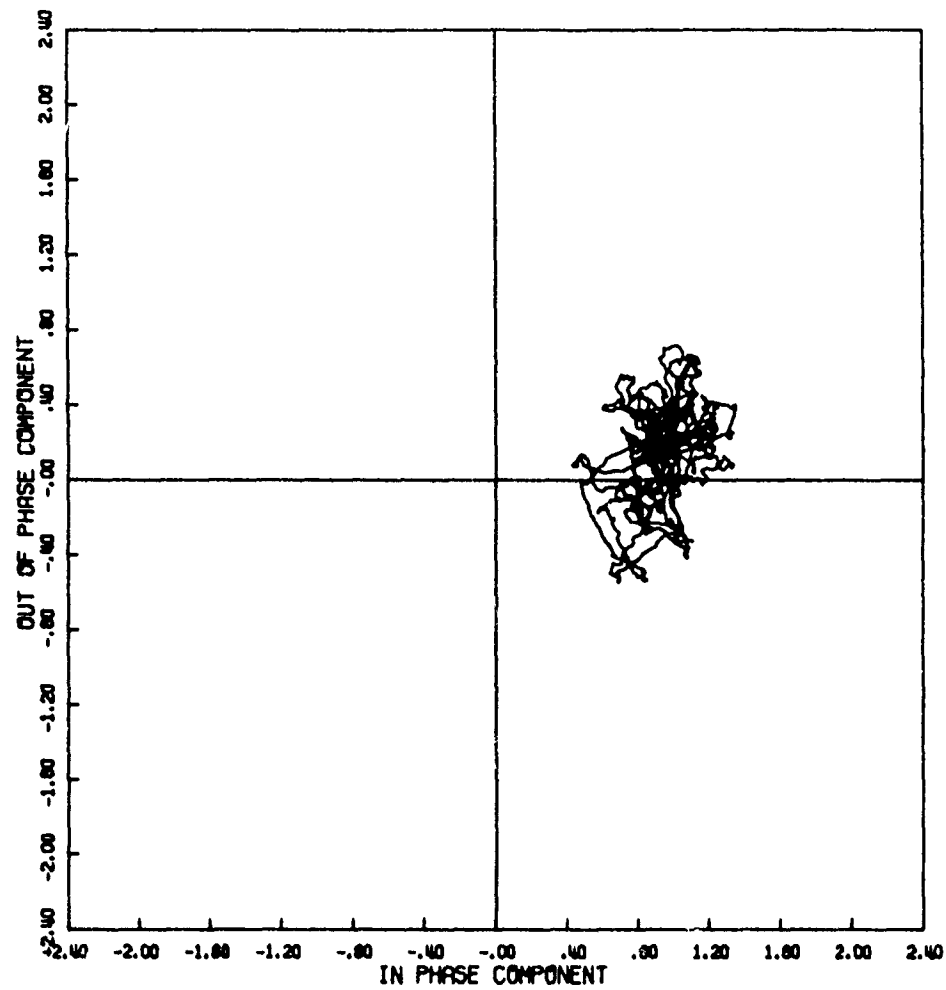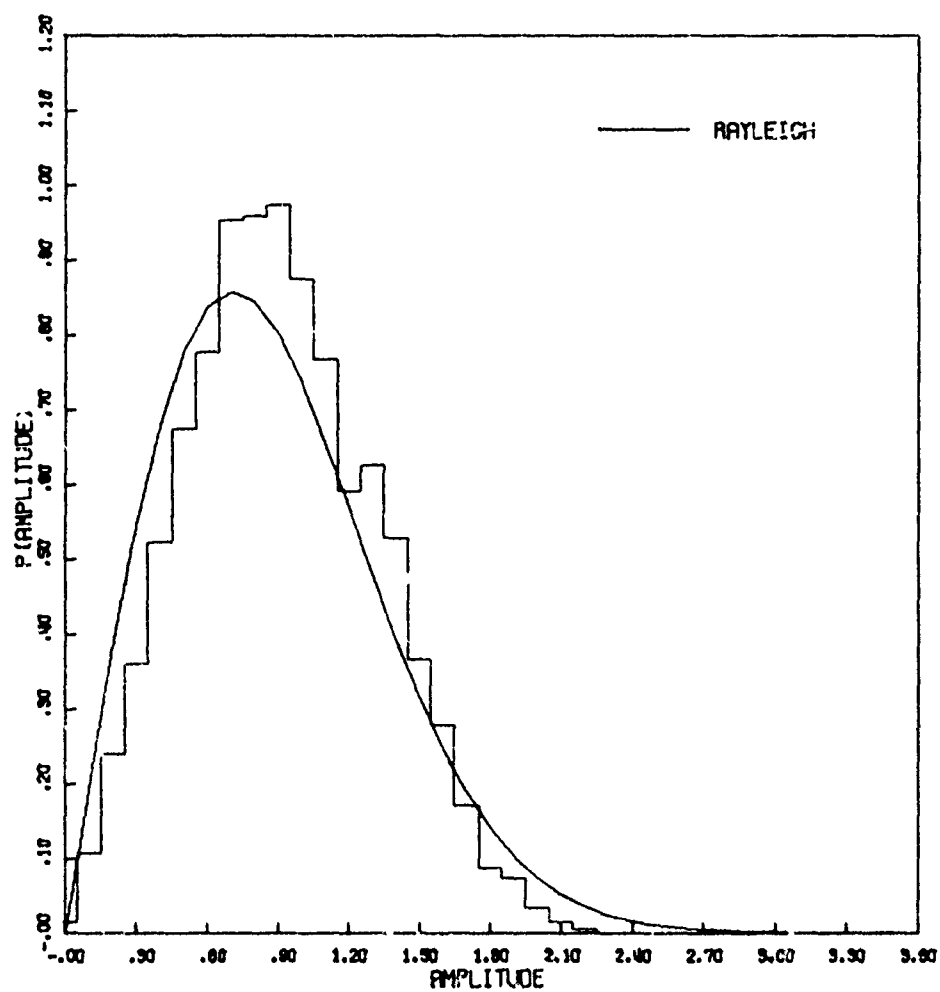
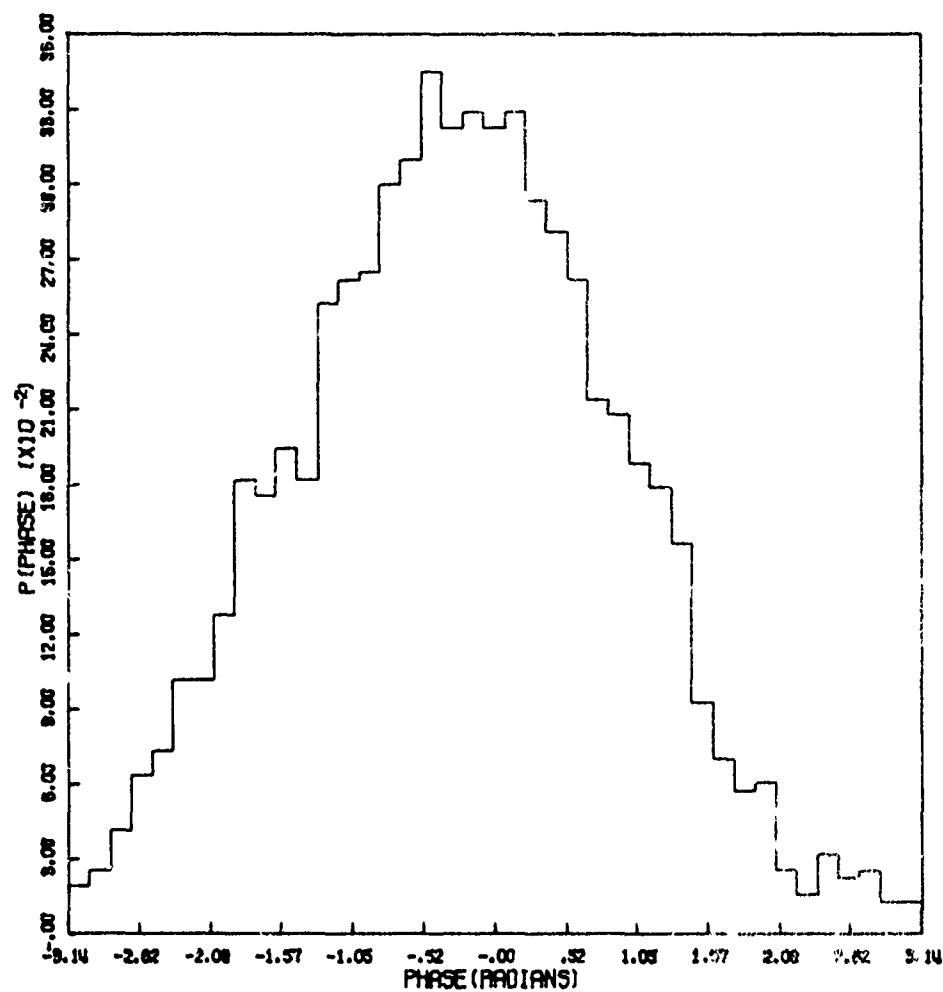Figure 26a.   Signal Phase Plot
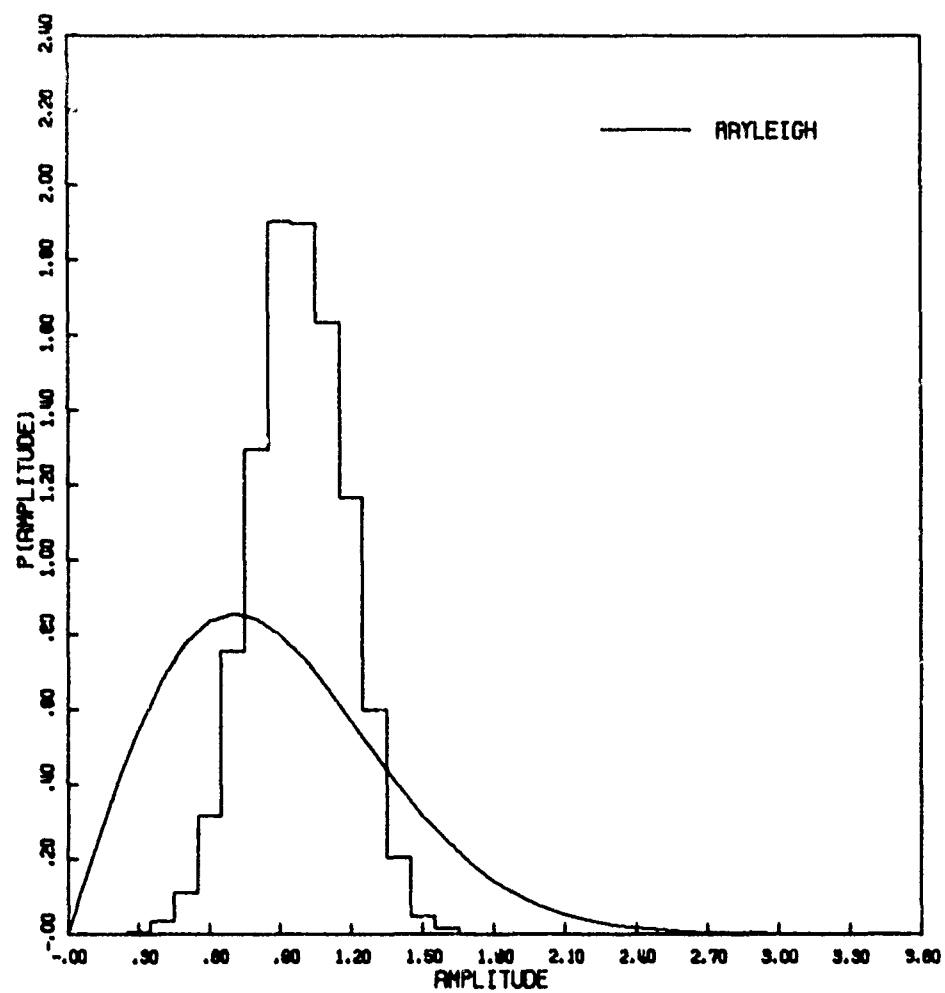
Figure 26b. Amplitude Distribution
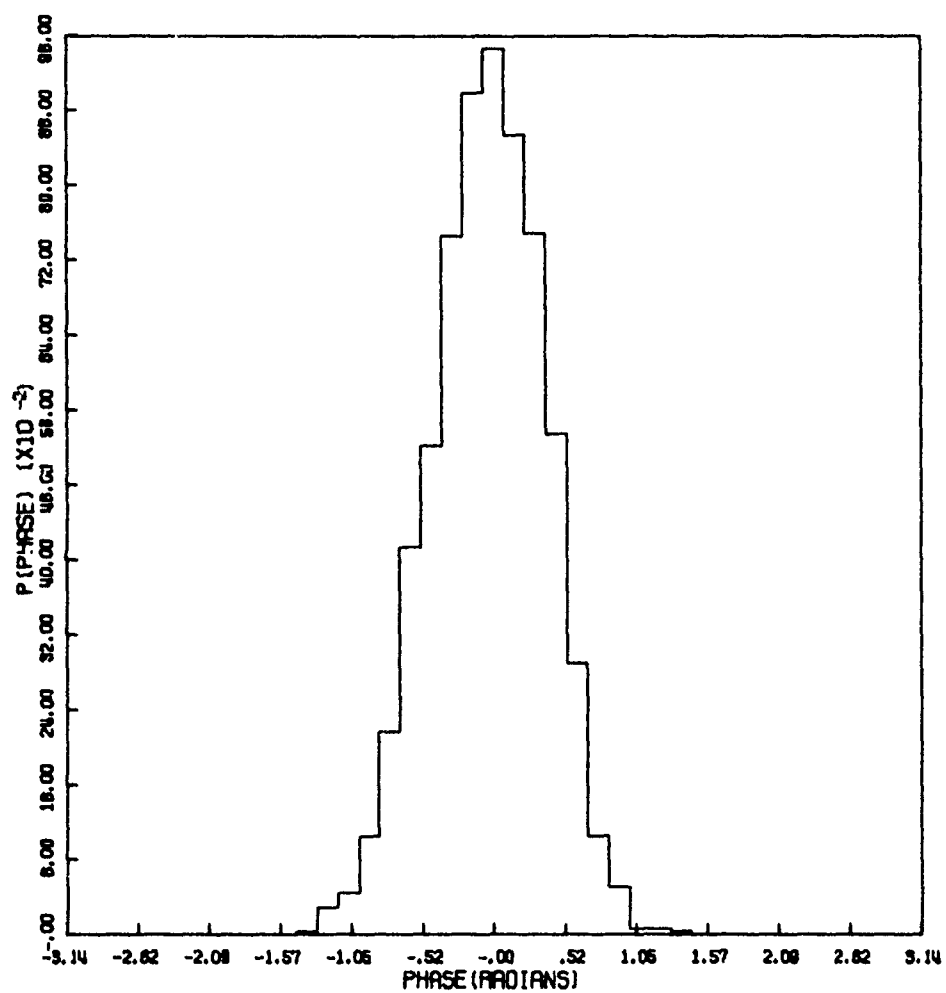
Figure 26c.   Phase Distribution
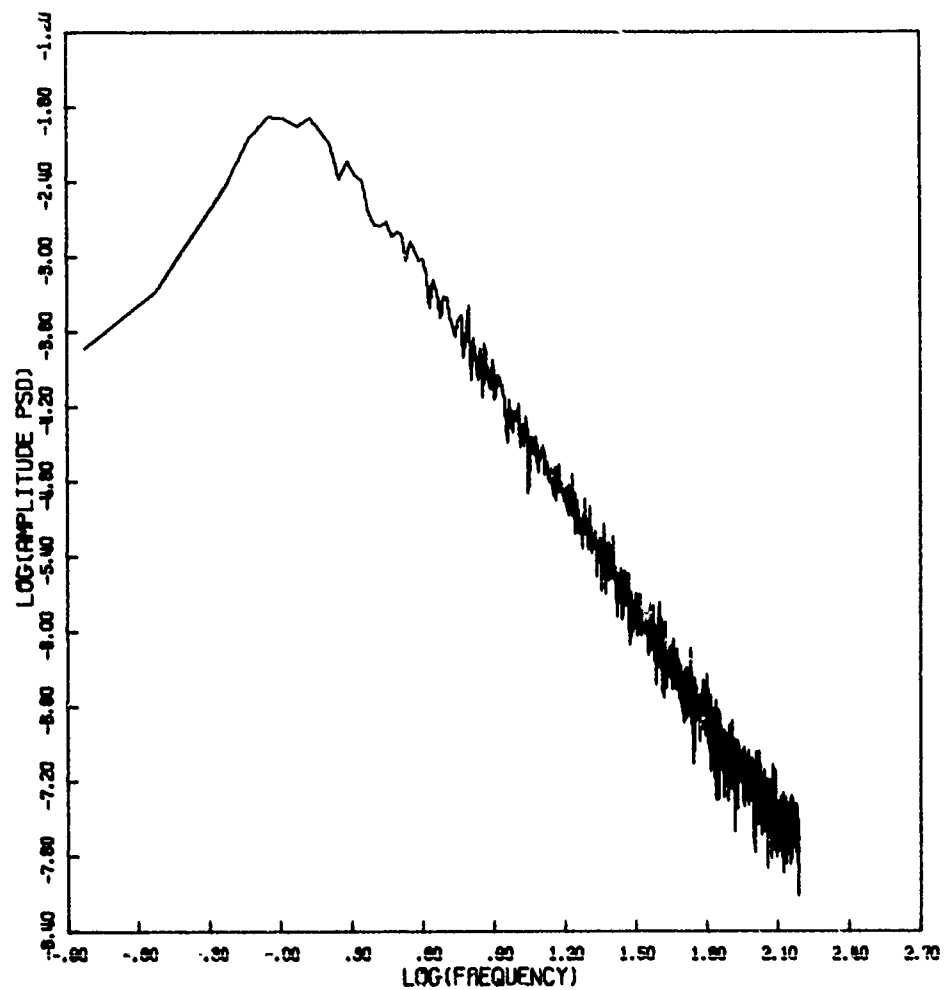
Figure 26d. Amplitude Power Spectral Density
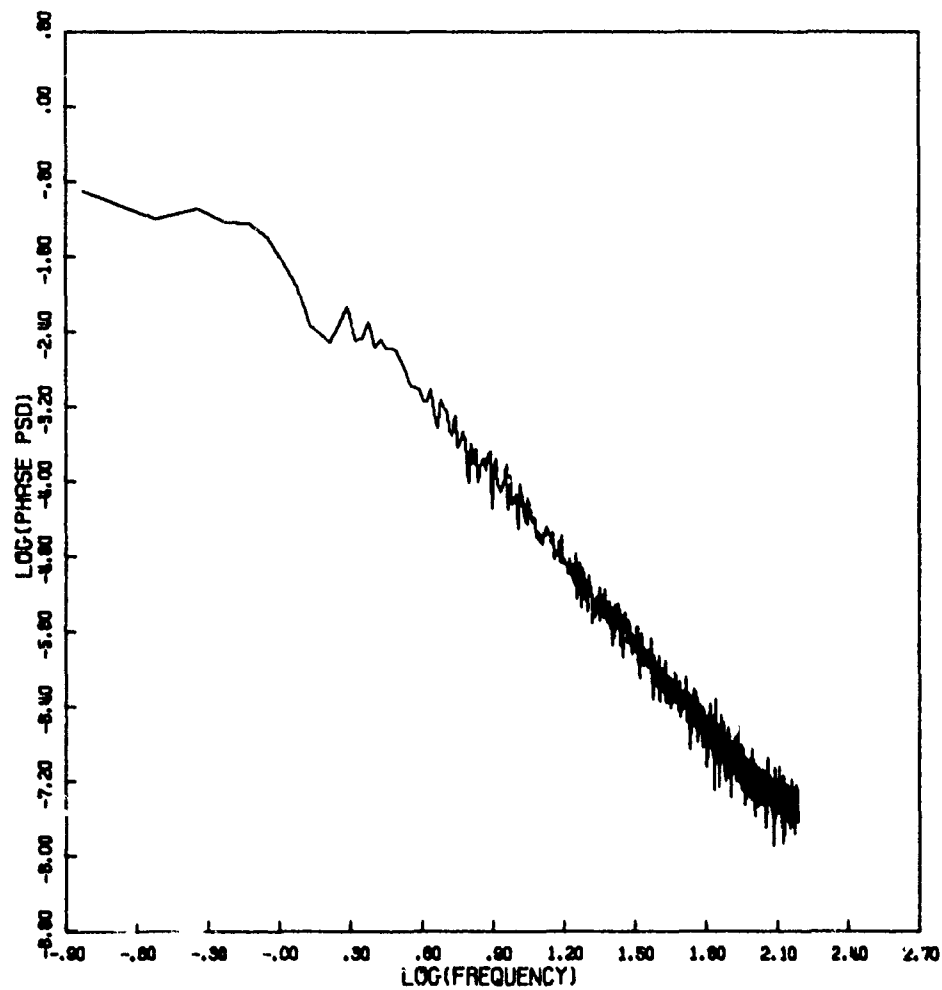
Figure 26e. Phase Power Spectra Density
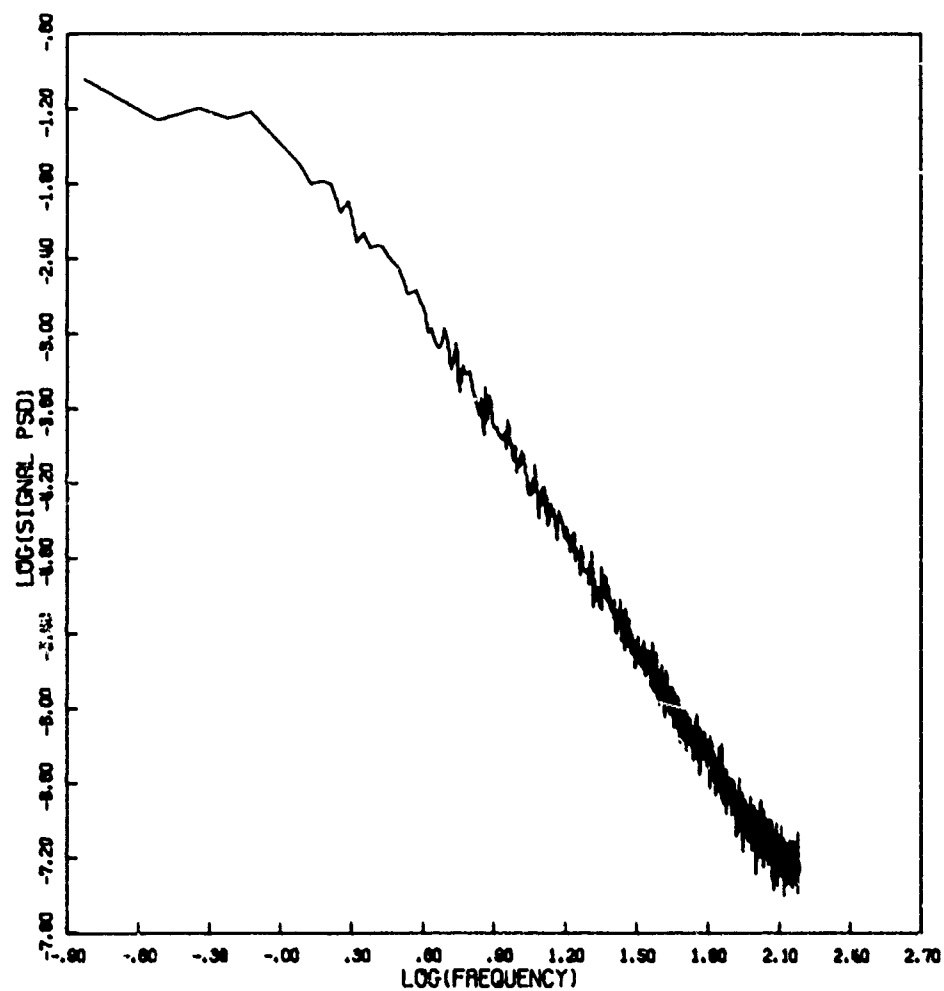
Figure 26f. Signal Power Spectral Density
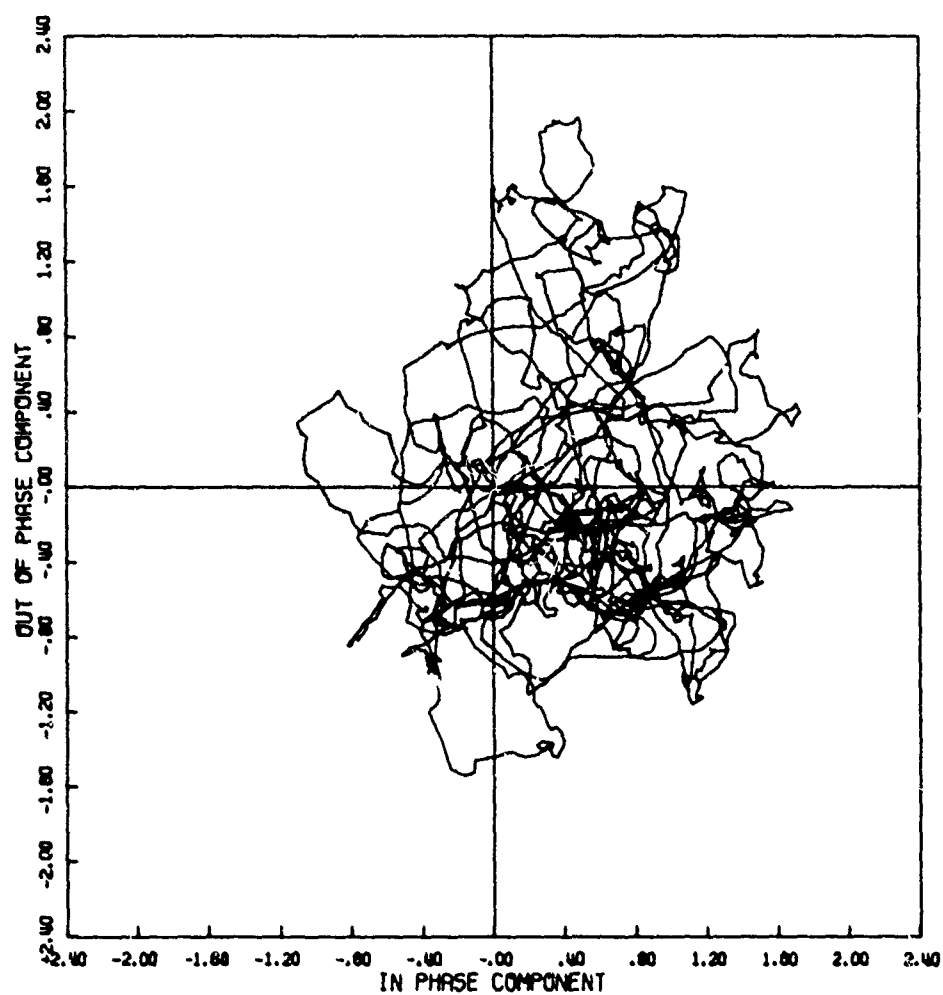
Figure 27a.   Signal Phase Plot
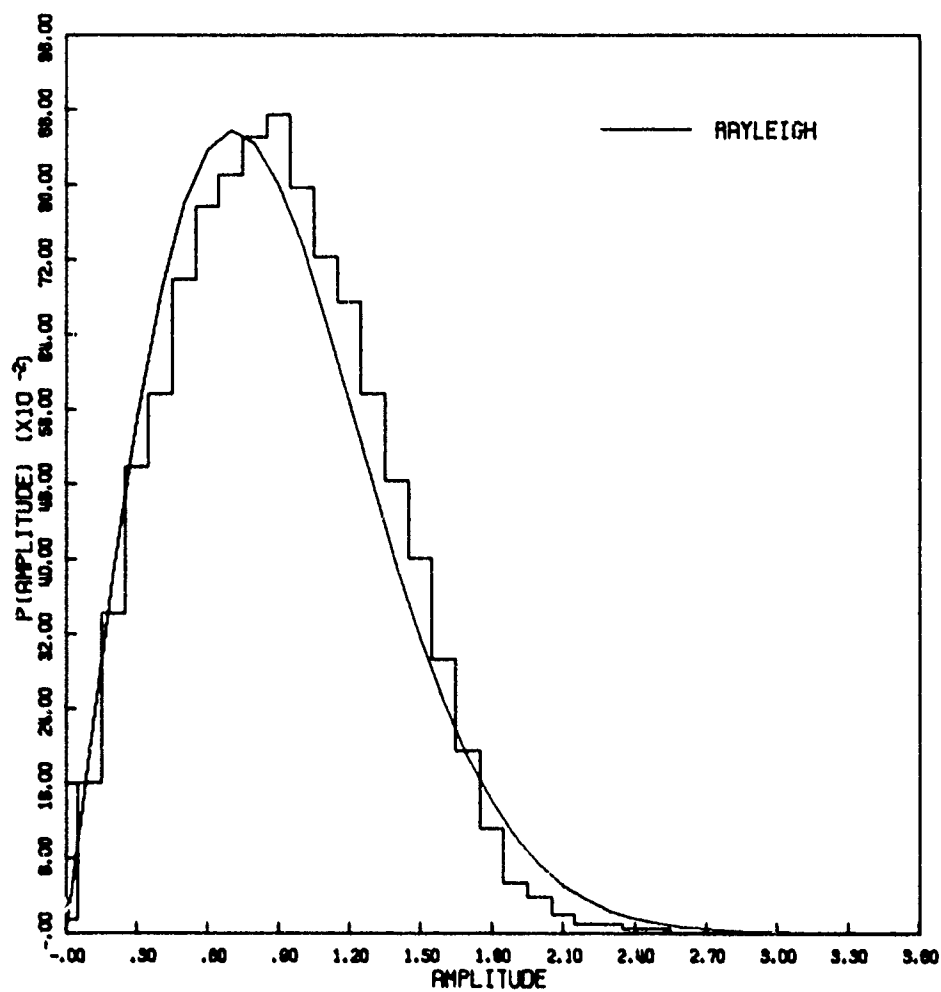
Figure 27b. Amplitude Distribution
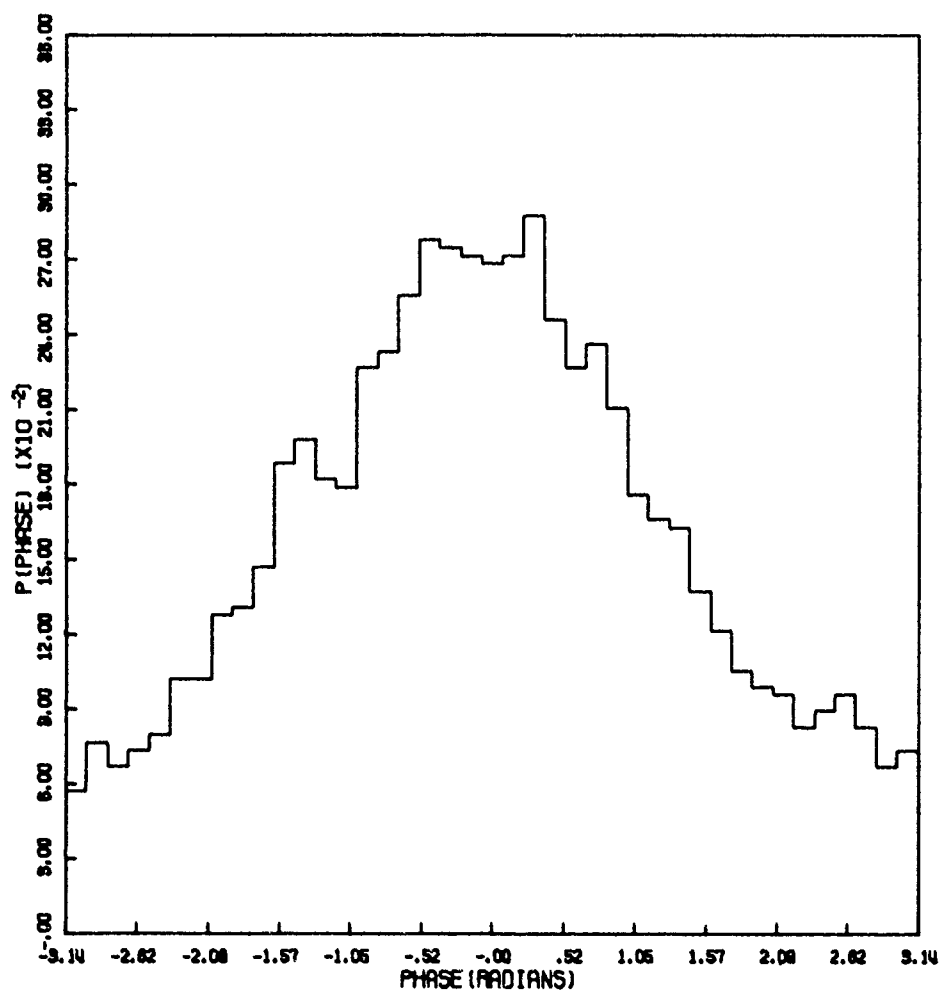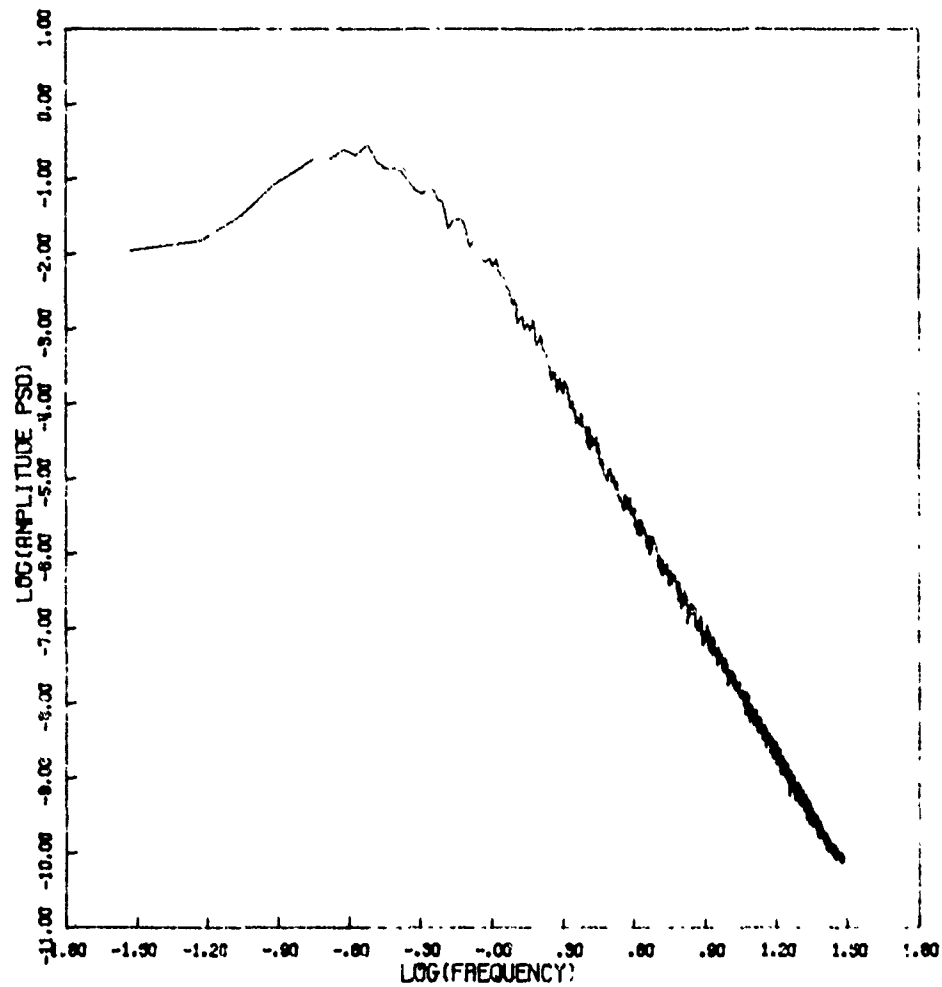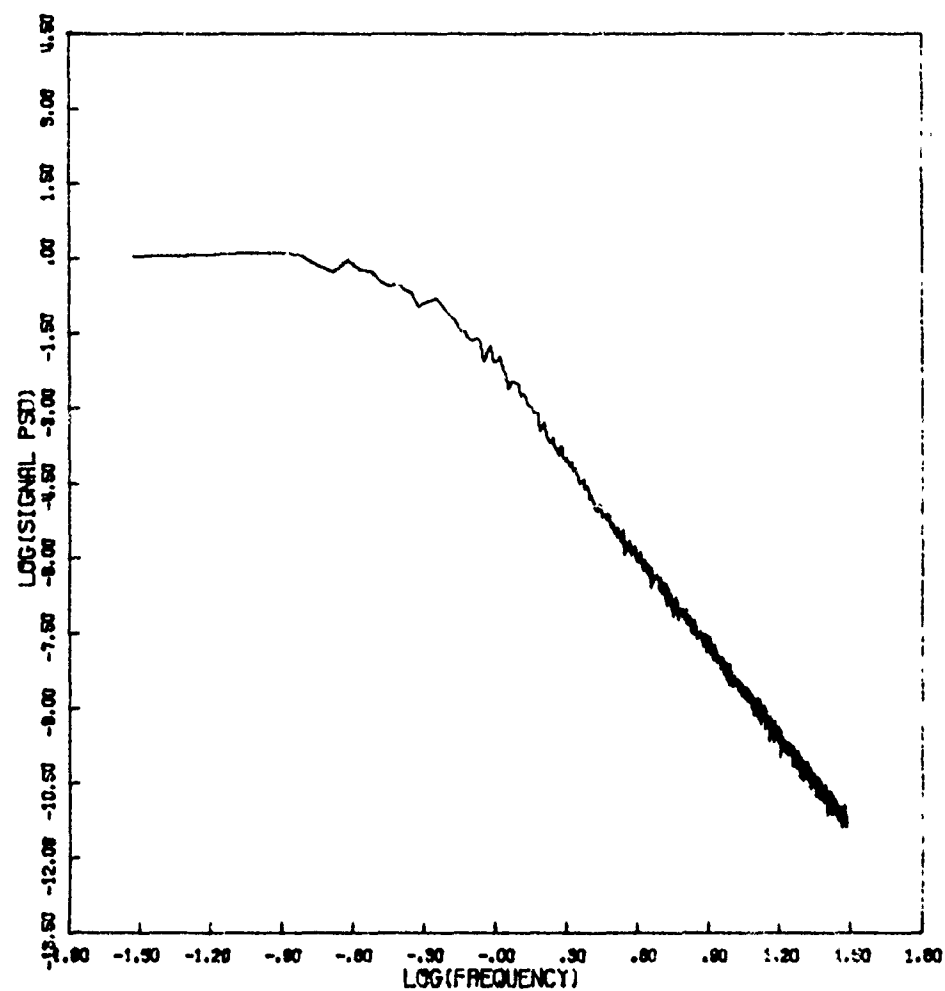
Figure 27c. Phase Distribution
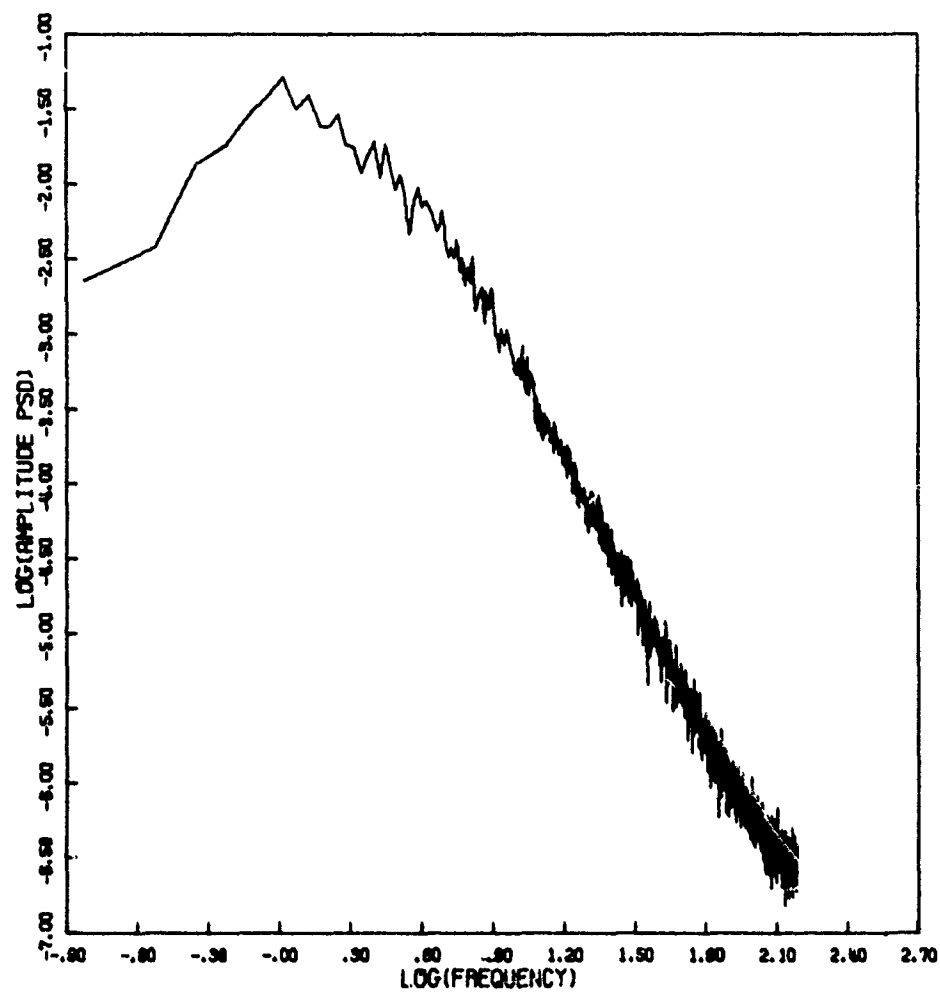
Figure 27d. Amplitude Power Spectral Density
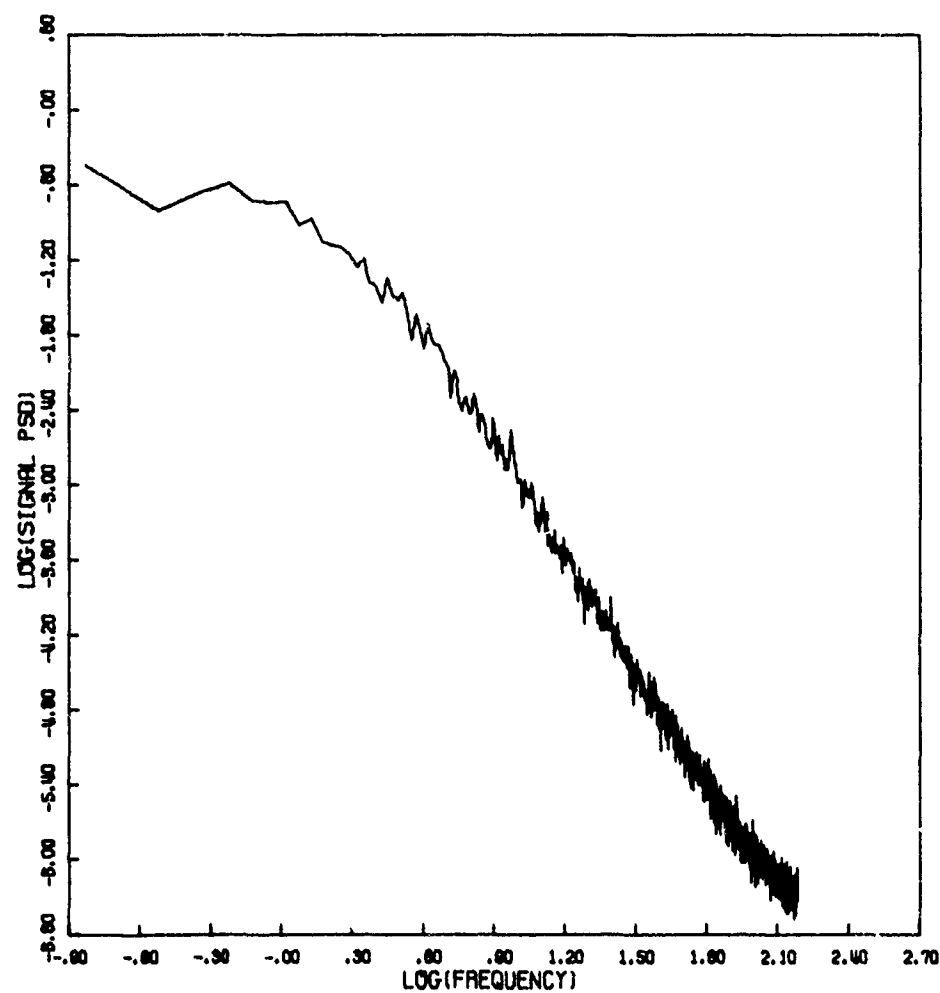
Figure 27e. Signal Power Spectral Density
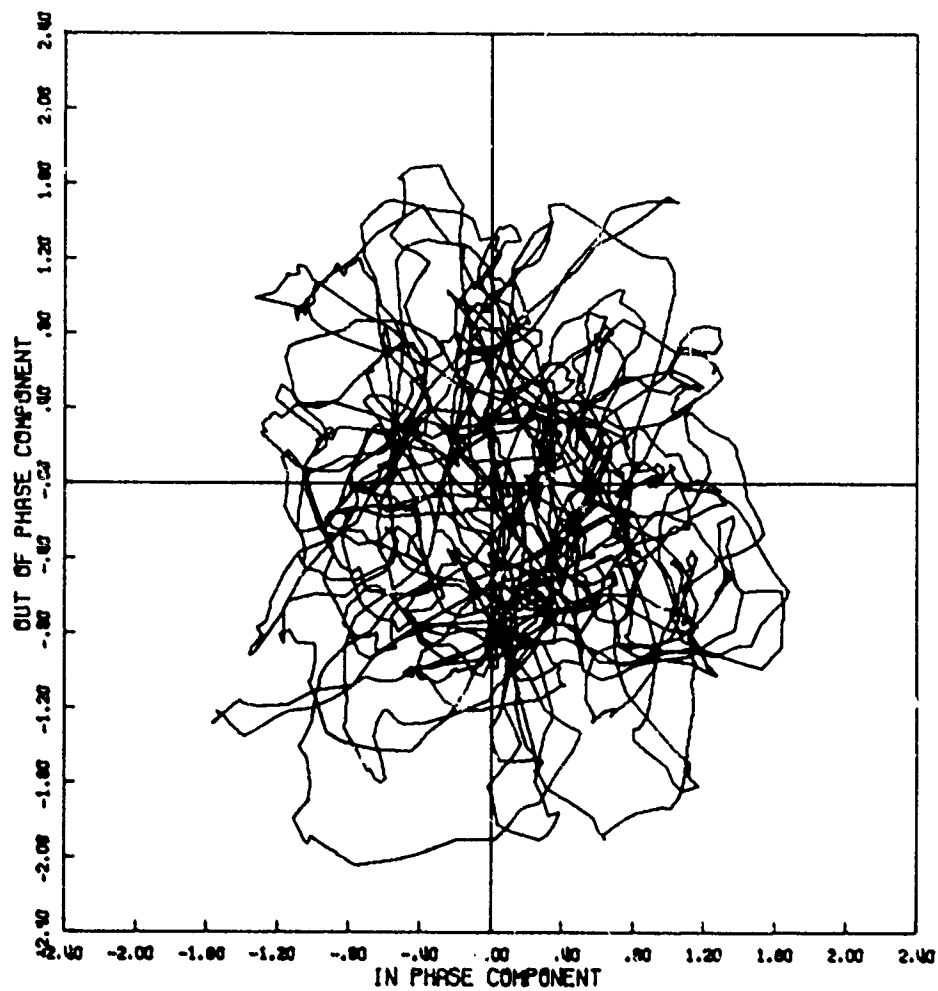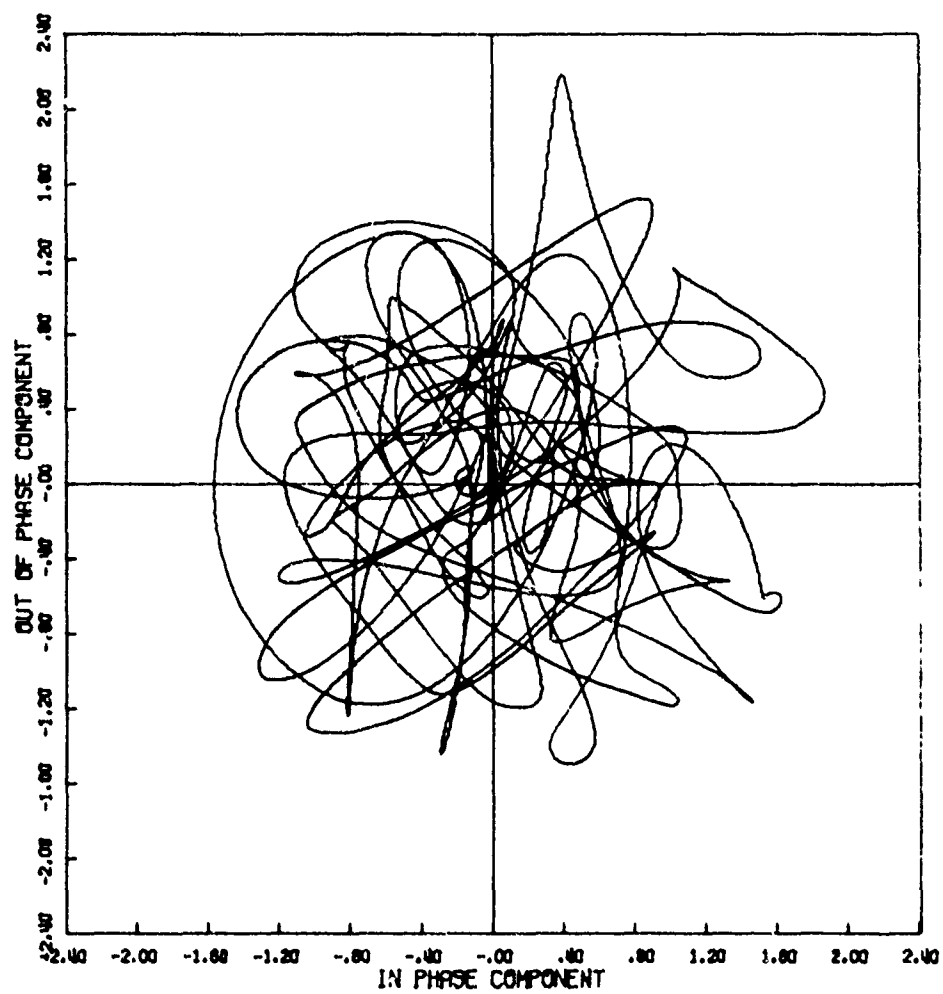
Figure 28a. Signal Phase Plot
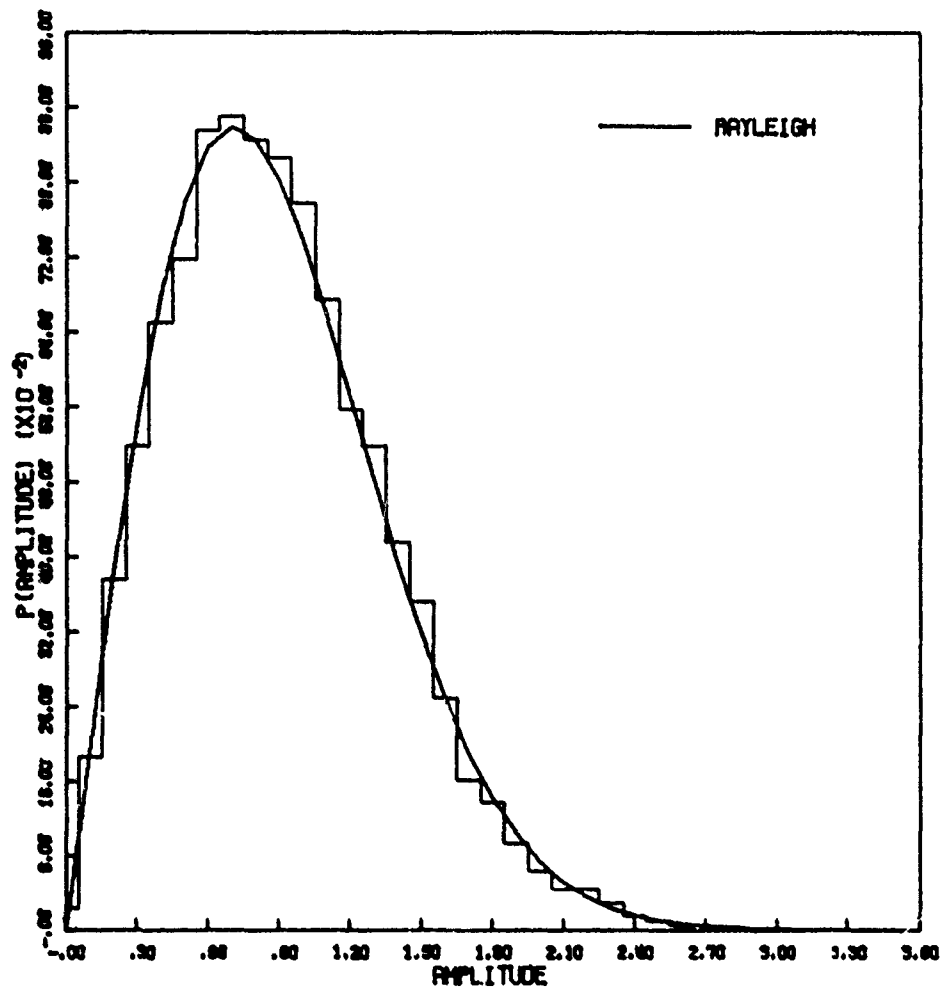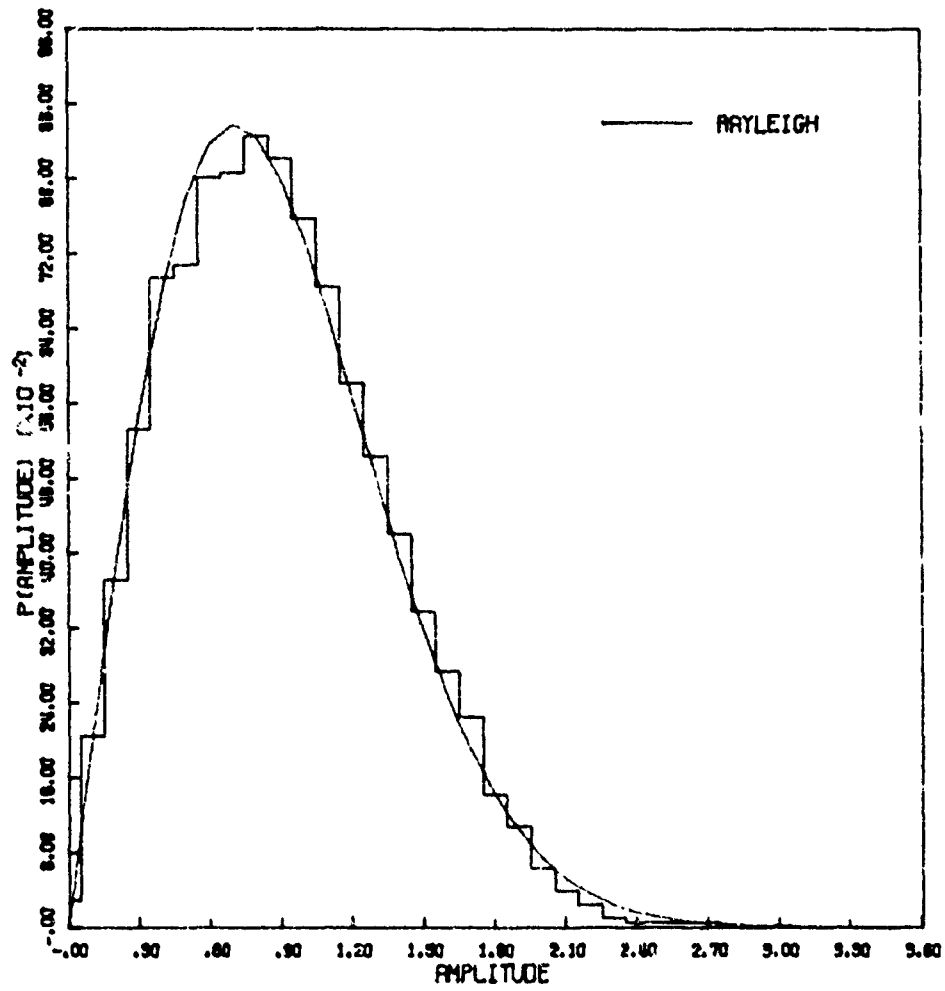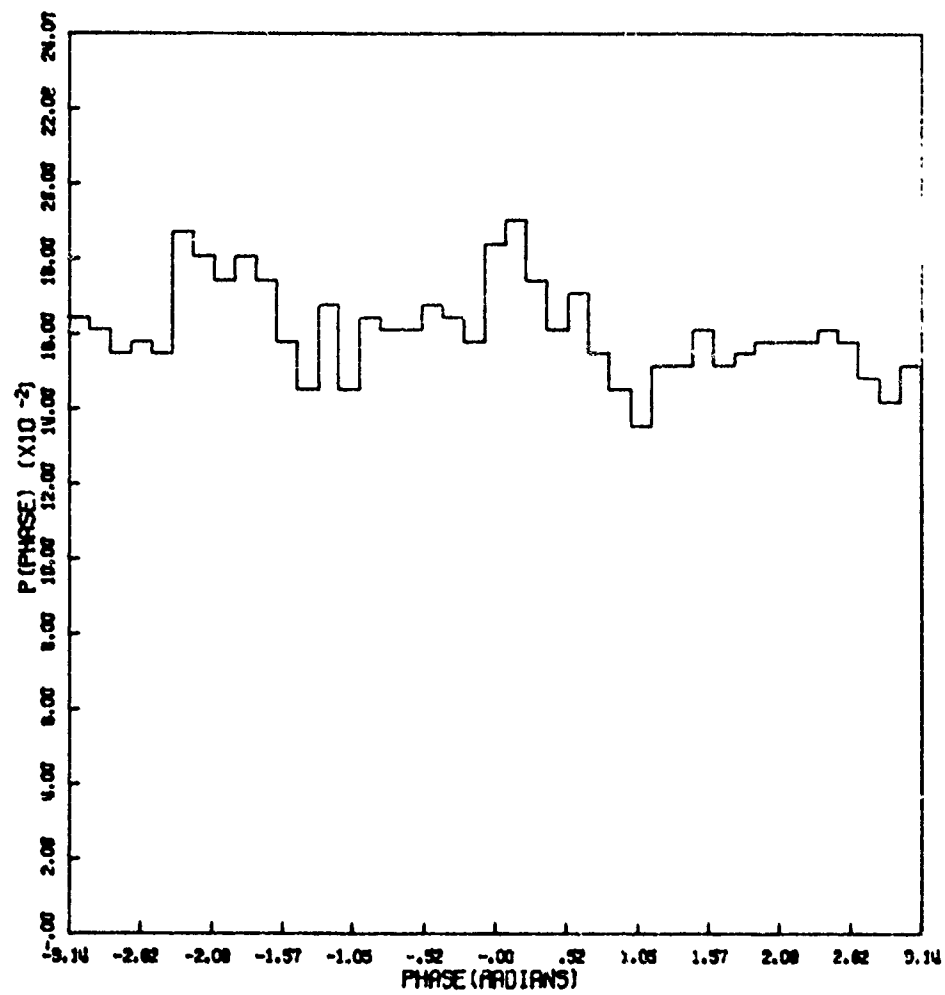
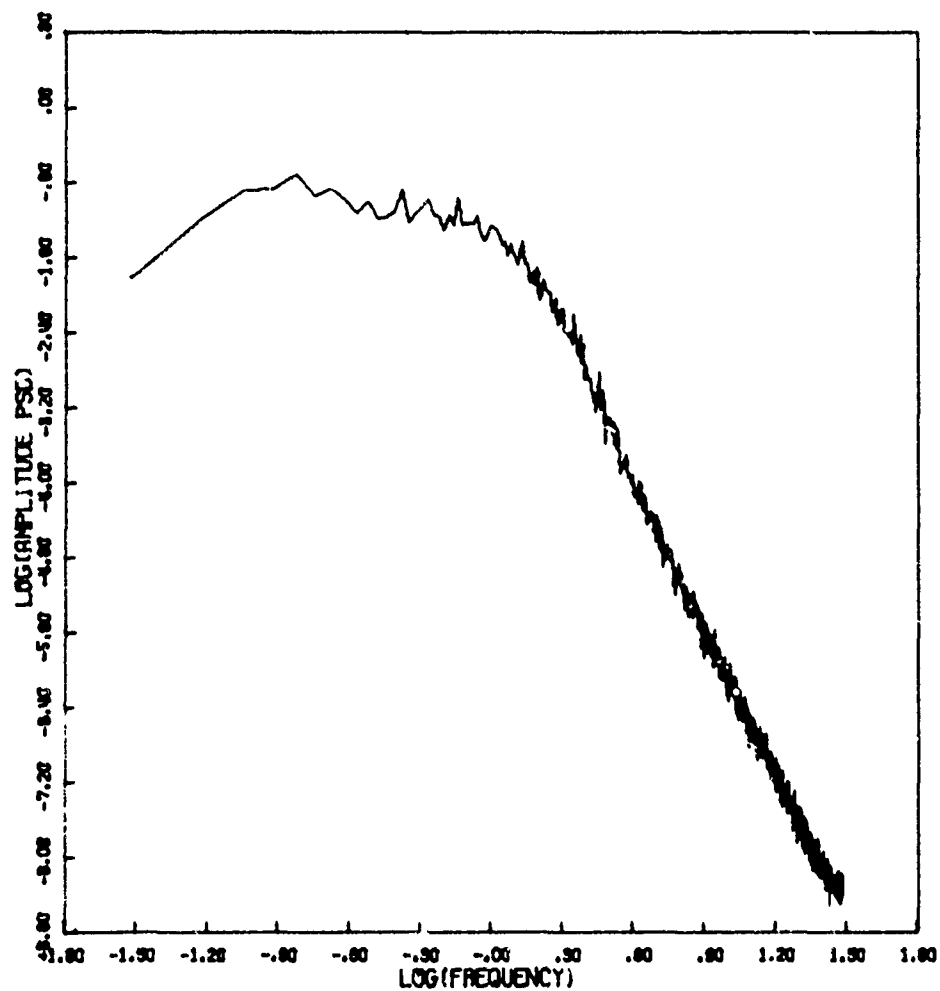Figure 28b. Amplitude Distribution
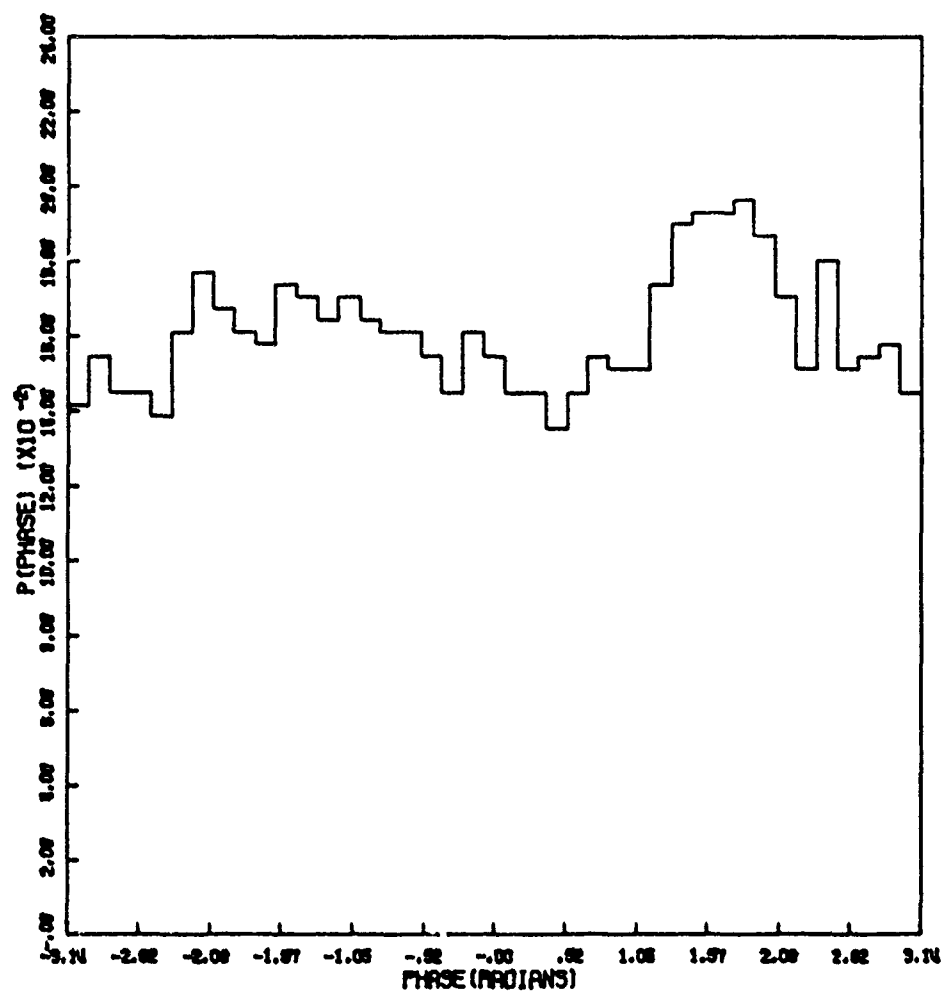
Figure 28c. Phase Distribution
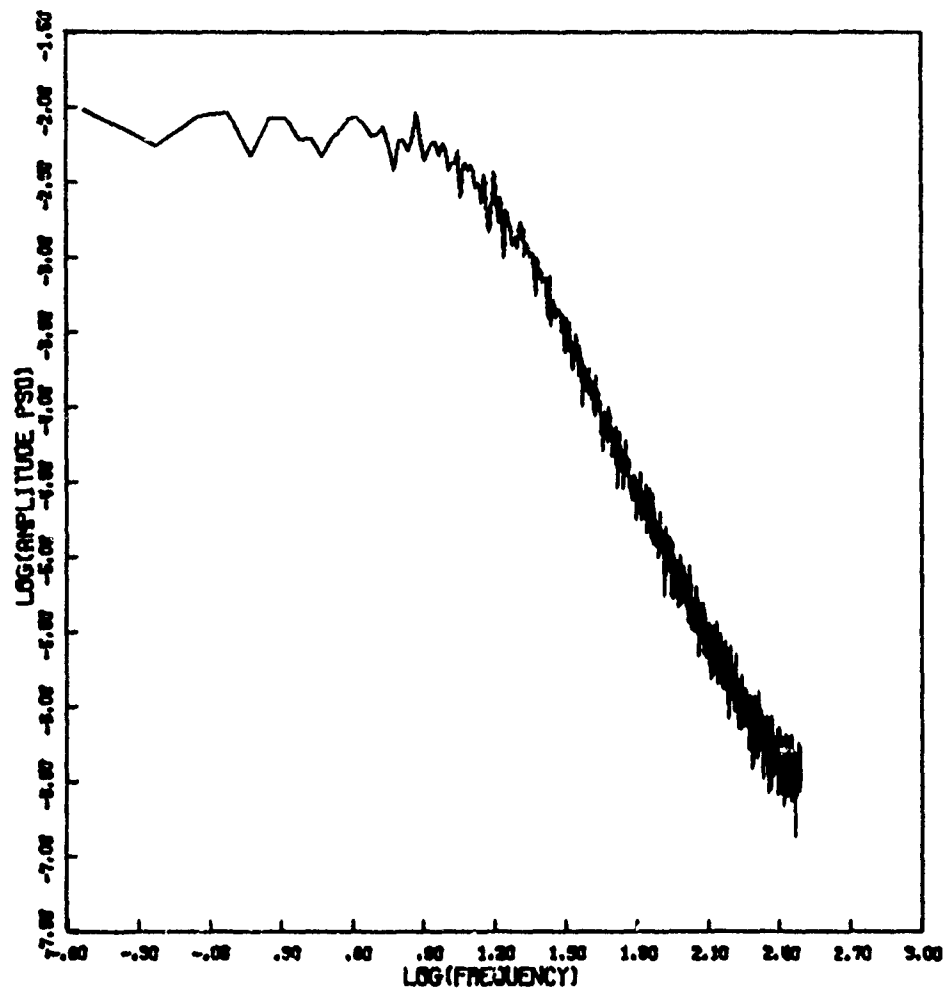
Figure 28d. Amplitude Power Spectral Density
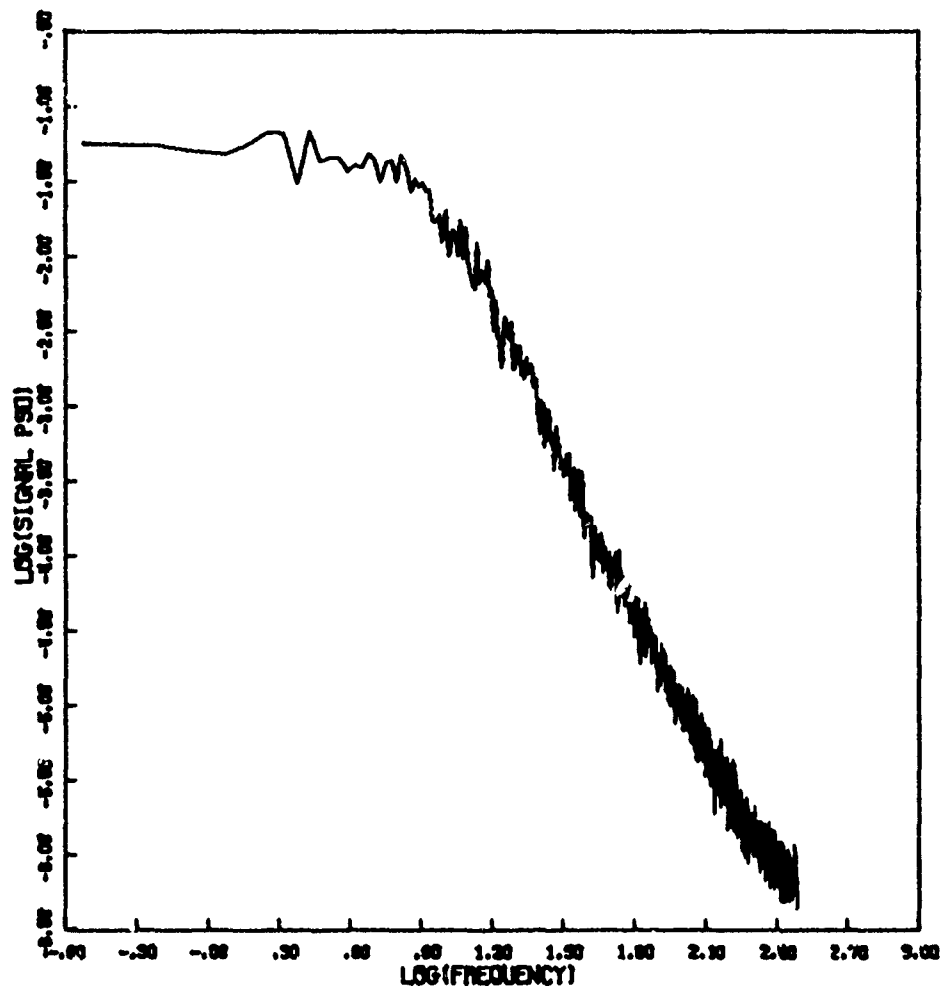
Figure 28f. Signal Power Spectral Density
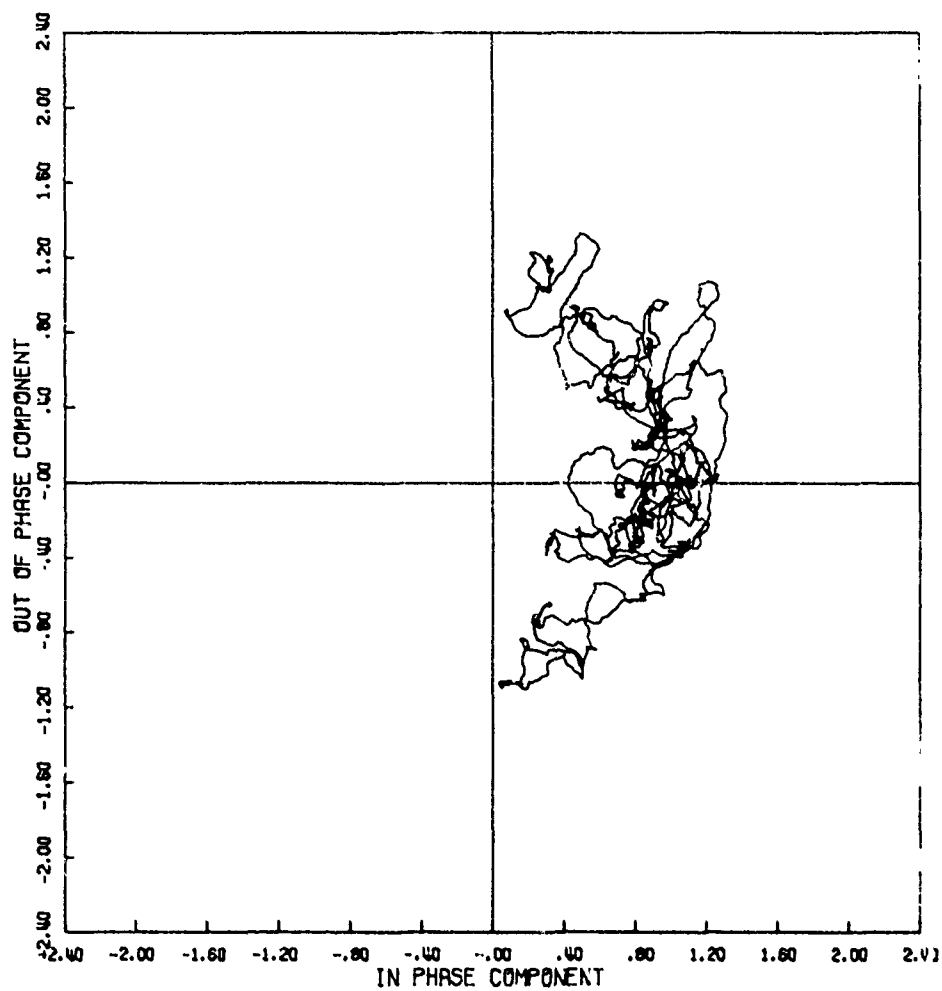
Figure 29a.   Signal Phase Plot
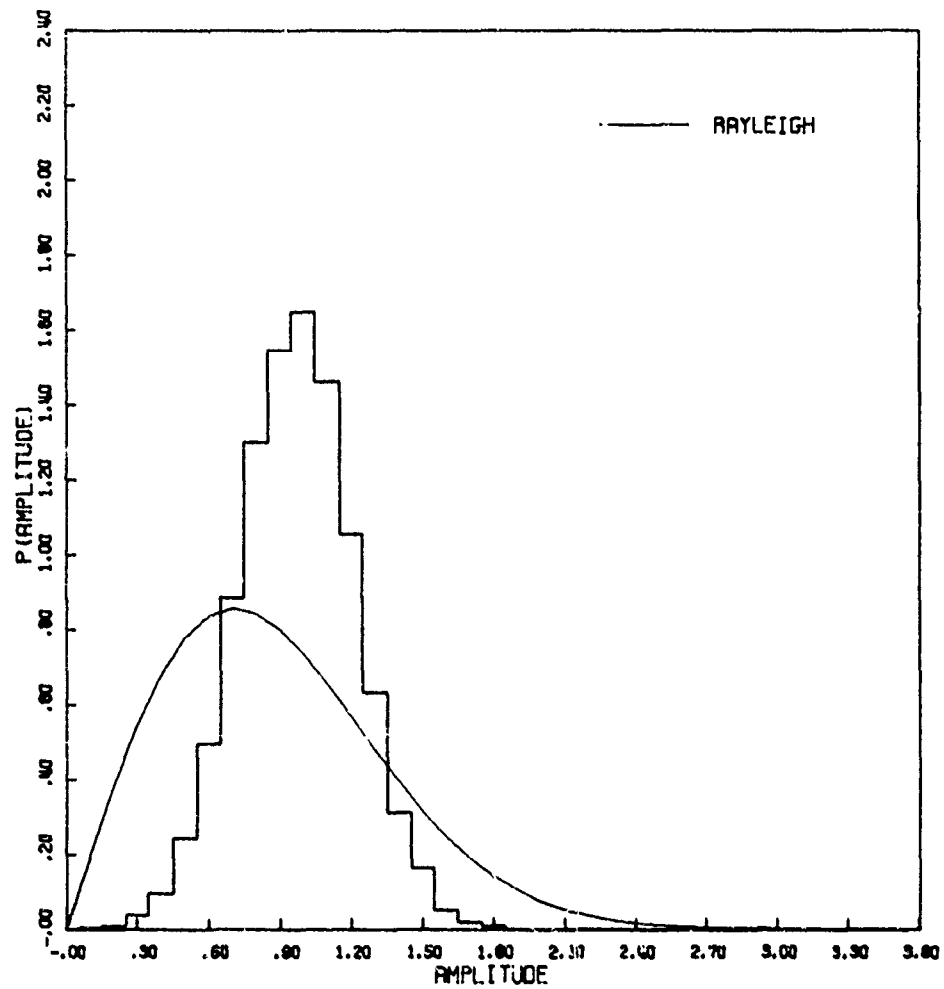
Figure 29b. Amplitude Distribution
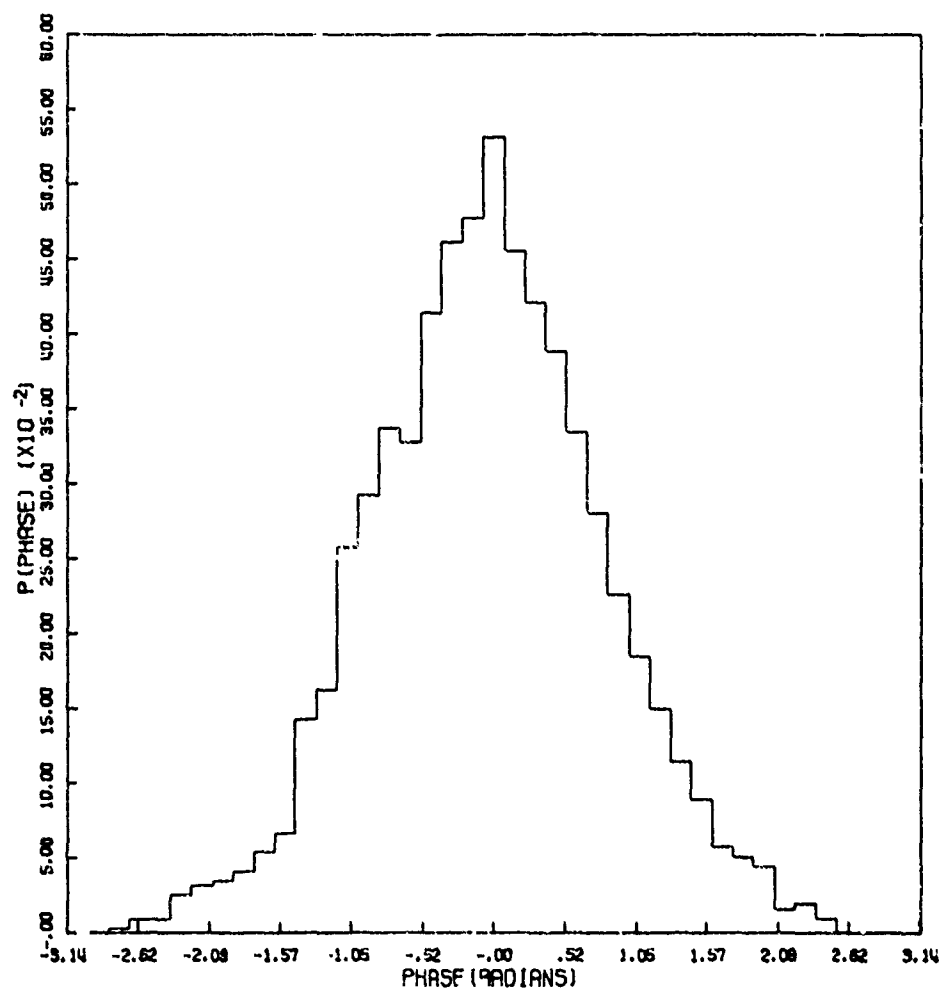
Figure 29c.   Phase Distribution
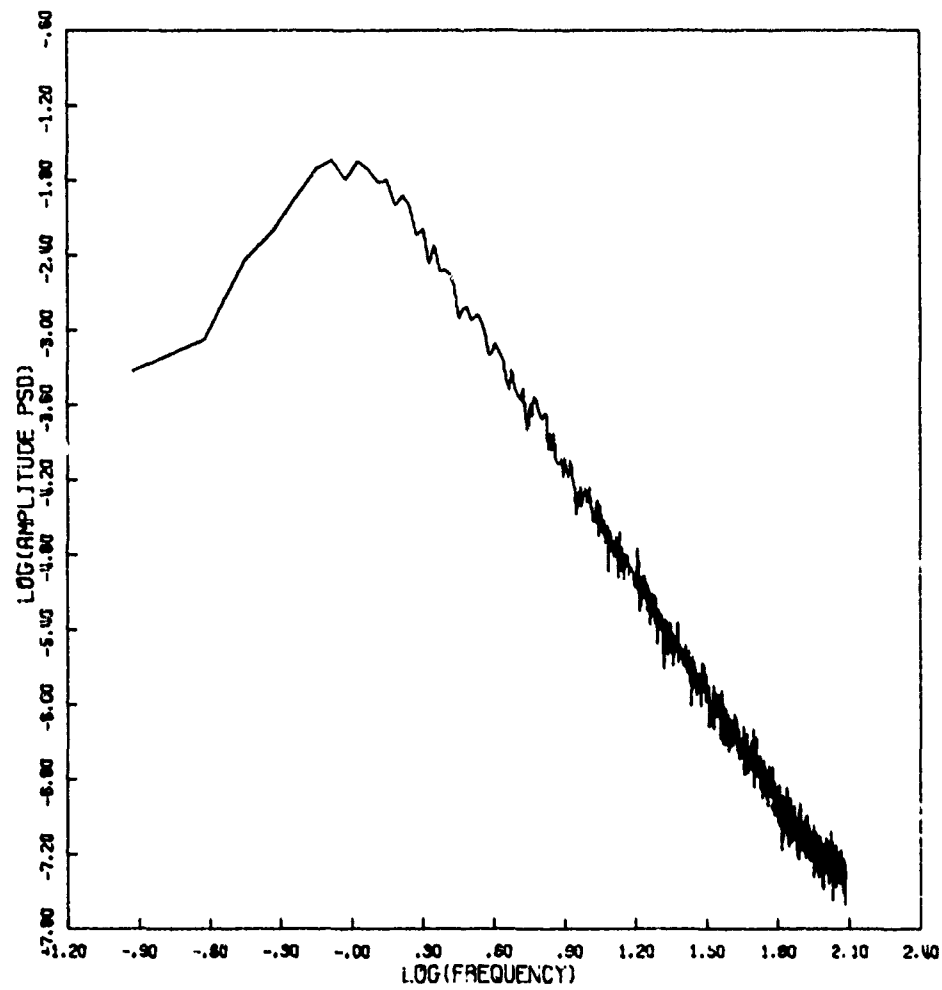
Figure 29d. Amplitude Power Spectral Density
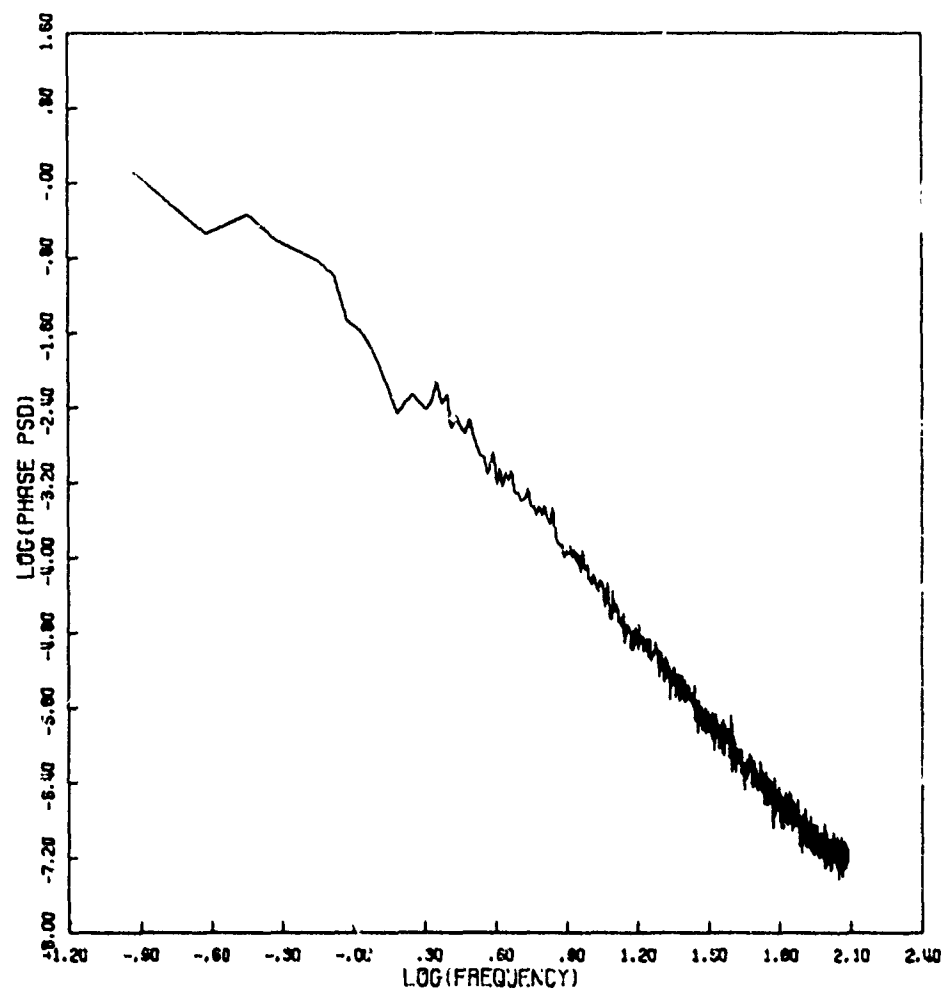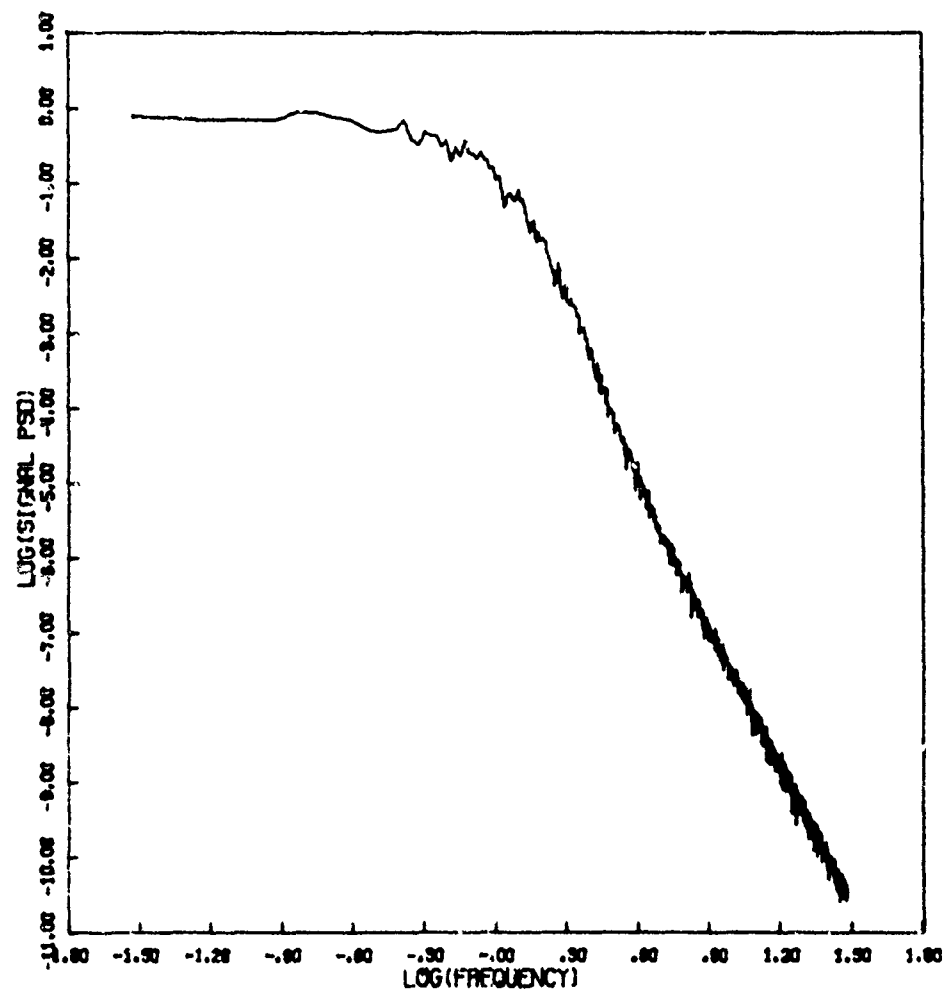
Figure 29e.   Phase Power Spectral Density
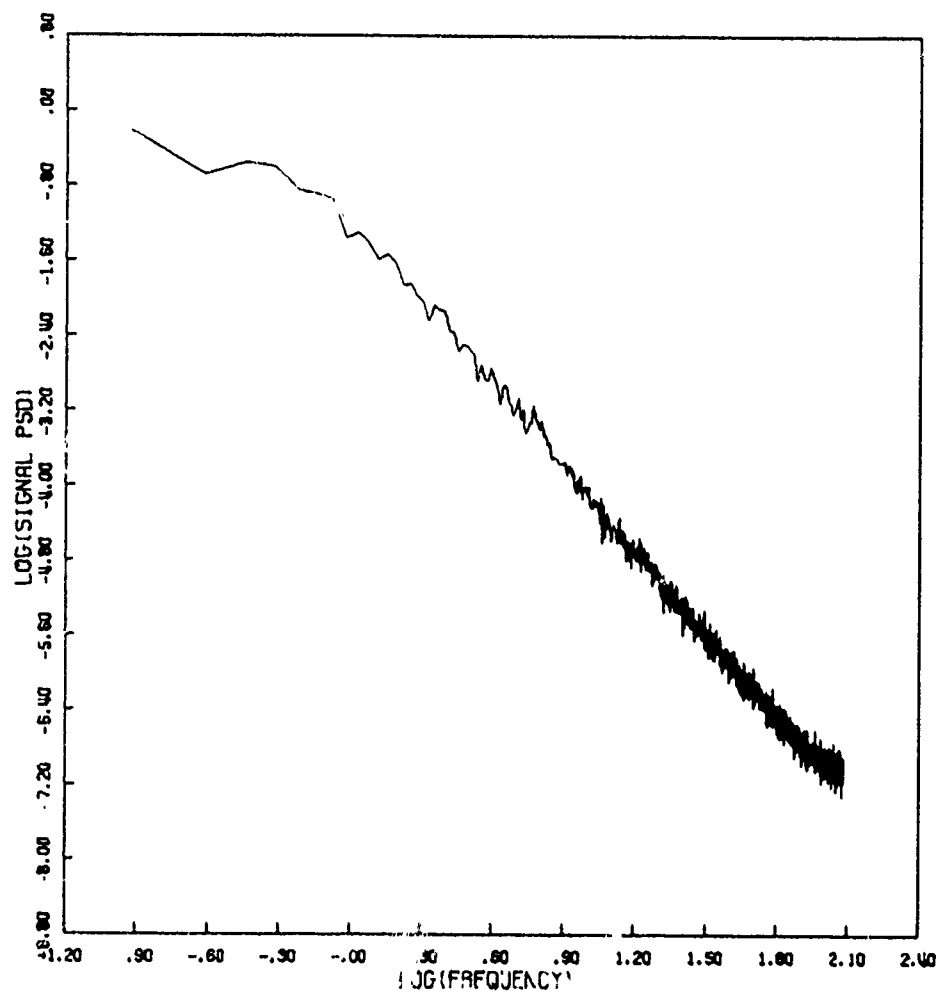
Figure 29f. Signal Power Spectral Density
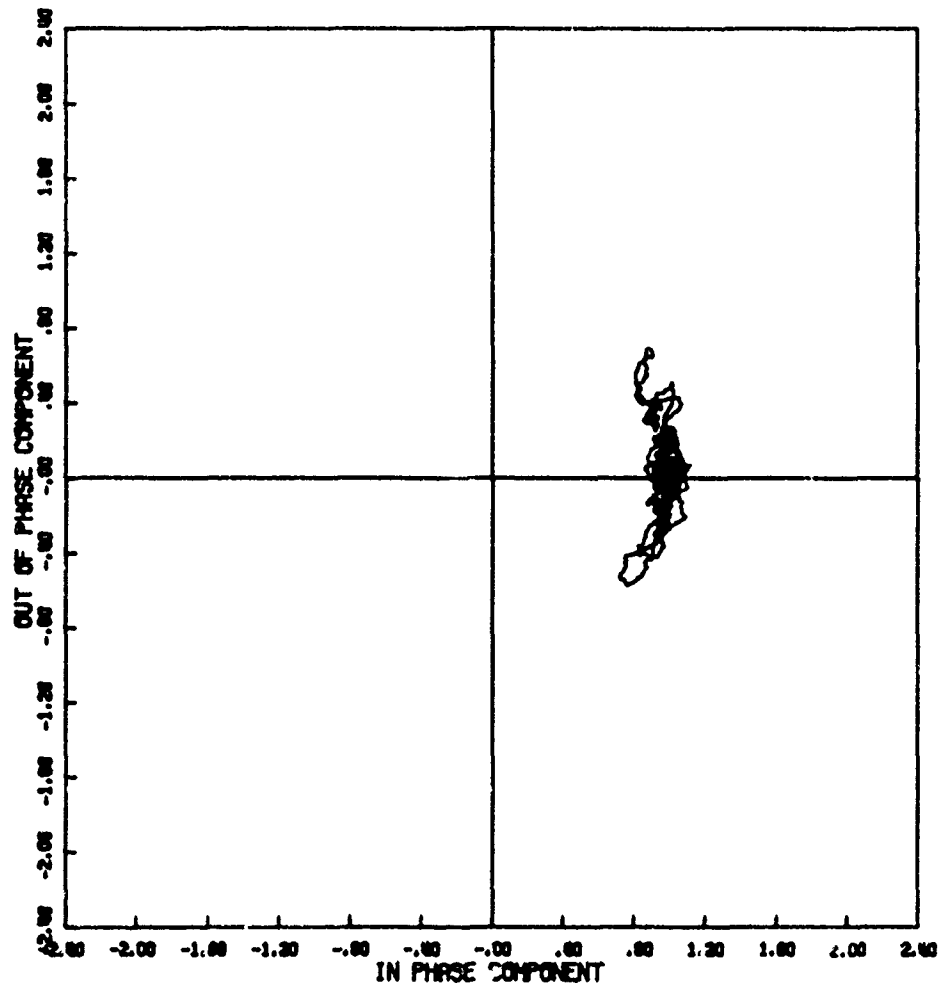
Figure 30a.   Signal Phase Plot
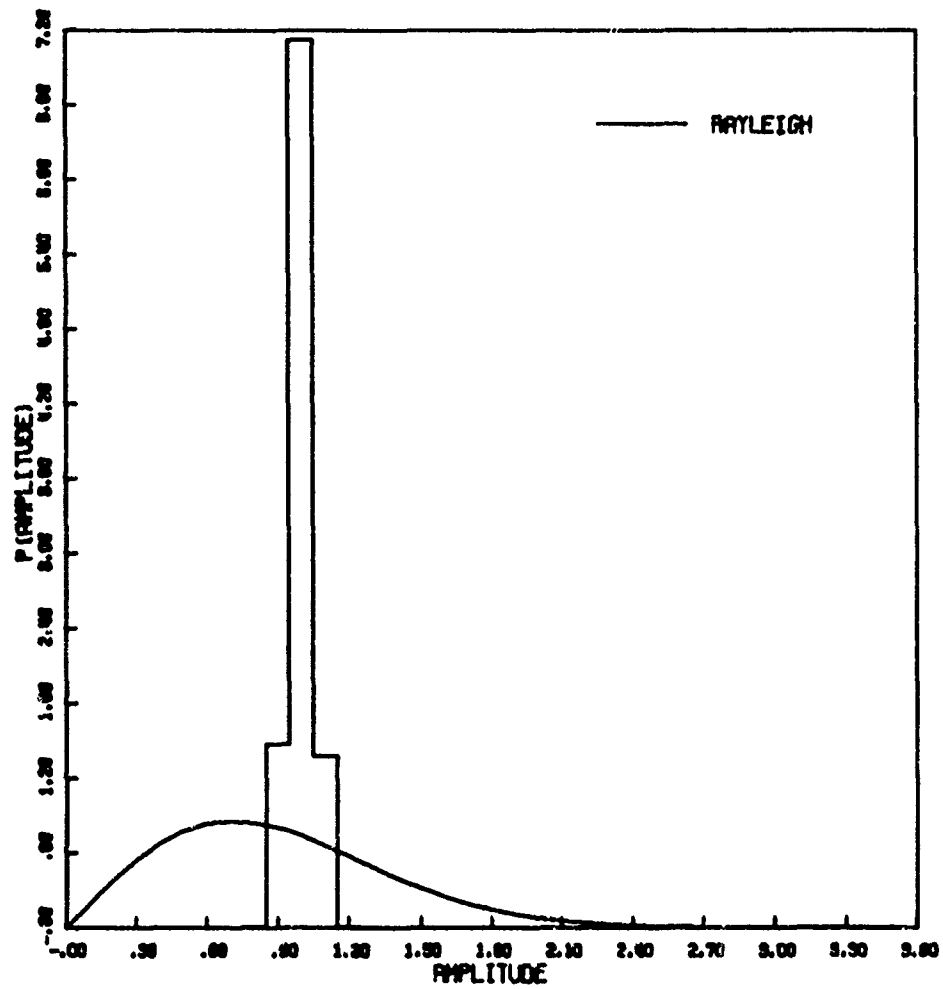
Figure 30b. Amplitude Distribution
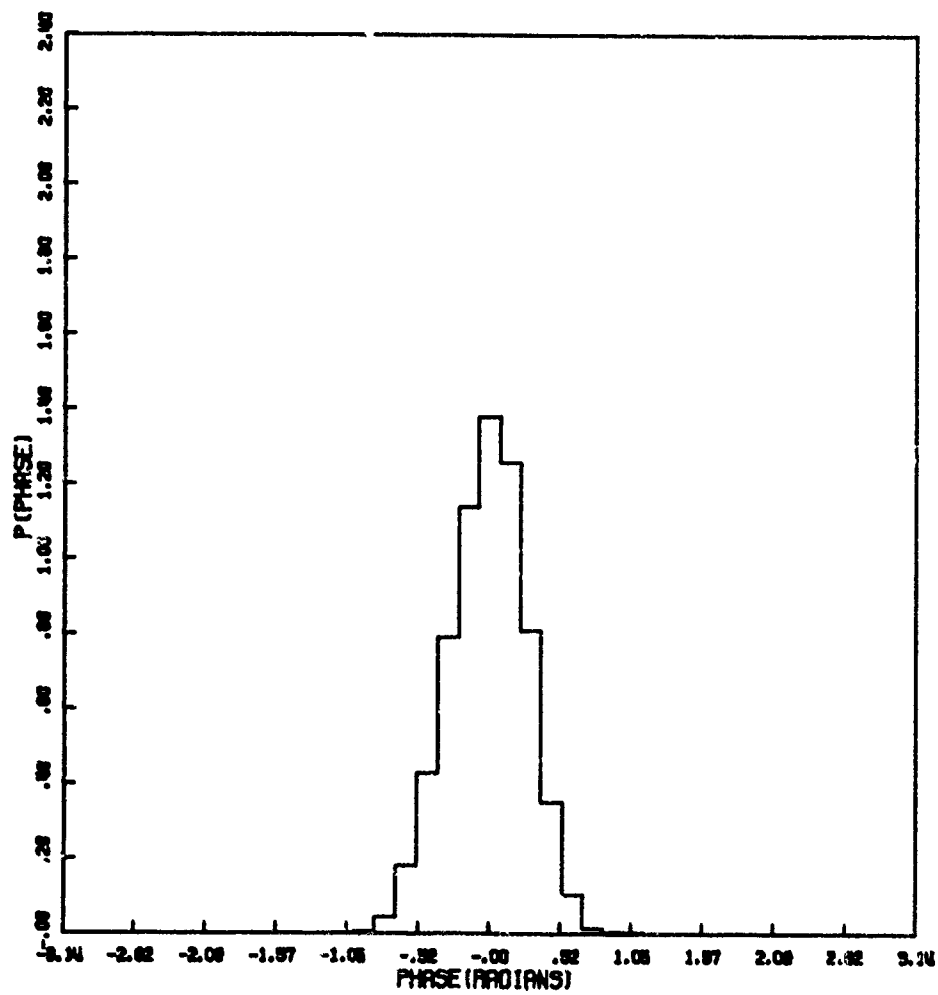
Figure 30c. Phase Distribution
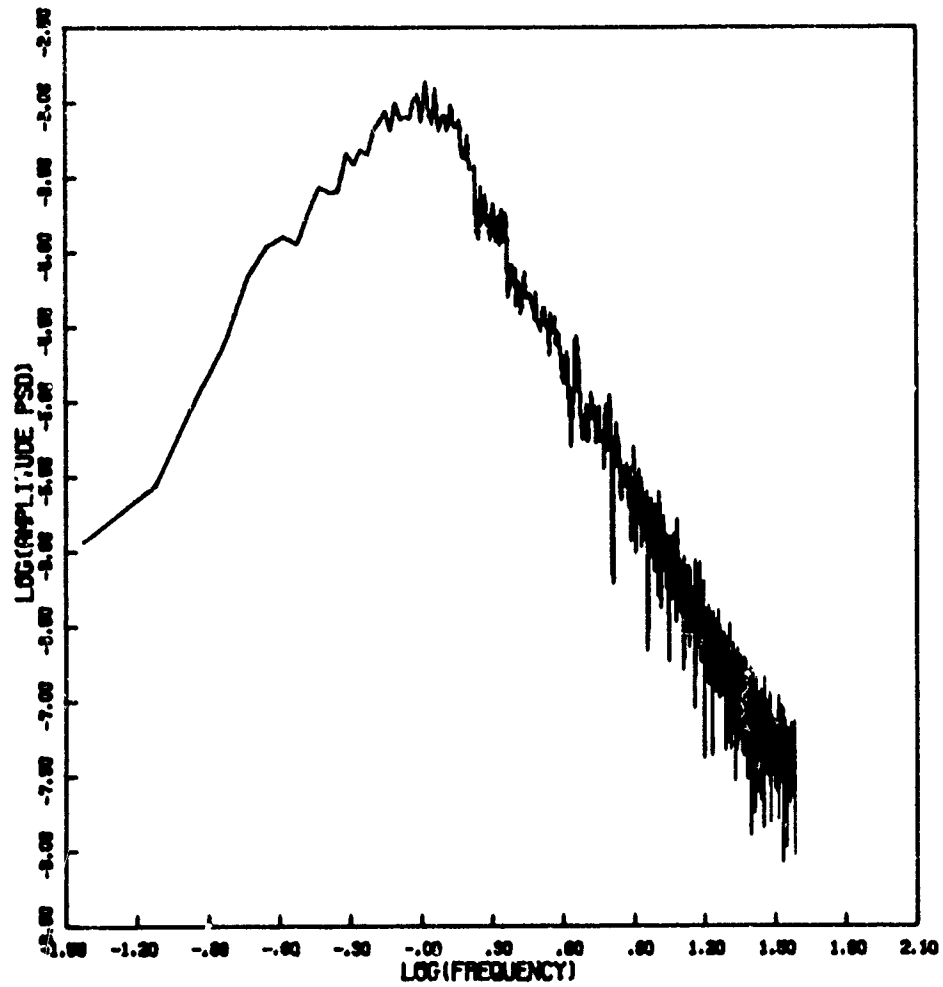
Figure 30d.   Amplitude Power Spectral Density
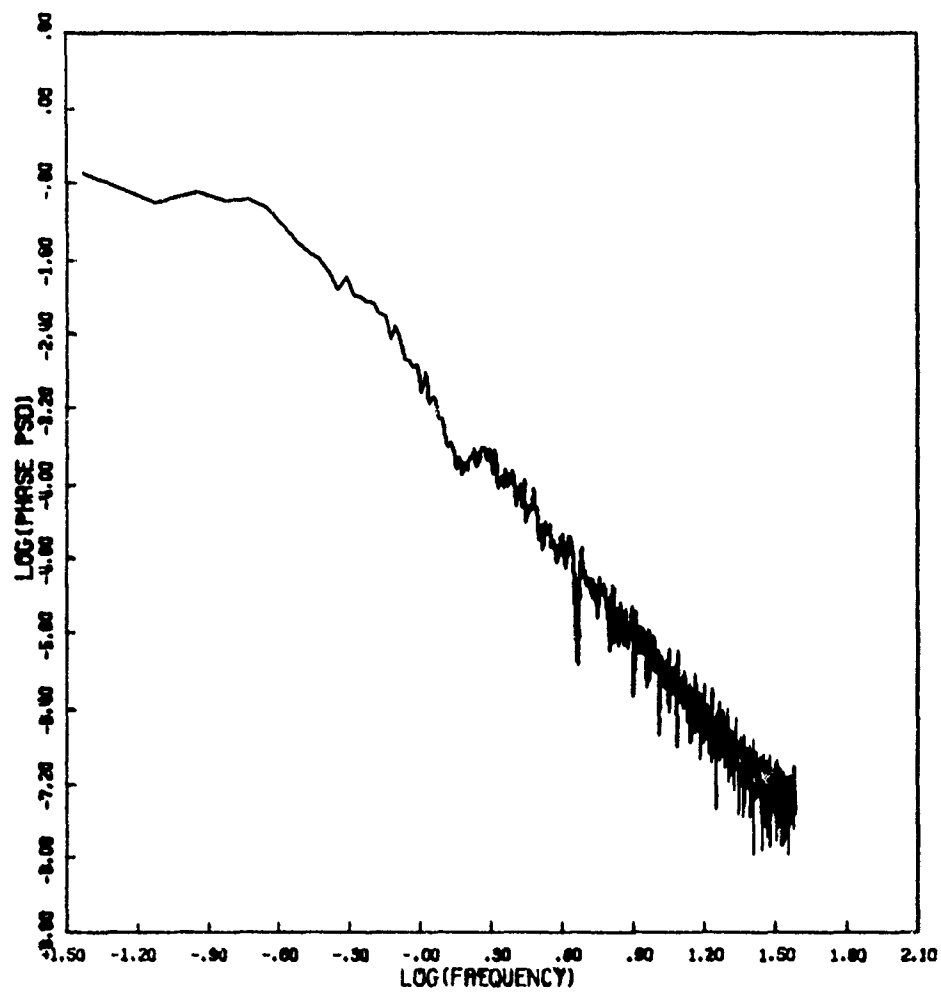
Figure 30e. Phase Power Spectral Density
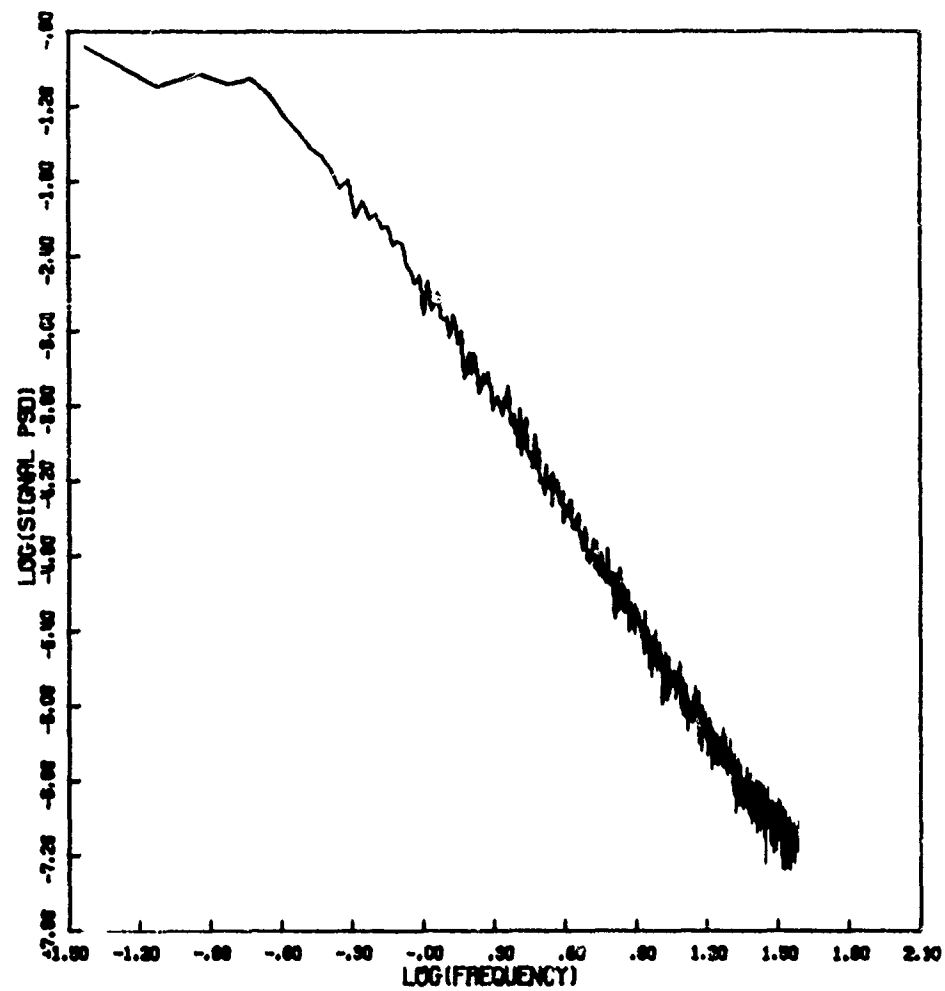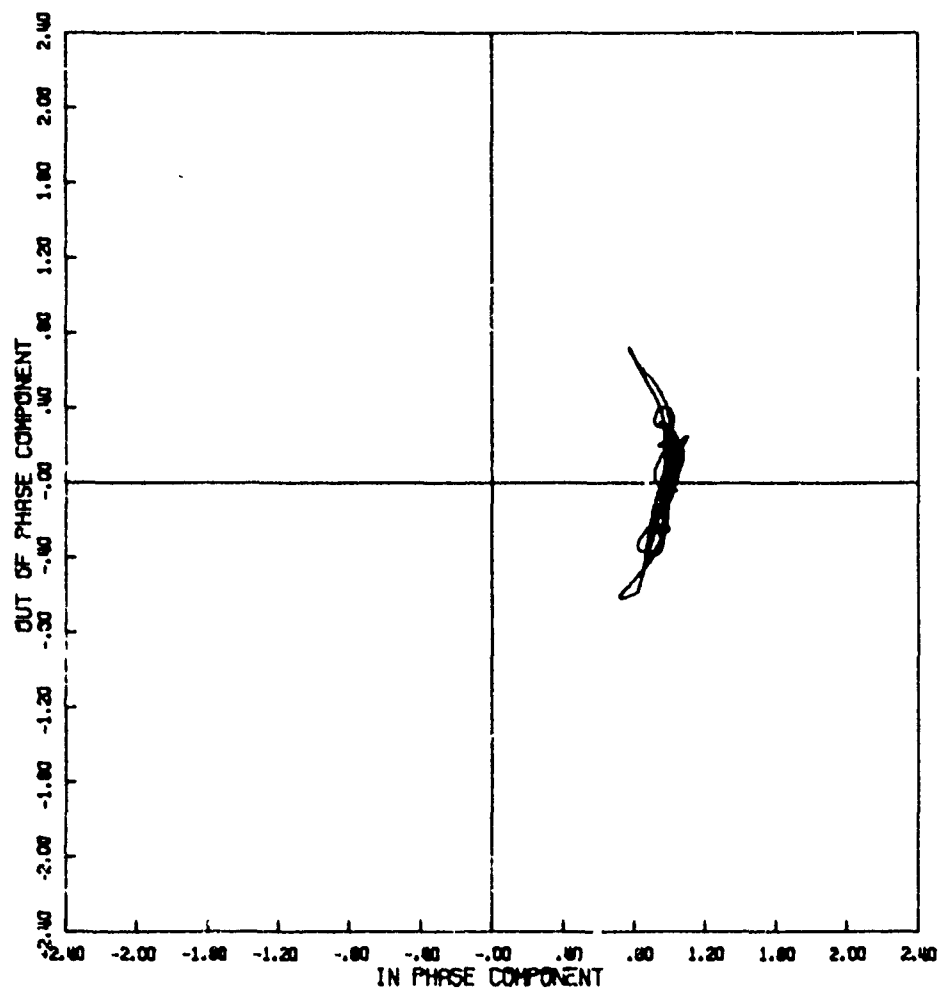
Figure 30f. Signal Power Spectral Density
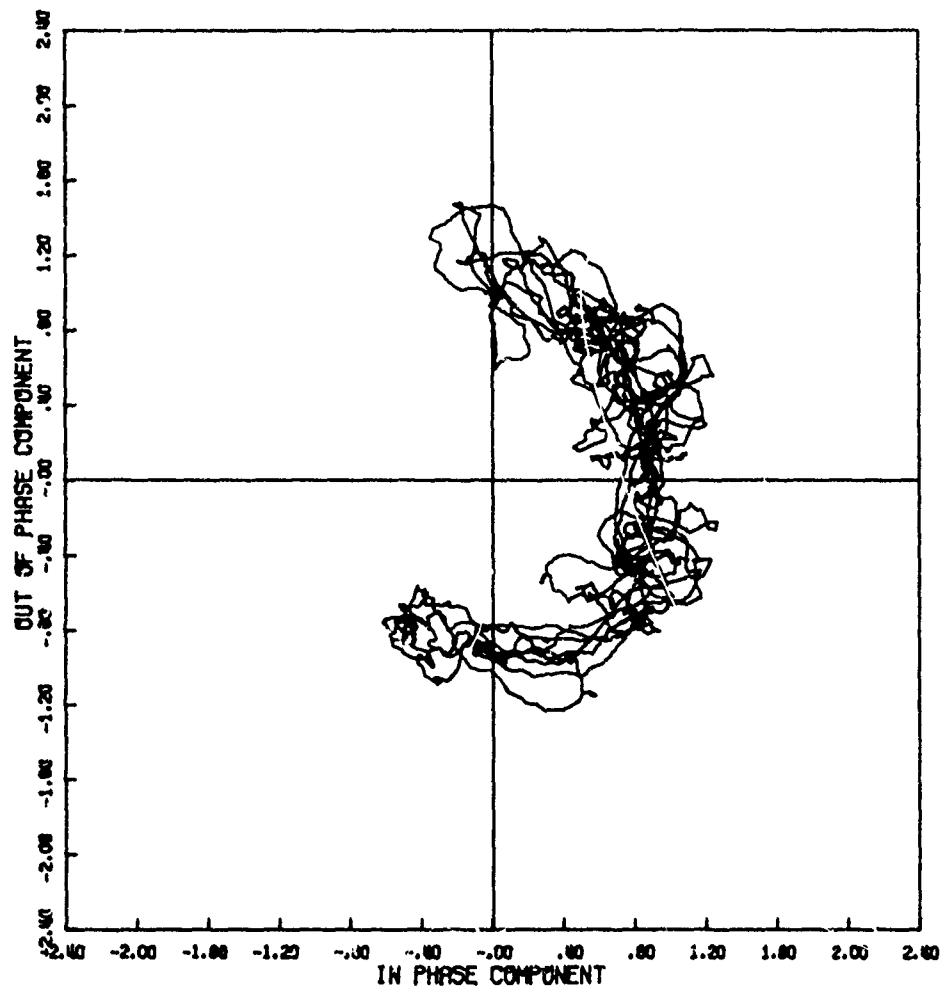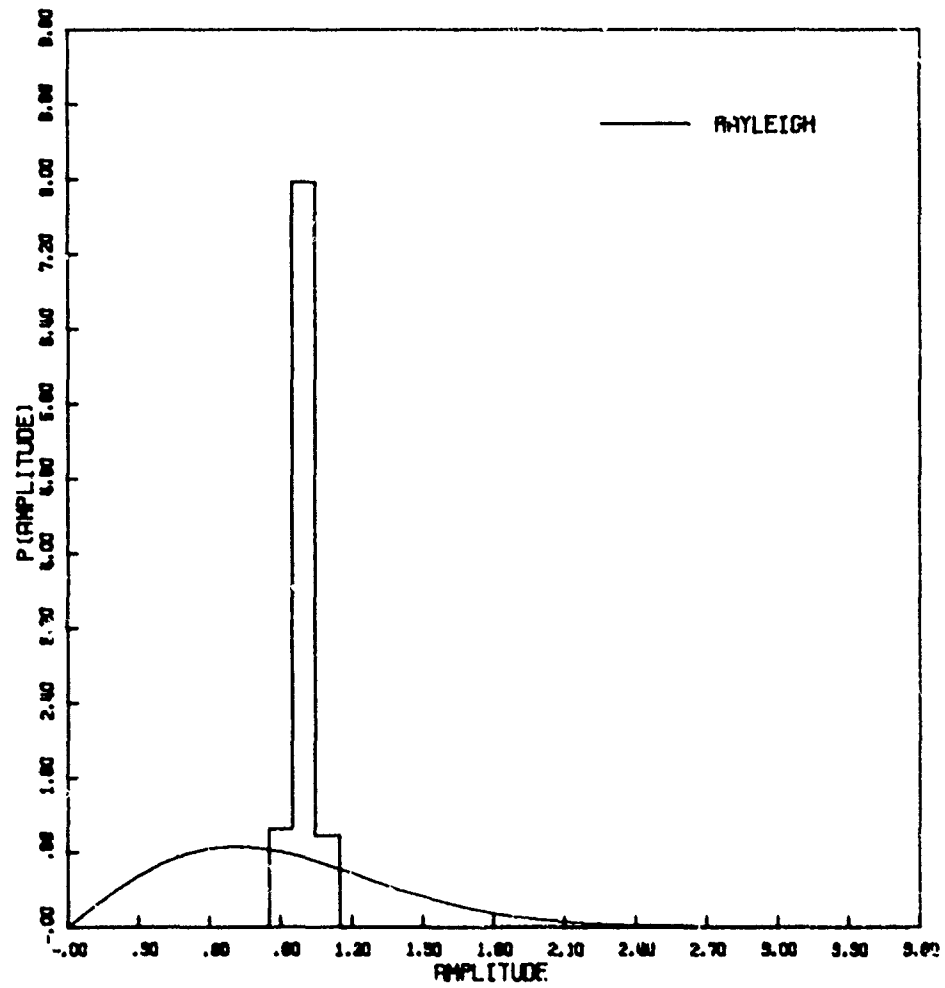
Figure 31a. Signal Phase Plot
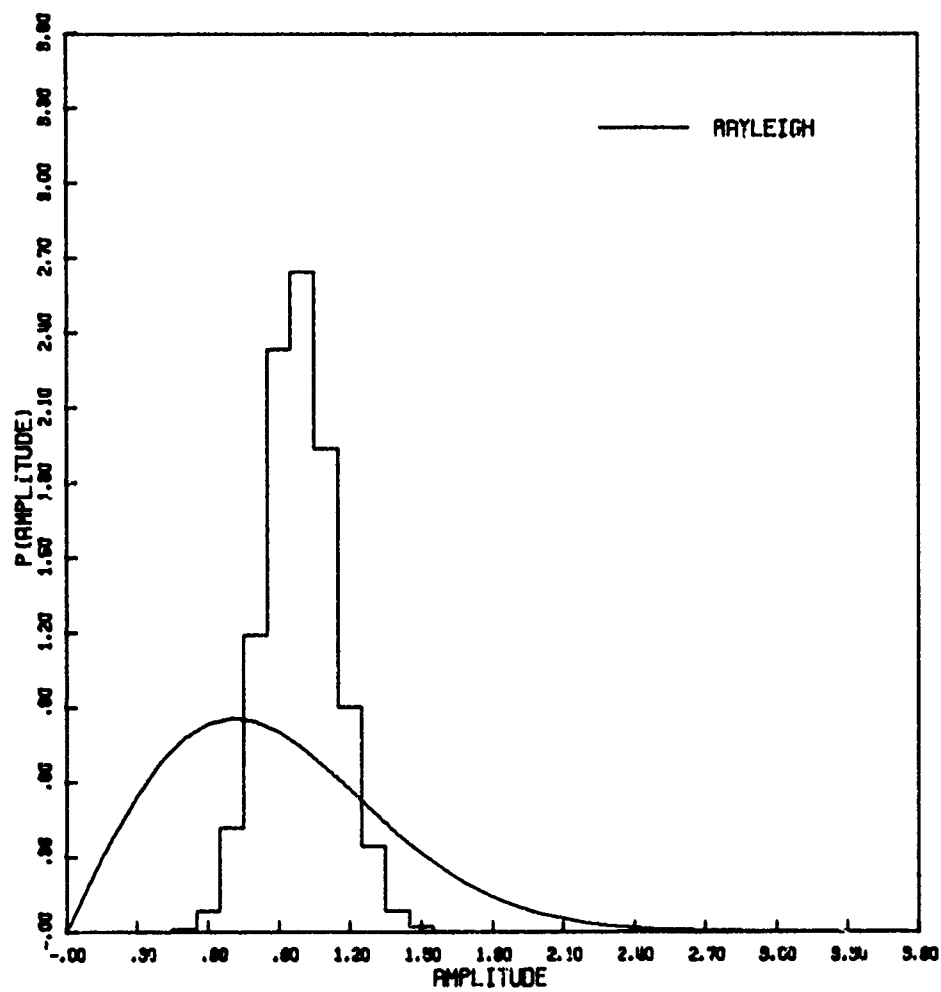
Figure 31b. Amplitude Distribution
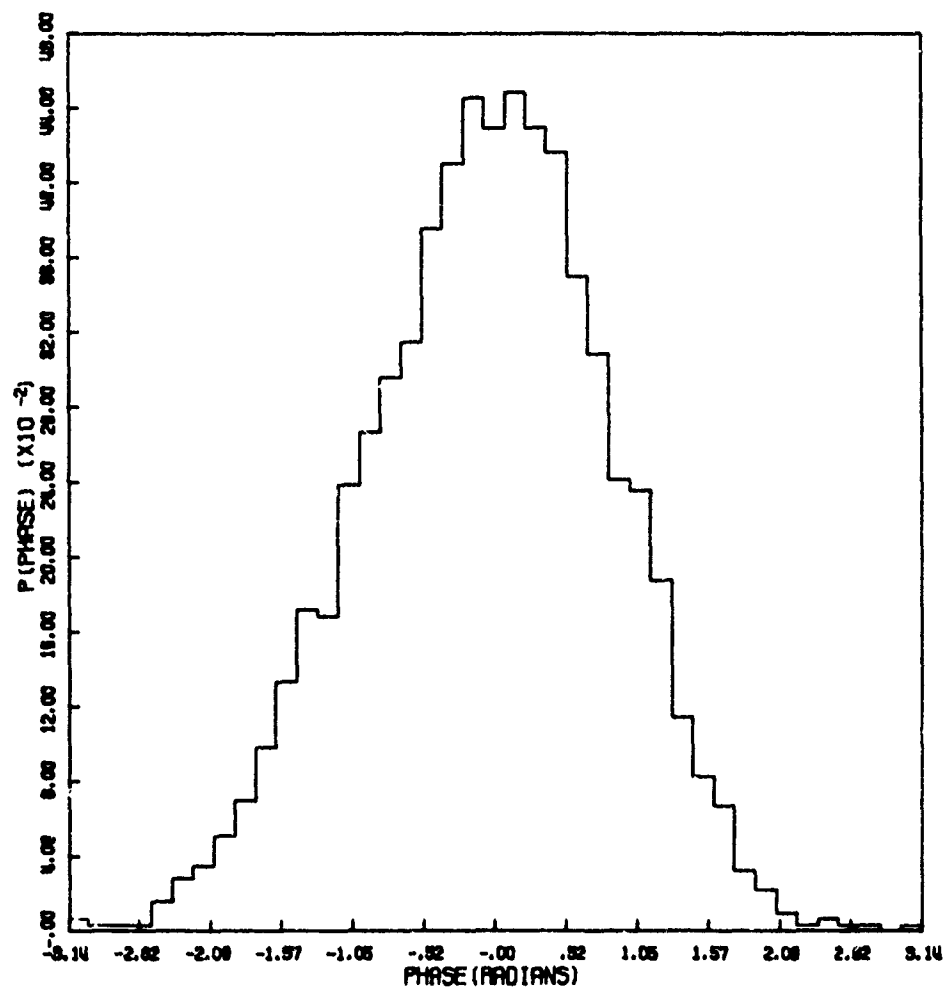
Figure 31c.   Phase Distribution
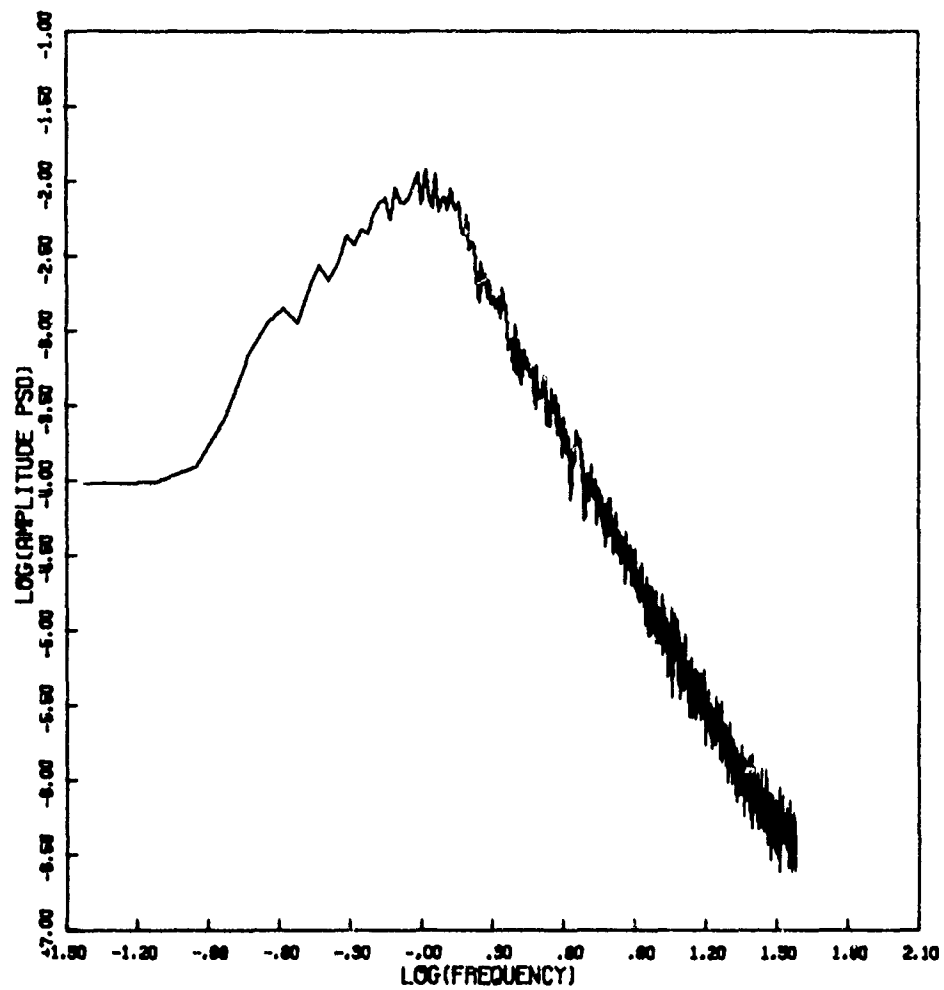
Figure 31d. Amplitude Power Spectral Density
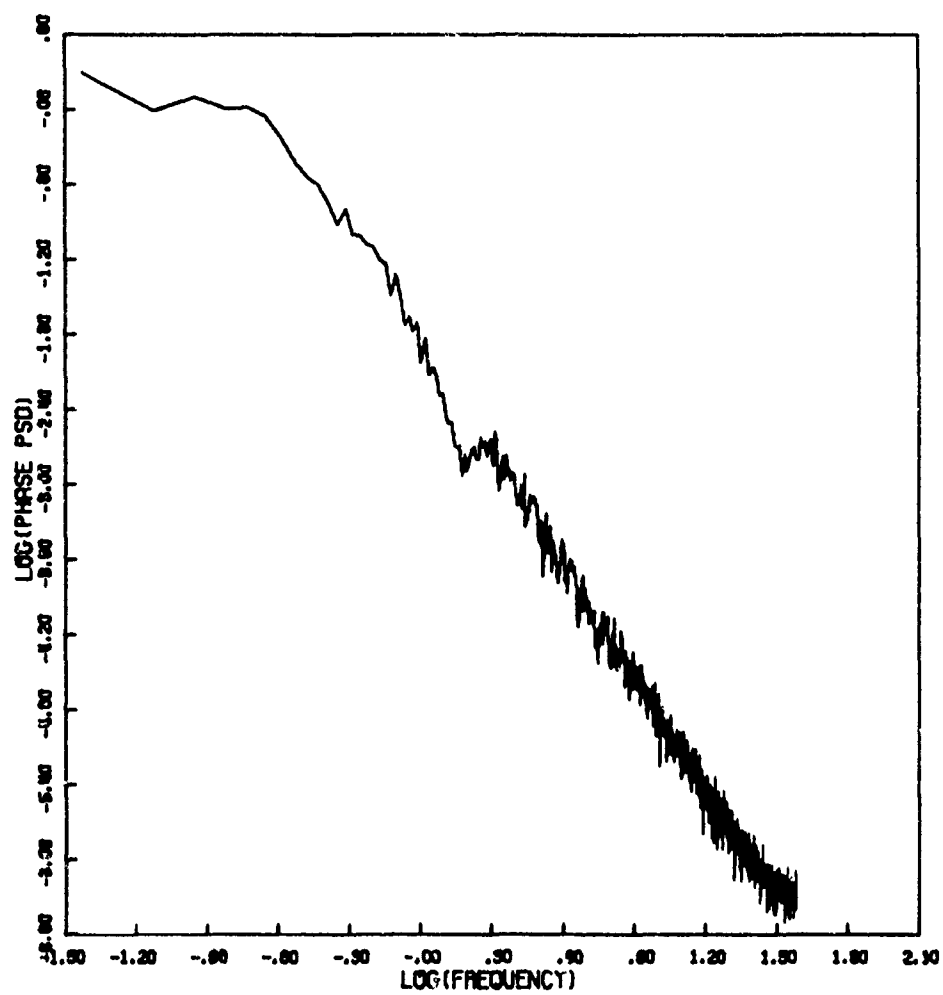
Figure 31e.   Phase Power Spectral Density
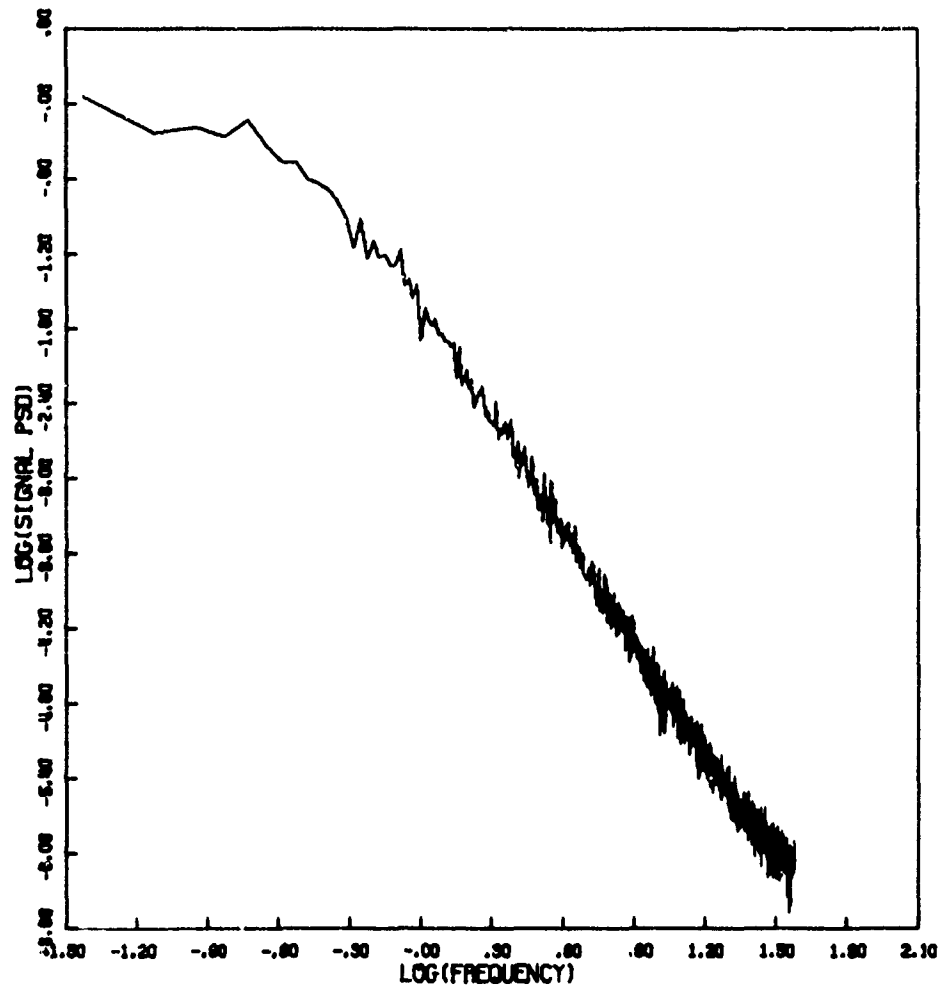
Figure 31f. Signal Power Spectral Density
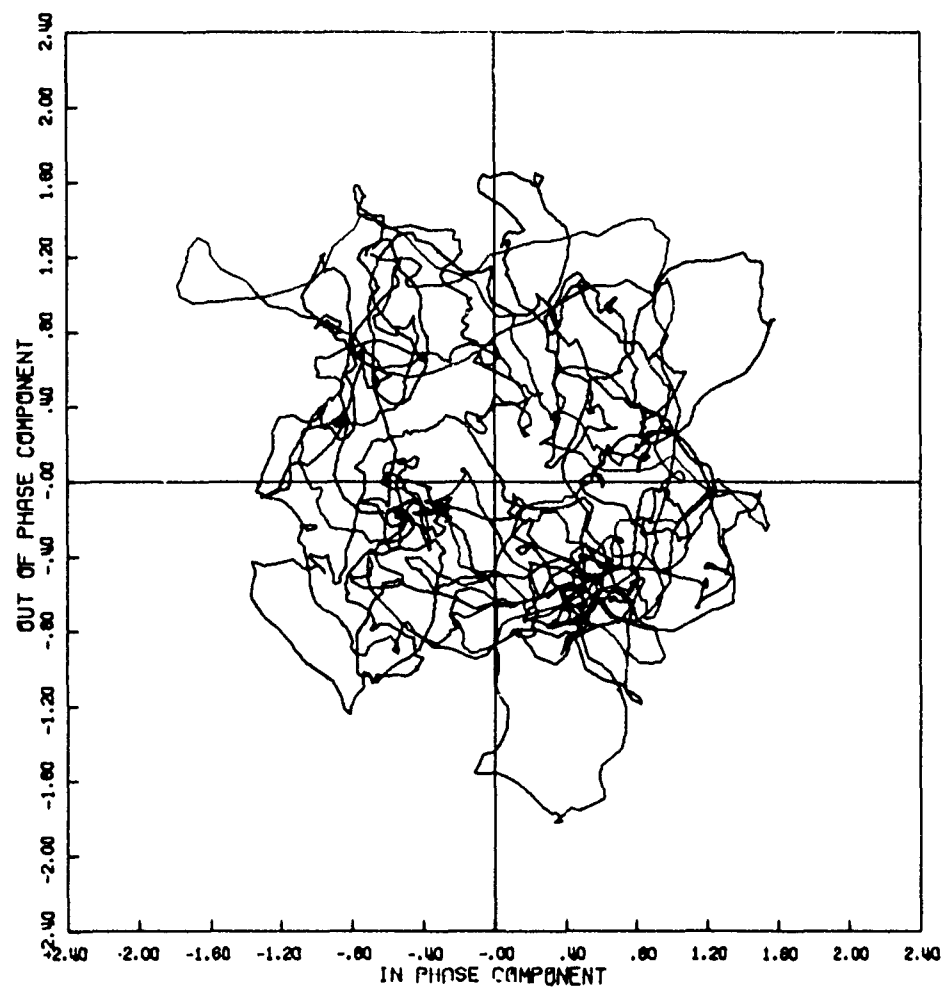
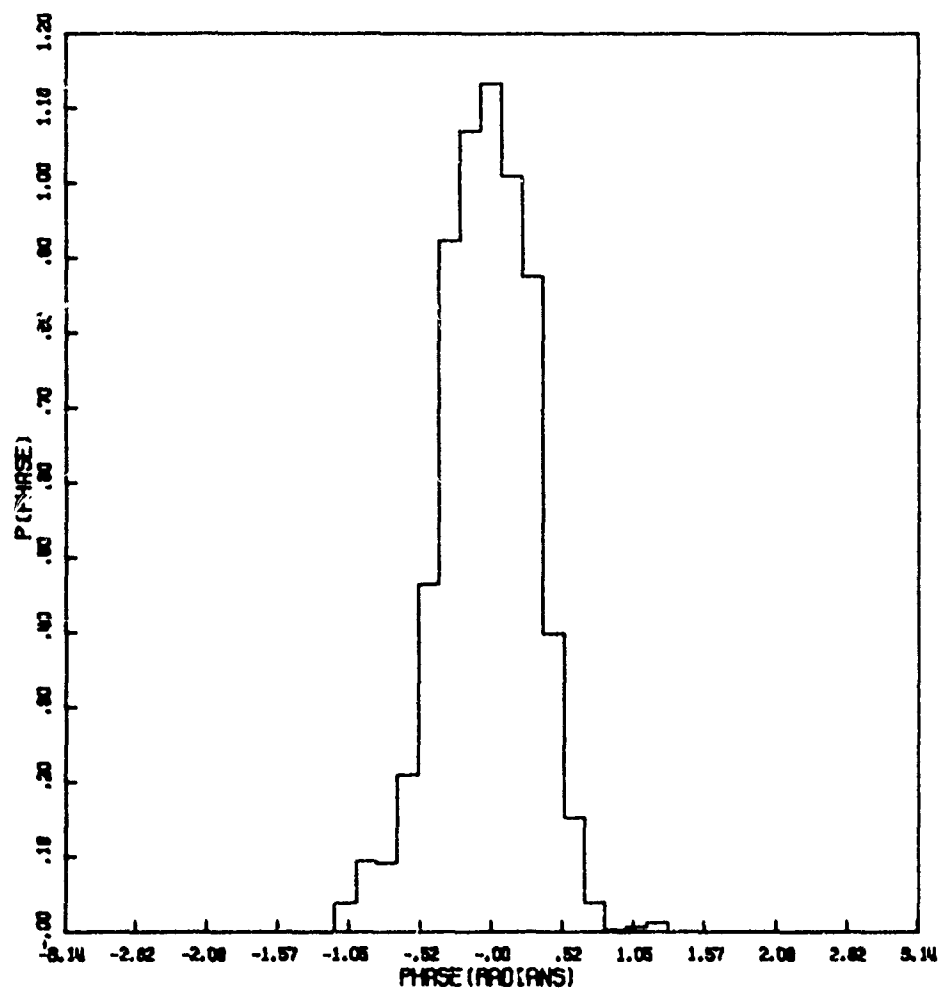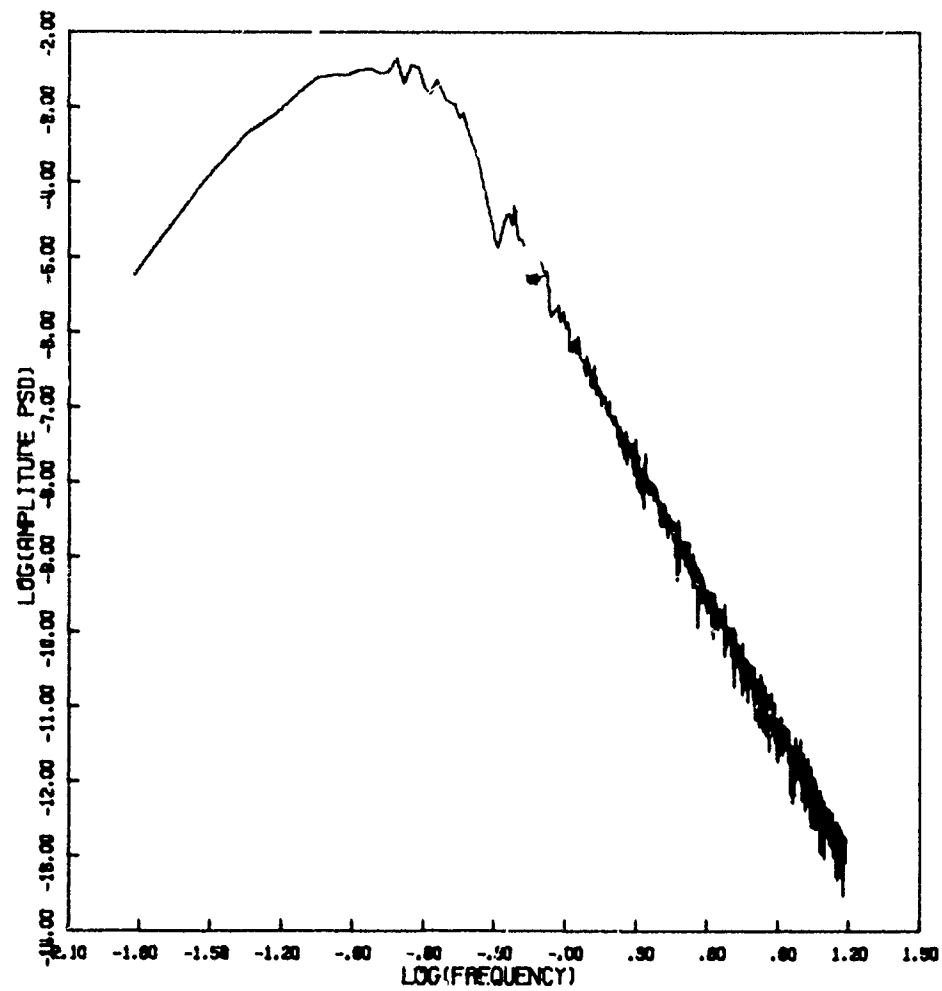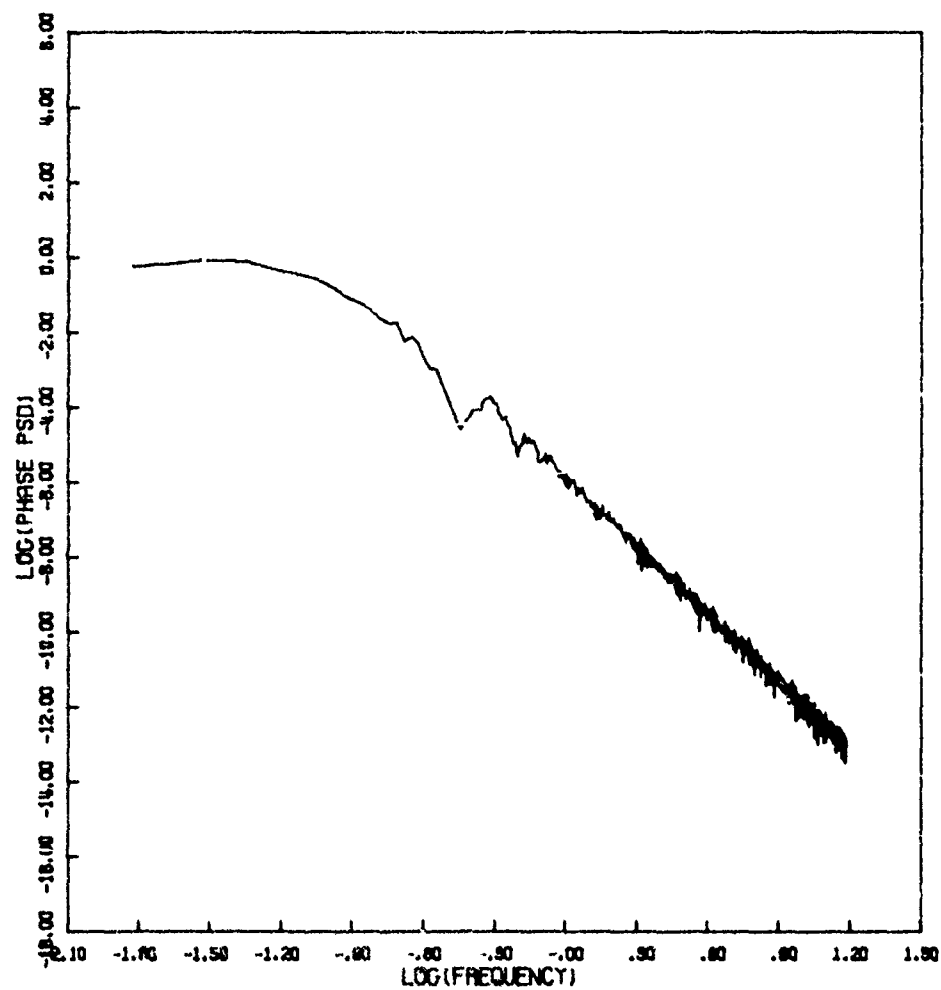Figure 32a. Signal Phase Plot
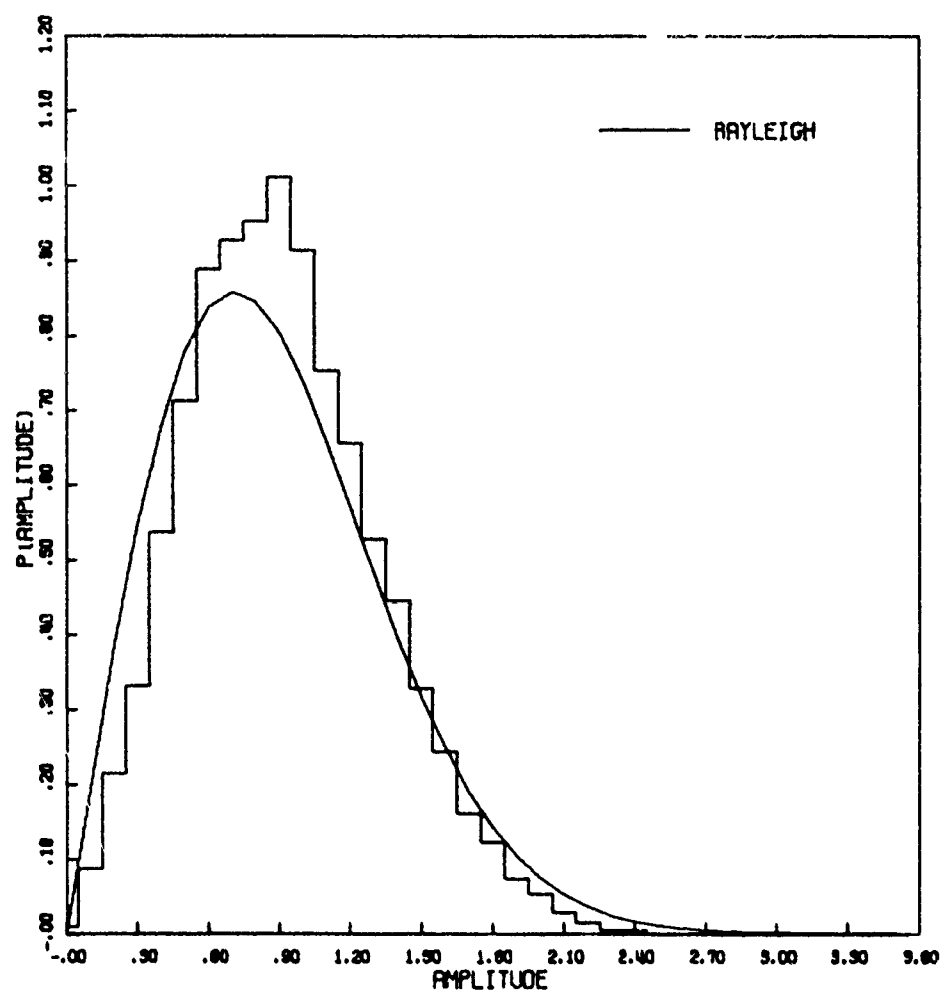
Figure 32b. Amplitude Distribution
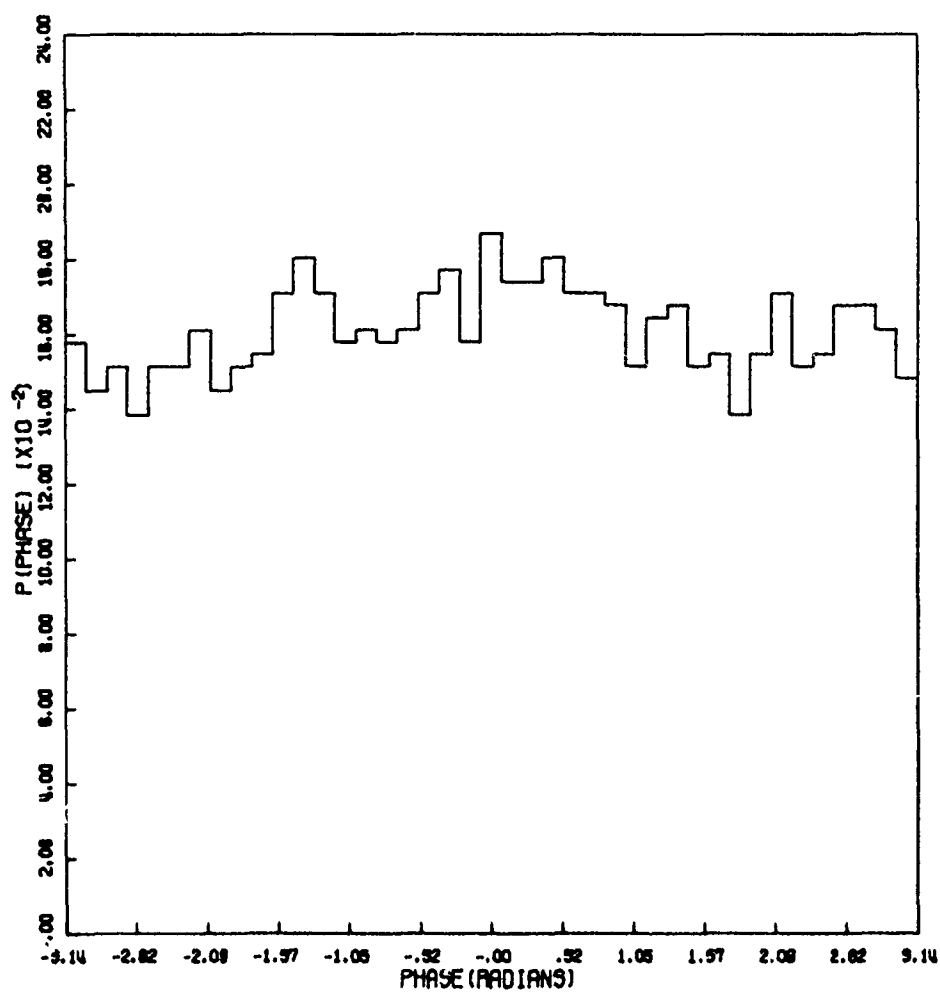
Figure 32c. Phase Distribution
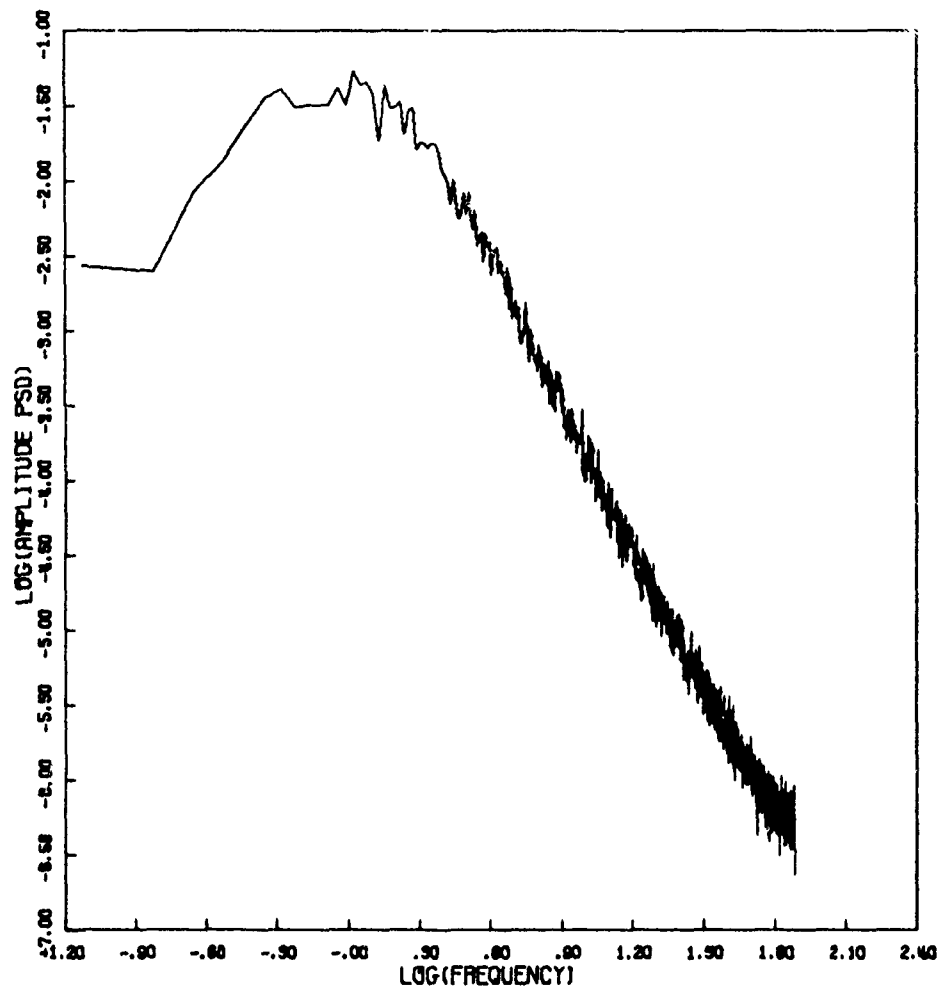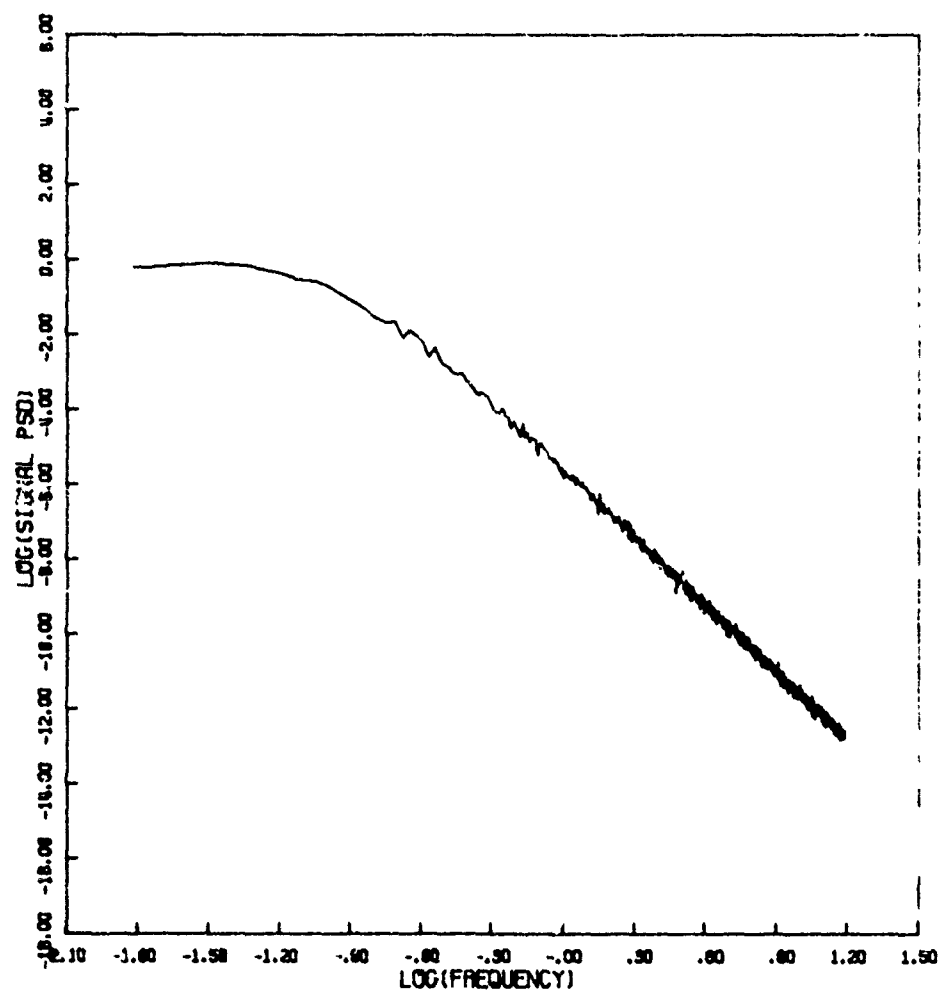
Figure 32d. Amplitude Power Spectral Density
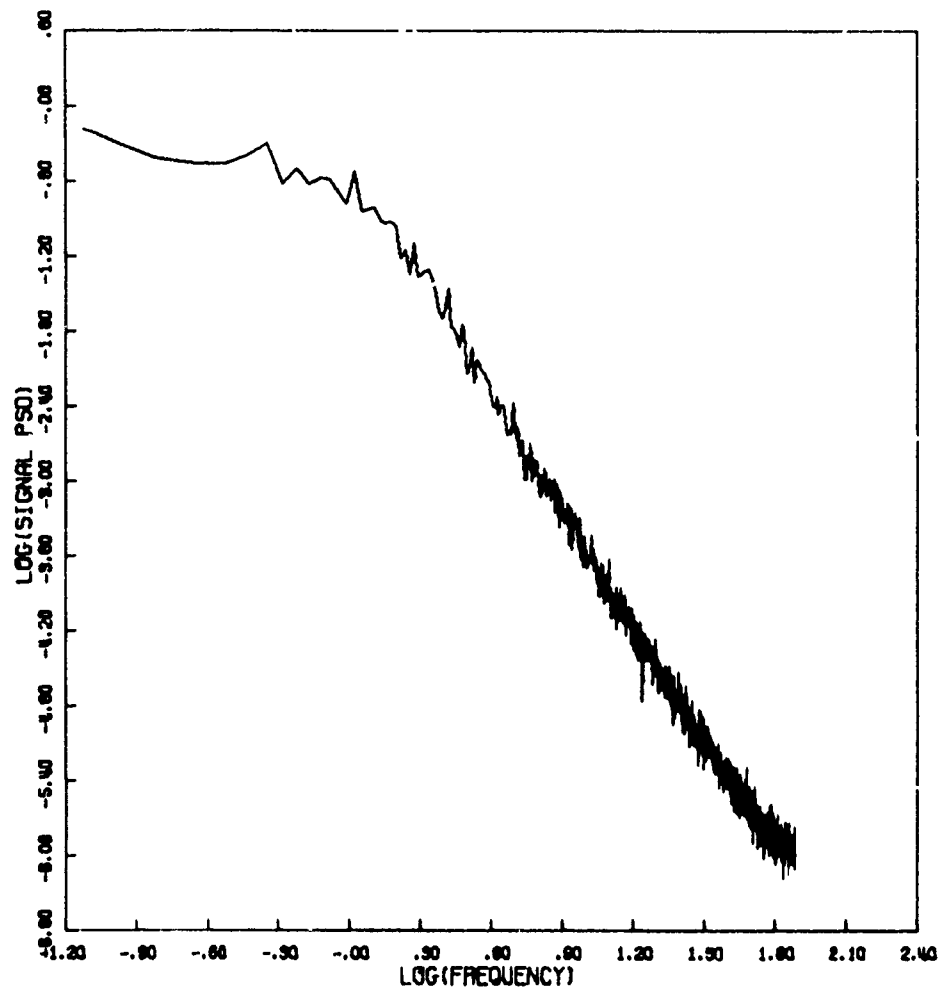
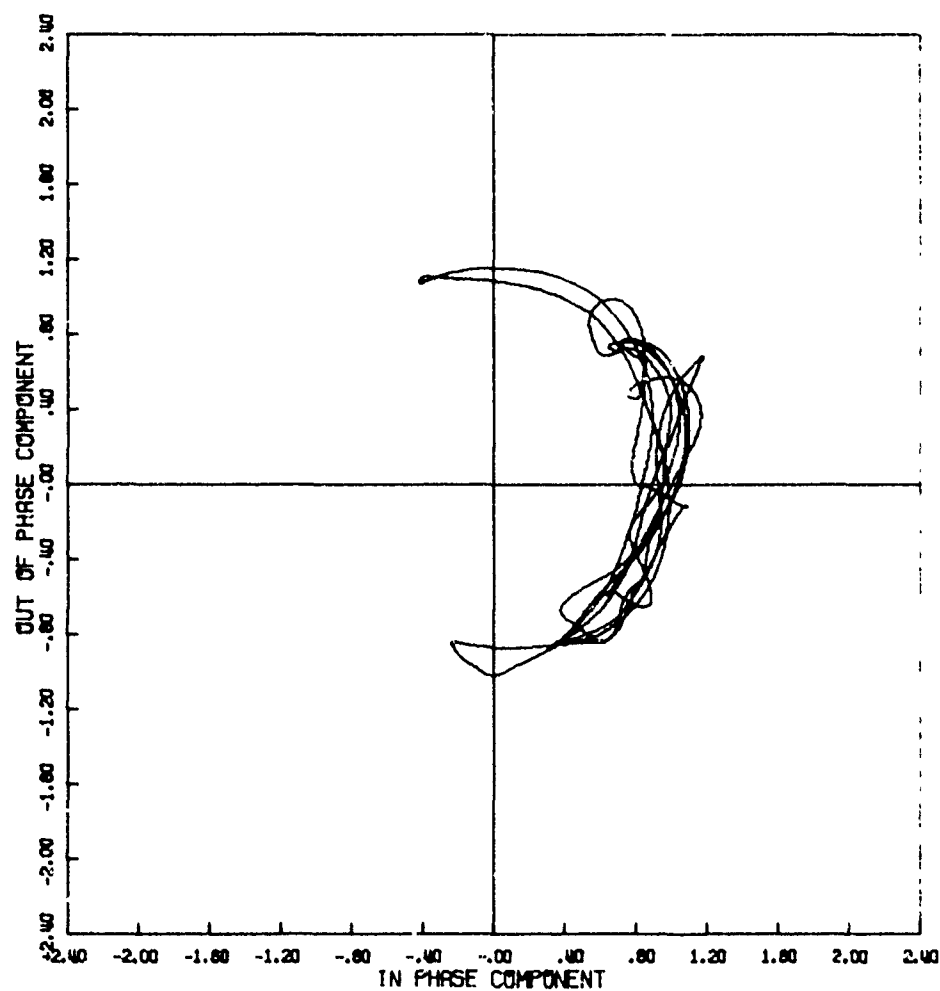Figure 32e. Signal Power Spectral Density
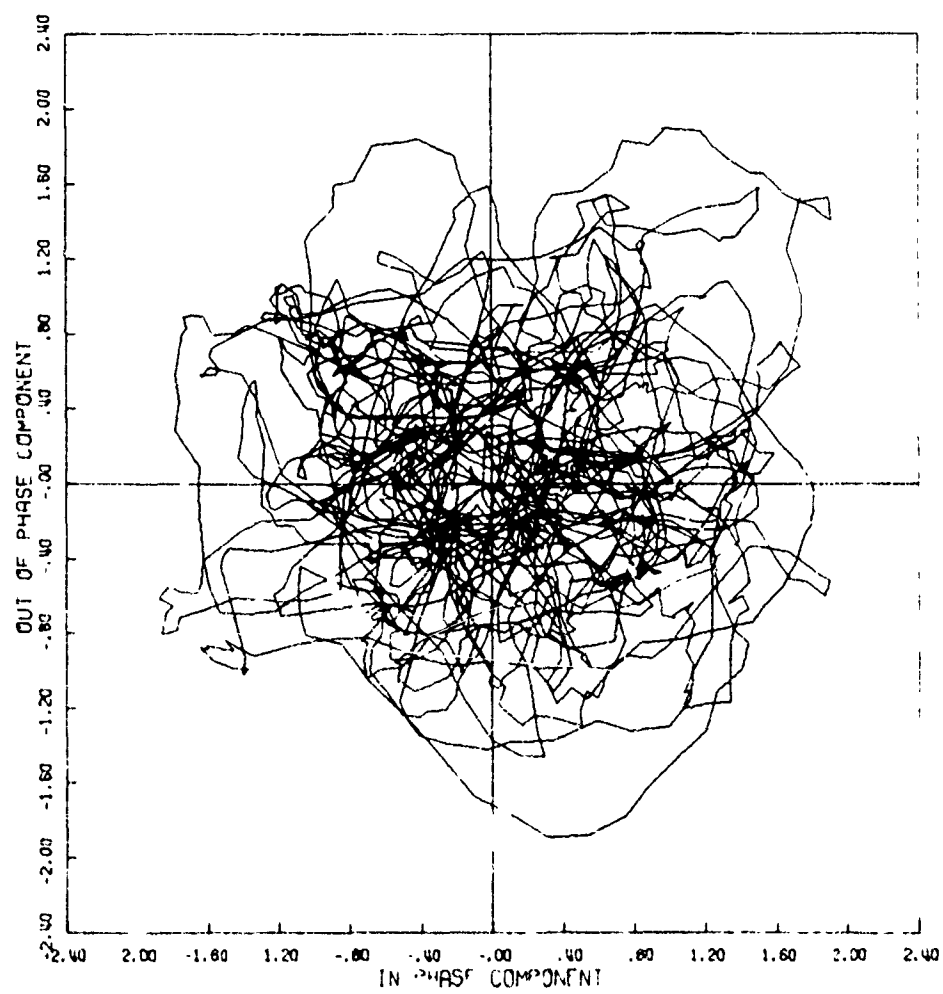
Figure 33a.   Signal Phase Plot
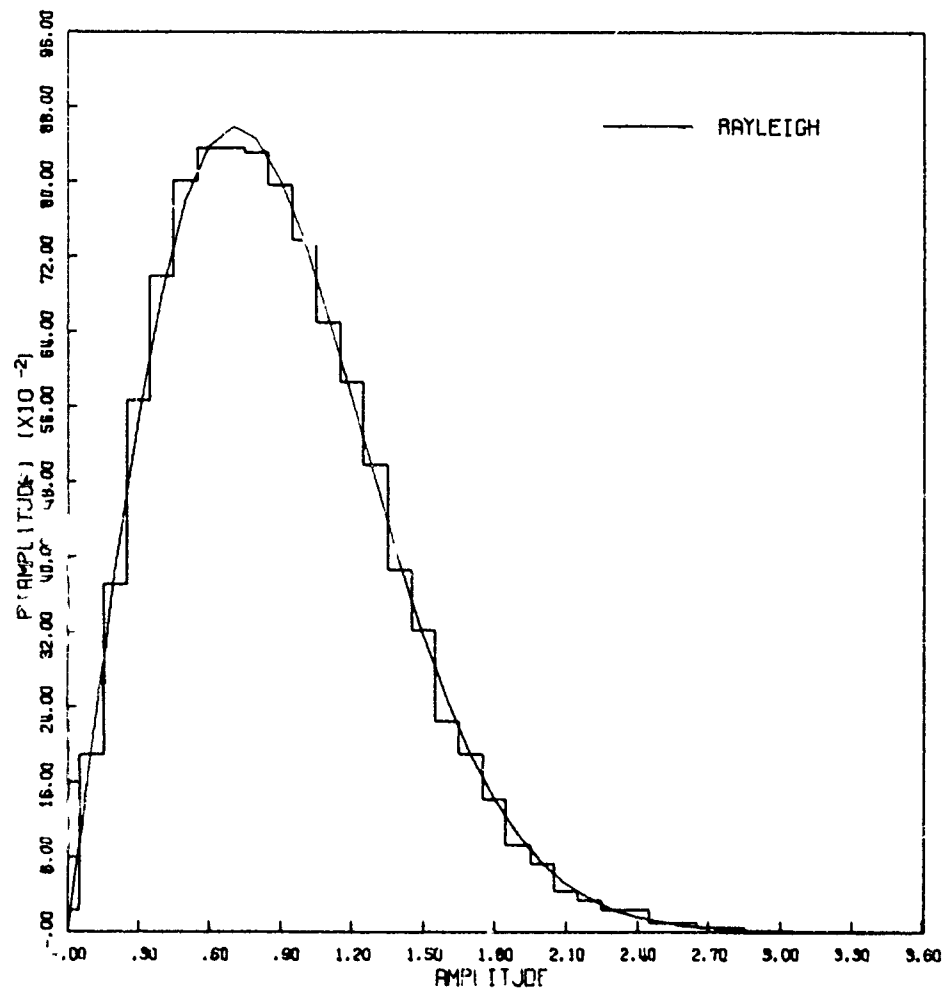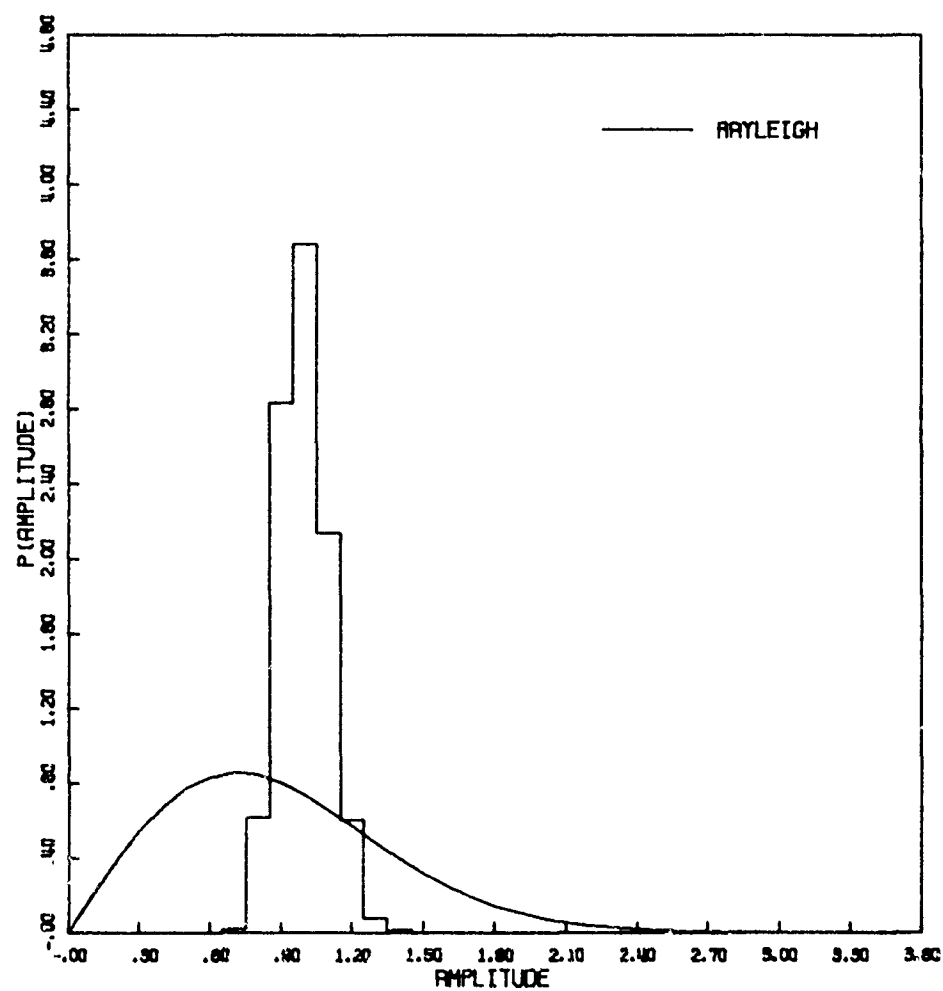
Figure 33b. Amplitude Distribution
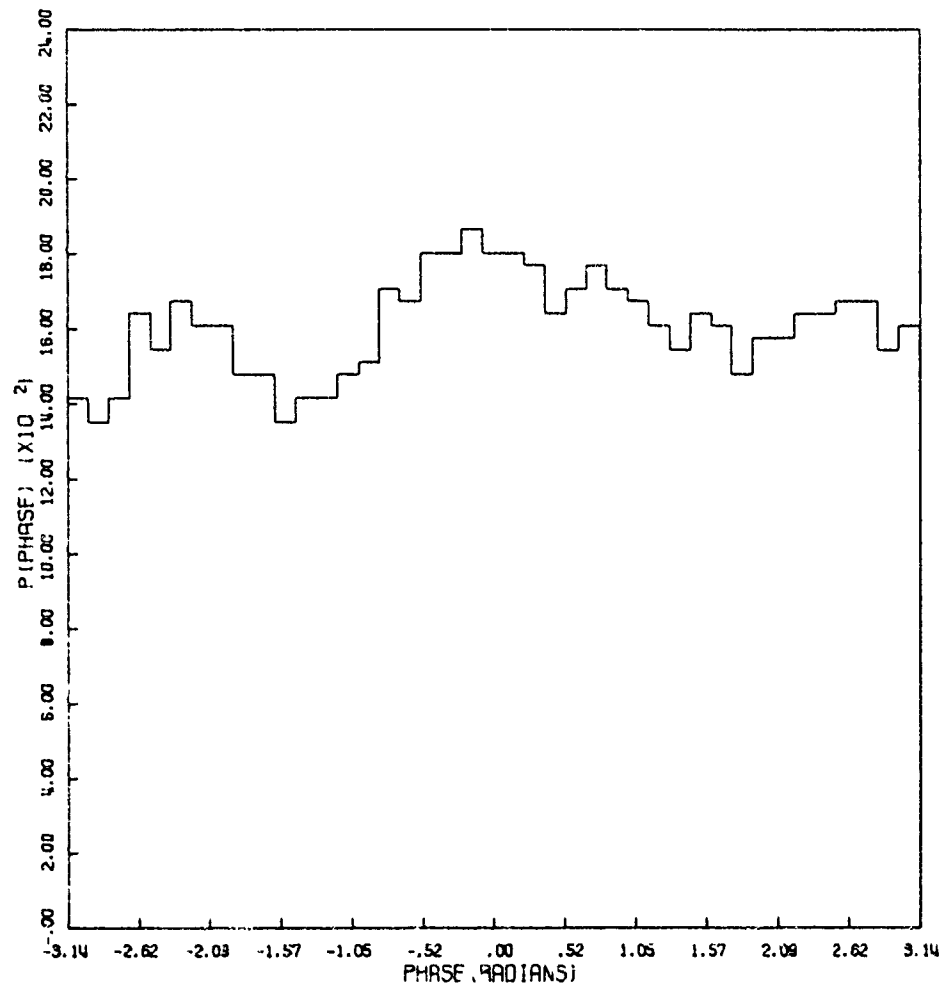
Figure 33c. Phase Distribution
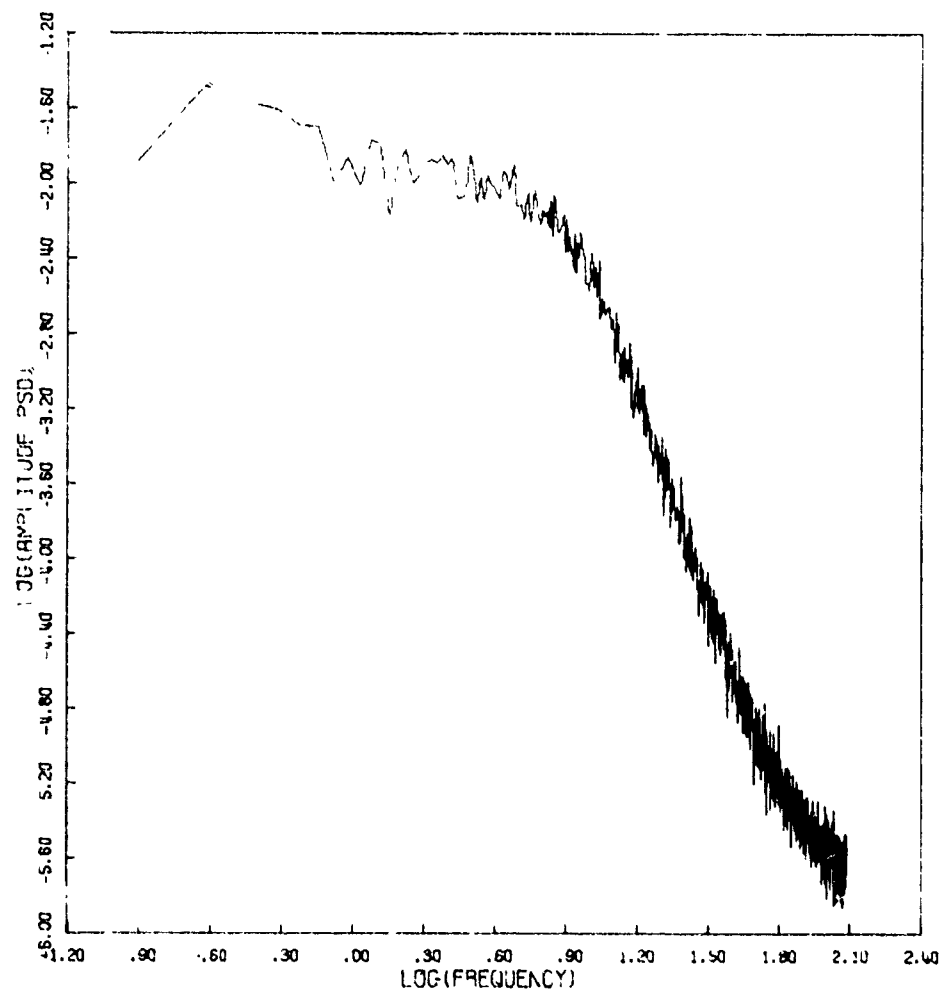
Figure 33d. Amplitude Power Spectral Density
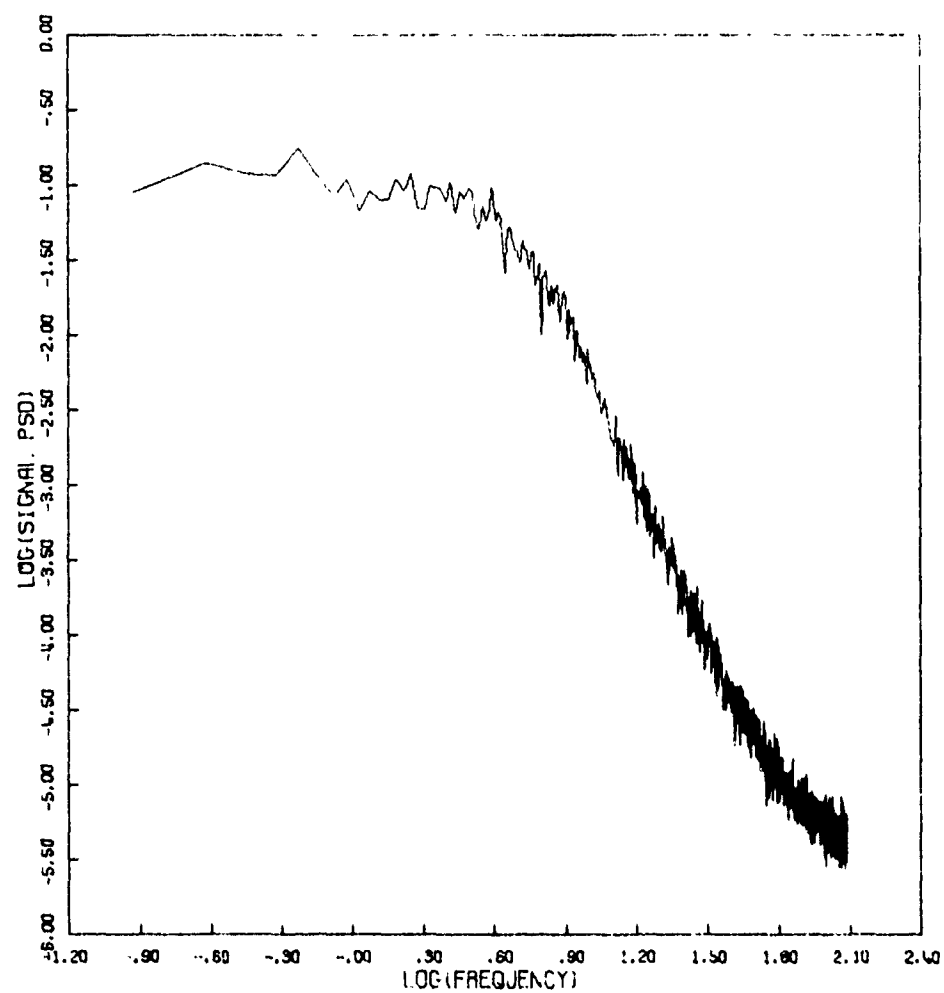
Figure 33e. Signal Power Spectral Density
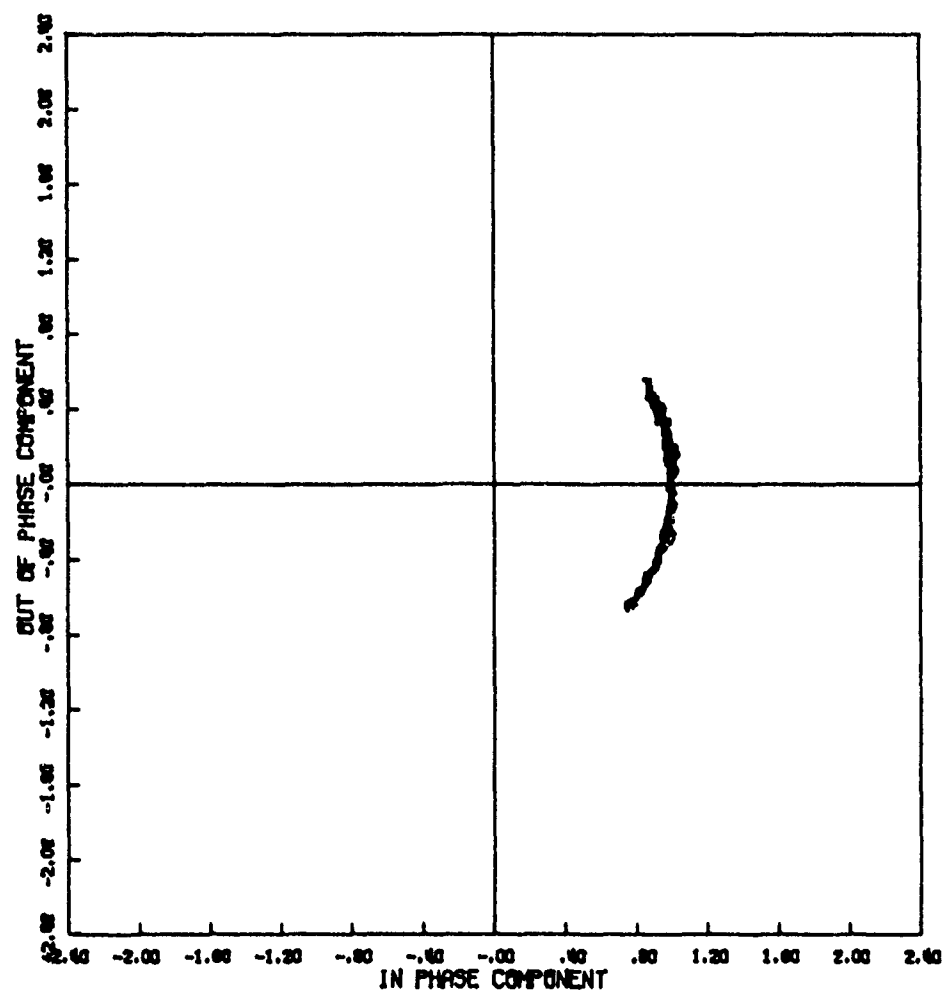
Figure 34a. Signal Phase Plot
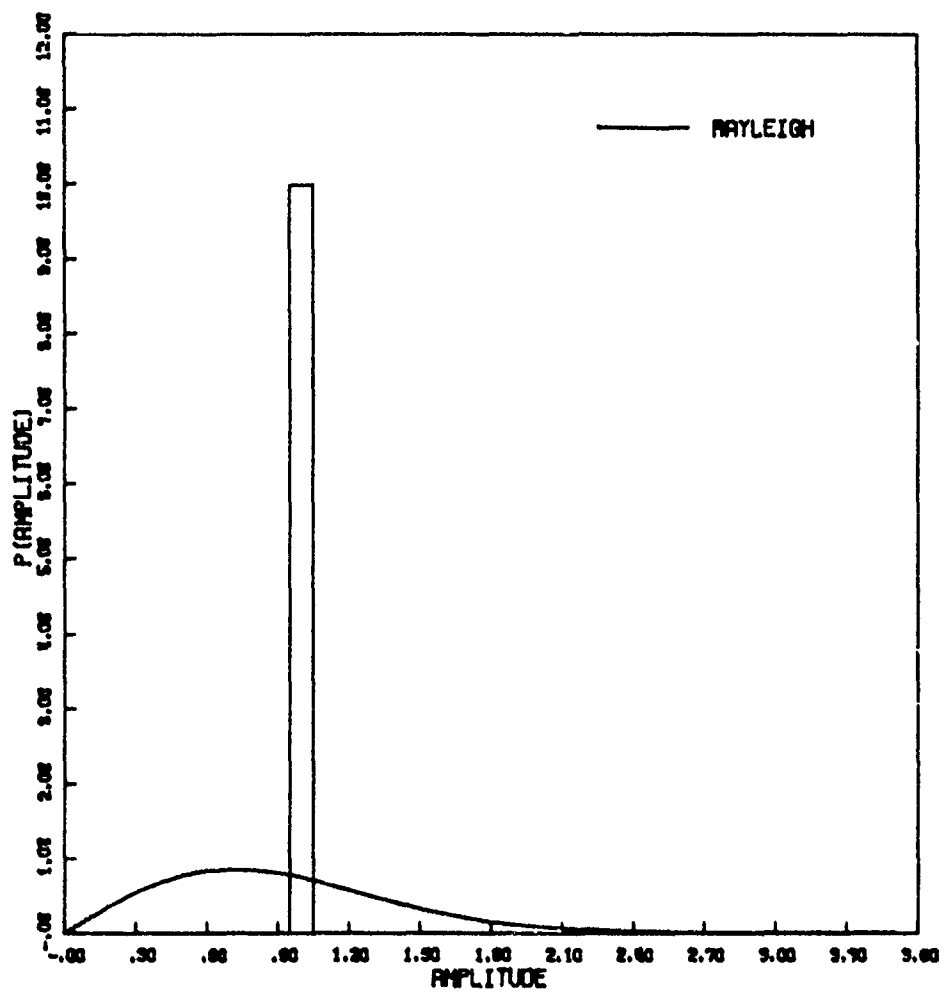
Figure 34b. Amplitude Distribution

169
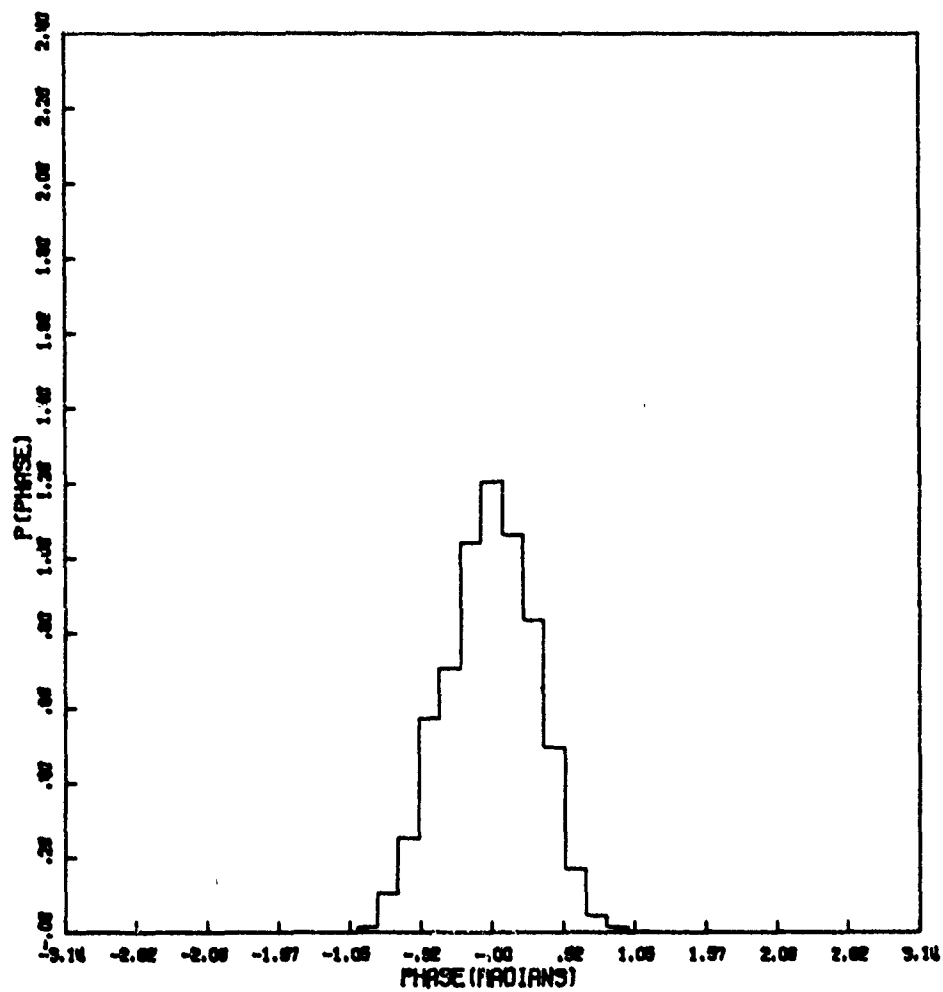
Figure 34c. Phase Distribution
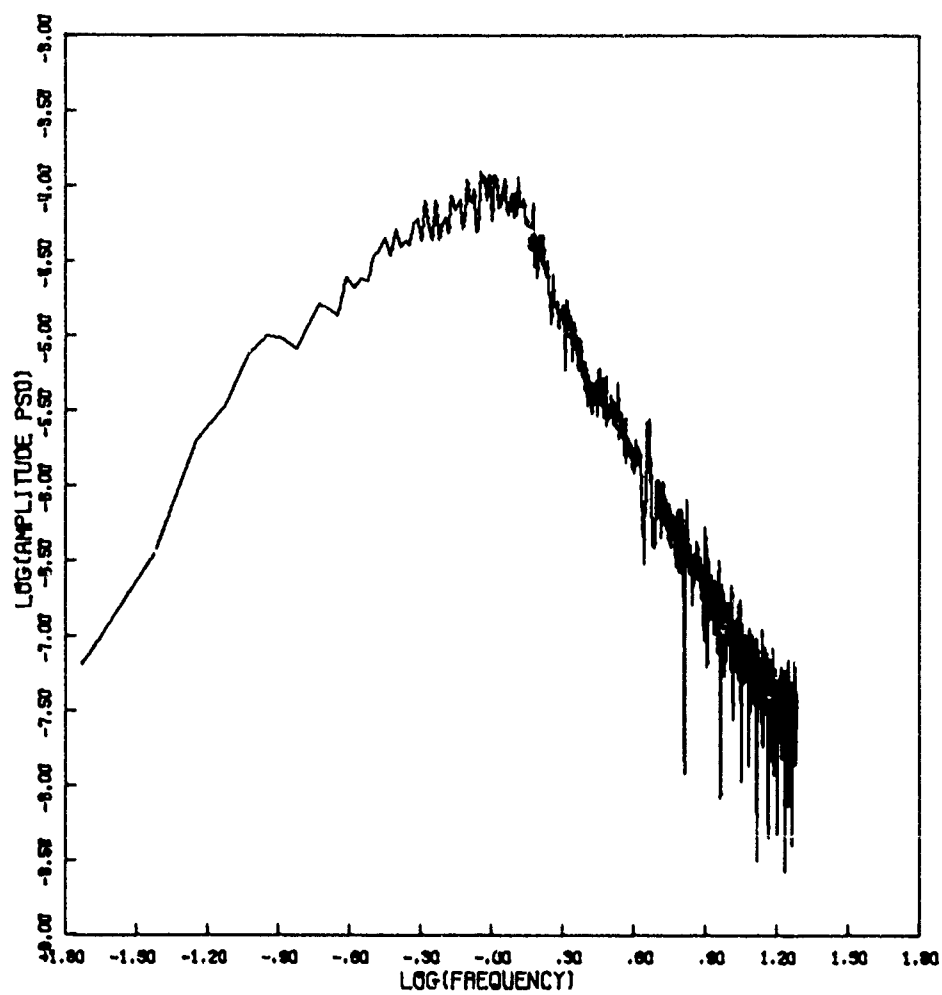
Figure 34d.   Amplitude Power Spectral Density

171
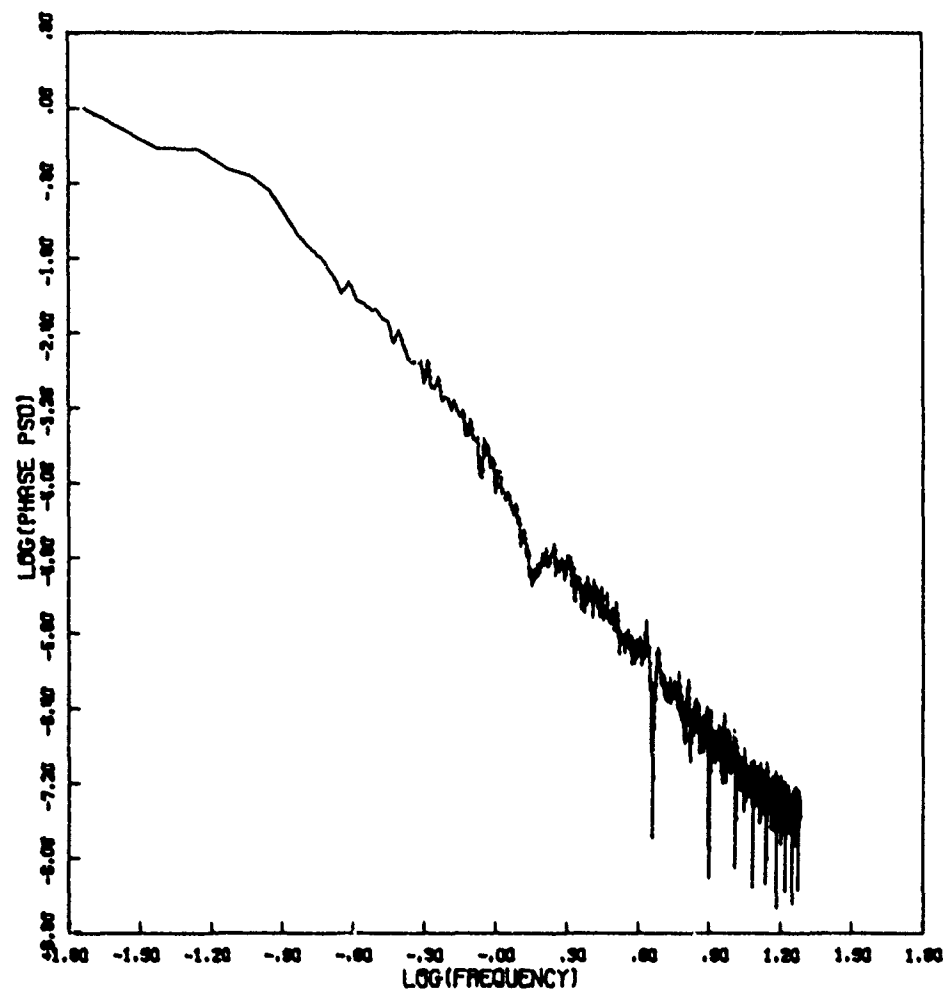
Figure 34e. Phase Power Spectral Density
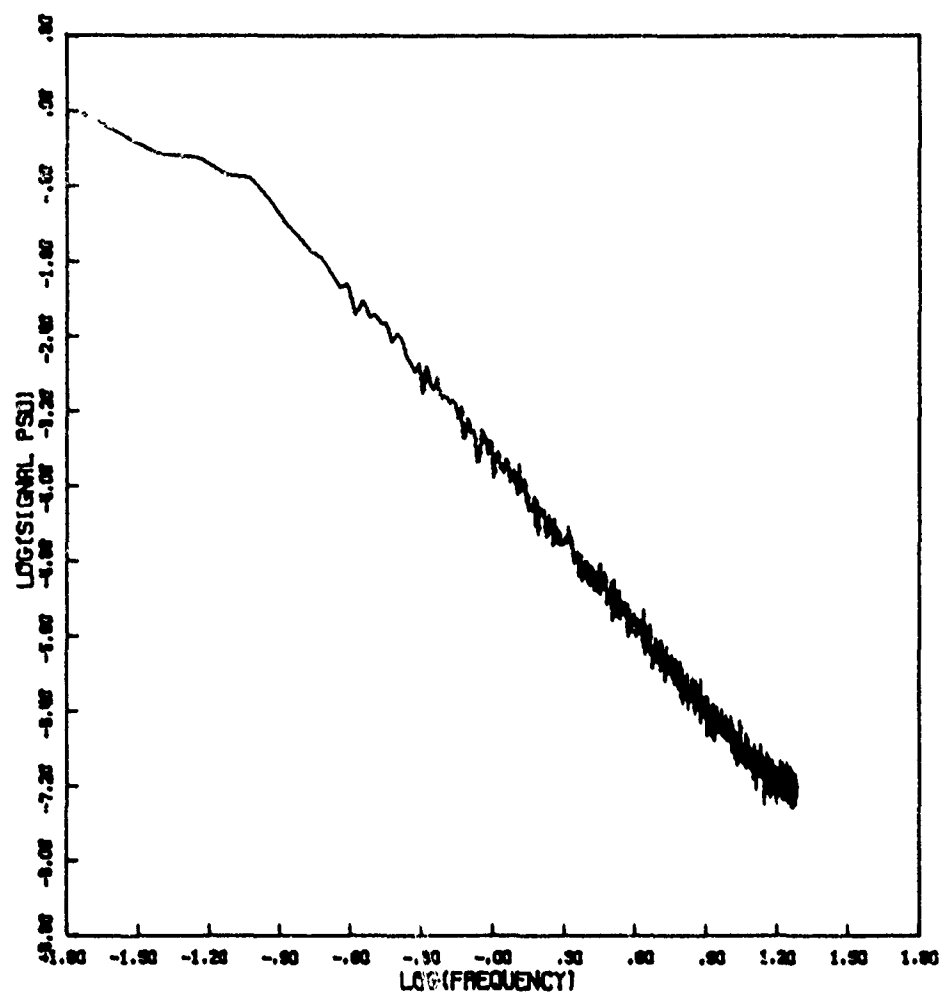
Figure 34f. Signal Power Spectral Density
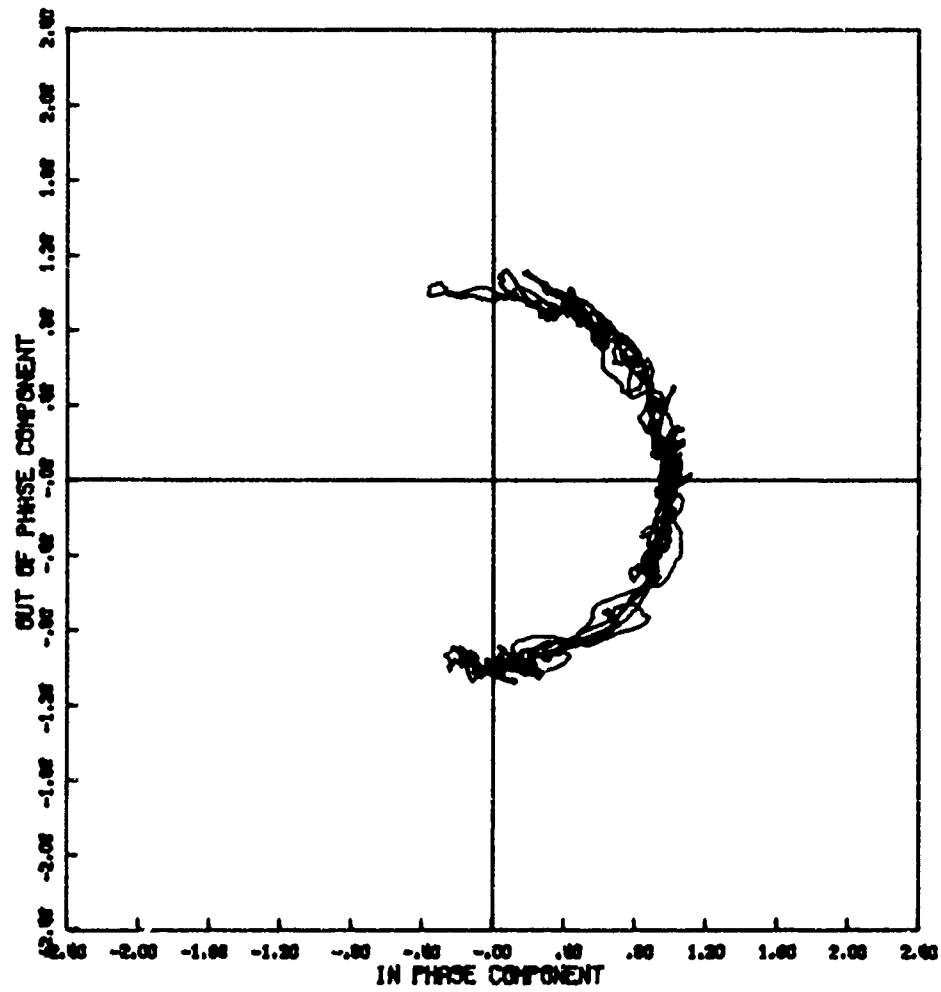
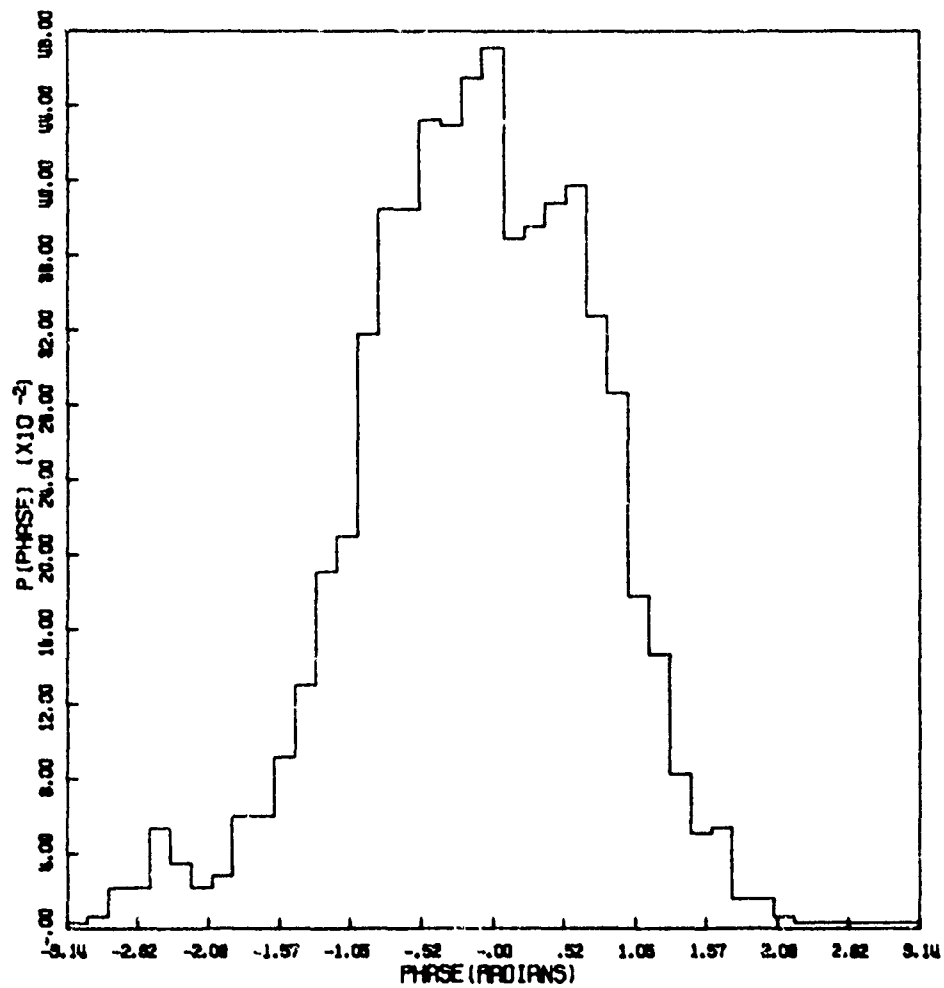Figure 35a. Signal Phase Plot
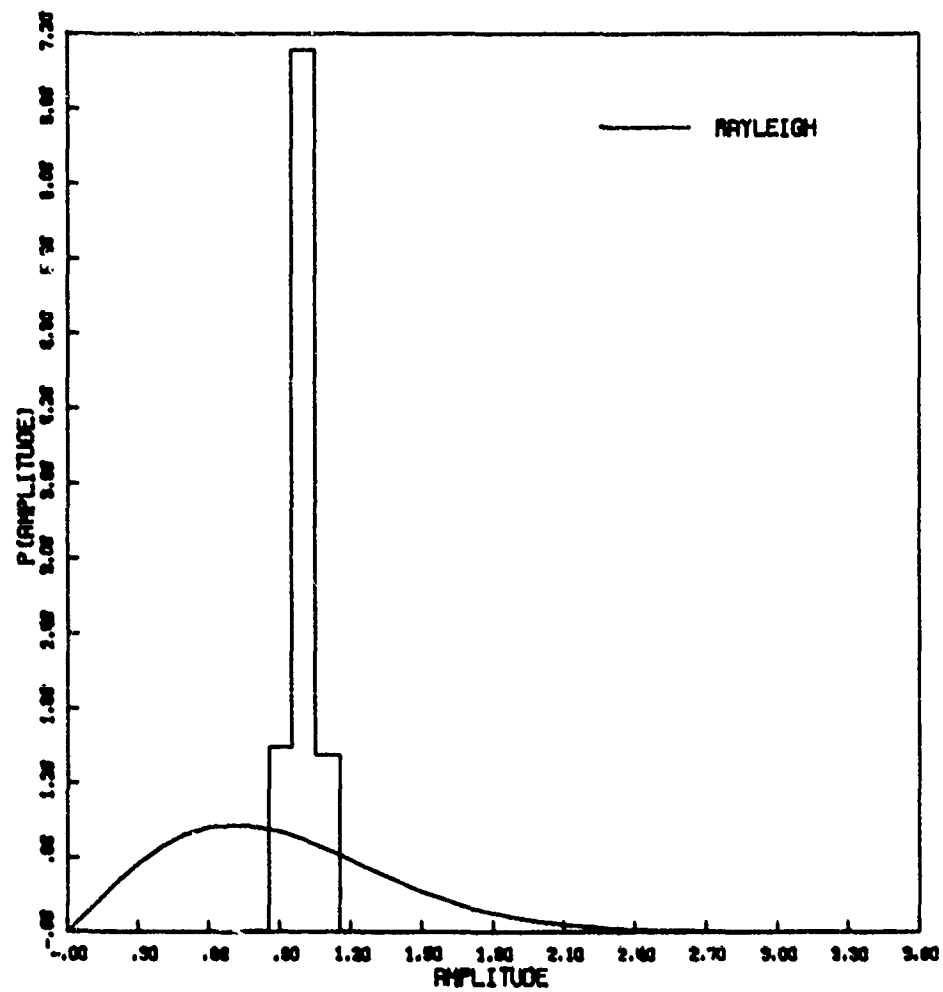
Figure 35b.   Amplitude Distribution
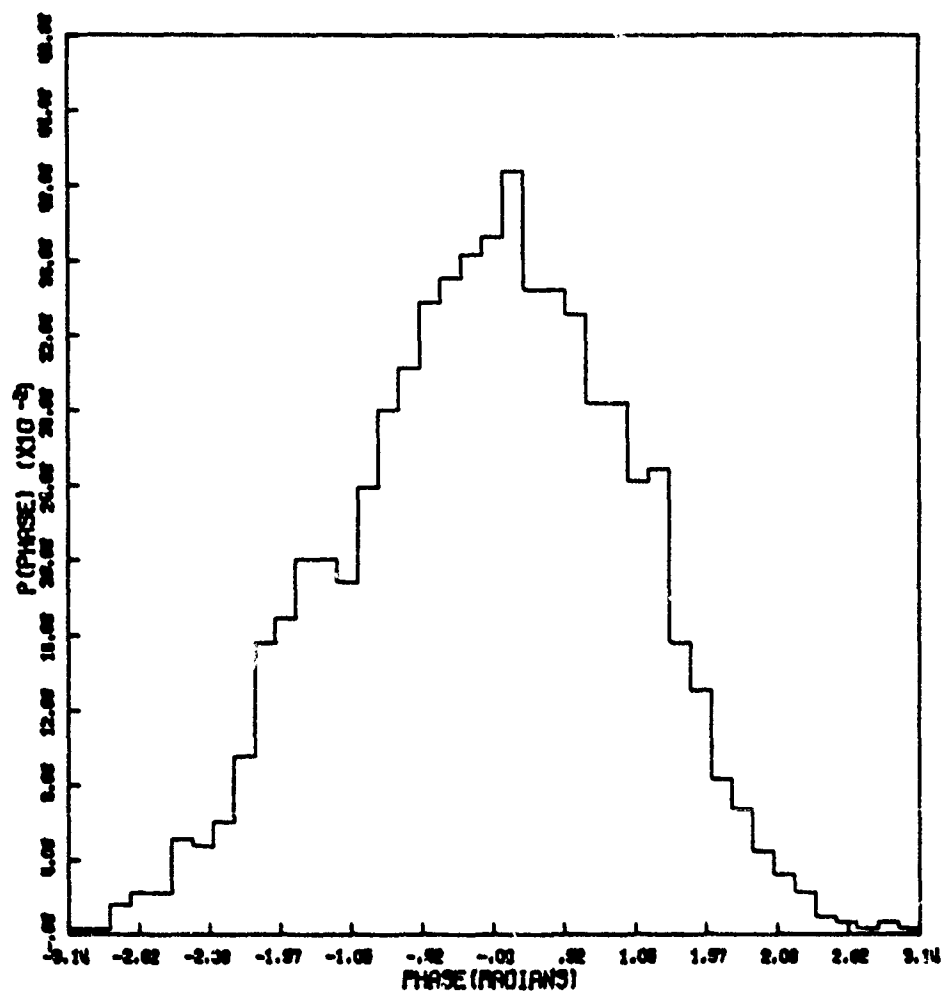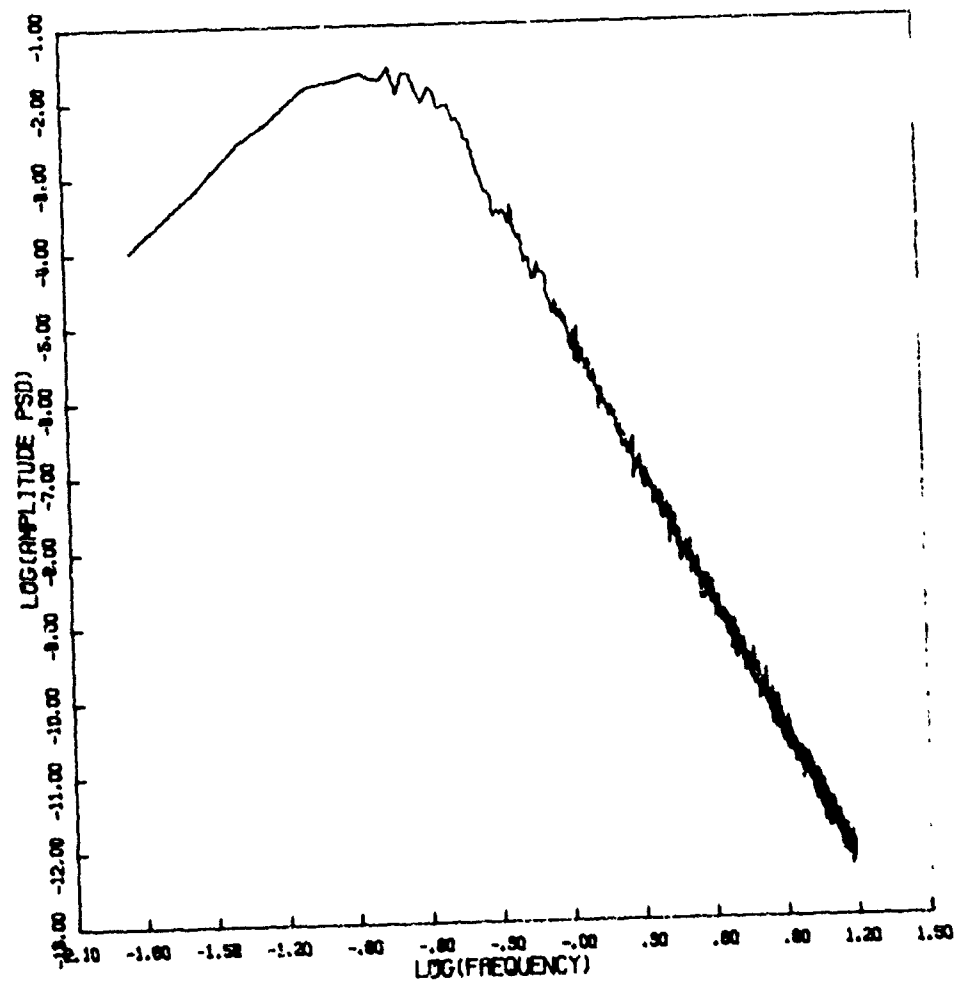
Figure 35c. Phase Distribution

176
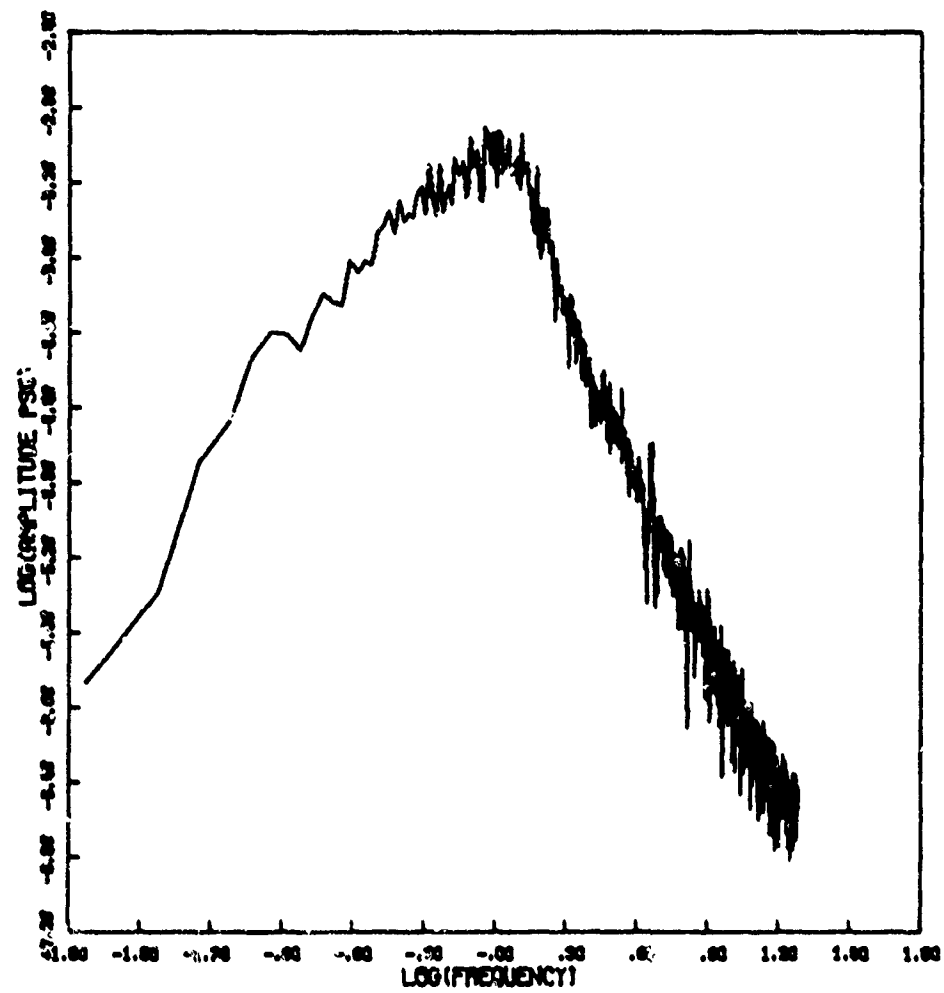
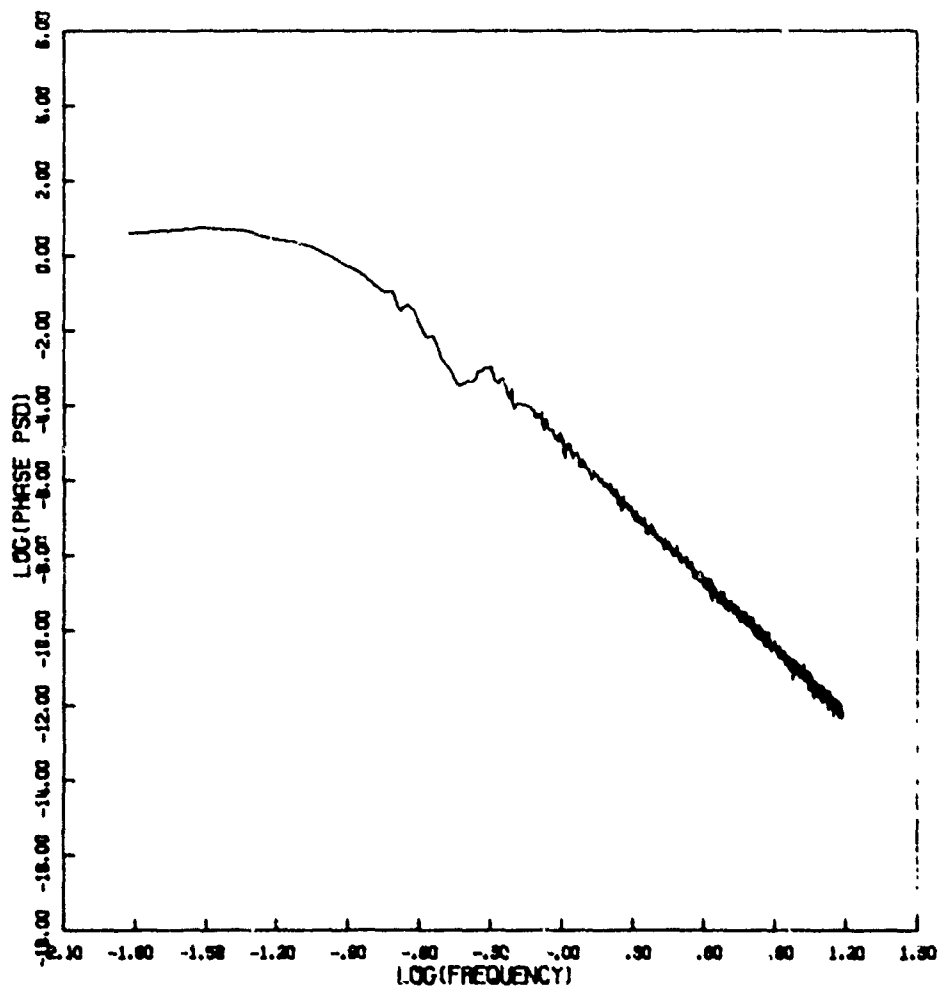Figure 35d. Amplitude Power Spectral Density
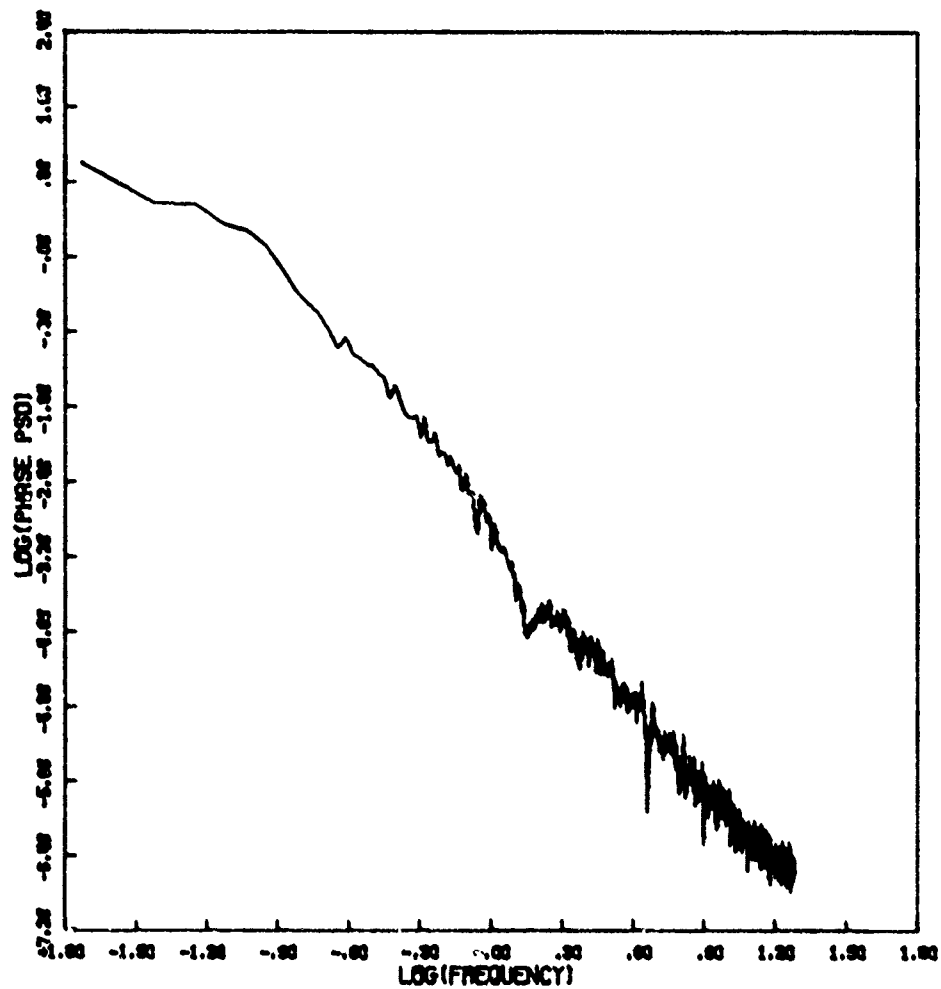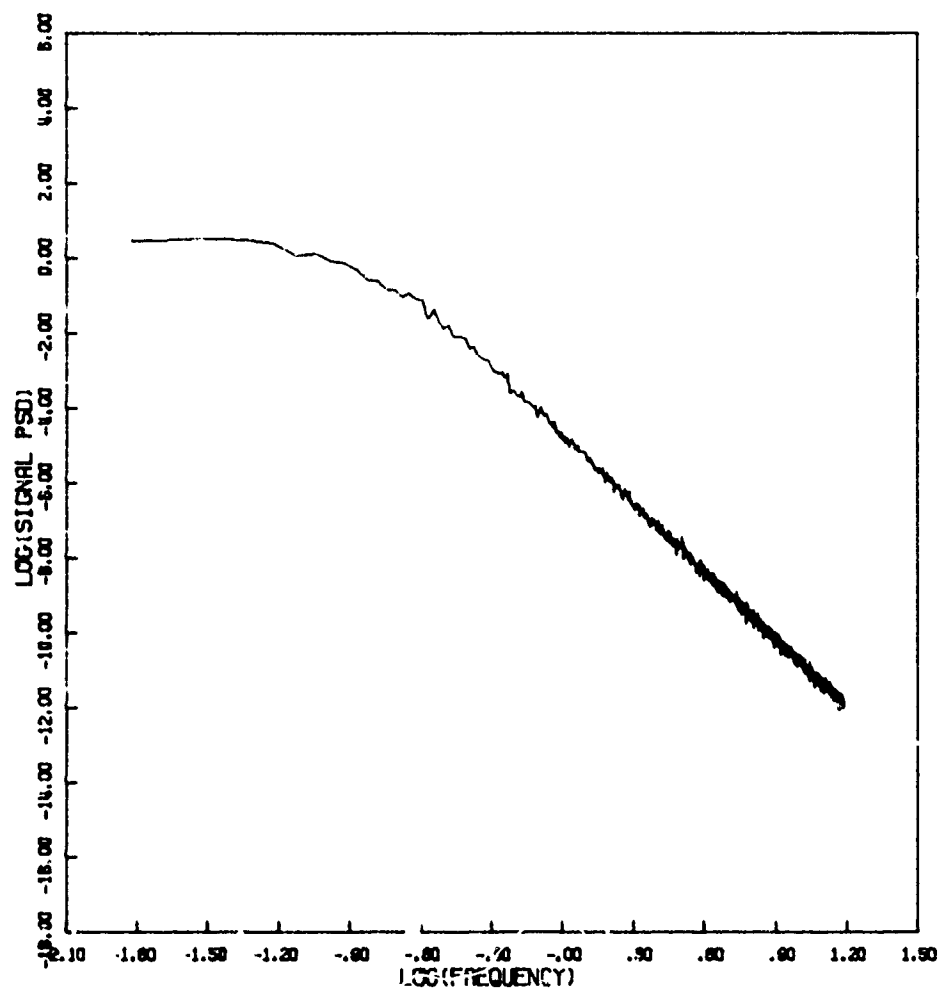
Figure 35e.   Phase Power Spectral Density
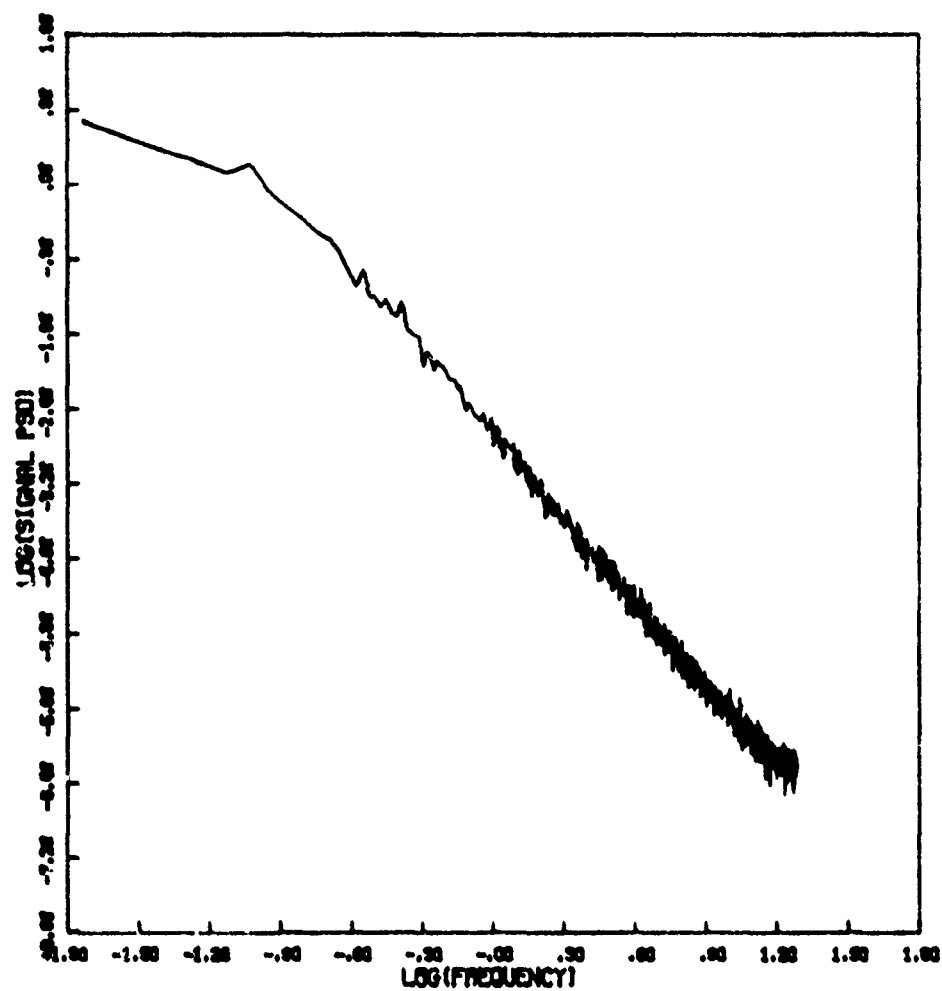
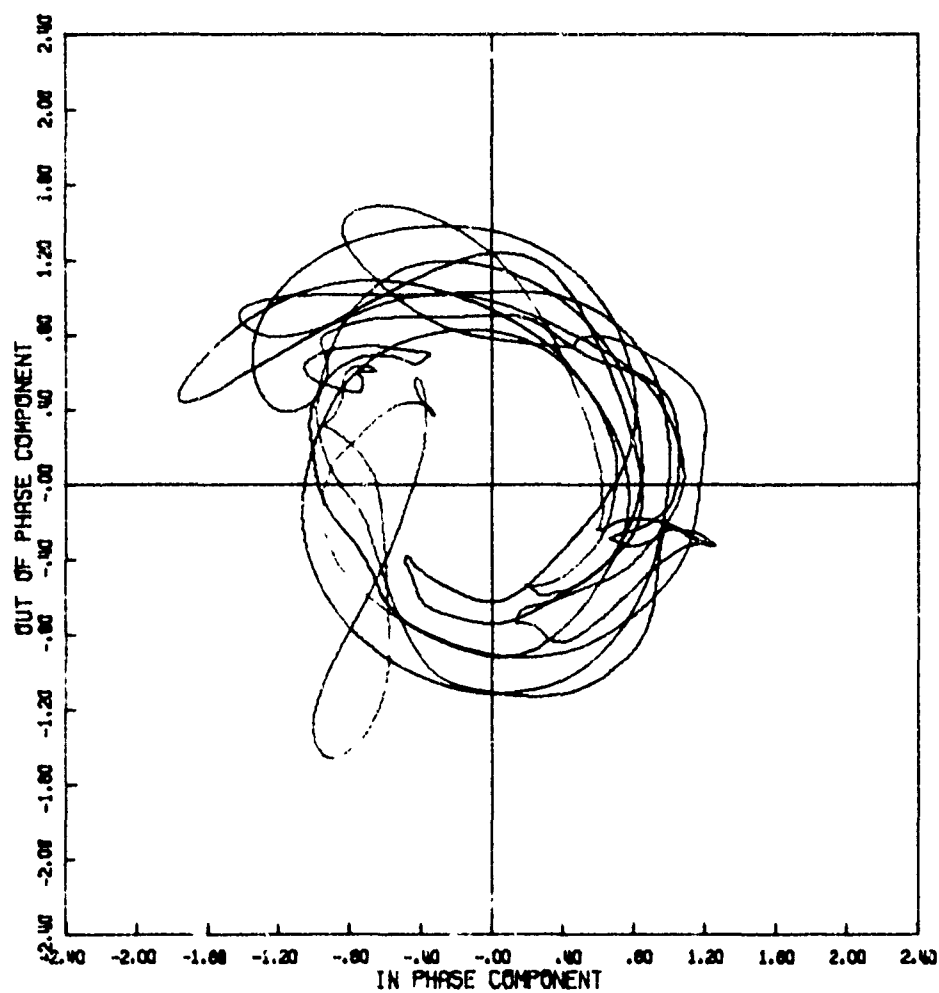Figure 35f. Signal Power Spectral Density
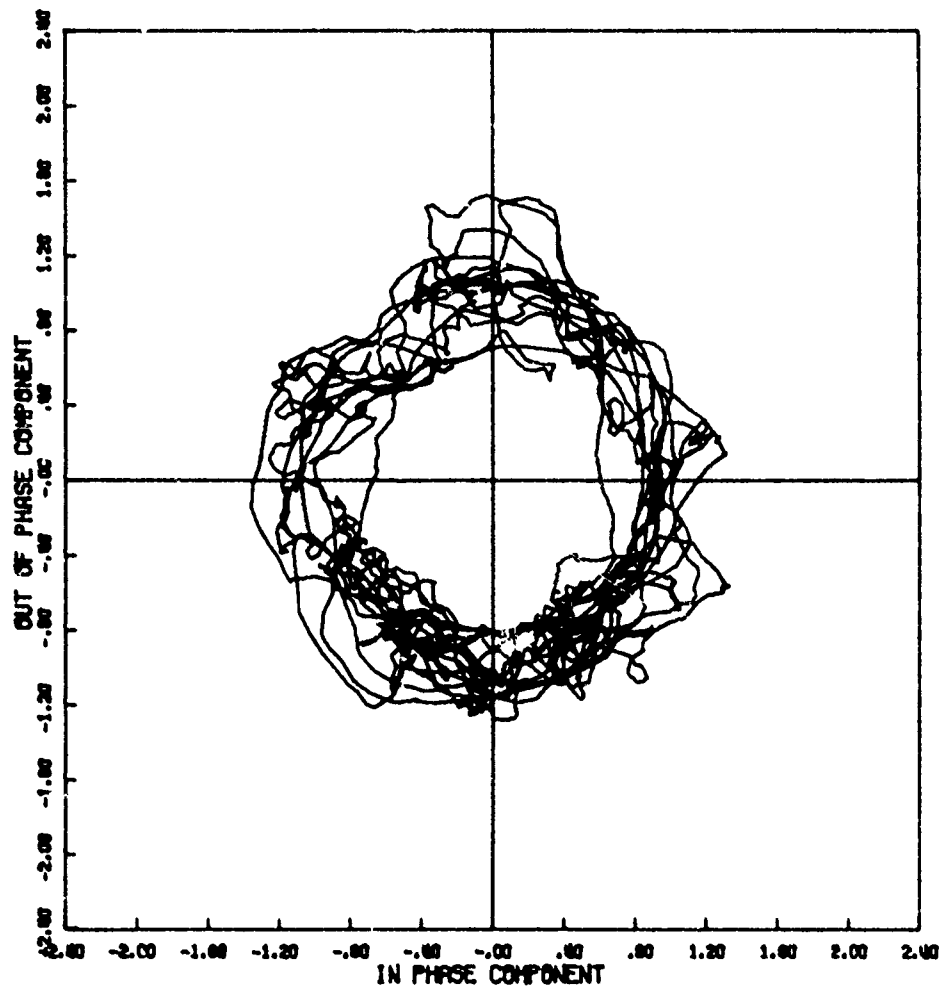
Figure 36a. Signal Phase Plot
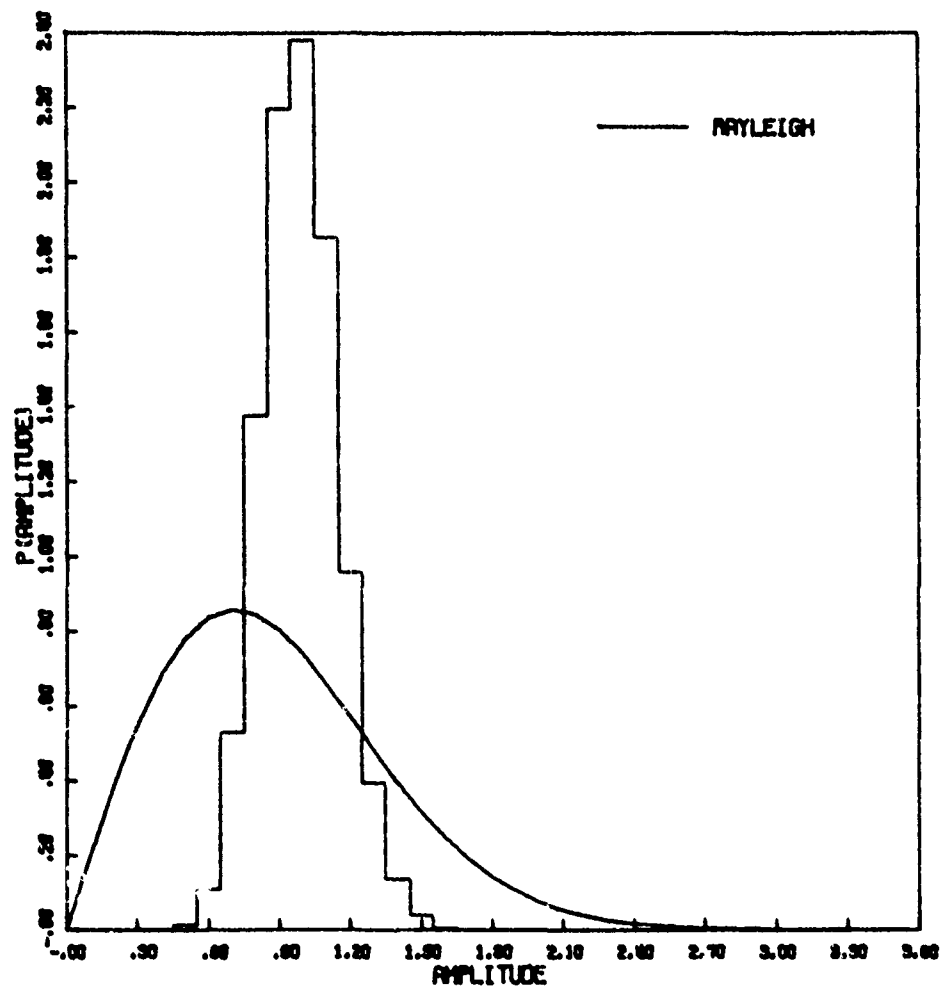
Figure 36b. Amplitude Distribution
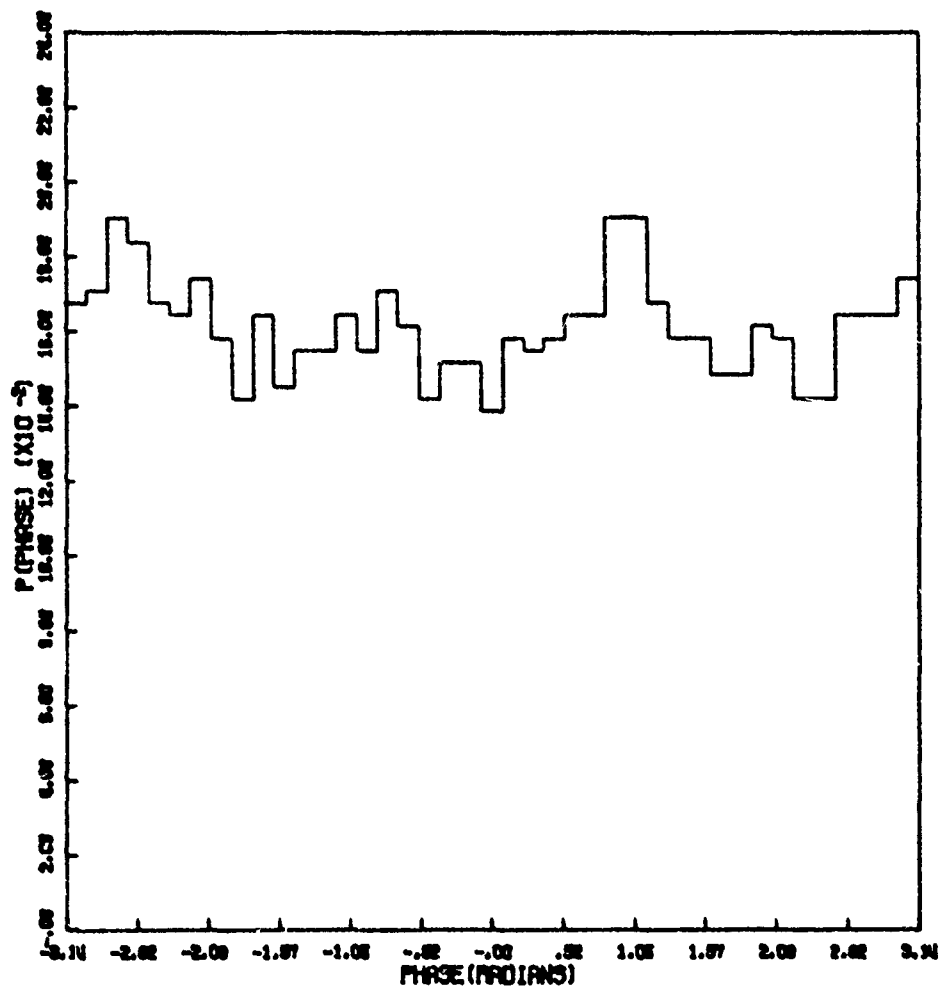
Figure 36c. Phase Distribution
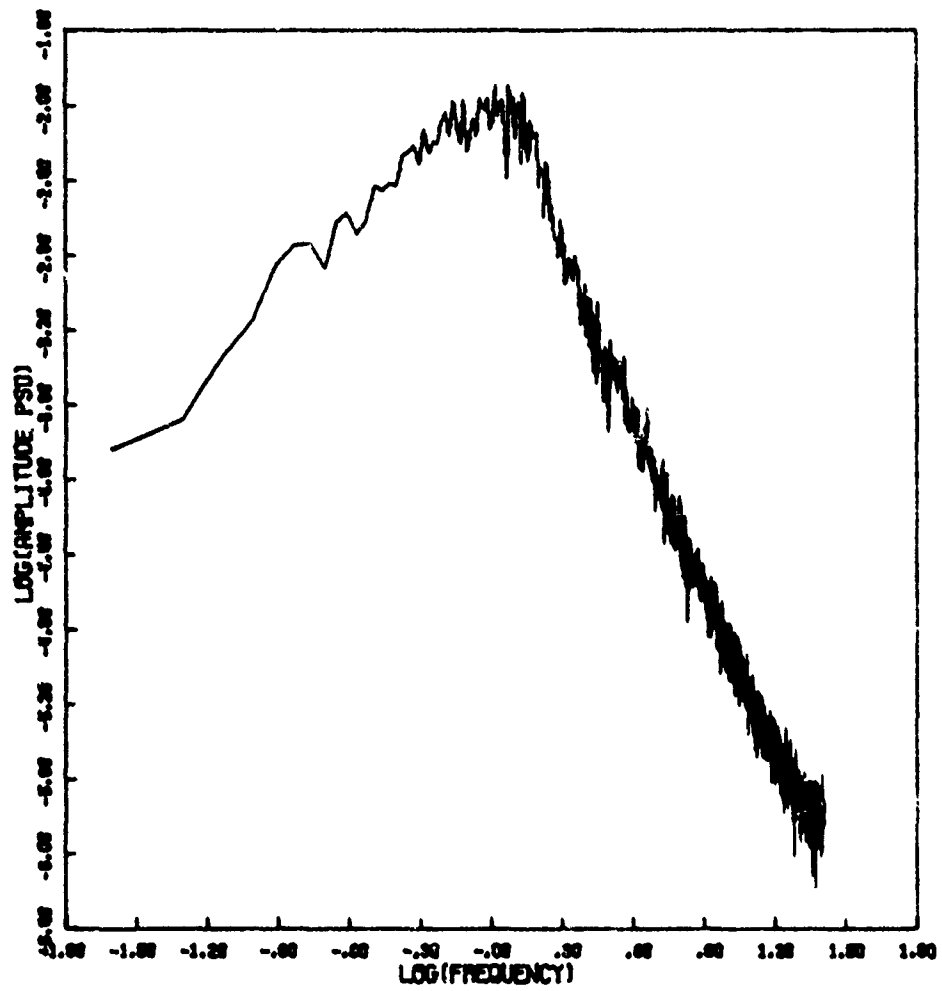
Figure 36d. Amplitude Power Spectral Density
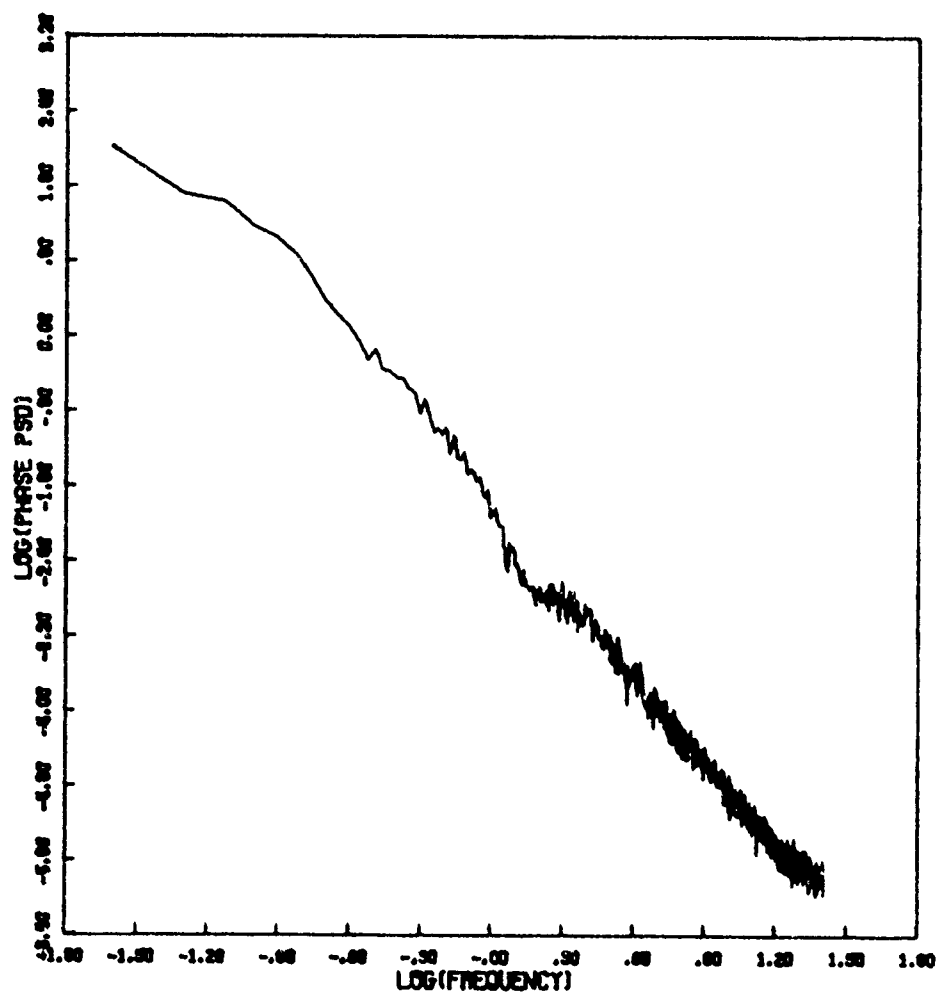
Figure 36e.   Phase Power Spectral Density
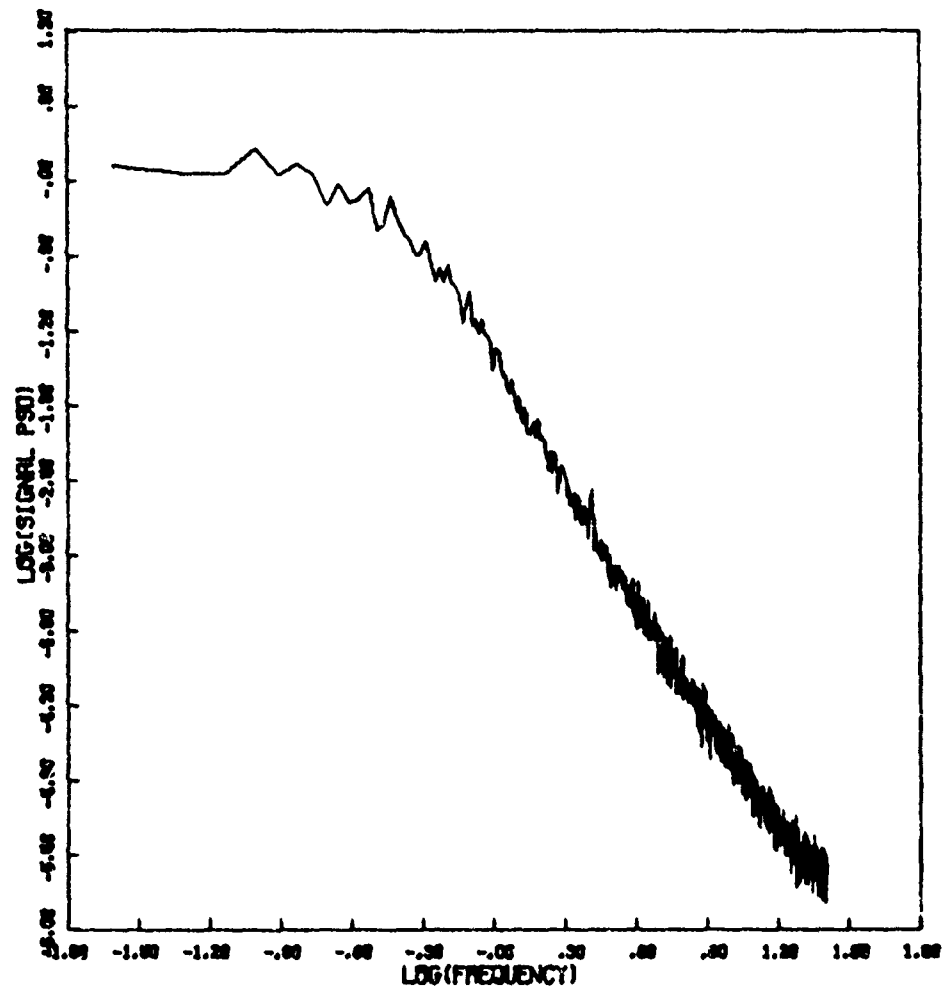
Figure 36f. Signal Power Spectral Density
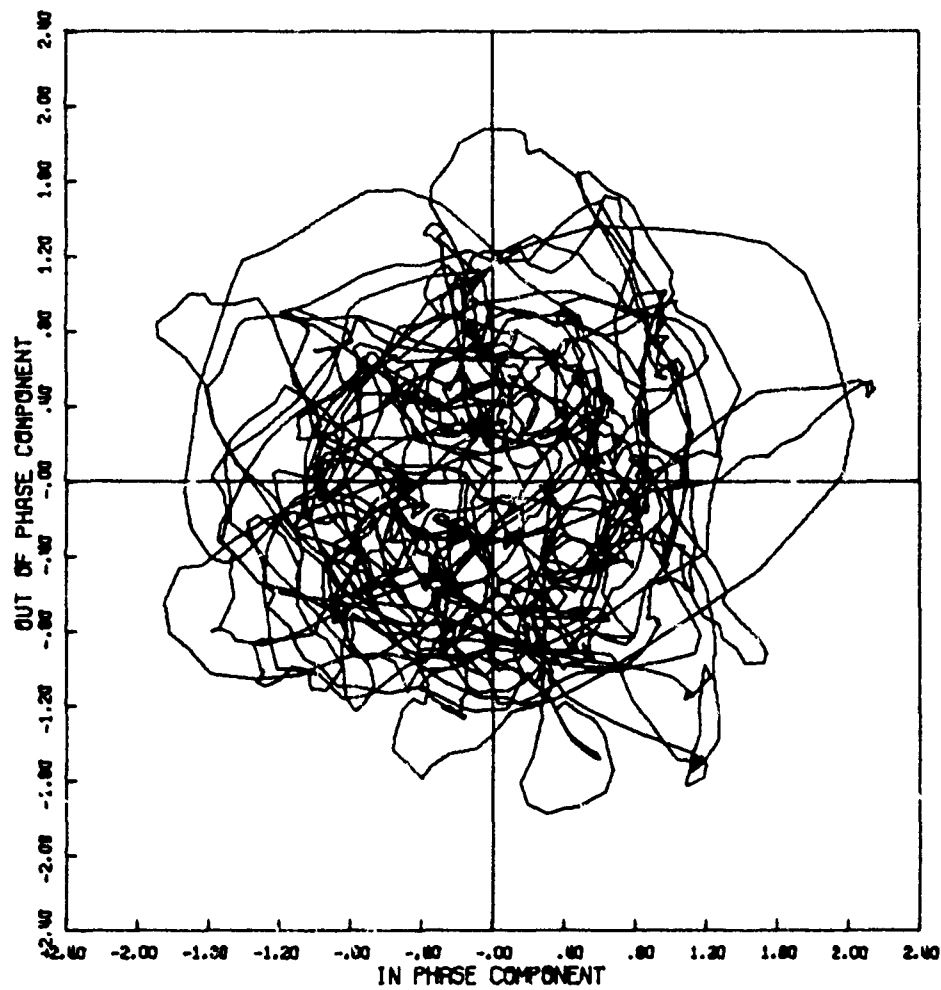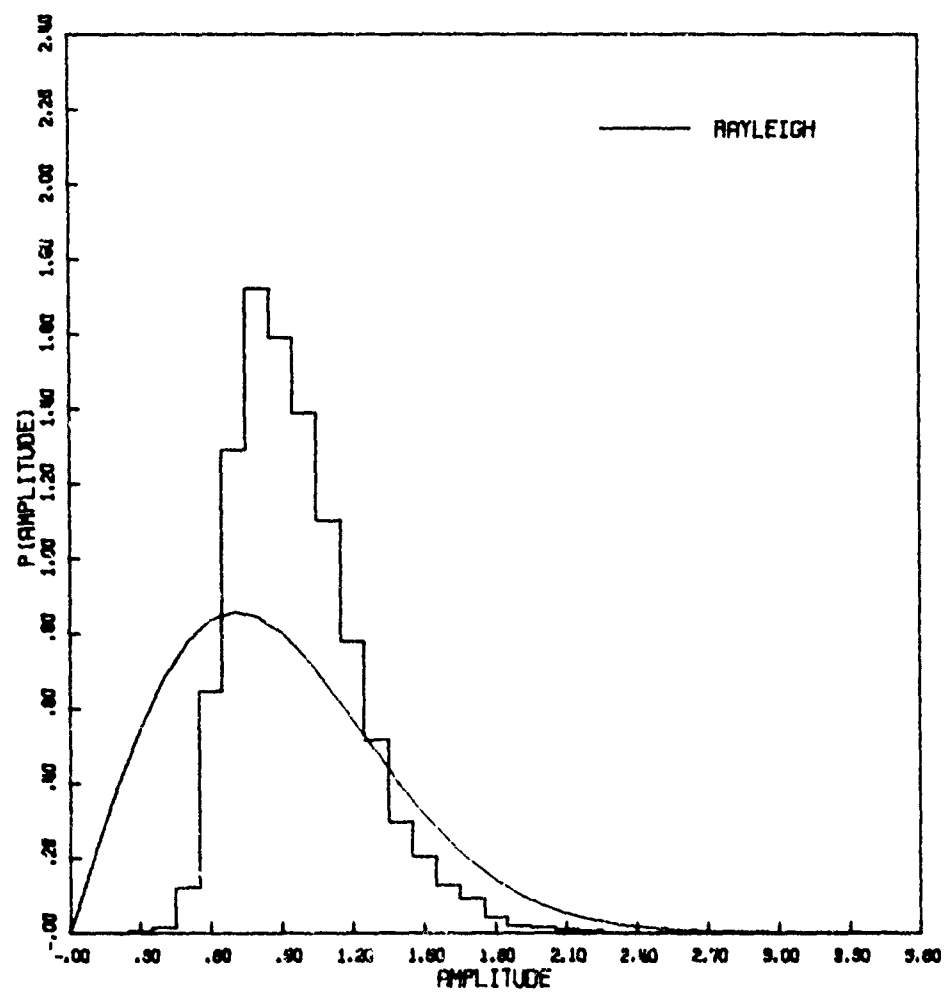
Figure 37a. Signal Phase Plot
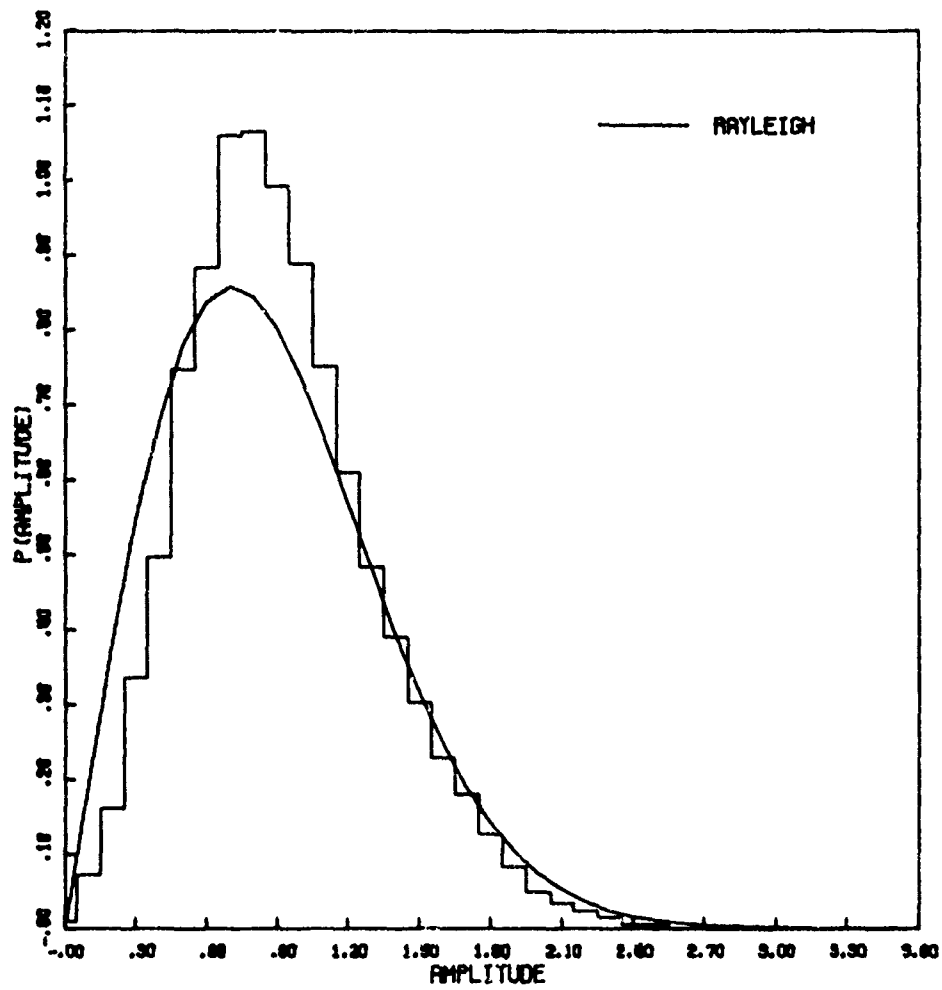
Figure 37b. Amplitude Distribution
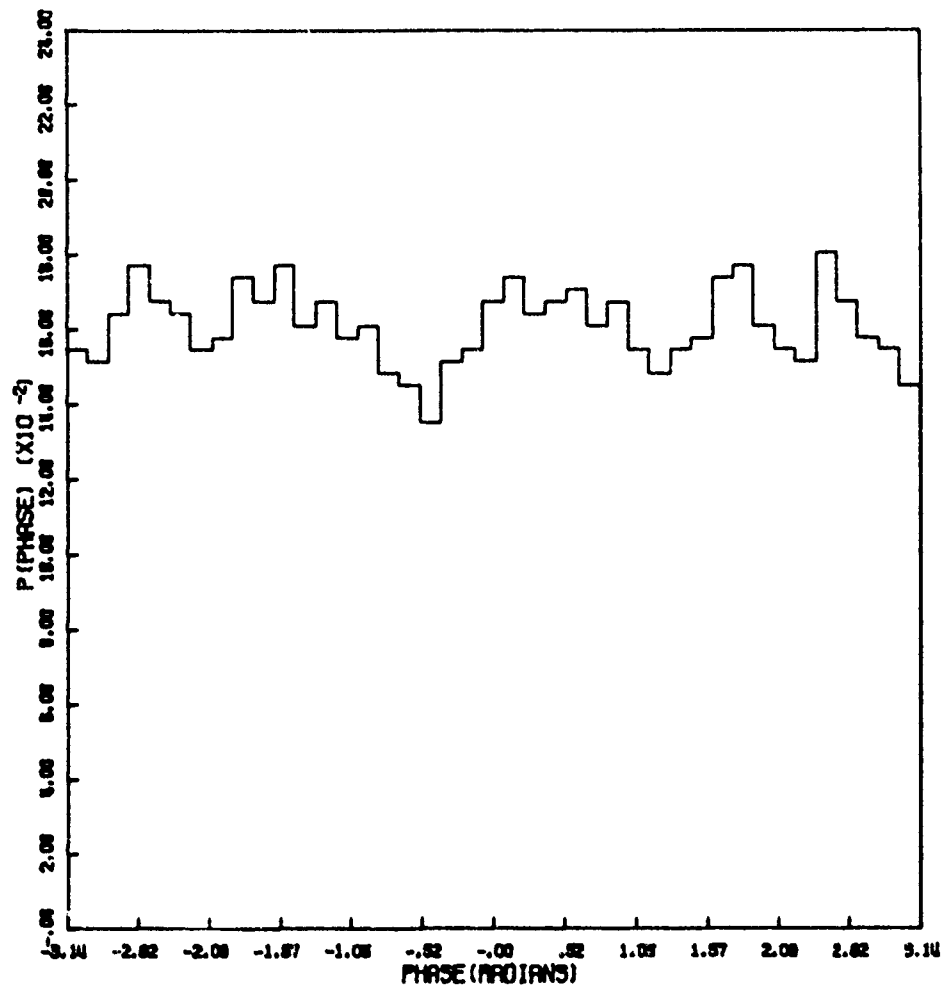
Figure 37c. Phase Distribution
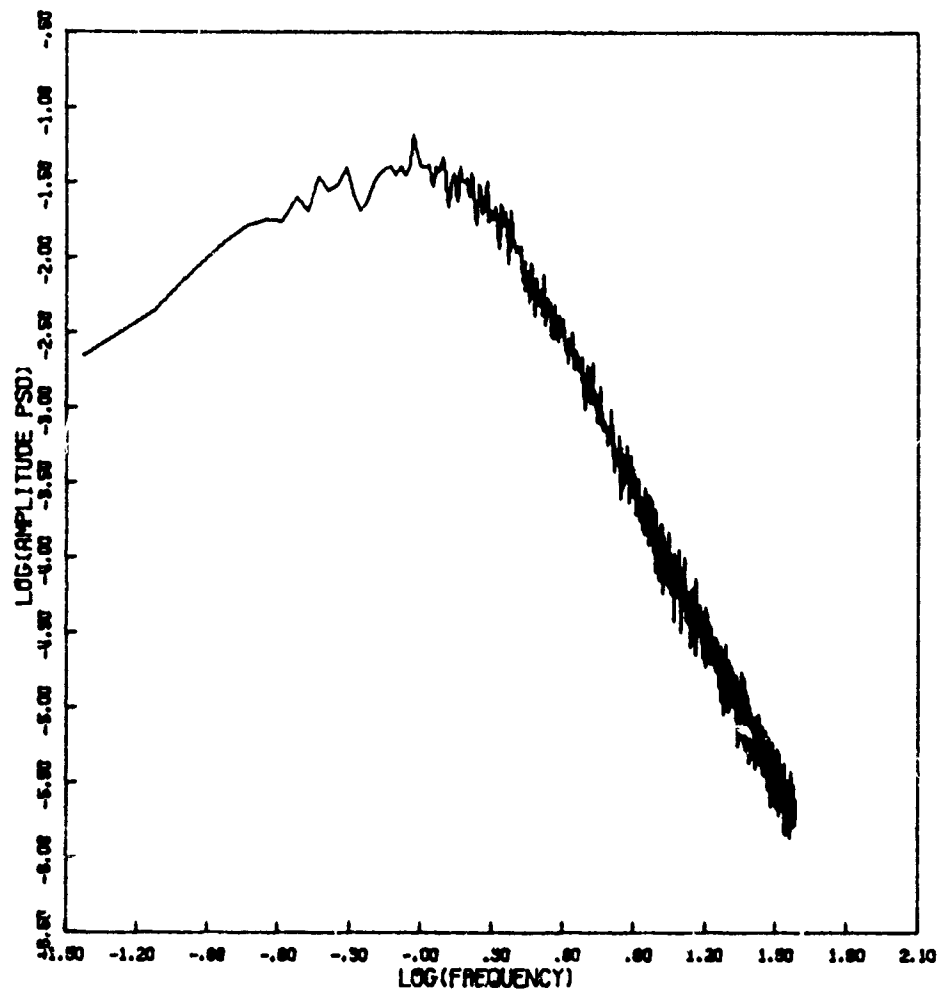
Figure 37d.   Amplitude Power Spectral Density
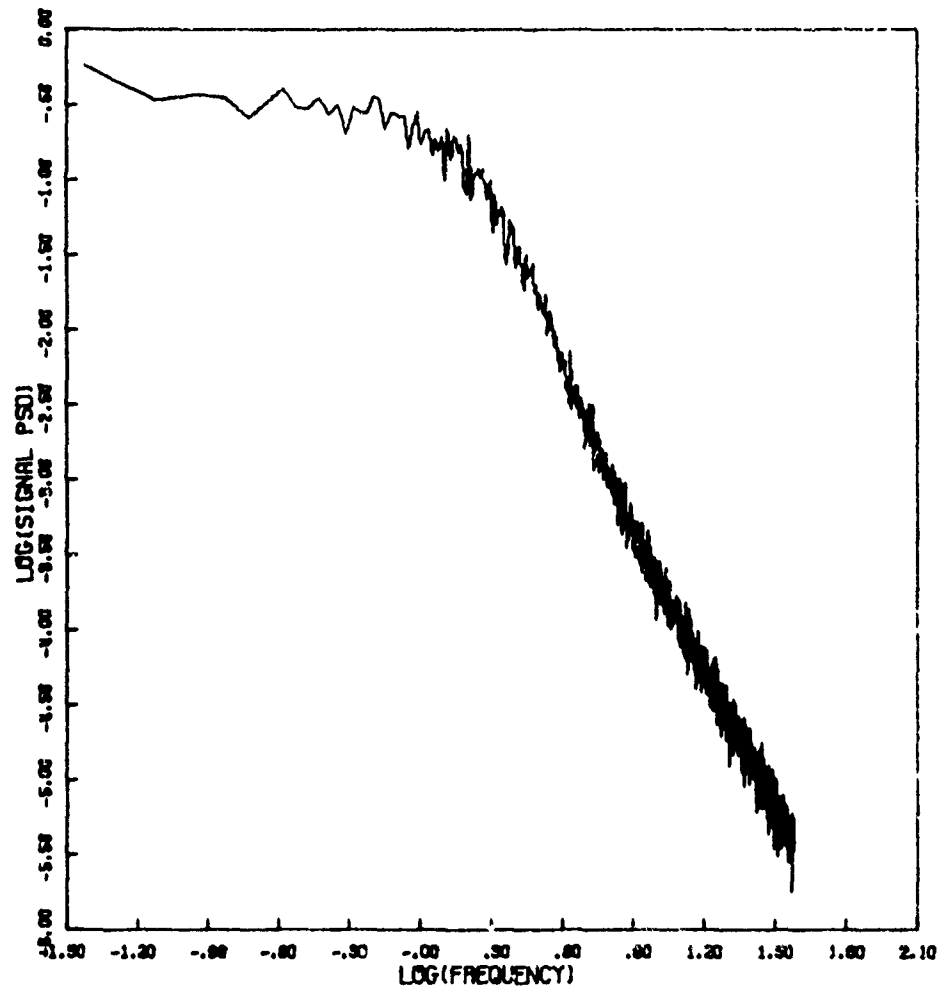
Figure 37e. Signal Power Spectral Density
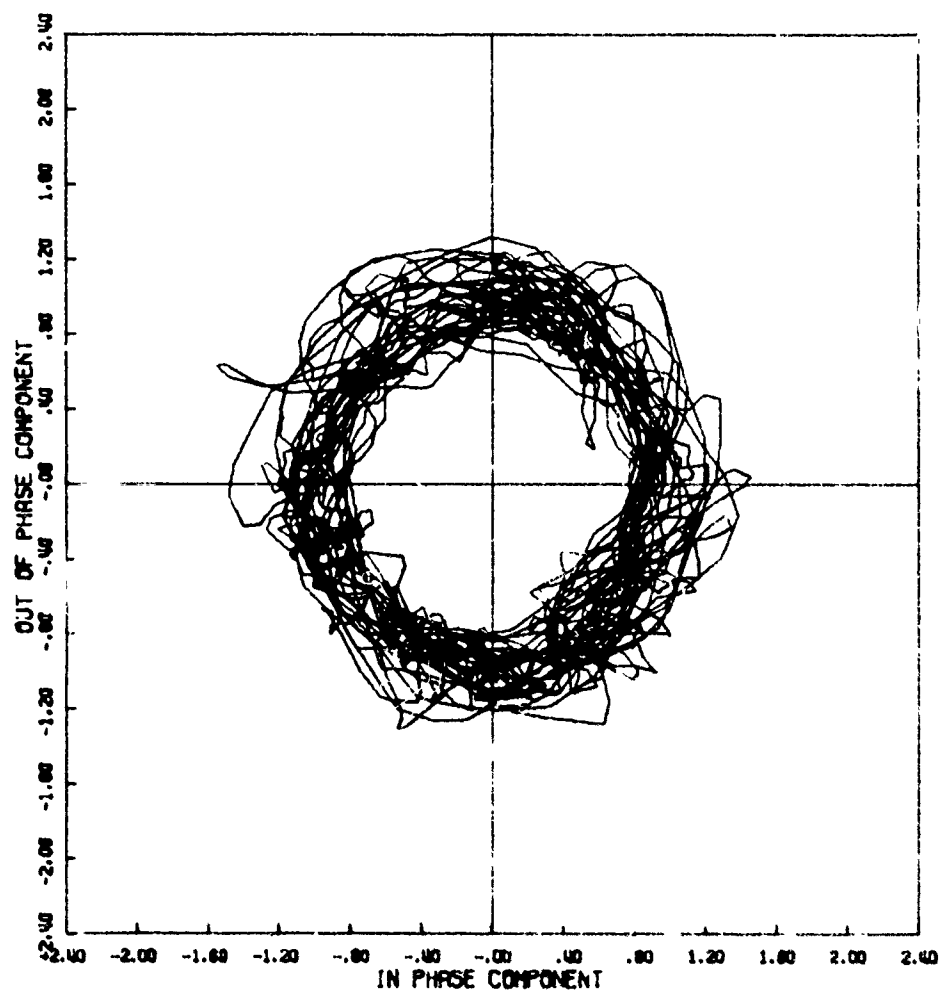
Figure 38a. Signal Phase Plot
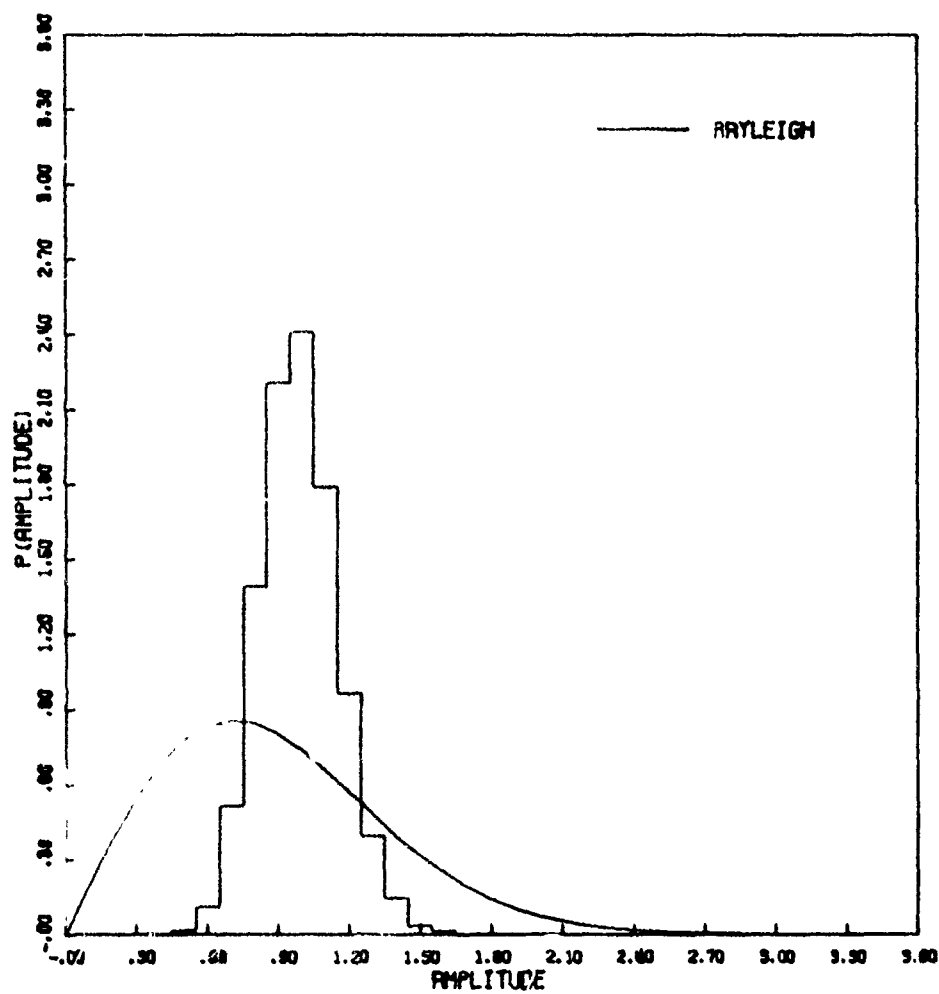
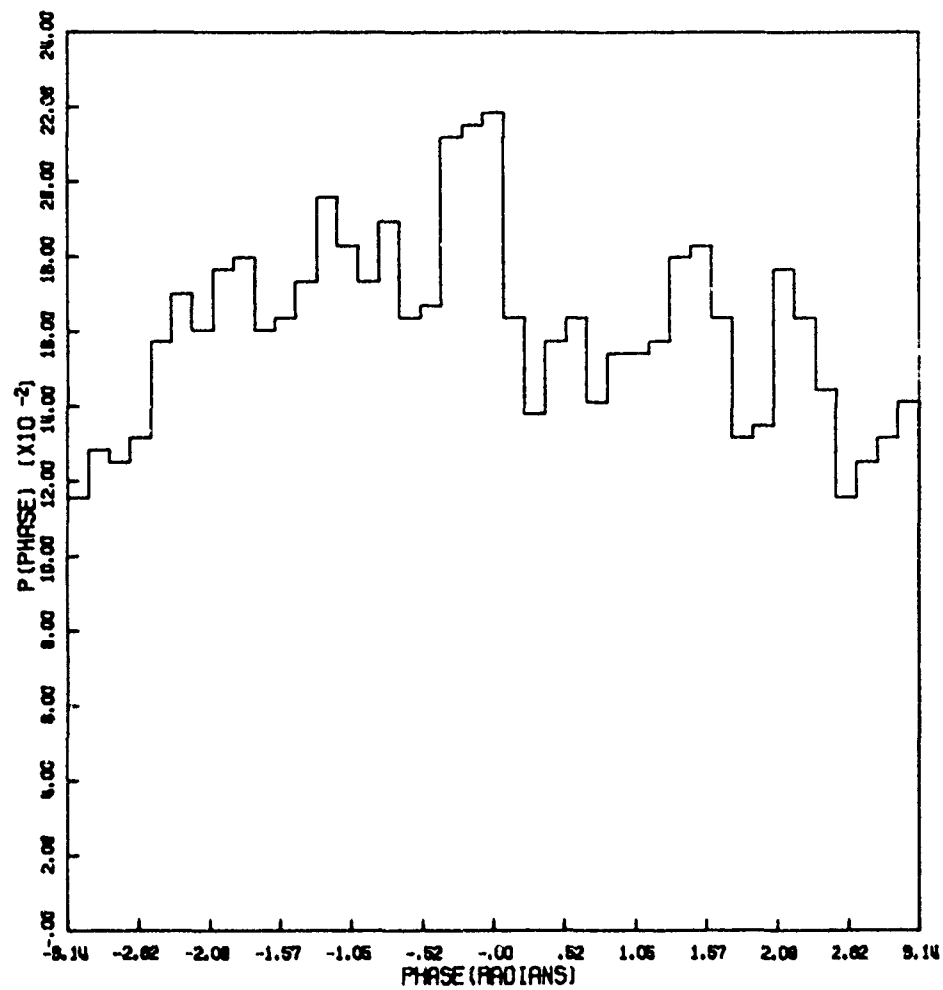Figure 38b. Amplitude Distribution
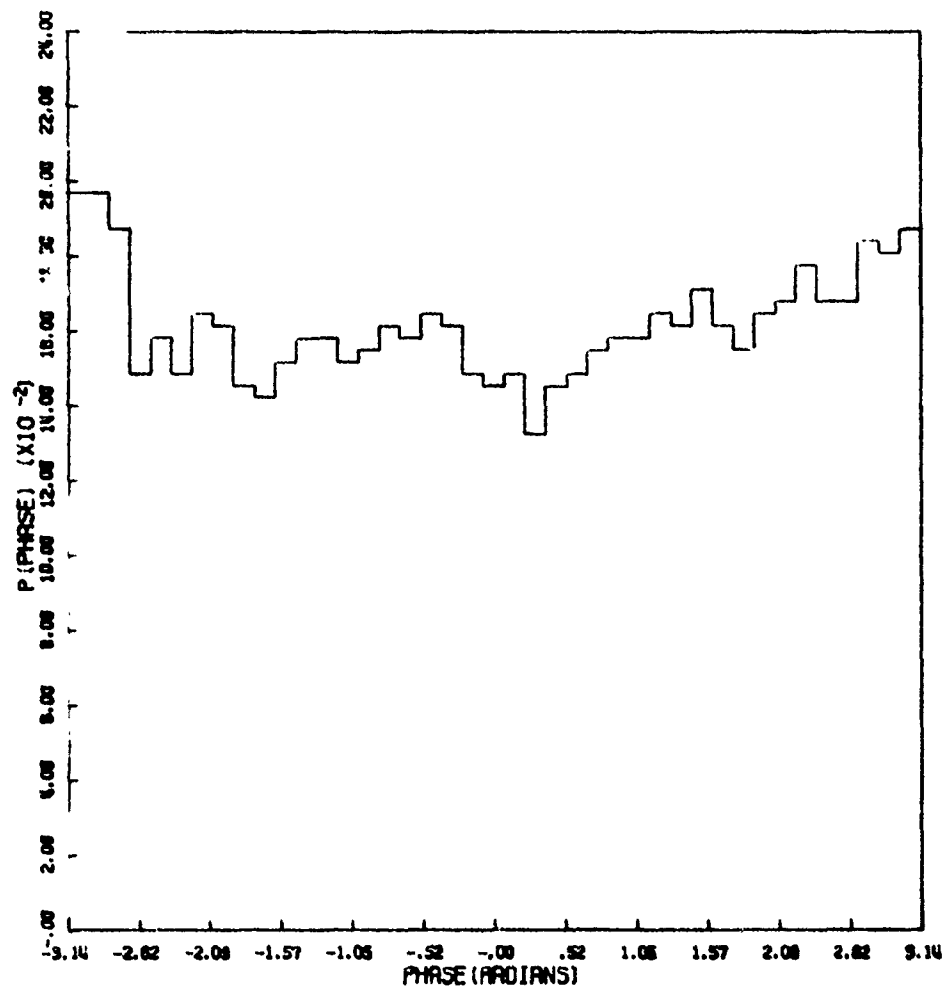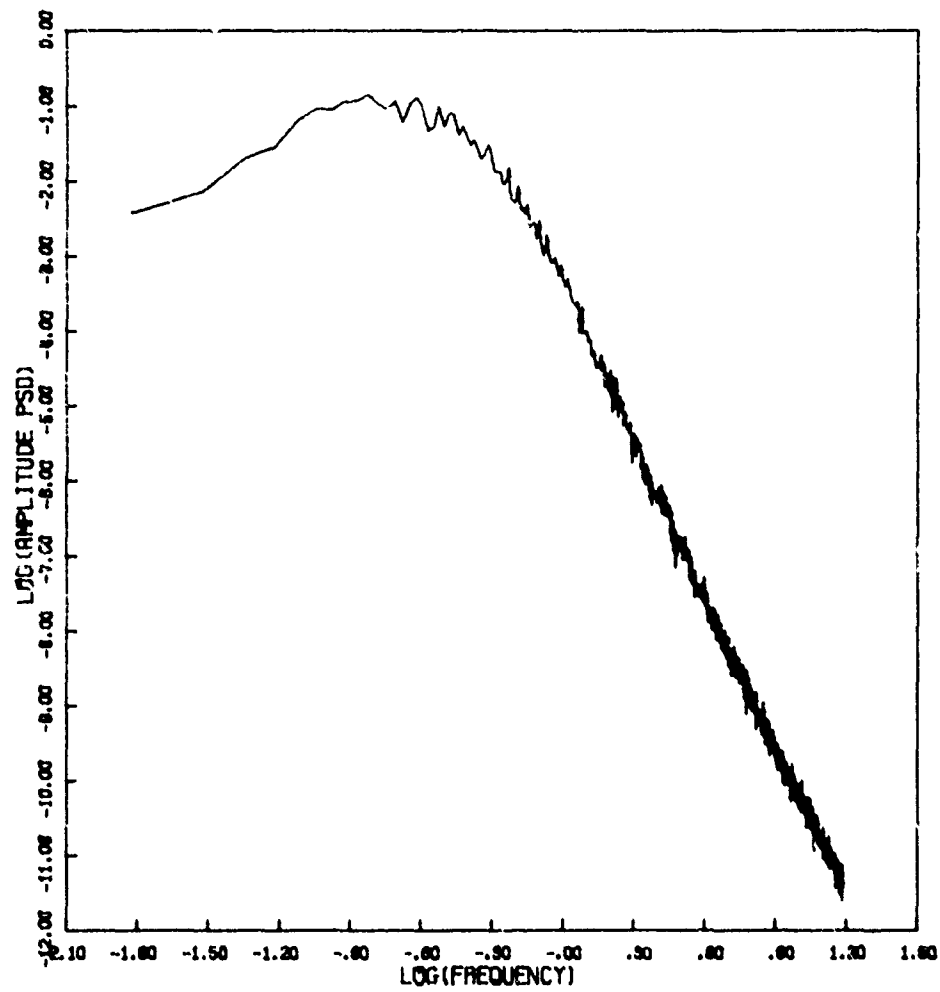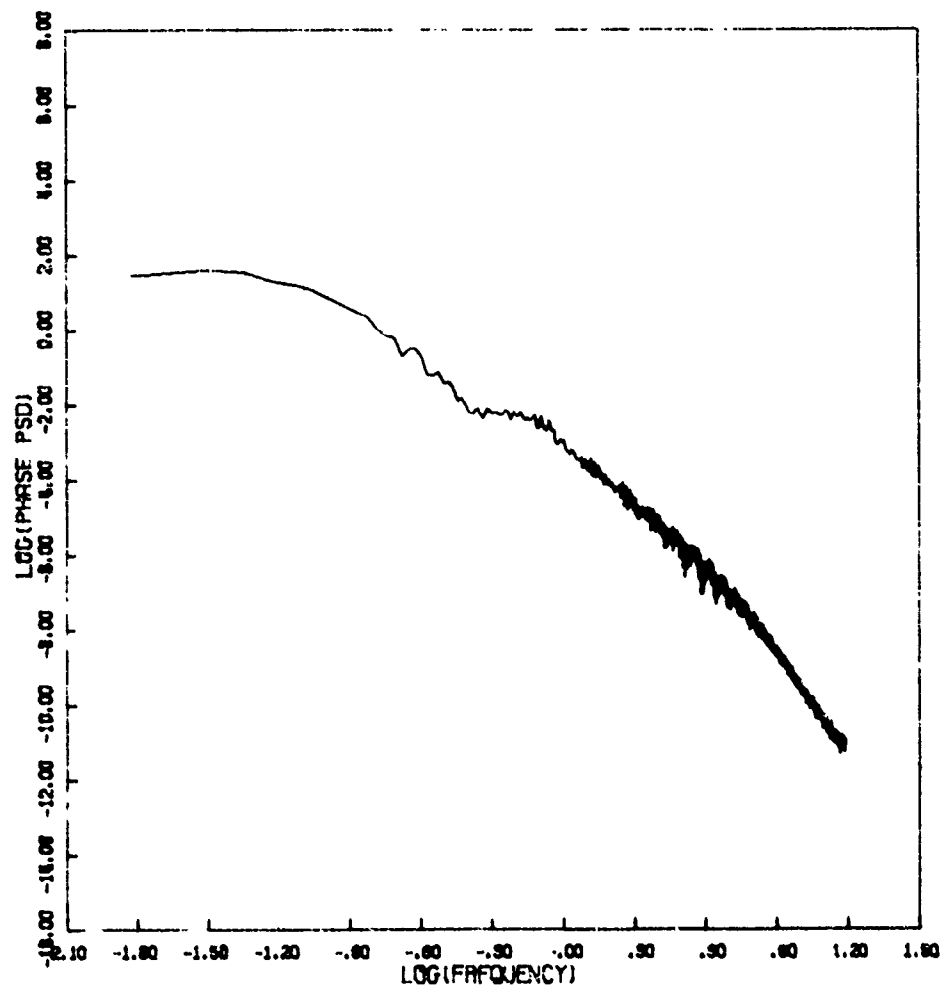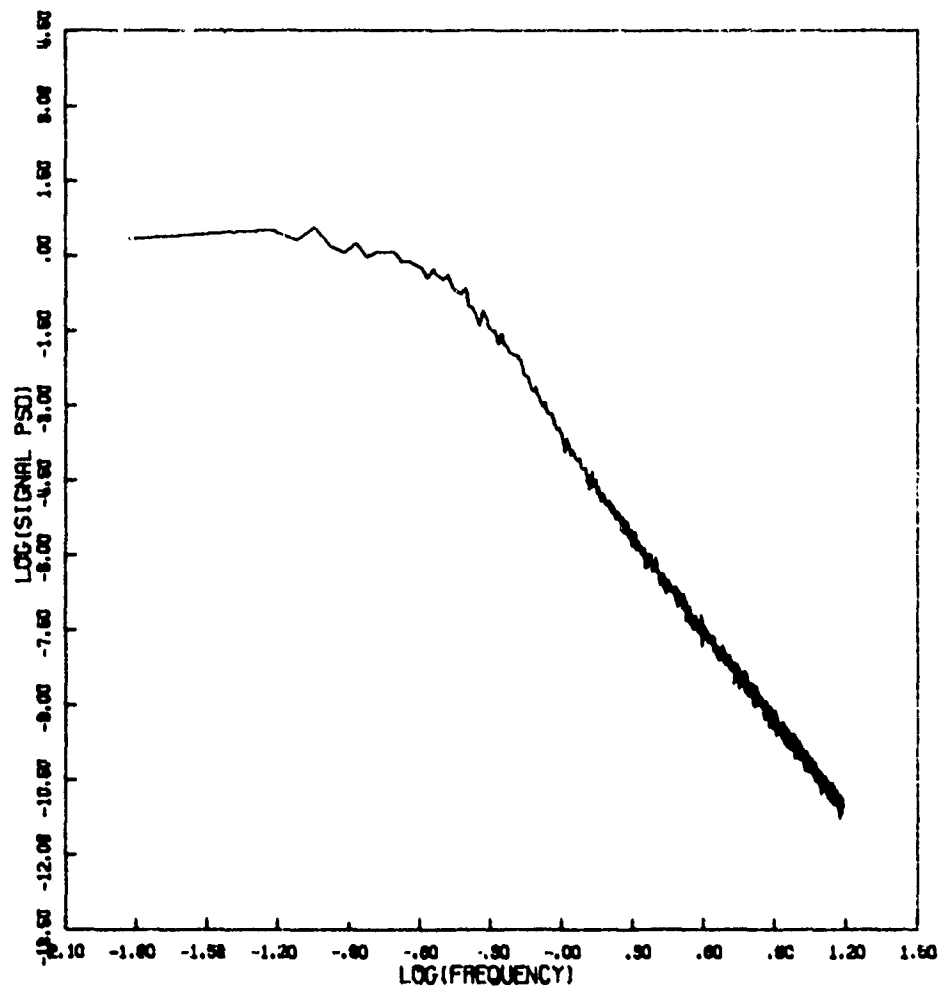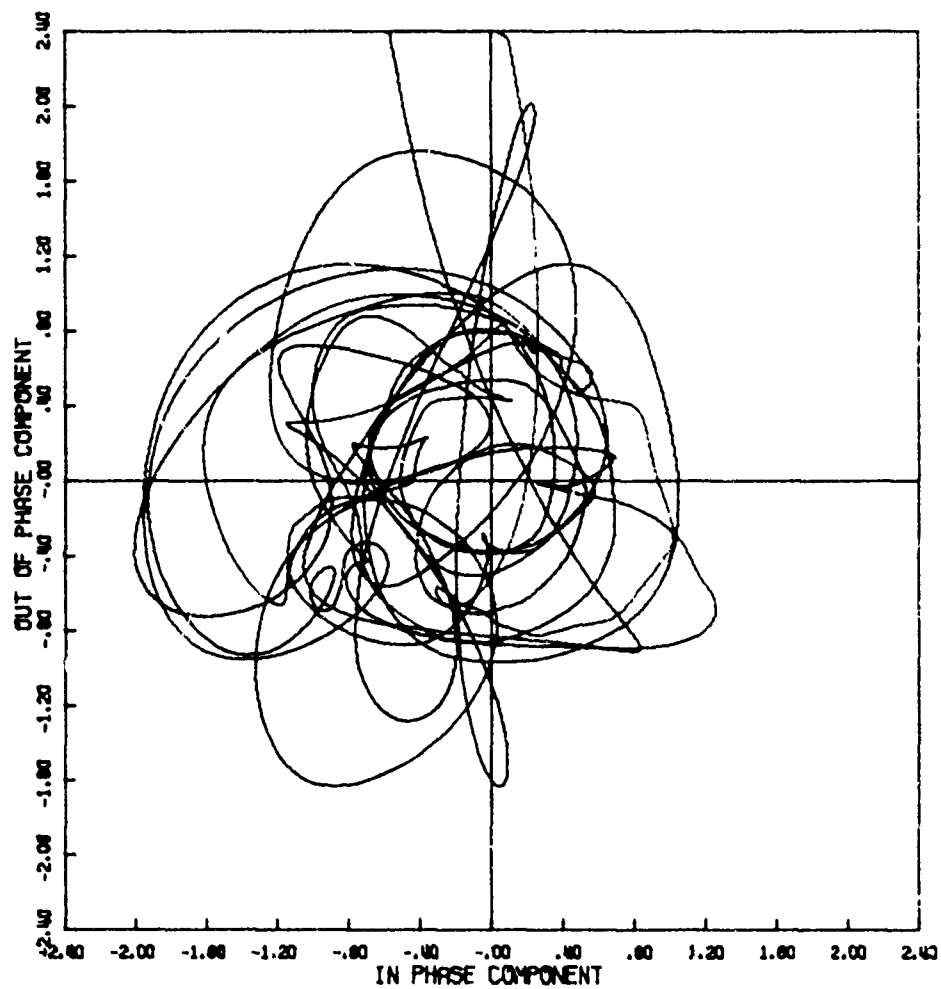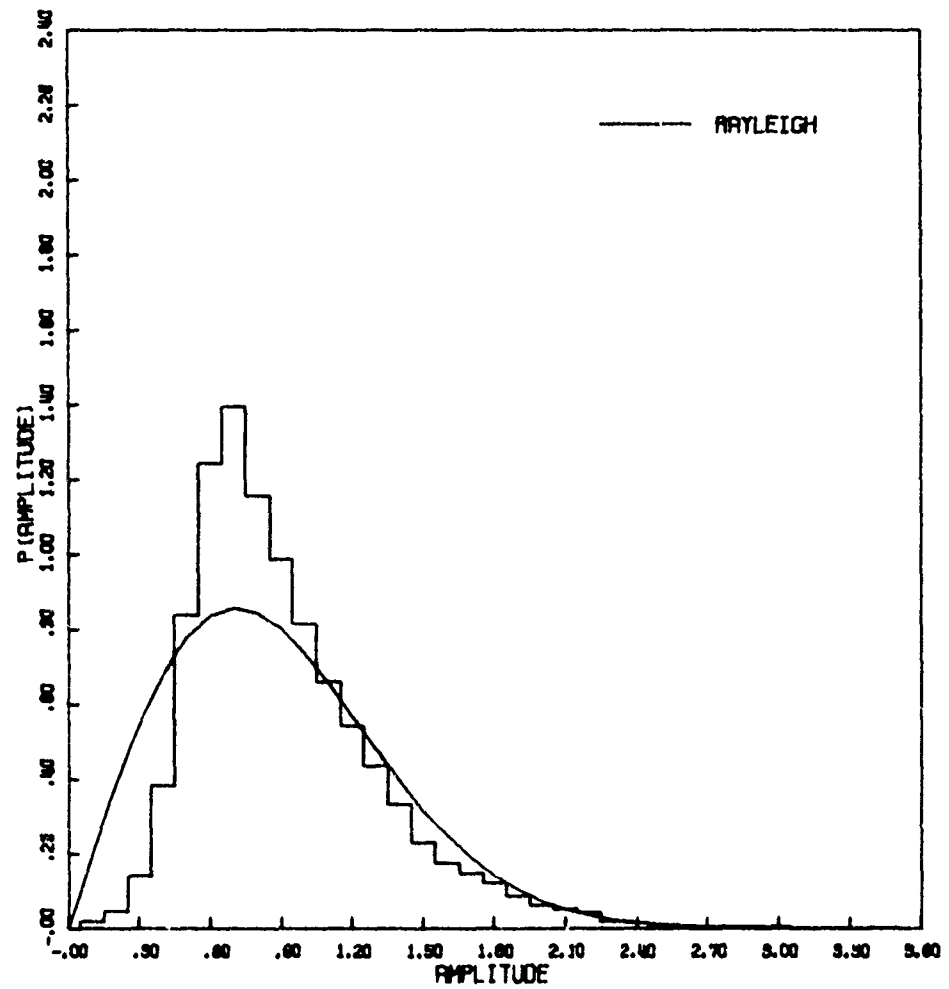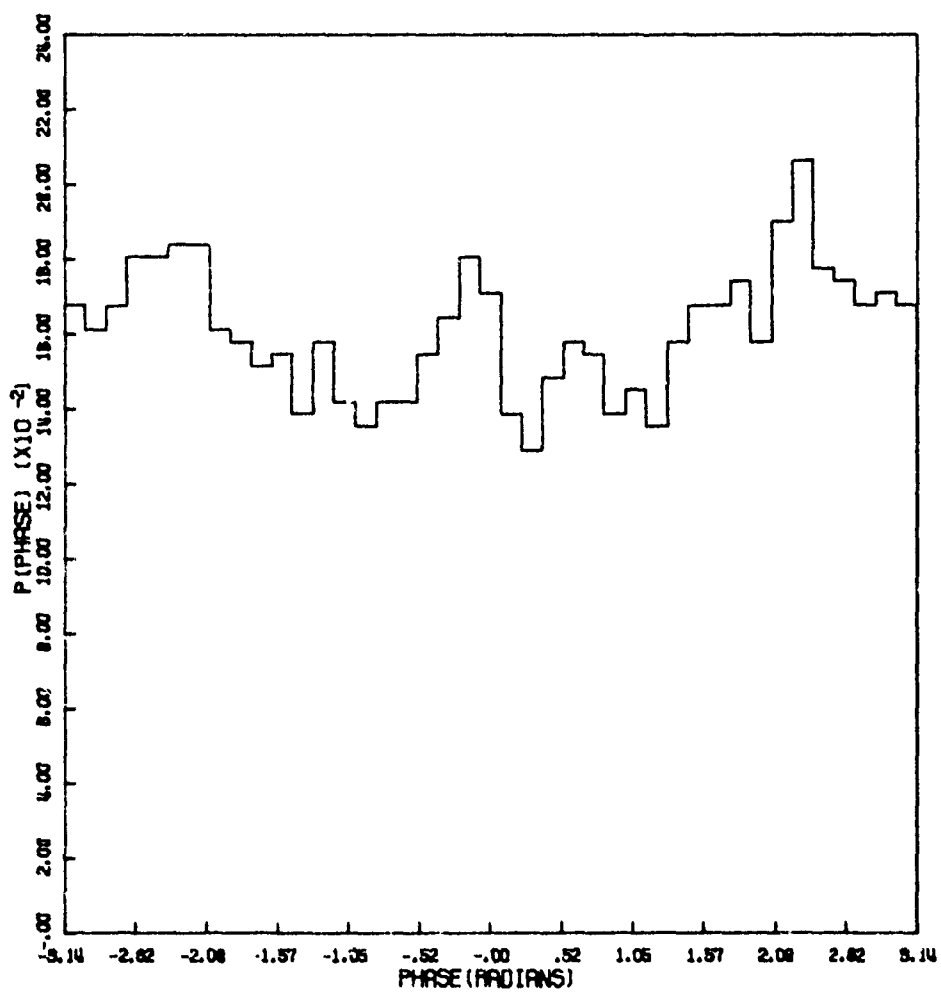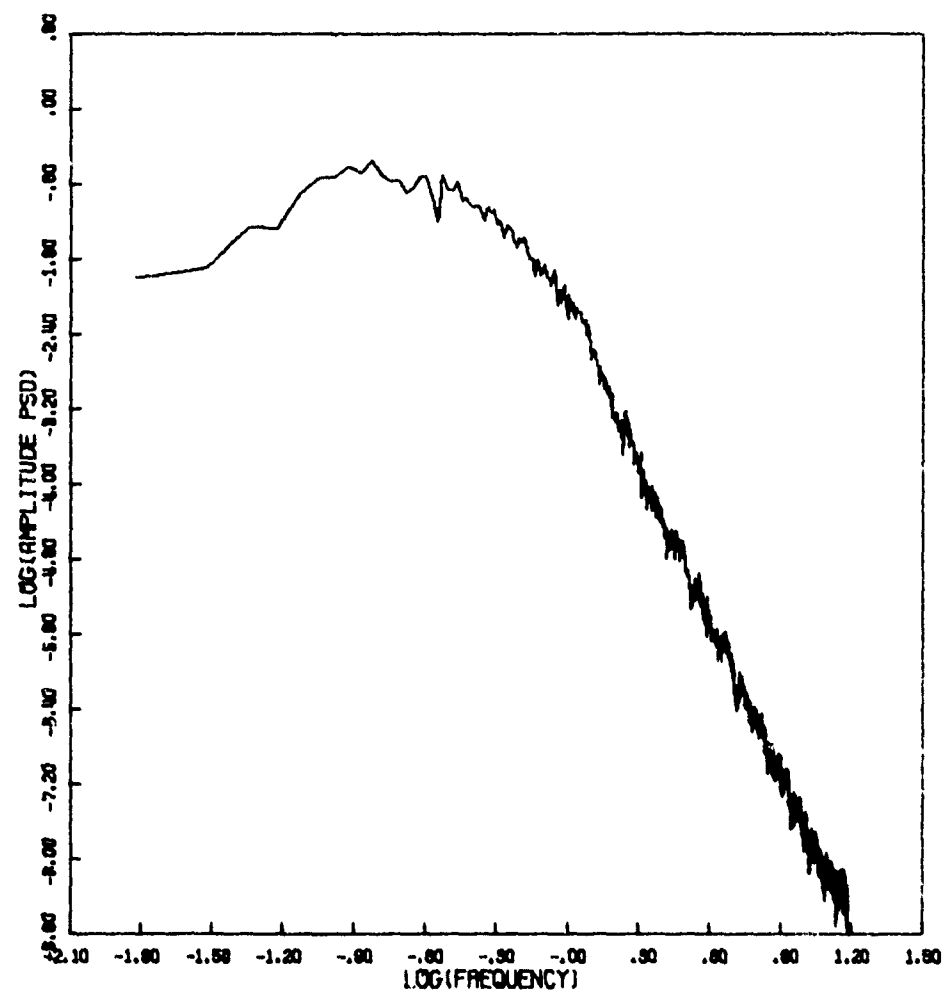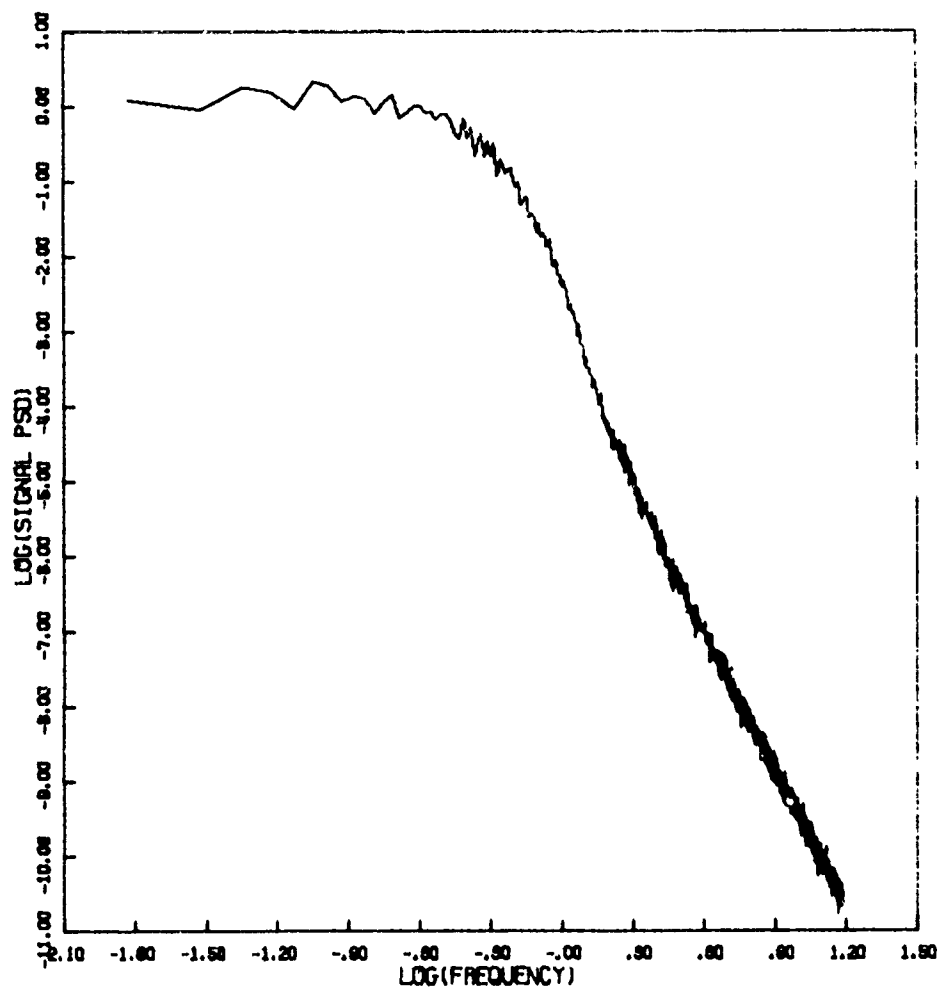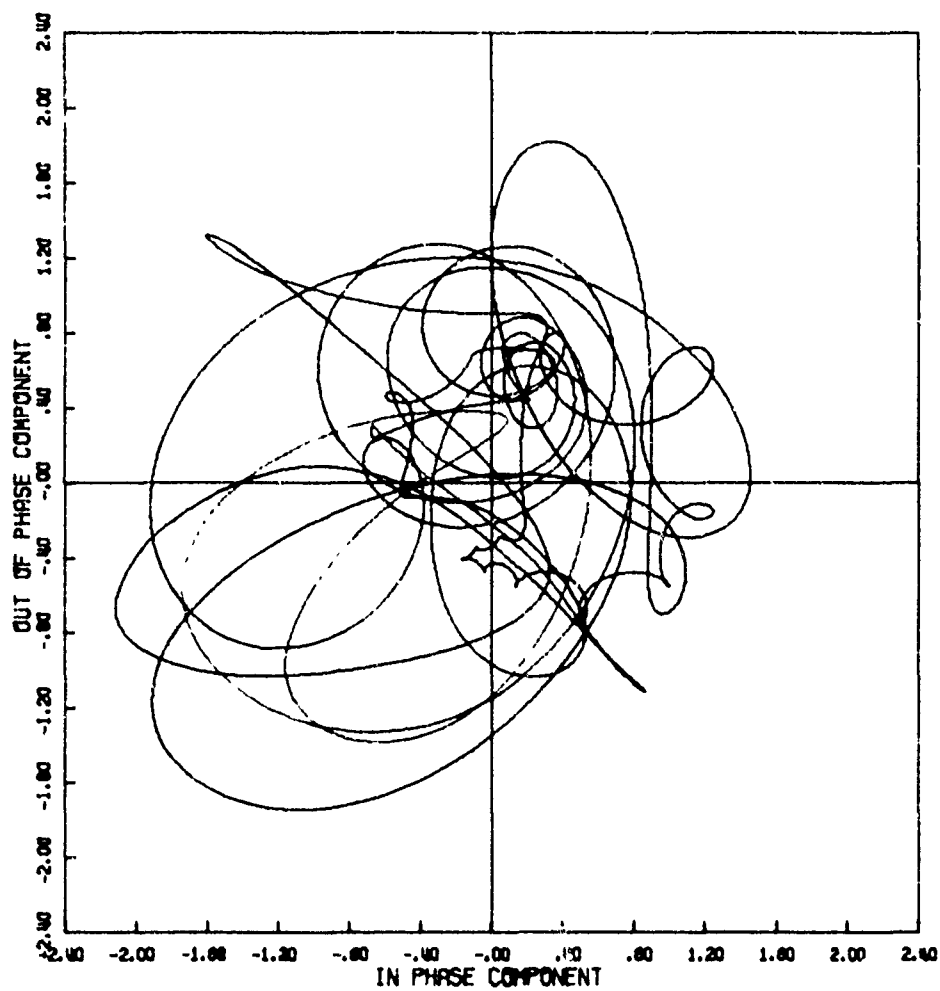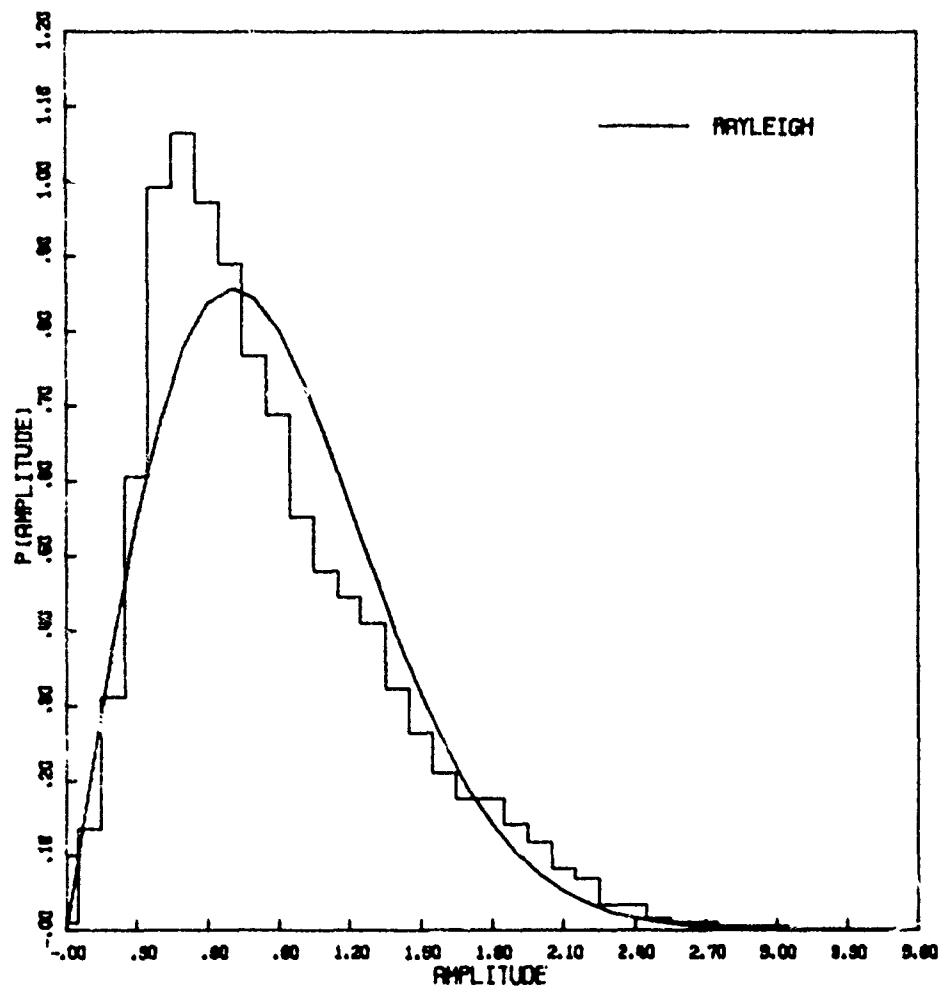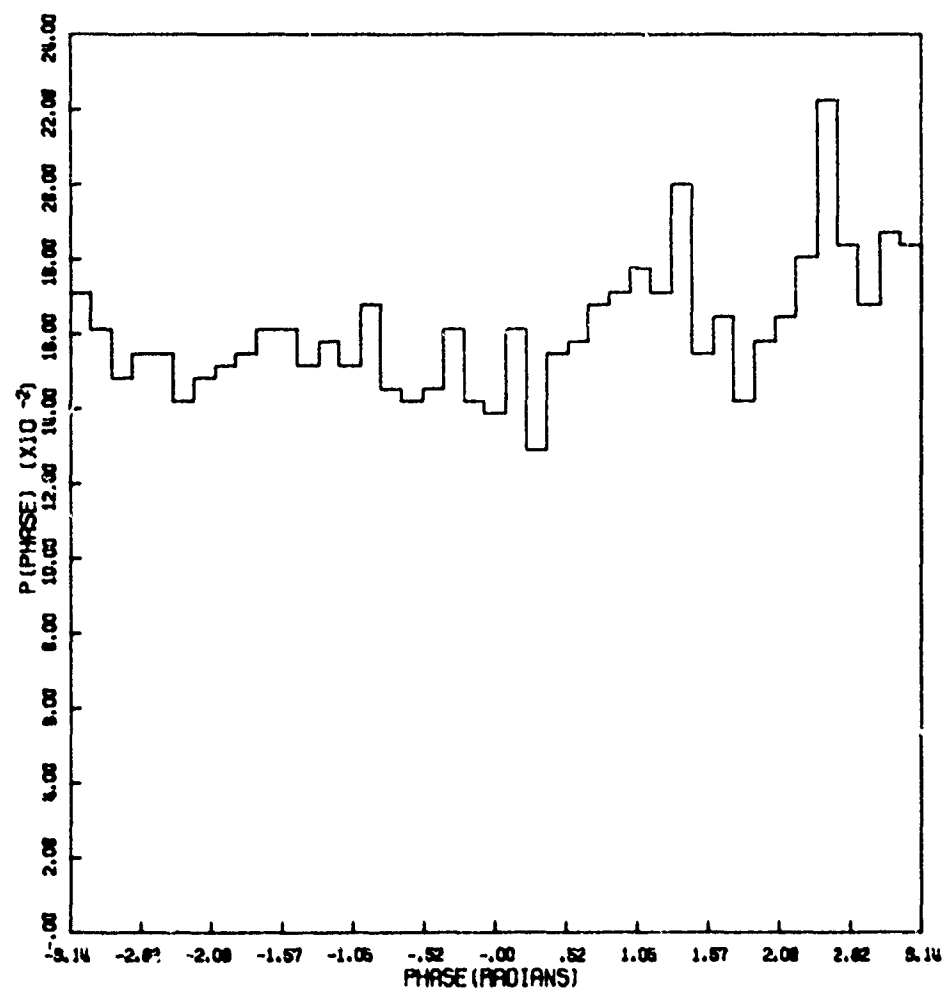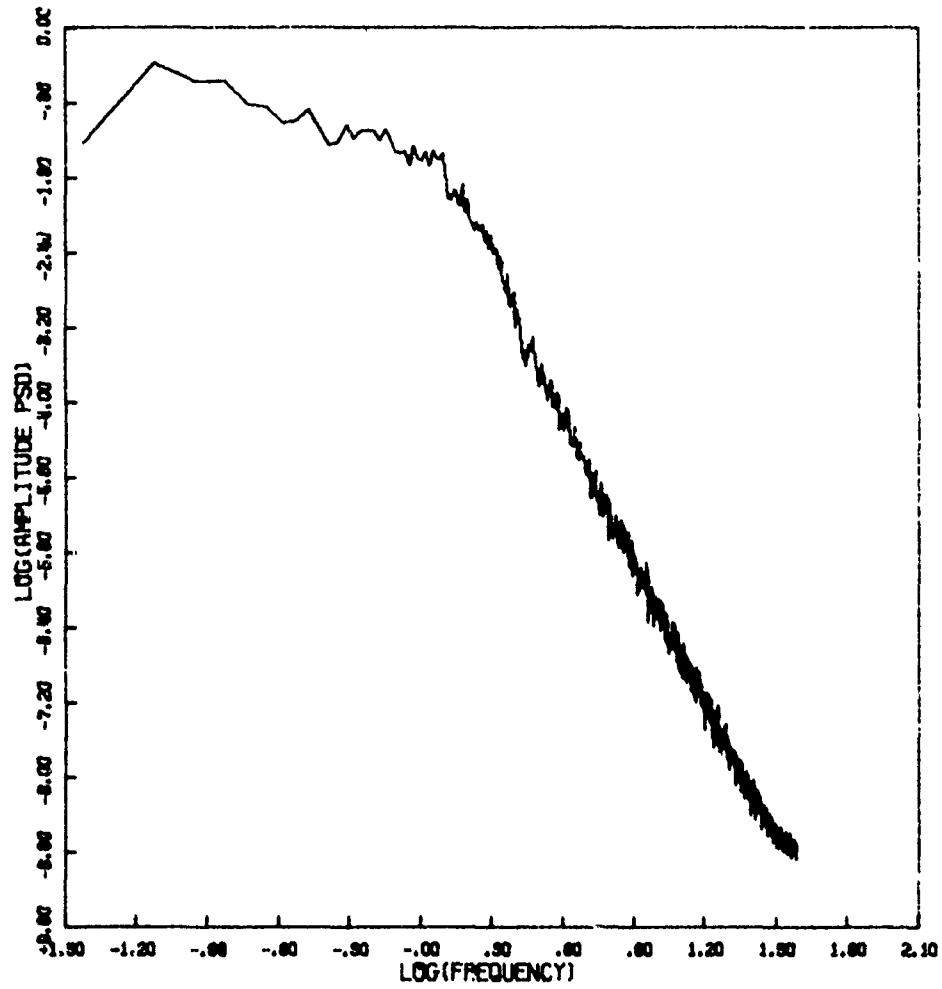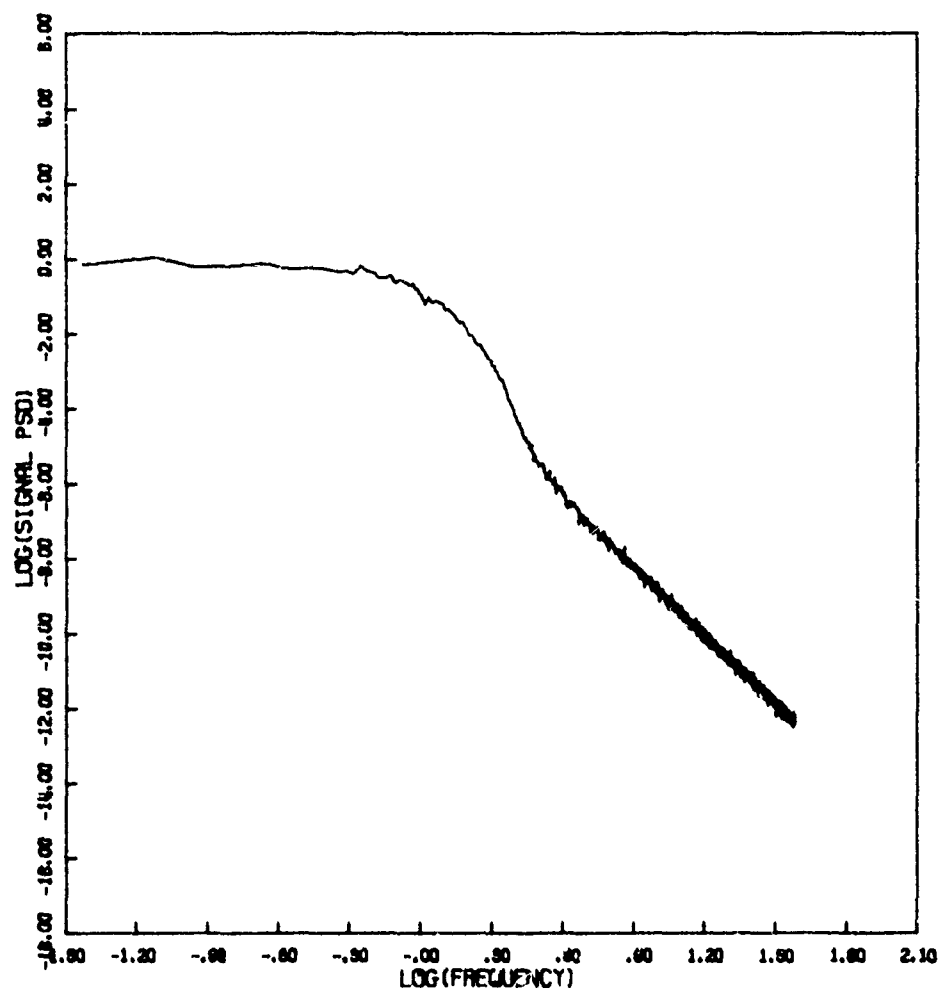
Figure 38c. Phase Distribution
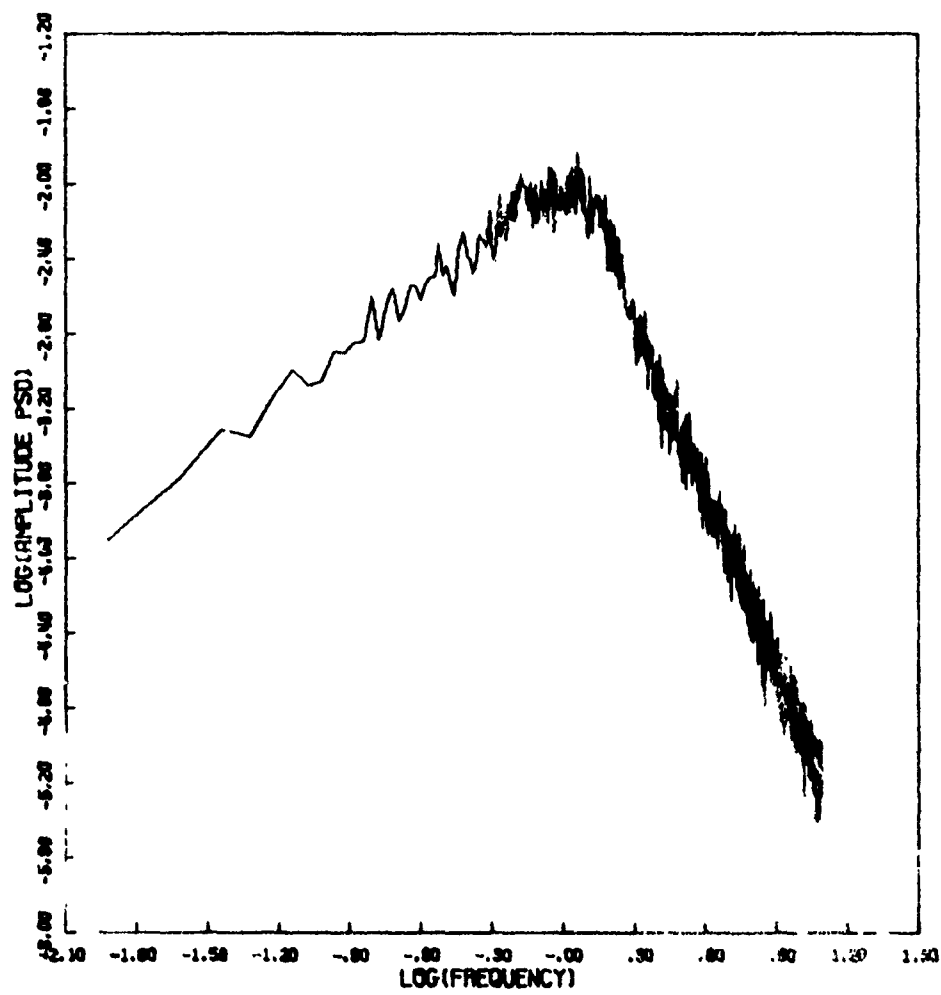
Figure 38d.   Amplitude Power Spectral Density
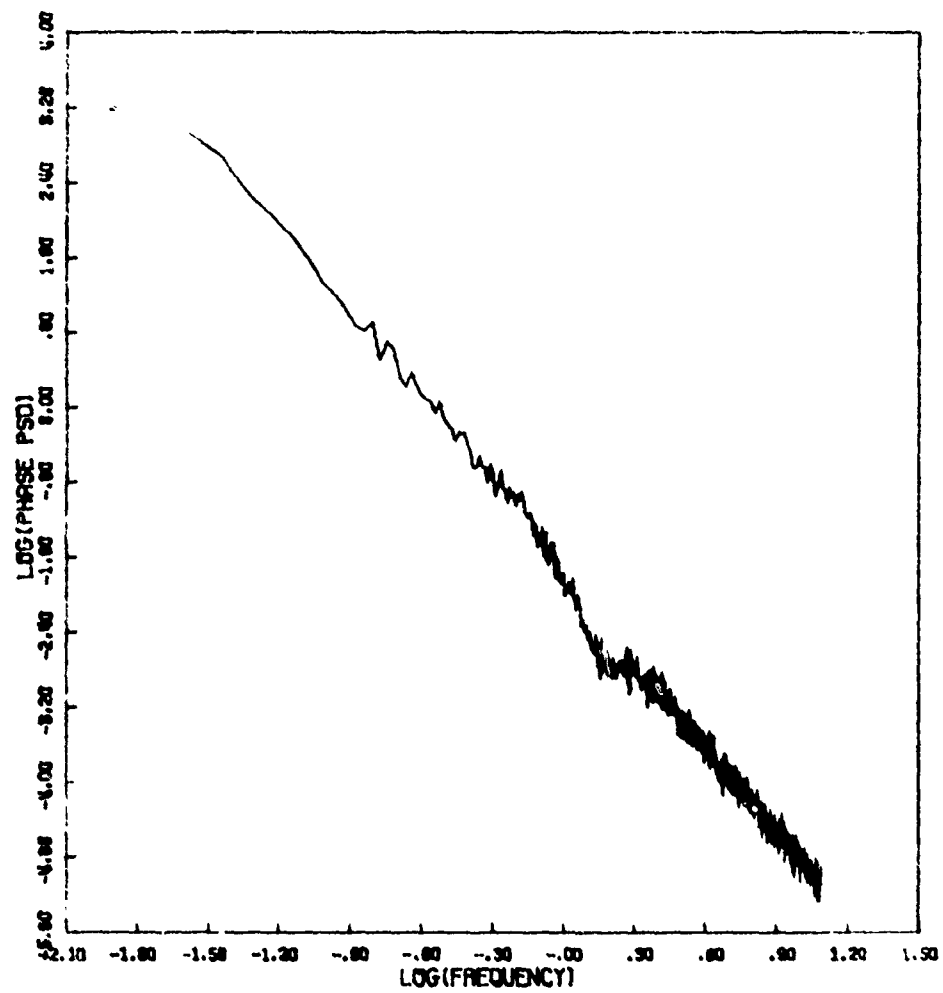
Figure 38e. Phase Power Spectral Density
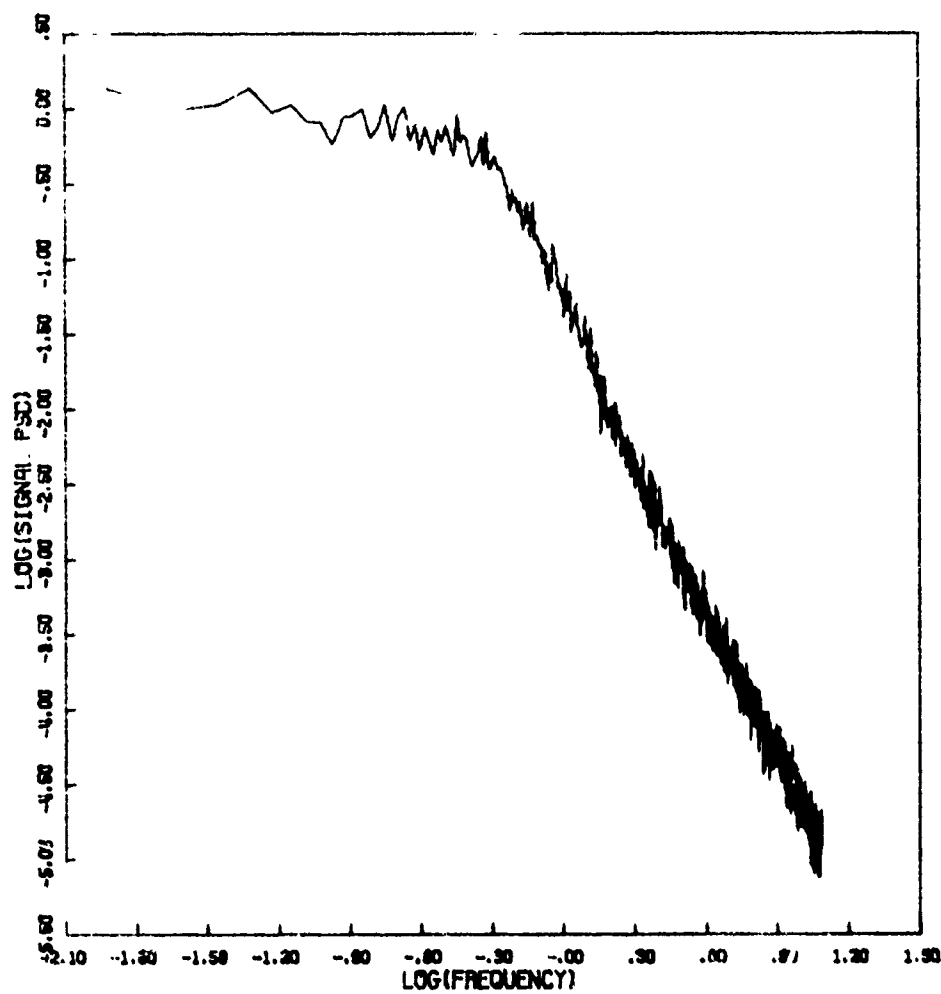
Figure 38f. Signal Power Spectral Density

Table 3

K_ρ^{-3} SPECTRUM

	$z_g = 3.0\times10^7$		$z_s = 1.0\times10^7$			$K = 6.28\times10^{-2}$			K_ρ^{-3} SPECTRUM		
FIG.	L	$\overline{\Delta n^2}$	$\overline{\phi^2}$	$\overline{\chi^2}$	S_4	ℓ_0	$\overline{E_R^2}$	$\overline{E_I^2}$	α_A	$\alpha_{\dot\phi}$	α_S
42	1.5×10^4	10^9	0.21	.05	0.40	3.9×10^4	0.05	0.13	4.1	4.1	4.1
43	1.5×10^4	5×10^9	1.0	0.35	0.78	2.5×10^4	0.24	0.39	4.2		4.2
44	1.5×10^4	3×10^{10}	6.3*	0.46	0.96	1.0×10^4	0.49	0.50	4.2		4.1
45	4×10^4	2×10^8	0.11	0.006	0.15	1.1×10^5	0.01	0.09	4.0	4.0	4.0
46	4×10^4	2×10^9	1.1	0.06	0.45	7.6×10^4	0.21	0.43	4.2	4.3	4.1
47	4×10^4	8.5×10^9	3.7*	0.21	0.75	4.0×10^4	0.48	0.49	4.4		4.3
48	4×10^4	2×10^{10}	11.2*	0.44	1.01	2.0×10^4	0.48	0.52	0.8, 4.9		G, 4.1
49	4×10^4	2×10^{11}	112*	0.49	1.01	5.6×10^3	0.50	0.50	0.7, 4.6		G, 4.6
50	10^5	10^8	0.14	0.001	0.05	2.7×10^5	0.01	0.11	4.0	4.0	4.0
51	10^5	10^9	1.4	0.008	0.17	1.8×10^5	0.25	0.47	4.1	4.1	4.1
52	10^5	10^{10}	14.	0.07	0.55	4.5×10^4	0.48	0.52	4.2	4.4	4.0
53	10^5	3.4×10^{10}	47.*	0.26	0.95	2.3×10^4	0.49	0.50	0.8, 4.9		G, 4.1
54	10^5	10^{11}	140.*	0.45	1.17	1.3×10^4	0.49	0.51	0.6, 4.8		G, 4.1
55	2.5×10^5	8.5×10^{10}	300.*	0.12	0.75	2.2×10^4	0.51	0.49	4.7	3.6	G, 4.1

Figure 39. Propagation Space Plot for K_ρ^{-3} Spectrum
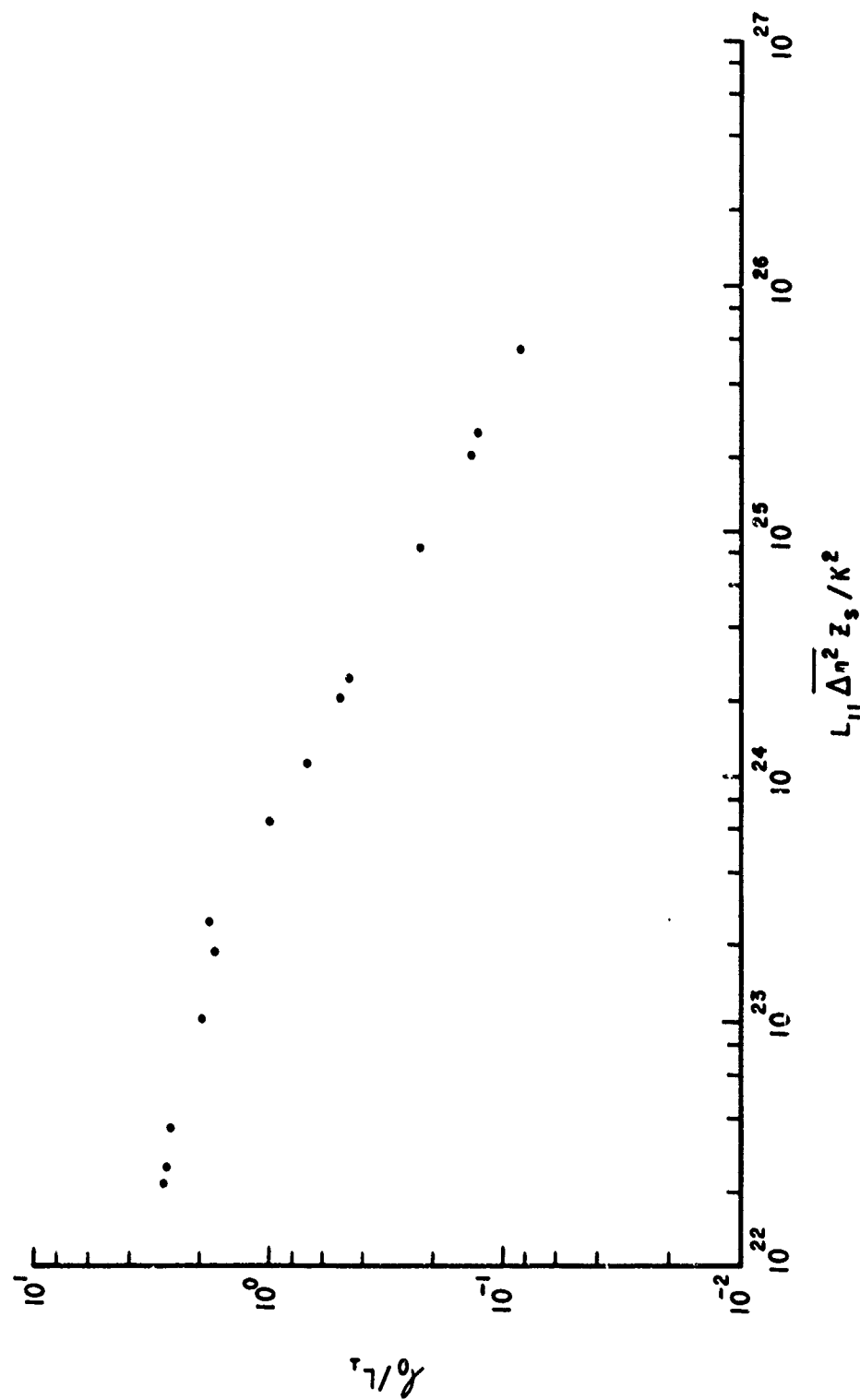
Figure 40. ℓ_0 for K_ρ^{-3} Spectrum
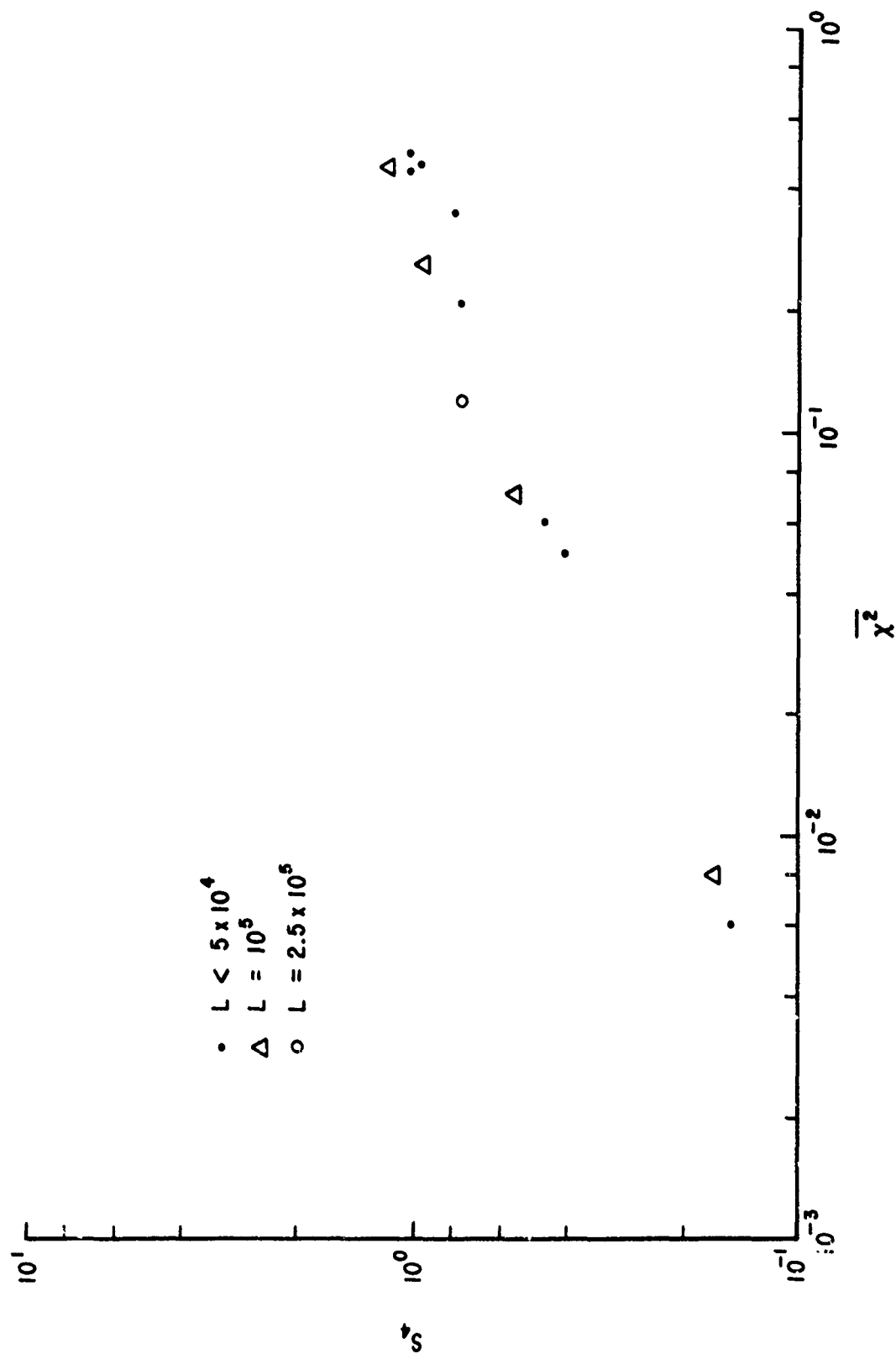
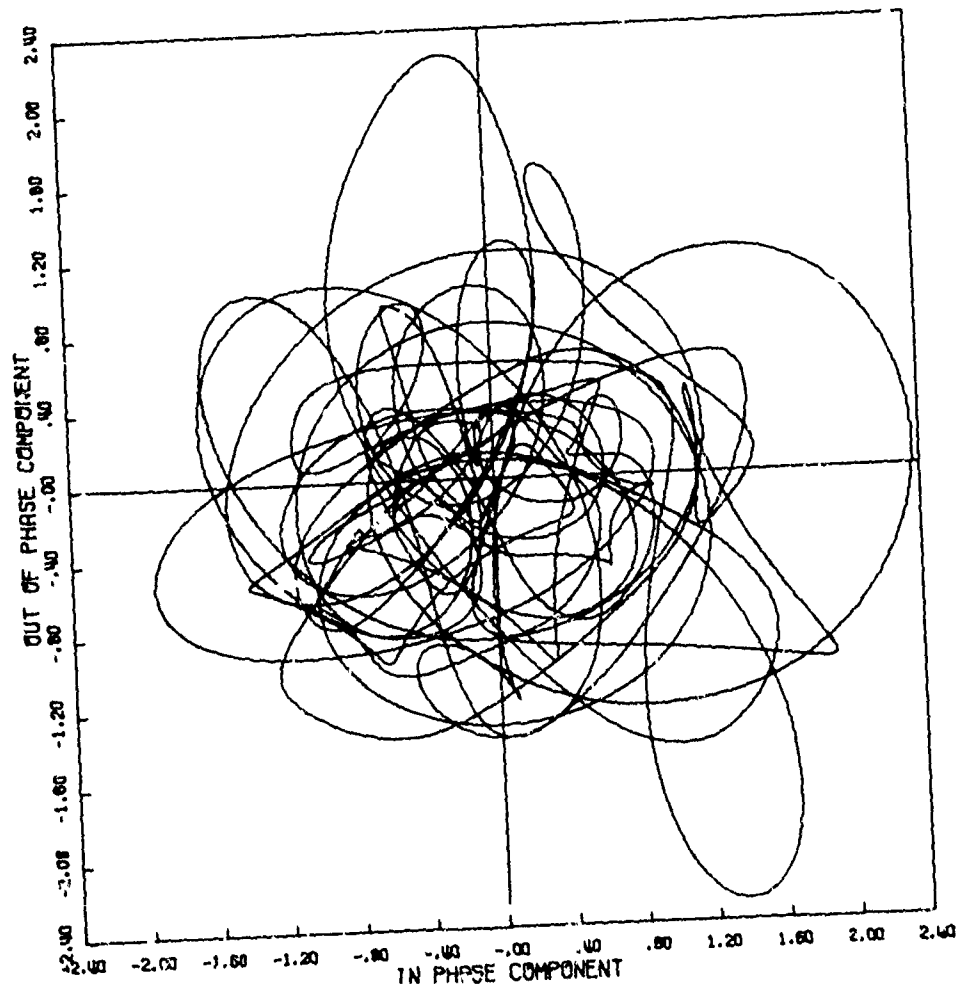Figure 41. S_4 vs. $\overline{\chi_2}$ for K_ρ^{-3} Spectrum
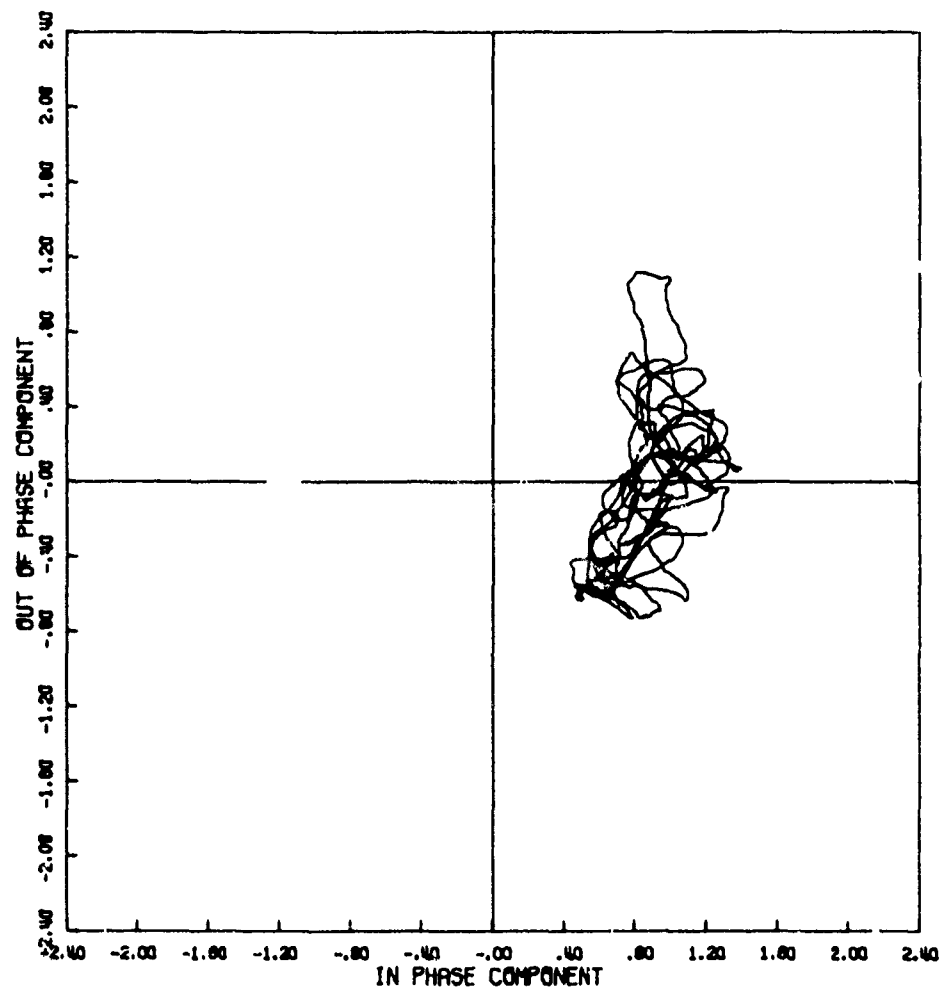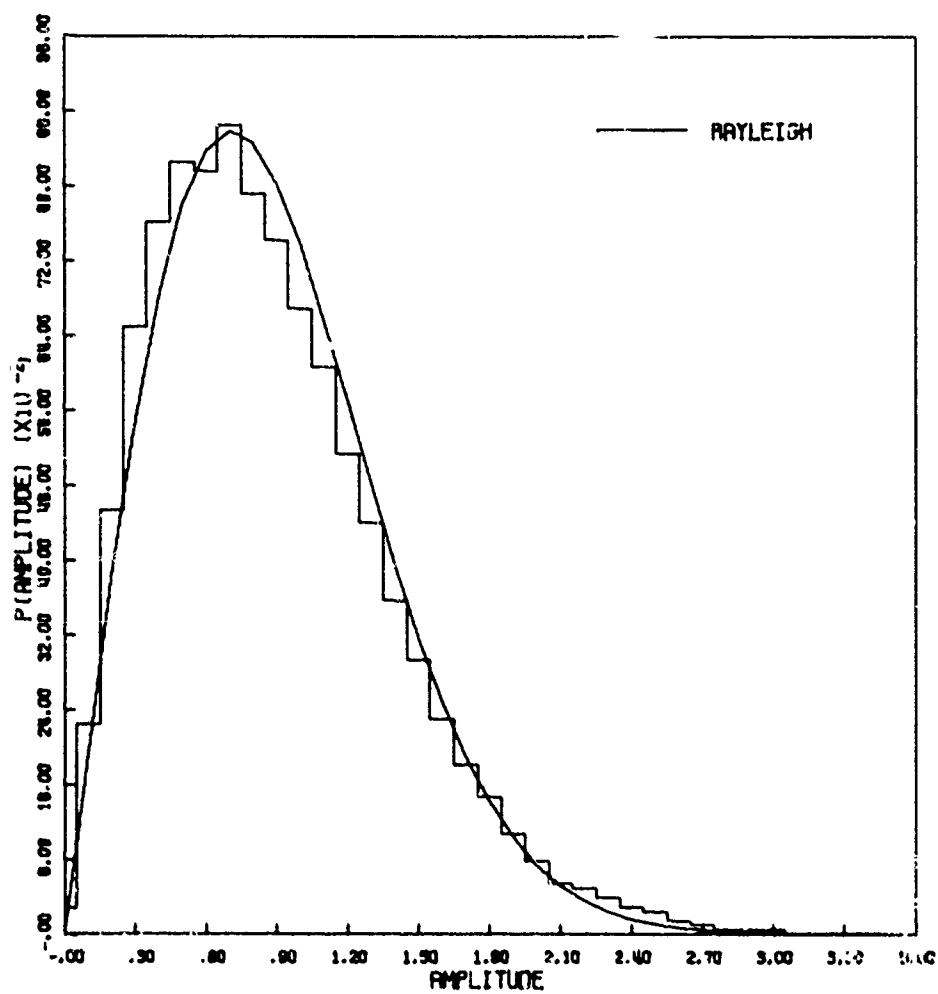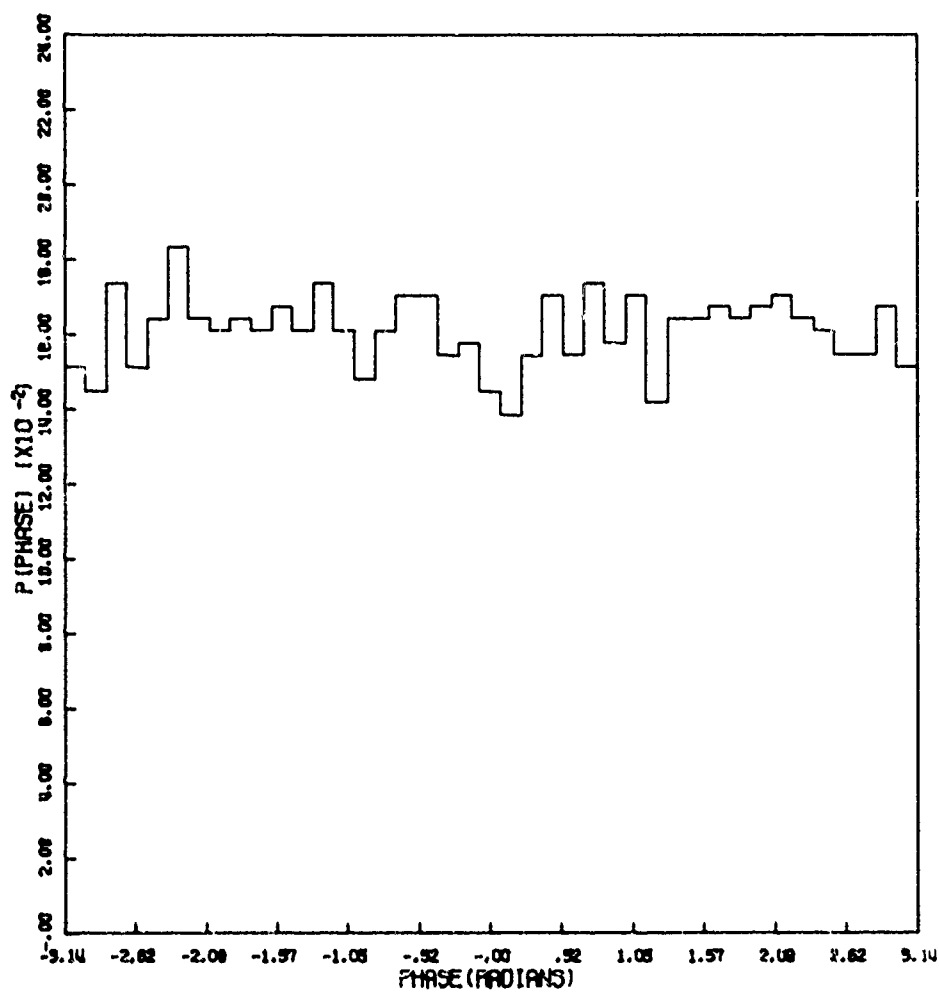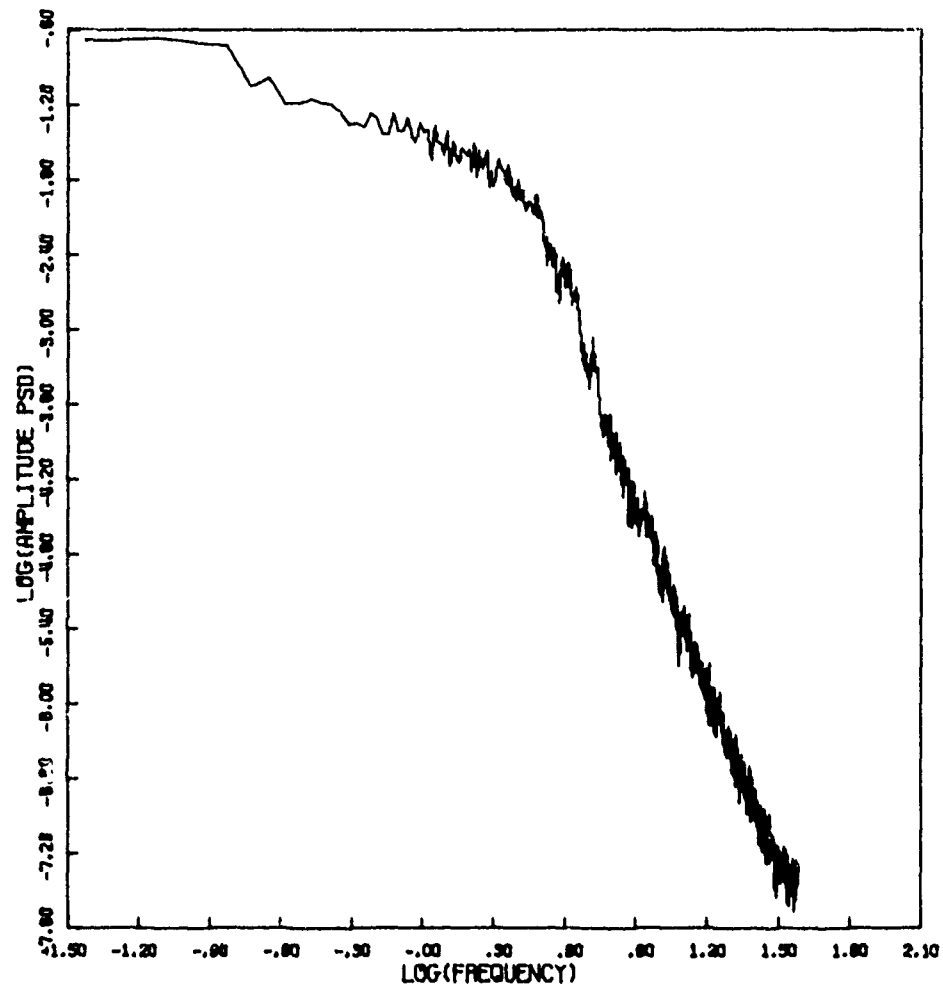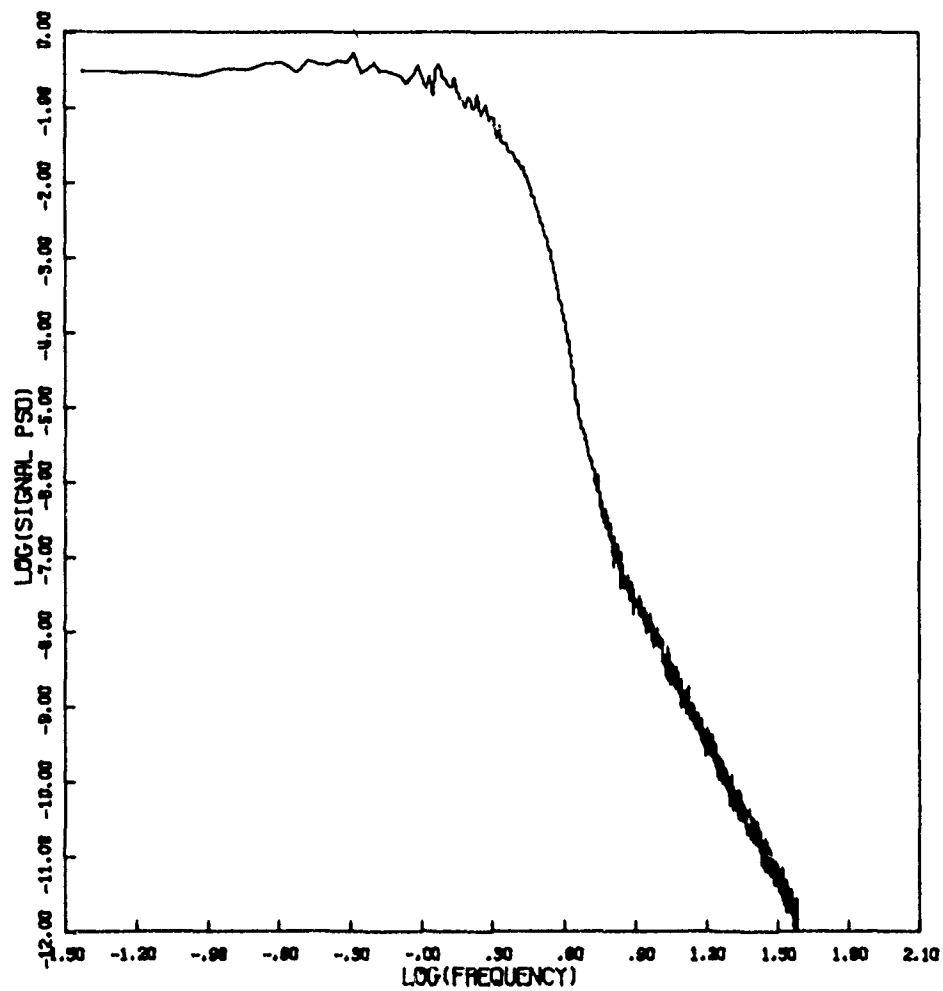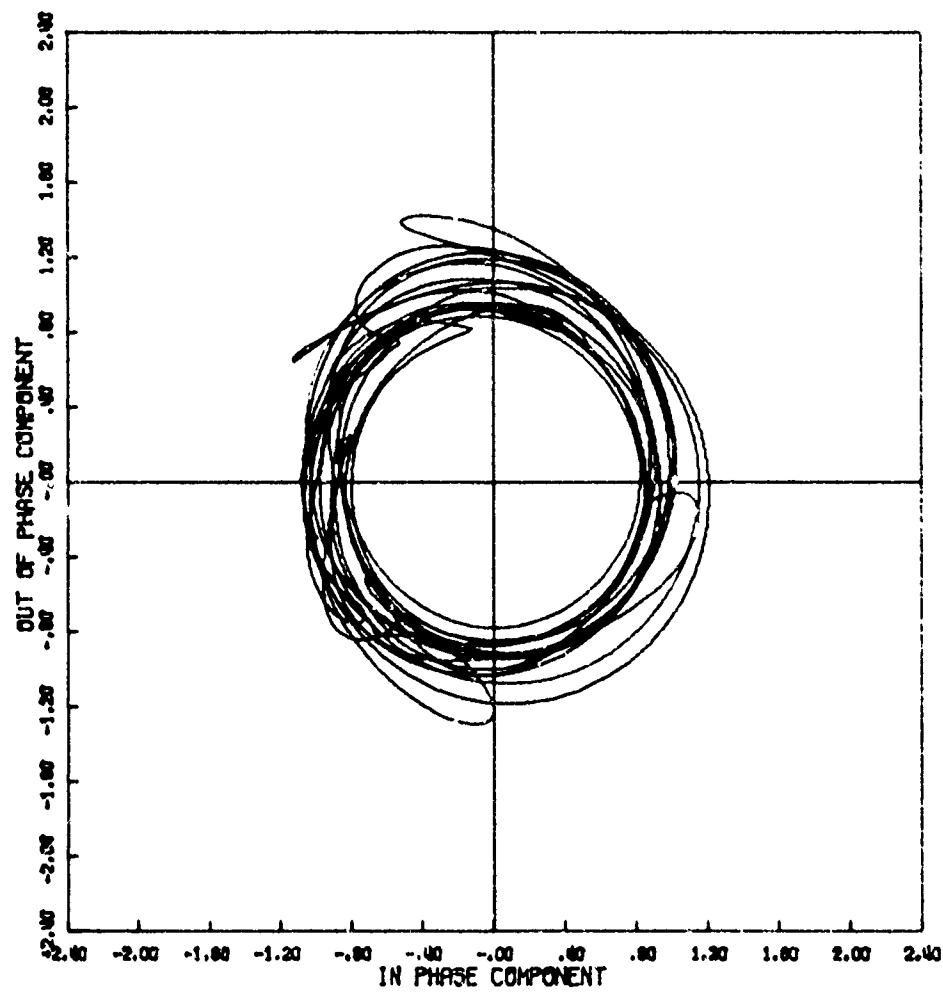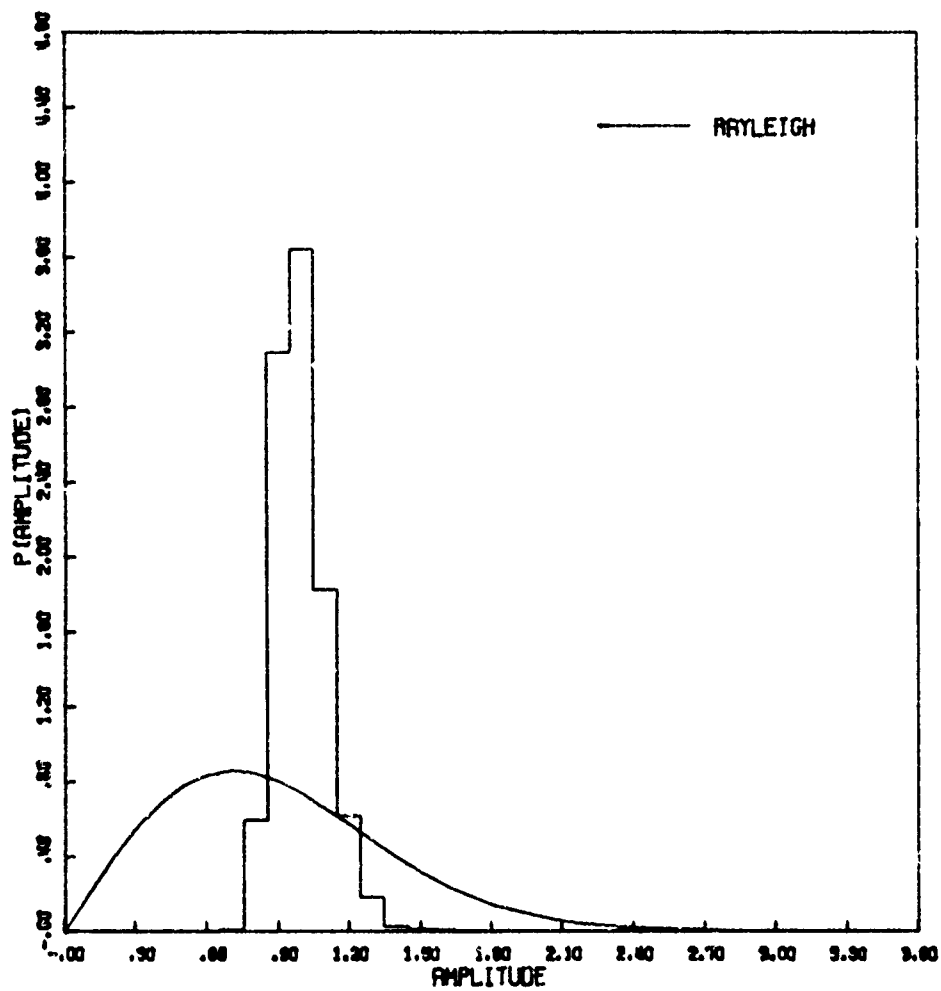
Figure 42a. Signal Phase Plot
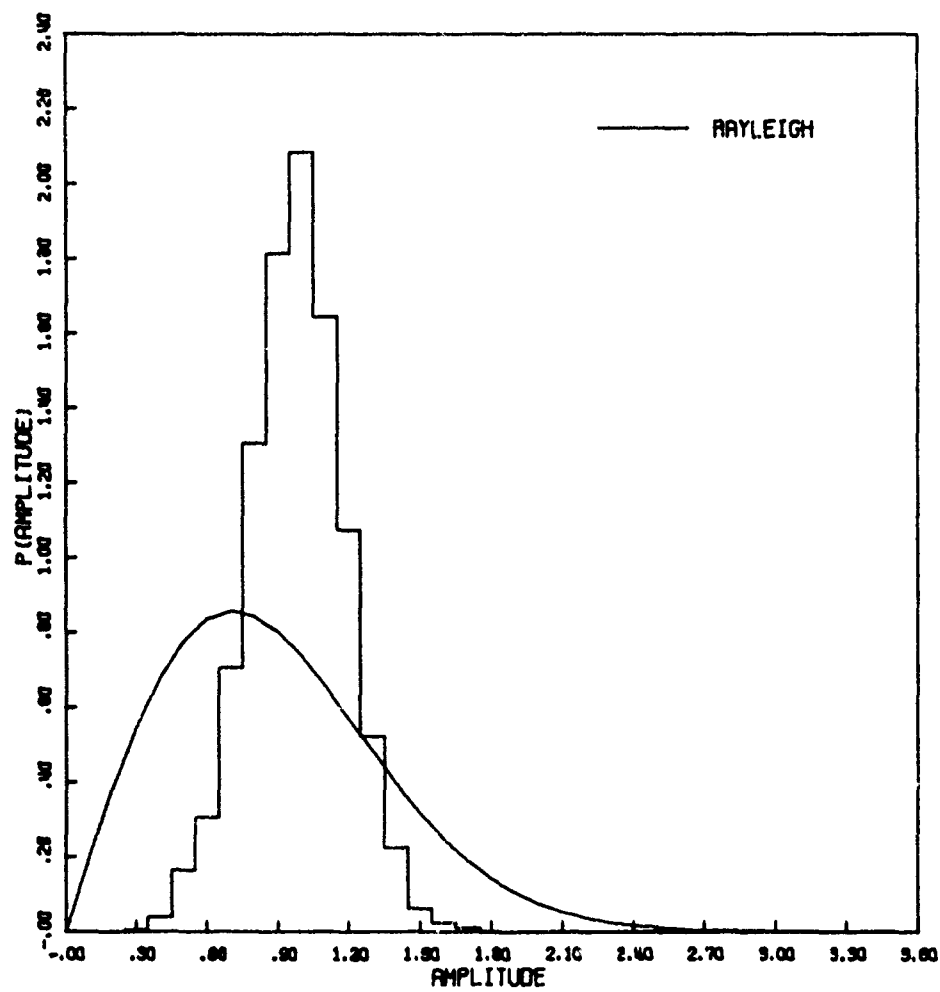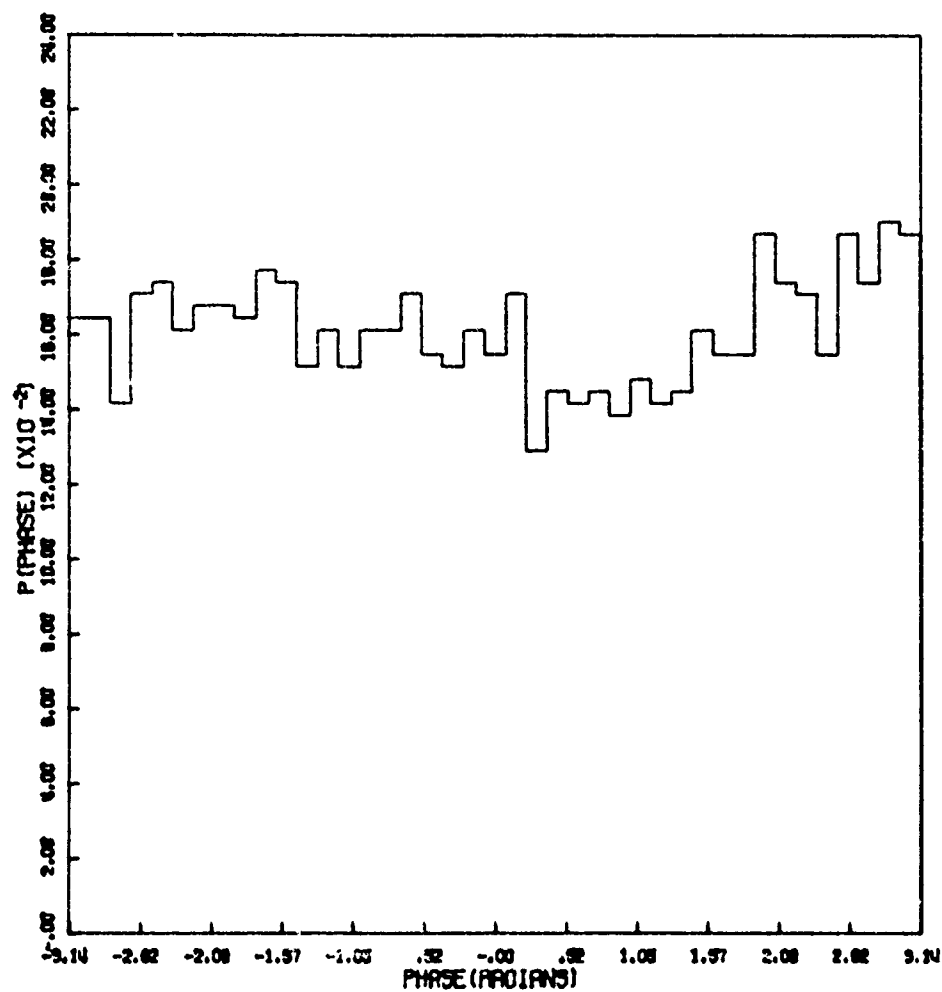
Figure 42b.   Amplitude Distribution
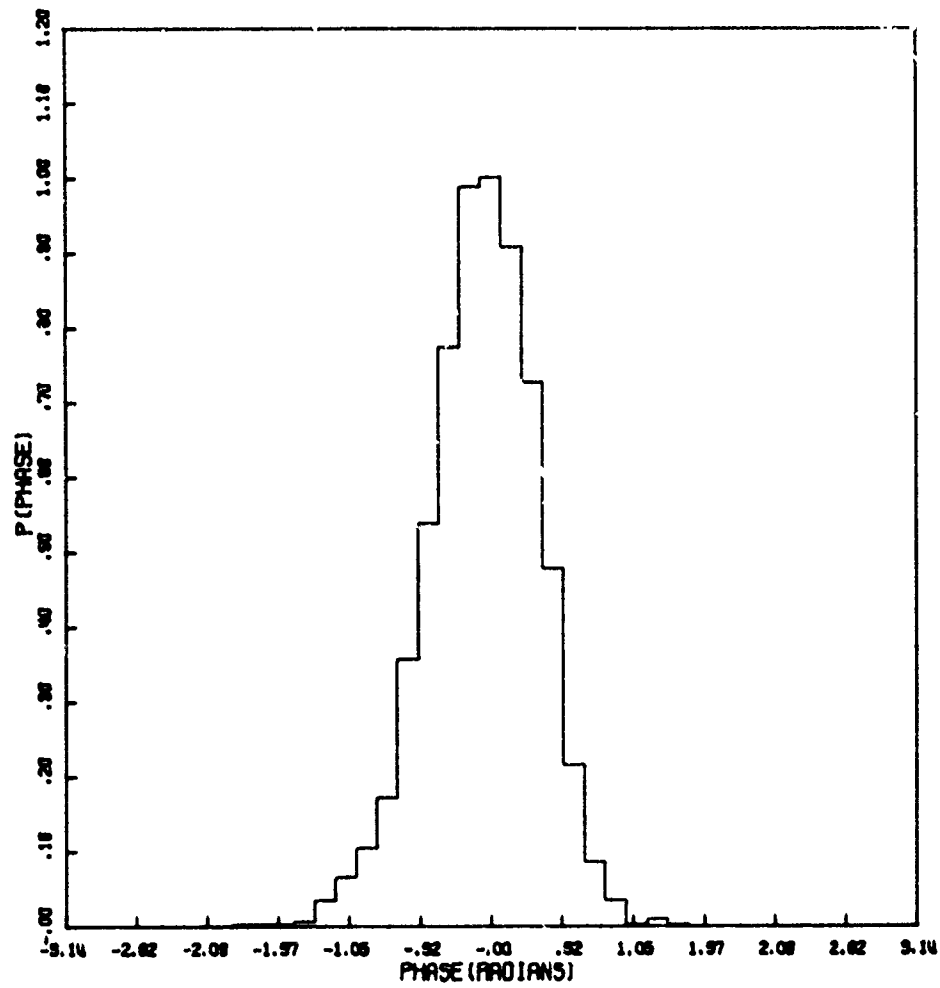
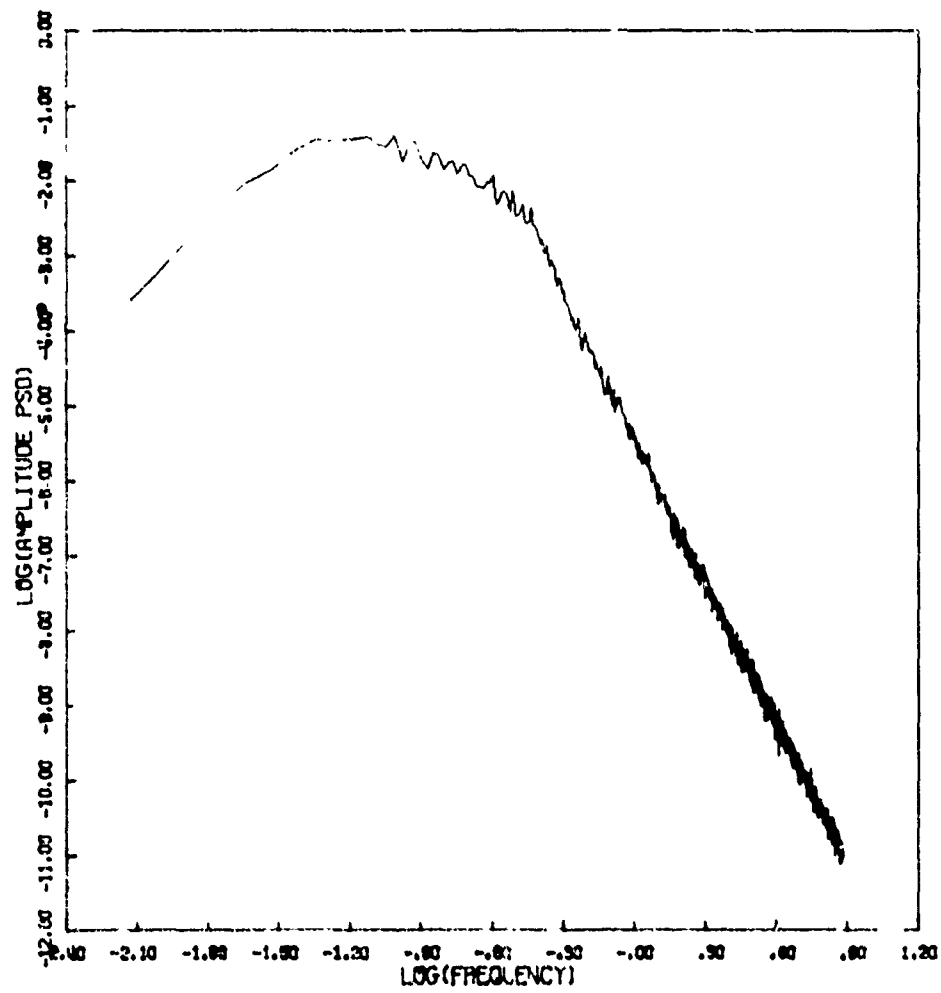Figure 42c.   Phase Distribution
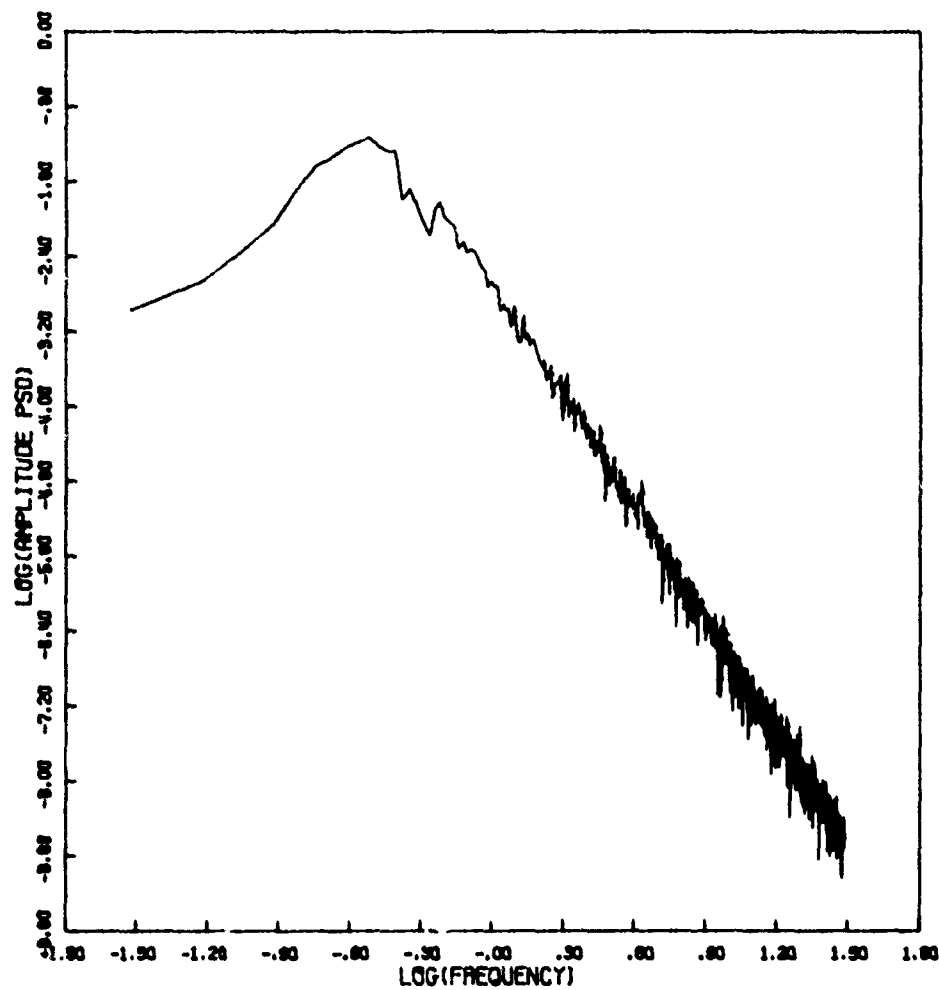
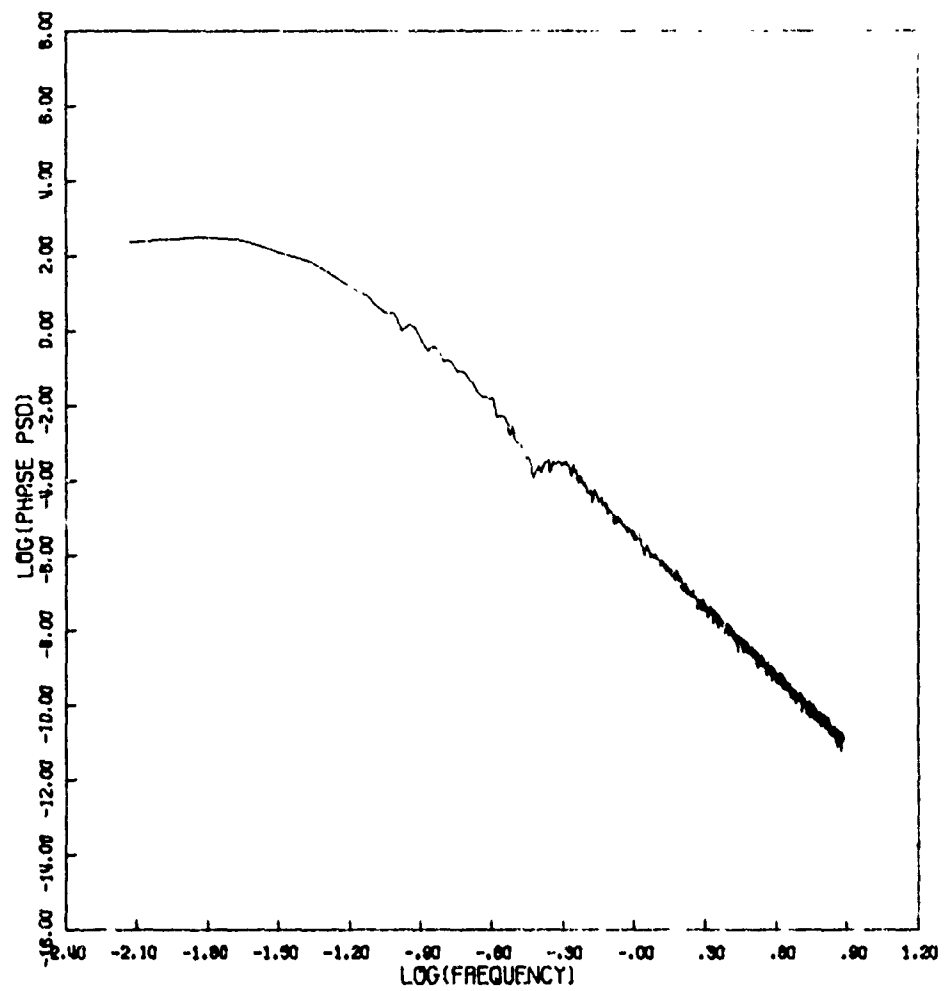Figure 42d. Amplitude Power Spectral Density
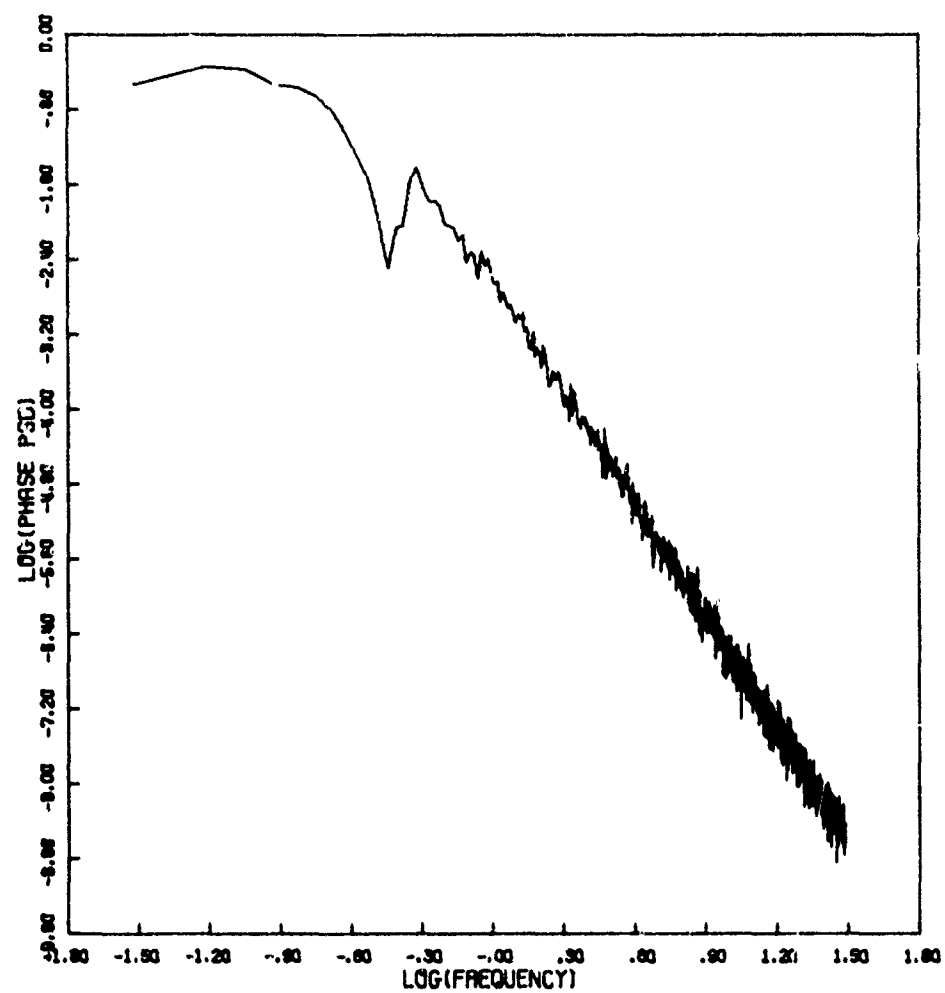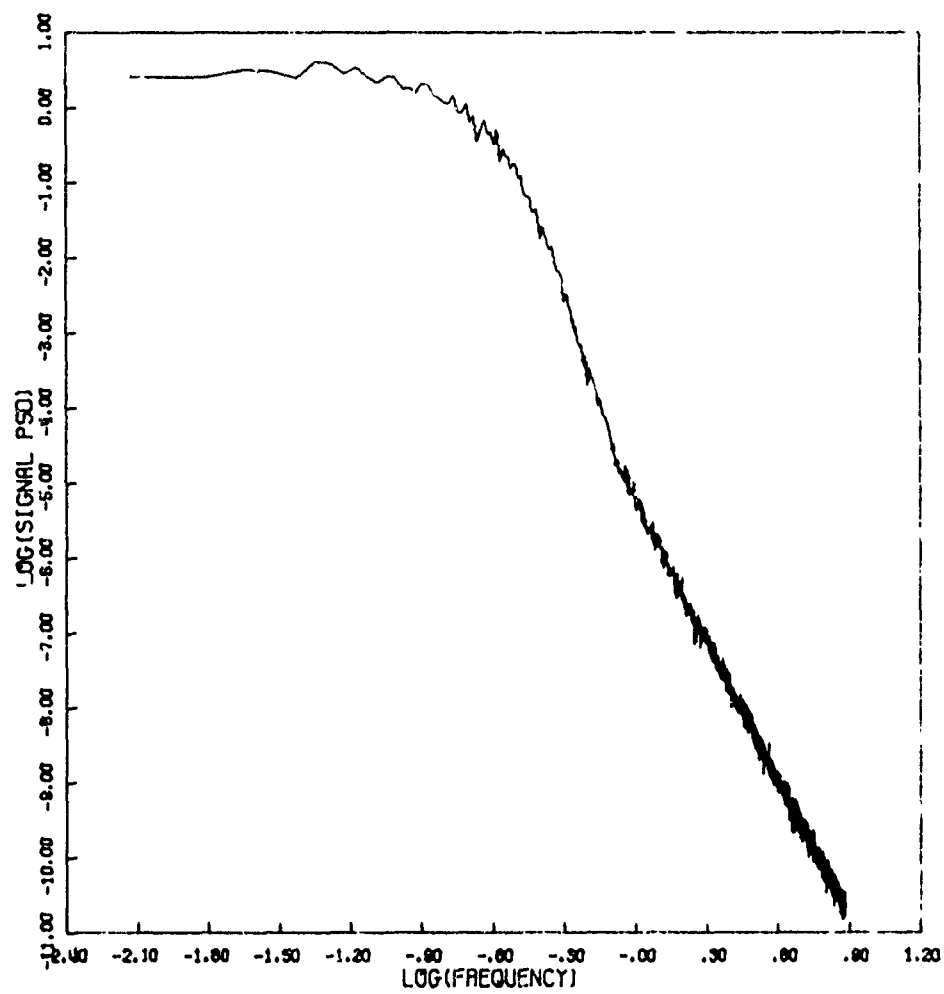
Figure 42e. Phase Power Spectral Density
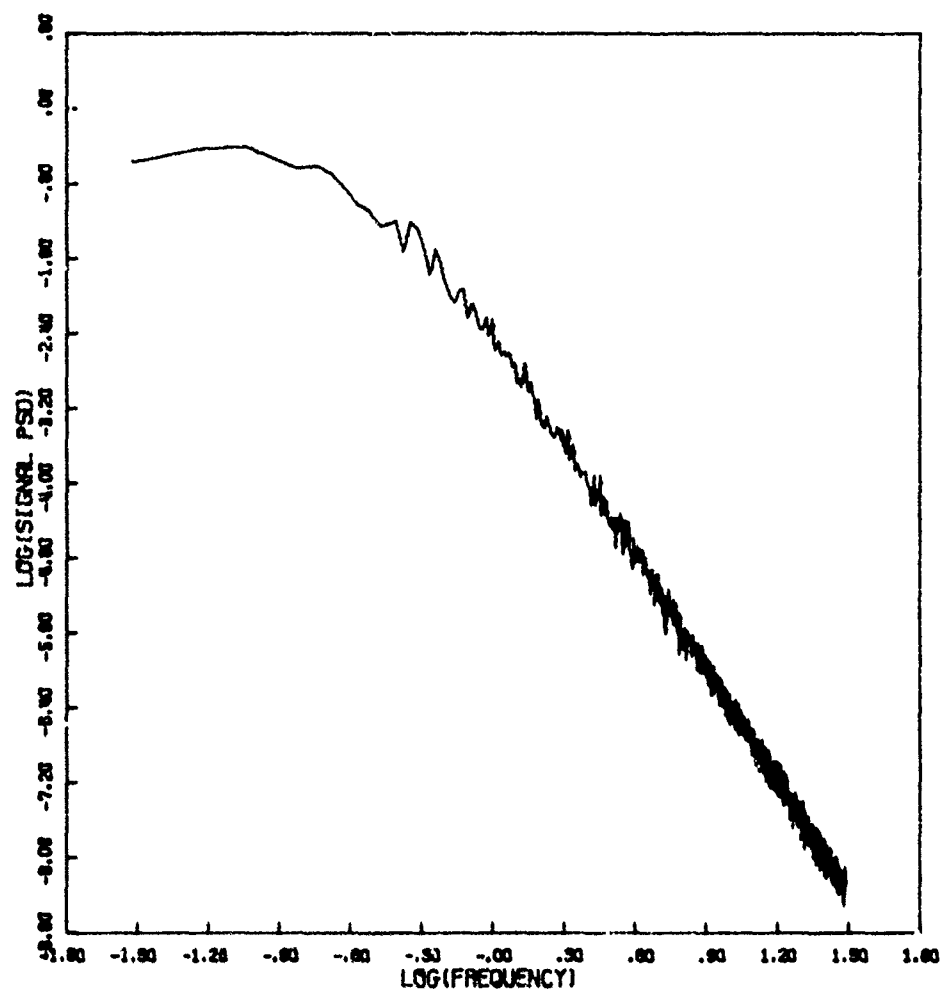
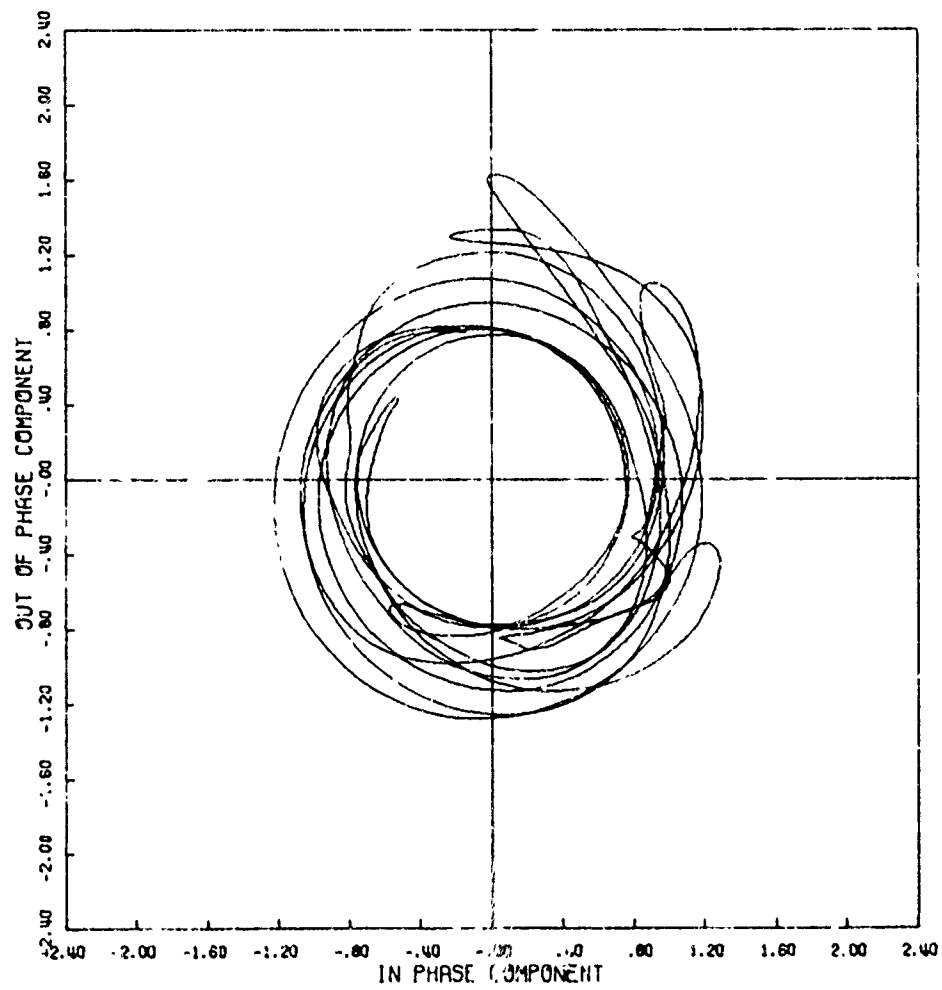Figure 42f. Signal Power Spectral Density
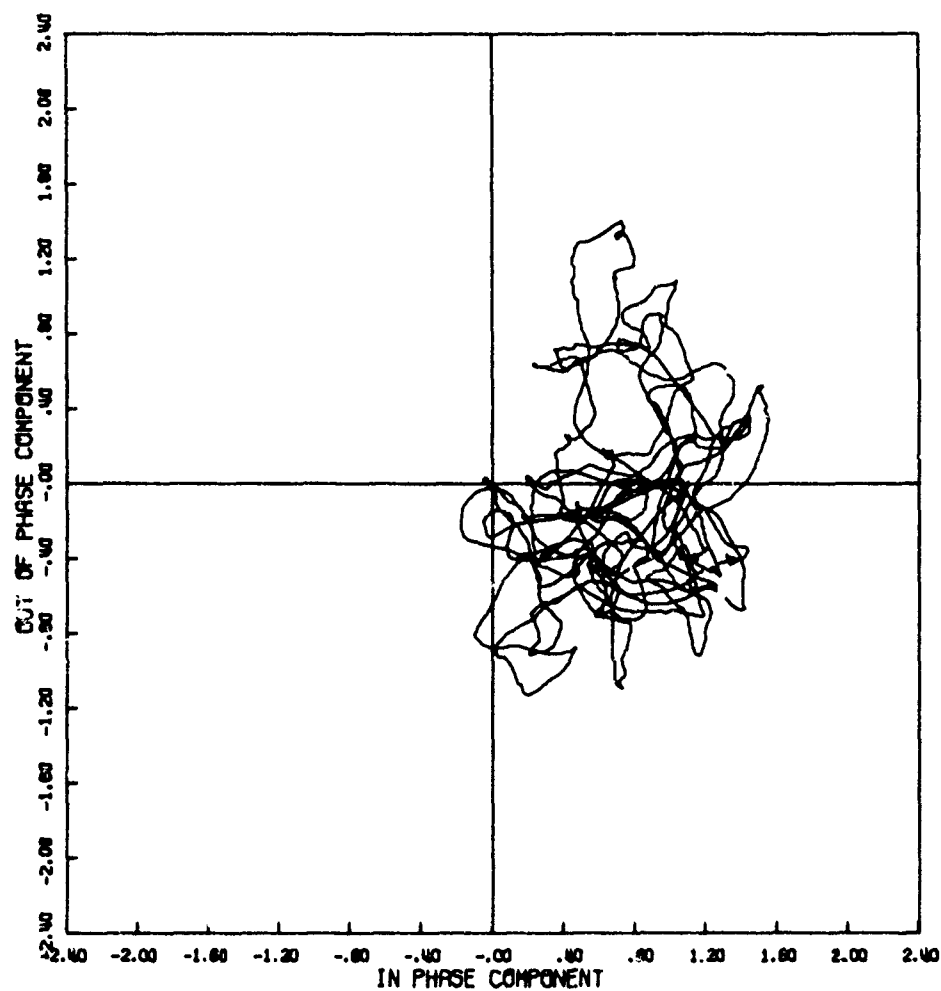
Figure 43a. Signal Phase Plot
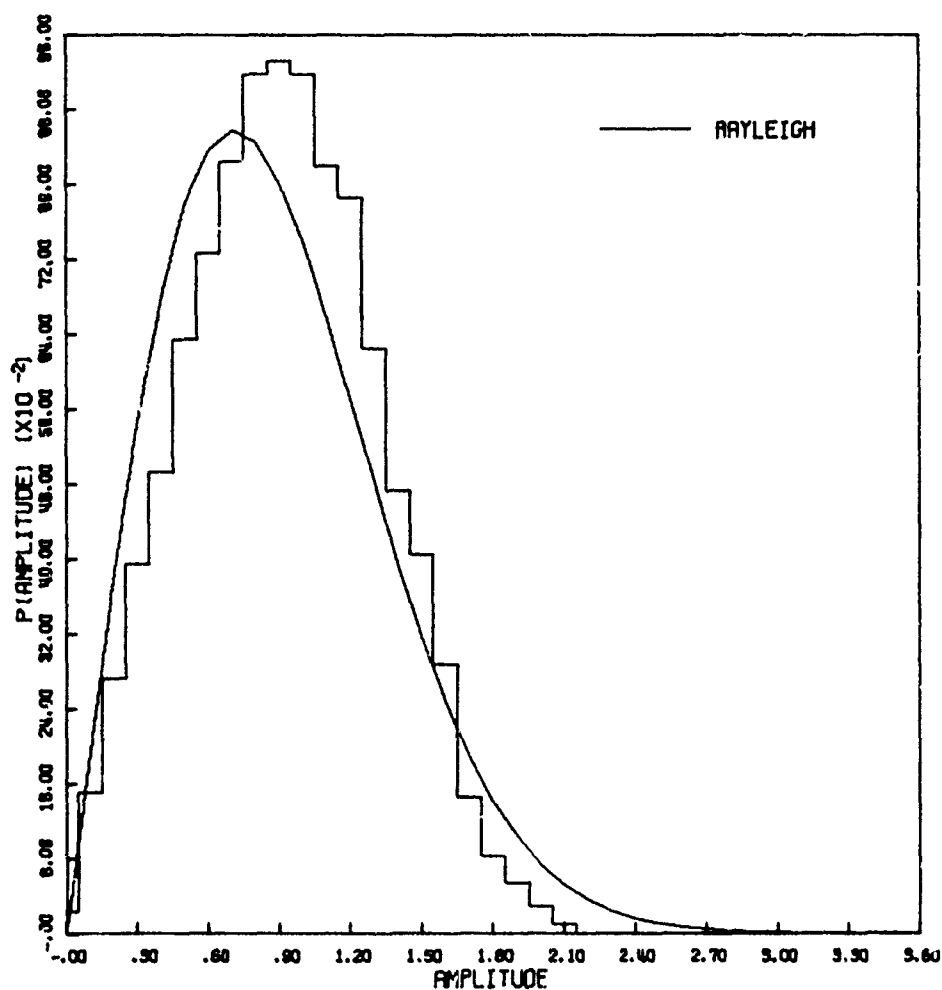
Figure 43b.   Amplitude Distribution
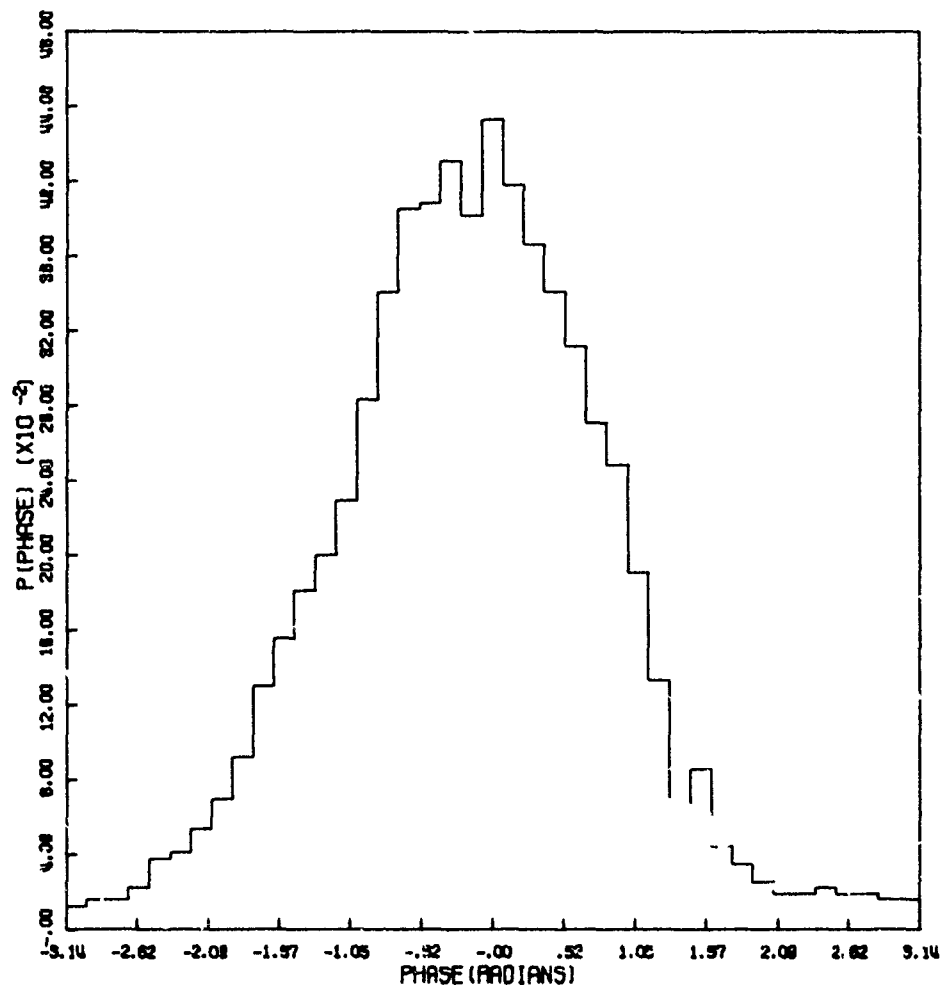
Figure 43c.   Phase Distribution
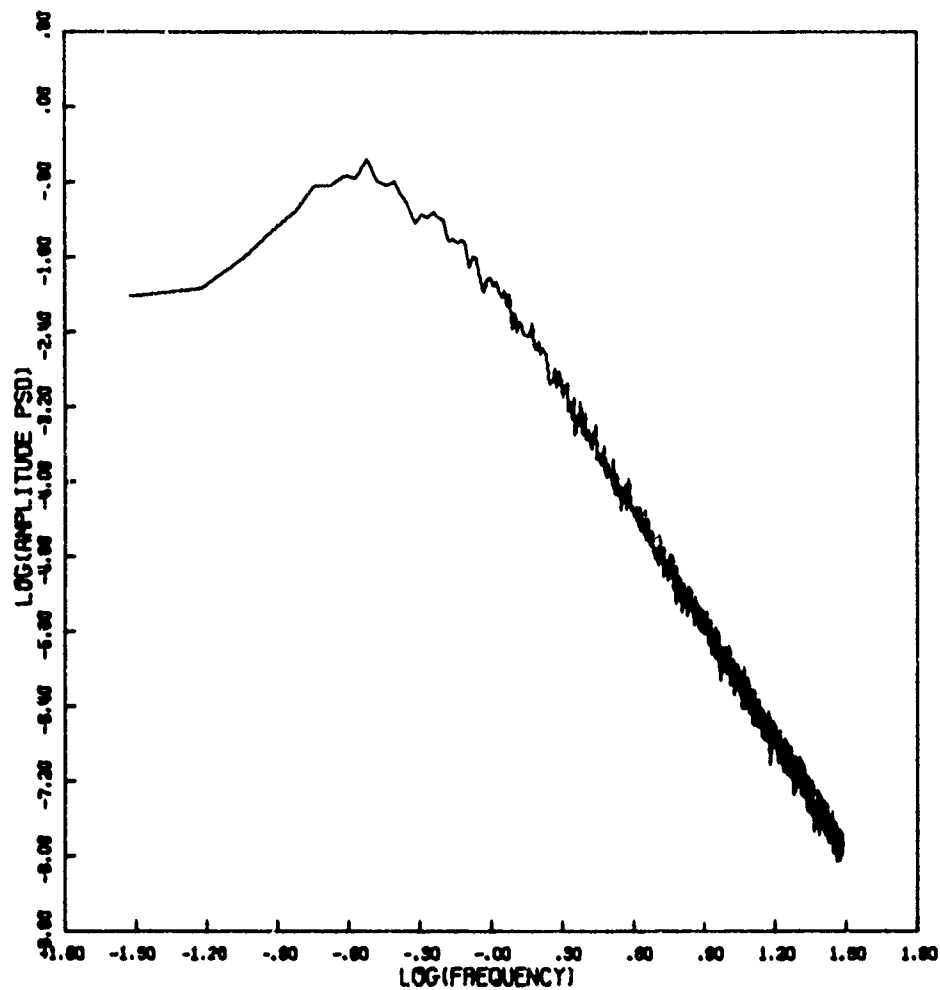
Figure 43d. Amplitude Power Spectral Density
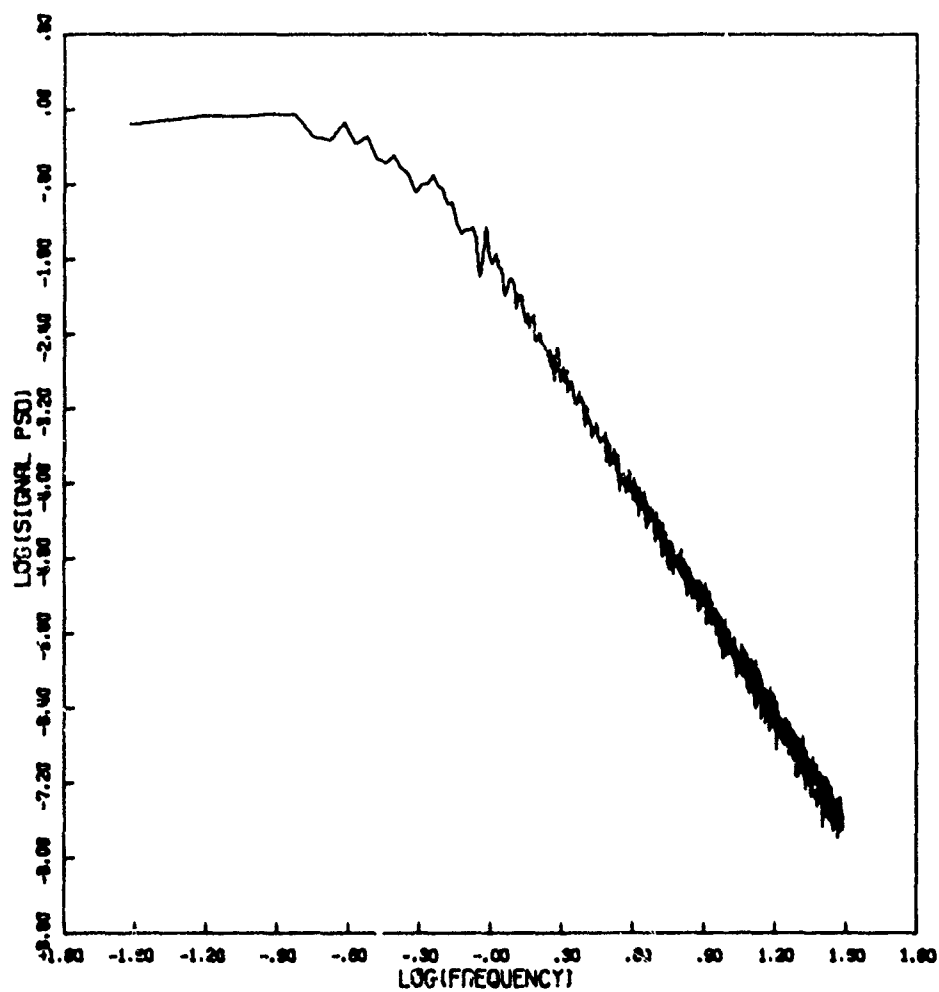
Figure 43f. Signal Power Spectral Density
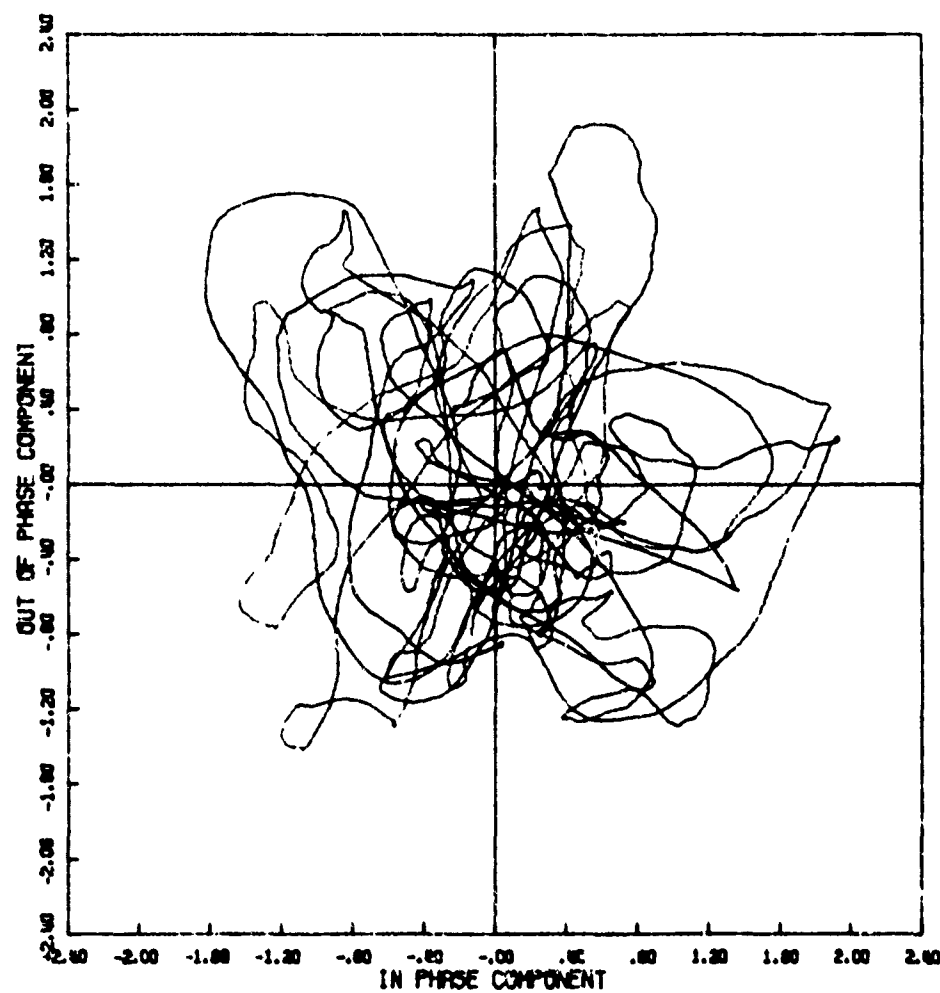
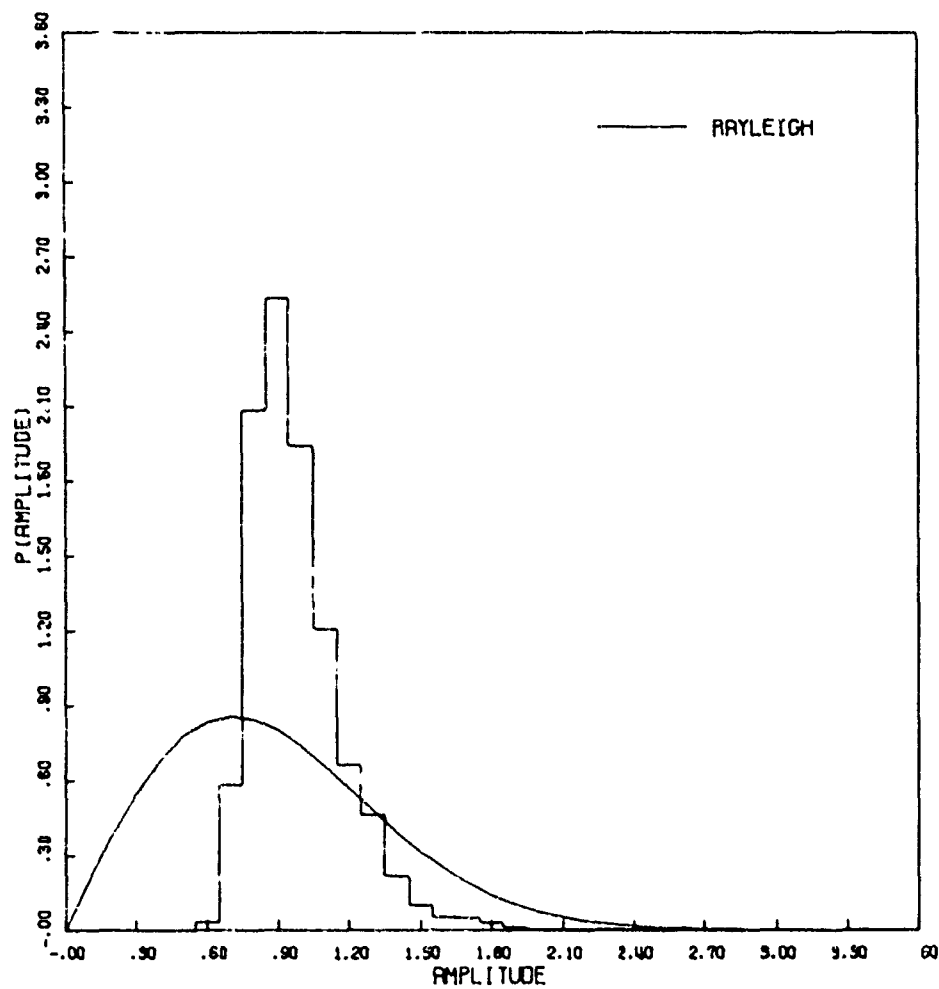Figure 44a. Signal Phase Plot
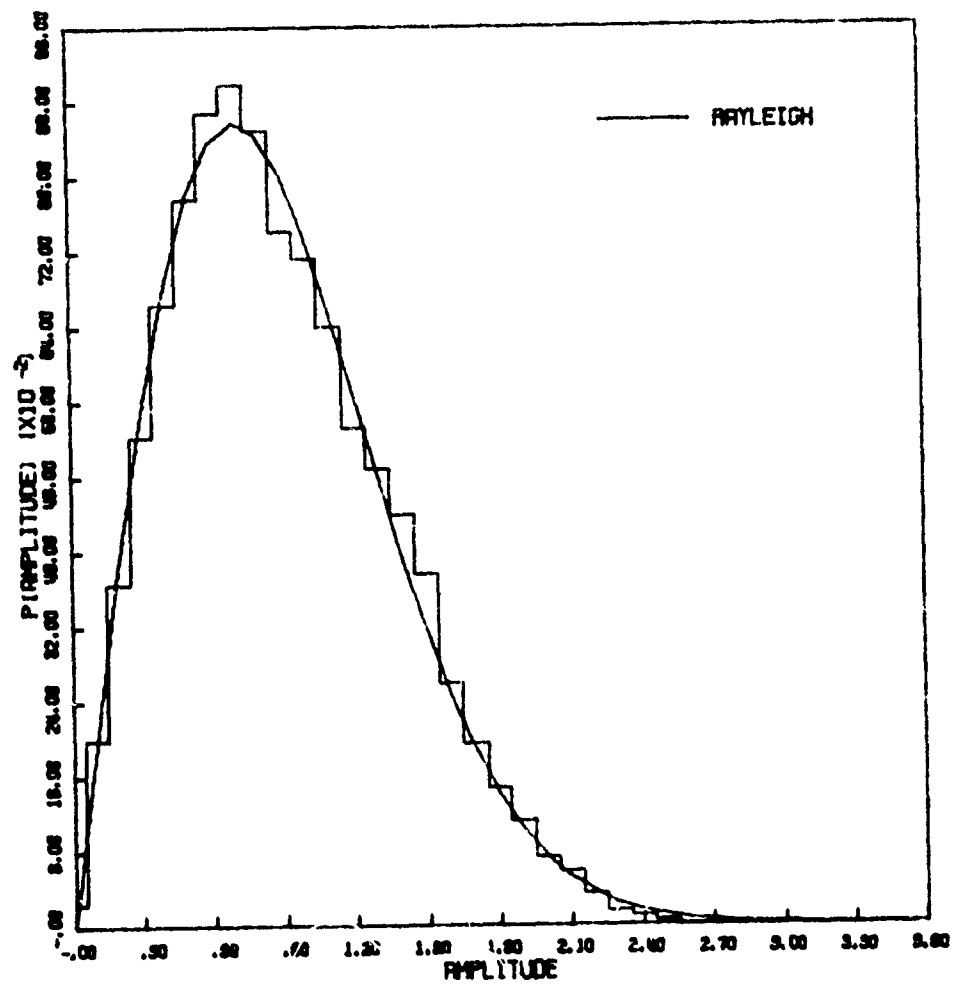
Figure 44b. Amplitude Distribution
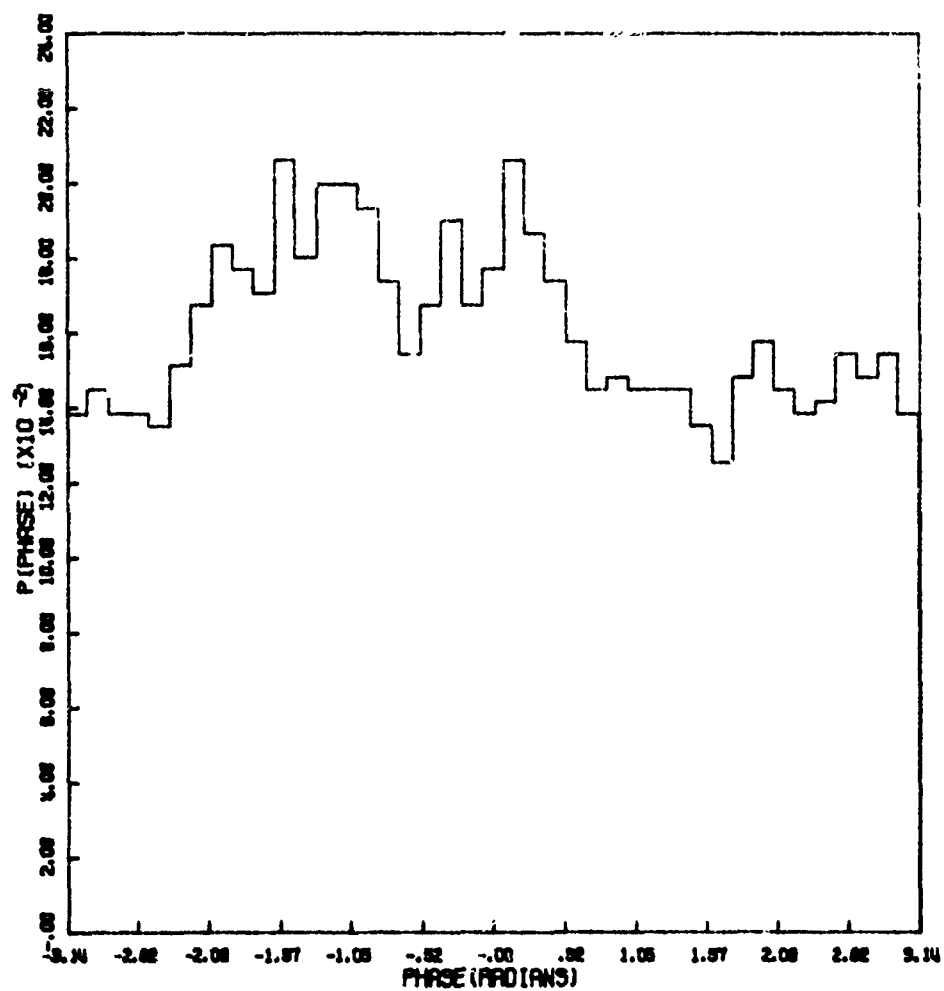
Figure 44c. Phase Distribution
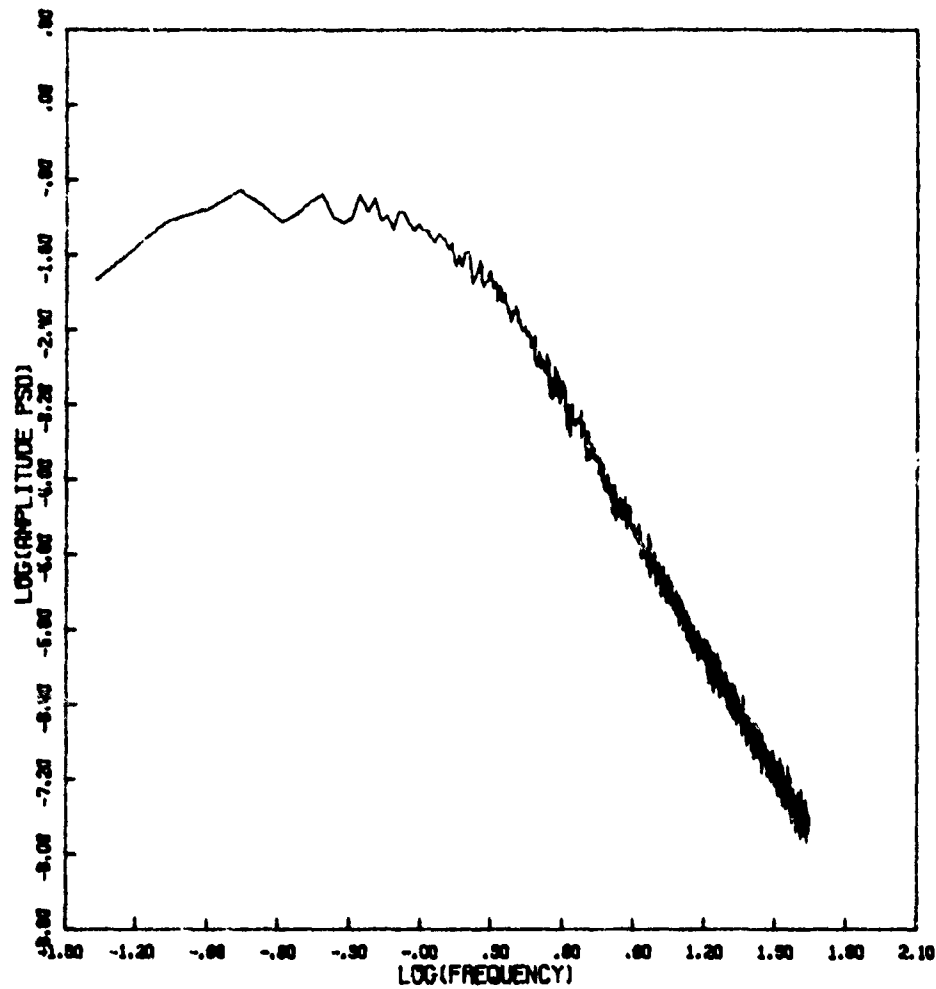
Figure 44d.   Amplitude Power Spectral Density
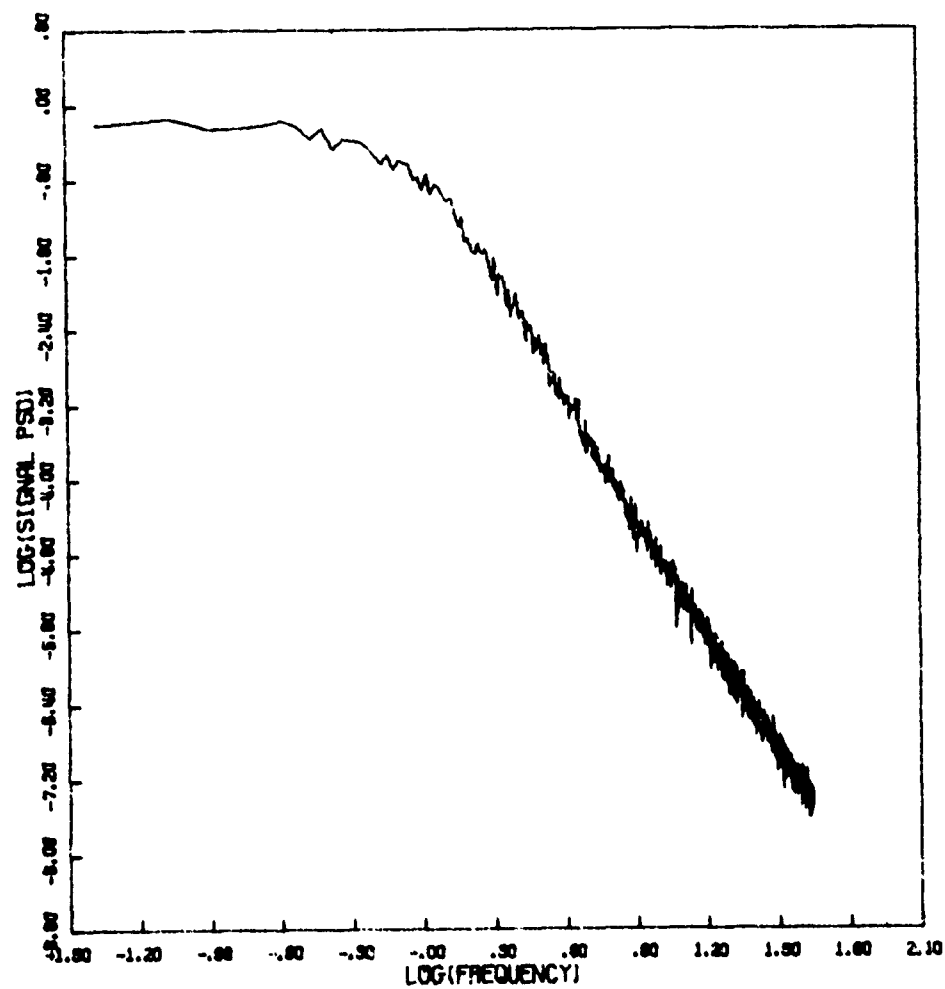
Figure 44f. Signal Power Spectral Density
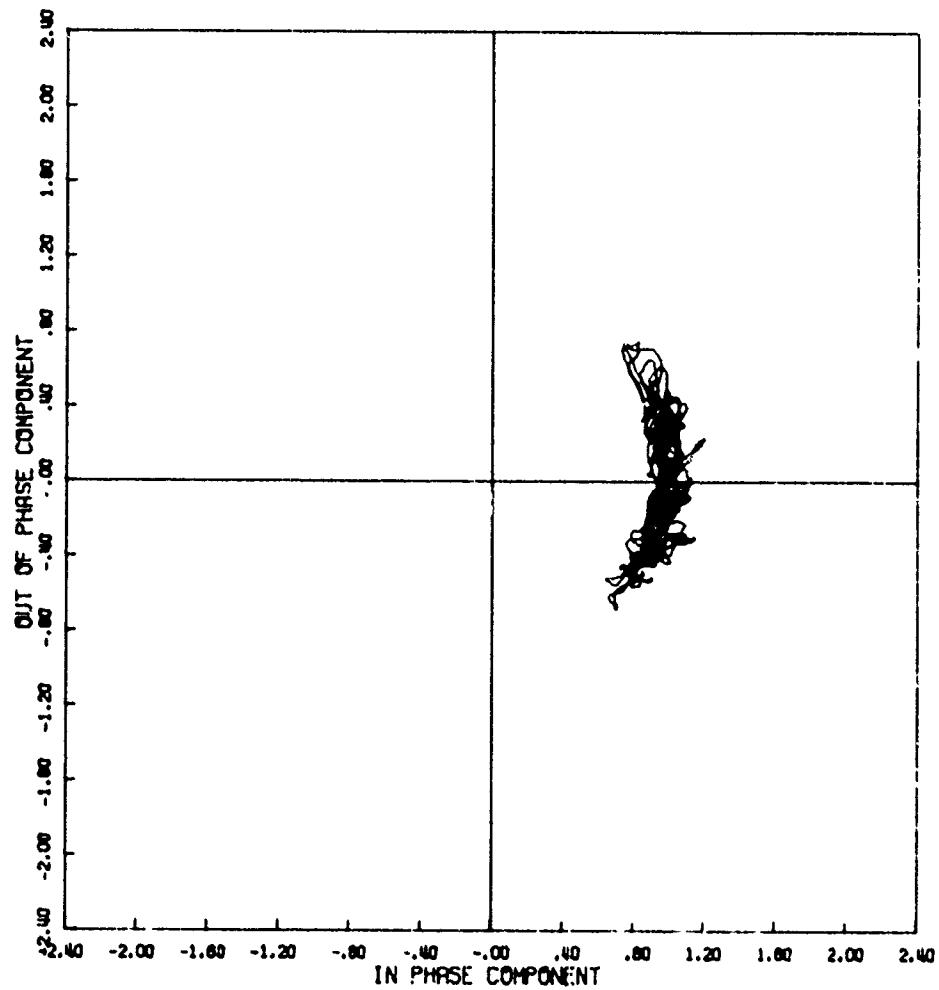
Figure 45a. Signal Phase Plot
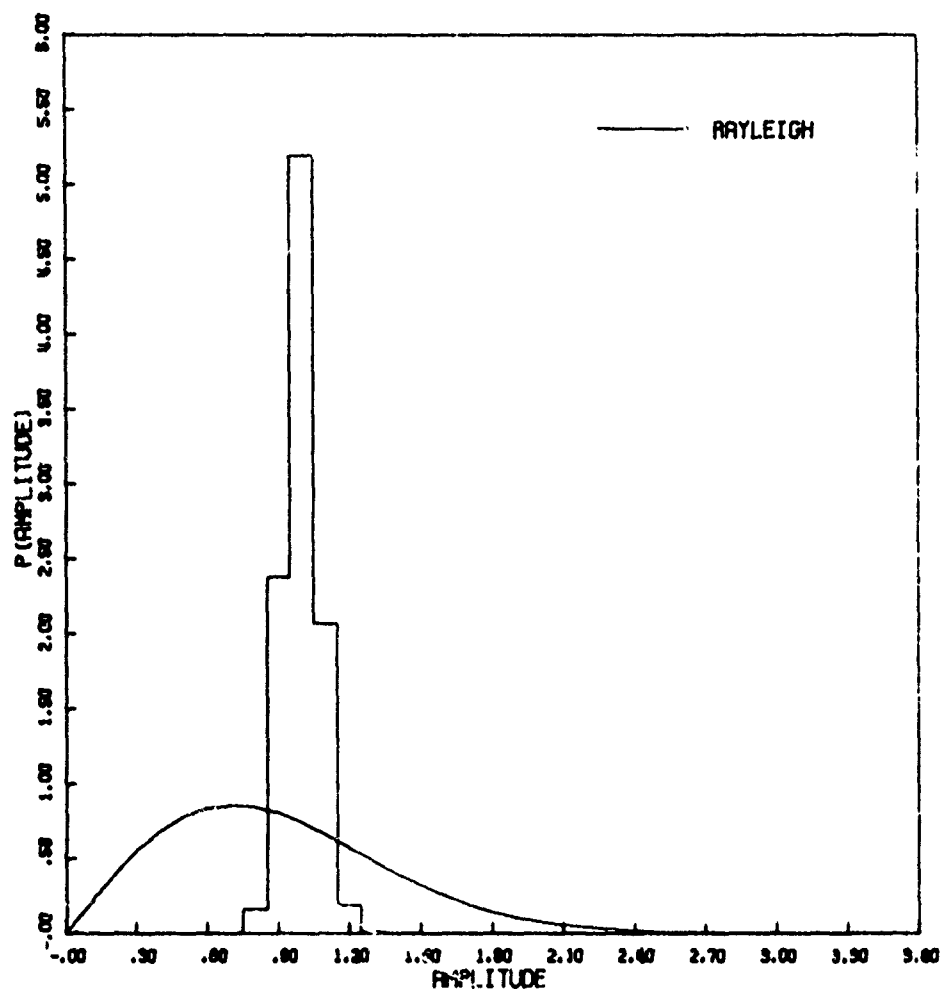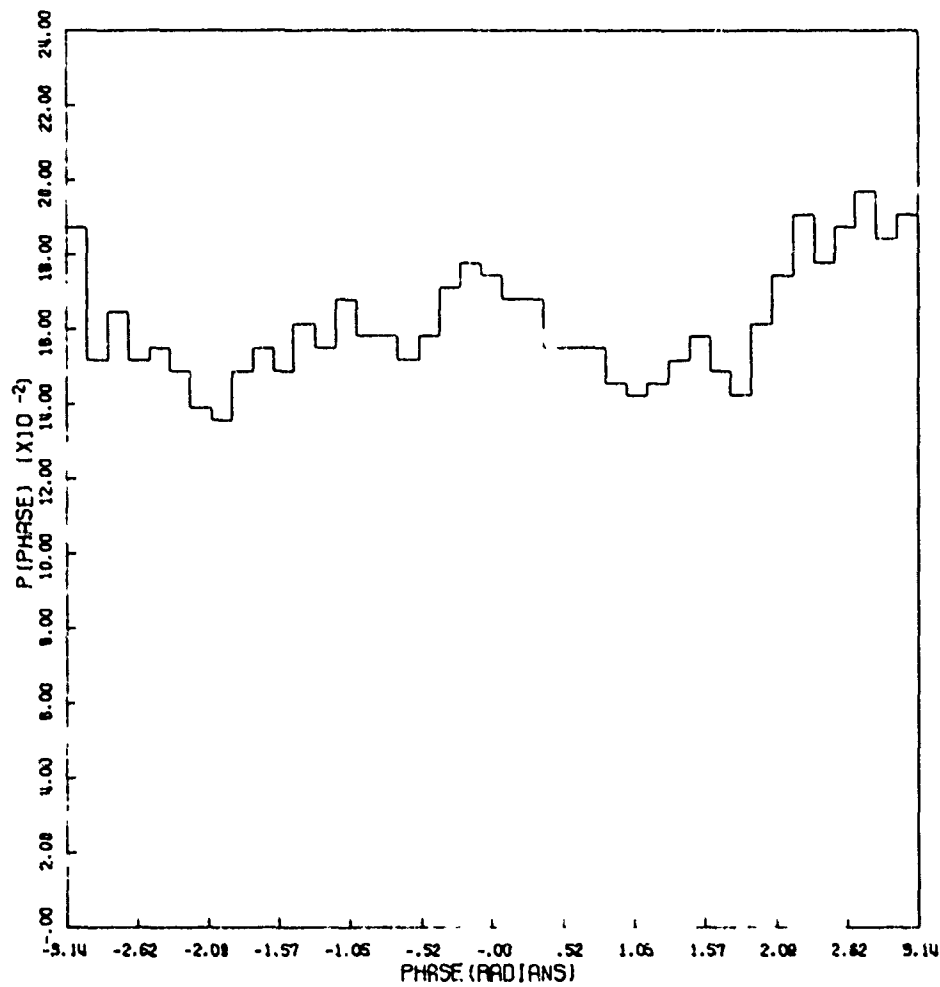
Figure 45b. Amplitude Distribution
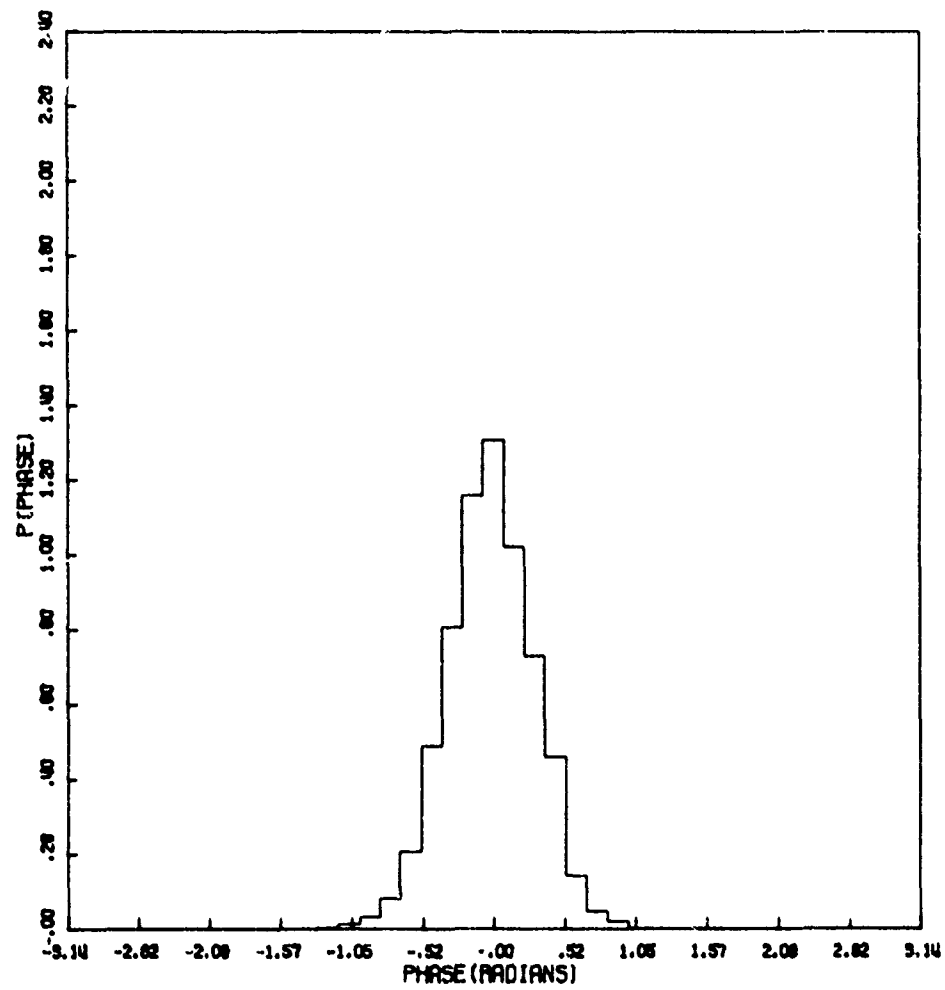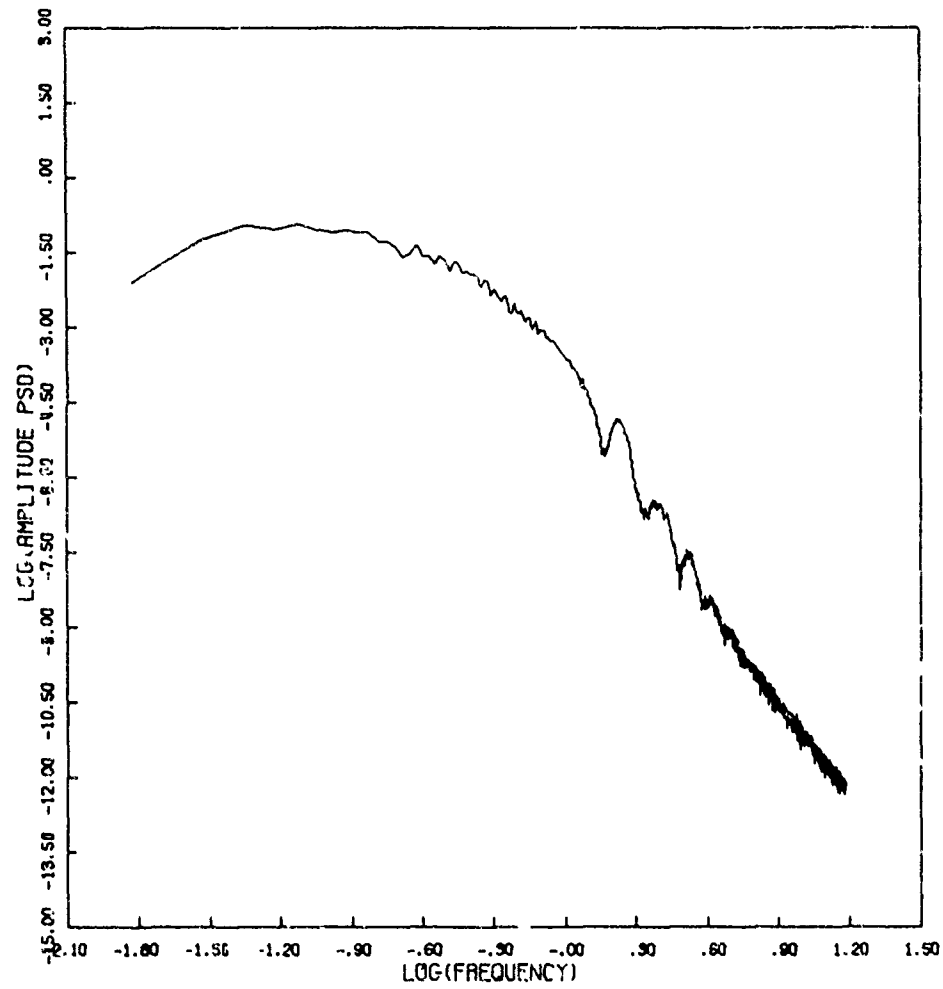
Figure 45c. Phase Distribution
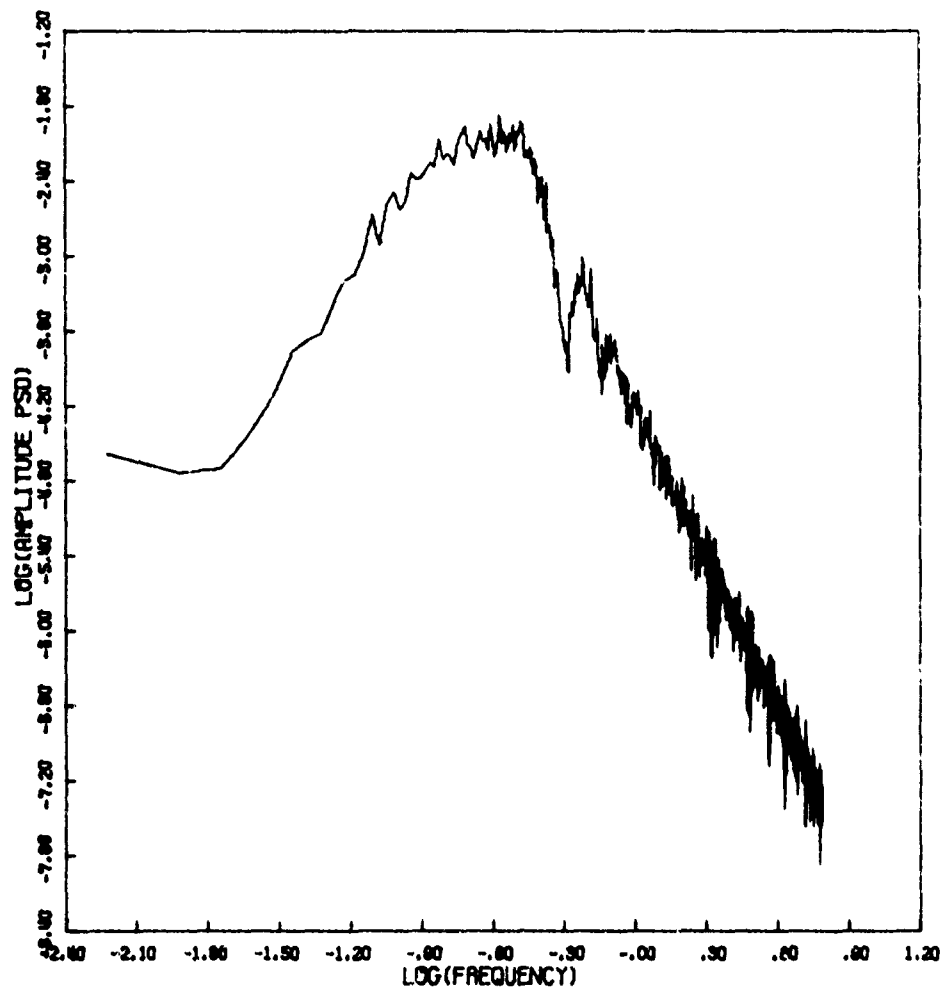
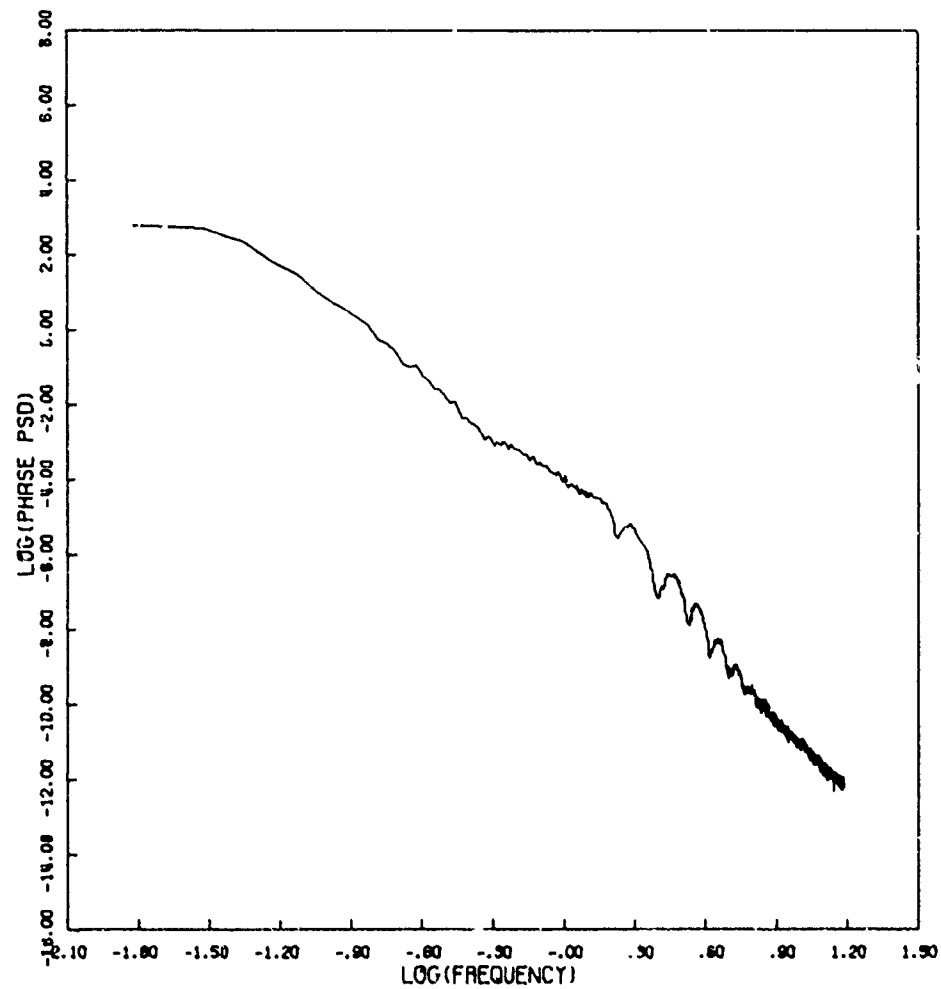Figure 45d. Amplitude Power Spectral Density
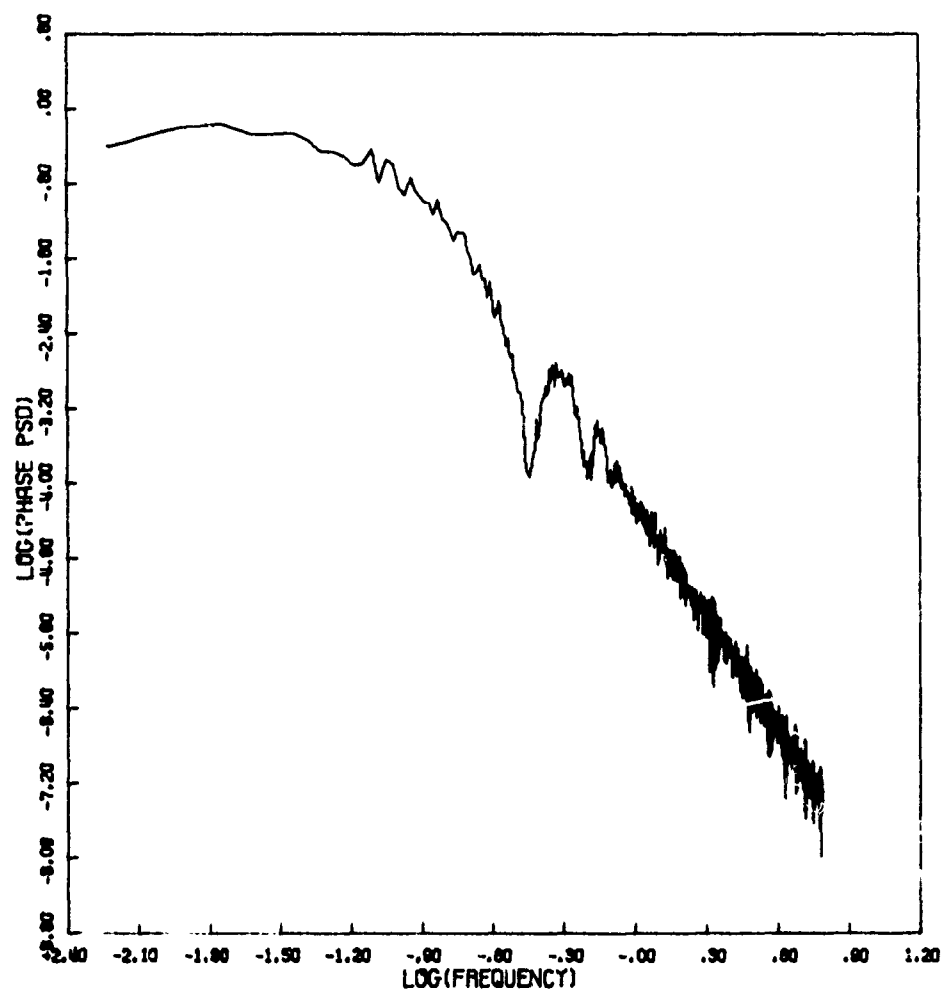
Figure 45e.   Phase Power Spectral Density
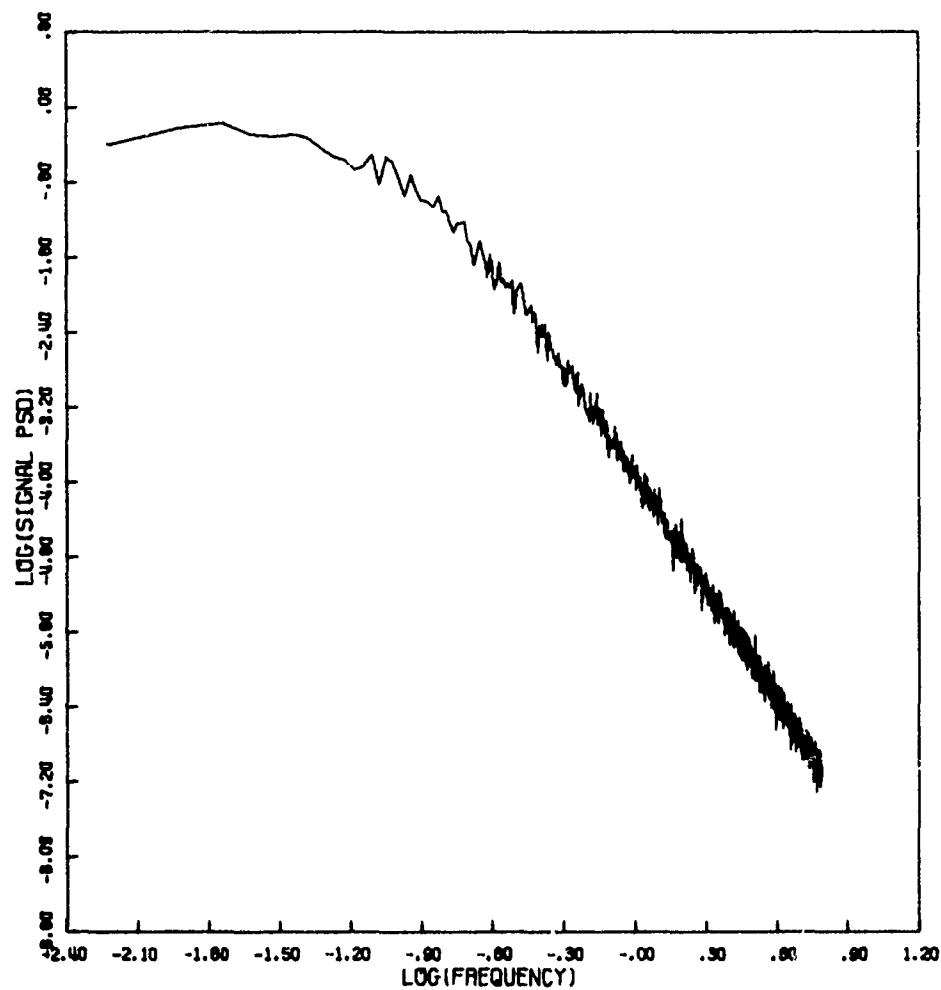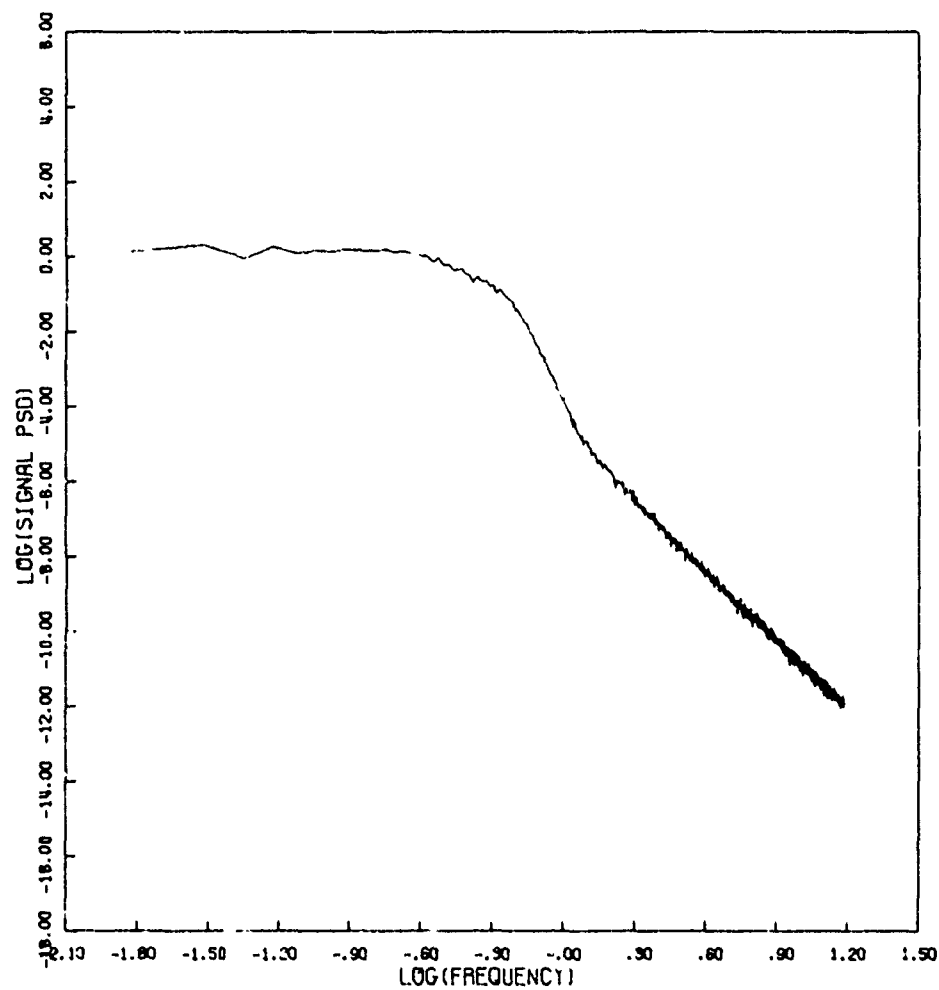
Figure 45f.   Signal Power Spectral Density
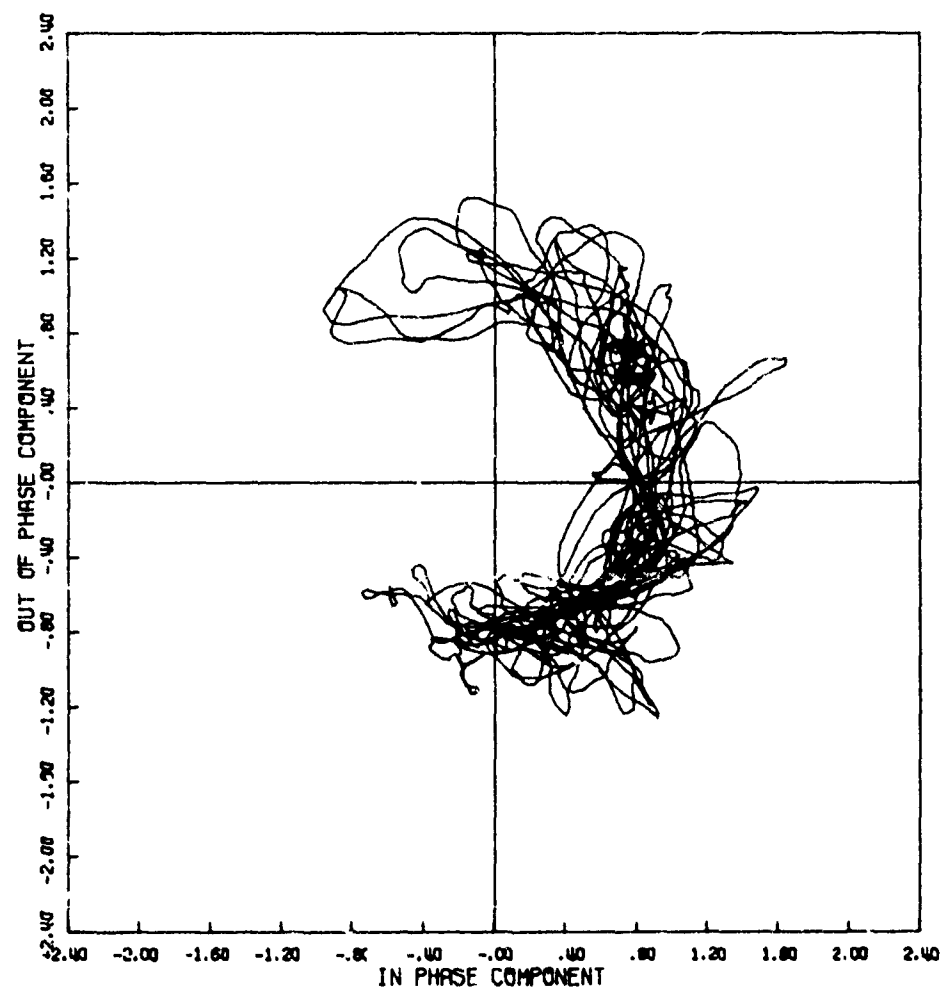
Figure 46a. Signal Phase Plot
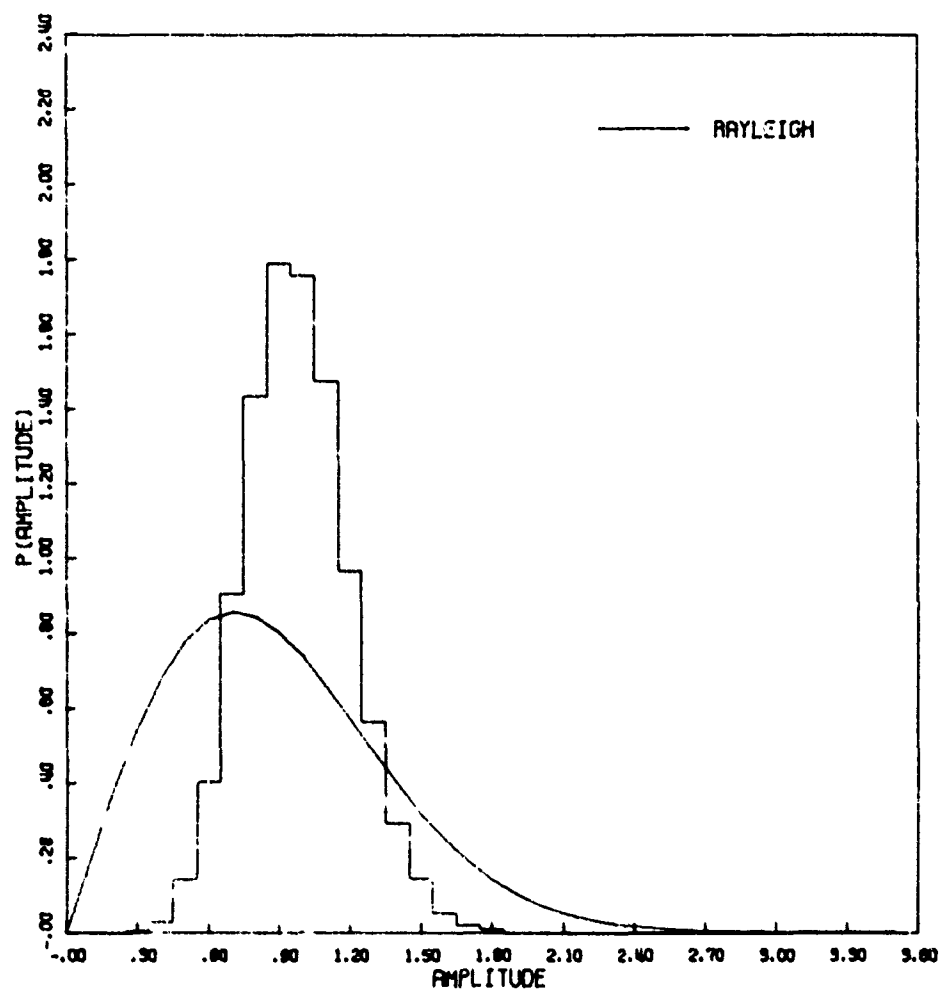
Figure 46b. Amplitude Distribution

Figure 46c. Phase Distribution

Figure 46d. Amplitude Power Spectral Density

Figure 46e. Phase Power Spectral Density
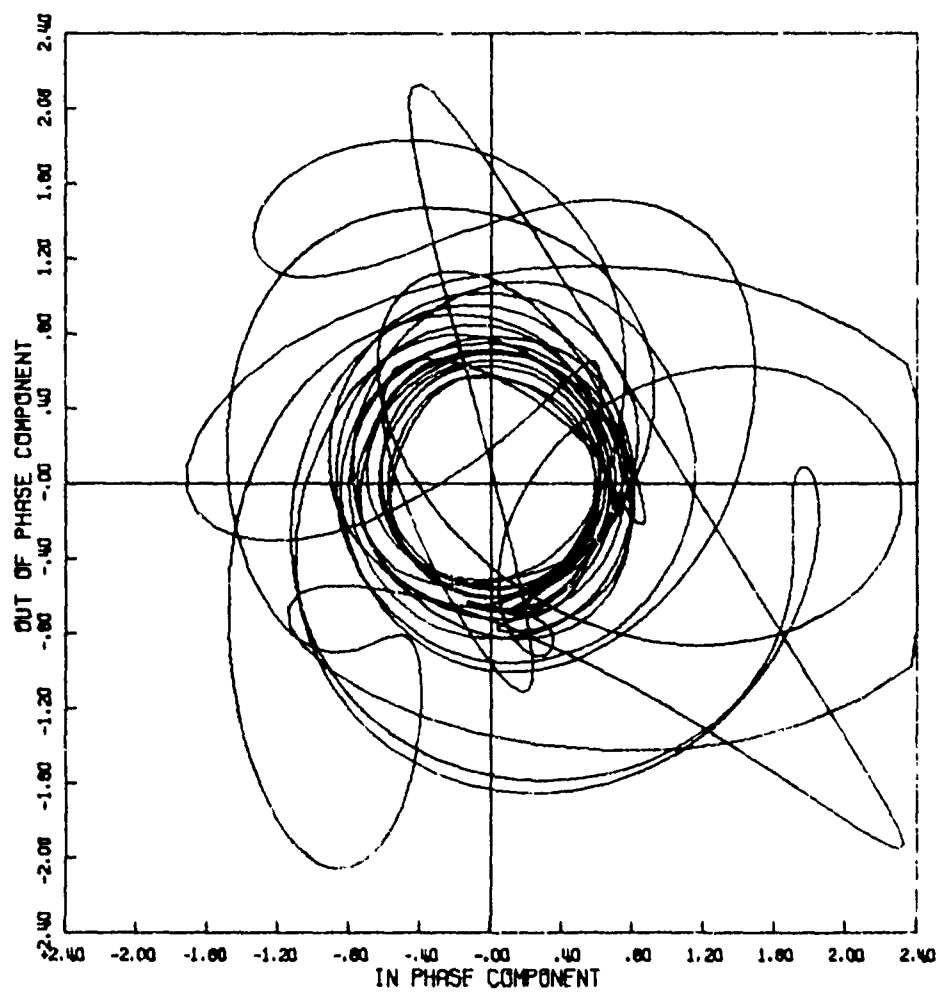
Figure 46f. Signal Power Spectral Density

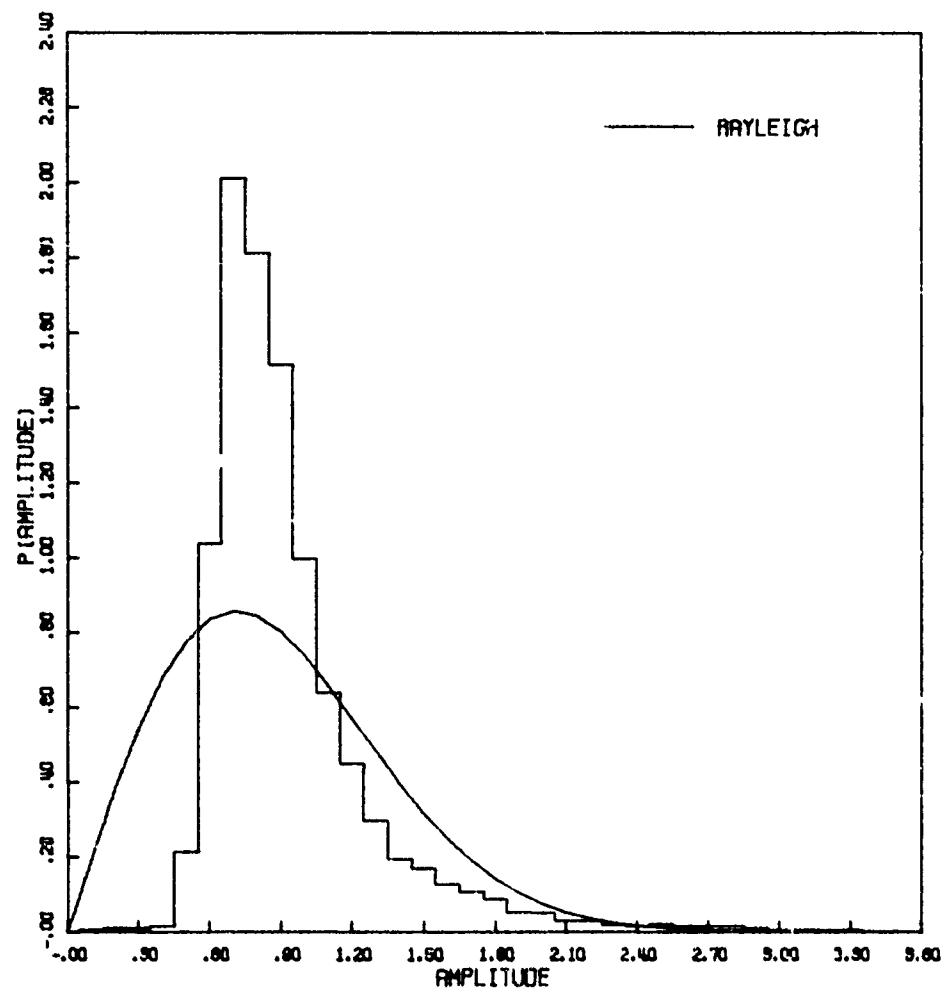Figure 47a.   Signal Phase Plot

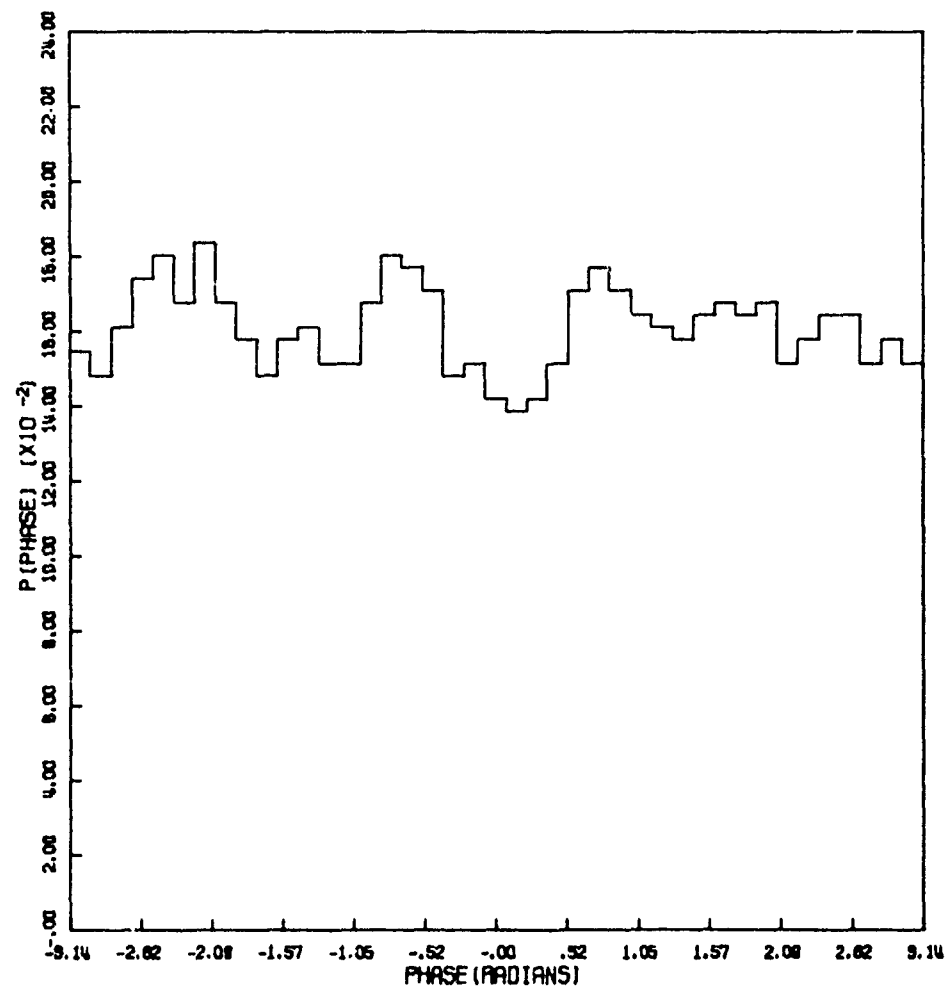Figure 47b. Amplitude Distribution
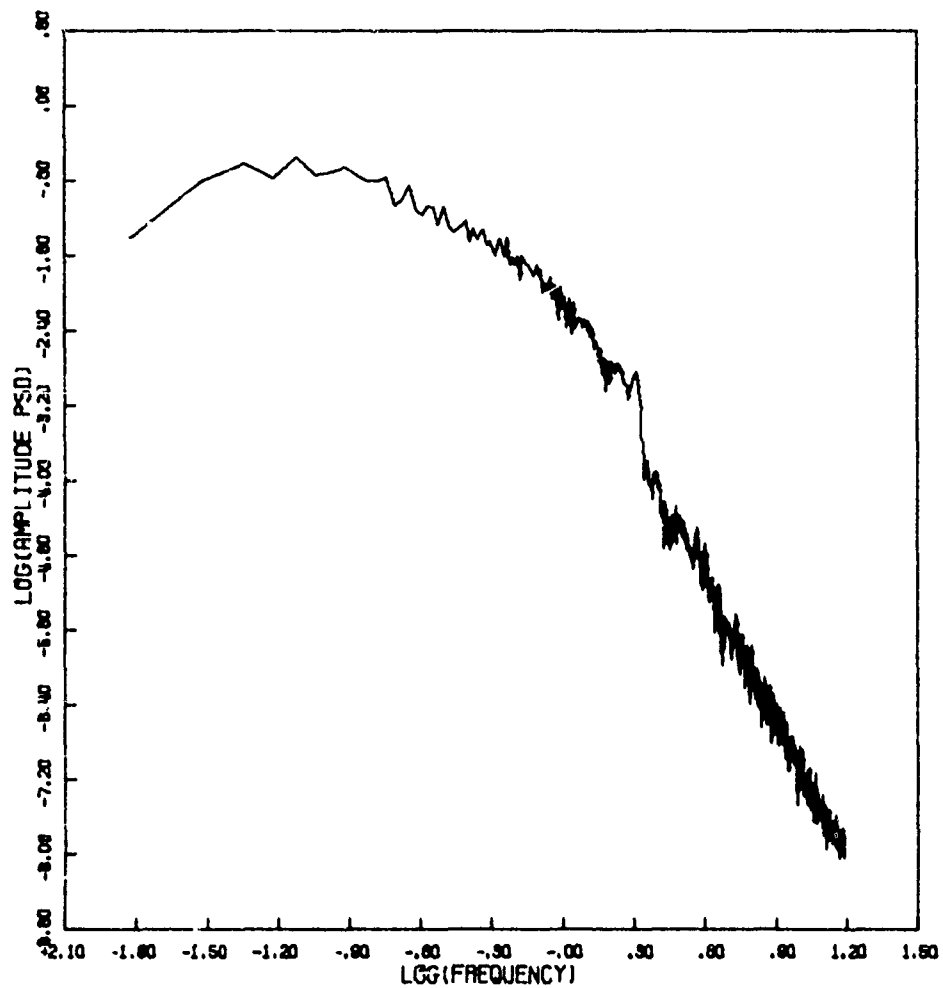
Figure 47c.   Phase Distribution

Figure 47d. Amplitude Power Spectral Density

Figure 47f. Signal Power Spectral Density

Figure 48a. Signal Phase Plot

Figure 48b. Amplitude Distribution

Figure 48c.   Phase Distribution

Figure 48d. Amplitude Power Spectral Density

Figure 48f. Signal Power Spectral Density

Figure 49a.   Signal Phase Plot

Figure 49b.   Amplitude Distribution

Figure 49c.   Phase Distribution
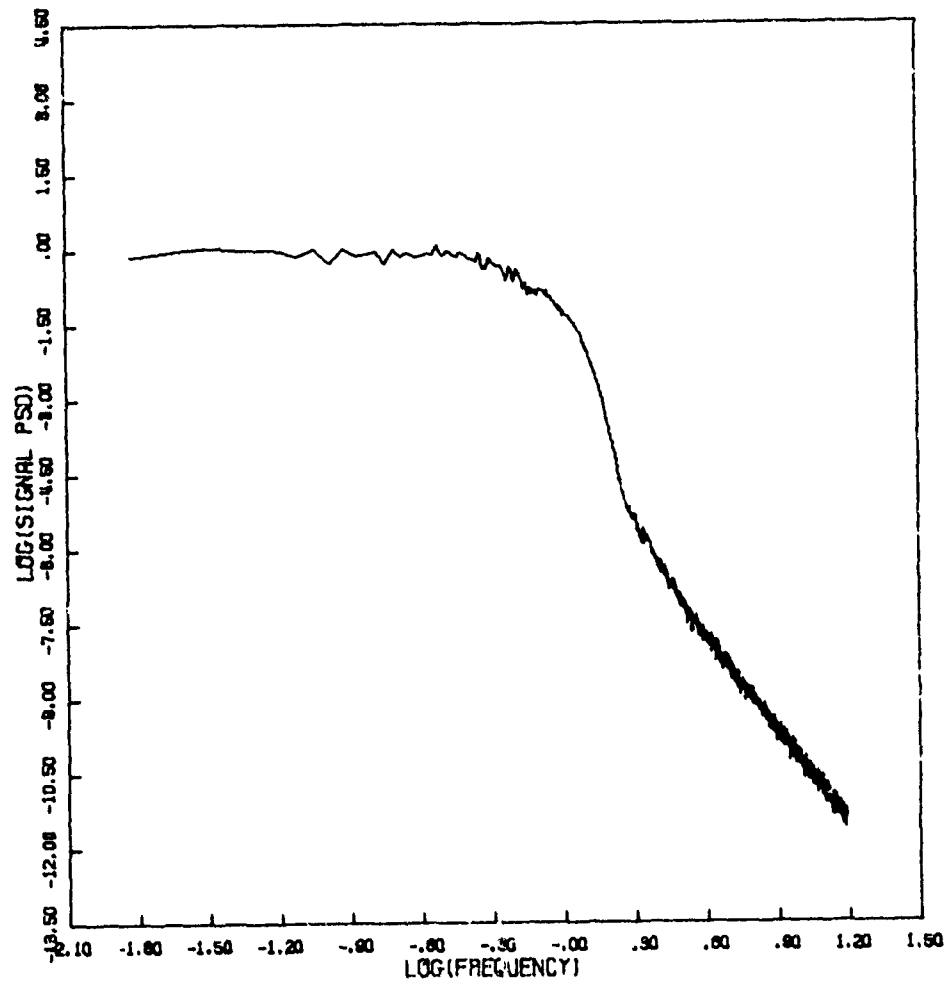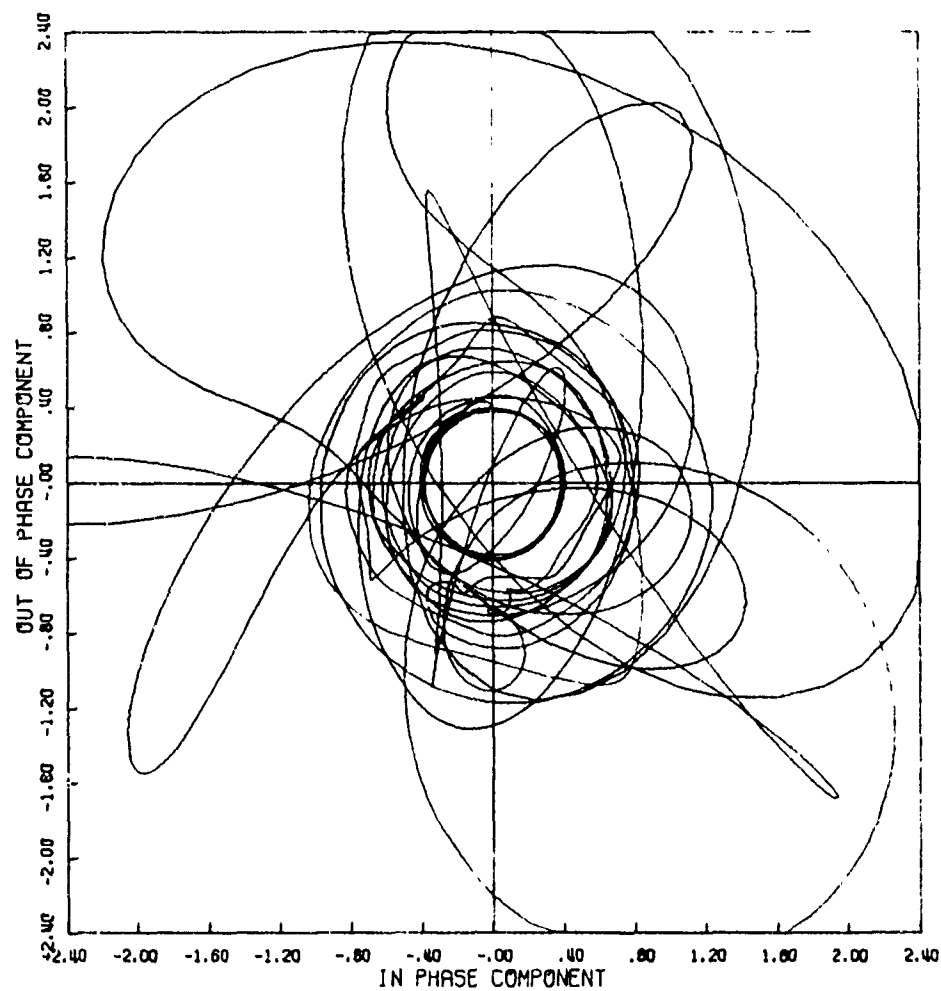
Figure 49d.   Amplitude Power Spectral Density

Figure 49e. Signal Power Spectral Density

Figure 50a. Signal Phase Plot

Figure 50b. Amplitude Distribution

Figure 50c.   Phase Distribution

Figure 50d. Amplitude Power Spectral Density

247

Figure 50e.   Phase Power Spectral Density

243

Figure 50f. Signal Power Spectral Density

Figure 51a.   Signal Phase Plot

Figure 51b. Amplitude Distribution

251

Figure 51c.   Phase Distribution

Figure 51d. Amplitude Power Spectral Density

Figure 51e.   Phase Power Spectral Density

254

Figure 51f. Signal Power Spectral Density

Figure 52a. Signal Phase Plot

Figure 52b.   Amplitude Distribution

Figure 52c. Phase Distribution

Figure 52d. Amplitude Power Spectral Density

Figure 52e.   Phase Power Spectral Density

Figure 52f. Signal Power Spectral Density

Figure 53a.   Signal Phase Plot

Figure 53b. Amplitude Distribution

Figure 53c. Phase Distribution

Figure 53d. Amplitude Power Spectral Density

265

Figure 53e. Signal Power Spectral Density

Figure 54a.   Signal Phase Plot

Figure 54b. Amplitude Distribution

Figure 54c.   Phase Distribution

Figure 54d. Amplitude Power Spectral Density

Figure 54f. Signal Power Spectral Density

Figure 55a.   Signal Phase Plot

Figure 55b. Amplitude Distribution

Figure 55c   Phase Distribution
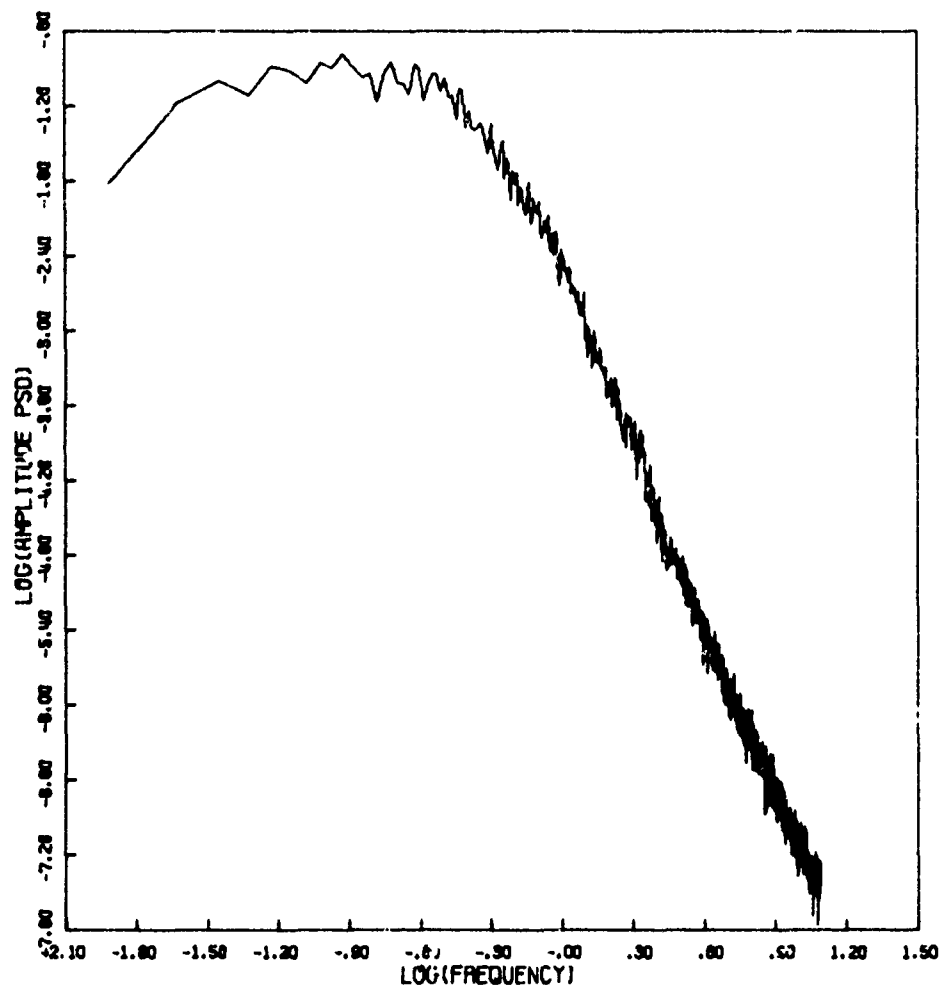
Figure 55d. Amplitude Power Spectral Density
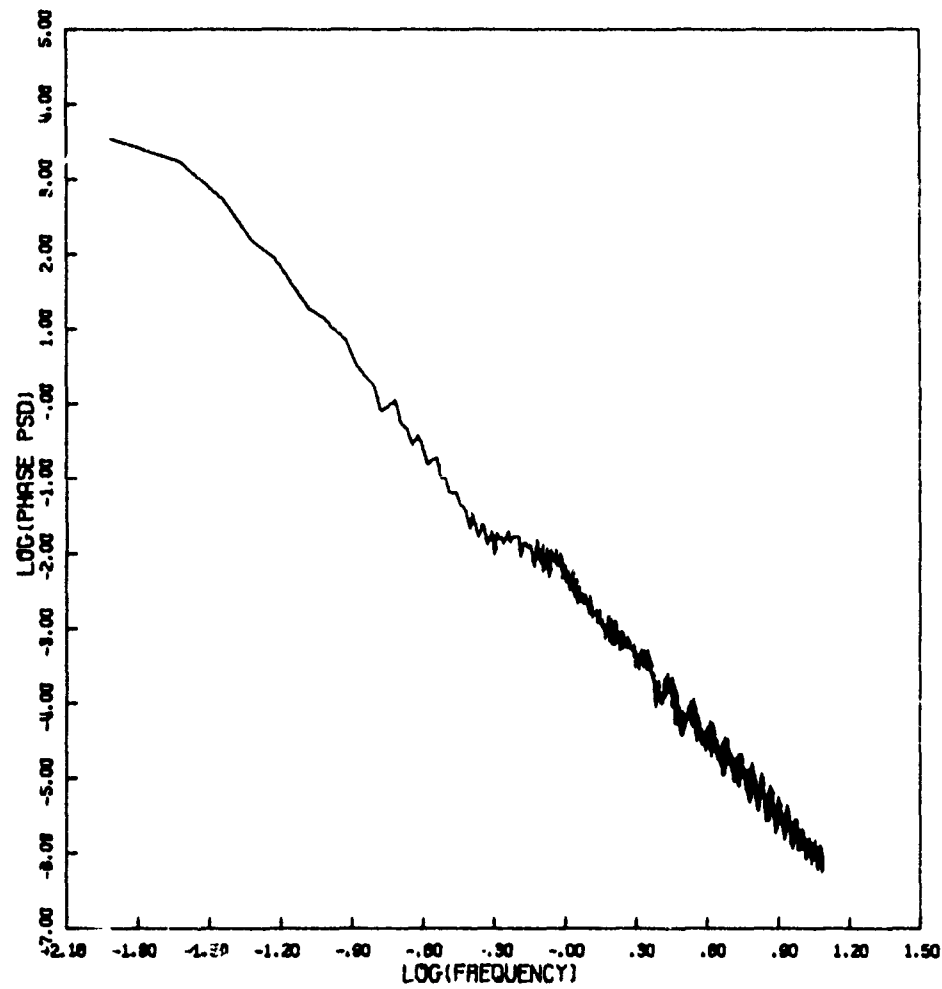
Figure 55e. Phase Power Spectral Density
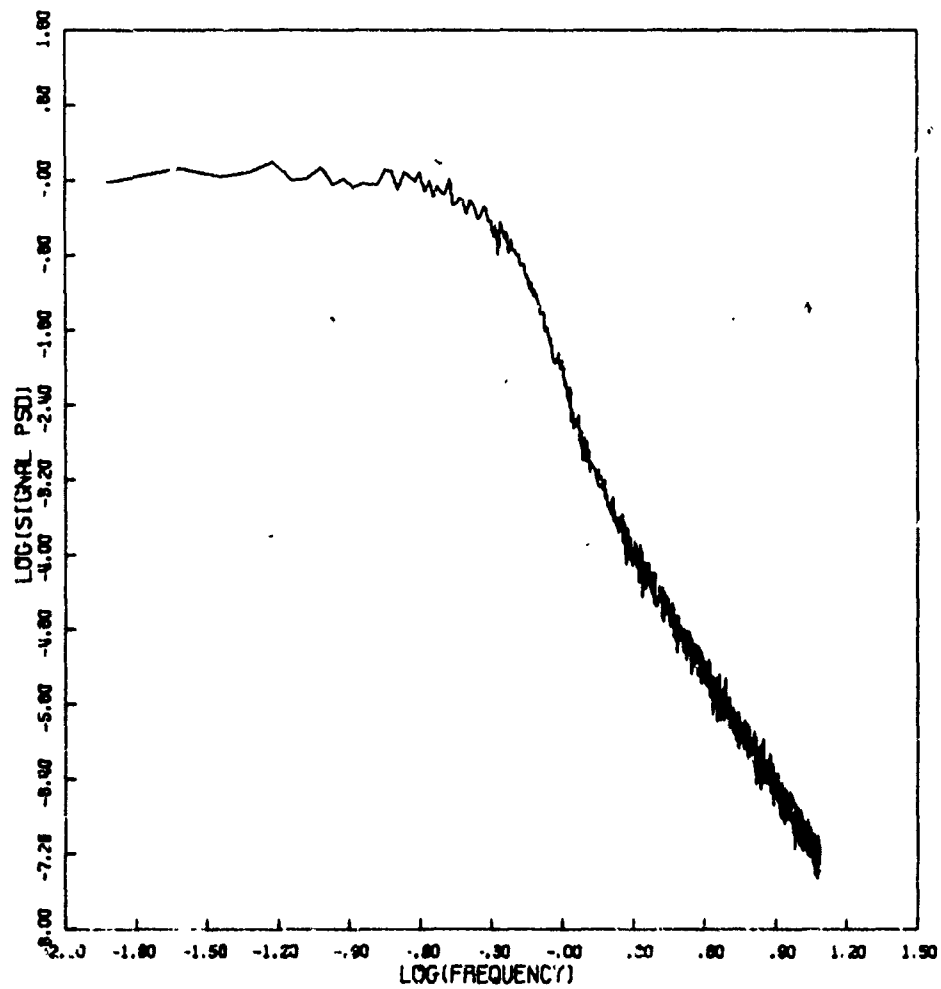
Figure 55f. Signal Power Spectral Density

Table 4

K_ρ^{-5} SPECTRUM

$z_g = 3 \times 10^7$			$z_s = 1 \times 10^7$			$K = 6.28 \times 10^{-2}$			K_ρ^{-5} SPECTRUM		
FIG.	L	$\overline{\Delta n^2}$	$\overline{\phi^2}$	$\overline{\chi^2}$	S_4	ℓ_0	$\overline{E_R^2}$	$\overline{E_I^2}$	α_A	α_ϕ	α_s
59	1.5×10^4	10^9	0.26	0.05	0.40	6.7×10^4	0.06	0.19	6.0	6.0	6.0
60	1.5×10^4	5×10^9	1.4	0.32	0.80	3.7×10^4	0.31	0.46	5.4		6.0
61	1.5×10^4	3×10^{10}	9.5*	0.46	0.94	1.3×10^4	0.51	0.49	5.1		G. 5.9
62	4×10^4	1.5×10^8	0.13	0.002	0.09	1.9×10^5	0.01	0.10	6.0	6.1	6.1
63	4×10^4	10^9	0.76	0.01	0.21	1.4×10^5	0.15	0.38	6.1	6.0	6.0
64	4×10^4	7×10^9	5.9	0.08	0.58	4.7×10^4	0.48	0.52	6.9	5.5	G. 6.1
65	4×10^4	2×10^{10}	17.*	0.22	0.97	2.6×10^4	0.51	0.49	2.8. 5.5		G. 6.3
66	4×10^4	8×10^{10}	67.*	0.48	1.14	1.2×10^4	0.51	0.49	0.9. 4.9		G. 6.1
67	4×10^4	3×10^{11}	252*	0.52	1.10	6.0×10^3	0.49	0.51	0.7. 5.3		G. 6.3
68	10^5	10^{10}	21.	0.01	0.23	5.9×10^4	0.50	0.50	1.6. 6.4	6.1	G. 6.2
69	10^5	3.3×10^{10}	69.	0.04	0.48	3×10^4	0.51	0.49	3.9. 7.8	6.1	G. 6.1
70	10^5	1.1×10^{11}	231.*	0.12	1.01	1.6×10^4	0.49	0.51	1.4. 5.1		G. 6.2
71	10^5	3×10^{11}	631.*	0.27	1.31	9.5×10^3	0.50	0.50	1.3. 4.6		G. 6.2

Figure 56. Propagation Space Plot for K_ρ^{-5} Spectrum
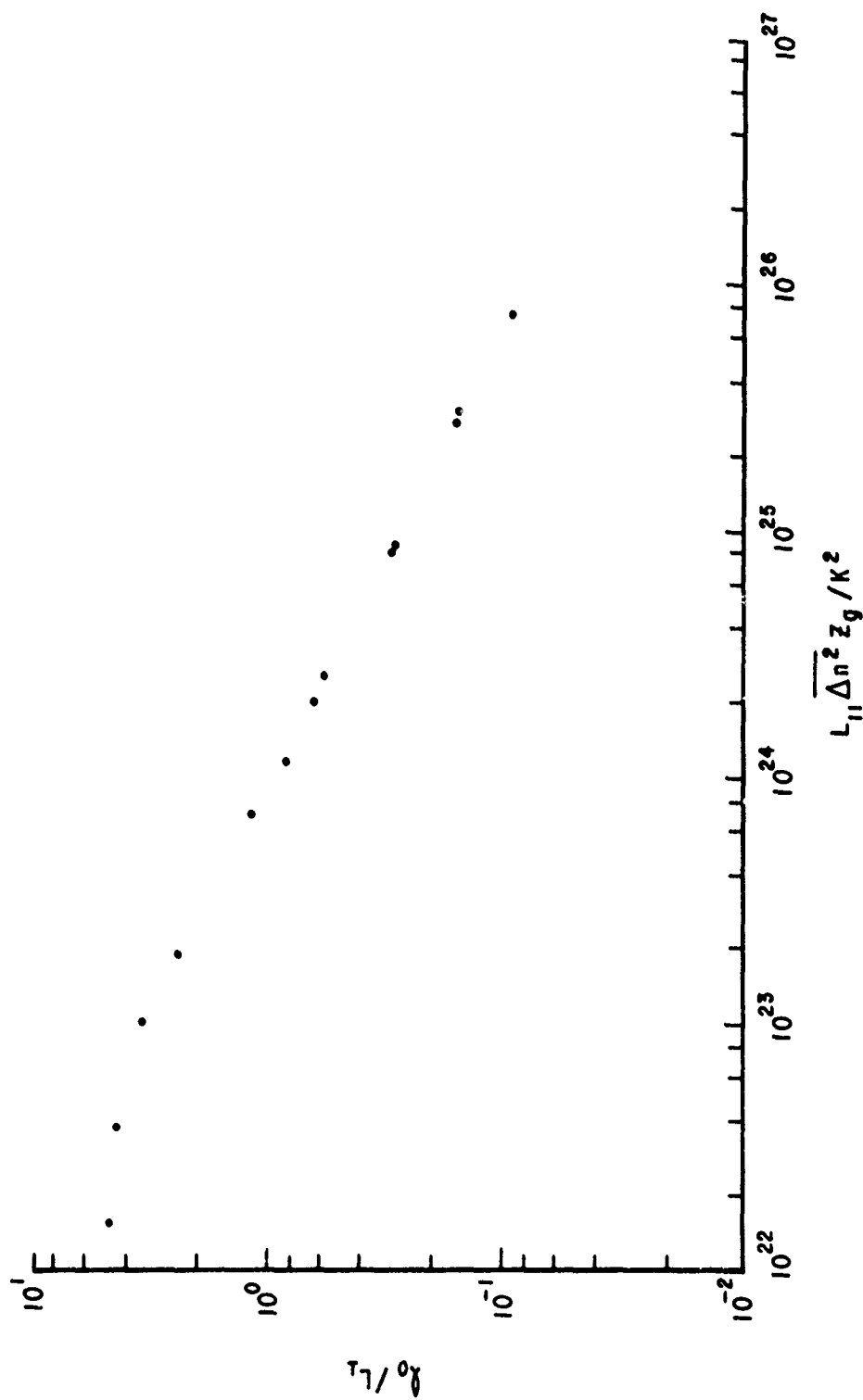
Figure 57. ν_0 for K_ρ^{-5} Spectrum
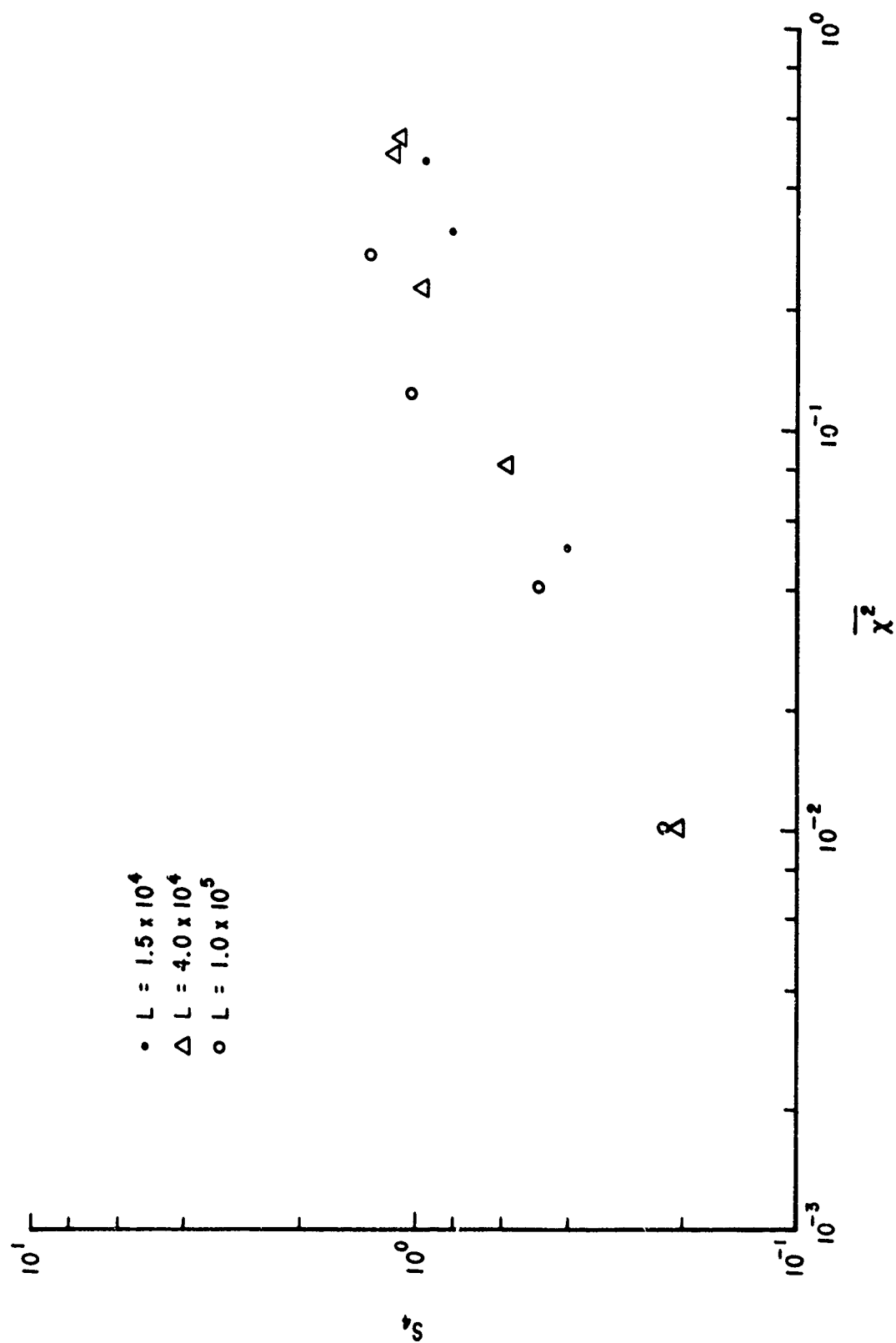
Figure 58. S_4 vs. $\overline{\chi^2}$ for K_ρ^{-5} Spectrum
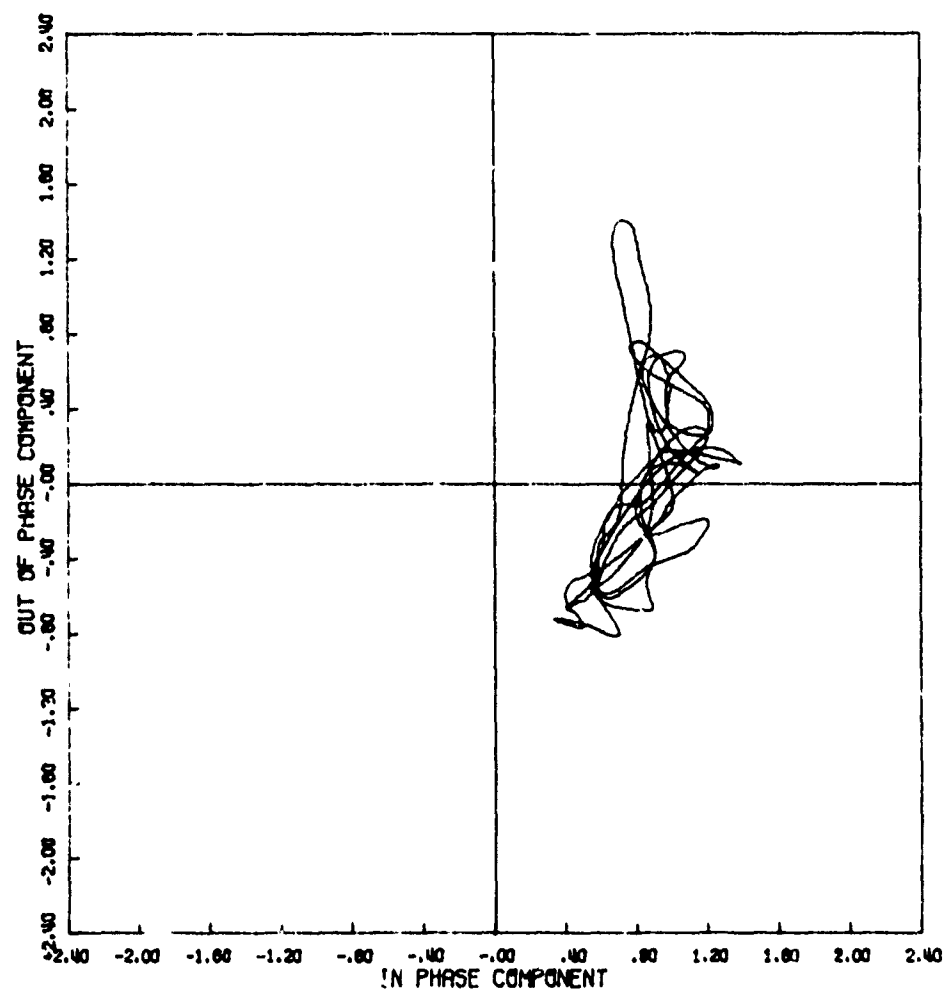
Figure 59a. Signal Phase Plot

Figure 59b. Amplitude Distribution

Figure 59c.   Phase Distribution
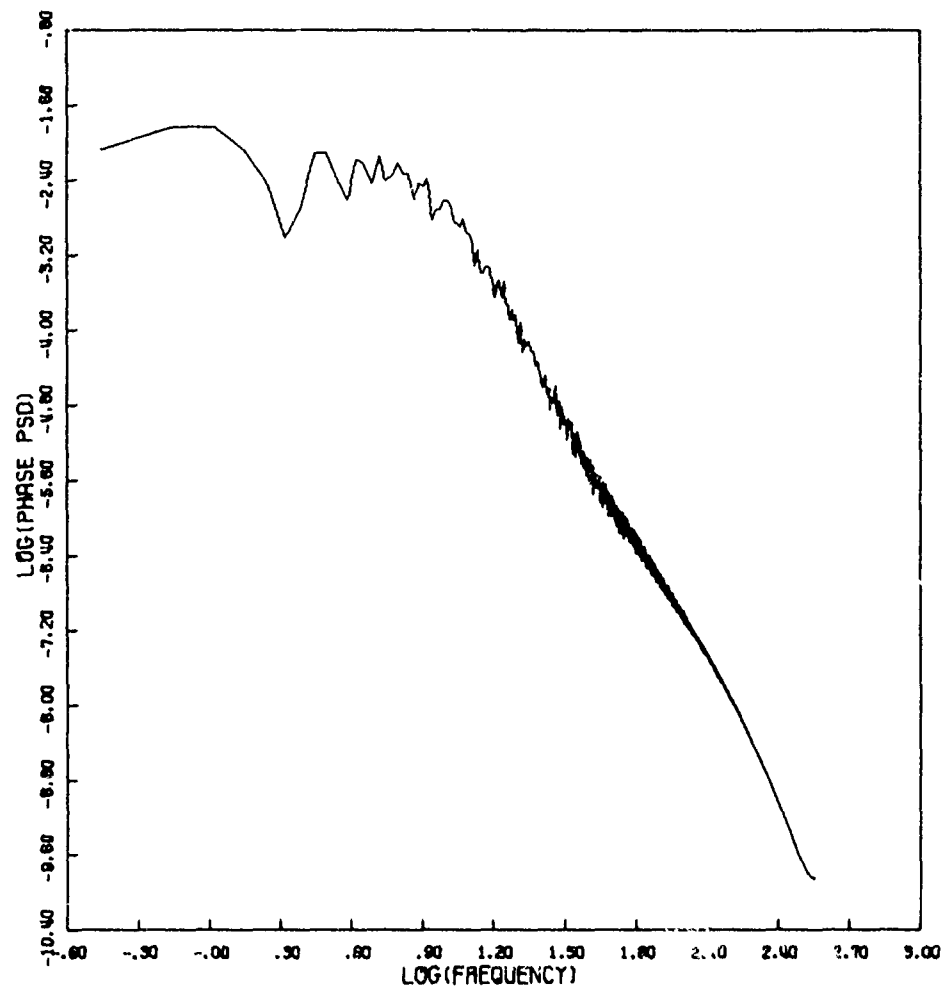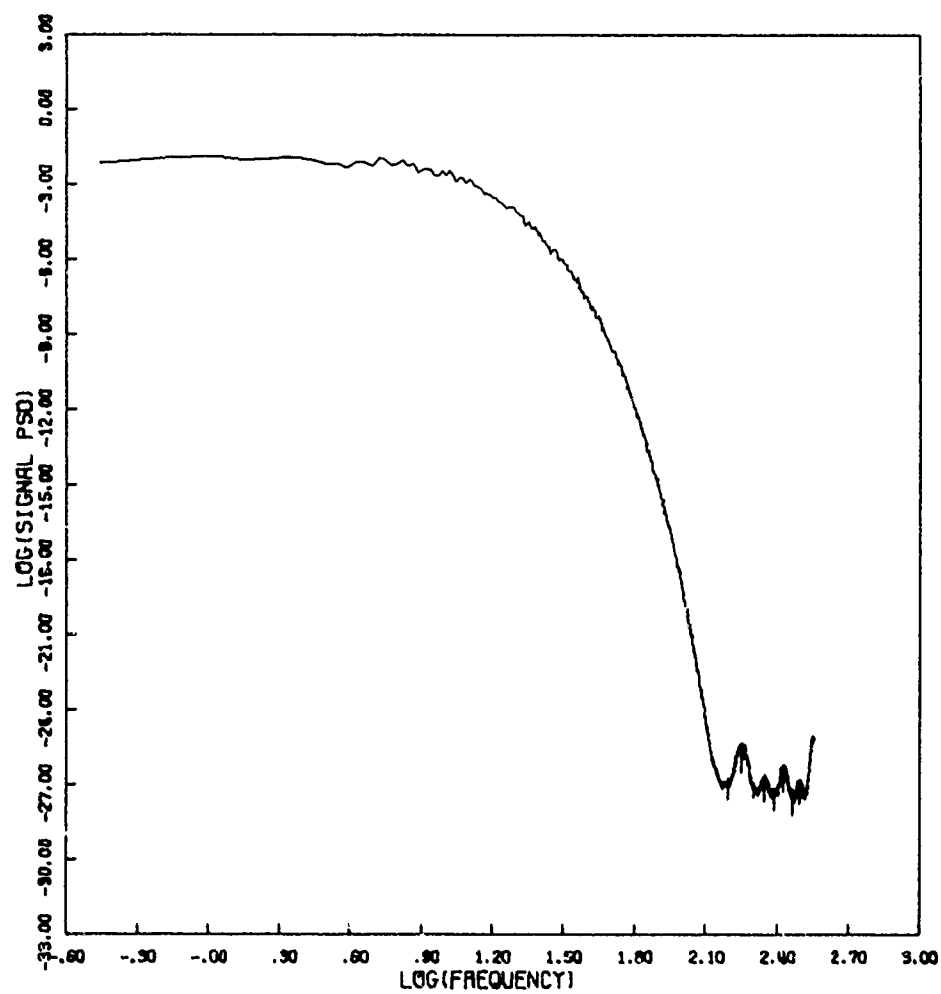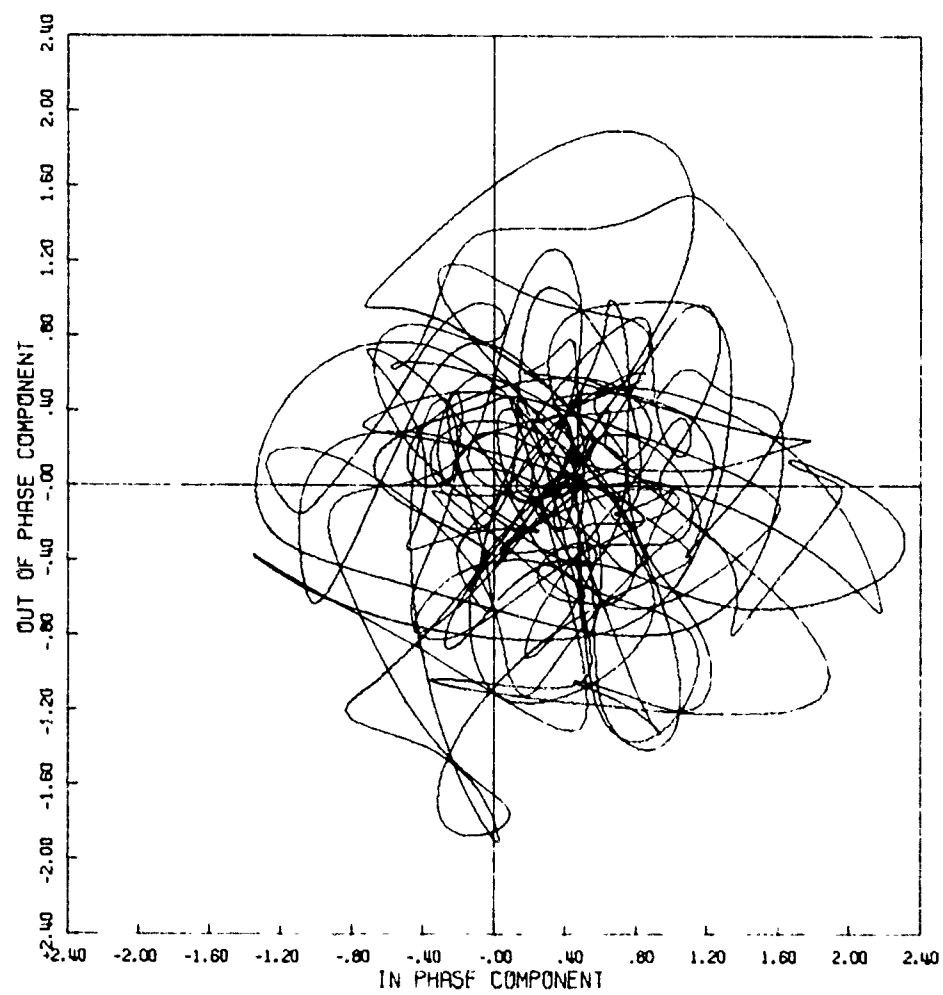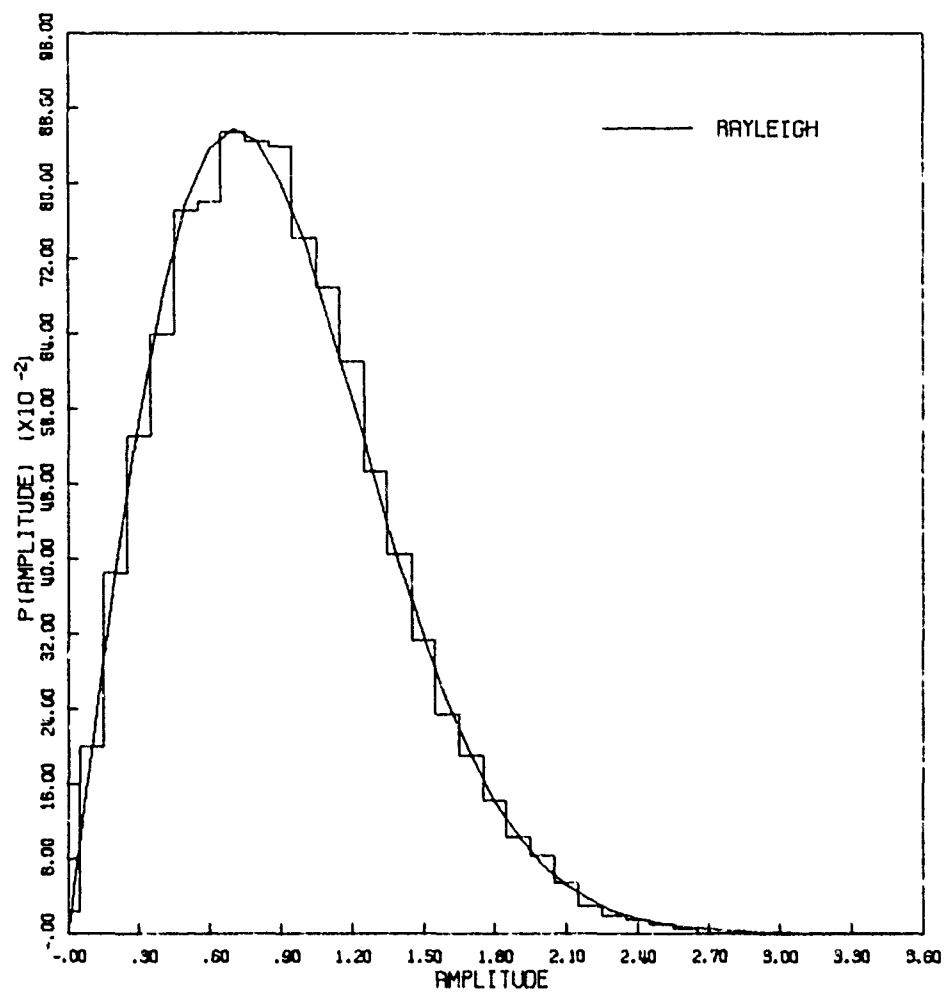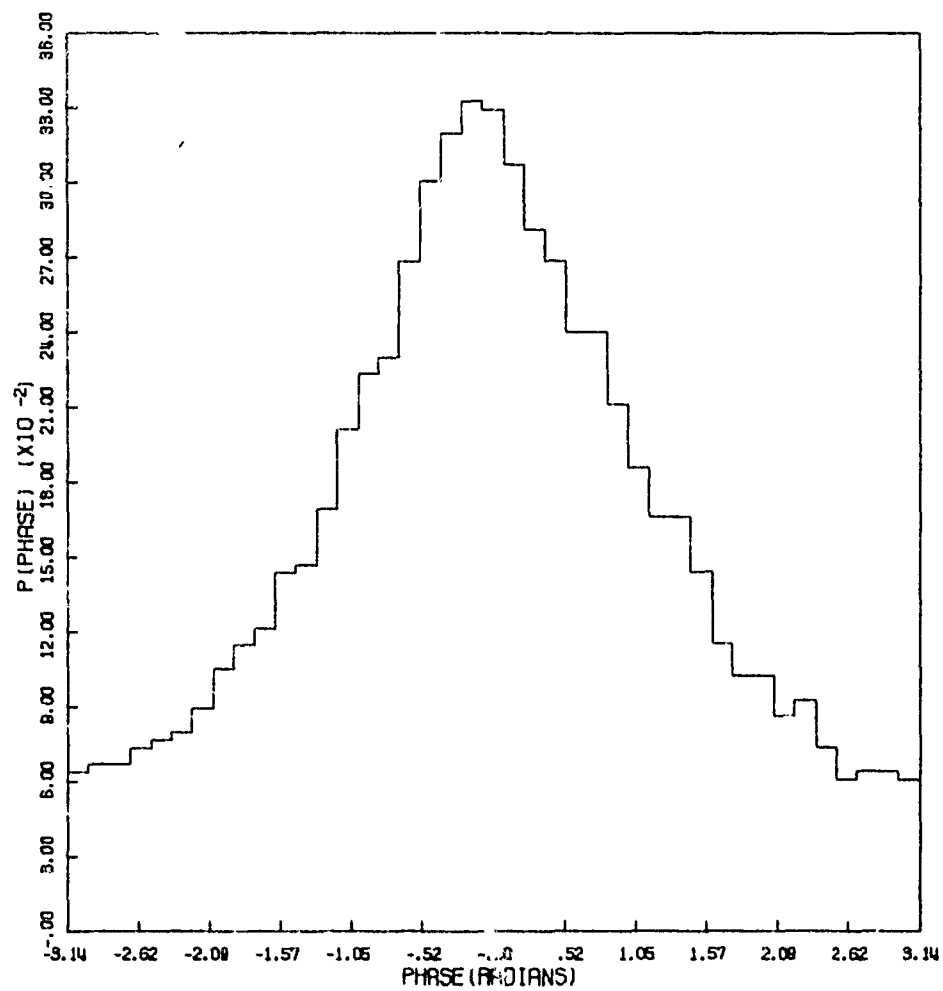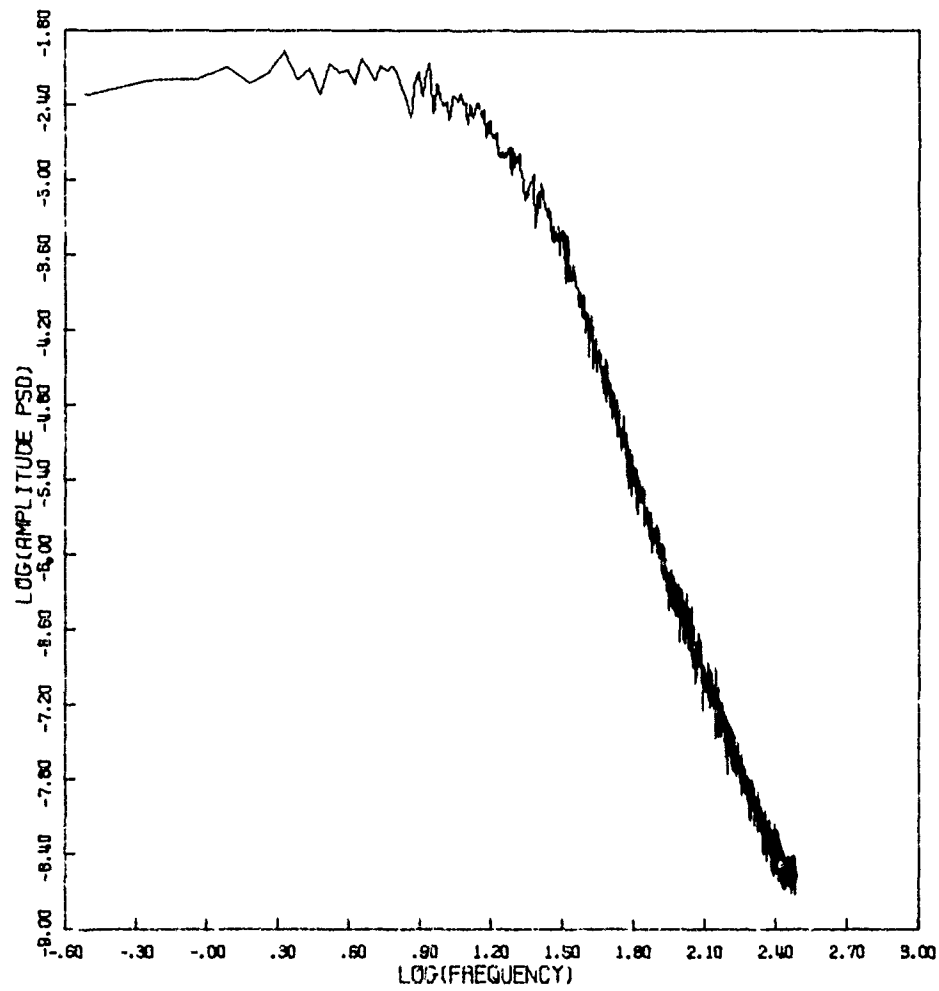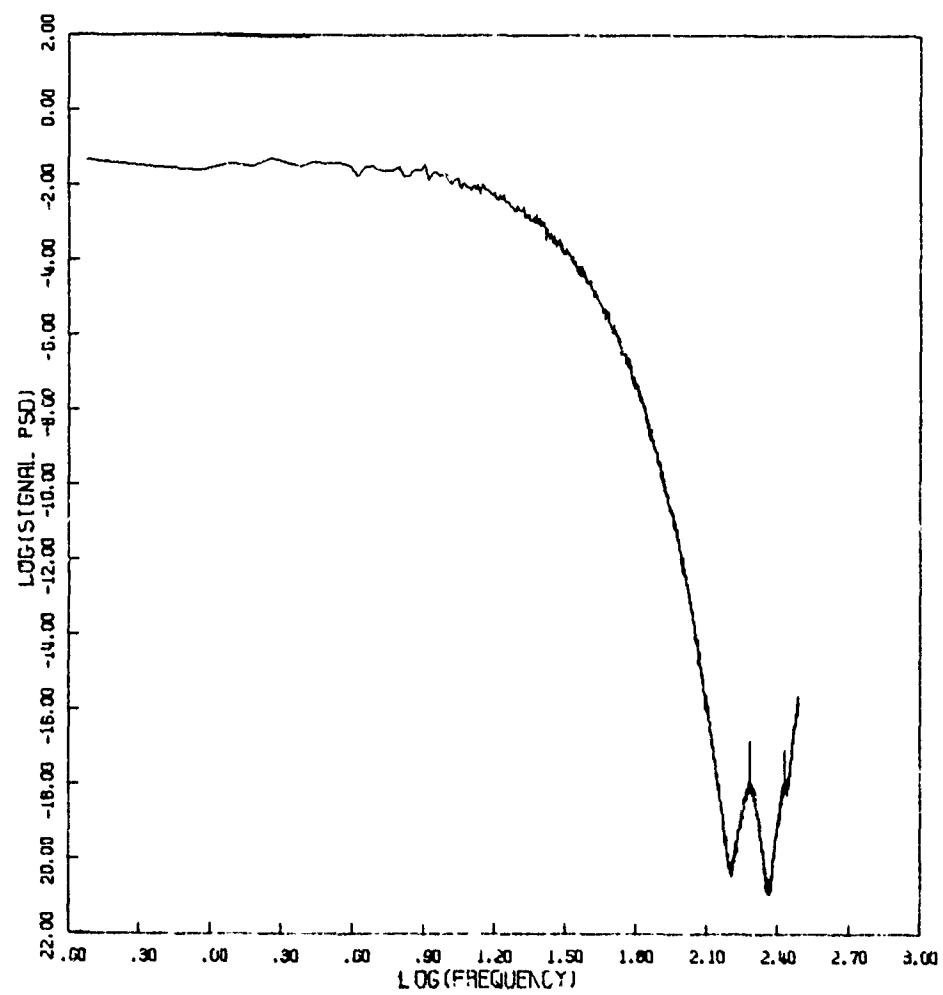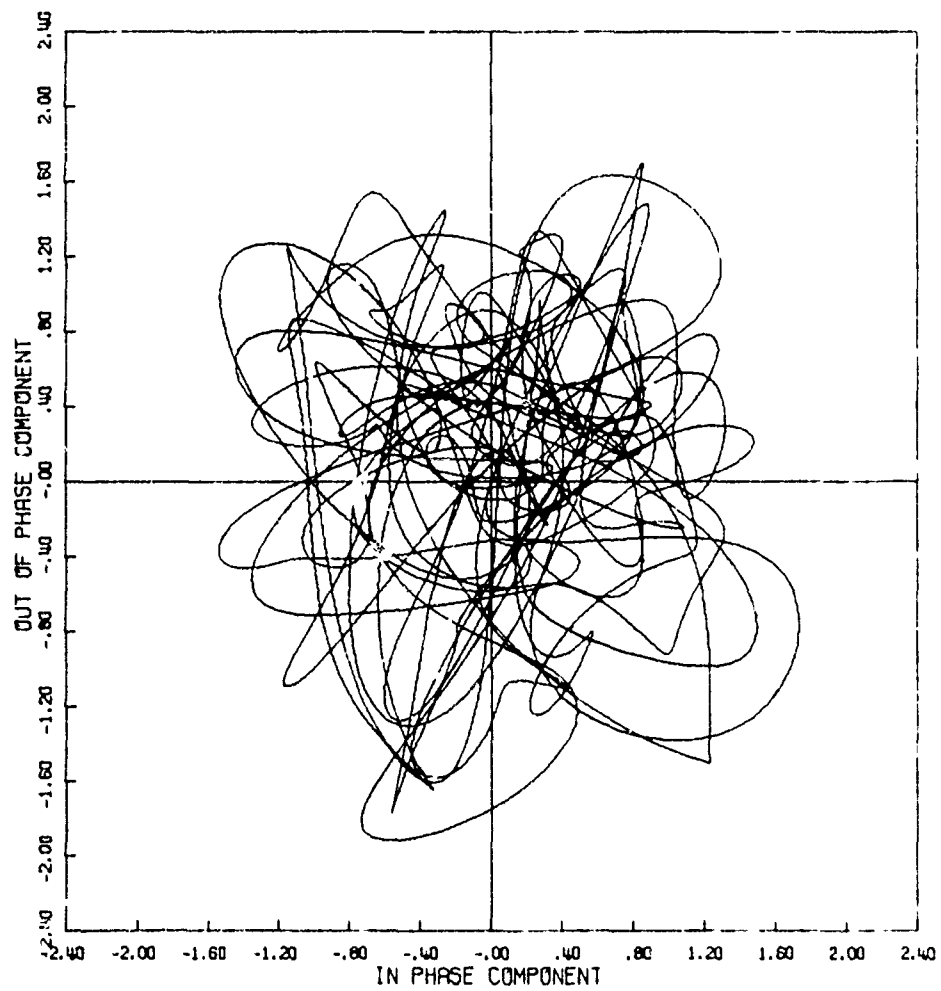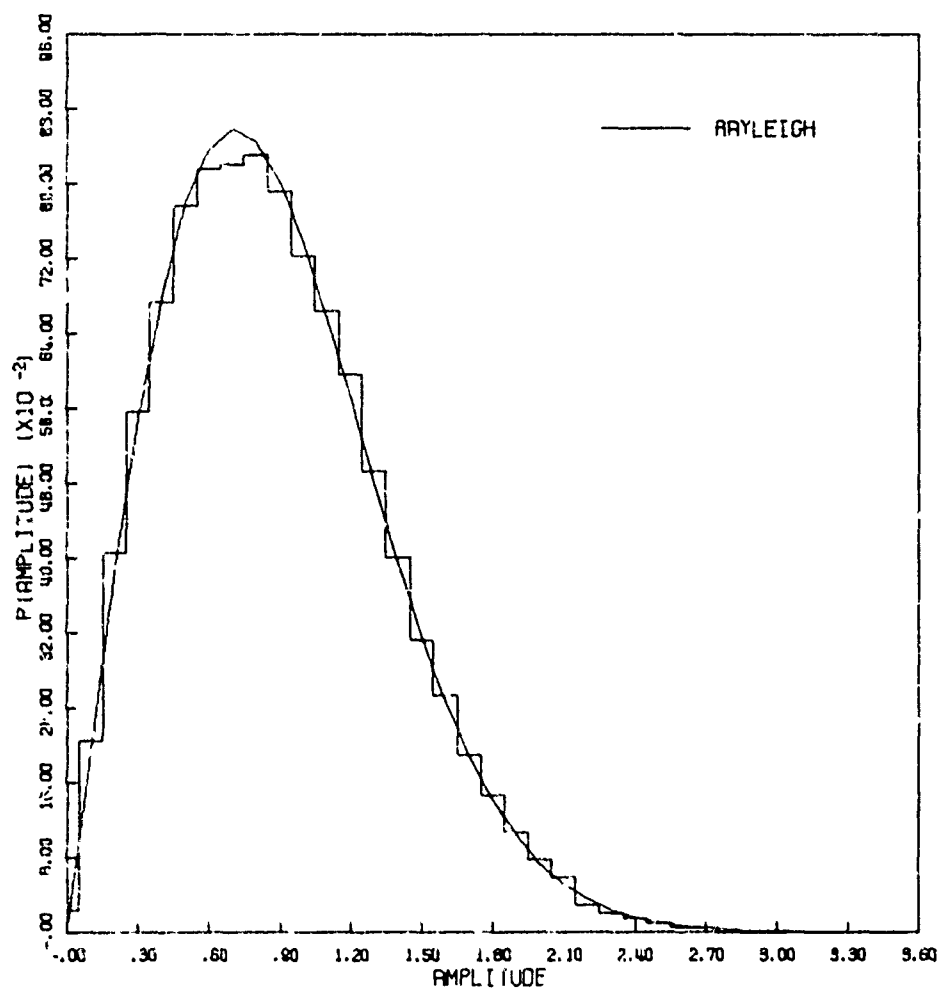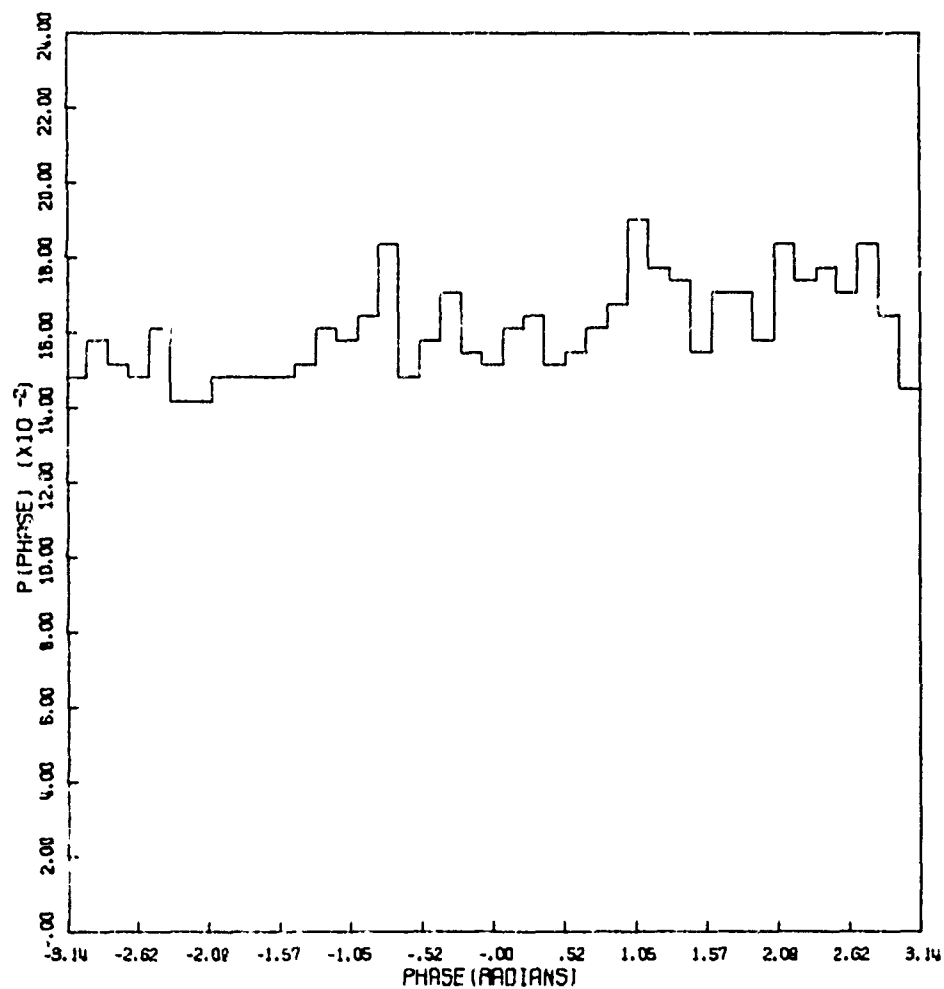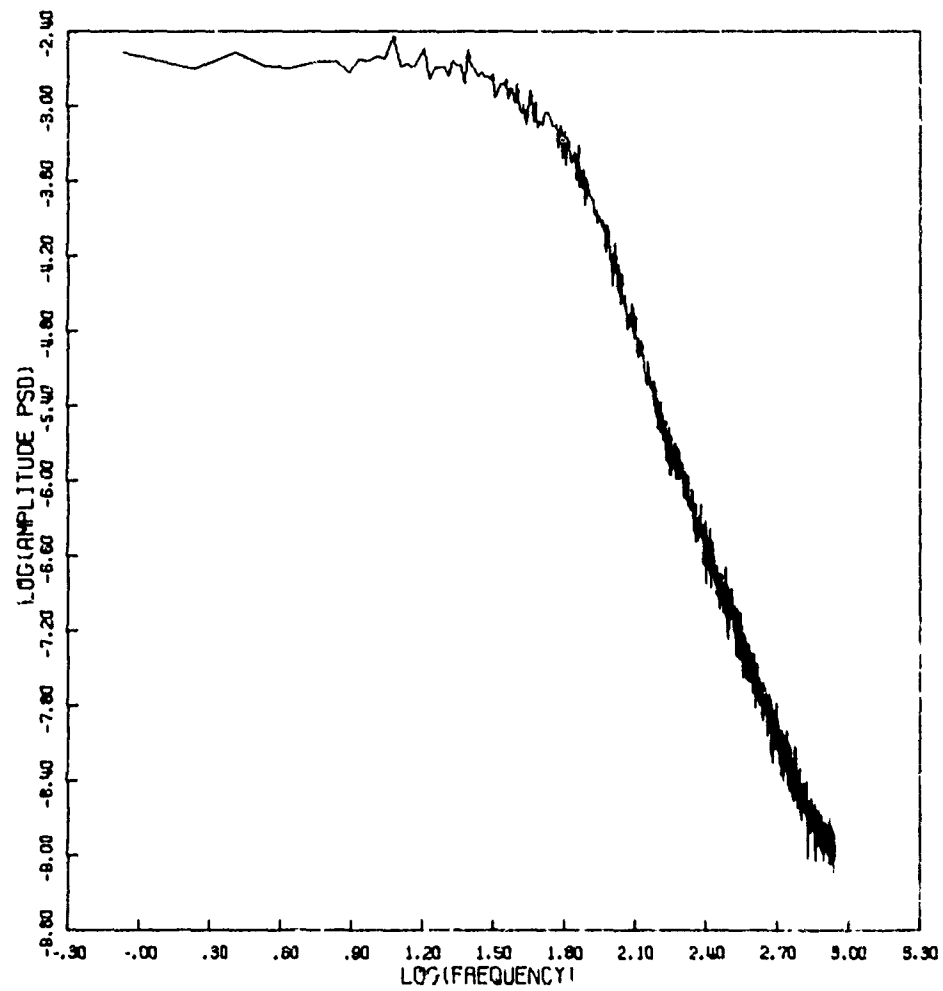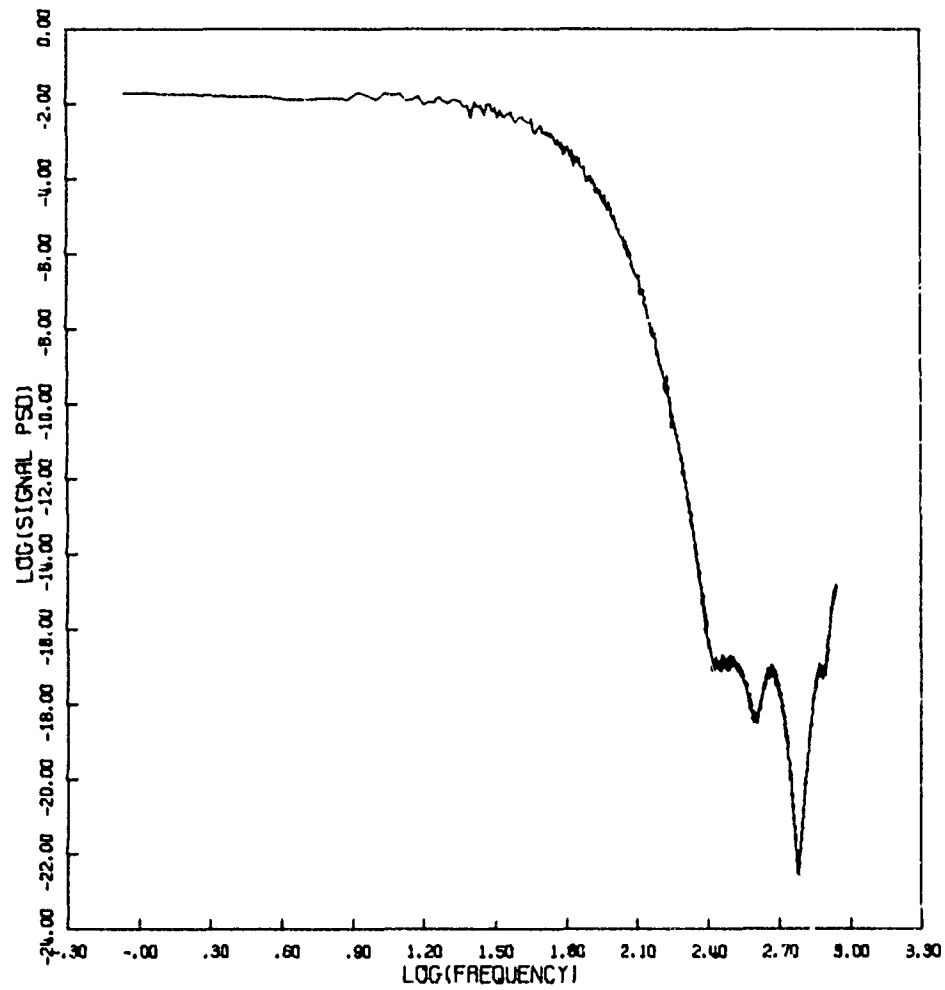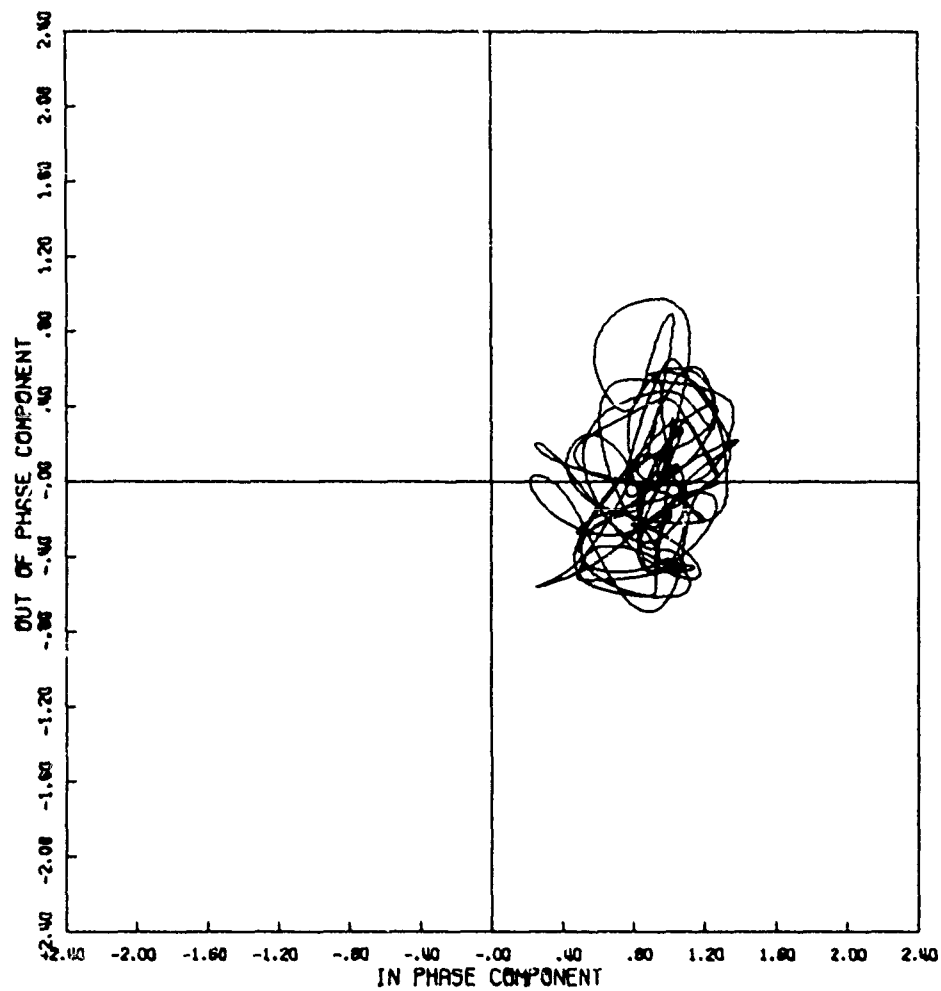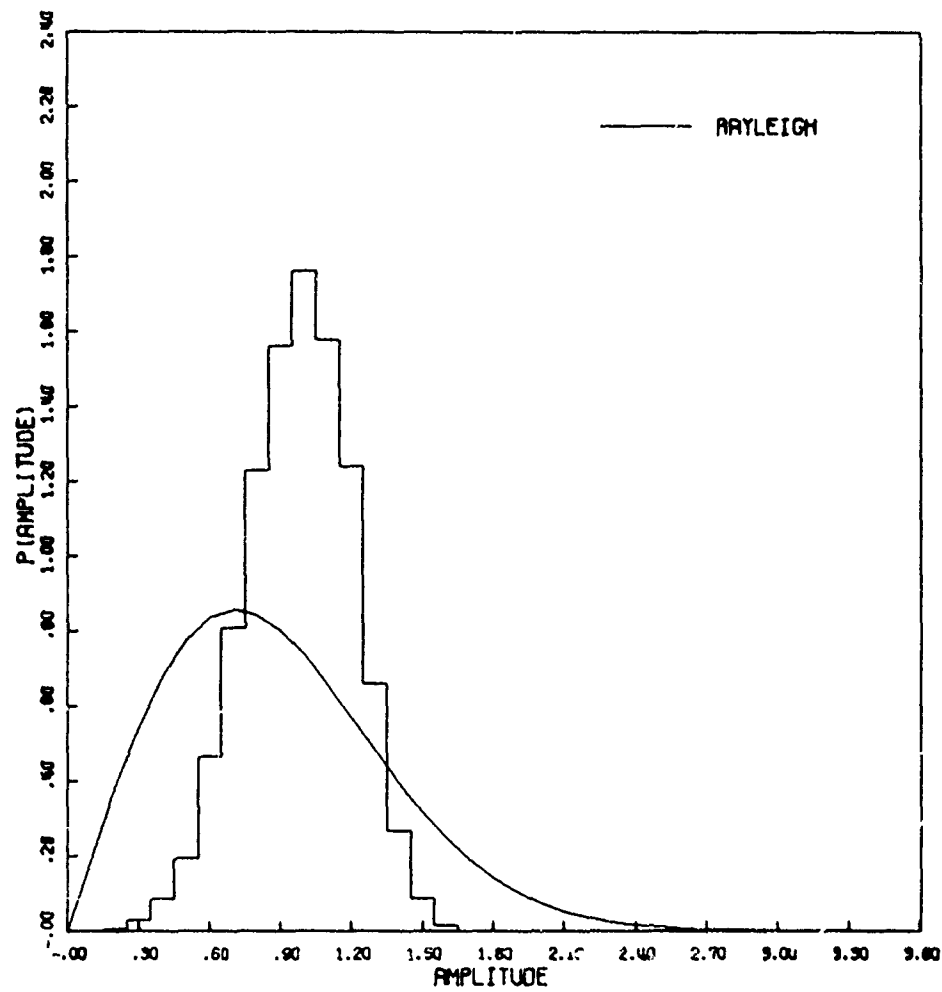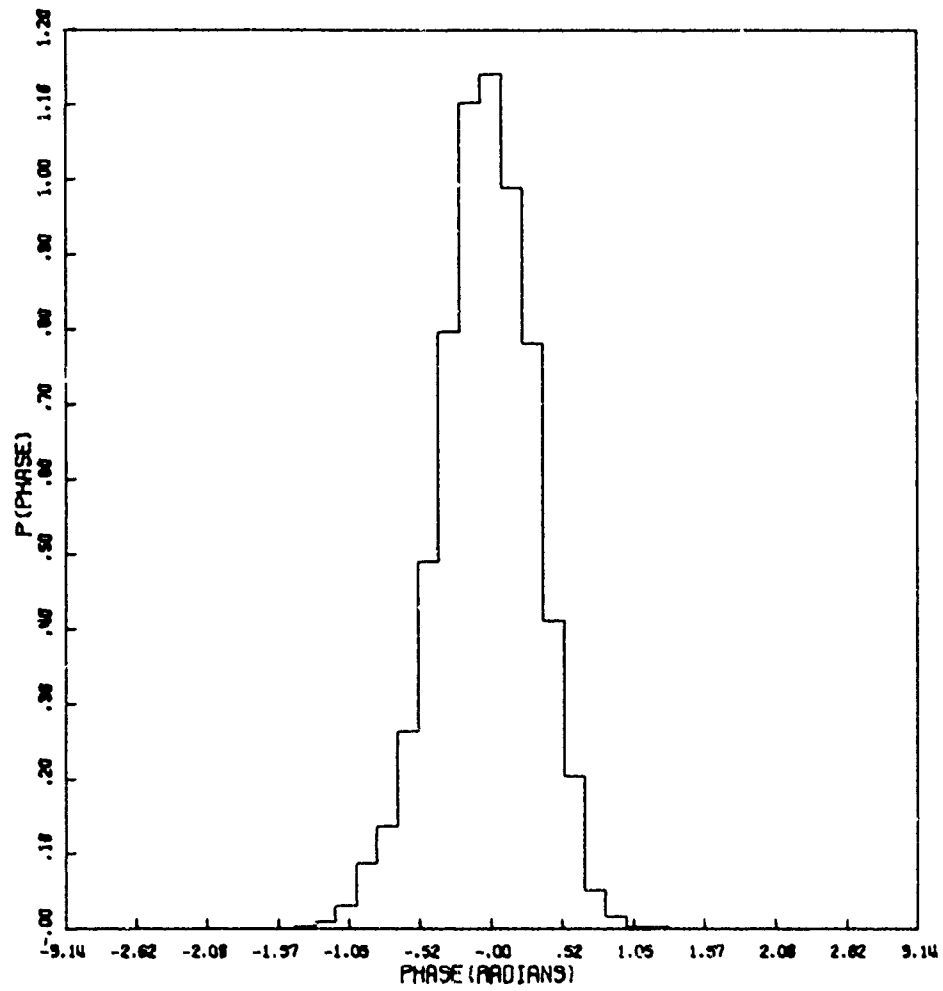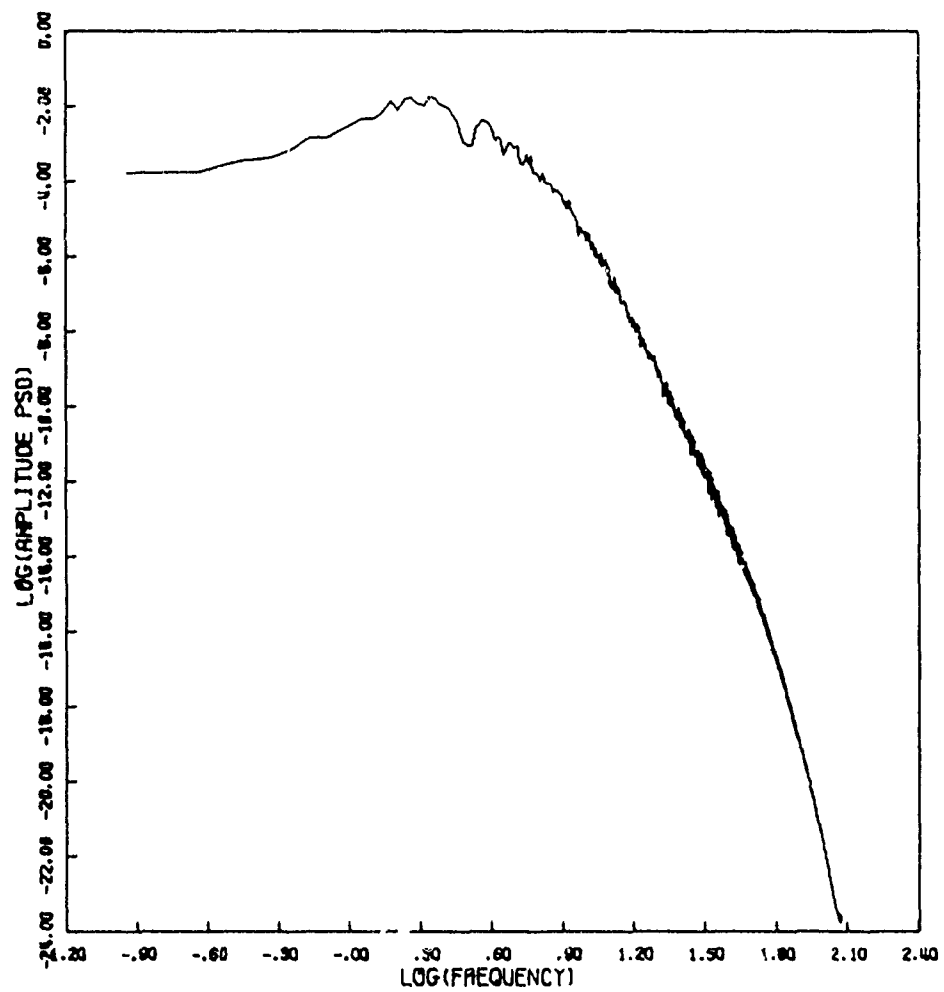
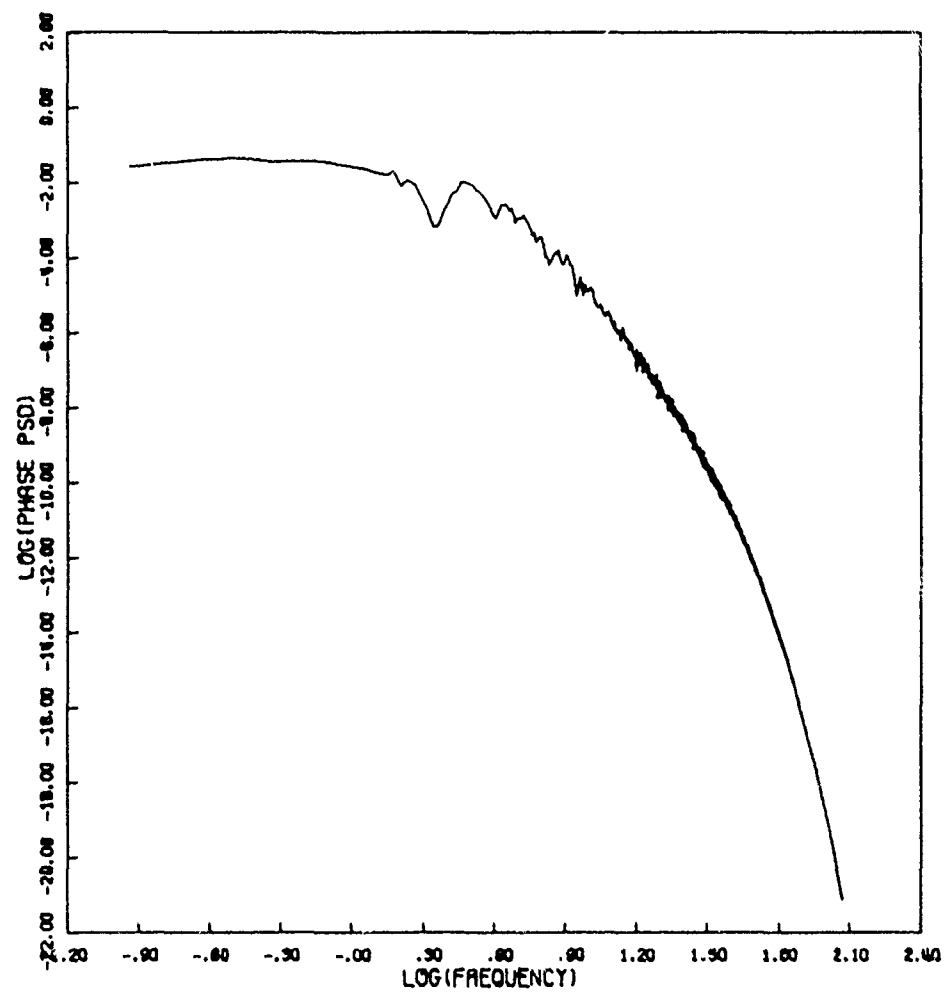Figure 59d.   Amplitude Power Spectral Density

Figure 59e.   Phase Power Spectral Density

Figure 59f. Signal Power Spectral Density

Figure 60a. Signal Phase Plot

Figure 60b. Amplitude Distribution

Figure 60c.   Phase Distribution

Figure 60d. Amplitude Power Spectral Density

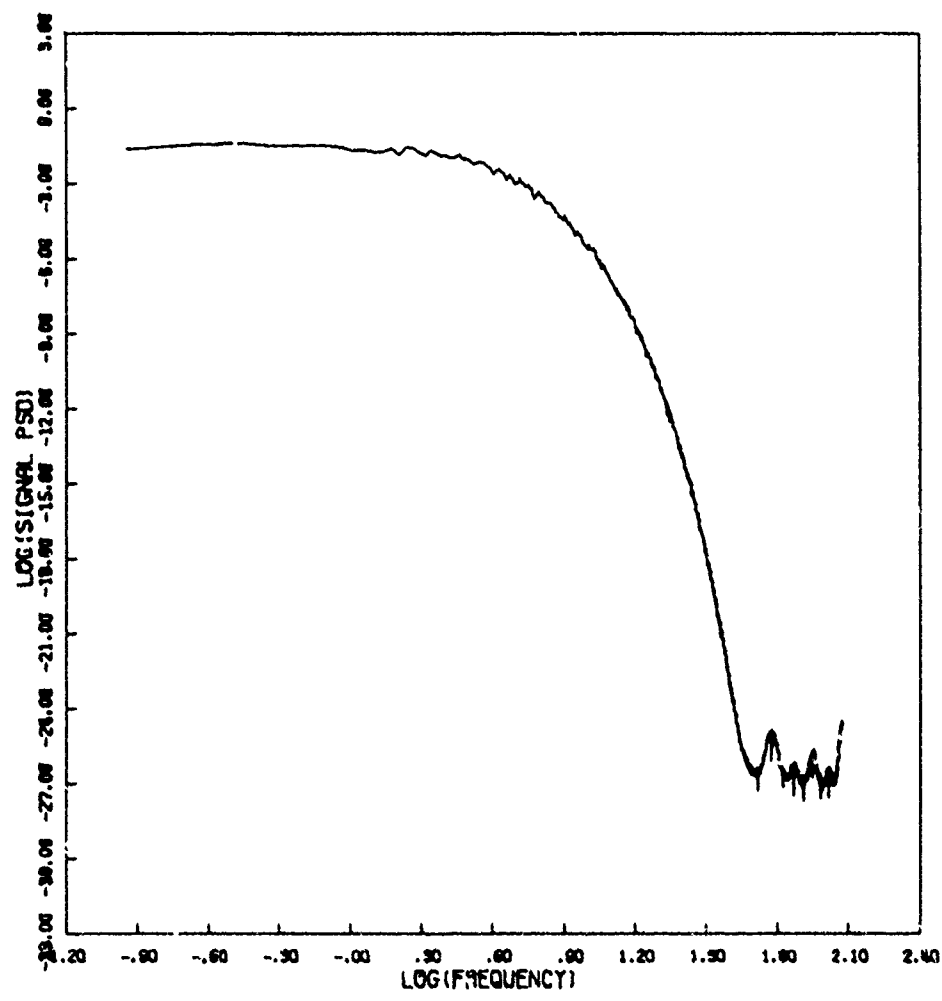Figure 60f. Signal Power Spectral Density
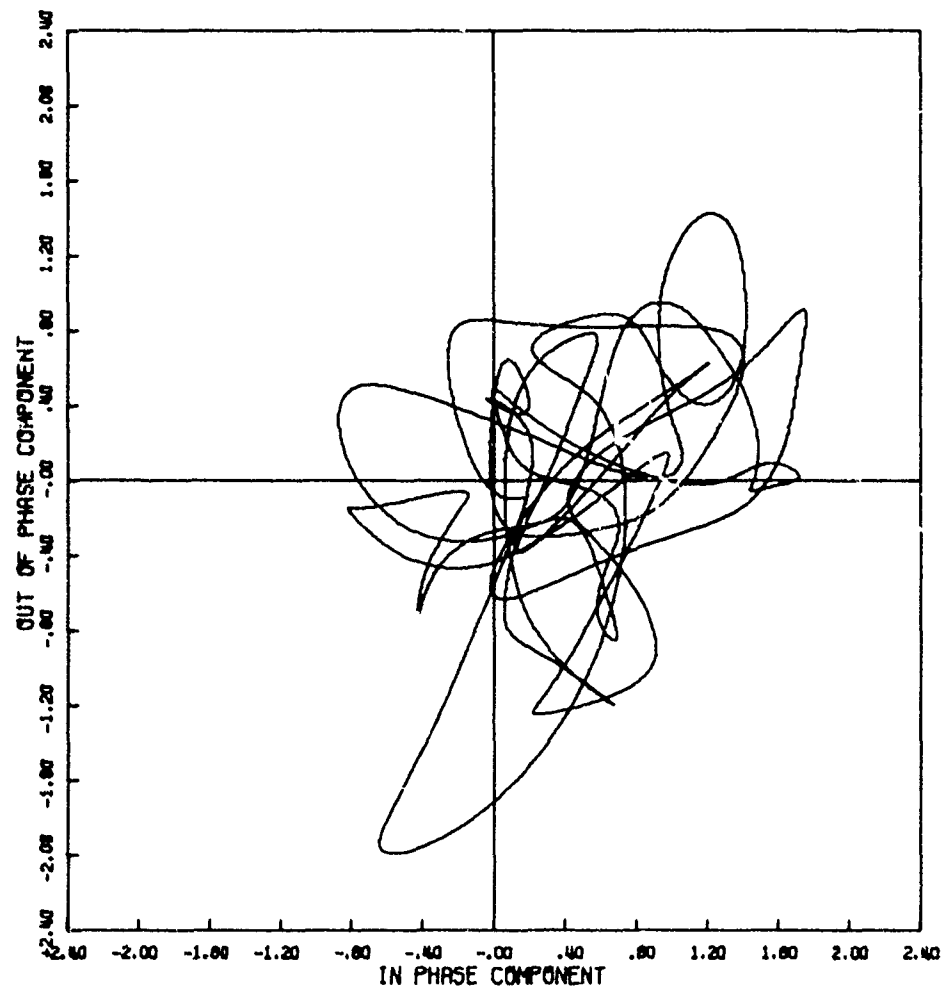
Figure 61a. Signal Phase Plot

Figure 61b. Amplitude Distribution

Figure 61c. Phase Distribution

Figure 61d. Amplitude Power Spectral Density

Figure 61f. Signal Power Spectral Density

Figure 62a. Signal Phase Plot
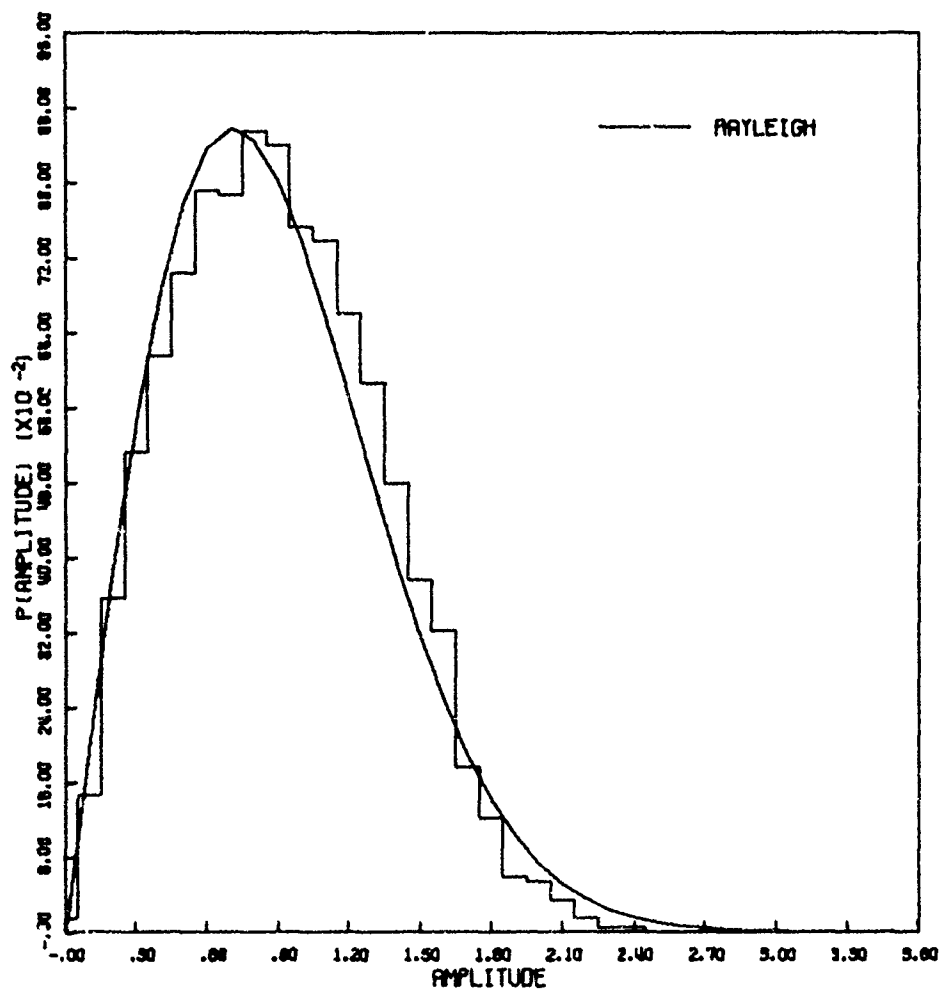
Figure 62b. Amplitude Distribution

Figure 62c.   Phase Distribution

Figure 62d.   Amplitude Power Spectral Density

Figure 62e.   Phase Power Spectral Density

Figure 62f. Signal Power Spectral Density

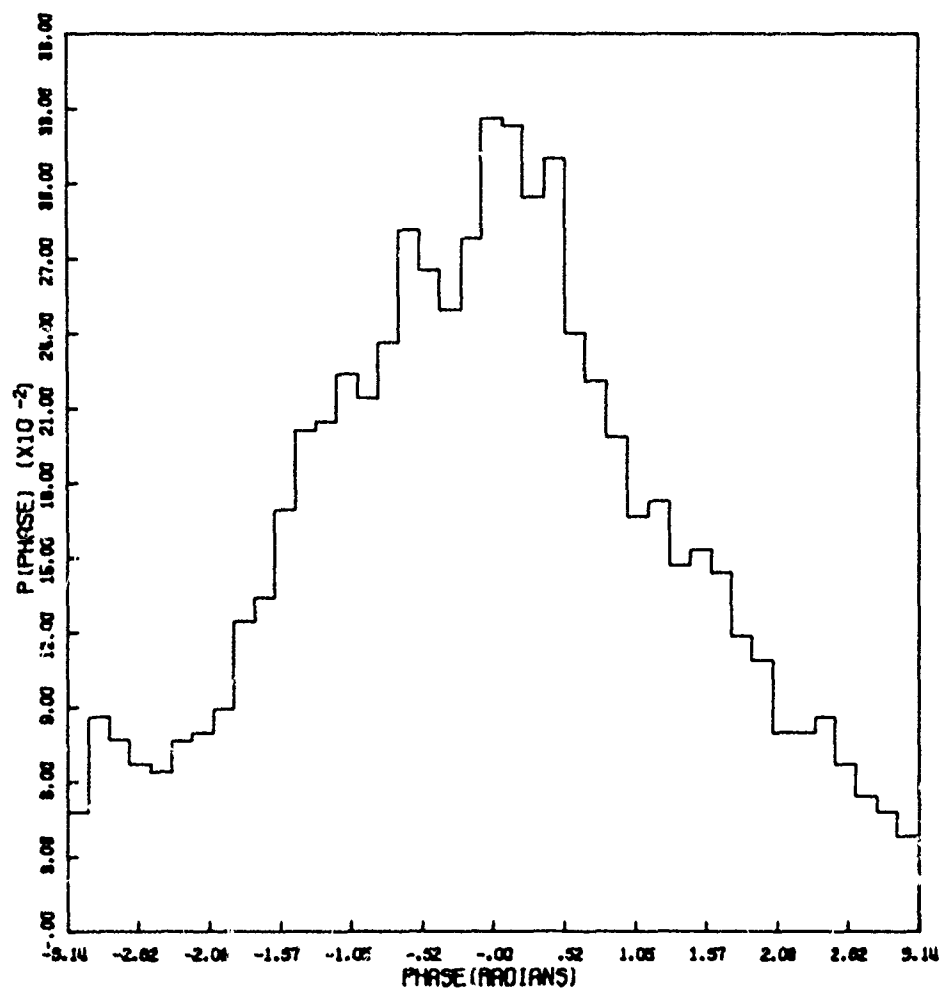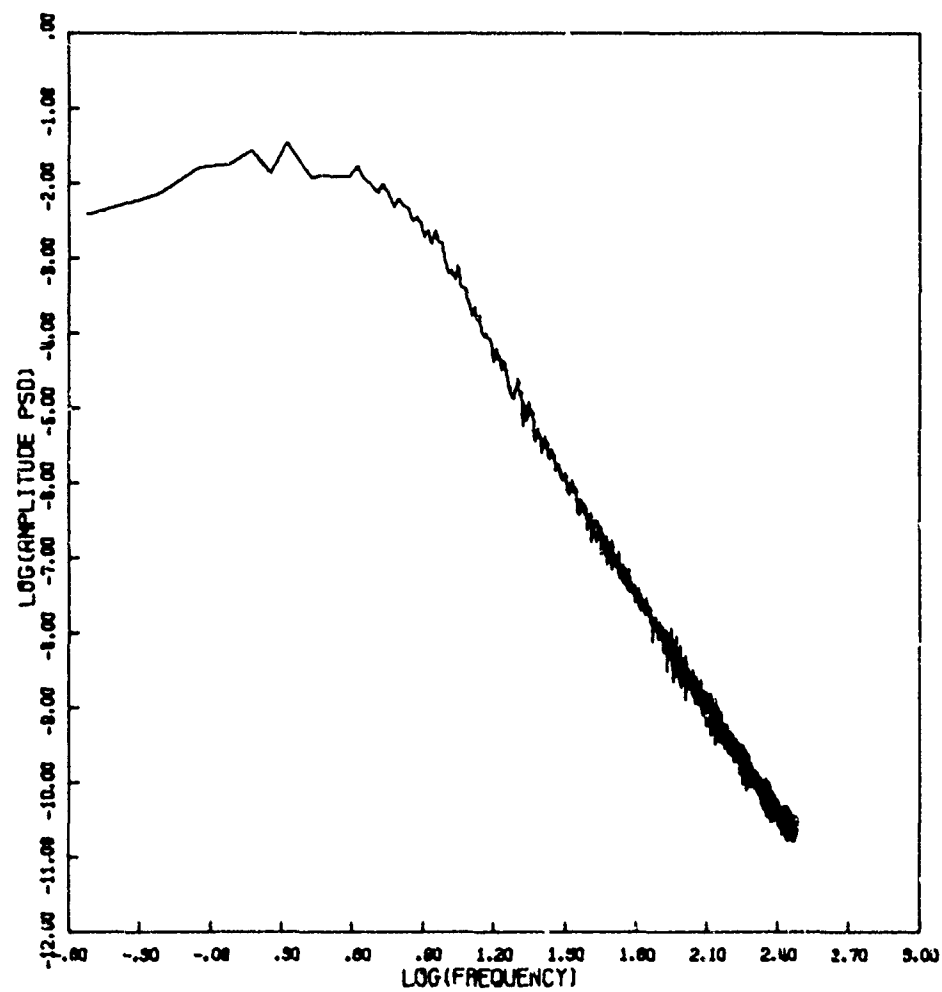Figure 63a. Signal Phase Plot

Figure 63b. Amplitude Distribution

Figure 63c. Phase Distribution

Figure 63d. Amplitude Power Spectral Density
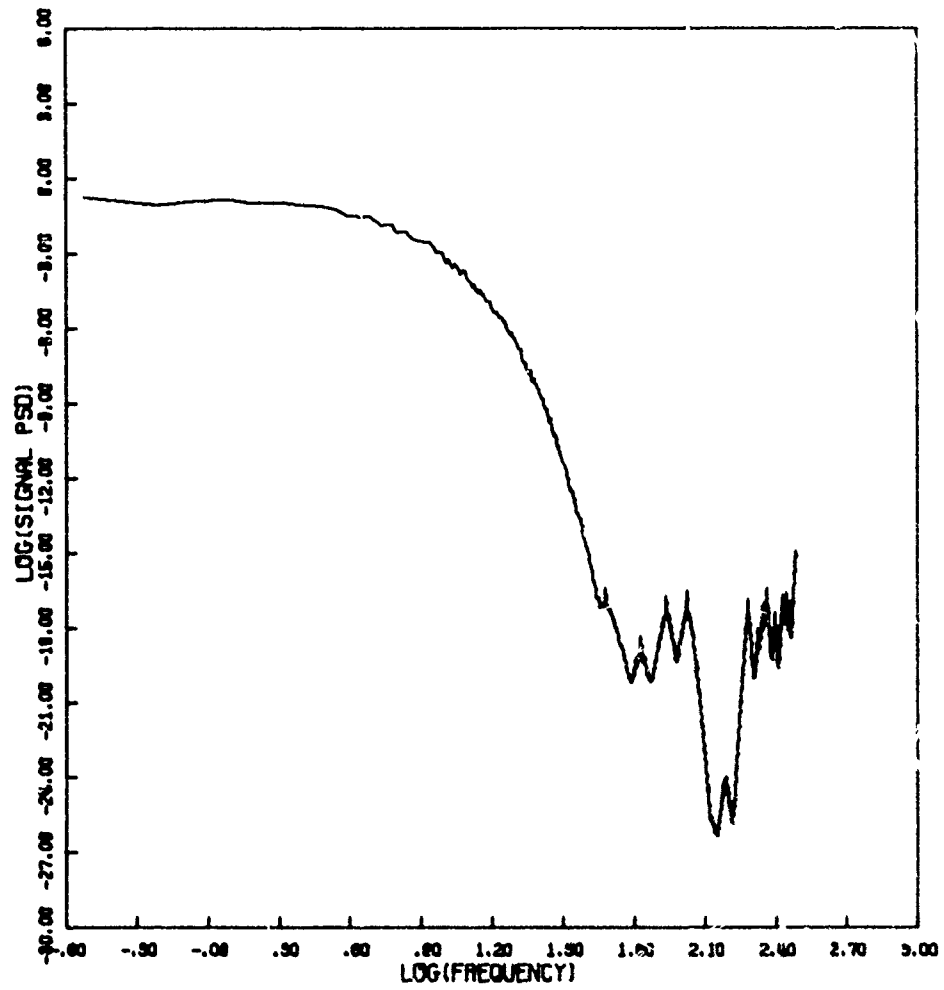
Figure 63f. Phase Power Spectral Density

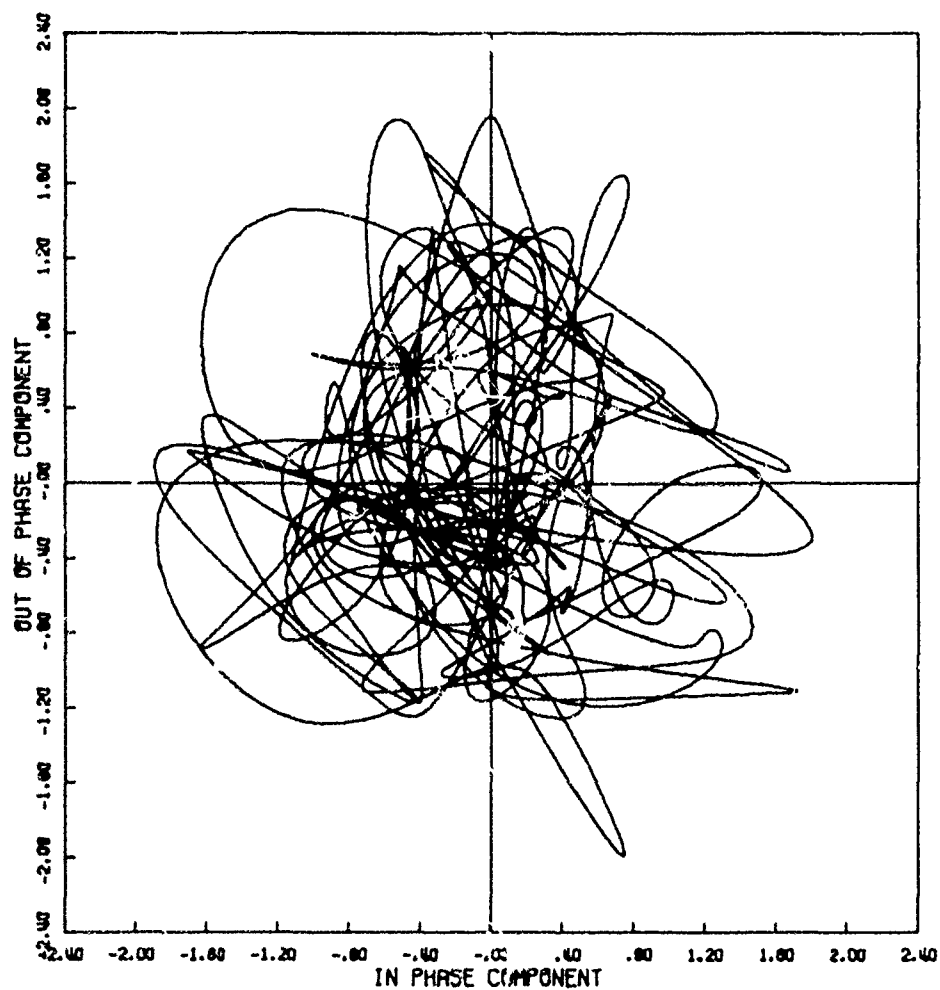Figure 63f.   Signal Power Spectral Density
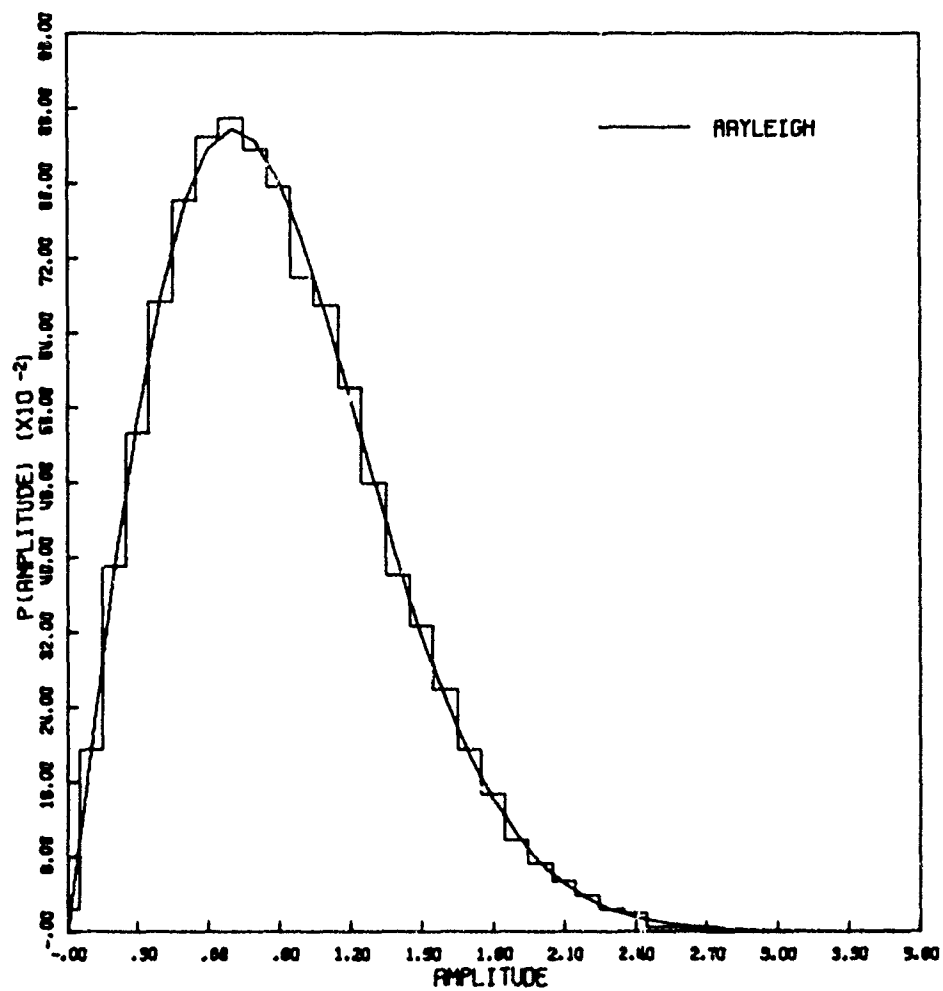
Figure 64a. Signal Phase Plot

Figure 64b. Amplitude Distribution

Figure 64c. Phase Distribution

Figure 64d.   Amplitude Power Spectral Density

Figure 64e.   Phase Power Spectral Density

Figure 64f. Signal Power Spectral Density

Figure 65a. Signal Phase Plot

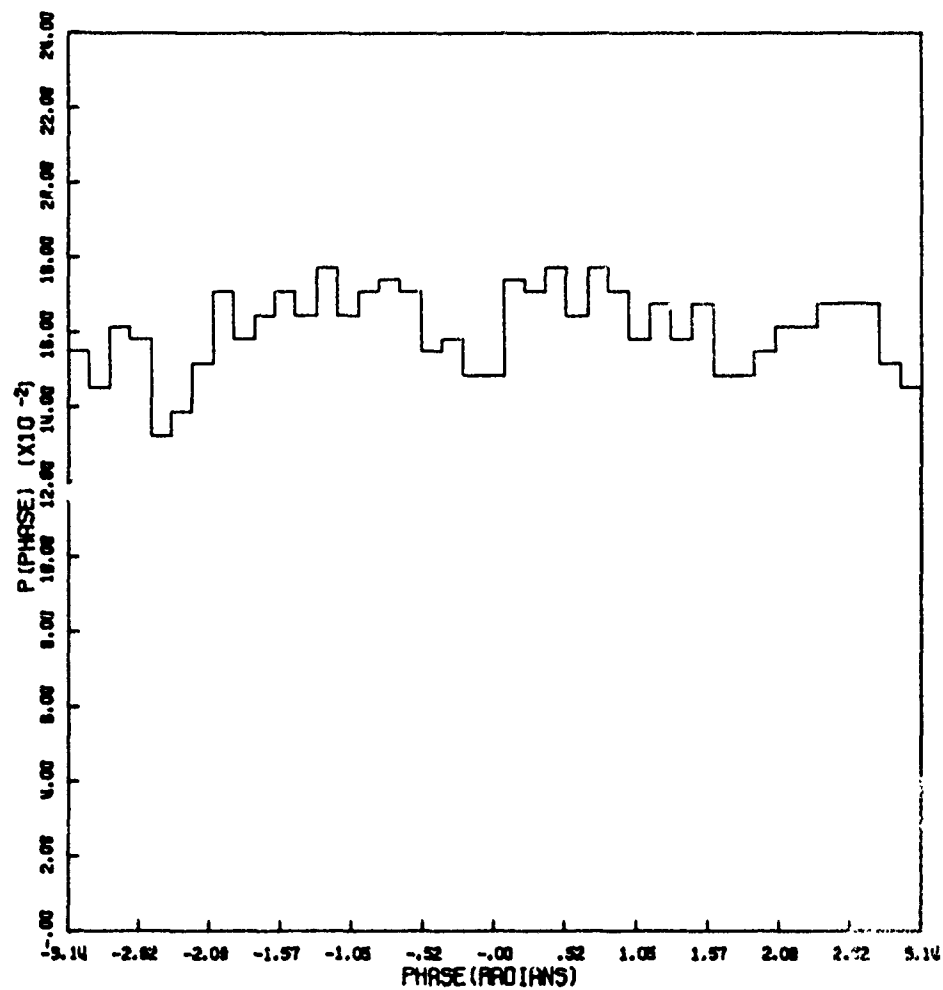Figure 65b. Amplitude Distribution
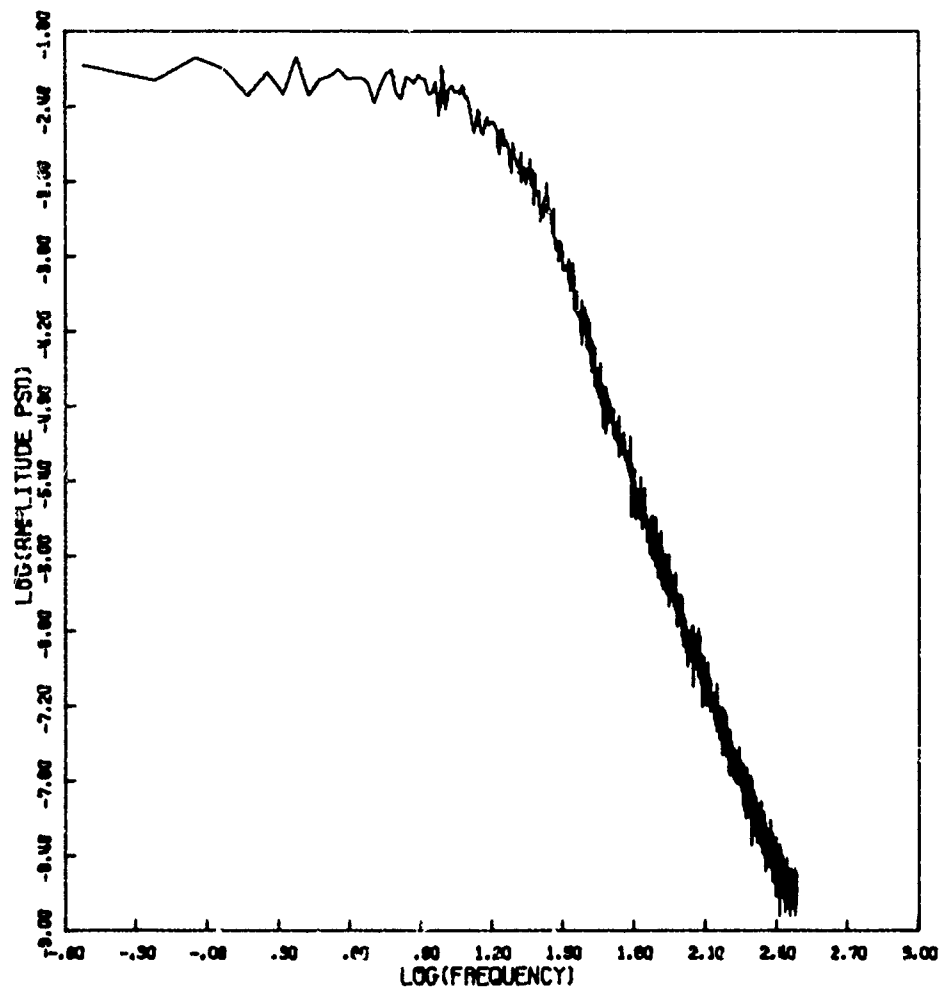
Figure 65c. Phase Distribution

Figure 65d. Amplitude Power Spectral Density
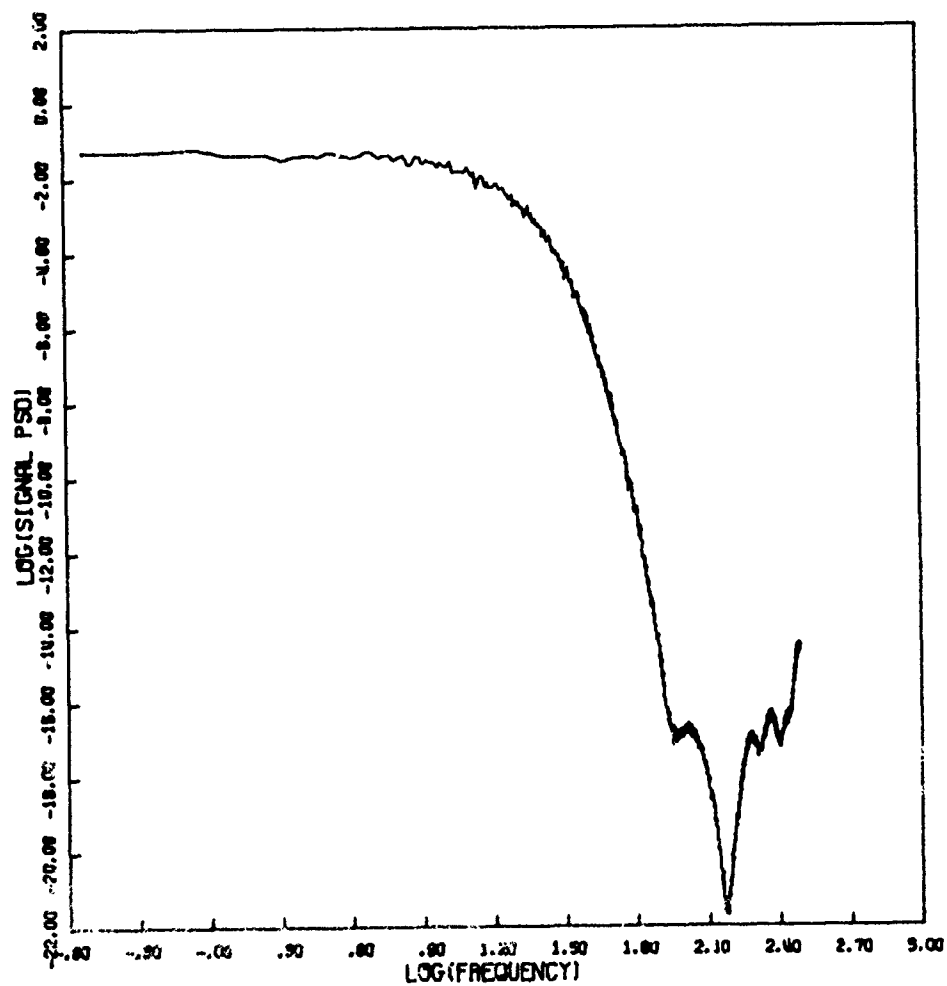
Figure 65e. Signal Power Spectral Density
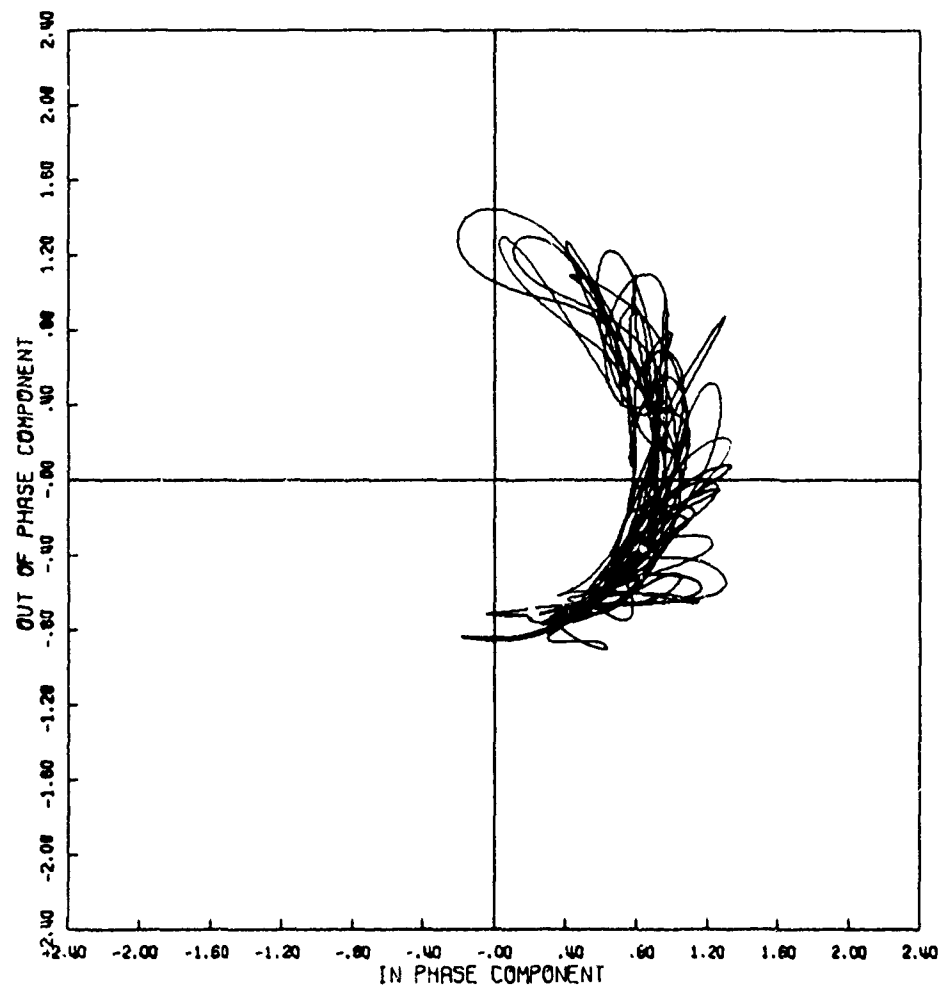
Figure 66a. Signal Phase Plot
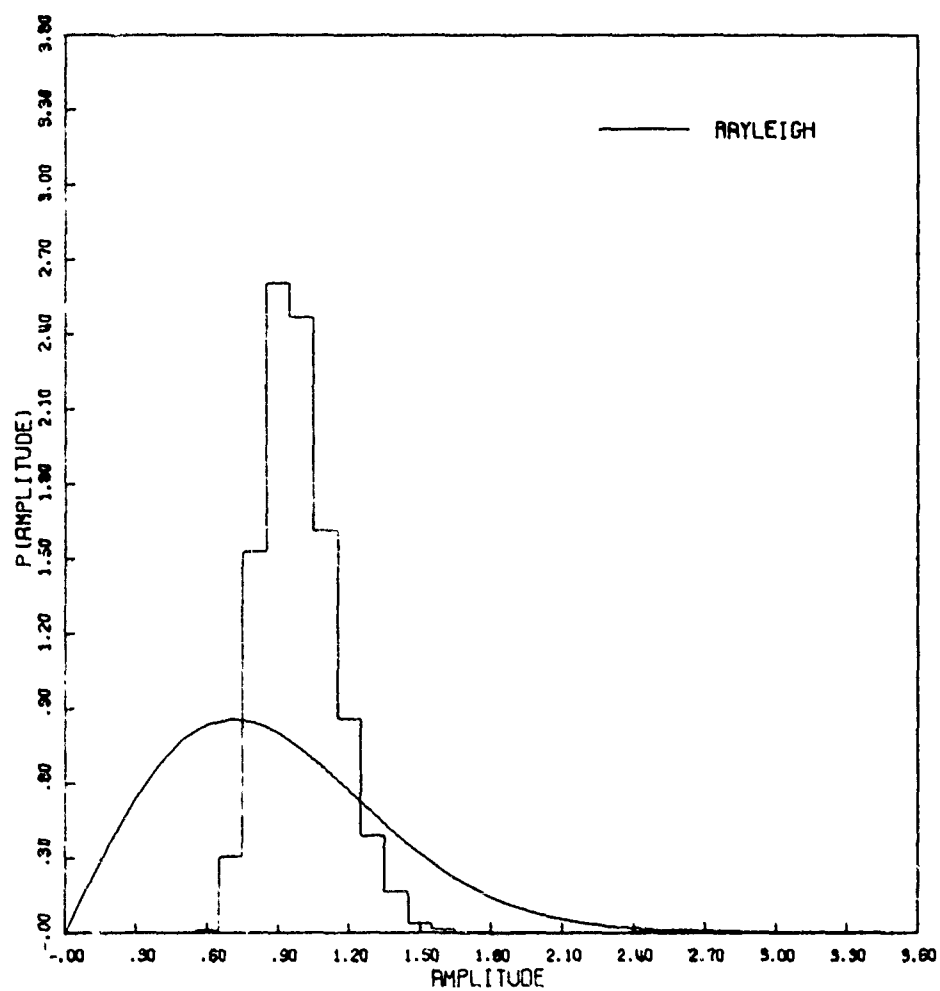
Figure 66b. Amplitude Distribution

Figure 66c.   Phase Distribution

Figure 66d. Amplitude Power Spectral Density

Figure 66e. Signal Power Spectral Density

Figure 67a. Signal Phase Plot

Figure 67b. Amplitude Distribution

Figure 67c.   Phase Distribution

Figure 67d. Amplitude Power Spectral Density

Figure 67e.   Signal Power Spectral Density

Figure 68a. Signal Phase Plot
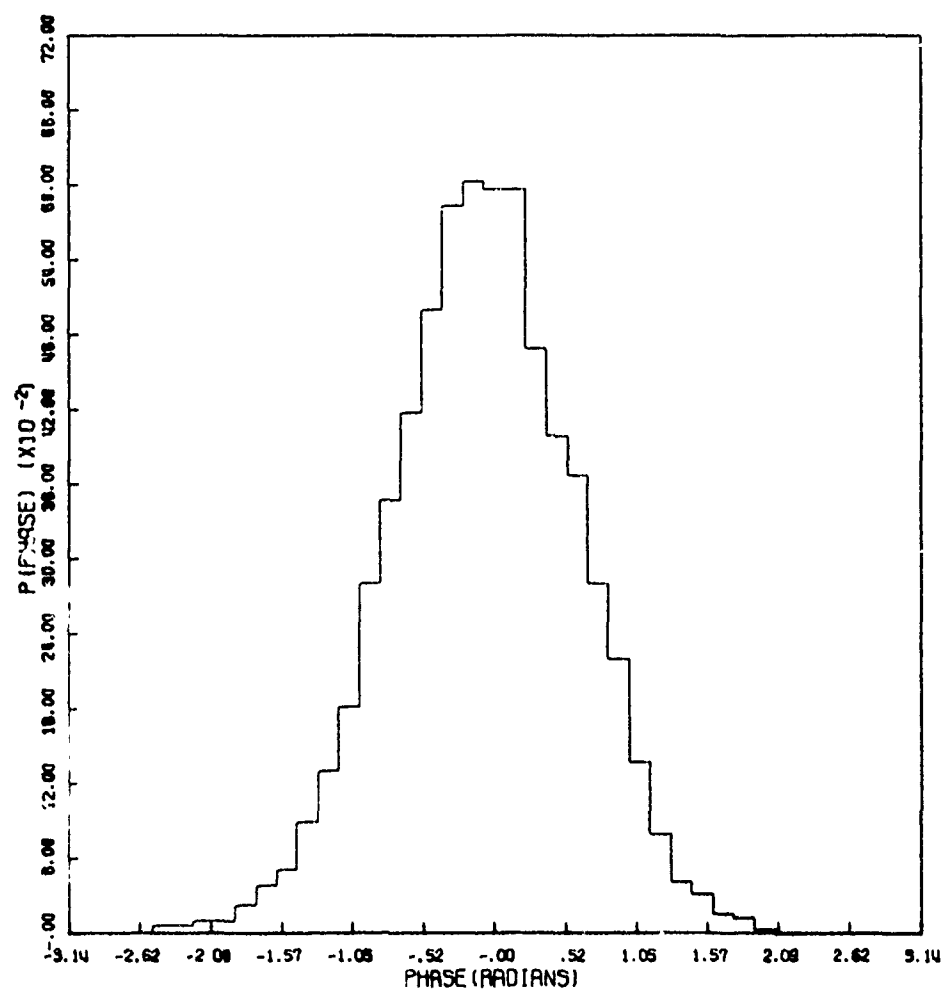
Figure 68b. Amplitude Distribution
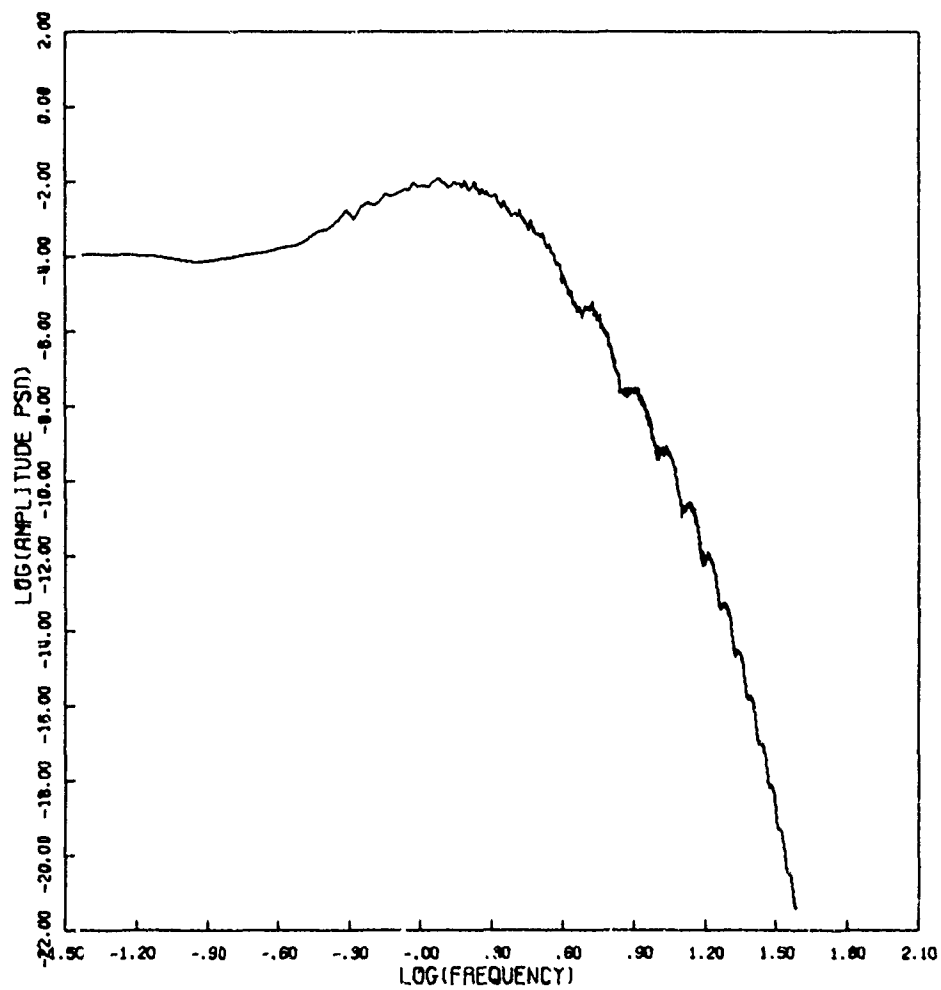
Figure 68c. Phase Distribution

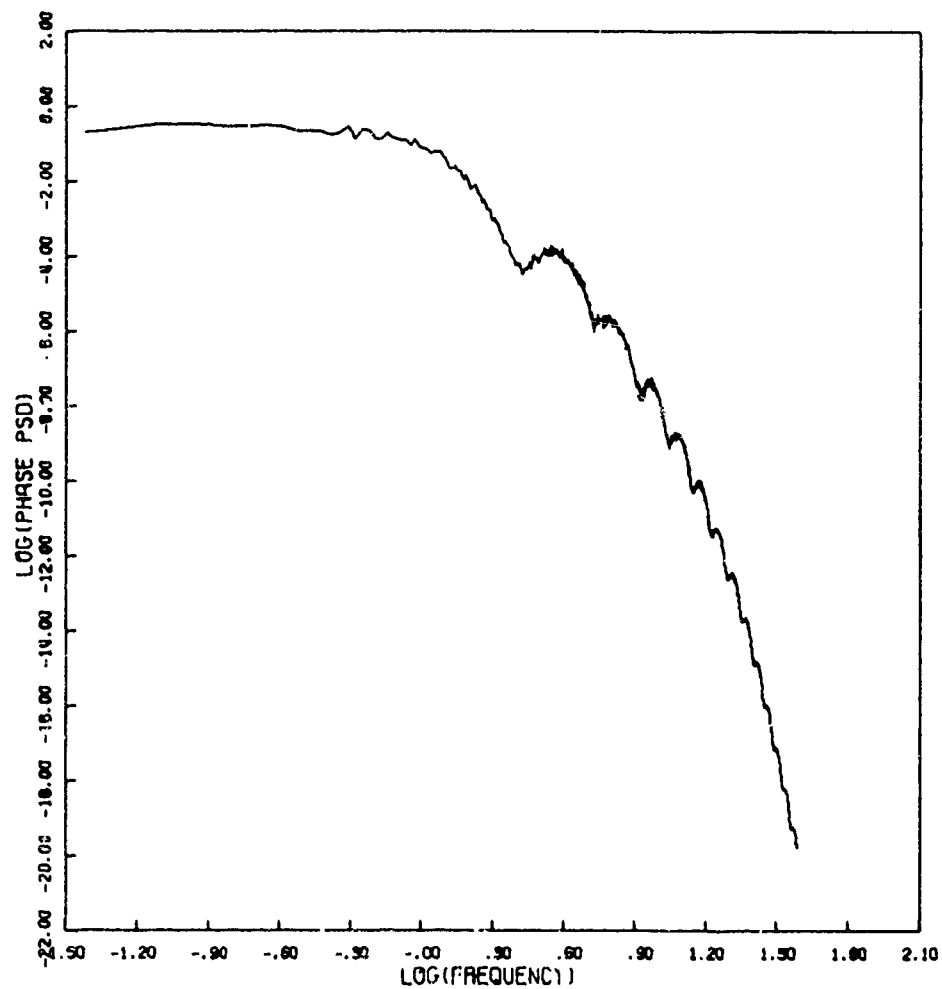Figure 68d.   Amplitude Power Spectral Density

Figure 68e. Phase Power Spectral Density
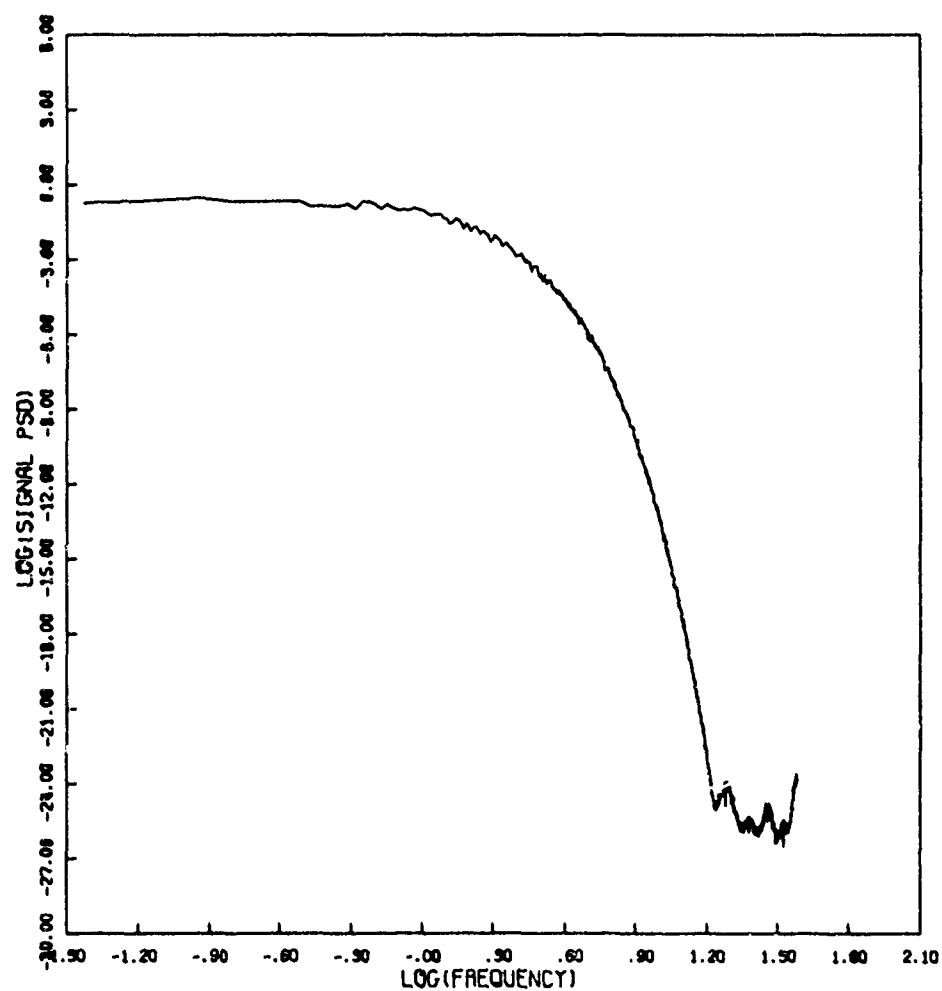
Figure 68f. Signal Power Spectral Density

Figure 69a. Signal Phase Plot

Figure 69b. Amplitude Distribution

Figure 69c. Phase Distribution

Figure 69d. Amplitude Power Spectral Density

Figure 69e.   Phase Power Spectral Density
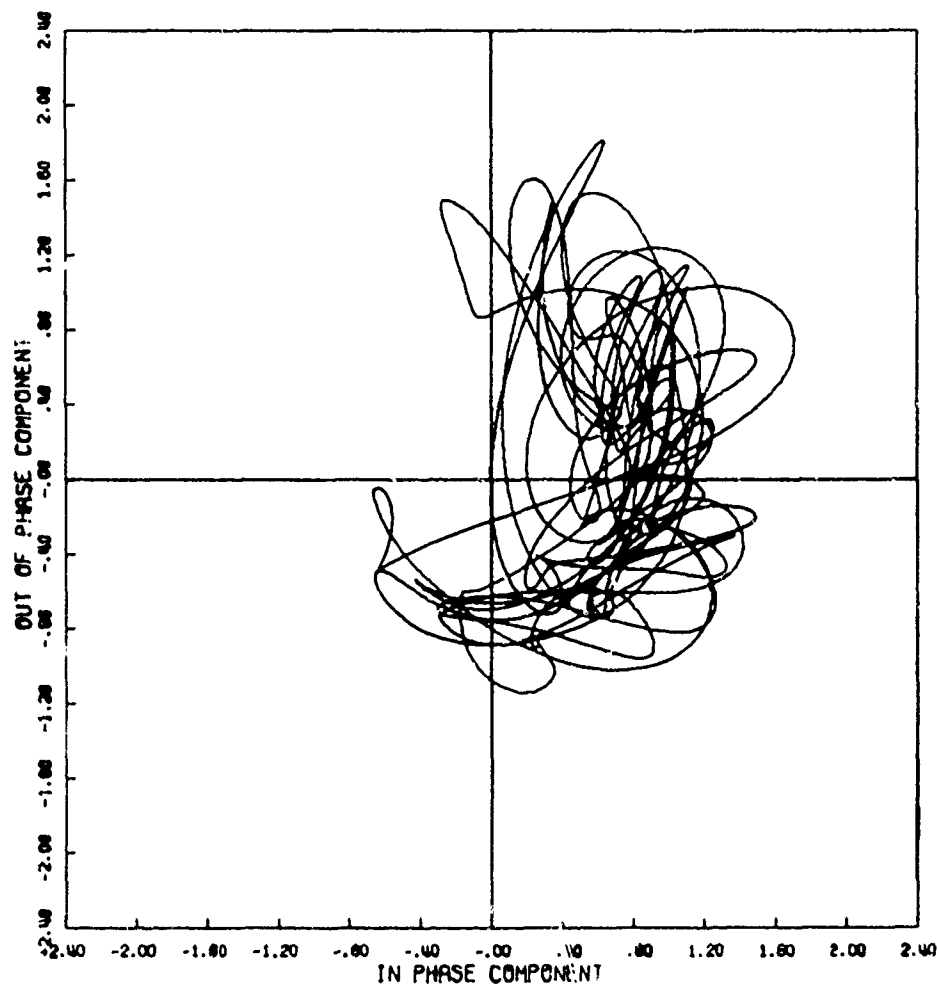
Figure 69f. Signal Power Spectral Density
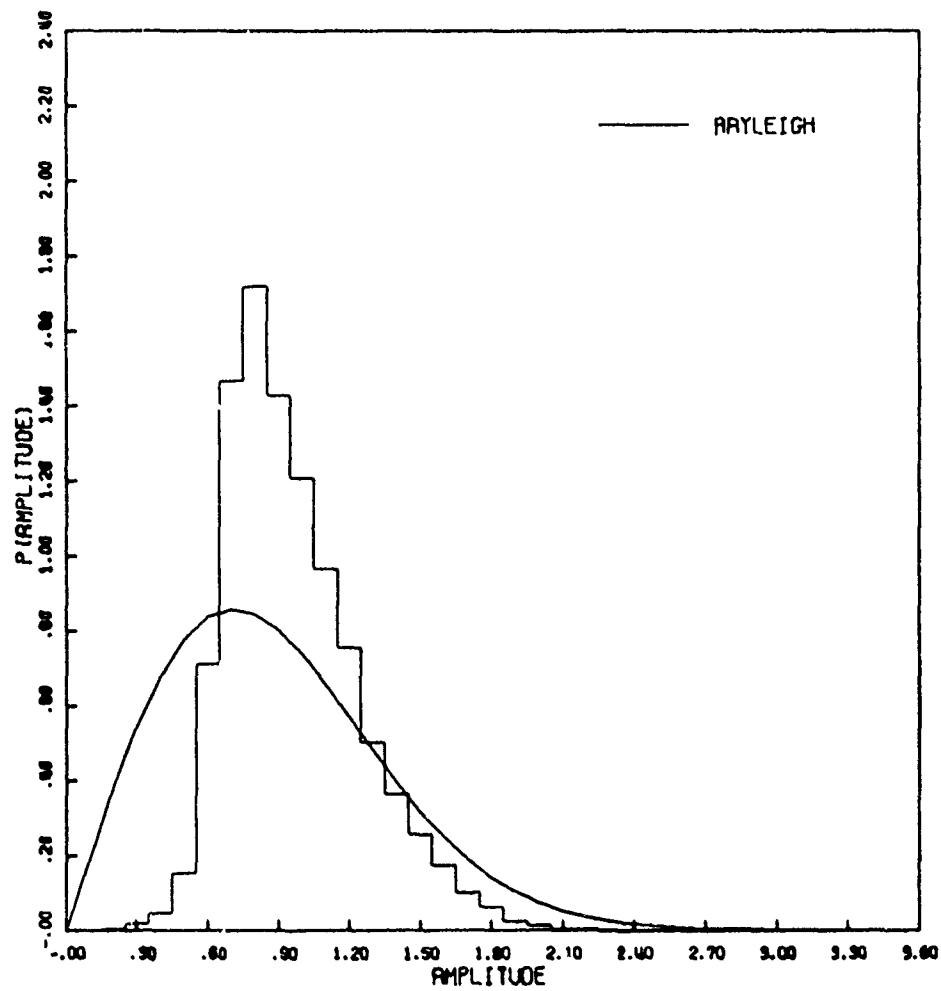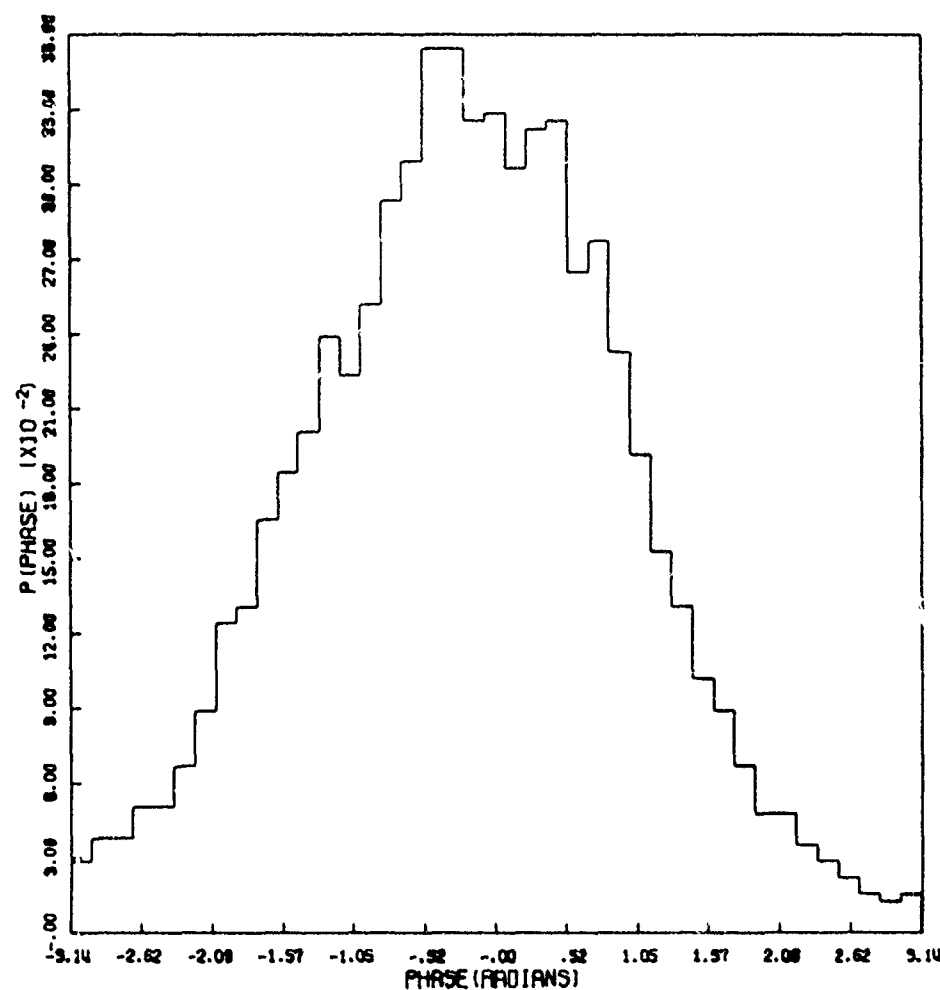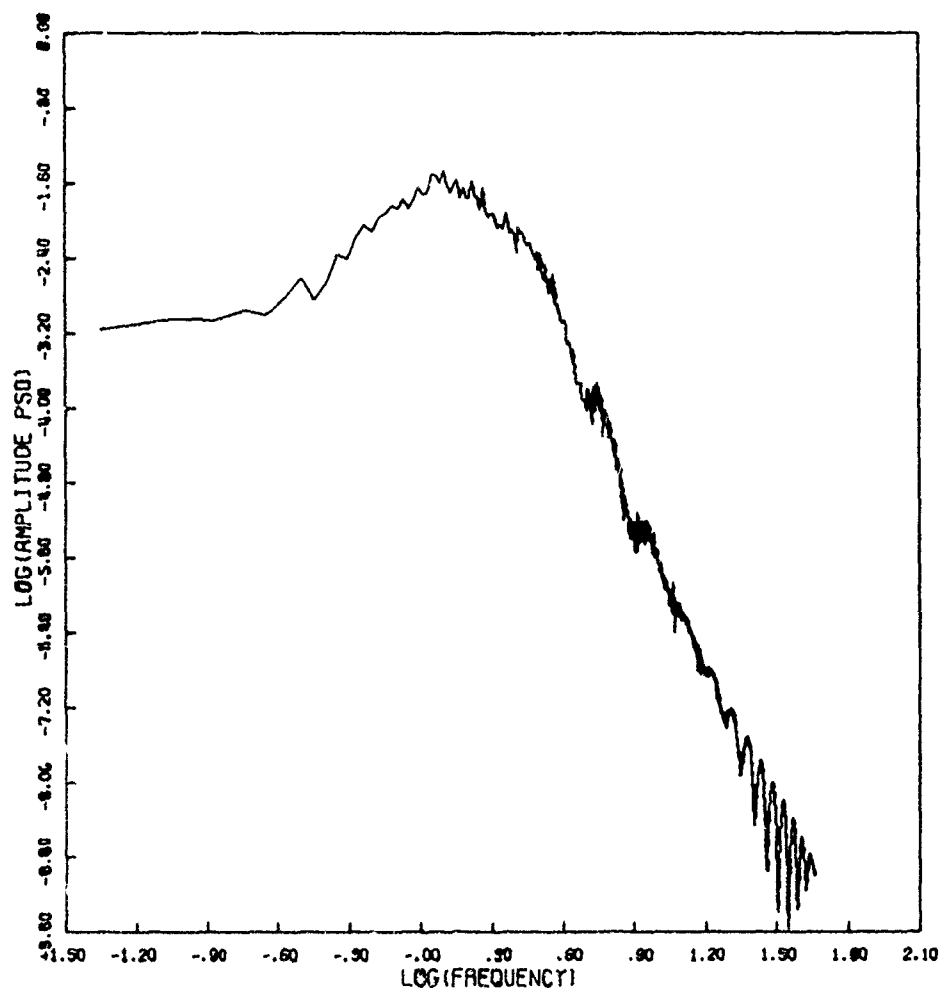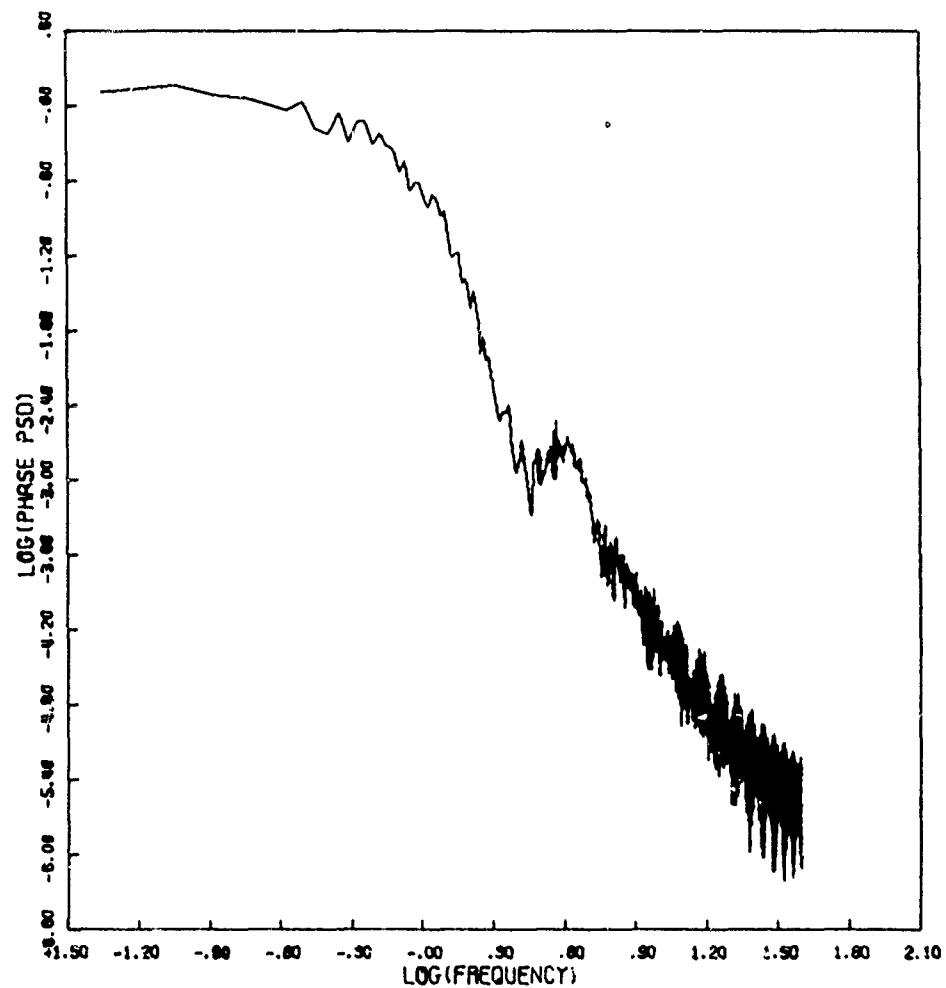
Figure 70a. Signal Phase Plot

Figure 70b. Amplitude Distribution

Figure 70c. Phase Distribution
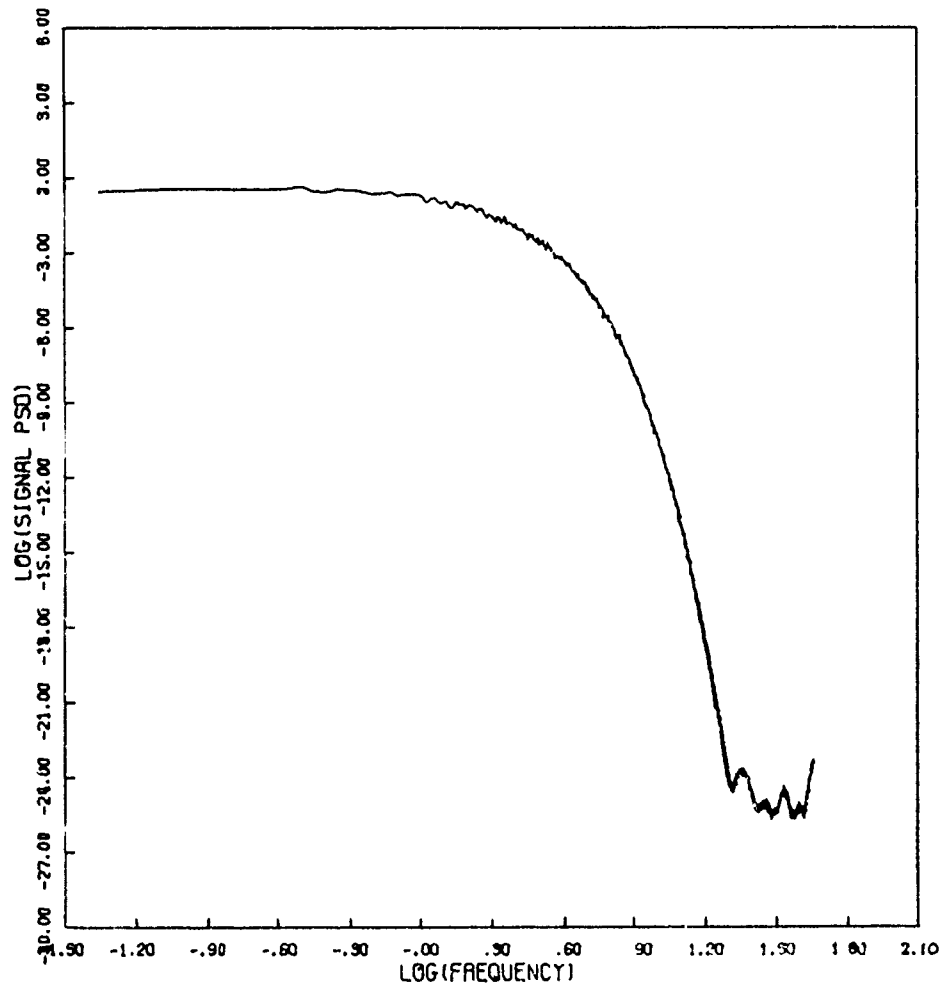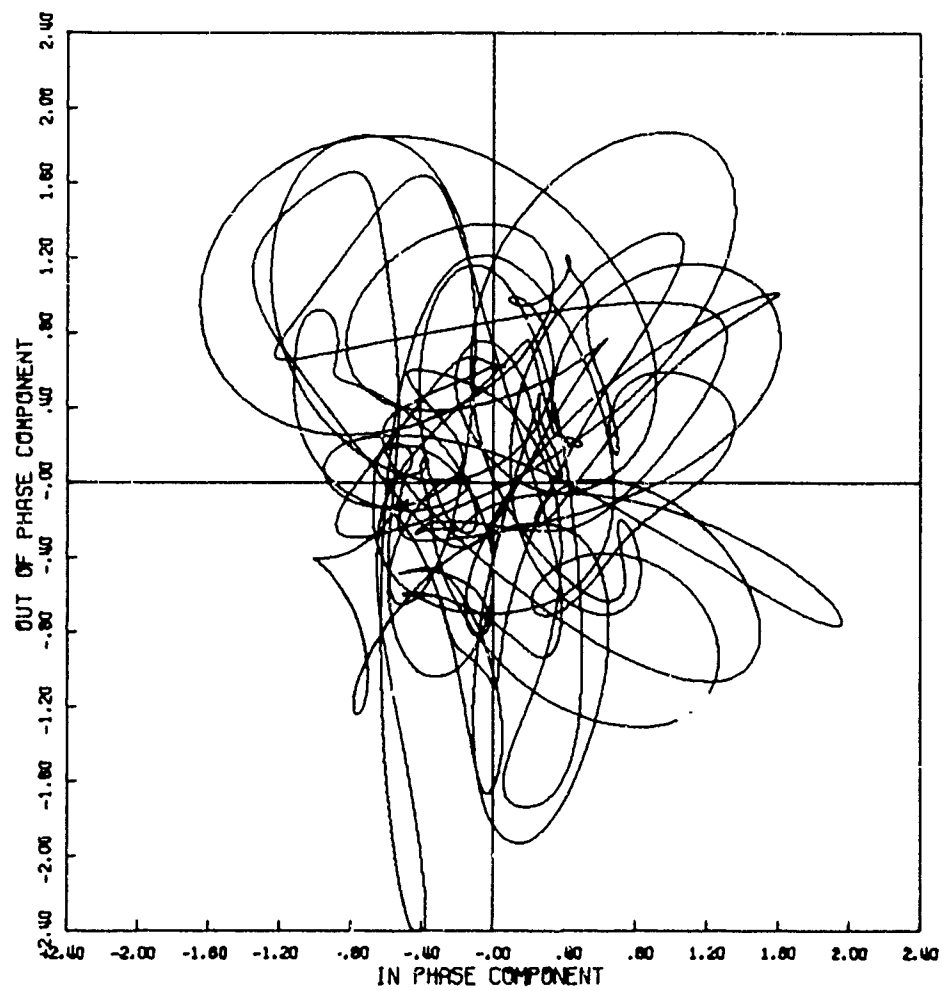
Figure 70d. Amplitude Power Spectral Density

Figure 70e. Signal Power Spectral Density

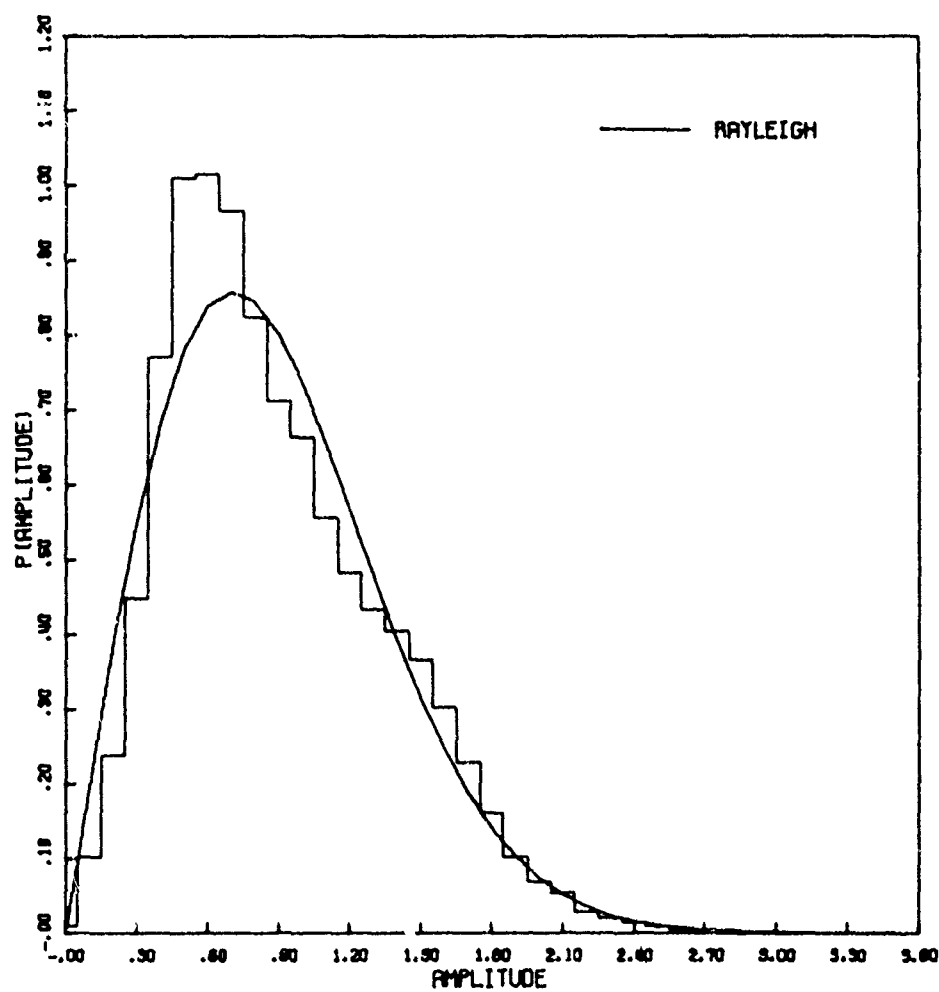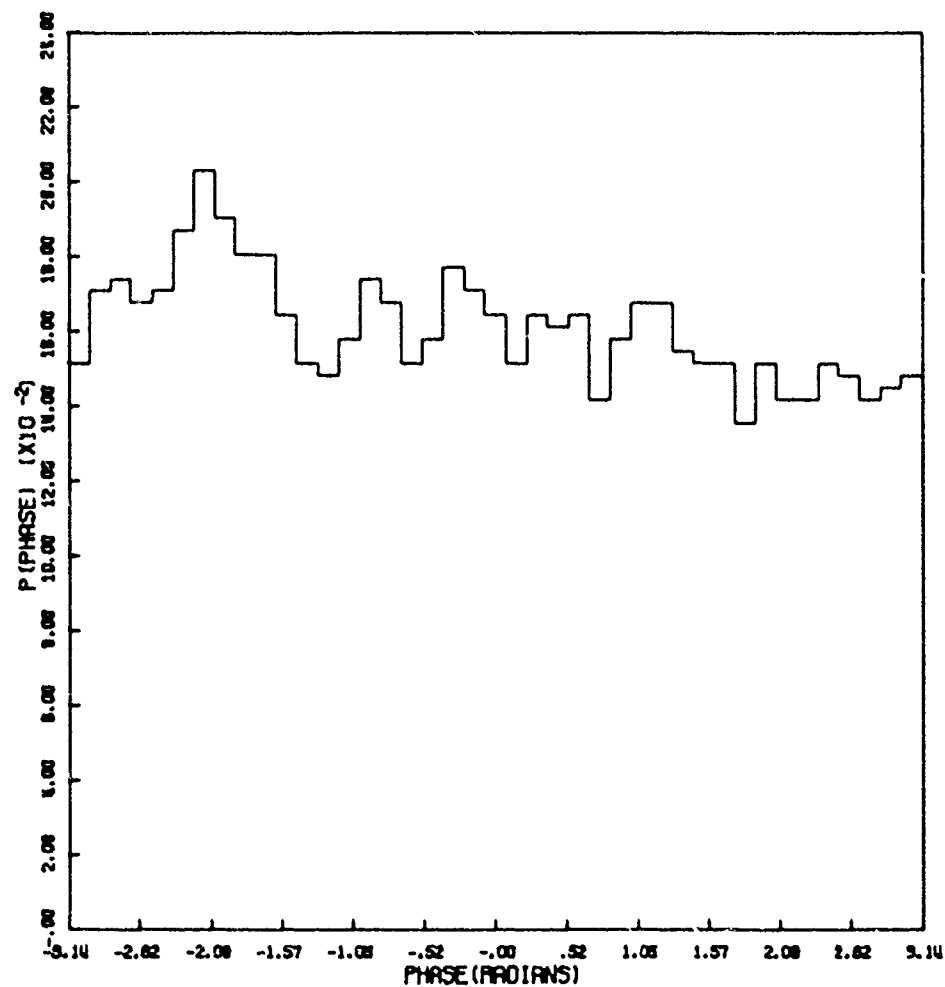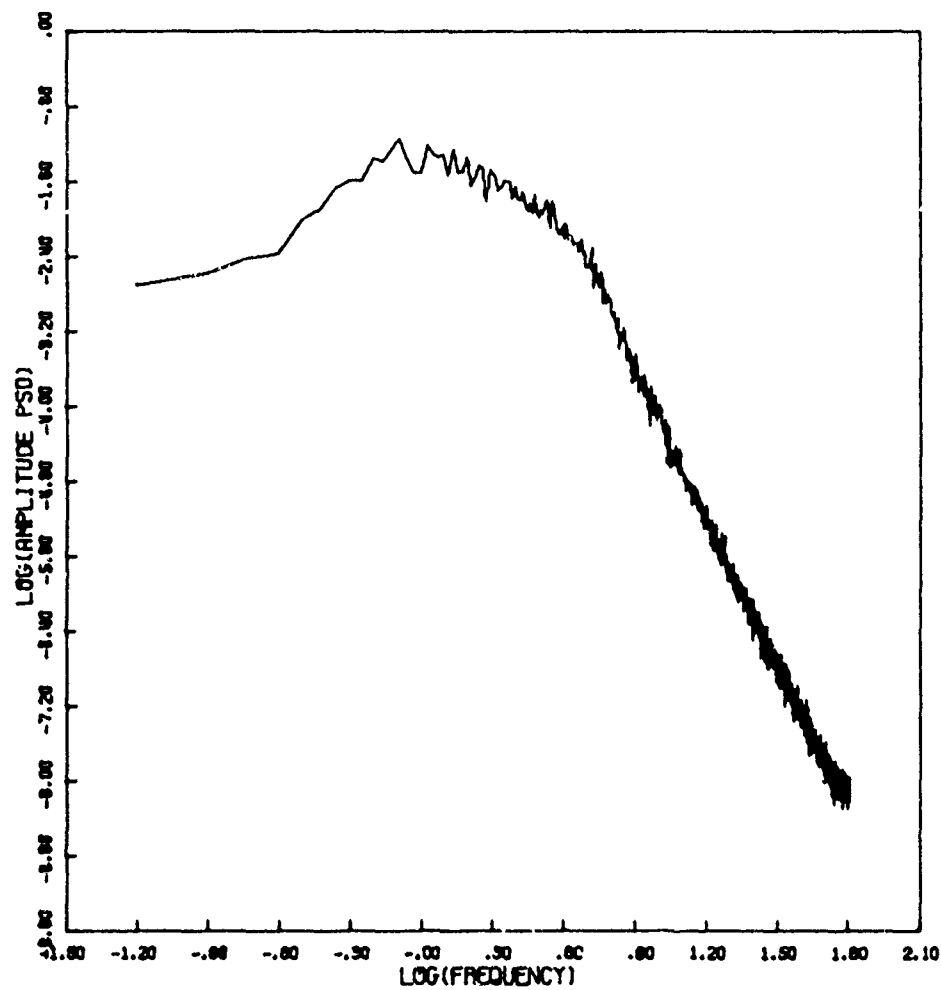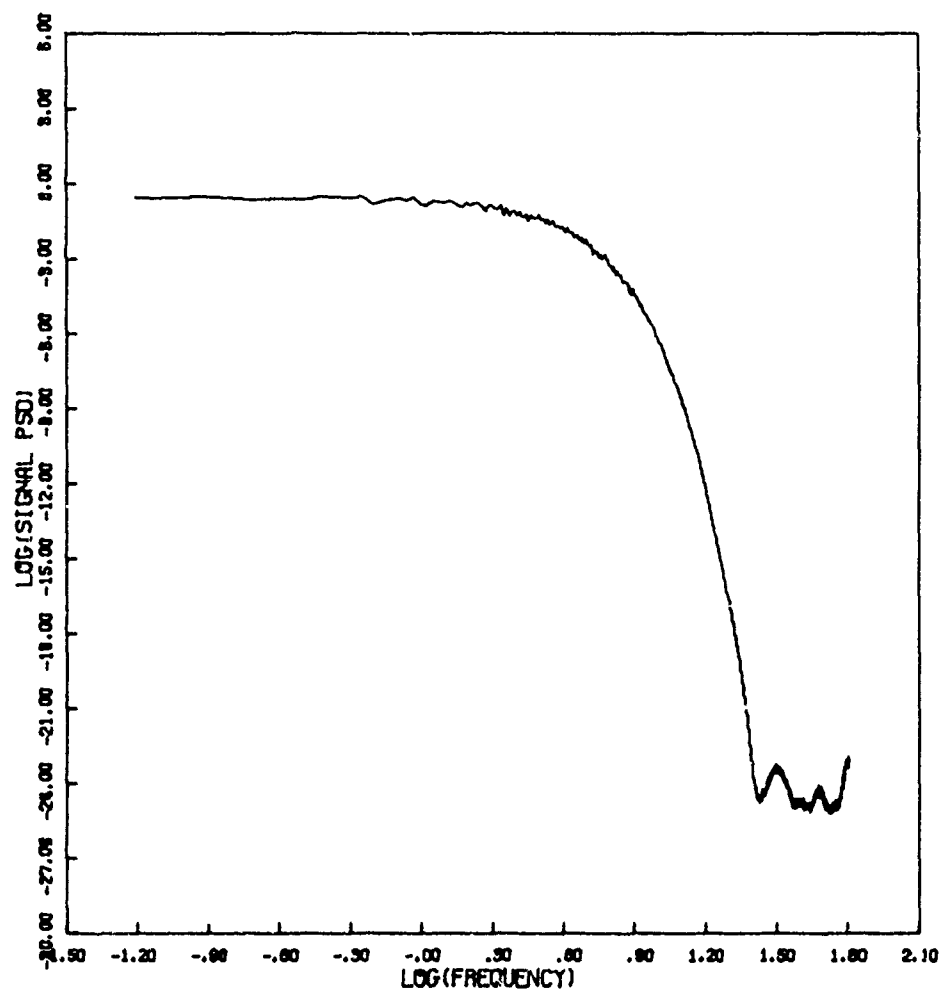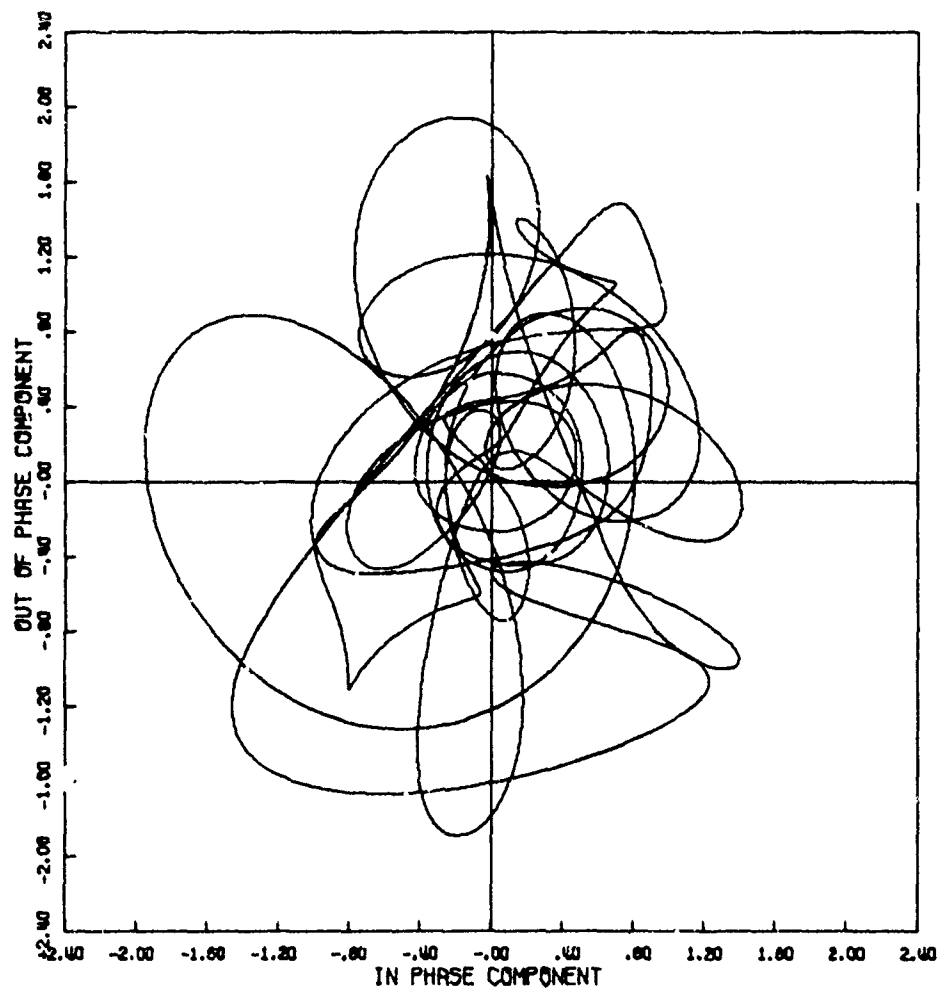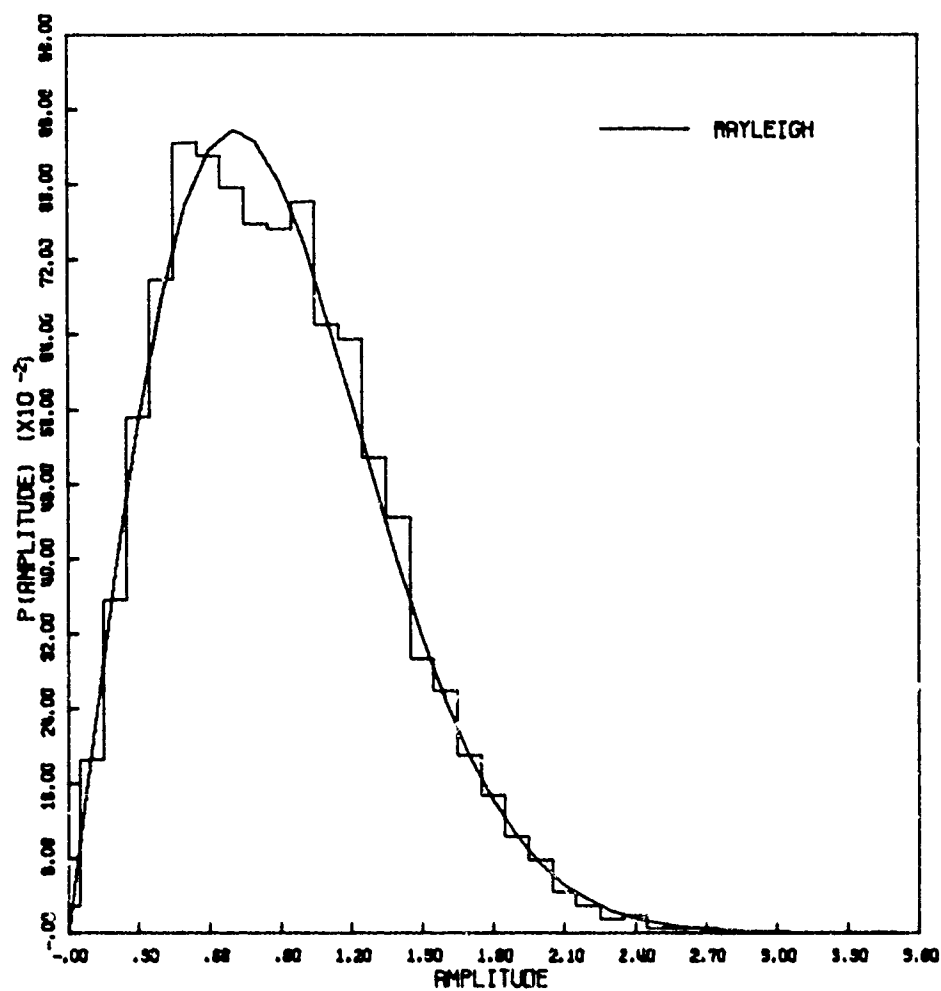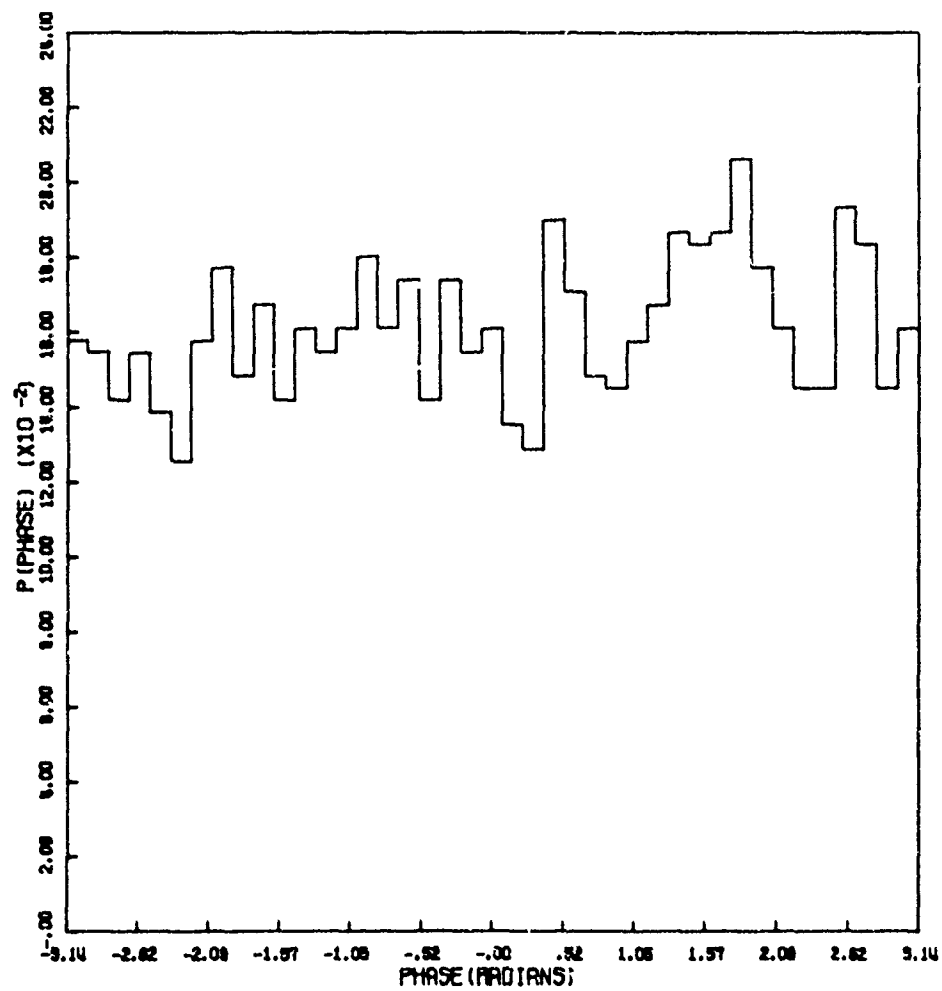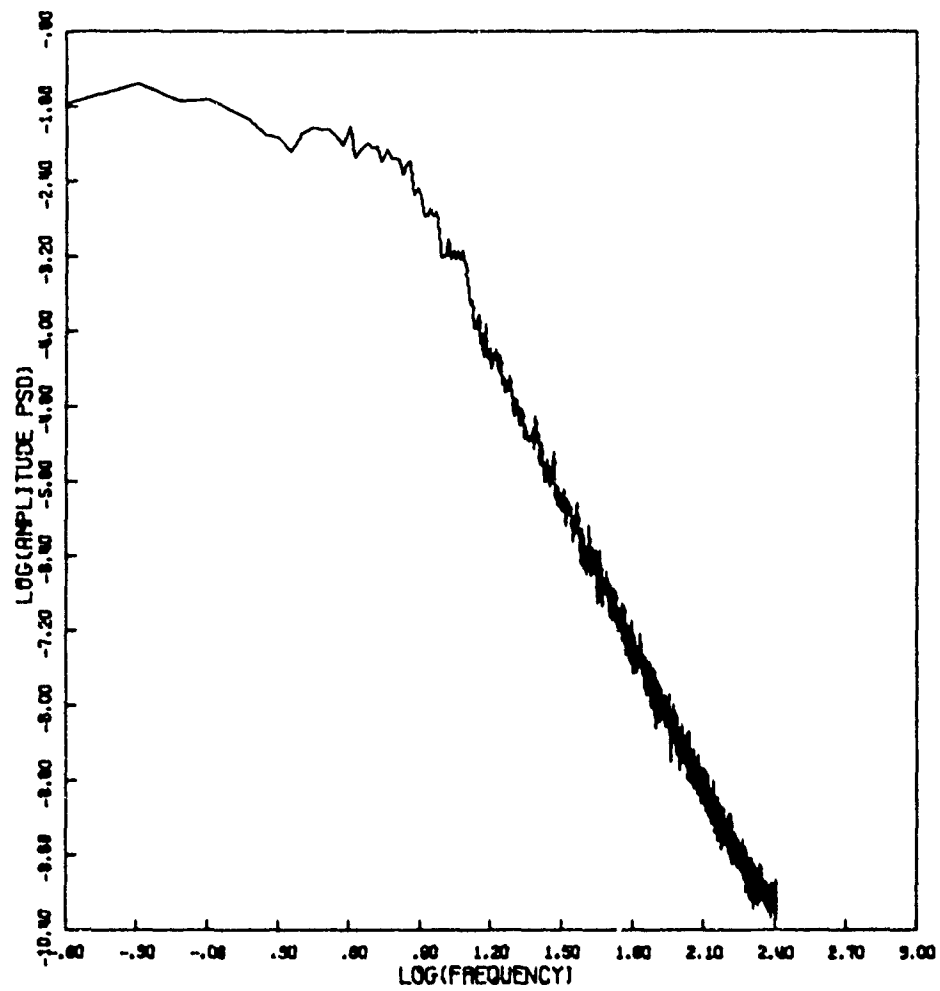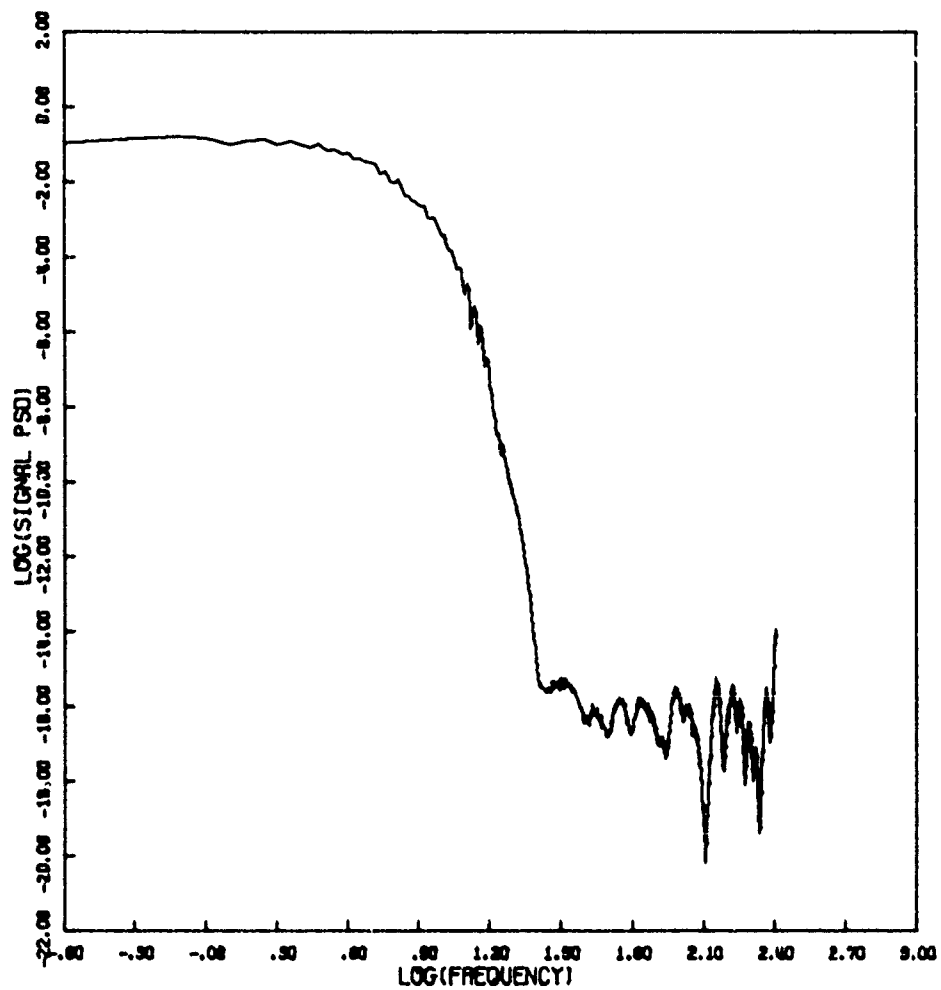Figure 71a.   Signal Phase Plot
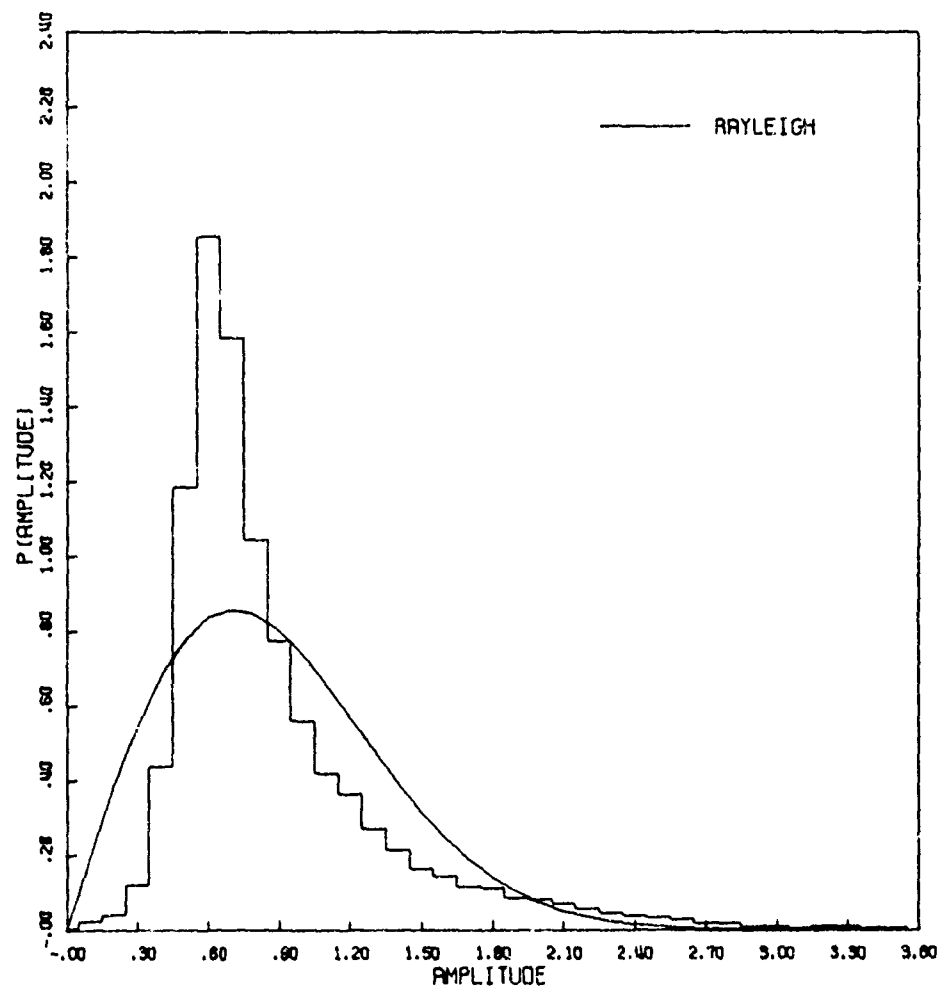
Figure 71b. Amplitude Distribution
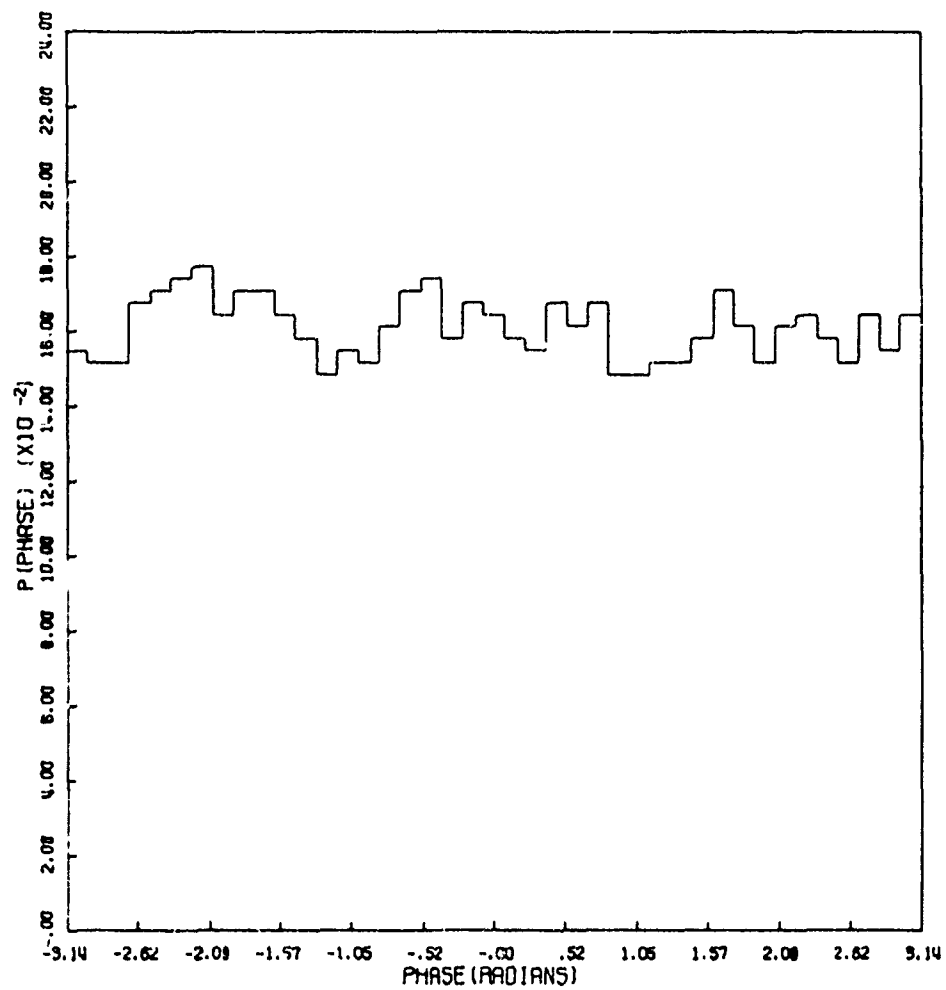
Figure 71c.   Phase Distribution
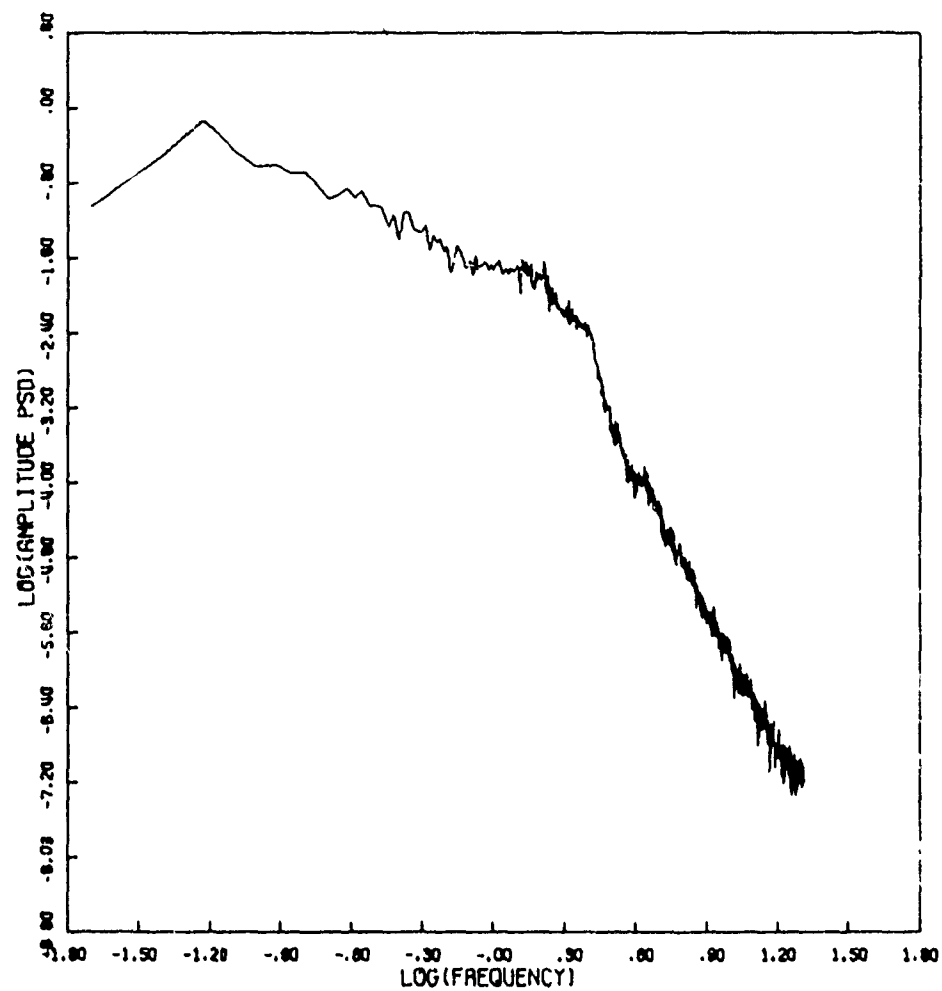
Figure 71d. Amplitude Power Spectral Density

351
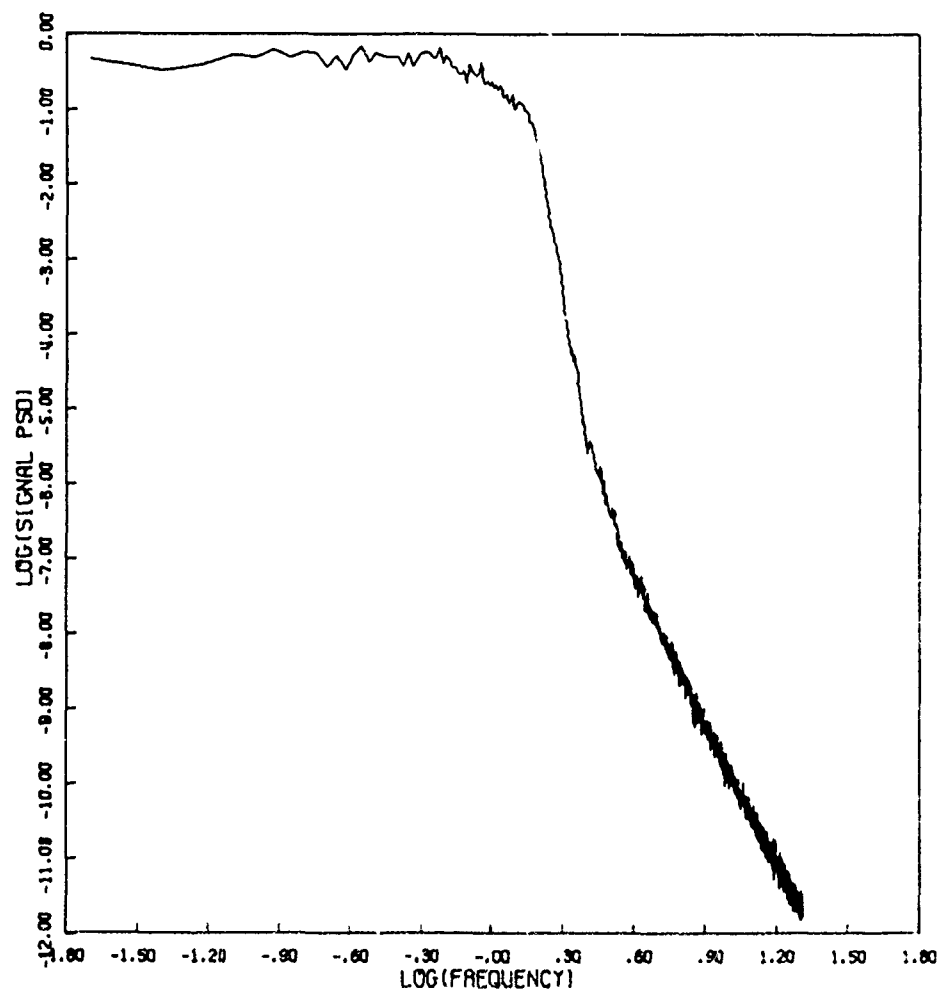
Figure 71e.   Signal Power Spectral Density

Table 5

GAUSSIAN SPECTRUM

	$Z_g = 2\times10^7$		$\overline{\Delta n^2} = 10^{13}$		K = 1.46				GAUSSIAN SPECTRUM		
FIG.	L	$\bar{Z}_s$	$\overline{\phi^2}$	$\overline{\chi^2}$	S_4	ℓ_0	$\overline{E_R^2}$	$\overline{E_I^2}$	α_A	α_ϕ	α_S
75	1.15×10^3	6×10^6	0.10	0.10	0.5?	$1.?\times10^3$	0.08	0.09	5.9	4.6	G
76	1.15×10^3	6×10^7	1.8*	0.46	0.9?	8.3×10^2	0.43	0.41	6.9		G
77	1.15×10^3	6×10^8	18.*	0.47	0.98	2.7×10^2	0.49	0.51	5.5		G
78	3.5×10^3	2×10^6	0.12	0.08	0.50	3.2×10^3	0.06	0.11	G	G	G
79	3.5×10^3	2×10^7	1.8*	0.41	0.87	2.6×10^3	0.39	0.46	4.8		G
80	3.5×10^3	2×10^8	18.*	0.46	0.98	8.3×10^2	0.49	0.51	5.5		G
81	10^4	2×10^6	0.52	0.03	0.33	1.0×10^4	0.08	0.30	G	G	G
82	10^4	6×10^6	1.6*	0.09	0.61	8.2×10^3	0.29	0.47	G	G	G
83	10^4	2.1×10^7	5.4*	0.36	0.98	4.7×10^3	0.52	0.47	1.3, 5.2		G
84	10^4	6×10^7	18.*	0.43	0.95	2.5×10^3	0.52	0.49	0.5, 5.1		G
85	10^4	6×10^8	155.*	?48	1.00	7.8×10^2	0.49	0.51	5.4		G
86	2.5×10^4	10^7	6.5	0.02	0.27	1.1×10^4	0.54	0.46	3.8, G	G	G
87	2.5×10^4	3×10^7	19.*	0.09	0.79	6.7×10^3	0.49	0.50	1.6, 5.5		G
88	2.5×10^4	5.6×10^7	36.*	0.26	1.21	4.2×10^3	0.53	0.47	1.3, 4.9		G
89	2.5×10^4	10^8	65.*	0.52	1.26	3.3×10^3	0.50	0.50	1.1, 5.7		G
90	2.5×10^4	3×10^8	194.*	0.54	1.16	1.8×10^3	0.50	0.50	0.6, 5.3		G
91	6×10^4	10^8	155.	0.09	0.97	5.3×10^3	0.50	0.50	1.6, 7.8		G
92	6×10^4	2×10^8	310.*	0.36	1.41	3.3×10^3	0.50	0.50	1.3, 3.3		G
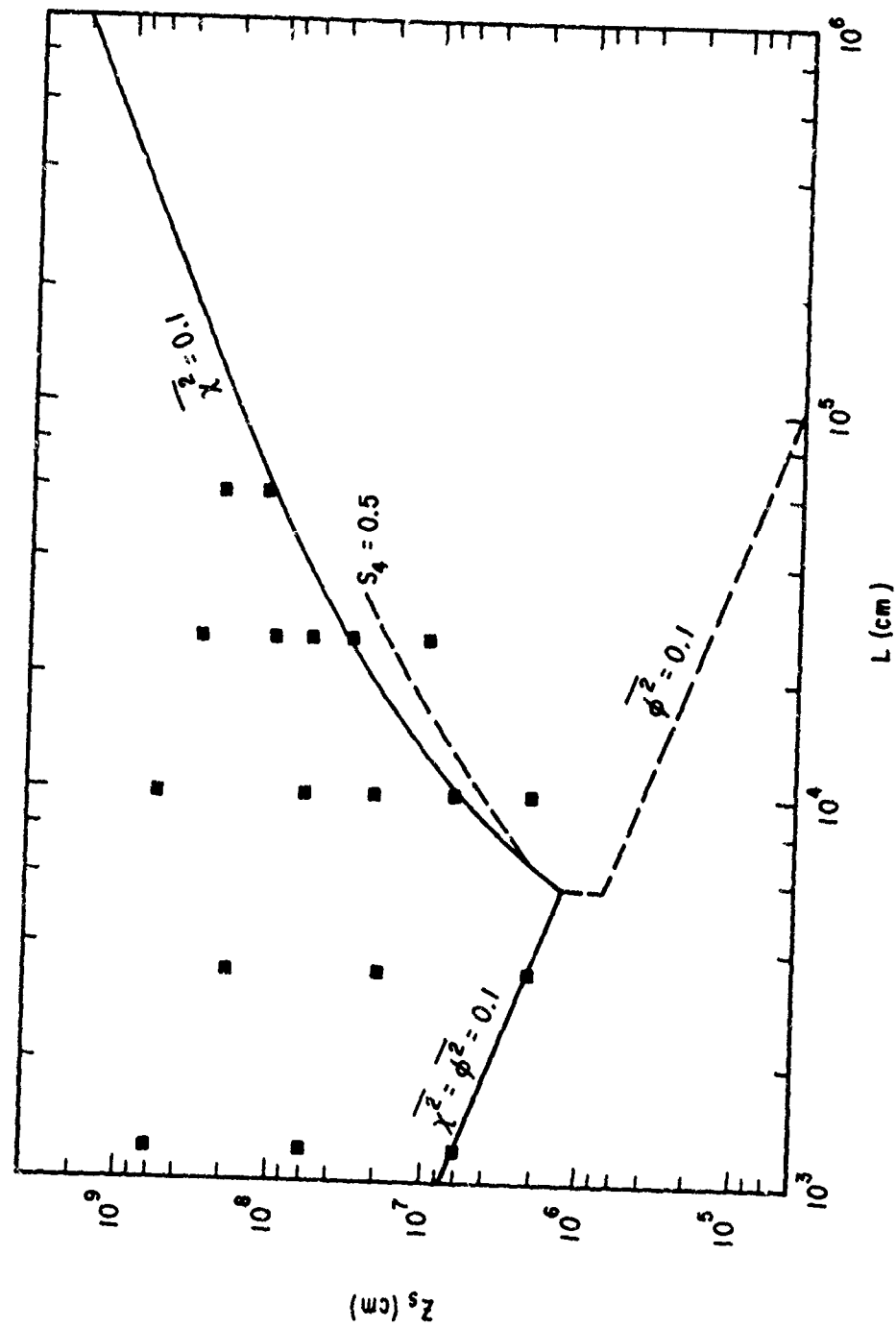
Figure 72. Propagation Space Plot for Gaussian Spectrum

354
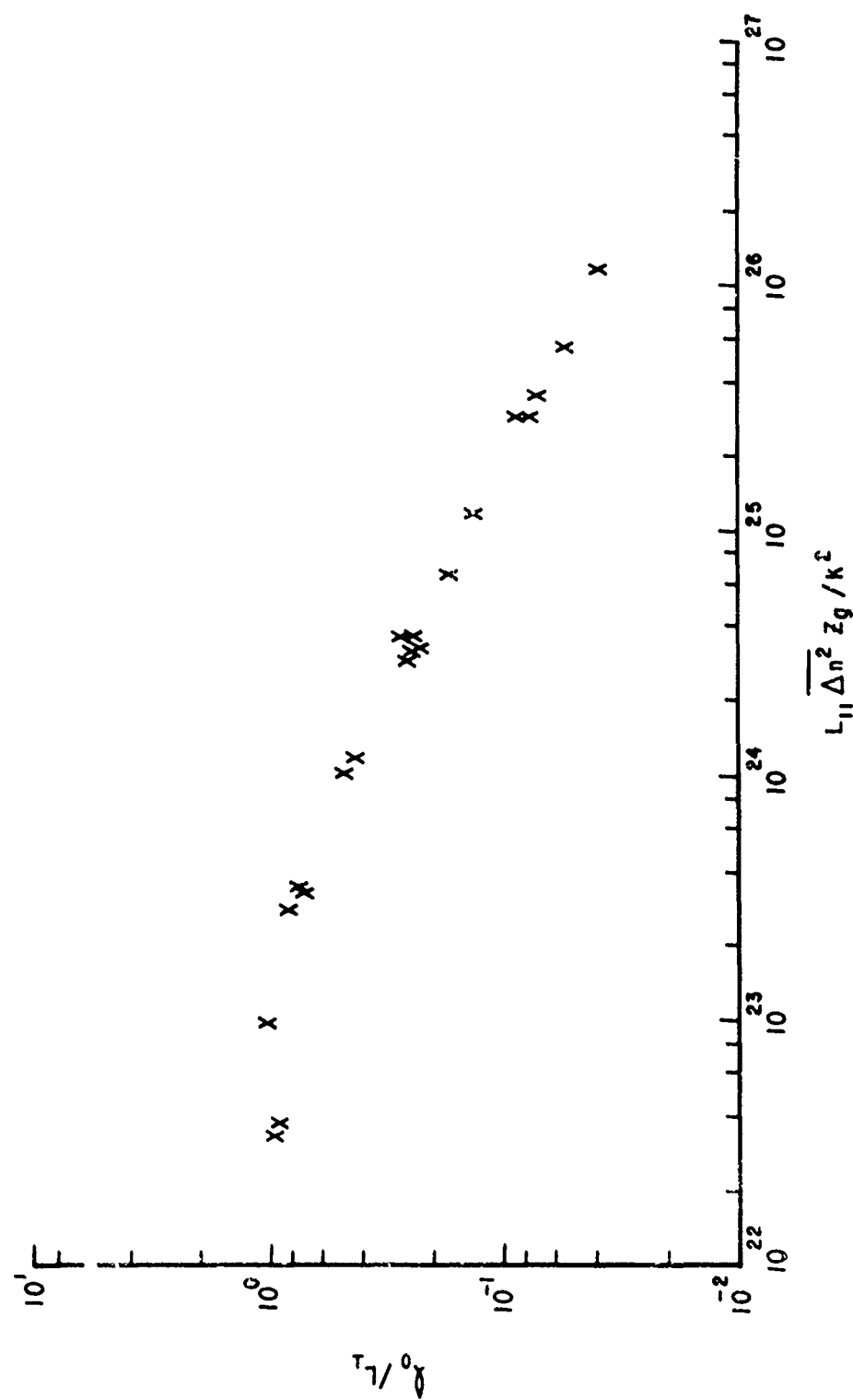
Figure 73. ℓ_0 for Gaussian Spectrum
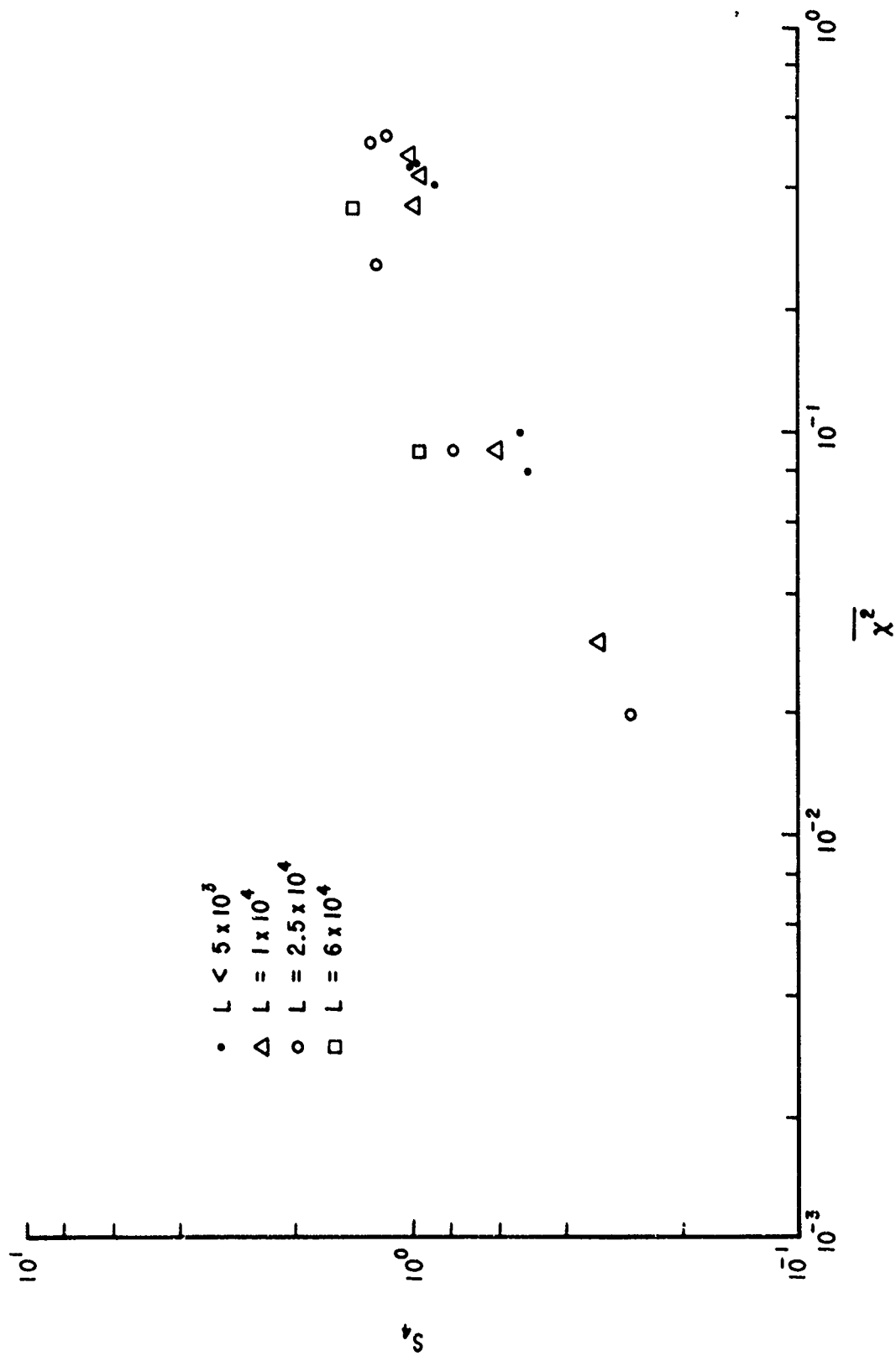
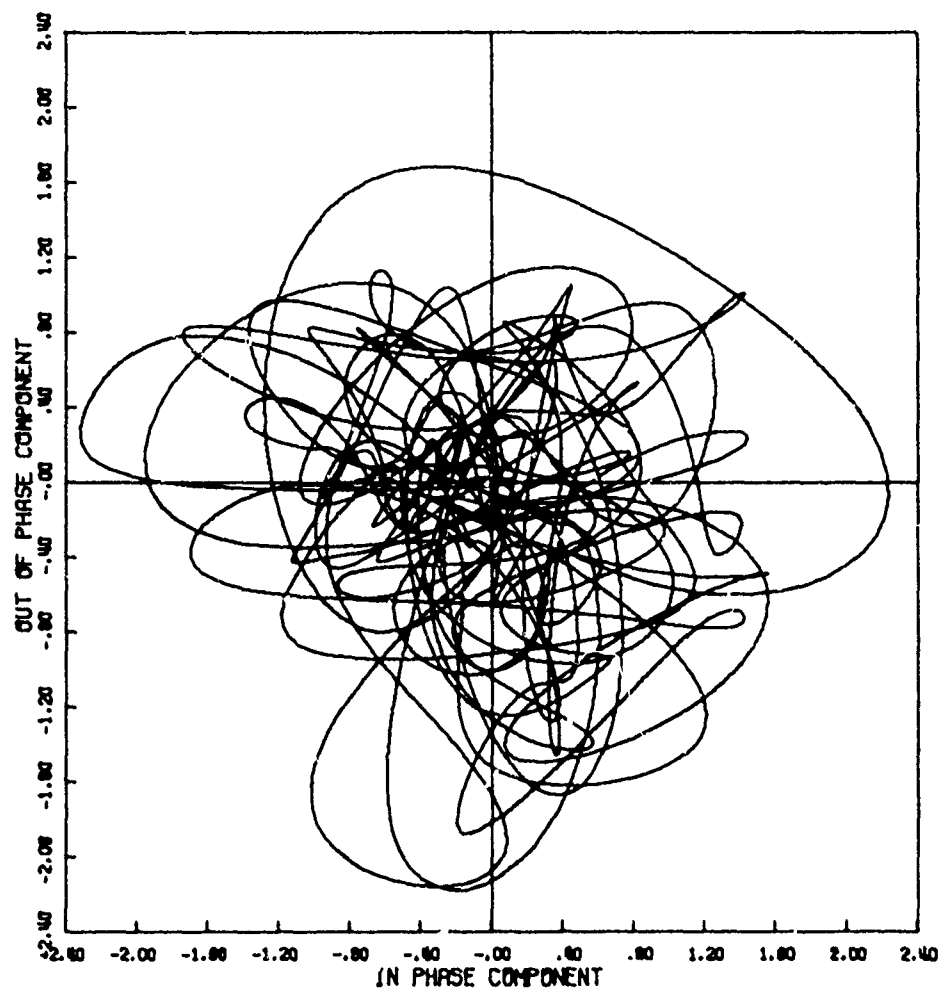Figure 74. S_4 vs. $\overline{\chi^2}$ for Gaussian Spectrum
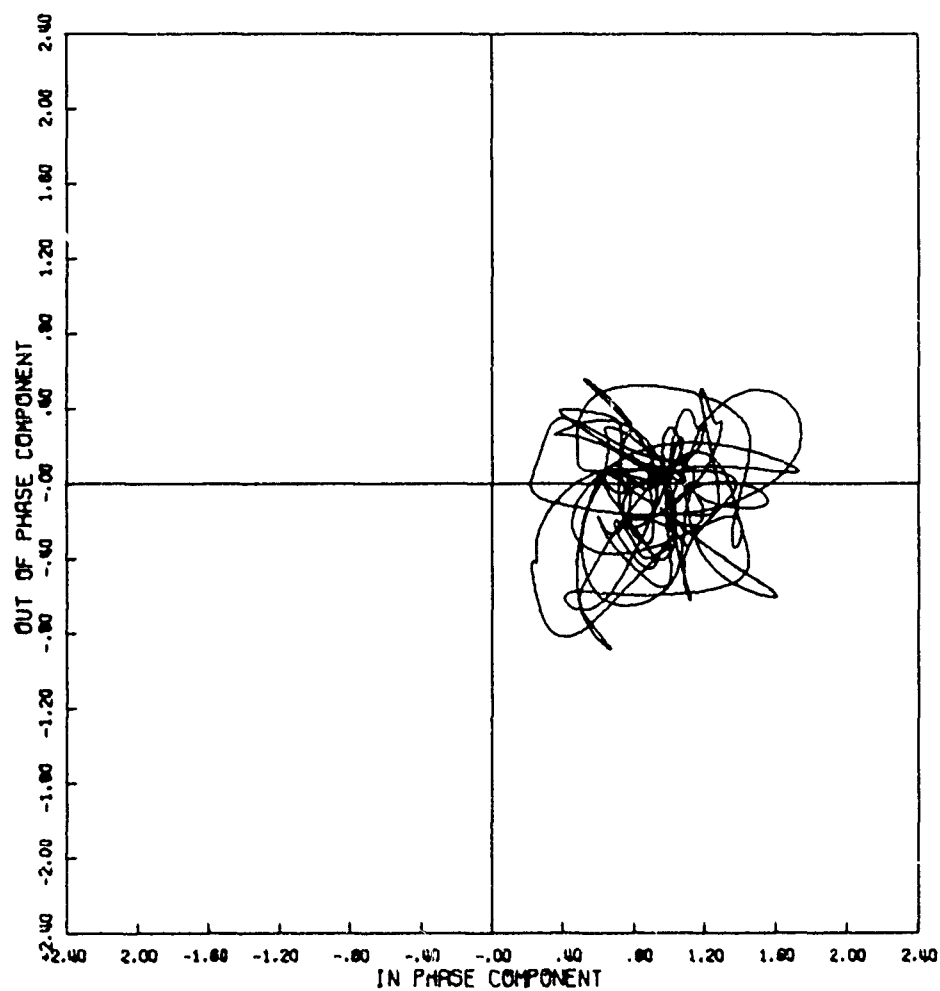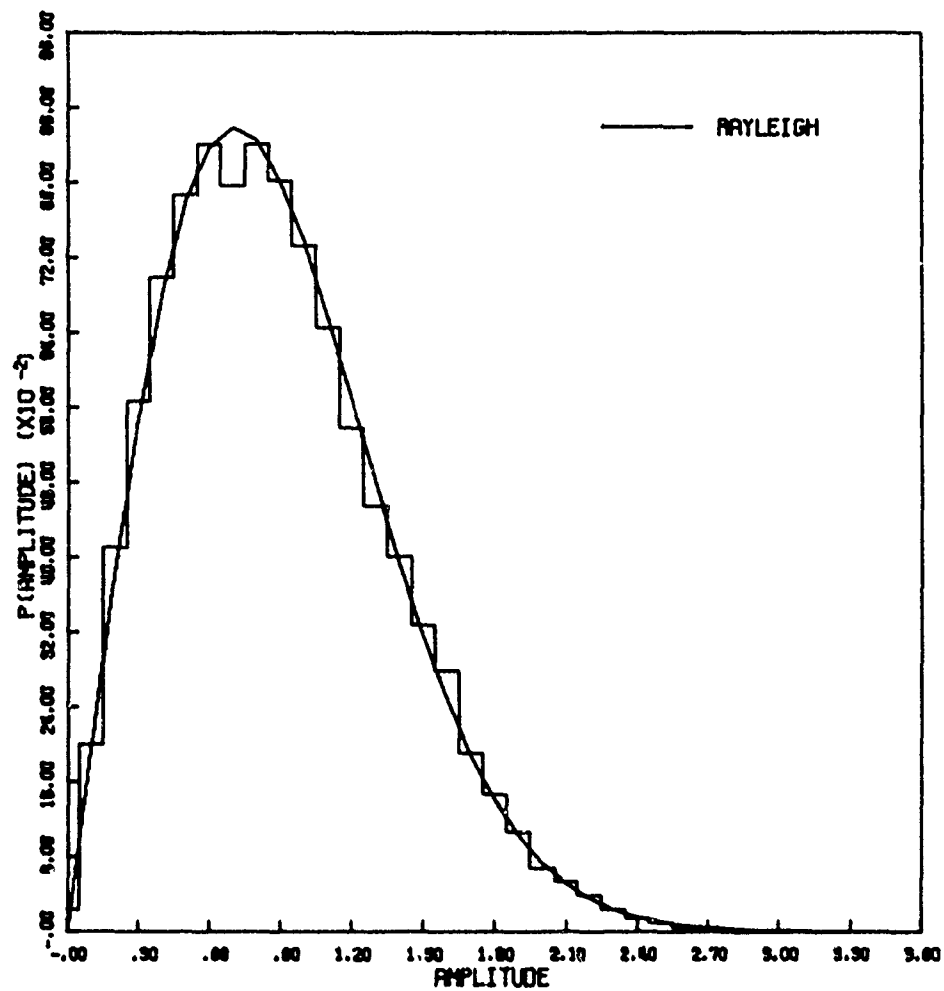
Figure 75a.   Signal Phase Plot
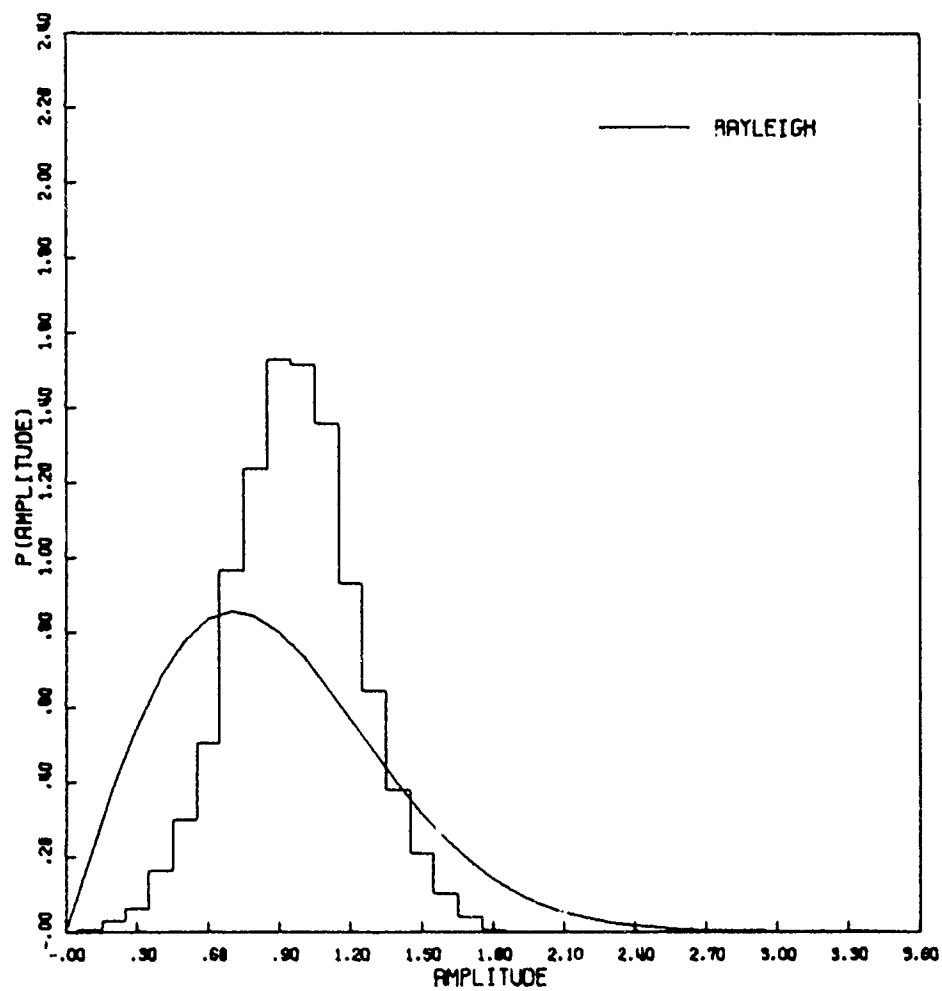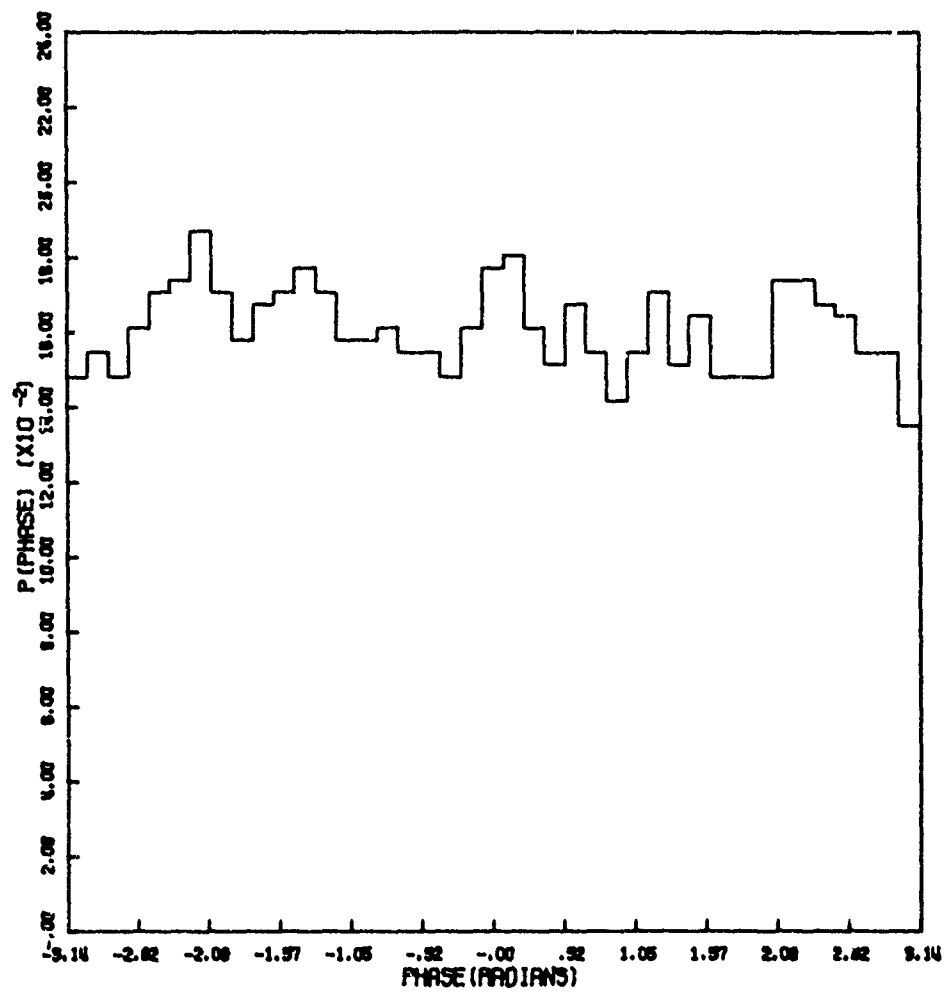
Figure 75b. Amplitude Distribution
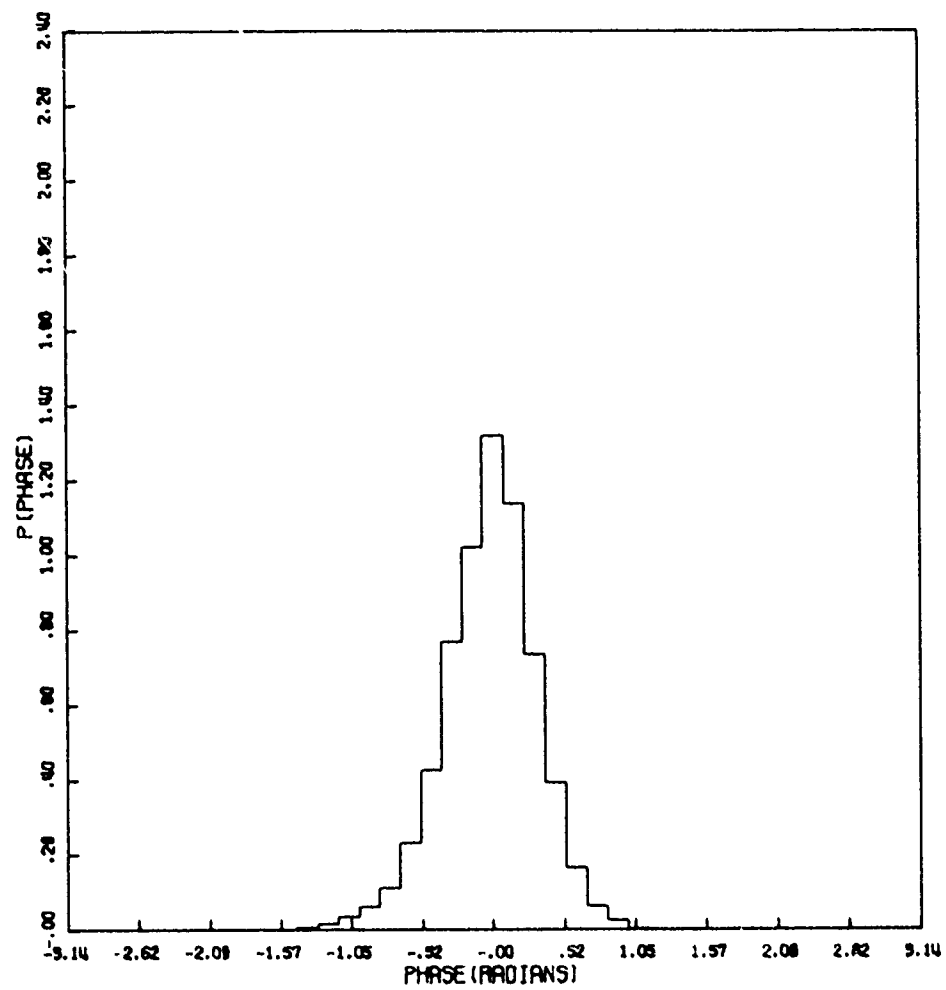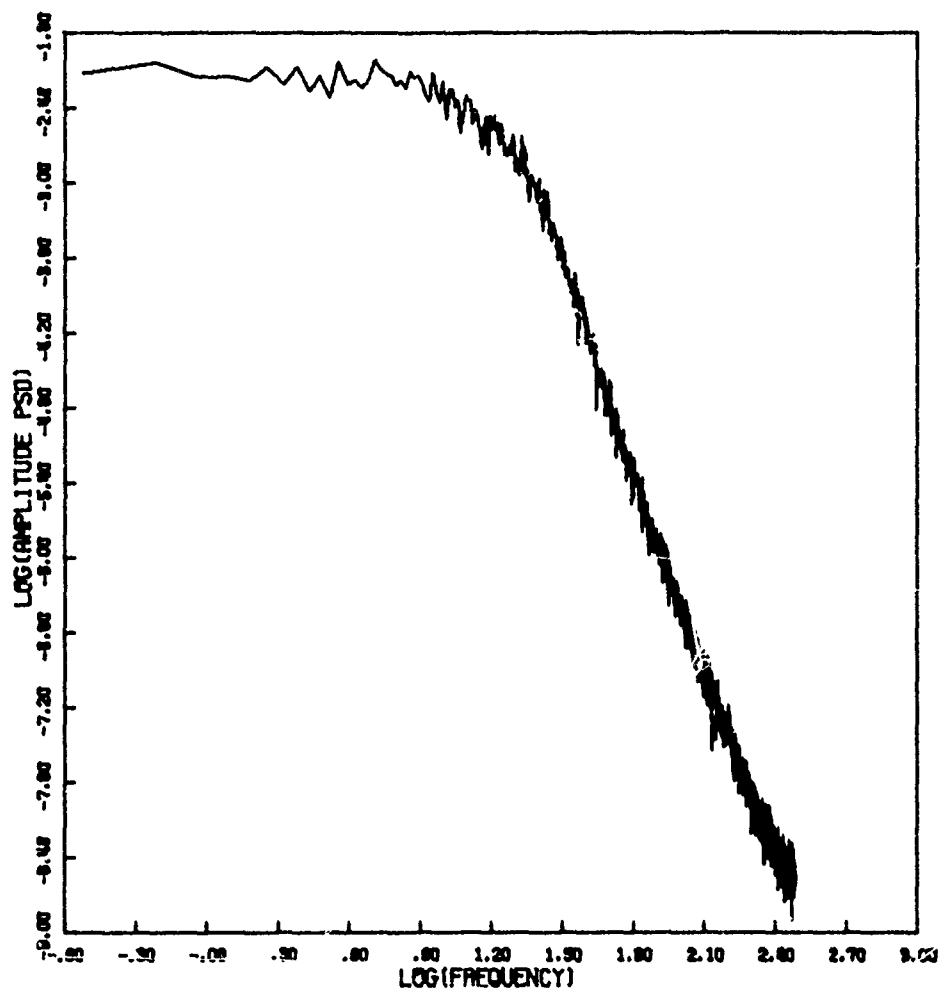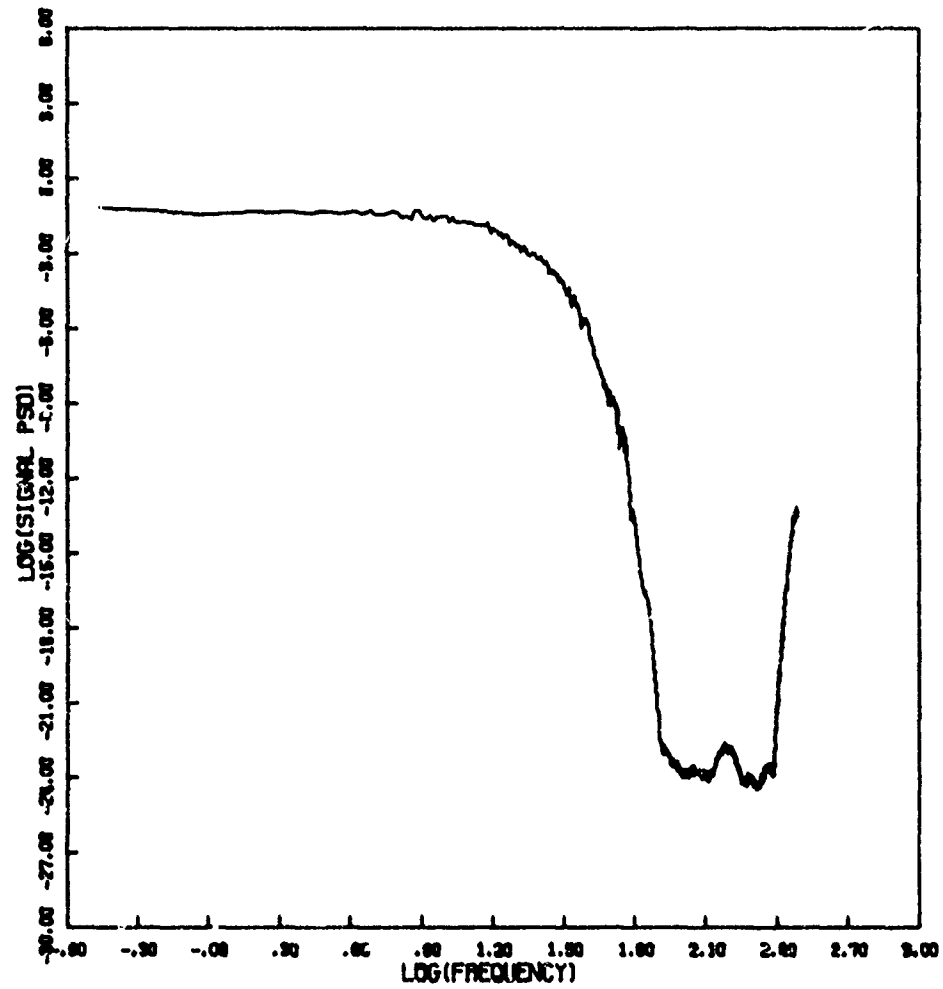
Figure 75c.   Phase Distribution
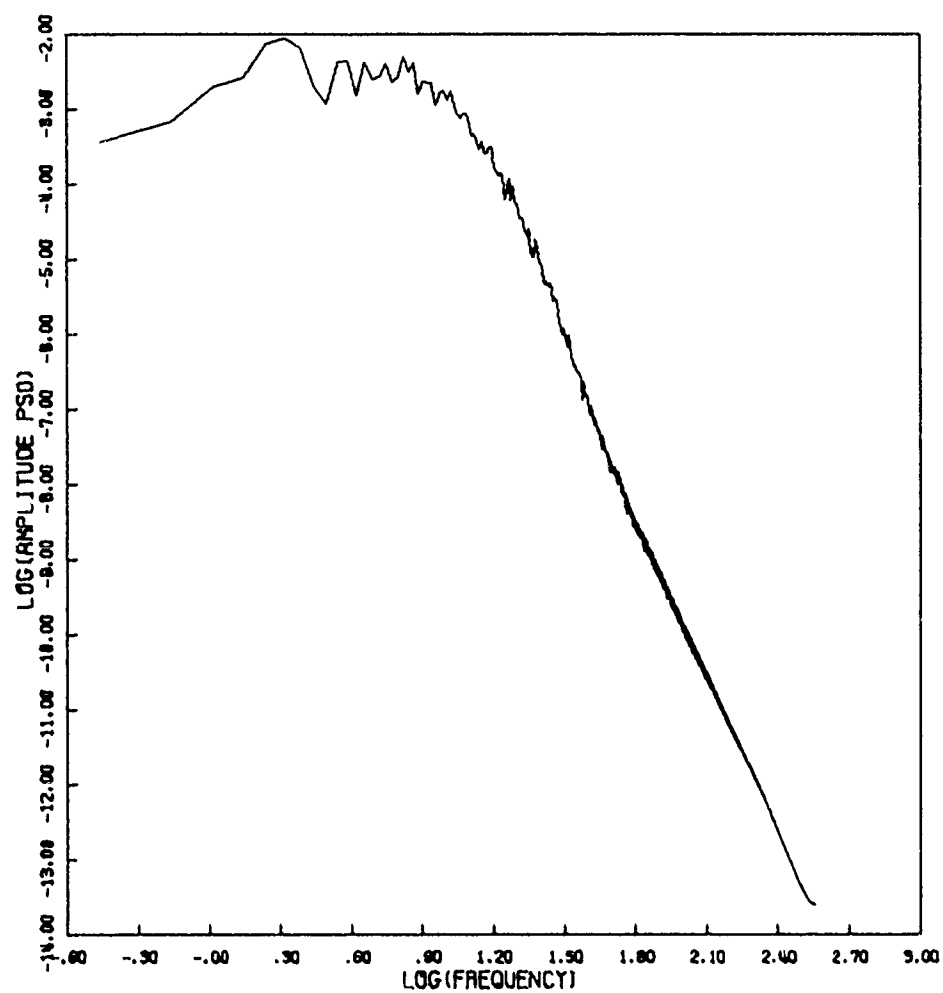
Figure 75d.   Amplitude Power Spectral Density

Figure 75e. Phase Power Spectral Density

Figure 75f. Signal Power Spectral Density
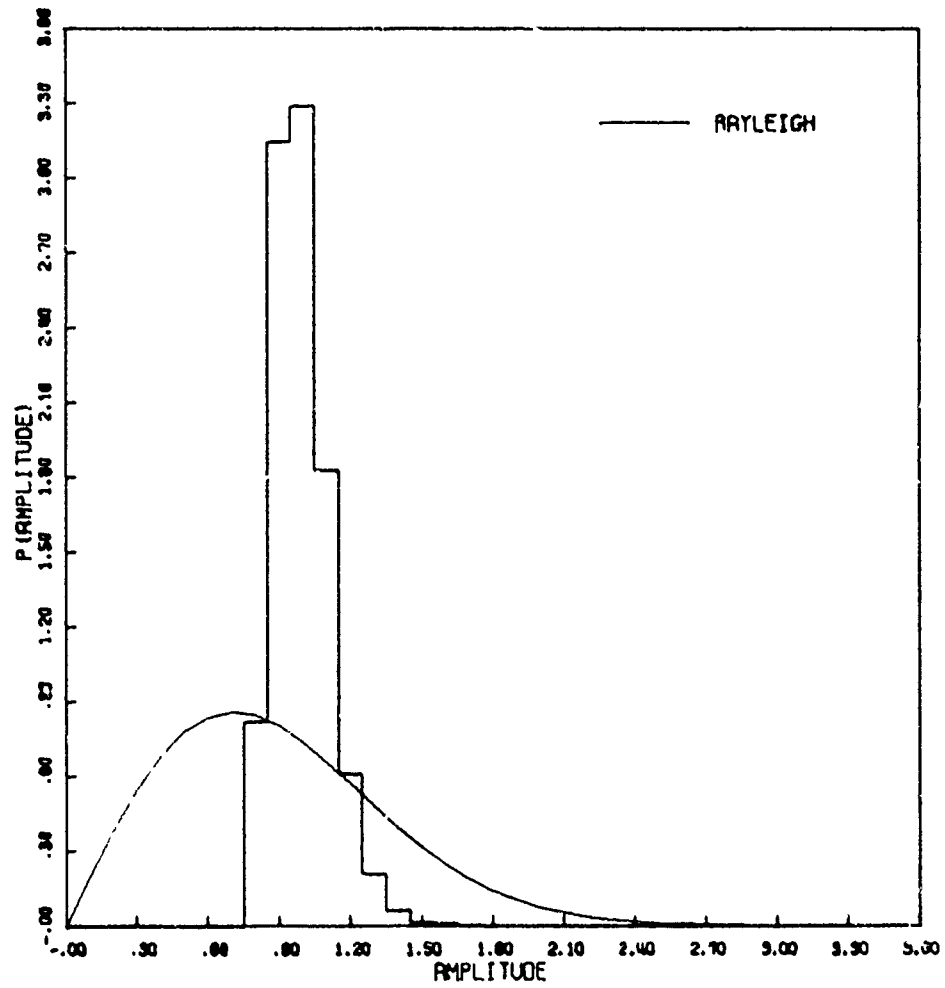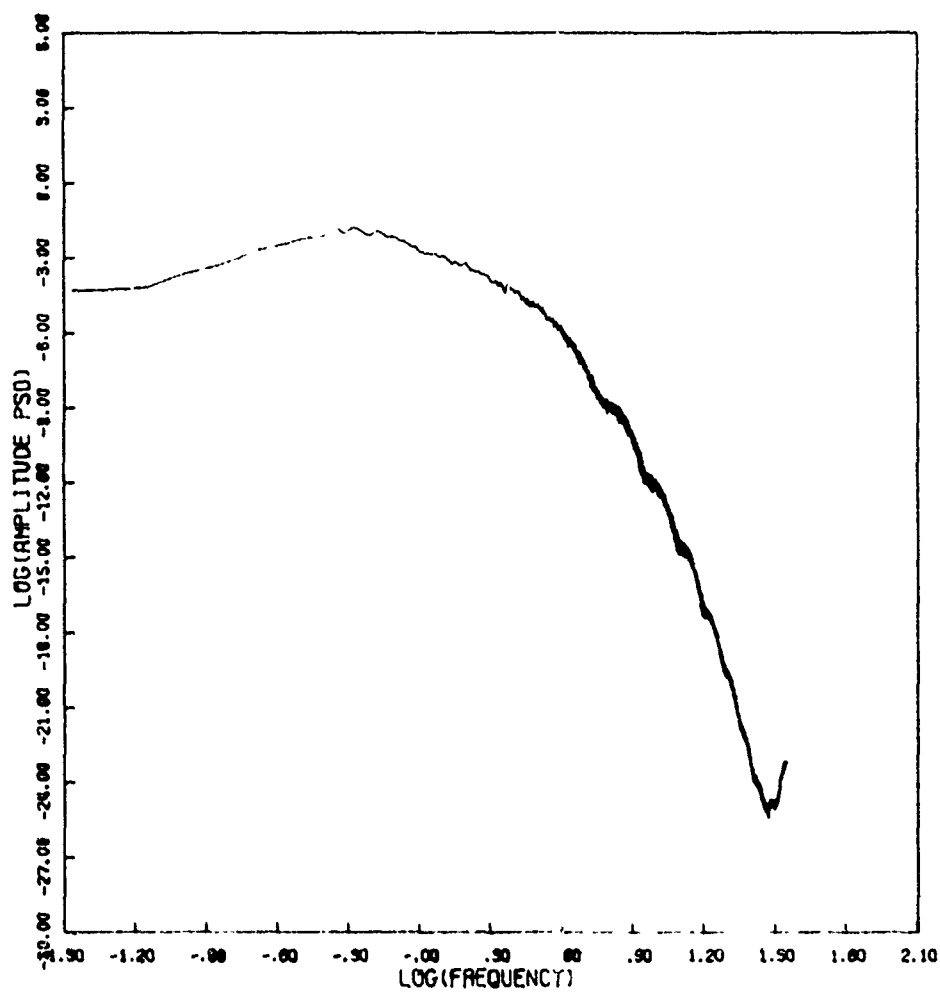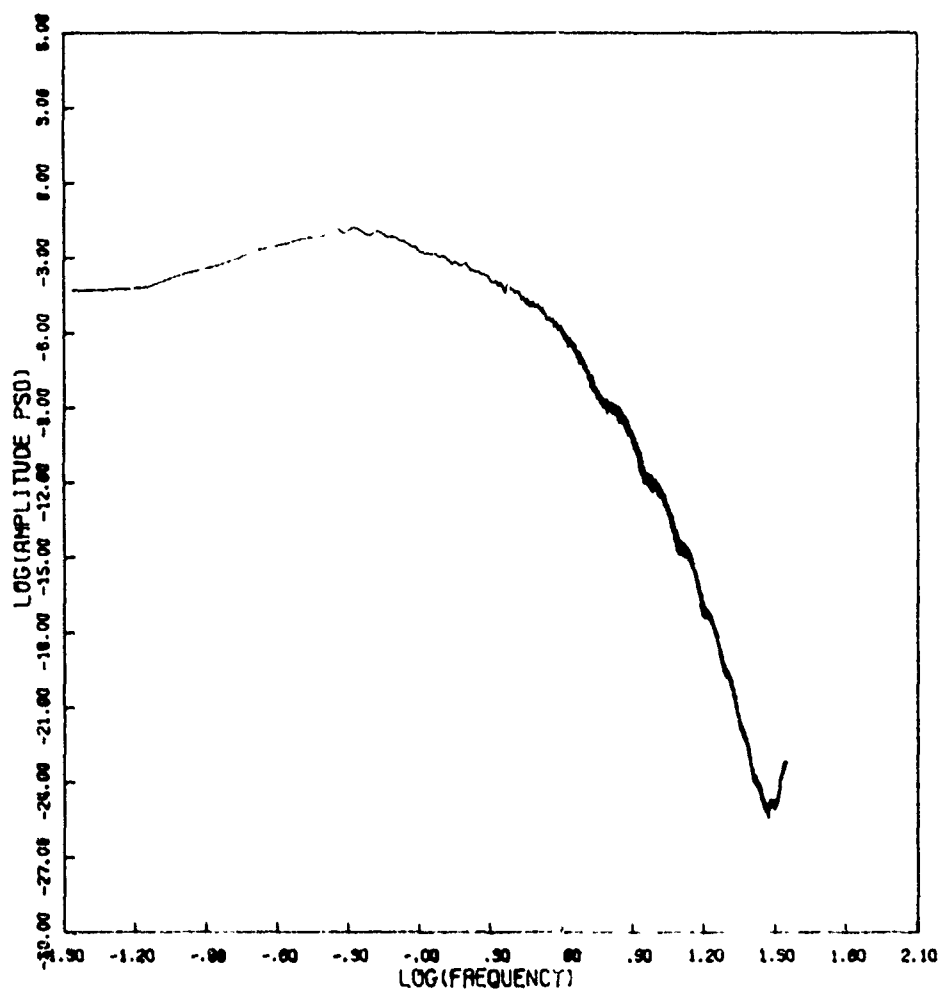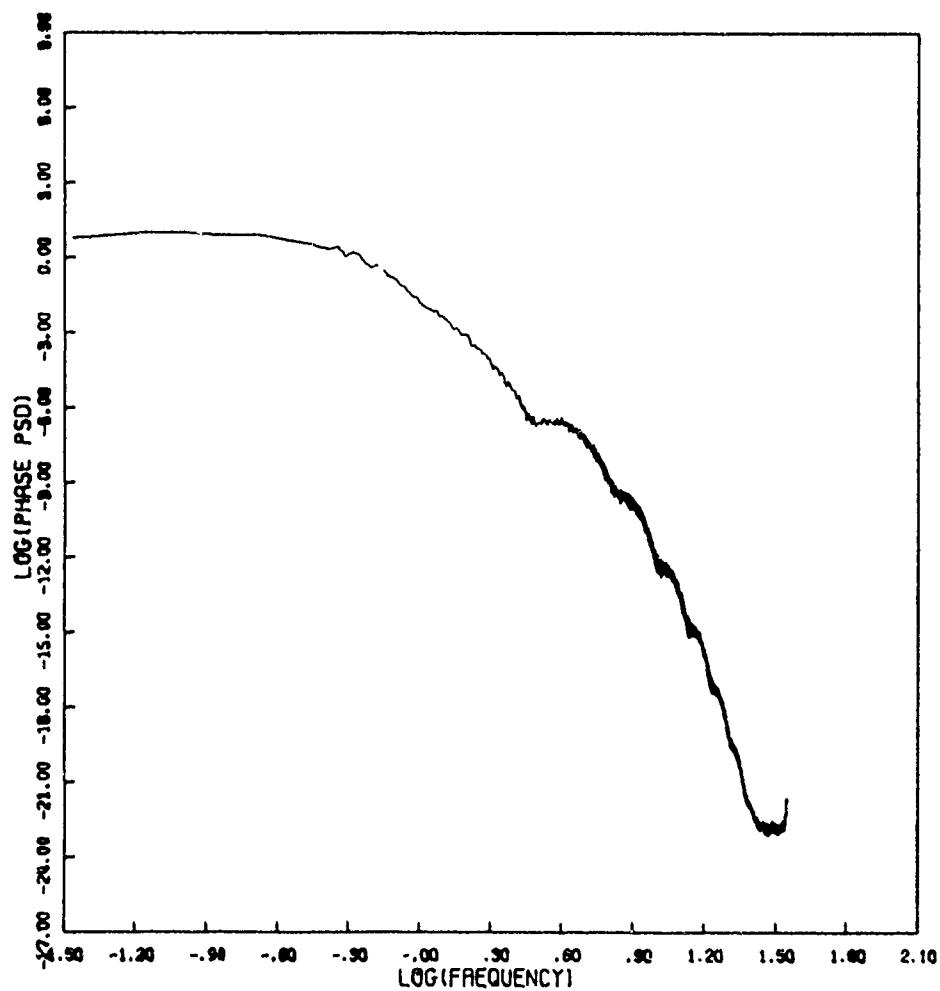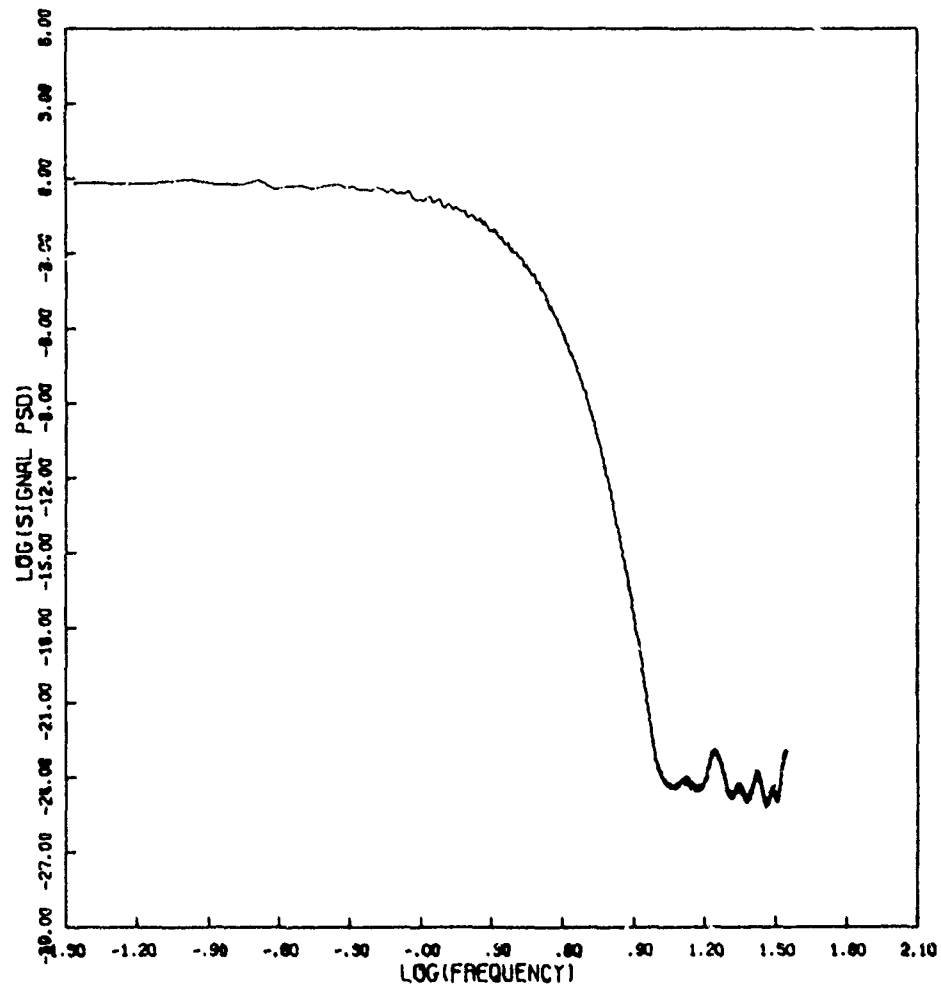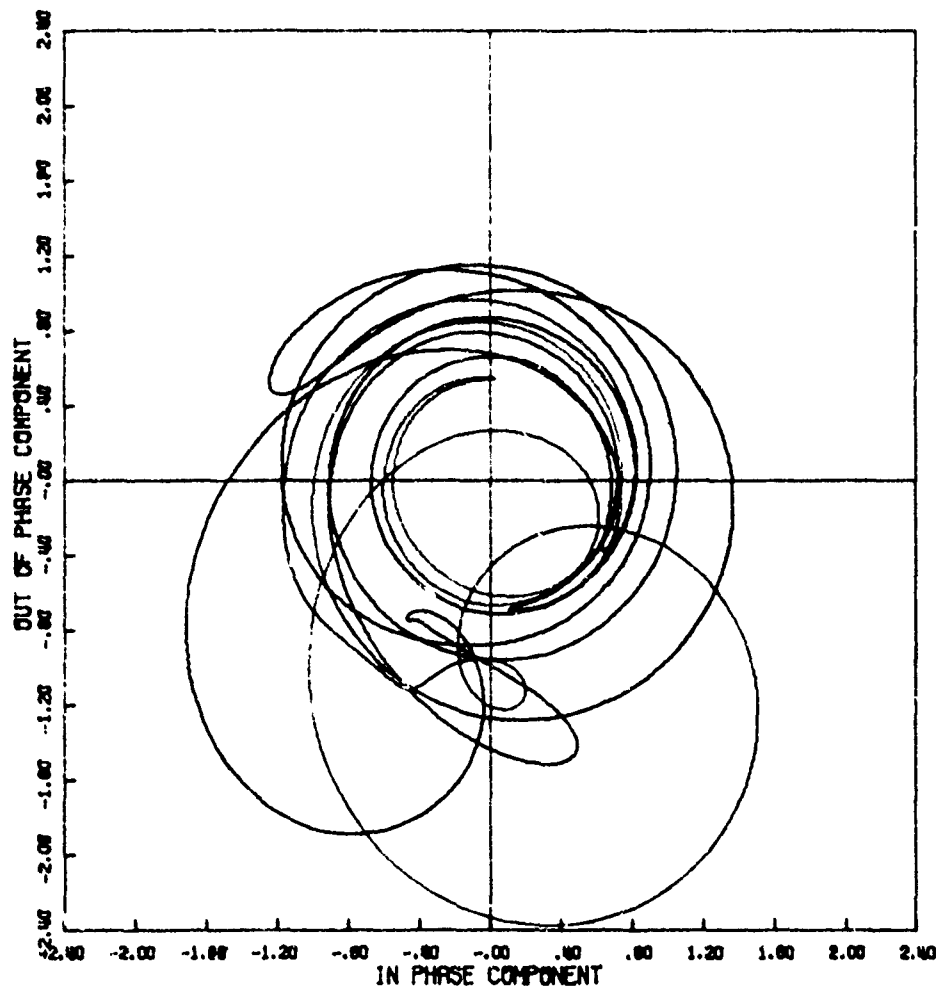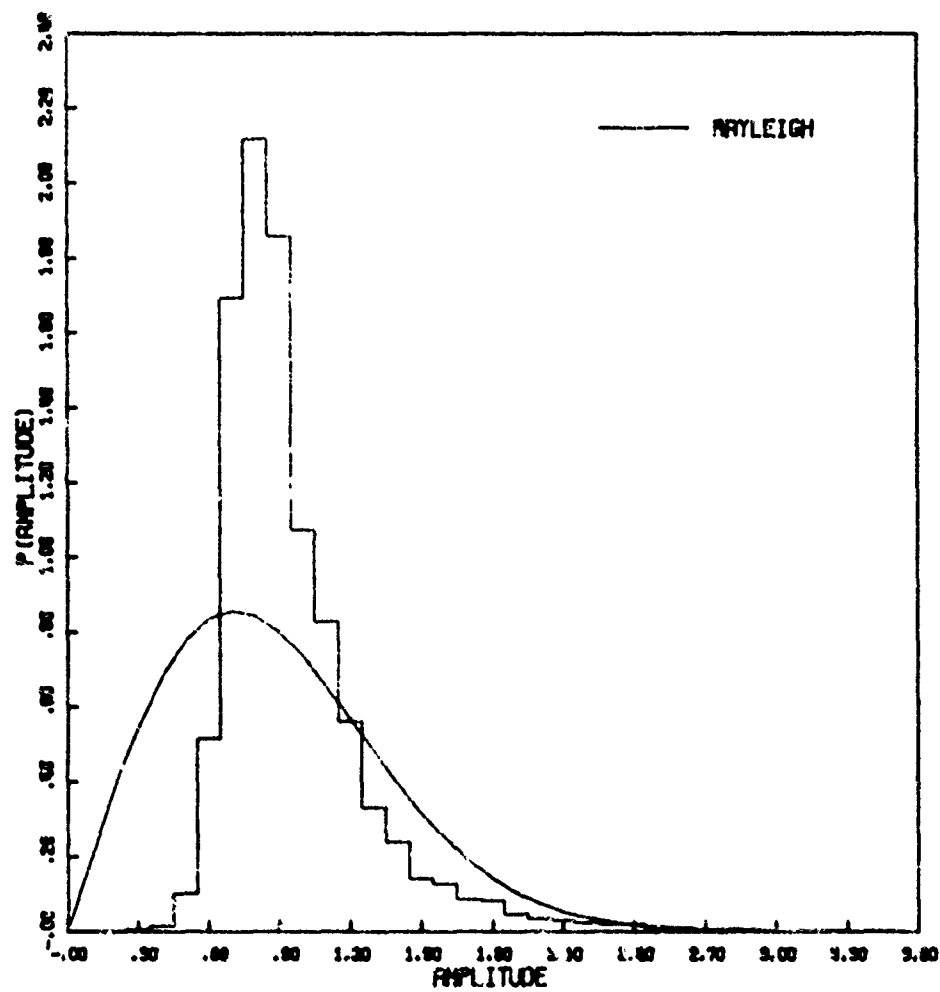
Figure 76a.   Signal Phase Plot

Figure 76b. Amplitude Distribution

Figure 76c.   Phase Distribution

Figure 76d. Amplitude Power Spectral Density

Figure 76e. Signal Power Spectral Density

Figure 77a. Signal Phase Plot

Figure 77b. Amplitude Distribution
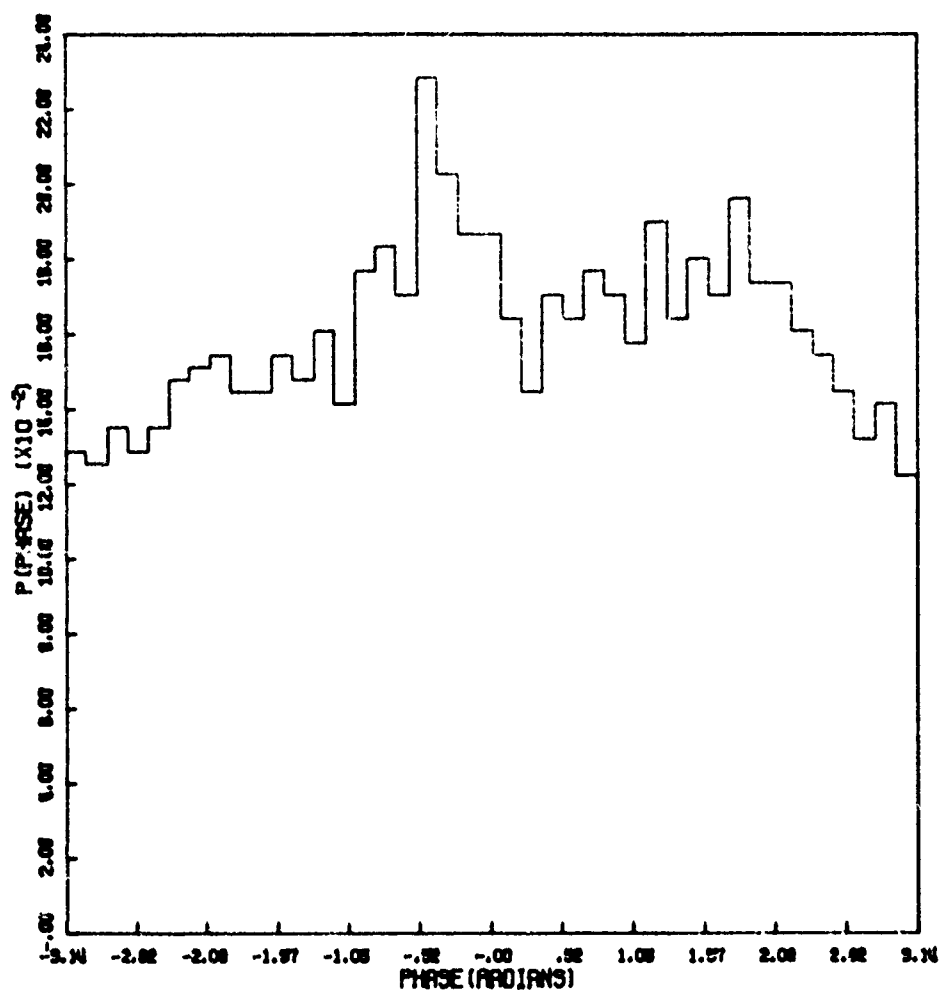
Figure 77c.   Phase Distribution
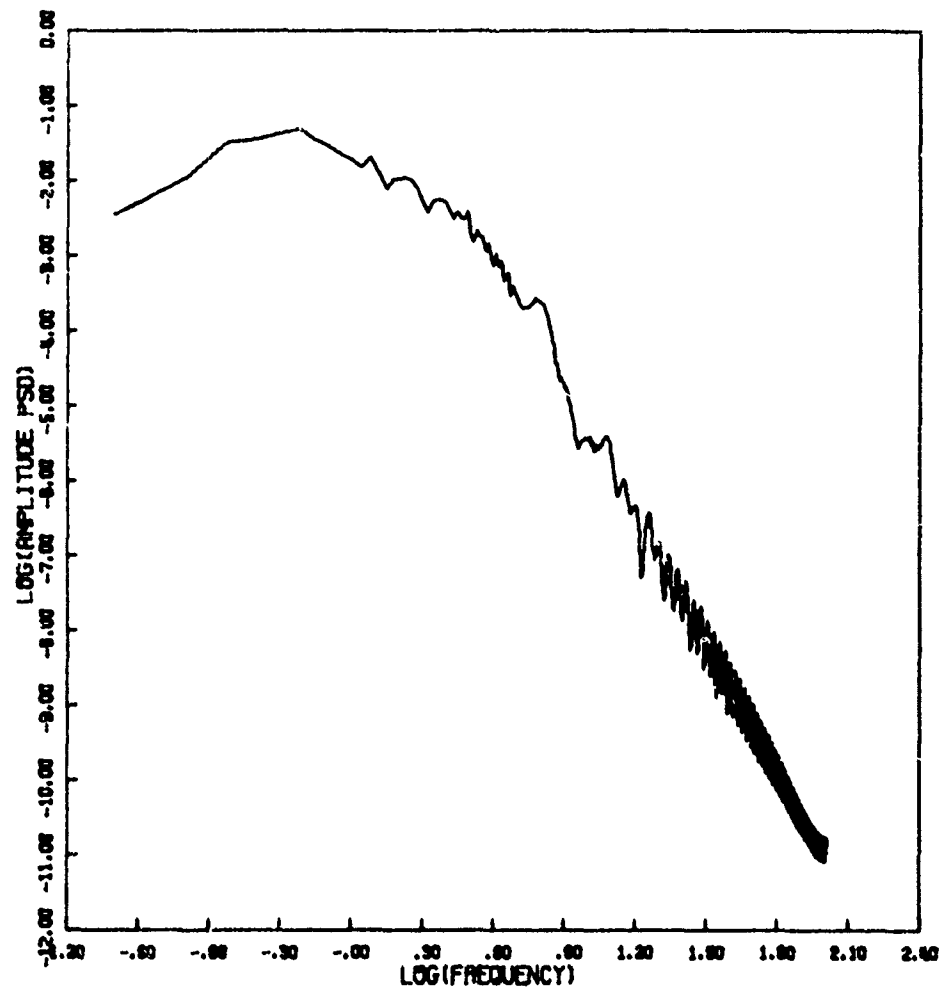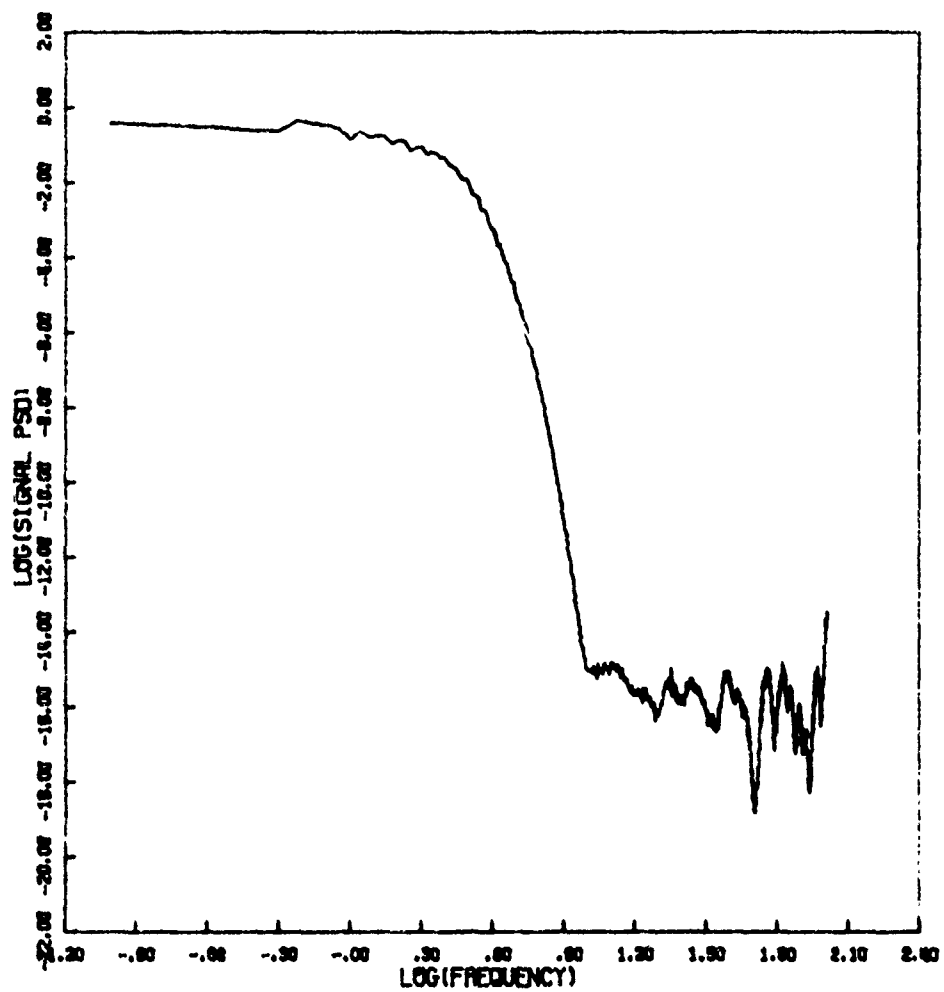
Figure 77d. Amplitude Power Spectral Density

Figure 77e.   Signal Power Spectral Density

Figure 78a. Signal Phase Plot

Figure 78b. Amplitude Distribution

Figure 78c. Phase Distribution

Figure 78d. Amplitude Power Spectral Density

Figure 78e. Phase Power Spectral Density
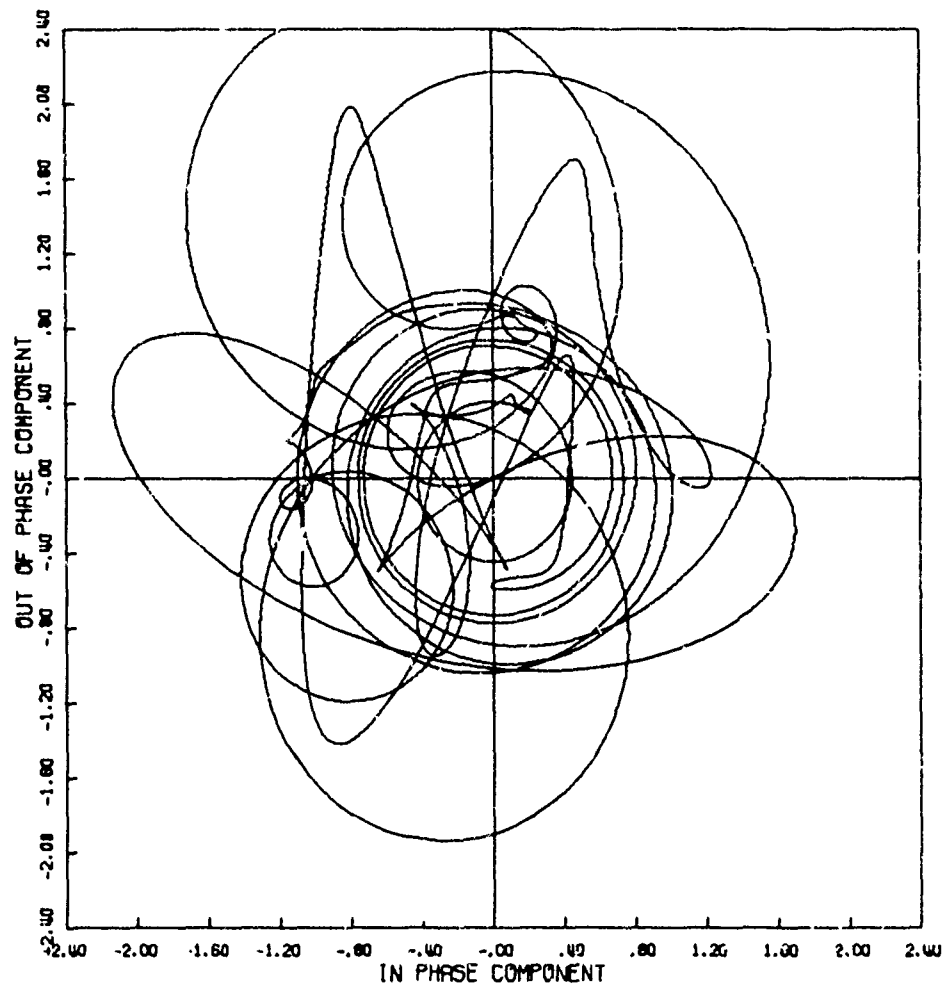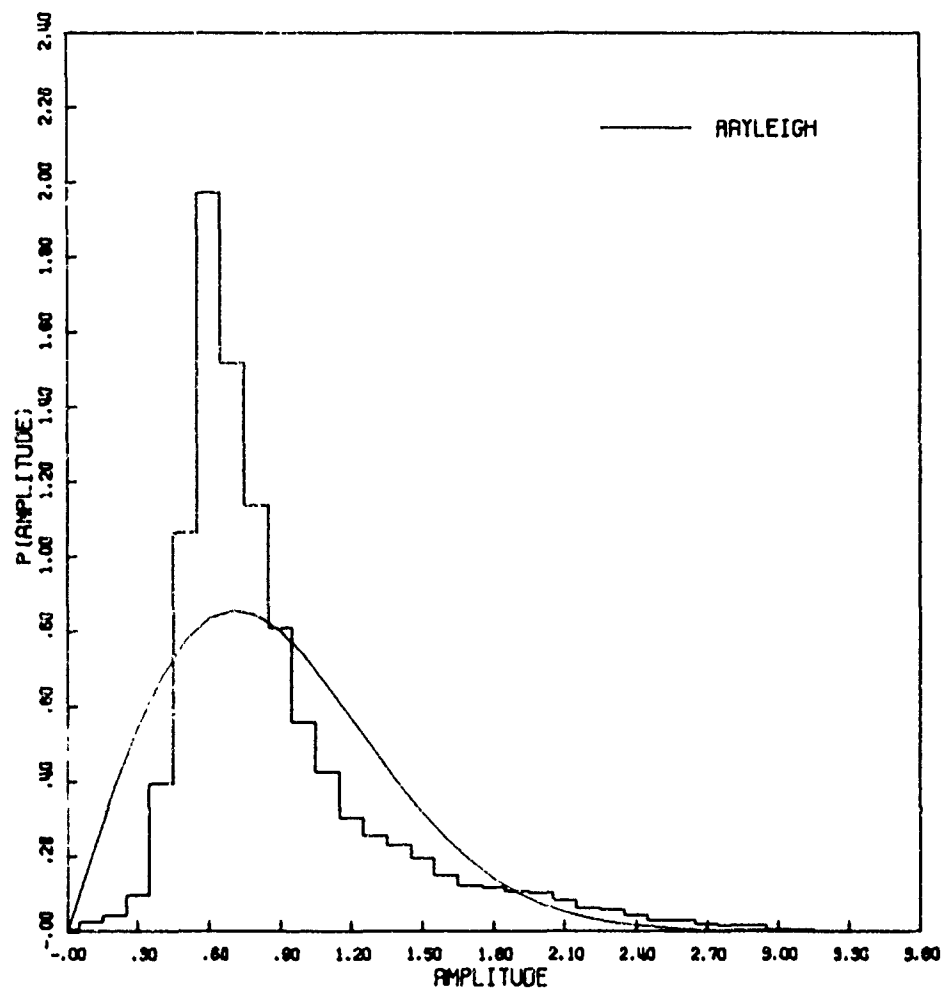
Figure 78f. Signal Power Spectral Density

Figure 79a. Signal Phase Plot

Figure 79b. Amplitude Distribution

Figure 79c.   Phase Distribution

Figure 79d.   Amplitude Power Spectral Density

Figure 79e.   Signal Power Spectral Density

Figure 80a. Signal Phase Plot

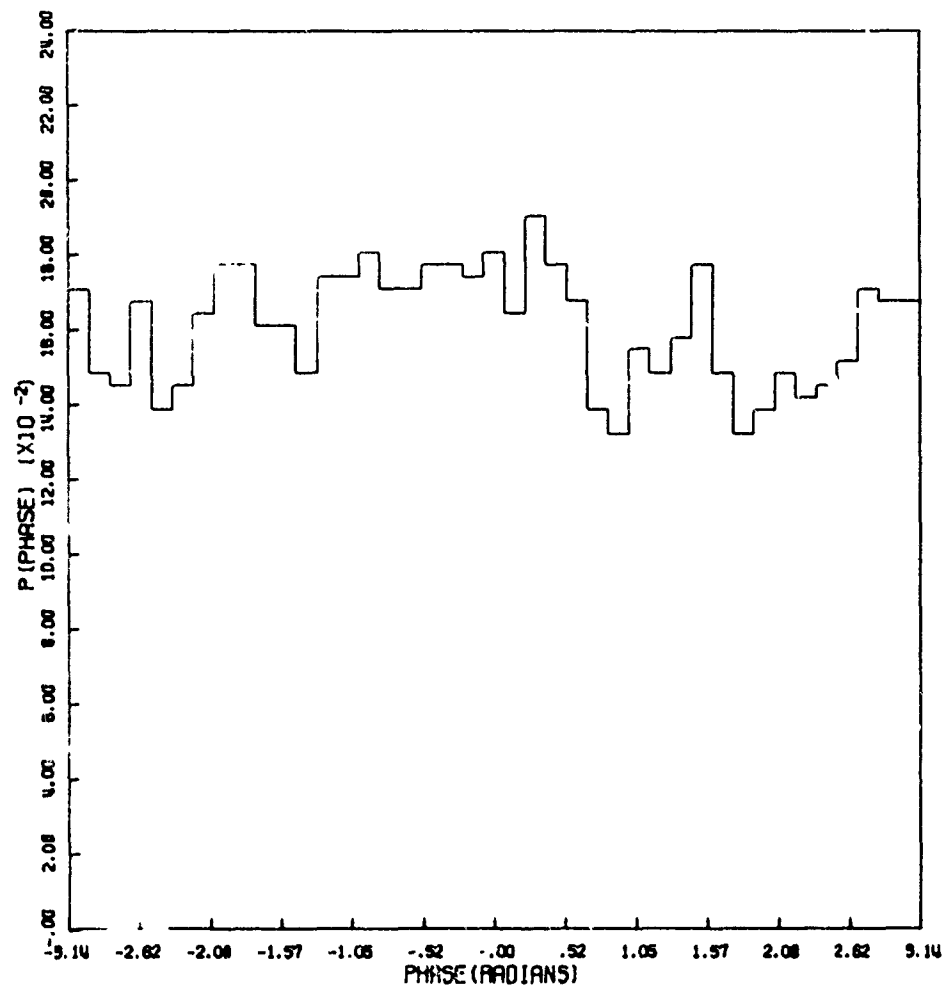Figure 80b. Amplitude Distribution
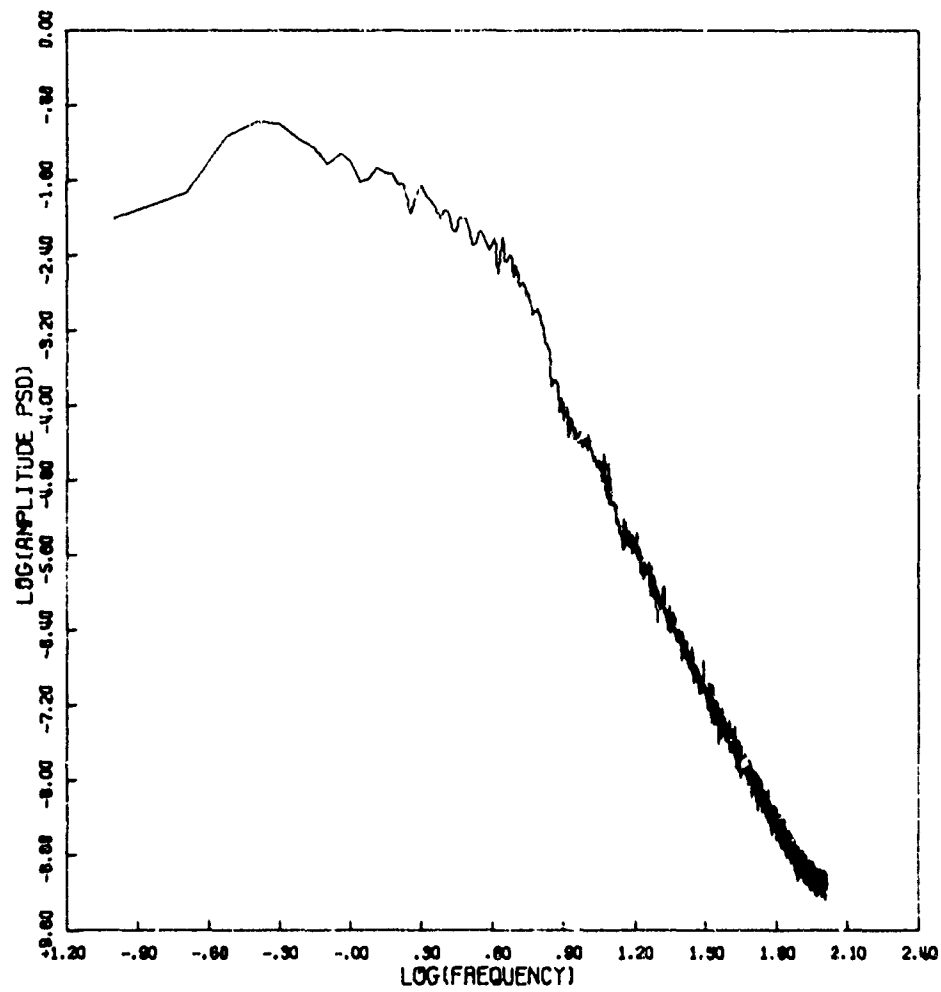
Figure 80c. Phase Distribution
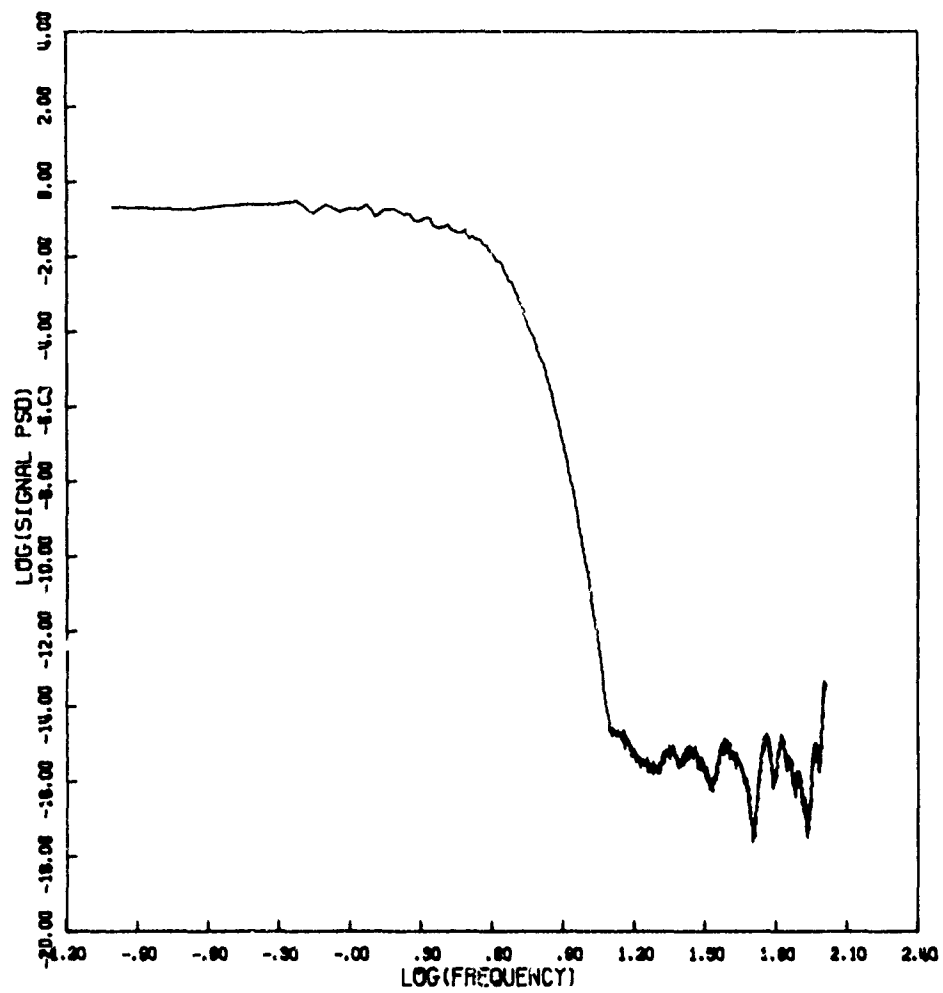
Figure 80d.   Amplitude Power Spectral Density

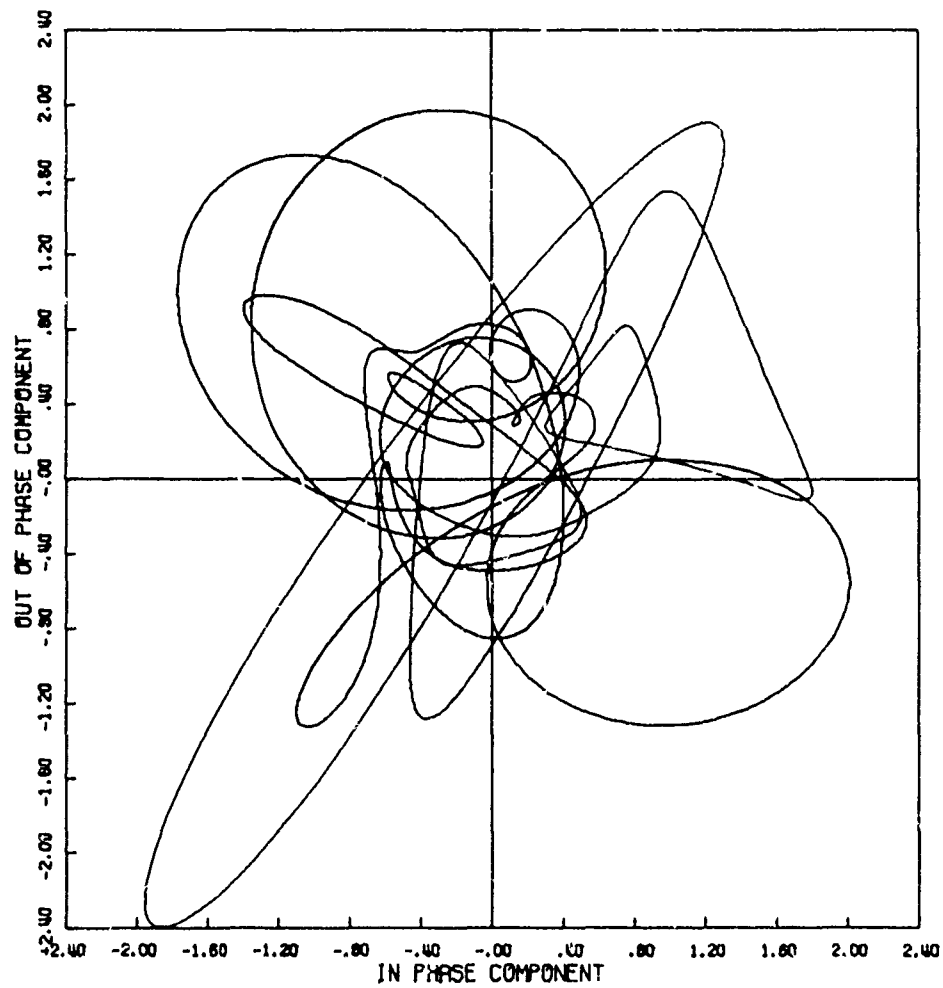Figure 80f. Signal Power Spectral Density

Figure 81a. Signal Phase Plot

Figure 81b. Amplitude Distribution

Figure 81c.   Phase Distribution

Figure 31d. Amplitude Power Spectral Density

Figure 81e.   Phase Power Spectral Density

Figure 81f. Signal Power Spectral Density
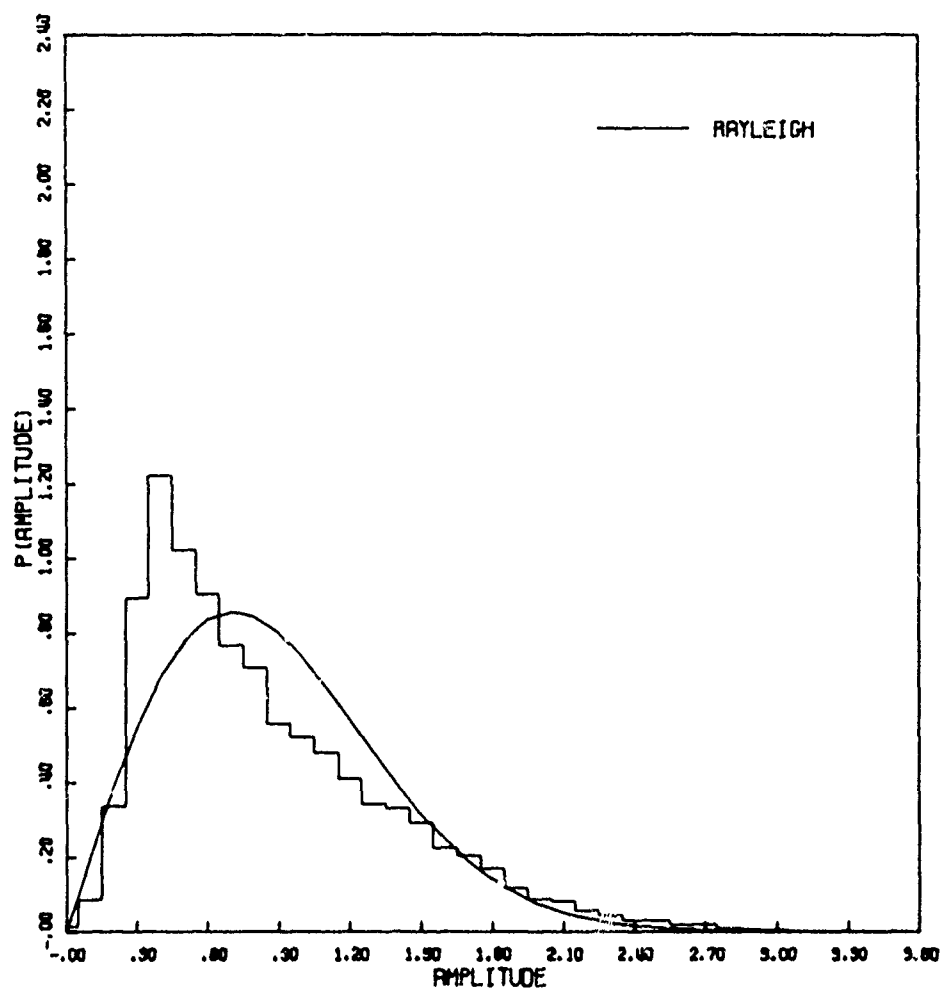
Figure 82a. Signal Phase Plot

Figure 82b. Amplitude Distribution

Figure 82c. Phase Distribution

Figure 82d. Amplitude Power Spectral Density

Figure 82e.   Phase Power Spectral Density

Figure 82f. Signal Power Spectral Density

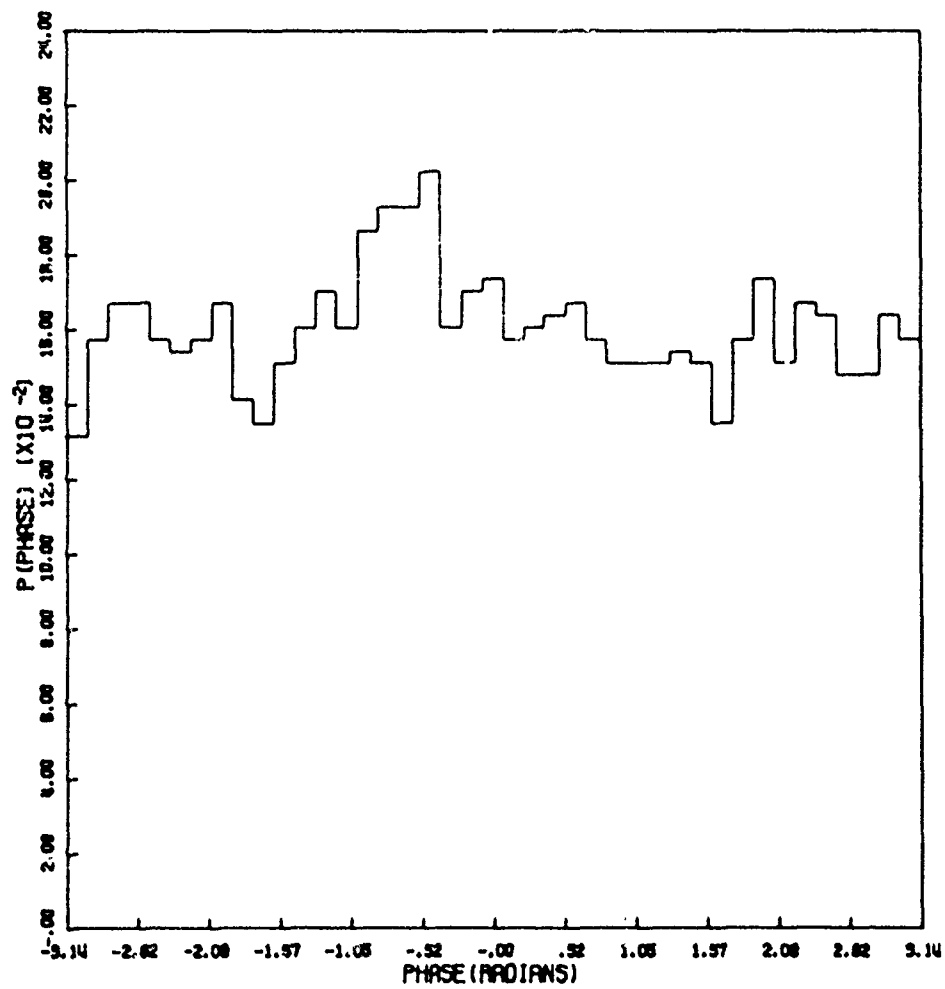Figure 83a.   Signal Phase Plot

Figure 83b. Amplitude Distribution

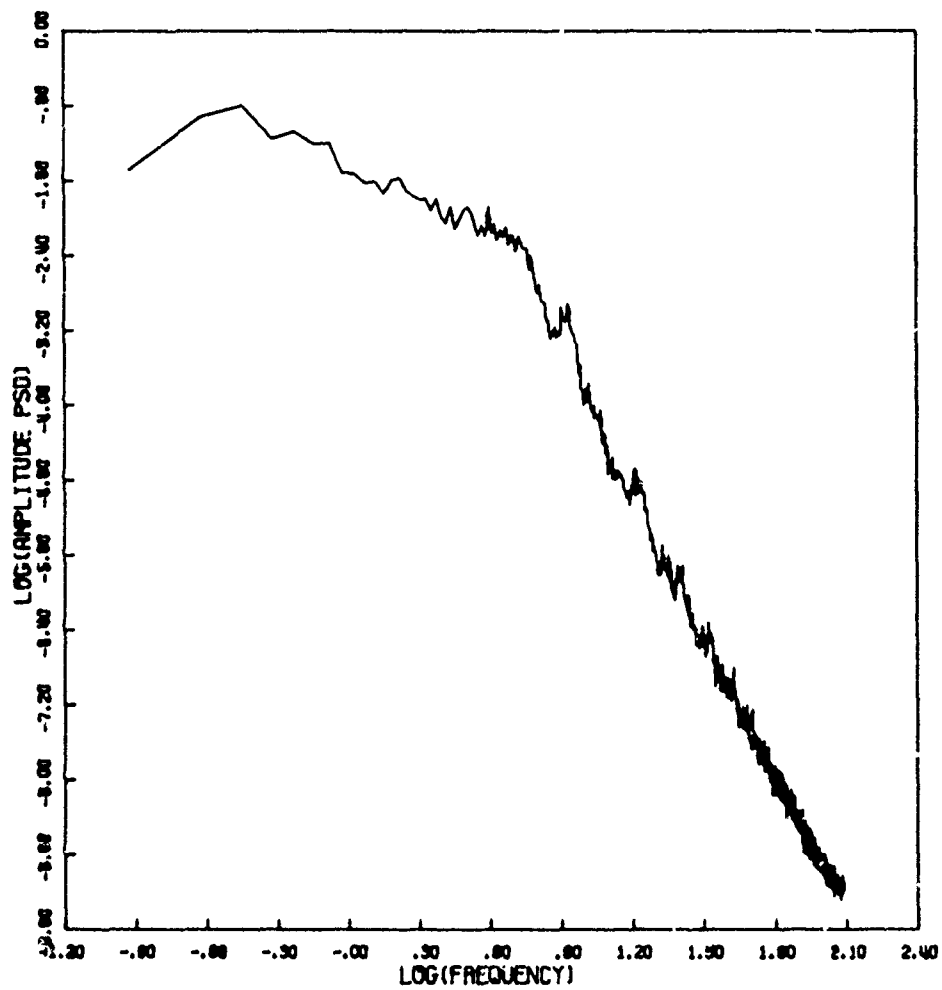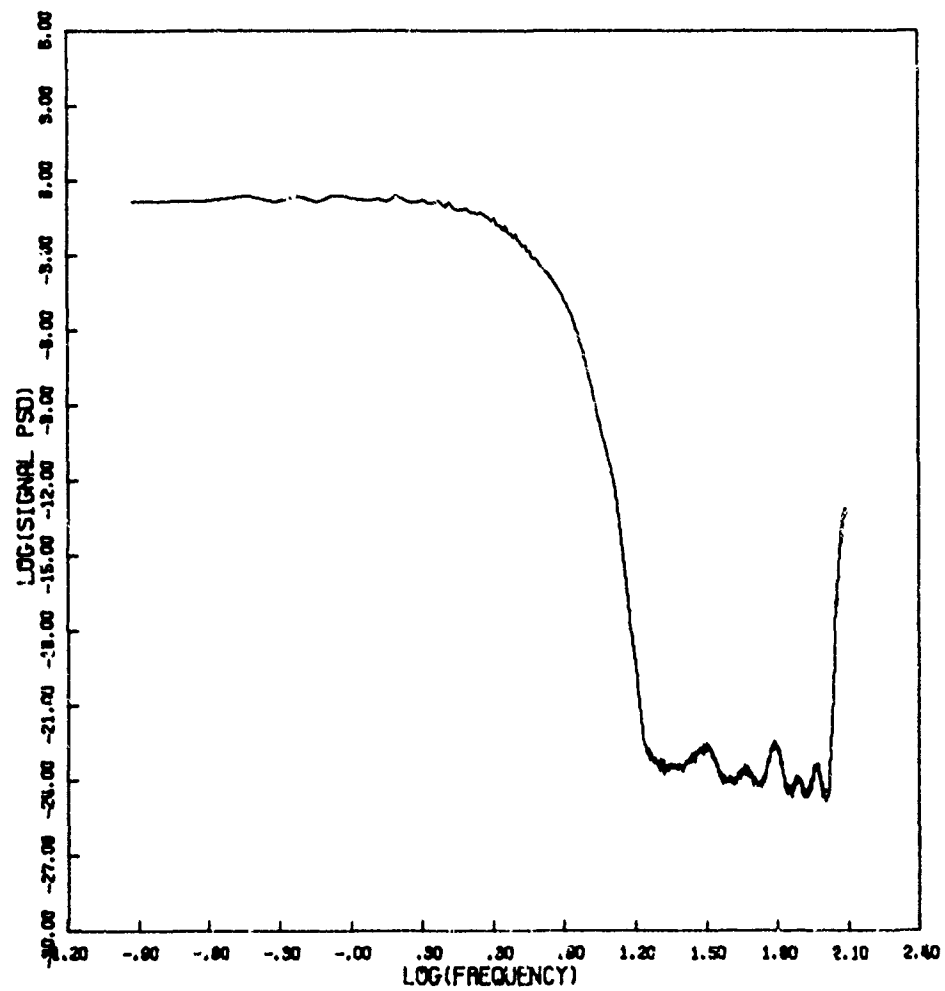Figure 83c.   Phase Distribution

Figure 83d. Amplitude Power Spectral Density

Figure 83f. Signal Power Spectral Density
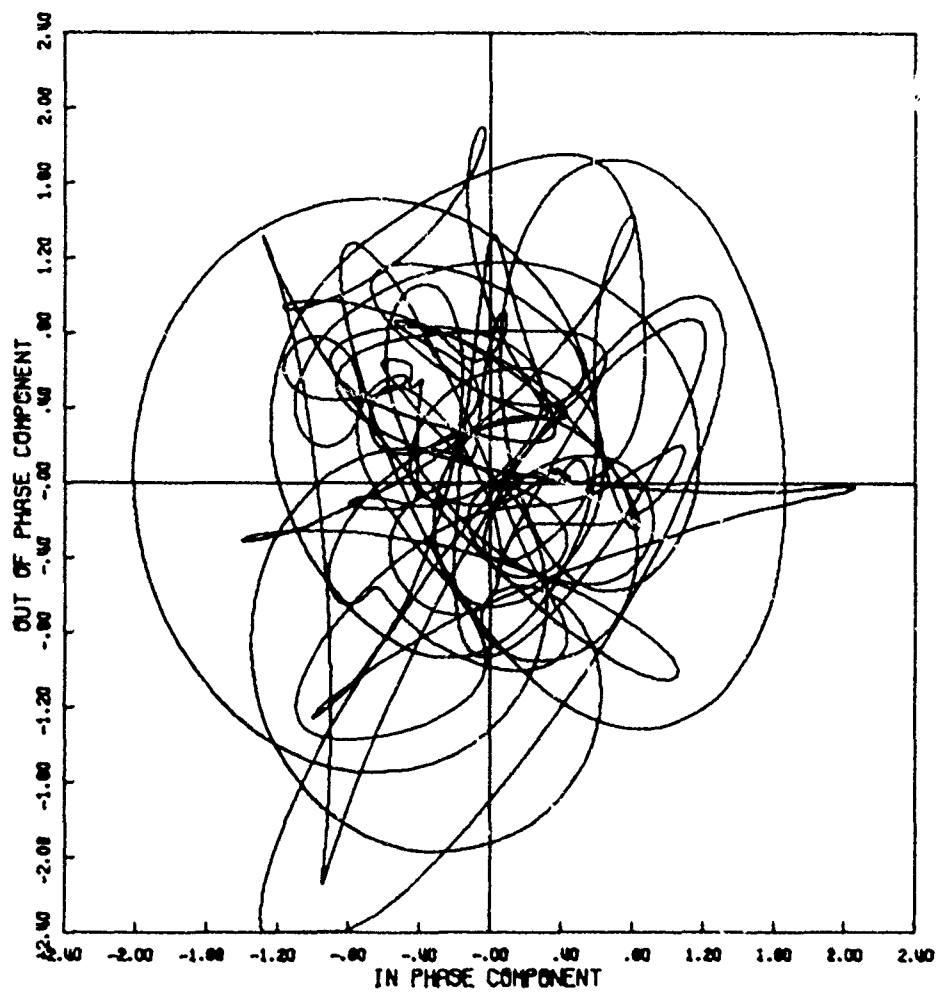
Figure 84a. Signal Phase Plot
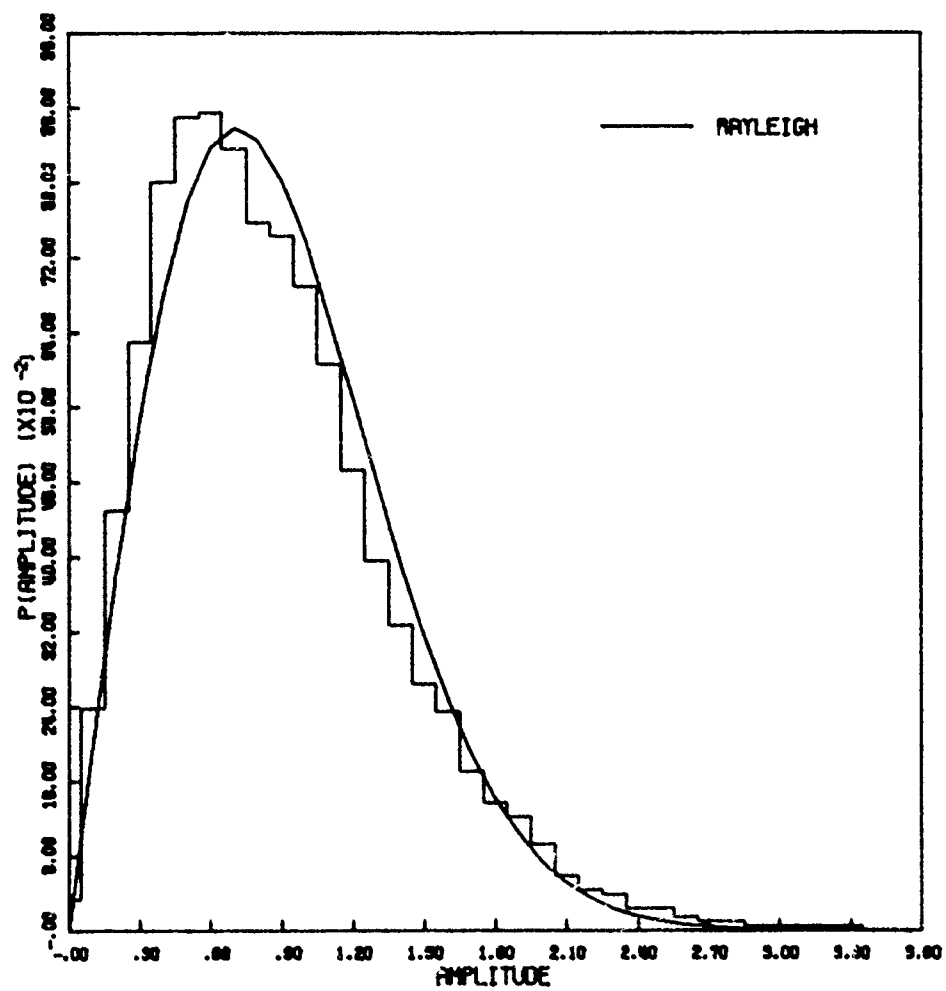
Figure 84b.   Amplitude Distribution

Figure 84c. Phase Distribution

Figure 84d.　Amplitude Power Spectral Density

Figure 84f. Signal Power Spectral Density

Figure 85a.   Signal Phase Plot

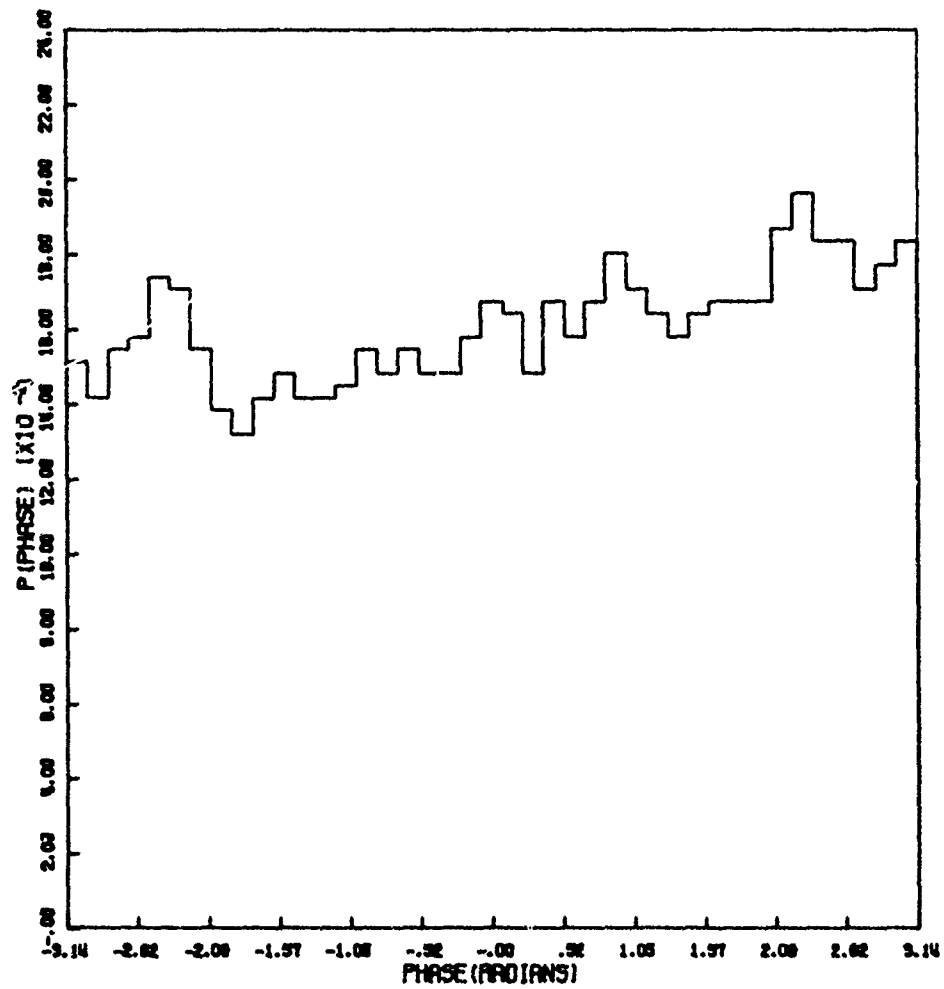Figure 85b. Amplitude Distribution
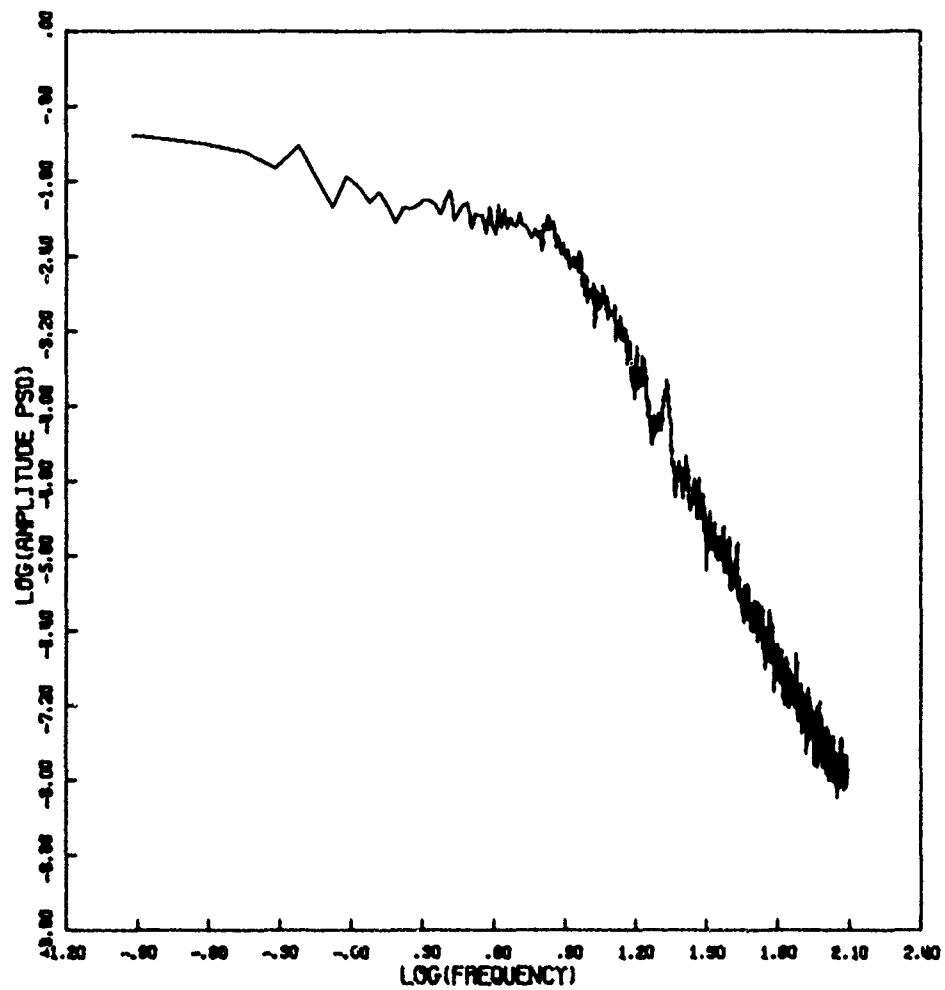
Figure 85c. Phase Distribution
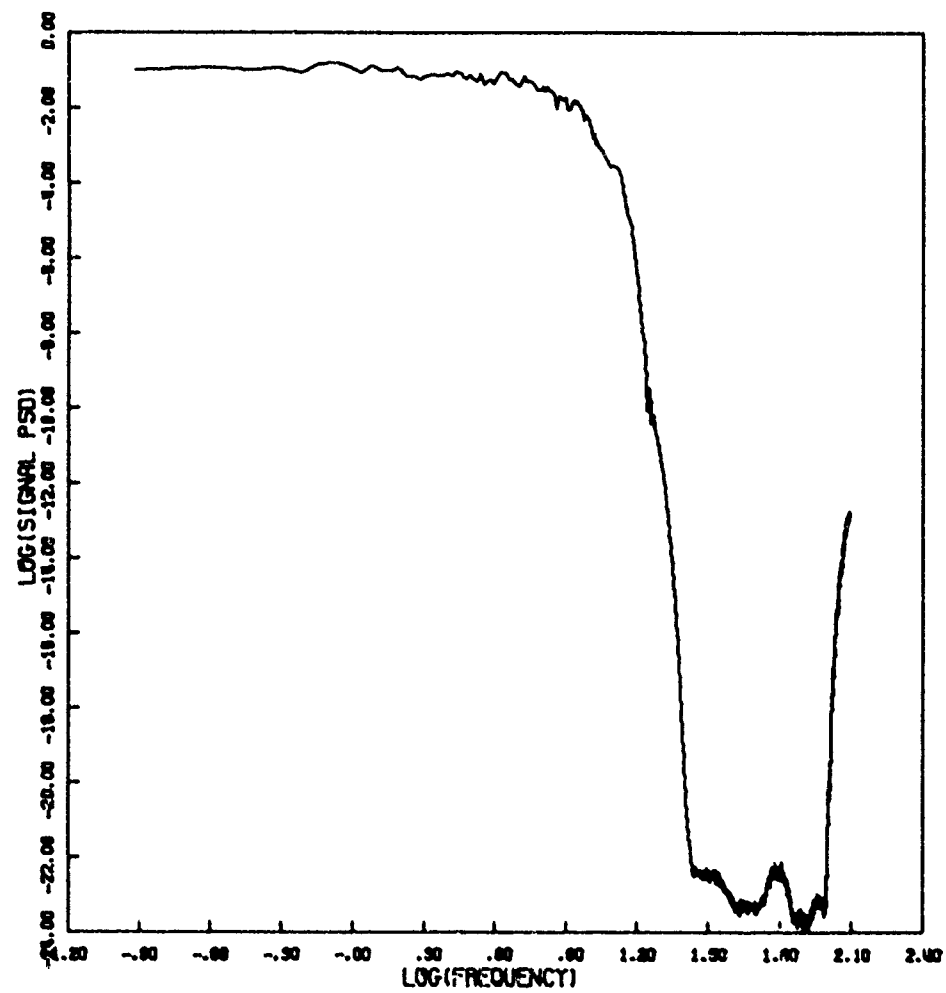
Figure 85d. Amplitude Power Spectral Density

Figure 85e. Signal Power Spectral Density
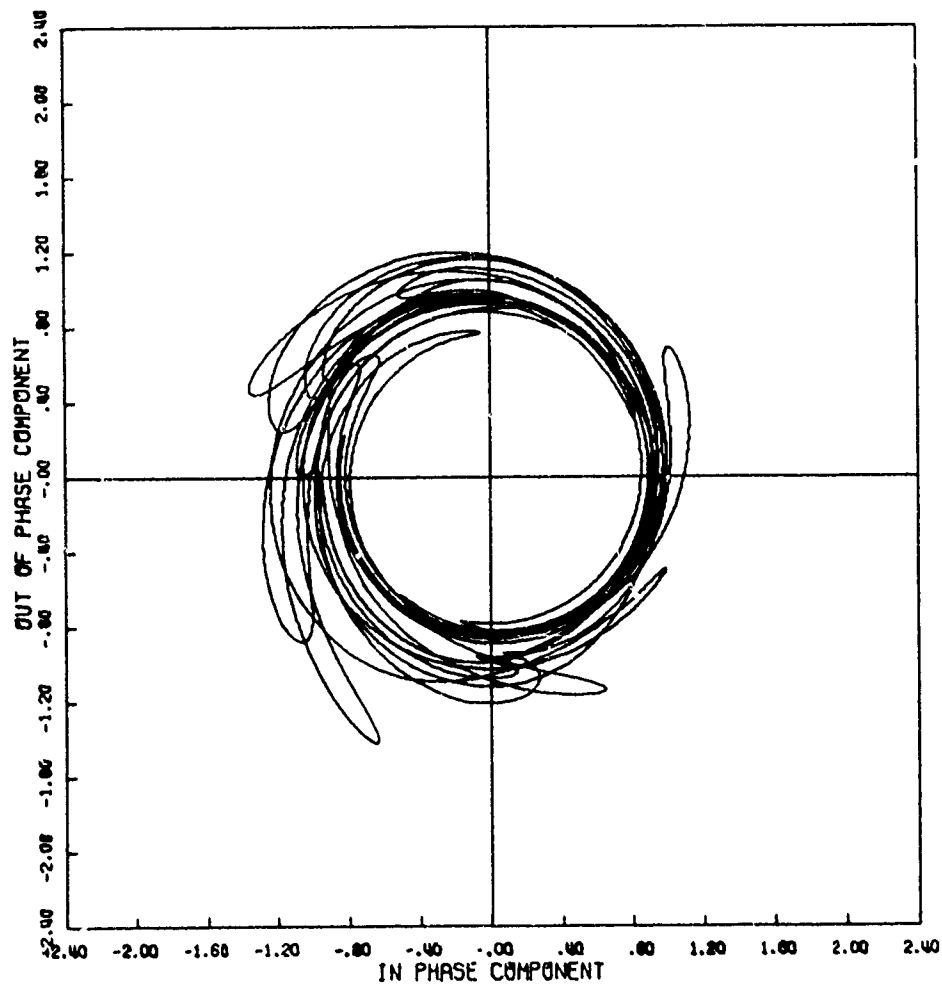
Figure 86a. Signal Phase Plot

Figure 86b. Amplitude Distribution

Figure 86d. Amplitude Power Spectral Density

Figure 86d. Amplitude Power Spectral Density

Figure 86e.   Phase Power Spectral Density
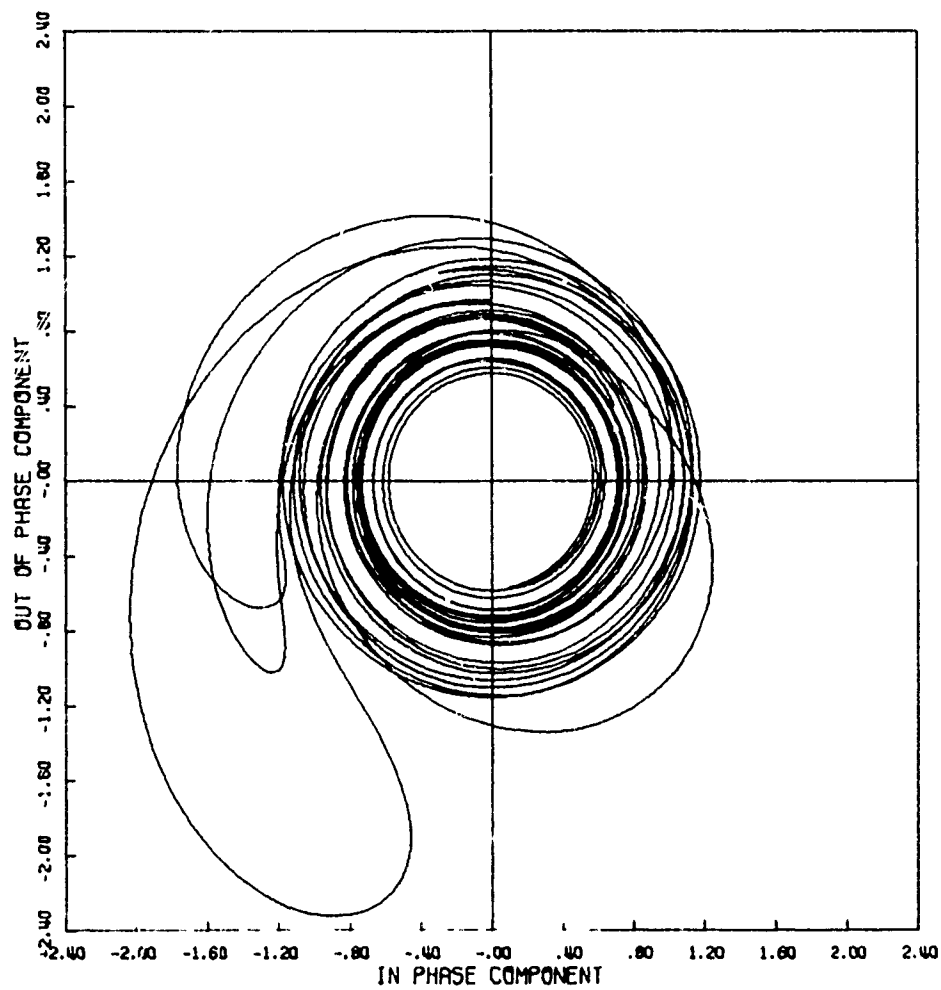
Figure 86f. Signal Power Spectral Density

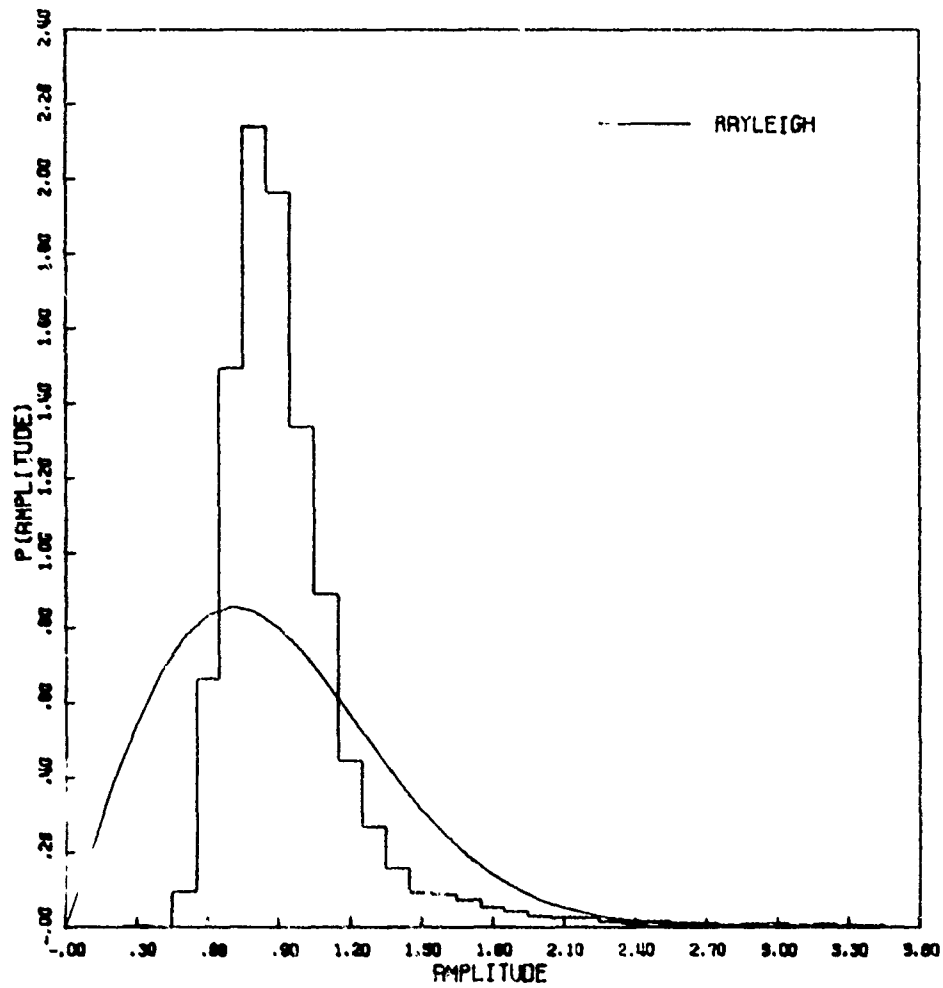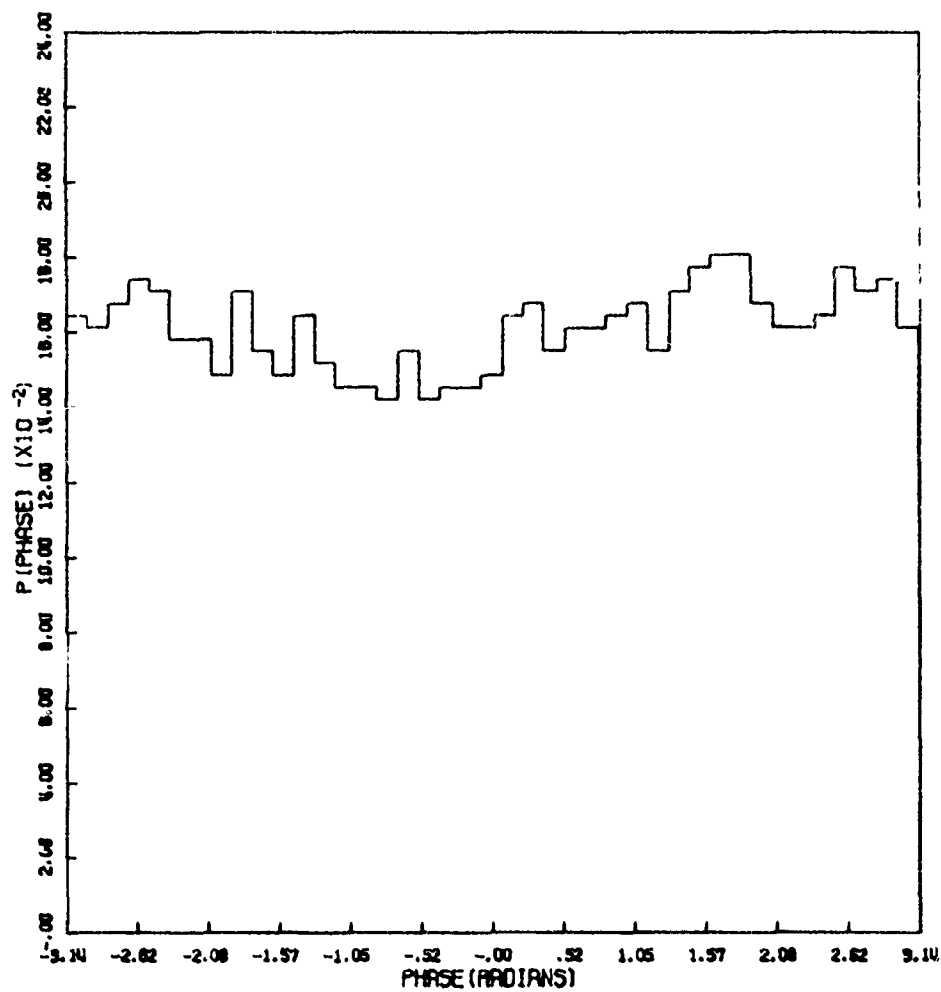Figure 87a. Signal Phase Plot

Figure 87b.   Amplitude Distribution

Figure 87c. Phase Distribution

Figure 87d.   Amplitude Power Spectral Density

Figure 87f. Signal Power Spectral Density

Figure 88a.   Signal Phase Plot

Figure 88b. Amplitude Distribution

Figure 88c. Phase Distribution

Figure 88d. Amplitude Power Spectral Density

Figure 88e. Signal Power Spectral Density

Figure 89a. Signal Phase Plot

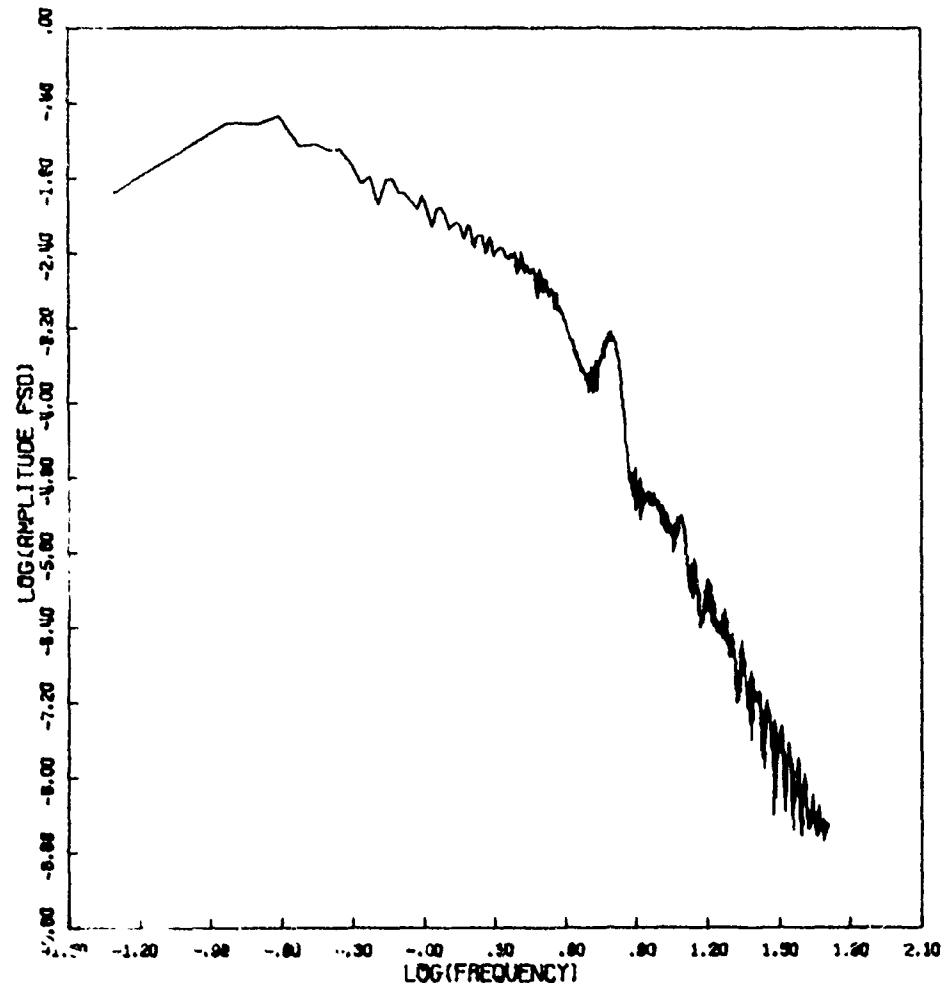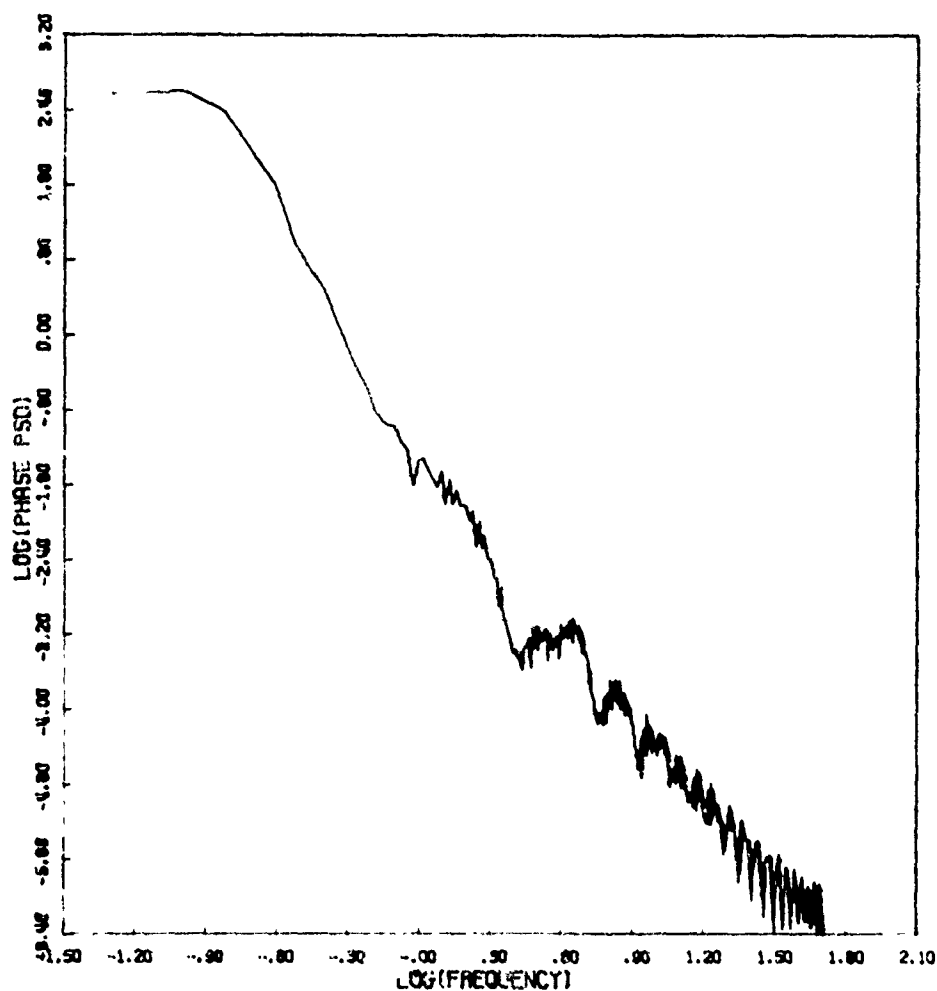Figure 89b. Amplitude Distribution

Figure 89c. Phase Distribution
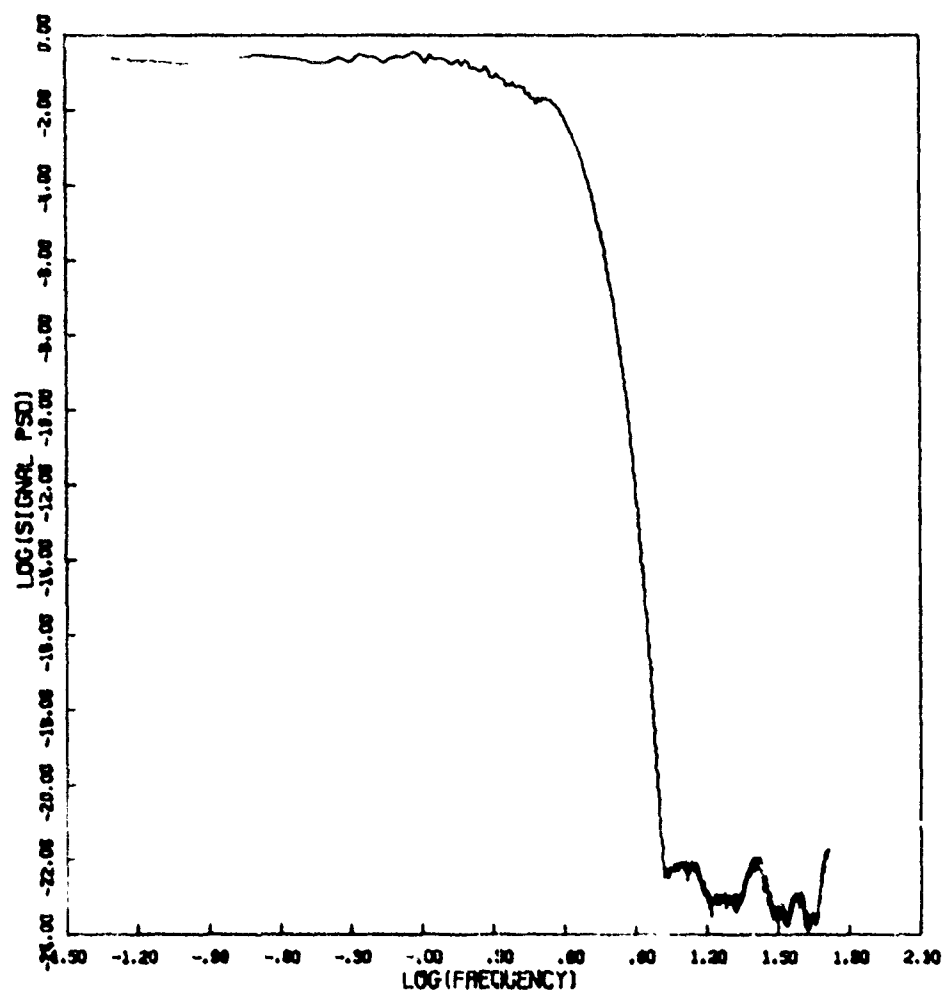
Figure 89d. Amplitude Power Spectral Density

Figure 89e. Signal Power Spectral Density
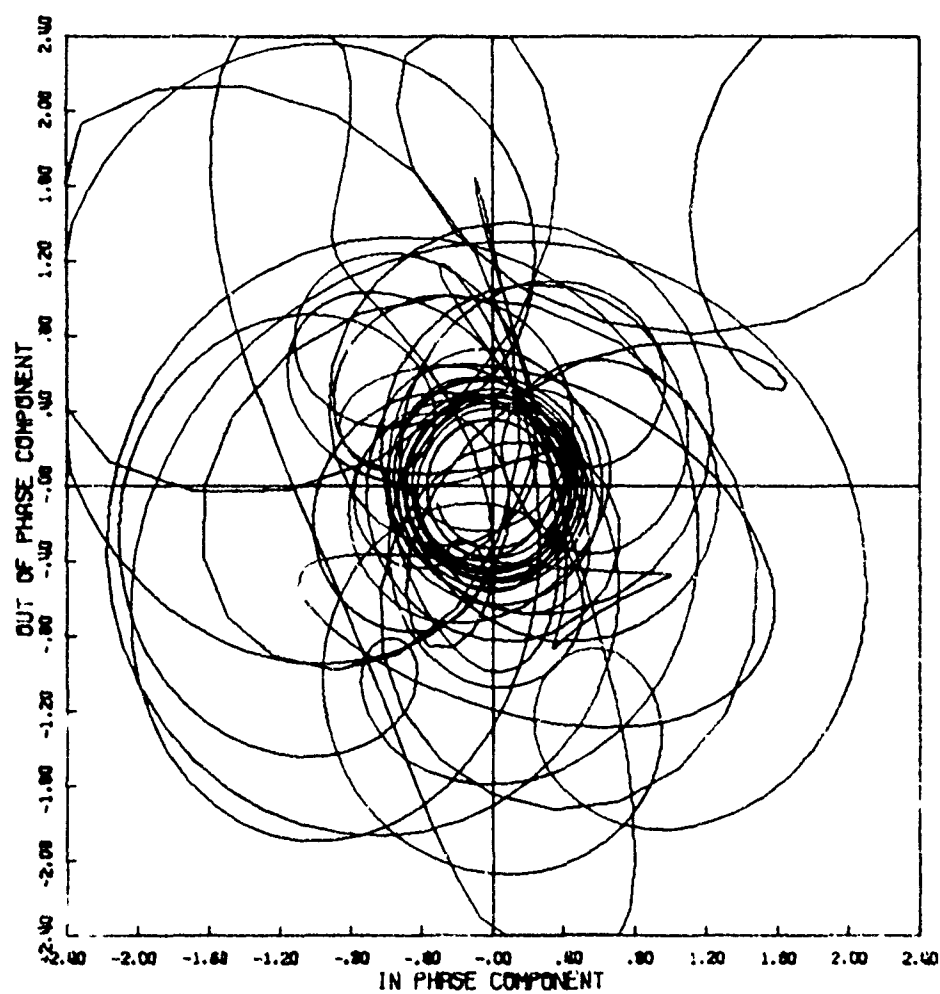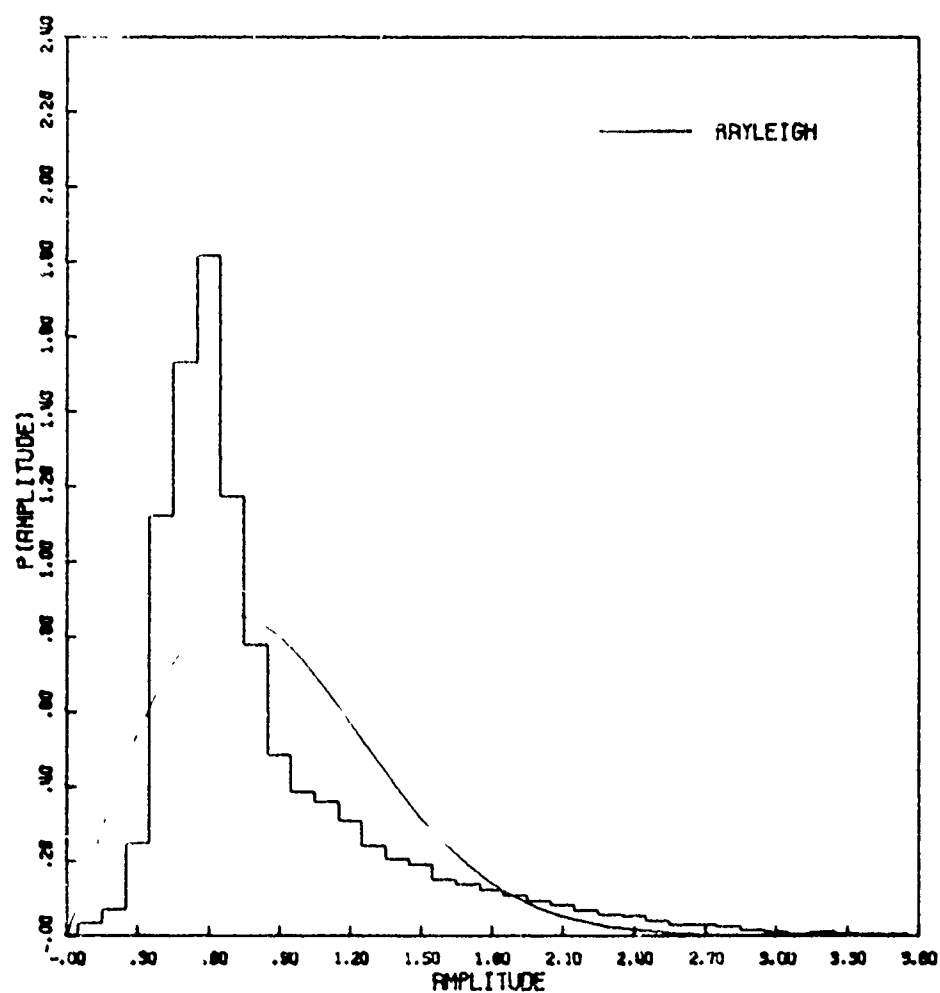
Figure 90a. Signal Phase Plot

Figure 90b. Amplitude Distribution

Figure 90c. Phase Distribution

Figure 90d.   Amplitude Power Spectral Density

Figure 90e. Signal Power Spectral Density

Figure 91a. Signal Phase Plot

Figure 91b.   Amplitude Distribution

Figure 91c.   Phase Distribution

Figure 91d. Amplitude Power Spectral Density

Figure 91e. Phase Power Spectral Density

Figure 91f.   Signal Power Spectral Density

Figure 92a. Signal Phase Plot
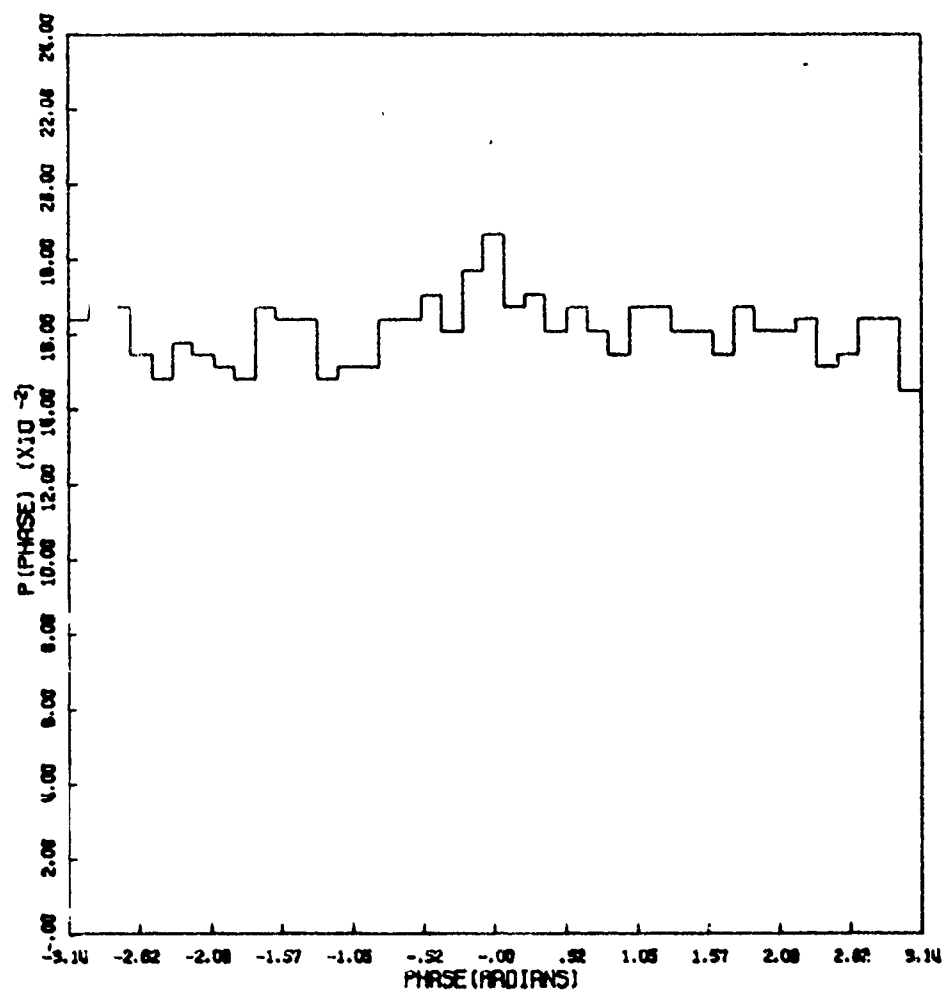
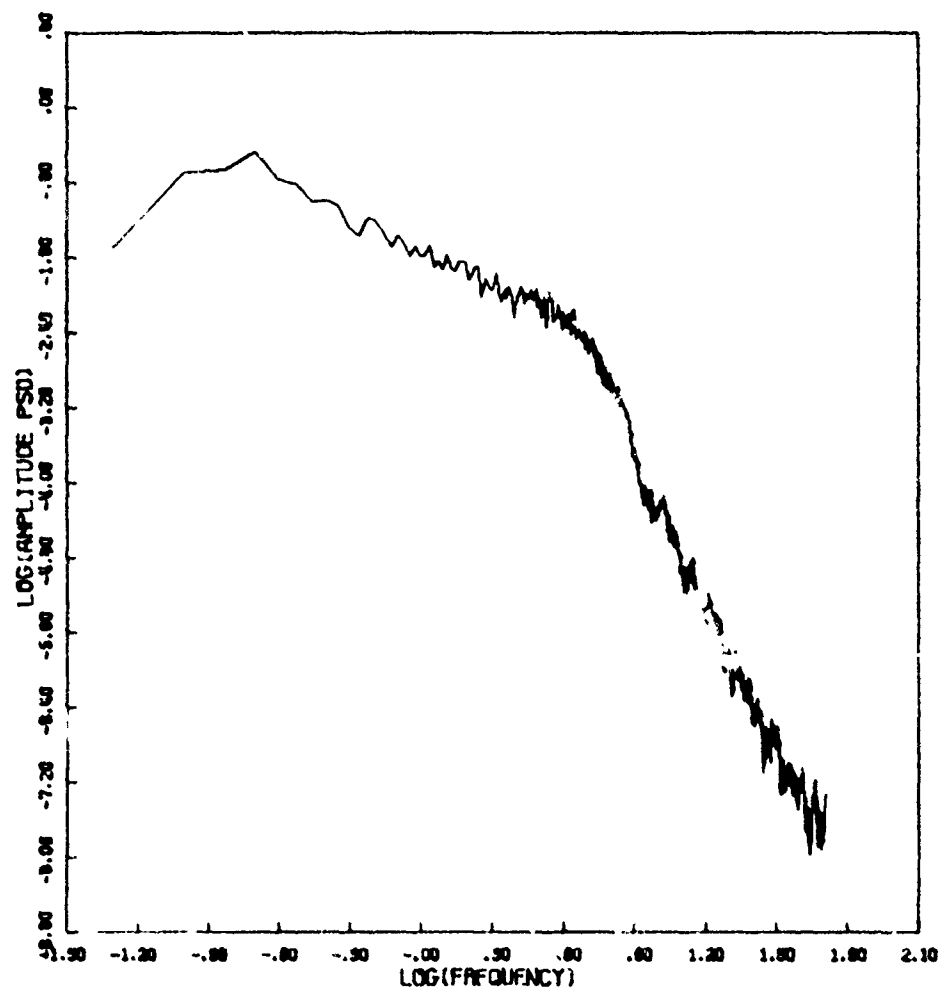Figure 92b. Amplitude Distribution

Figure 92c. Phase Distribution

450

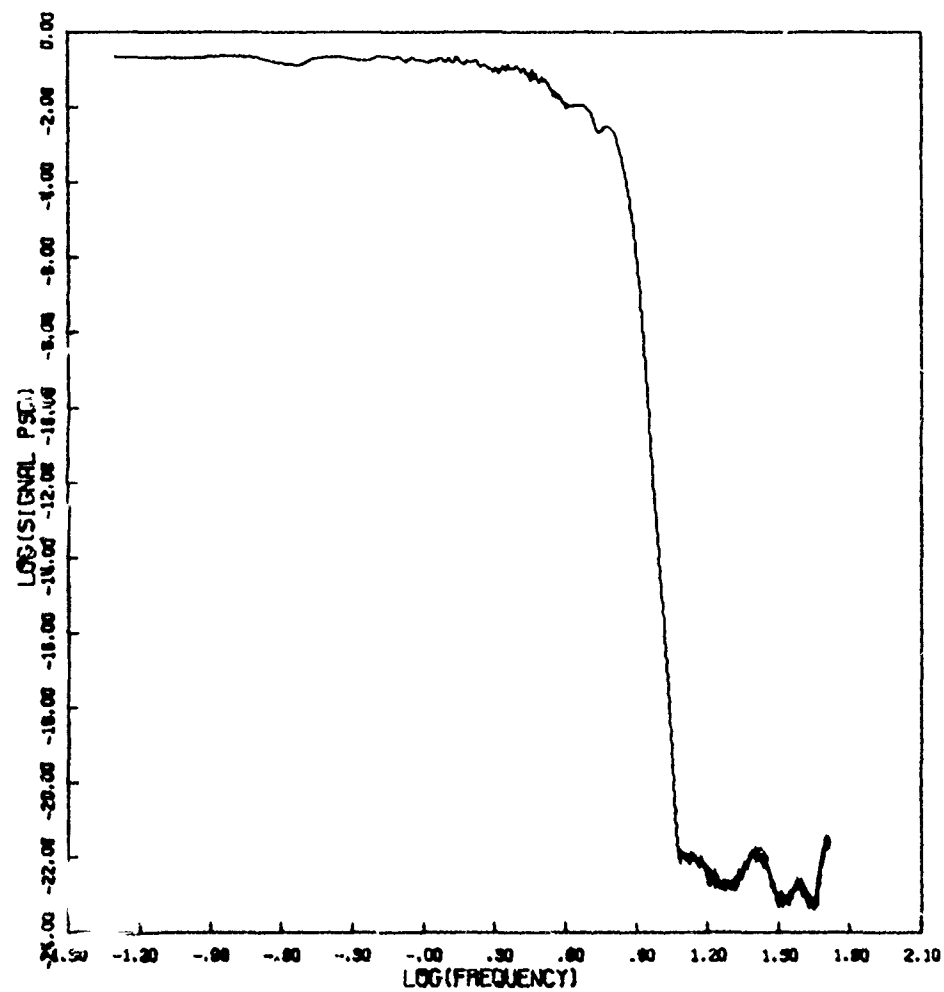Figure 92d. Amplitude Power Spectral Density

Figure 92e.   Signal Power Spectral Density

Table 6

THICKNESS DATA

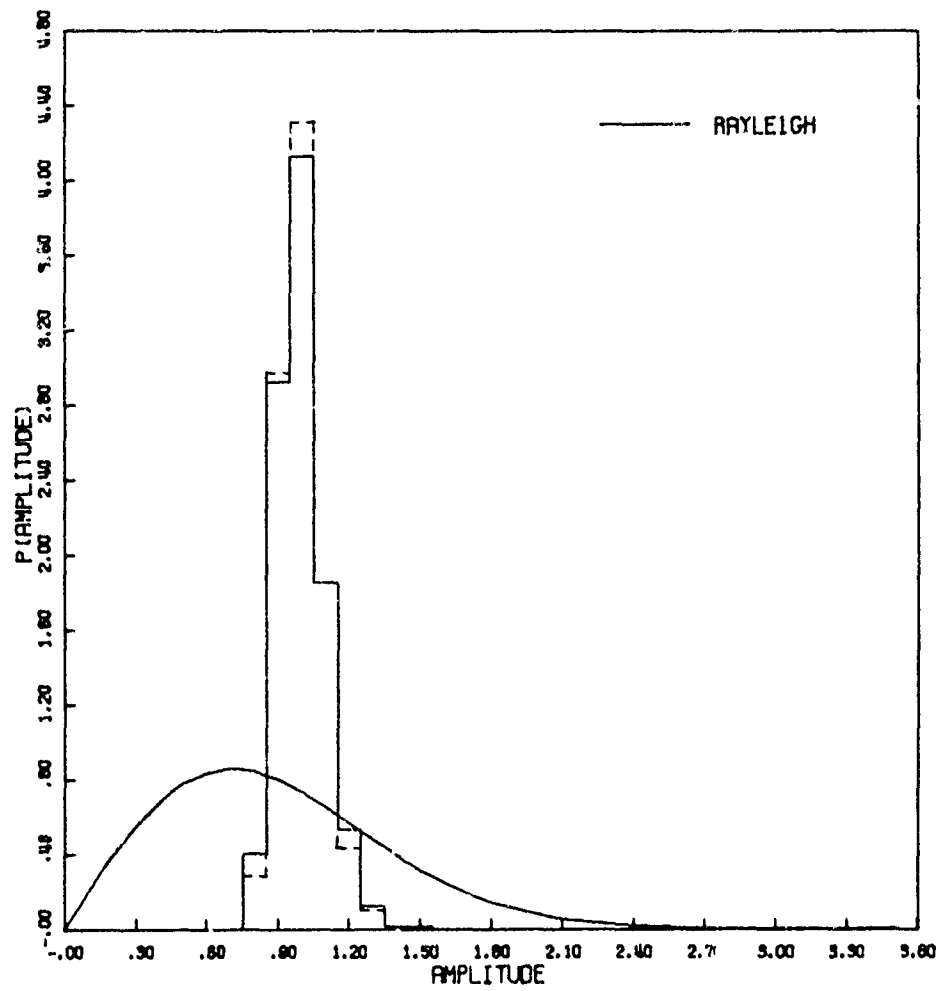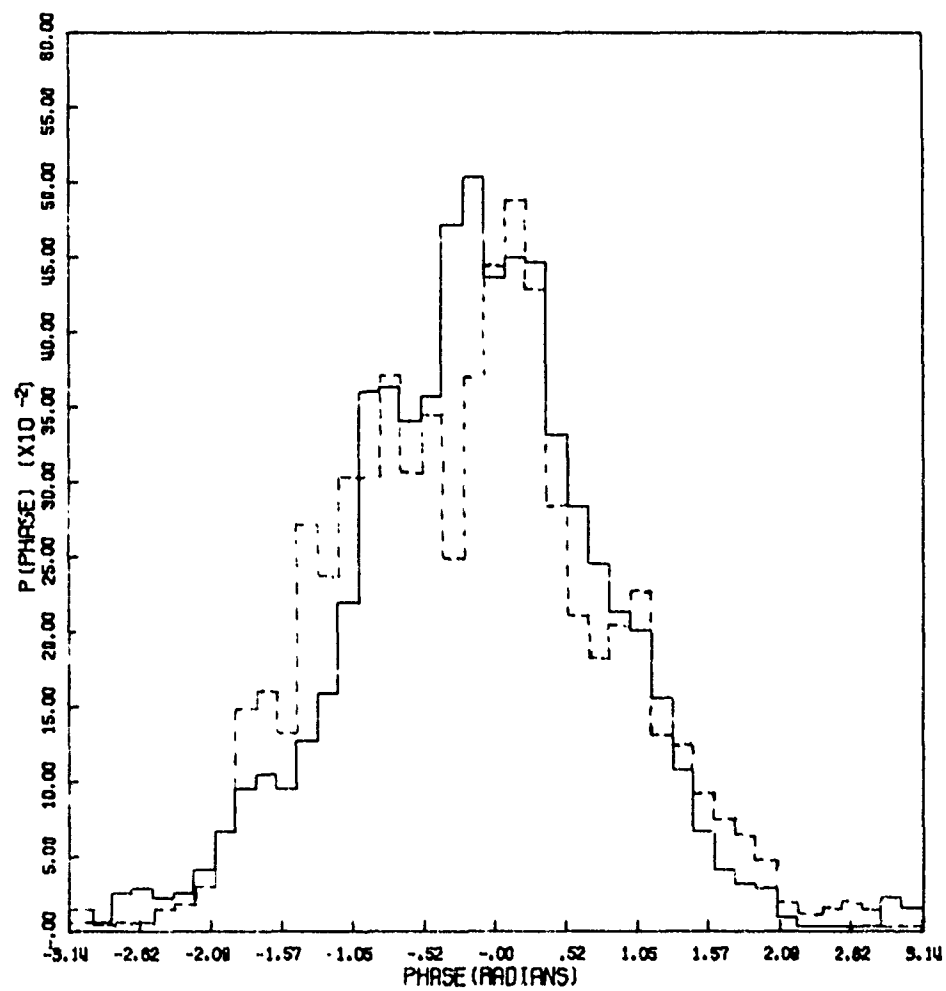|	$z_g = 3\times10^7$		$z_s = 10^7$			$K = 6.28\times10^{-2}$		THICKNESS DATA		
FIG.	L	$\overline{\Delta n^2}$	$\overline{\phi^2}$	$\overline{\chi^2}$	S_4	ℓ_0	$\overline{E_R^2}$	$\overline{E_I^2}$	$\overline{N}/A$	MFP
J3				GAUSSIAN						
	10^5	7.1×10^8	0.86	0.01	0.21	8.2×10^4	0.18	0.38		∞
	10^5	7.1×10^8	1.01	0.009	0.20	9.0×10^4	0.20	0.44	3.5×10^{-12}	5
94				CYLINDRICAL ROD						
	10^5	7.4×10^8	0.80	0.02	0.26	9.2×10^4	0.17	0.37		∞
	10^5	7.4×10^8	0.96	0.02	0.25	1.0×10^5	0.20	0.44	3.5×10^{-12}	5
95				K_ρ^{-2}						
	10^5	6.3×10^8	0.74	0.02	0.28	1.3×10^5	0.17	0.35		∞
	10^5	6.3×10^8	0.84	0.02	0.28	1.4×10^5	0.17	0.41	7.1×10^{-11}	5
96				K_ρ^{-1}						
	10^5	3.6×10^8	0.79	0.11	0.55	7.1×10^4	0.20	0.36		∞
	10^5	3.6×10^8	0.97	0.11	0.53	7.9×10^4	0.21	0.42	9.4×10^{-10}	5

Figure 93a. Amplitude Distribution
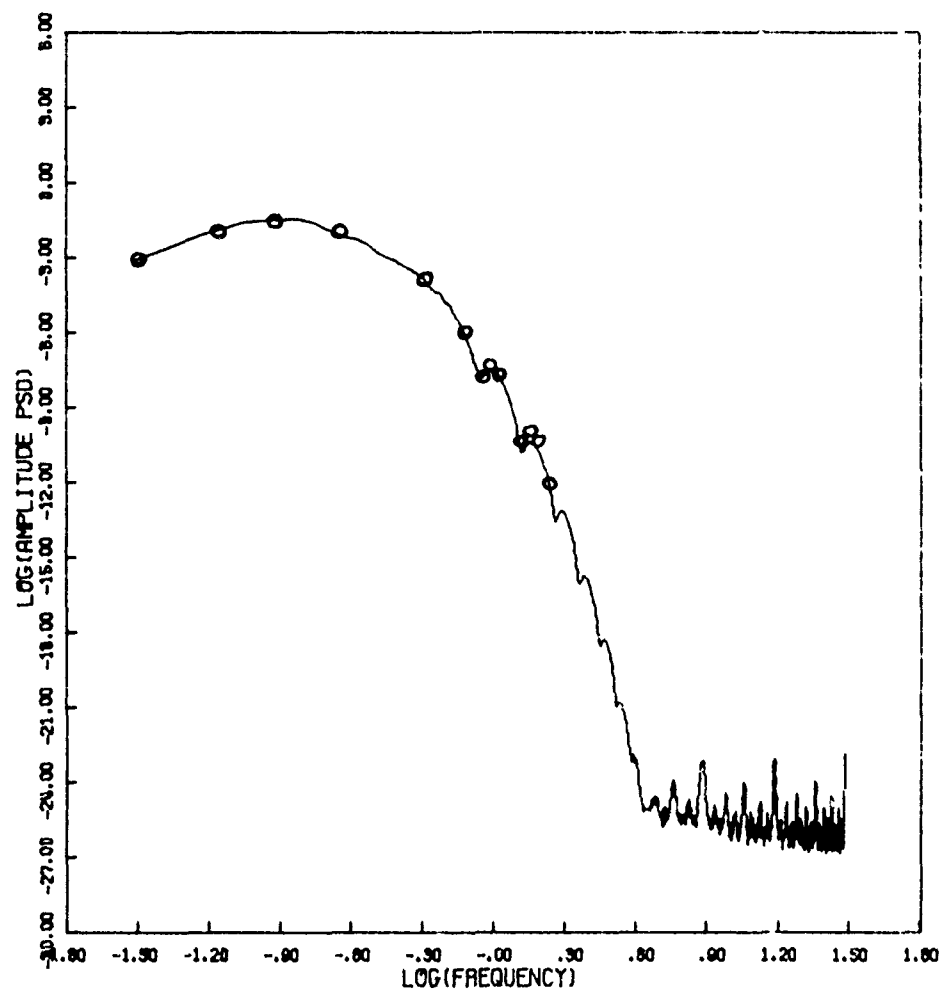
Figure 93b. Phase Distribution

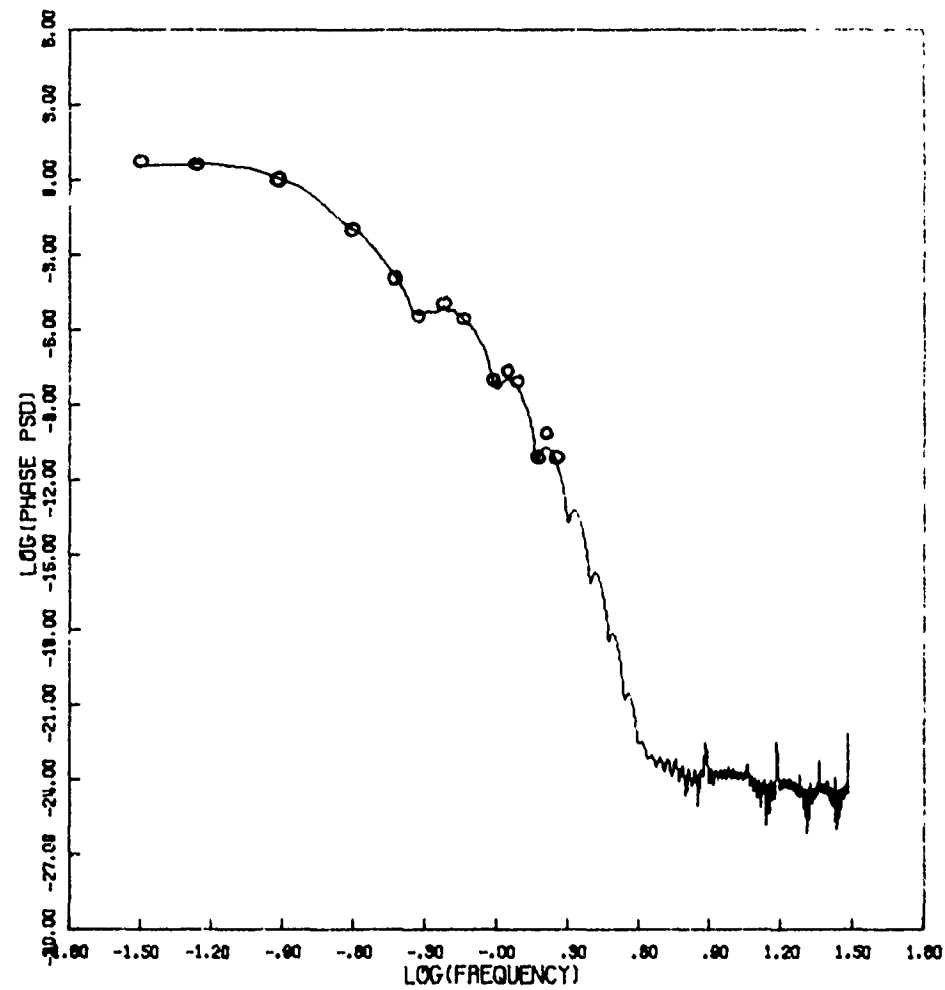Figure 93c. Amplitude Power Spectral Density

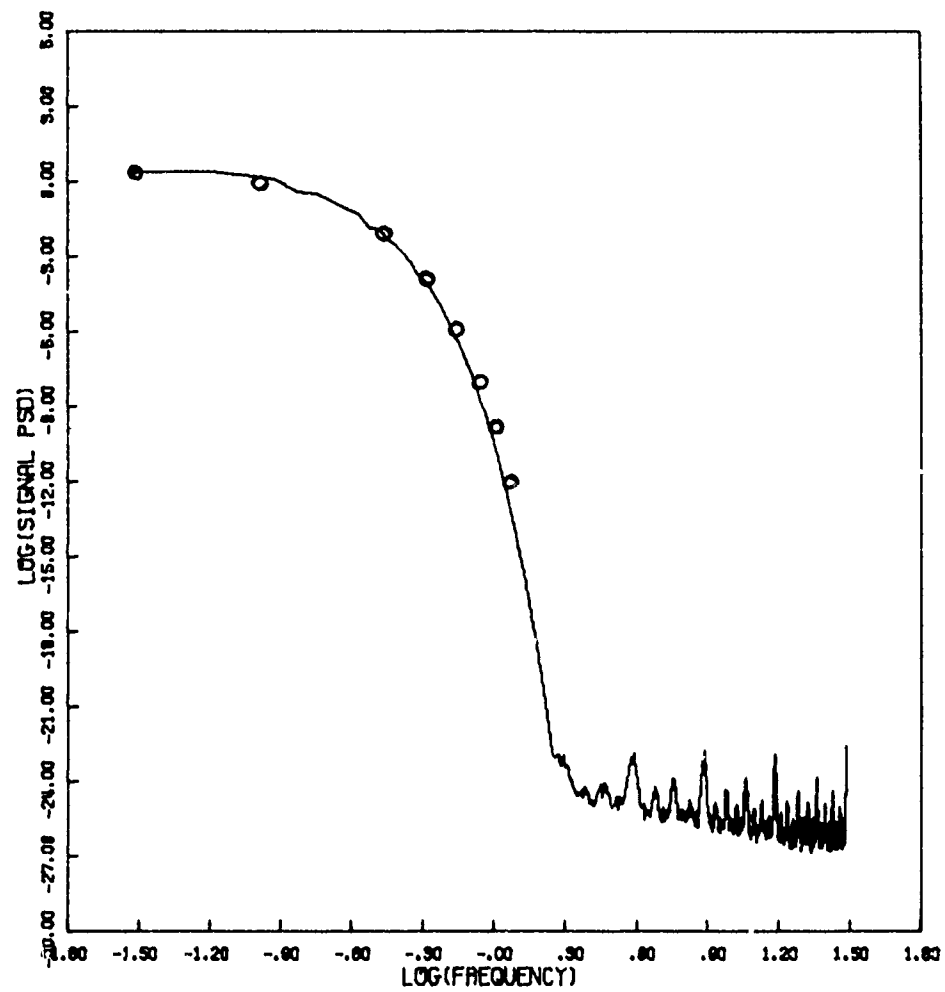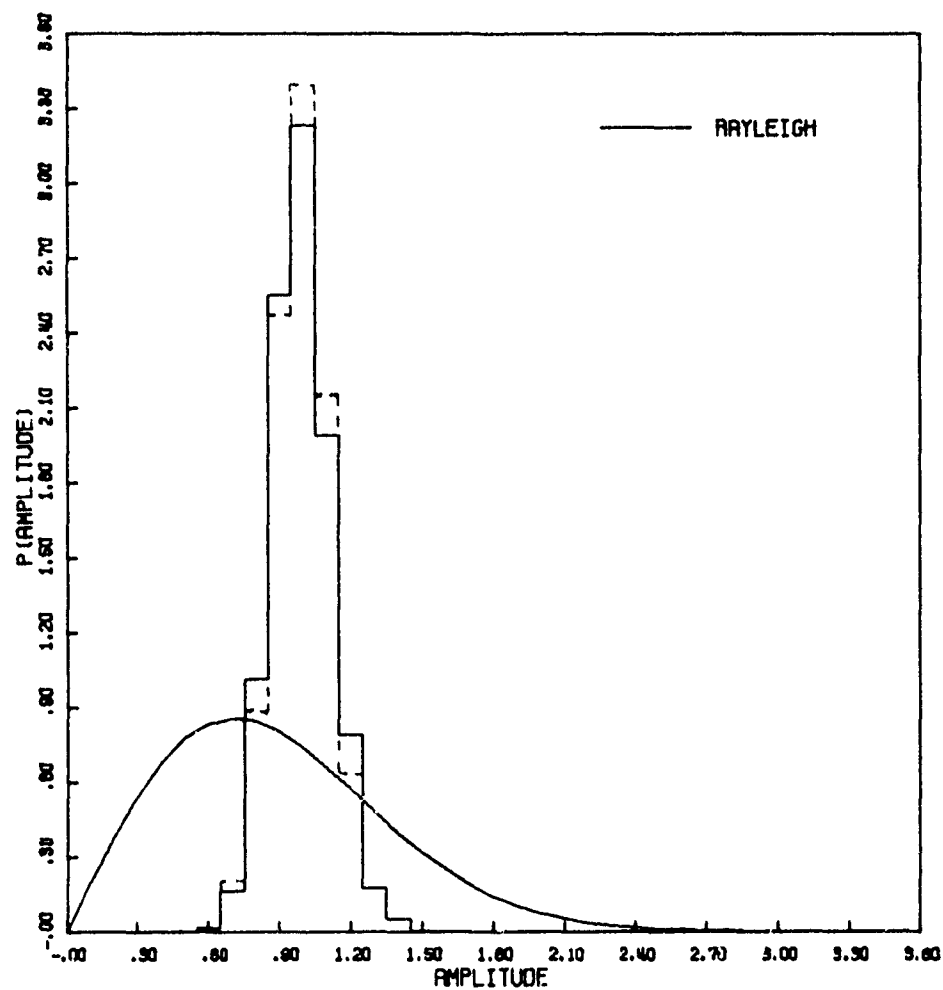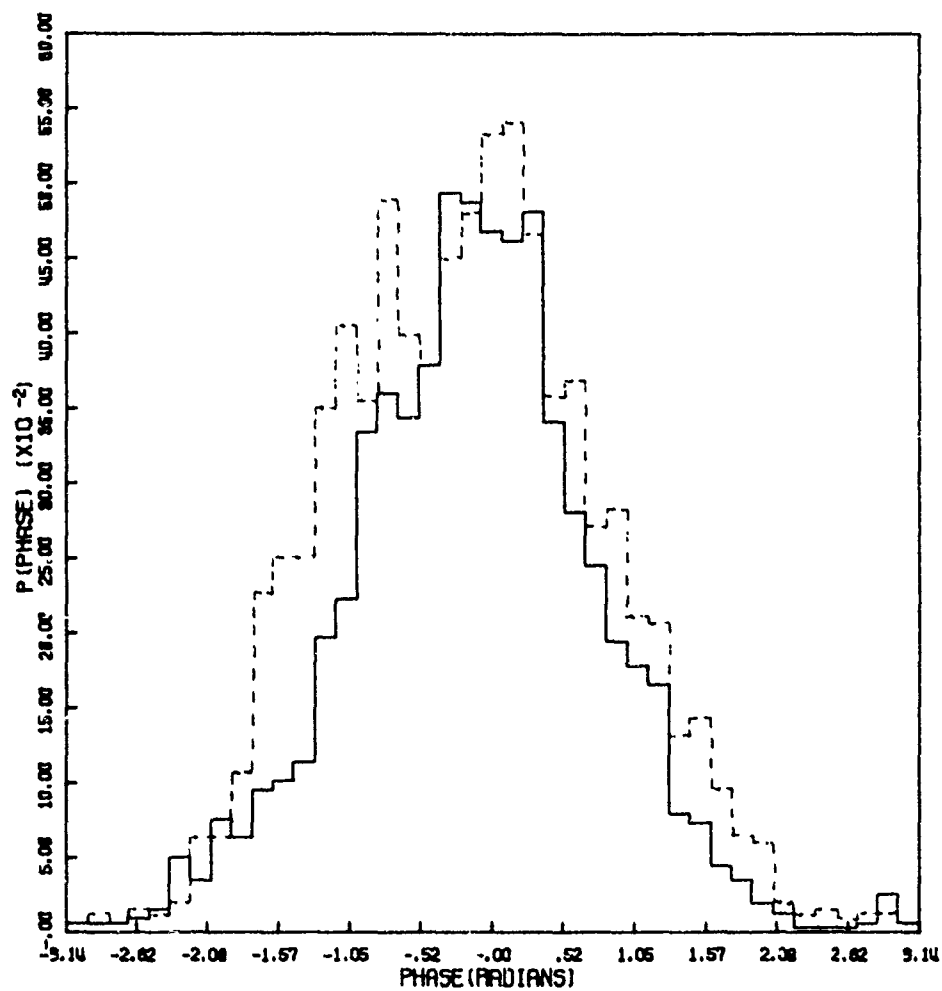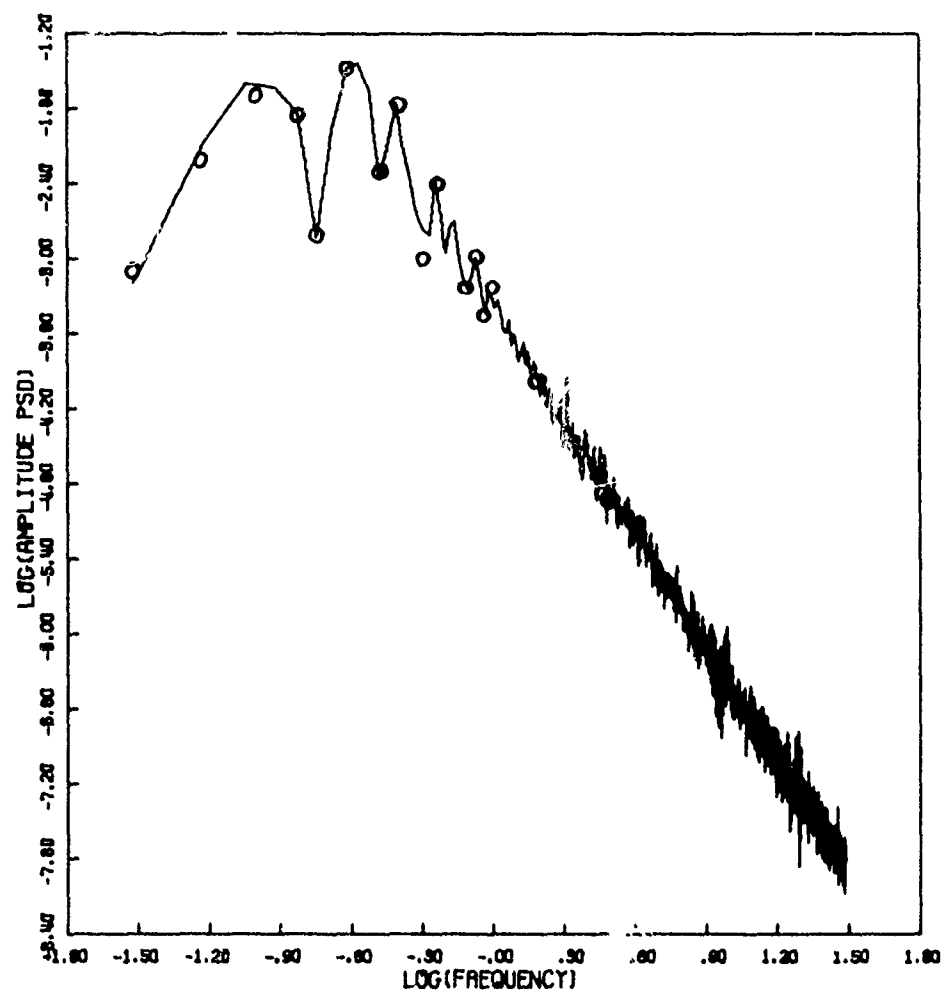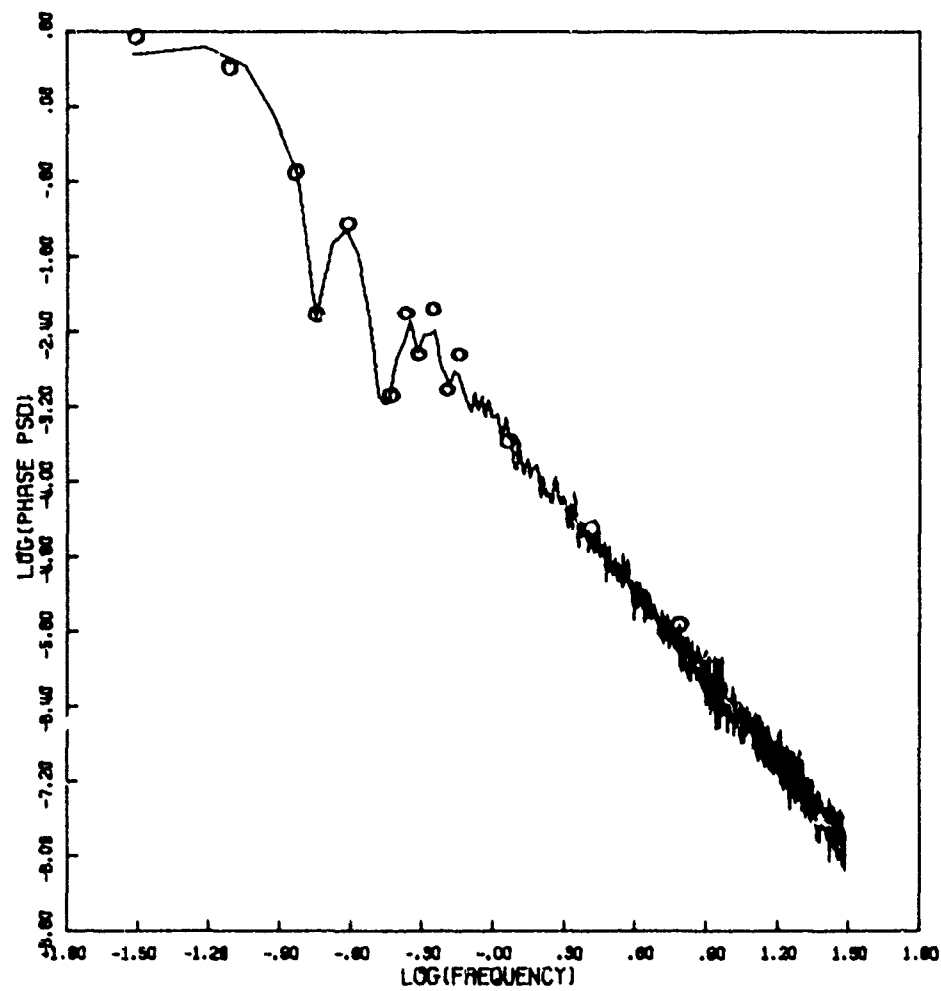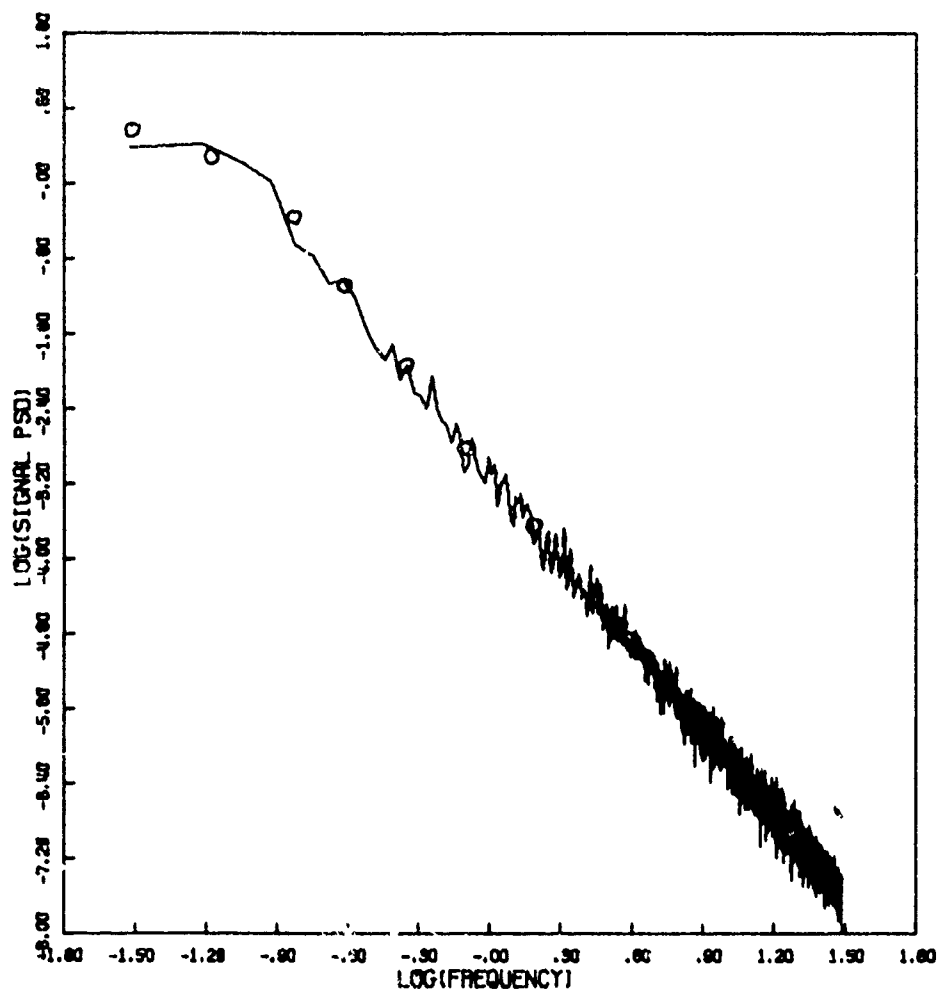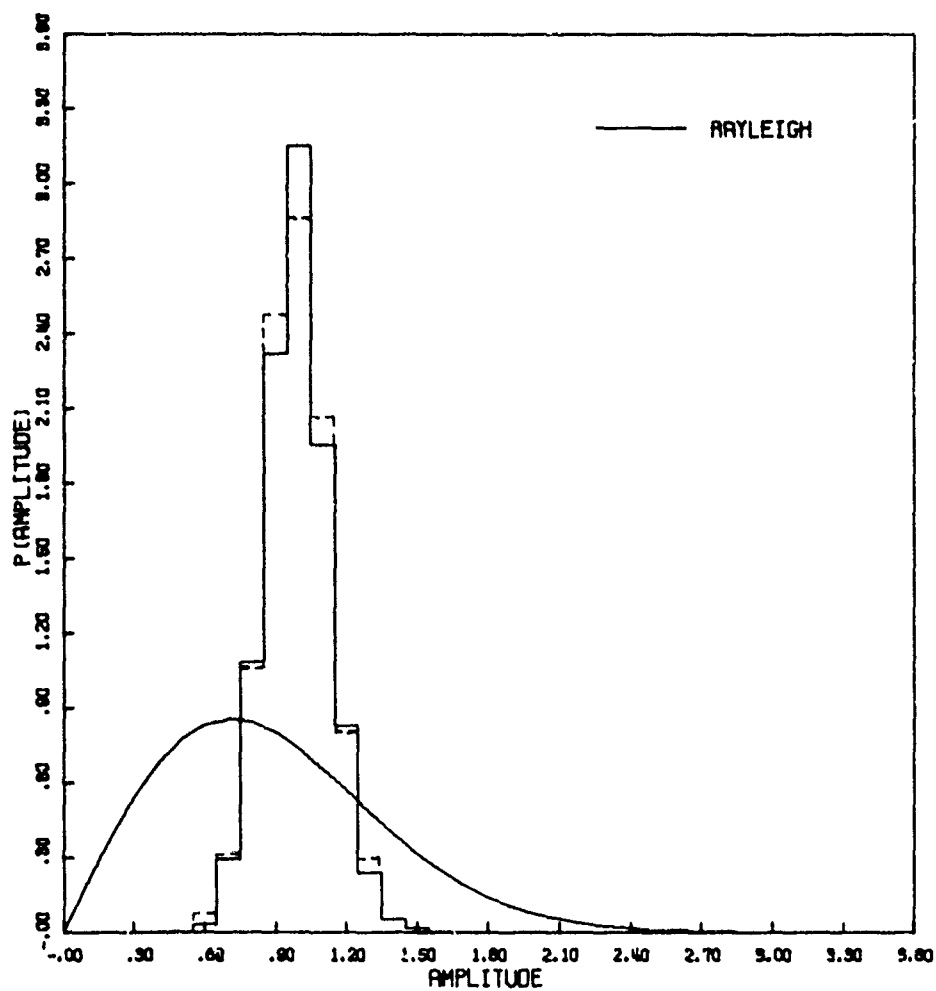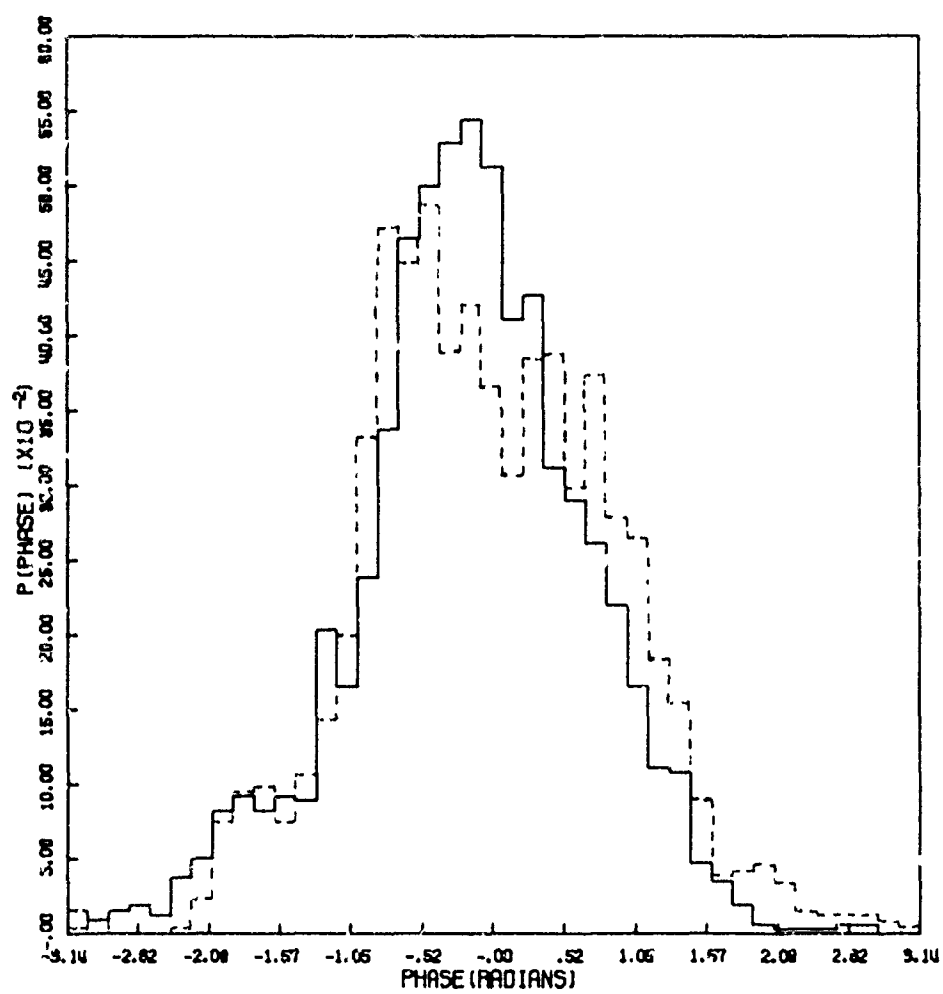Figure 93d.   Phase Power Spectral Density

Figure 93e.   Signal Power Spectral Density

458

Figure 94a. Amplitude Distribution

Figure 94b.   Phase Distribution

460

Figure 94c. Amplitude Power Spectral Density

461

Figure 94d.   Phase Power Spectral Density

Figure 94e. Signal Power Spectral Density

Figure 95a. Amplitude Distribution
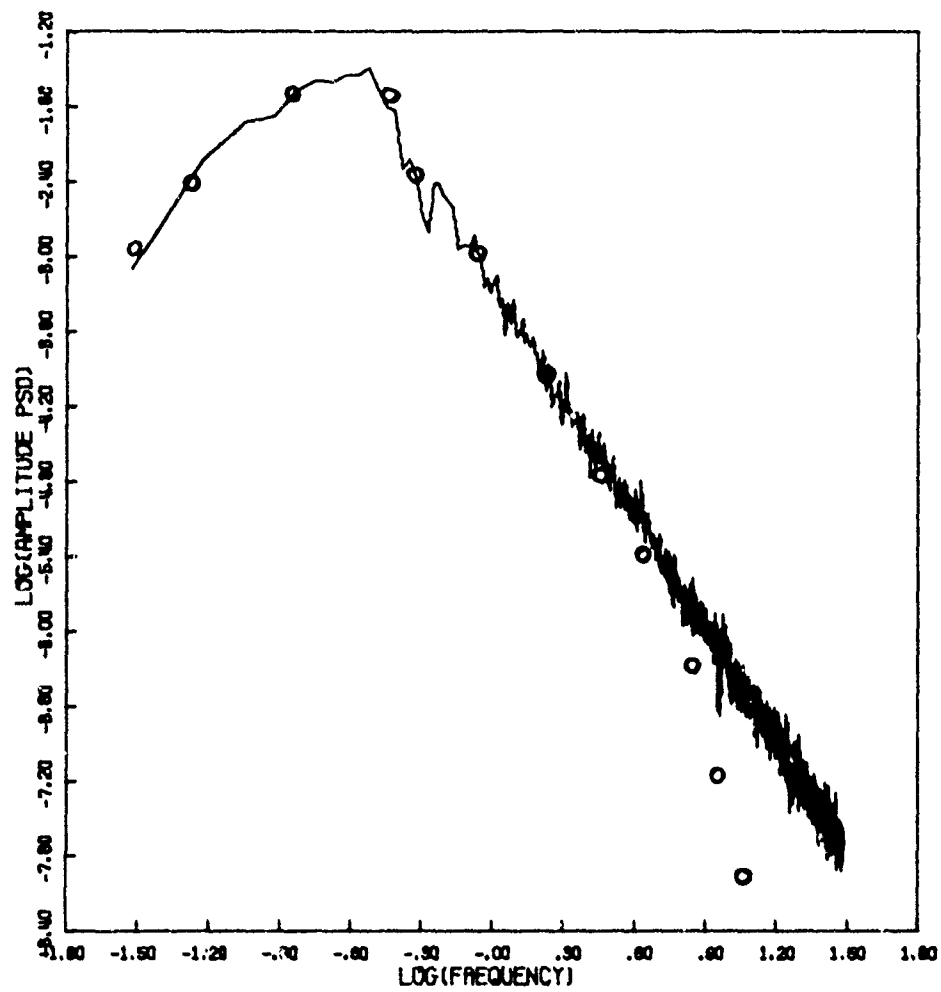
Figure 95 Phase Distribution
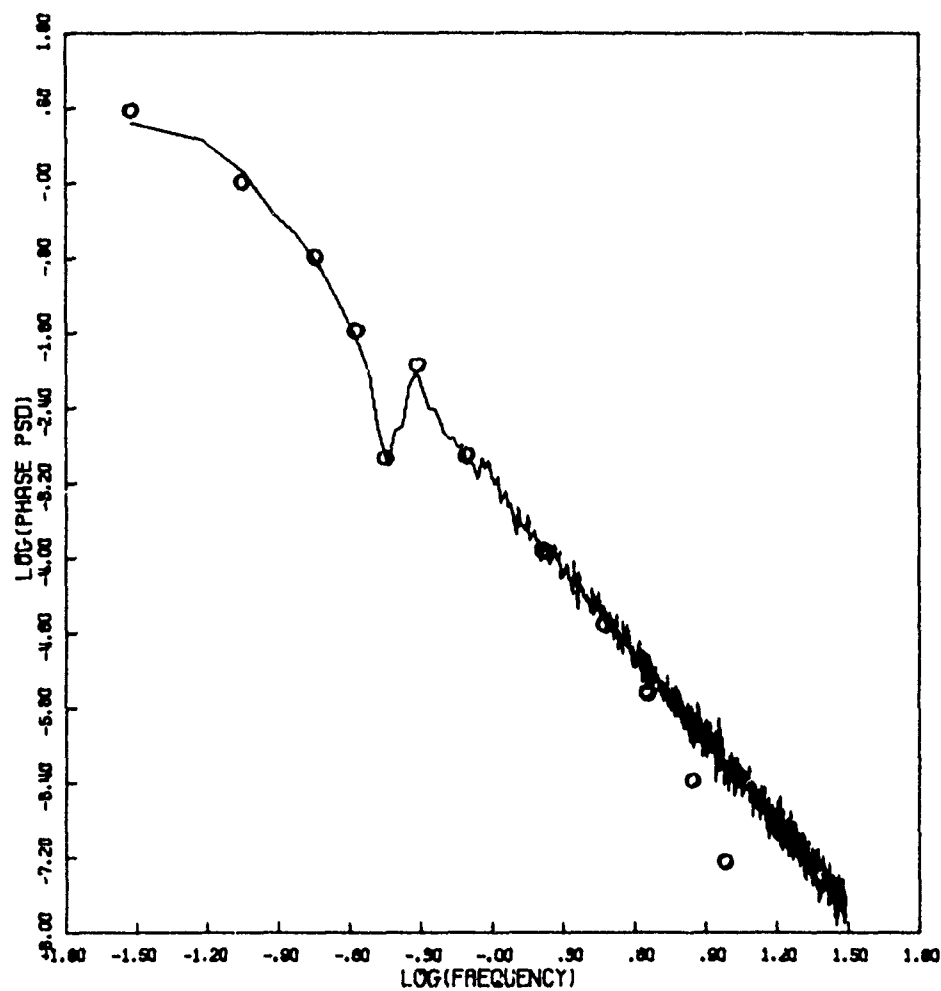
Figure 95c. Amplitude Power Spectral Density
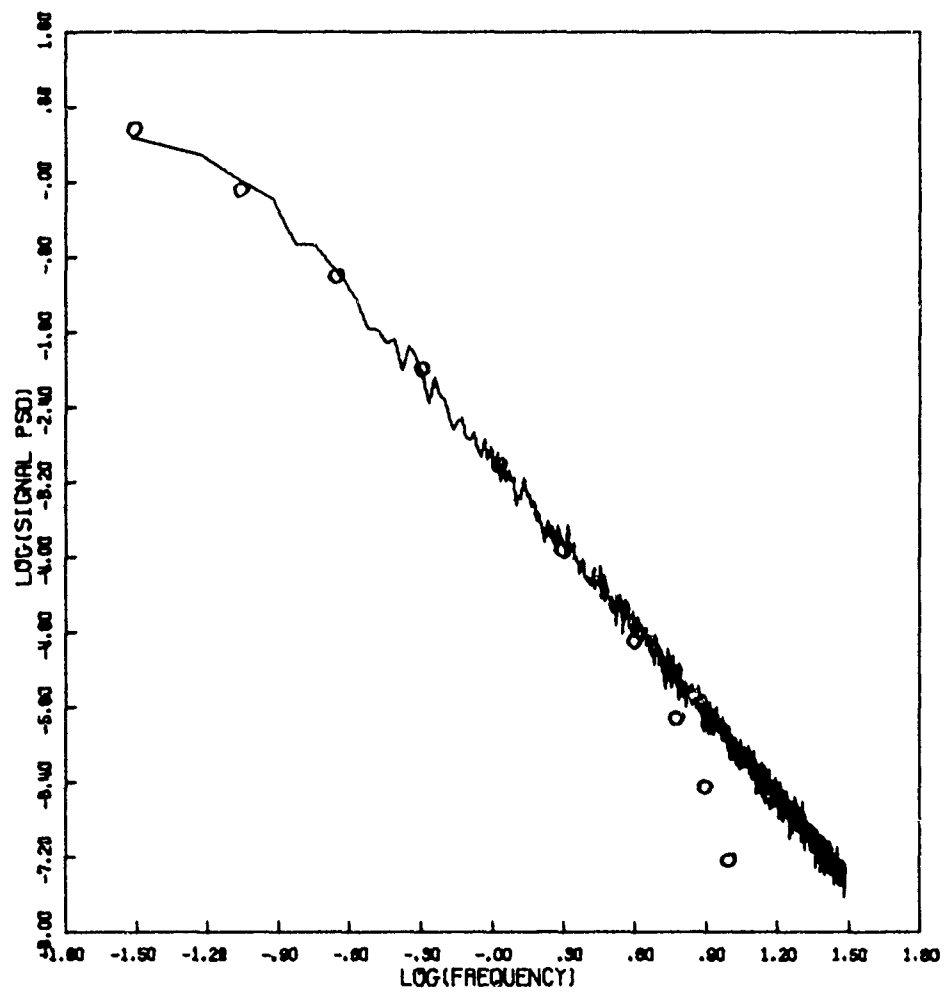
Figure 95d. Phase Power Spectral Density
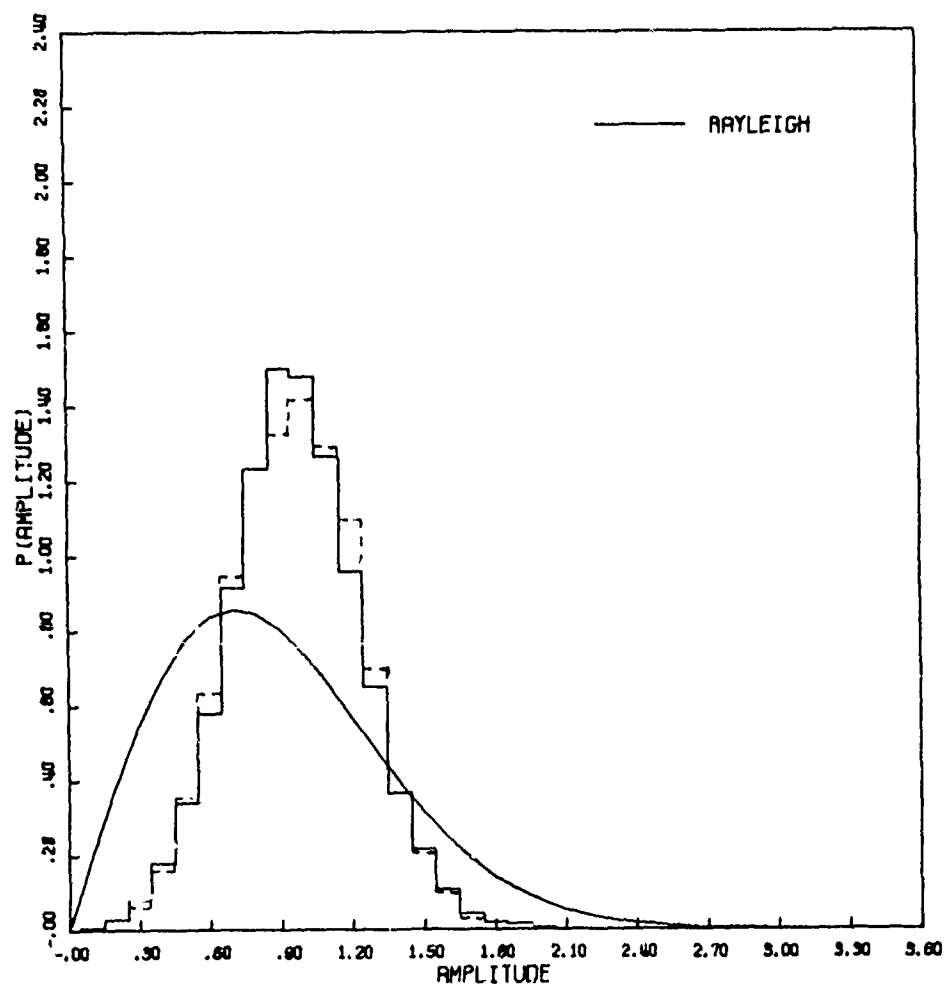
Figure 95e. Signal Power Spectral Density

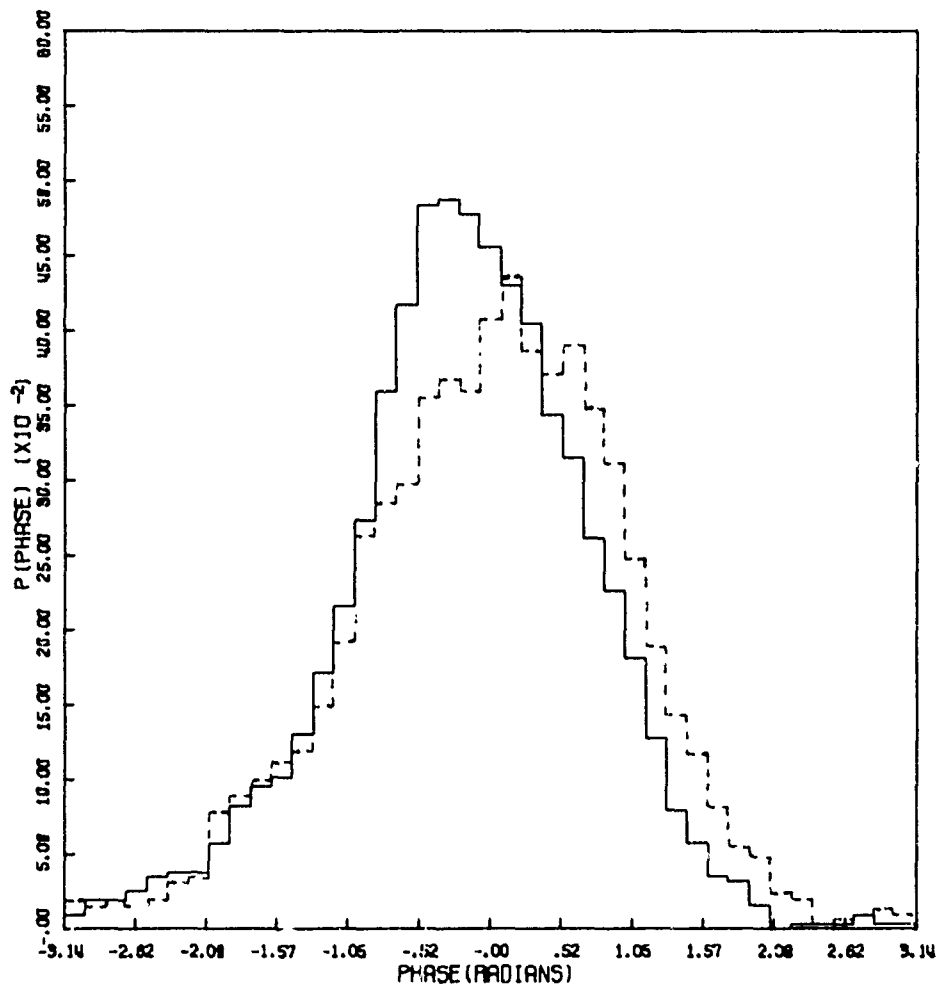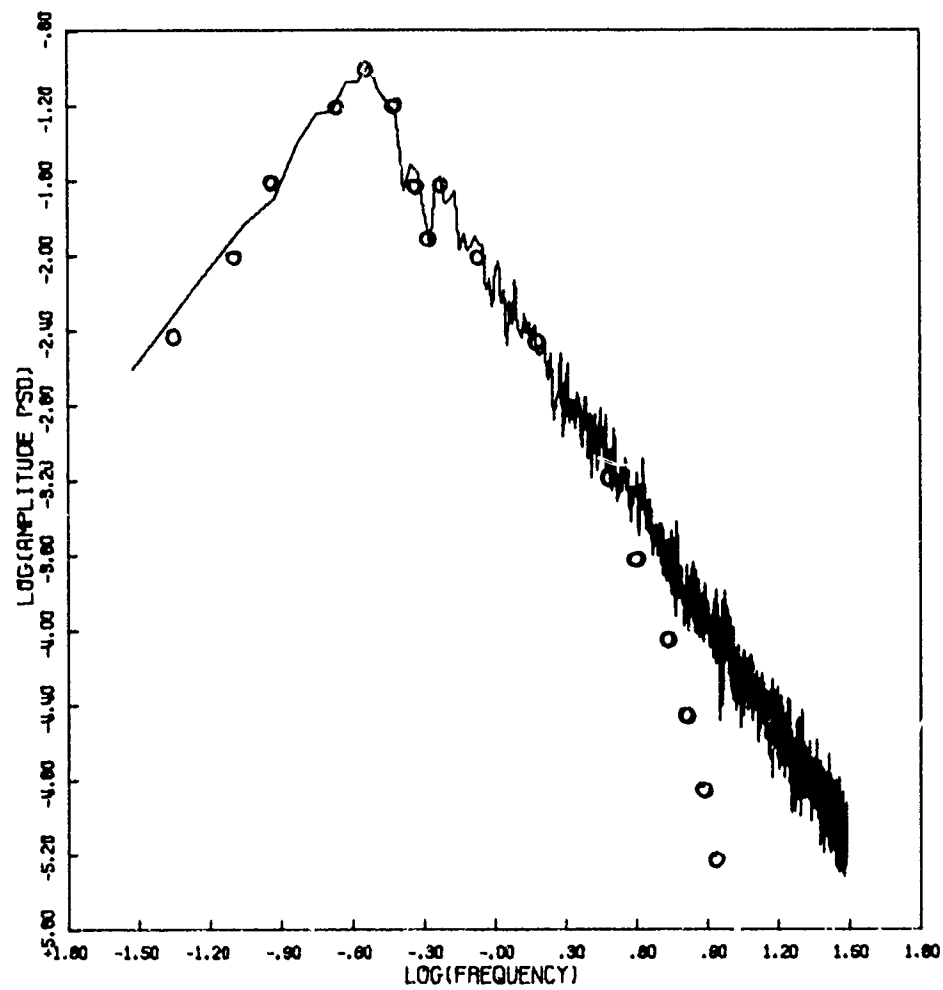Figure 96a. Amplitude Distribution

Figure 96b. Phase Distribution

Figure 96c.   Amplitude Power Spectral Density

Figure 96d.   Phase Power Spectral Density
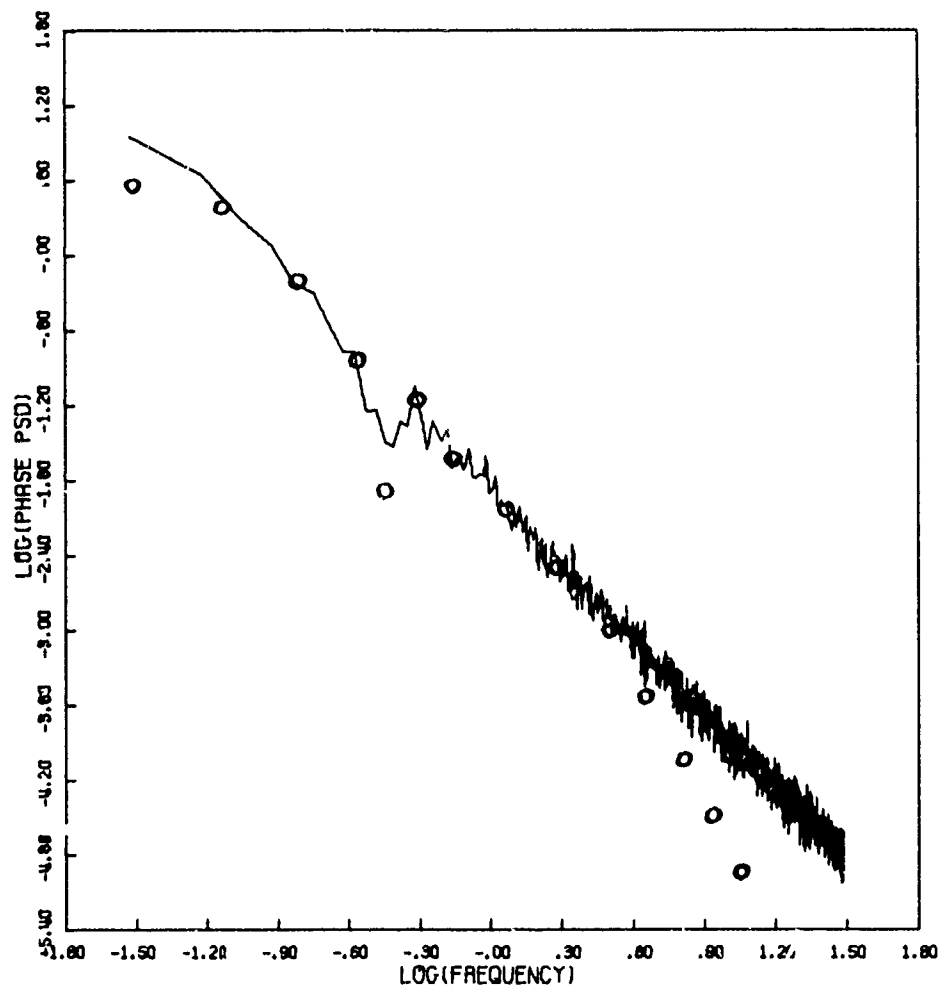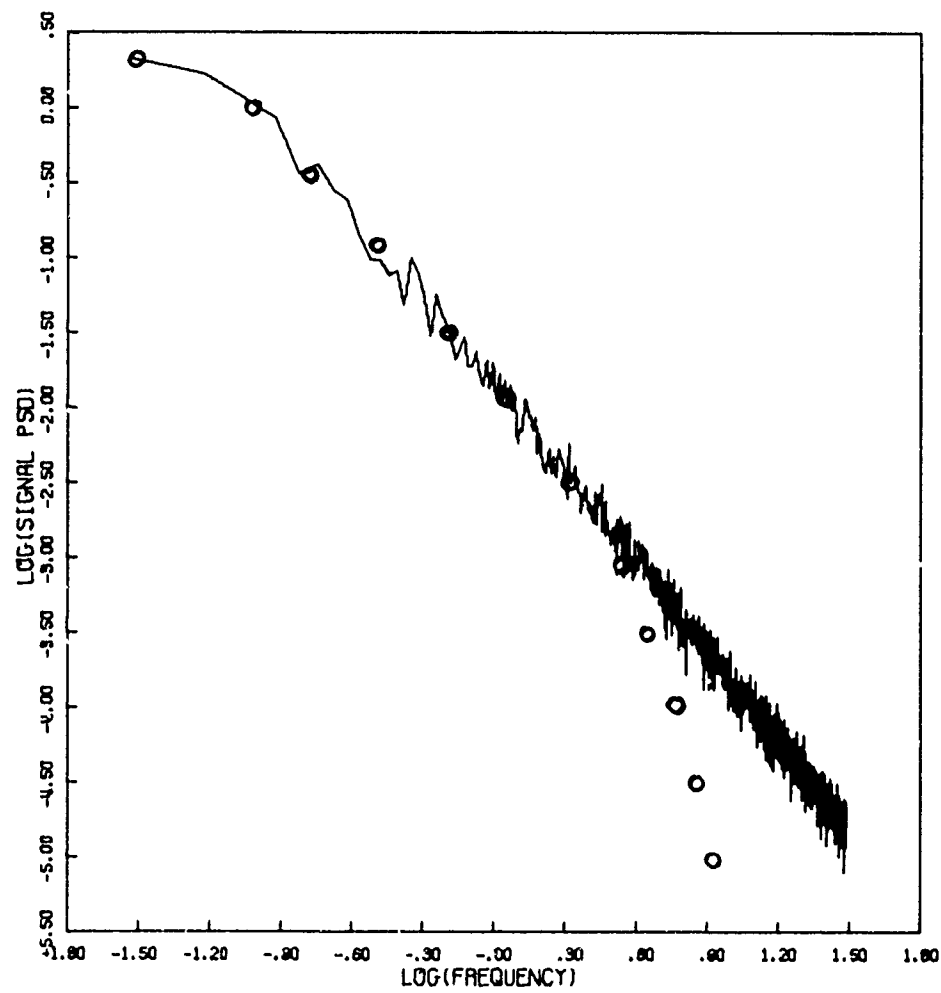
Figure 96e.   Signal Power Spectral Density

NO. OF COPIES		NO. OF COPIES	
1	Hq USAF (RDQPM/1D425)	1	Dir, DIA
1	AFTAC (TAP)	1	OSD, ARPA (NMR)
1	Dir Nuc Surety (SN)	1	FCDNA (FCPR)
1	AUL (LDE)	1	LVLO (FCTCL)
1	AFIT (Tech Lib/Bldg 640)	1	WSEGp (Doc Con)
1	USAF, SCLO (Maj Pierson/Ch,LO)	1	JSTPS (JLTW)
1	AFSC (DLSP)	1	LLL (TID)
1	(DLCAM)	1	LASL (Rpt Lib)
1	CINSAC (DOXS)	12	DDC (TC)
1	ADC (XPQY)	1	SRI (C. Rino)
1	SAMSO (SEN)	1	Aerosp Corp (R. Fox)
1	AFGL	1	NELC (M. Paulson)
1	AFWL (HO/Dr. Minge)	1	SAI (D. Sachs)
2	(SUL)		
5	(DYC)		
2	(NTS)		
1	AFOSR	1	MRC (R. Bogusch)
1	Dir, DNA (TISI)	1	Phys Dyn Inc. (J. Workman)
3	(TITL)		
1	(DDST)		
2	(G. Soper/R. Bigoni)	1	NRL (S. Ossakow)
1	USDR&E (S&SS (OS))	1	Elec Sys Lab (J. Marshall)

475